Investigation of the Role of G3BP in Stress Granule Formation in Senescence

AL-RUSHADI, MAHA,RASHID,MUSABAH

Durham University

Department of Biosciences

Investigation of the Role of G3BP in Stress Granule Formation in Senescence

Maha R. M. Al-Rushadi

A thesis submitted for the degree of Doctor of Philosophy

2022

Abstract

Senescent cells accumulate with age and are defined as the cells that irreversibly lose their ability to proliferate. They are characterized by an enlarged flat cell phenotype, enlarged nucleus with persistent DNA damage foci, and an increase in senescence-associated β-galactosidase (SA-β-GAL) activity. The accumulation of senescent cells with ageing is associated with physiological decline and age-related diseases.

Cells experience stress and damage from internal or external sources which induce various responses ranging from recovery to cell death. They respond to stress by regulating RNA translation to allow the expression of proteins required for cell viability. During stress, untranslated mRNAs are re-directed from polysomes to cytoplasmic aggregates known as stress granules. The assembly of stress granules is promoted by RNA-binding proteins including G3BP which is the nucleating protein of stress granule assembly.

Mammalian cells have three G3BP proteins: G3BP1, G3BP2a and G3BP2b, encoded by 2 genes G3BP1 and 2. We investigated the formation of stress granules in proliferative, stress induced premature senescent (SIPS) and replicative senescent cells in primary human dermal fibroblast cells and U2OS cell lines. Senescence phenotype, stress granule formation, lipid droplet accumulation and differential proteome-wide expression were investigated in WT U2OS cells and in cells lacking G3BP1/2 as well as in cells that were reconstituted with a single form of G3BP.

Table of Contents

1 Introduction 19
1.1 Cellular Senescence 19
1.1.1 Replicative Senescence 21
1.1.2 Stress Induced Premature Senescence (SIPS) 24
1.1.3 Hallmarks of Senescence 27
1.2 The Consequences of Senescence 39
1.2.1 Ageing 39
1.2.2 Cancer 40
1.3 Cellular Response to Stress 41
1.3.1 Oxidative Stress 41
1.3.2 Stress Granules 42
1.3.3 Formation of Stress Granules 42
1.3.4 Detection of Stress Granules 46
1.4 Conclusion 46
1.5 Project Aims and Objectives 49
1.5.1 Project Aims 49
1.5.2 Project Objectives 49

2 Materials and Methods 50
2.1 Materials 50
2.1.1 Cell Lines 50
2.1.2 Antibodies 51
2.1.3 Cell Culture Reagents 52
2.1.4 Reagents 52
2.1.5 Cell Culture Consumables 54
2.1.6 Lipid Staining Reagents 54
2.1.7 Solutions for Protein Work 54
2.1.8 Senescence Associated ß-Galactosidase Reagents 55
2.2 Methodology 56
2.2.1 Mammalian Cell Culture 56
2.2.2 Induction of Senescence 59
2.2.3 Senescence Associated *B*-Galactosidase Detection 60
2.2.4 Induction of Oxidative Stress 61
2.2.5 Cell Treatment with Puromycin and Cycloheximide 61
2.2.6 Immunofluorescence 61
2.2.7 DAPI Staining 62
2.2.8 Mitotracker 62
2.2.9 Oleate Medium Preparation 62
2.2.10 Oil Red O Staining 63
2.2.11 Western Blotting 63
2.2.12 Microscopy 66
2.2.13 Quantification and Statistical Analysis 66
2.2.14 Proteomics Analysis 67

3 Senescence in Primary Cells and Cancer Cell Lines 68
3.1 Cellular Senescence in Primary Cells 68
3.1.1 Introduction 68
3.1.2 Aims and Objectives 76
3.1.3 Materials and Method 77
3.1.4 Results 78
3.2 Induction of Cellular Senescence in Osteosarcoma Cells (U2OS) 89
3.2.1 Introduction 89
3.2.2 Aims and Objectives 90

3.2.3 Materials and Method 91
3.3 Results 92
3.4 Conclusion 96

4 Stress Granules in Senescence 98
4.1 Introduction 98
4.2 Aims and Objectives 102
4.2.1 Aims 102
4.2.2 Objectives 103
4.3 Materials and Methods 104
4.3.1 Materials 104
4.3.2 Methods 104
4.4 Results 105
4.4.1 Stress Granules in Proliferative and Senescent HDF Cells 105
4.4.2 Stress Granules in U2OS Cells 116
4.4.3 Puromycin and Cycloheximide Treatment 144
4.5 Comparison of Different Routes to Senescence in HDF Cells 151
4.6 Conclusion 152

5 Senescence in WT U2OS and G3BP Knock-out Cells 155
5.1 Introduction 155
5.2 Aims and Objectives 157
5.2.1 Aims 157
5.2.2 Objectives 158
5.3 Materials and Methods 159
5.3.1 Materials 159
5.3.2 Methods 159
5.4 Results 160
5.4.1 Loss of G3BP1/2 Significantly Reduced Stress Granule Formation 160
5.4.2 Stress Granule Markers 162
5.4.3 G3BP Knockout Promotes Senescence in Most of the Population 171
5.4.4 Stress in Cells Re-Constituted with G3BP1 182
5.4.5 Senescence in GFP-G3BP1 Cells 192
5.4.6 Stress Granules in GFP-G3BP2a and GFP-G3BP2b Cells 197
5.4.7 Senescence in GFP-G3BP2a and GFP-G3BP2b Cells 208
5.5 Conclusion 215

6 Lipid Droplets in WT U2OS and Knockout Cells 218
6.1 Introduction 218
6.2 Aims and Objectives 221
6.2.1 Aims 221
6.2.2 Objectives 222
6.3 Materials and Methods 223
6.3.1 Materials 223
6.3.2 Methods 223
6.4 Results 224
6.4.1 Lipid Droplets in WT U2OS Cells 224
6.4.2 Lipid Droplets in G3BP Knockout (ΔΔG3BP1/2) Cells 237
6.4.3 Lipid Droplets in GFP-G3BP1 Cells 245
6.4.4 Lipid Droplets in GFP-G3BP2a Cells 251
6.4.5 Lipid Droplets in GFP-G3BP2b Cells 258
6.4.6 Proteomics Analysis of Lipid Proteins (Perilipin) 264
6.5 Conclusion 269

7 Proteomics Analysis of Stress Granules and Senescence Proteins in U2OS Cell Lines 272
7.1 Introduction 272
7.2 Aims and Objectives 275
7.2.1 Aims 275
7.2.2 Objectives 275
7.3 Materials and Method 276
7.3.1 Materials 276
7.3.2 Methods 276
7.4 Results 277
7.4.1 WT U2OS Cells 277
7.4.2 ΔΔG3BP1/2 Cells 294
7.4.3 GFP-G3BP1 Cells 311
7.4.4 GFP-G3BP2a Cells 324
7.4.5 GFP-G3BP2b Cells 339
7.5 Conclusion 353
8 Discussion and Conclusion 357
8.1 Senescence Phenotype in HDF and U2OS Cells 359
8.2 Stress Granule Formation in HDF and U2OS Cells 359
8.3 Knockout of G3BP Increases Number of Senescent Cells 361
8.4 Knockout of G3BP Inhibits Lipid Droplet Formation 362
8.5 Elevated CDKN1A and PLIN2 Protein Levels in ΔΔG3BP1/2 Cells 363
9 Bibliography 366
10 Appendices 393

List of Figures

Chapter 1

Figure 1.1 Schematic of senescence development.

Figure 1.2 Schematic of replicative senescence.

Figure 1.3 Schematic of stress-induced premature senescence (SIPS).

Figure 1.4 Senescence hallmarks.

Figure 1.5 Schematic represents SASP phenotype in senescence.

Figure 1.6 DNA damage response and p53 pathway.

Figure 1.7 Lipid droplet synthesis.

Figure 1.8 Stress granule formation.

Chapter 3

Figure 3.1. Senescence inducing factors and cell response.

Figure 3.2 Ionizing radiation promotes senescence.

Figure 3.3 Chemical structure of (N-(5,5-Diacetoxypent-1-yl)) doxorubicin.

Figure 3.4 X-gal is used for in situ staining to measure activity of SA-ß-Gal.

Figure 3.5 A simplified scheme of cell cycle.

Figure 3.6 Cell growth pattern and population doubling curves of human fibroblast (HDF) cells.

Figure 3.7 Human fibroblast cells developed senescence-associated phenotypes by continual passaging

Figure 3.8 The structural changes in senescent HDF cells.

Figure 3.9 Mitochondrial mass in proliferative and senescent cells.

Figure 3.10 Ionizing radiation induces senescence in HDF cells.

Figure 3.11 Structural changes in SIPS senescent cells

Figure 3.12 Stress-induced premature senescence in U2OS cells using ionizing radiation.

Figure 3.13 Doxorubicin-induced senescence in U2OS cells

Chapter 4

Figure 4.1 Schematic of cell response to stress.

Figure 4.2 Schematic of regulatory components of stress granule assembly.

Figure 4.3 Sodium arsenite optimal dose to induce stress granules in proliferative HDF cells.

Figure 4.4 1.0 mM SA induces the highest number of stress granule aggregation in proliferative HDF cells.
Figure 4.5 Proliferative HDF cells exposed to 1.0 mM SA for different time periods.
Figure 4.6 Proliferative HDF cells treated with SA at different exposure time.
Figure 4.7 1.0 mM SA induces stress granules in senescent fibroblast cells
Figure 4.8 Senescent HDF cells were exposed to SA at different exposure times
Figure 4.9 Senescent HDF cells were exposed to SA at different time length.
Figure 4.10 WT U2OS cells treated with different concentrations of SA.
Figure 4.11 The optimal dose of SA to induce stress granule assembly inU2OS cells.
Figure 4.12 Determination of the optimal time length of SA exposure in U2OS cells.
Figure 4.13 WT U2OS cells exposed to 0.5 mM SA for different time periods.
Figure 4.14 G3BP1 recruitment to SA-induced stress granules in HDF proliferative and IR-induced senescent cells.
Figure 4.15 Stress granule formation and recruitment of G3BP1 in replicative senescent HDF cells.
Figure 4.16 Stress granule number in SA-treated proliferative, IR-induced and replicative senescent cells.
Figure 4.17 TIA-1 recruitment to SA-induced stress granules in HDF proliferative, IR-induced senescent cells and replicative senescent cells.
Figure 4.18 Caprin-1 recruitment to sites of stress granule assembly in proliferative and IR-induced senescent HDF cells.
Figure 4.19 Replicative senescent HDF cells showed formation of few small stress granules and localization of Caprin-1 at sites of stress granule assembly.
Figure 4.20 Count of Caprin-1 in HDF cells.
Figure 4.21 Assembly of TDP-43 in proliferative, IR-induced senescent and replicative senescent cells.
Figure 4.22 Assembly of stress granules in U2OS cells.
Figure 4.23 G3BP1 in senescent U2OS.
Figure 4.24 Number of stress granules in proliferative and senescent U2OS cells.
Figure 4.25 eIF4G in proliferative U2OS cells.
Figure 4.26 Quantitative representation of eIF4G and G3BP1 in proliferative U2OS cells.
Figure 4.27 FXR1 in proliferative U2OS cells.
Figure 4.28 Quantitative representation of FXR1 and G3BP1 in proliferative U2OS cells.

Figure 4.29 Cycloheximide (CHX) and puromycin shows counteract effect on stress granules in proliferative HDF cells.
Figure 4.30 Cycloheximide (CHX) and puromycin treatment in senescent HDF cells.
Figure 4.31 Quantitative comparison of stress granules in HDF cells treated with Cycloheximide (CHX) and puromycin (Puro.).
Figure 4.32 Treatment of proliferative U2OS cells with Cycloheximide (CHX) and Puromycin.
Figure 4.33 Quantitative representation of stress granules in U2OS under Cycloheximide (CHX) and Puromycin (Puro.).

Chapter 5

Figure 5.1 Schematic representation of G3BP domains.
Figure 5.2 WT U2OS were used to generate cells lacking G3BP1 and G3BP2 (ΔΔG3BP1/2).
Figure 5.3 Knockout of G3BP1 and G3BP2 inhibited stress granule formation in ΔΔG3BP1/2 cells.
Figure 5.4 Sodium arsenite induced formation of stress granules in WT U2OS but not ΔΔG3BP1/2 cells.
Figure 5.5 FXR1 is recruited to stress granules in WT U2OS cells and detected to be diffused in ΔΔG3BP1/2 cells.
Figure 5.6 G3BP1 and FXR1 were detected at sites of stress granule assembly in WT U2OS cells.
Figure 5.7 EIF4G is involved in stress granule formation in WT U2OS cells and detected to be diffused in ΔΔG3BP1/2 cells.
Figure 5.8 EIF4G was detected at sites of stress granule assembly in WT U2OS cells.
Figure 5.9 SA-ß-Gal positive cells were detected in WT U2OS and ΔΔG3BP1/2 cells.
Figure 5.10 Knockout of G3BP1/2 accelerates development of senescence phenotype in ΔΔG3BP1/2 cells.
Figure 5.11 WT U2OS and ΔΔG3BP1/2 cells showed gradual formation of SAHF.
Figure 5.12 Absence of G3BP1/2 promotes senescence phenotype in mostly all ΔΔG3BP1/2 cells.
Figure 5.13 High p21 protein level was detected in ΔΔG3BP1/2 cells.
Figure 5.14 Schematic diagram shows the development of ΔΔG3BP1/2+GFP-G3BP1 through transient transfection of ΔΔG3BP1/2 with GFP-G3BP1.
Figure 5.15 Stress granule formation is rescued in GFP-G3BP1 cells.

Figure 5.16 G3BP1 promotes formation of stress granules in GFP-G3BP1 under oxidative stress.
Figure 5.17 FXR1 is recruited to stress granules in GFP-G3BP1 cells.
Figure 5.18 EIF4G is recruited to stress granules in GFP-G3BP1 cells.
Figure 5.19 GFP-G3BP1 cells showed gradual formation of SA-ß-Gal and SAHF
Figure 5.20 G3BP1 slows cells' progression towards senescence.
Figure 5.21 Low p21 protein level was detected in GFP-G3BP1 cells.
Figure 5.22 Schematic diagram shows the development of ΔΔG3BP1/2+GFP-G3BP2a and ΔΔG3BP1/2+GFP-G3BP2b cells.
Figure 5.23 Stress granule formation is rescued in GFP-G3BP2a and GFP-G3BP2b cells.
Figure 5.24 G3BP2a and G3BP2b promotes formation of stress granules.
Figure 5.25 FXR1 is recruited to stress granules in GFP-G3BP2a cells.
Figure 5.26 FXR1 but not EIF4G is recruited to stress granules in GFP-G3BP2b cells.
Figure 5.27 Senescence phenotype in GFP-G3BP2a and GFP-G3BP2b cells.
Figure 5.28 GFP-G3BP2b showed an increased cell's progression towards senescence.
Figure 5.29 Low p21 protein level was detected in GFP-G3BP2b cells.

Chapter 6

Figure 6.1 Oleate (C18H33O2).
Figure 6.2 Oleate induced formation of lipid droplets in WT U2OS cells.
Figure 6.3 Oleate induced lipid droplet accumulation in WT U2OS cells.
Figure 6.4 WT U2OS cells formed stress granules and lipid droplets under SA treatment.
Figure 6.5 Oleate induced lipid droplet accumulation in SA-treated WT U2OS cells.
Figure 6.6 Oxidative stress reduced lipid droplet accumulation in WT U2OS cells.
Figure 6.7 Oleate induced lipid droplet accumulation in senescent WT U2OS cells.
Figure 6.8 Oleate induced lipid droplet accumulation in SA-treated senescent WT U2OS cells.
Figure 6.9 Lipid droplet accumulation is reduced in senescent and proliferative cells in response to oxidative stress.
Figure 6.10 Inhibition of stress granules inhibits lipid droplet formation in ΔΔG3BP1/2 cells.
Figure 6.11 Oxidative stress induces formation of small lipid droplets in ΔΔG3BP1/2 cells.
Figure 6.12 Formation of lipid droplets in senescent ΔΔG3BP1/2 cells.
Figure 6.13 Oxidative stress induced formation of small and large lipid droplets in senescent ΔΔG3BP1/2 cells.

Figure 6.14 Re-constitution of cells with G3BP1 promotes lipid droplet formation.
Figure 6.15 Formation of lipid droplets increased under oxidative stress in GFP-G3BP1.
Figure 6.16 Formation of lipid droplets in senescent GFP-G3BP1 cells.
Figure 6.17 Oxidative stress induced formation of lipid droplets in senescent GFP-G3BP1 cells.
Figure 6.18 Re-constitution of cells with G3BP2a promotes lipid droplet formation.
Figure 6.19 Formation of lipid droplets increased under oxidative stress in GFP-G3BP2a.
Figure 6.20 Formation of lipid droplets in senescent GFP-G3BP2a cells.
Figure 6.21 Oxidative stress reduced formation of lipid droplets in senescent GFP-G3BP2a cells.
Figure 6.22 Re-constitution of cells with G3BP2b promotes lipid droplet formation.
Figure 6.23 Formation of lipid droplets increased under oleate and oxidative stress in GFP-G3BP2b cells.
Figure 6.24 Formation of lipid droplets in senescent GFP-G3BP2b cells.
Figure 6.25 Oxidative stress reduced formation of lipid droplets in senescent GFP-G3BP2b cells.
Figure 6.26 Levels of lipid proteins in WT U2OS cells.
Figure 6.27 Levels of Perilipin proteins in proliferative and senescent ΔΔG3BP1/2 cells.
Figure 6.28 Levels of Perilipin proteins in proliferative and senescent GFP-G3BP1 cells.
Figure 6.29 Levels of Perilipin proteins in proliferative and senescent GFP-G3BP2a cells.
Figure 6.30 Levels of Perilipin proteins in GFP-G3BP2b cells.

Chapter 7

Figure 7.1 Schematic of SWATH-MS workflow.
Figure 7.2 Proteomics analysis of proliferative (Day 0) and senescent (Day 9) WT U2OS cells.
Figure 7.3 Level of cytoskeletal proteins in senescent WT U2OS cells.
Figure 7.4 Overrepresentation of GO biological process terms in the upregulated proteins.
Figure 7.5 Level of H1 proteins in WT U2OS cells.
Figure 7.6 Biological processes that are underrepresented in senescence.
Figure 7.7 Change in cyclin-dependent kinase inhibitors level.
Figure 7.8 Change in the level of LMNB1 and PML proteins.
Figure 7.9 level of stress granule proteins WT U2OS cells.
Figure 7.10 Proteomics analysis of proliferative (Day 0) compared to senescent (Day 9) ΔΔG3BP1/2 cells.

Figure 7.11 Overrepresentation of GO biological process terms.
Figure 7.12 Biological processes that are underrepresented in senescence.
Figure 7.13 Level of cyclin-dependent kinase inhibiting proteins in ΔΔG3BP1/2 cells.
Figure 7.14 Change in the level of LMNB1 and PML proteins.
Figure 7.15 Change in the level of RNA-binding proteins from proliferative to senescent ΔΔG3BP1/2 cells.
Figure 7.16 Proteomics analysis of proliferative (Day 0) and senescent (Day 9) GFP-G3BP1 cells.
Figure 7.17 Overrepresentation of GO biological process terms.
Figure 7.18 Level of minichromosome maintenance proteins varies from proliferative to senescent GFP-G3BP1 cells.
Figure 7.19 Biological processes that are underrepresented in senescence.
Figure 7.20 Level of cyclin-dependent kinase inhibiting proteins varies from proliferative to senescent cells.
Figure 7.21 Change in the level of LMNB1 and PML proteins.
Figure 7.22 Change in the level of RNA-binding proteins from proliferative to senescent GFP-G3BP1 cells.
Figure 7.23 Proteomics analysis of proliferative (Day 0) and senescent (Day 9) GFP-G3BP2a cells.
Figure 7.24 Level of Caspase proteins varies from proliferative to senescent GFP-G3BP2a cells.
Figure 7.25 Overrepresentation of GO biological process terms.
Figure 7.26 Level of Histone H1 proteins in GFP-G3BP2a cells.
Figure 7.27 Biological processes that are underrepresented in senescence.
Figure 7.28 Level of cyclin-dependent kinase inhibitors varies from proliferative to senescent GFP-G3BP2a cells.
Figure 7.29 Change in the level of LMNB1 and PML proteins in GFP-G3BP2a cells.
Figure 7.30 Change in the level of RNA-binding proteins from proliferative to senescent GFP-G3BP2a cells.
Figure 7.31 Proteomics analysis of proliferative (Day 0) and senescent (Day 9) GFP-G3BP2b cells.
Figure 7.32 Overrepresentation of GO biological process terms.
Figure 7.33 Level of Histone H1 proteins in GFP-G3BP2b cells.

Figure 7.34 Level of CDK proteins in GFP-G3BP2b cells.
Figure 7.35 Biological processes that are underrepresented in senescence.
Figure 7.36 Level of cyclin-dependent kinase inhibitors in GFP-G3BP2b cells.
Figure 7.37 Change in the level of LMNB1 and PML proteins in GFP-G3BP2b cells.
Figure 7.38 Change in the level of RNA-binding proteins from proliferative to senescent GFP-G3BP2b cells.
Figure 7.39 Level of senescence proteins in WT U2OS, ΔΔG3BP1/2, GFP-G3BP1, GFP-G3BP2a and GFP-G3BP2b cells.

List of Tables

Chapter 2

Table 2.1 List of cell lines

Table 2.2: List of antibodies

Table 2.3: List of cell culture reagents

Table 2.4: List of reagents

Table 2.5: List of lipid staining reagents

Table 2.6: List of solutions used for protein work

Table 2.7: List of senescence associated ß-galactosidase reagents

Chapter 7

Table 7.3: List of proteins involved in DNA damage-repair and cell growth regulation pathway.

Table 7.4: Nuclear and mitochondrial proteins that are significantly down-regulated from proliferative to senescent ΔΔG3BP1/2 cells.

Table 7.5: Lysosomal proteins that are significantly up-regulated from proliferative to senescent ΔΔG3BP1/2 cells.

Appendices

Table 7.1: Enriched GO terms (BP) (Overrepresented) in WT U2OS

Table 7.2: Enriched GO terms (BP) (Underrepresented) in WT U2OS

Table 7.6: Enriched GO terms (BP) (Overrepresented) in ΔΔG3BP1/2 cells

Table 7.7: Enriched GO terms (BP) (Underrepresented) in ΔΔG3BP1/2 cells

Table 7.8: Enriched GO terms (BP) (Overrepresented) in GFP-G3BP1 cells

Table 7.9: Enriched GO terms (BP) (Underrepresented) in GFP-G3BP1 cells

Table 7.10: Enriched GO terms (BP) (Overrepresented) in GFP-G3BP2a cells

Table 7.11: Enriched GO terms (BP) (Underrepresented) in GFP-G3BP2a cells

Table 7.12: Enriched GO terms (BP) (Overrepresented) in GFP-G3BP2b cells

Table 7.13: Enriched GO terms (BP) (Underrepresented) in GFP-G3BP2b cells

Abbreviations

ATM	Ataxia telangiectasia mutated
ATR	Ataxia telangiectasia and Rad3-related
CAD	Coronary heart disease
CDC25	Cell-division cycle 25
CHK2	Checkpoint kinase 2
DDR	DNA-damage Response
DIA	Data-independent acquisition
DMEM	Dulbecco's Modified Eagle Medium
DSB	Double-strand Breaks
dsRNA	Double-stranded RNA
eIF2α	Eukaryotic initiation factor 2α
eIF4G	Eukaryotic initiation factor 4G
ER	Endoplasmic reticulum
FMRP	Fragile X mental retardation protein
FXR1	Fragile X mental retardation-related protein1
G3BP	Ras-GTPase-activating protein SH3-domain-binding protein
GAPDH	Glyceraldehyde-3-phosphate dehydrogenase
GO	Gene Ontology
Gy	Gray
HDF	Human Dermal Fibroblast
HRI	Heme-regulated eIF2α kinase
IGF-II	Insulin-like growth factor II
IL	Interleukin
IR	Ionizing Radiation
L	Litre
LDs	Lipid Droplets
LMNB1	Lamin-B1
MAPK	Mitogen-activated protein kinase
mL	millilitre
mM	millimolar
MMPs	Matrix metalloproteinases
nM	nanomolar

PAI-1	Plasminogen activator inhibitor-1
PD	Population Doubling
PERK	PKR-like ER kinase
PKR	Protein kinase R
PLIN	Perilipin
PML	Protein PML
Rb	Retinoblastoma
RIPA	Radio-immunoprecipitation assay
SA	Sodium Arsenite
SA-ß-Gal	Senescence-associated ß-galactosidase
SAHF	Senescence-associated heterochromatic foci
SASP	Senescence-associated secretory phenotype
SDS-PAGE	Sodium dodecyl sulphate–polyacrylamide gel electrophoresis
SGs	Stress granules
SIPS	Stress Induced Premature Senescence
SMN	Survival of motor neurons
SWATH-MS	Sequential Windowed Acquisition of All Theoretical Fragment Ion Mass Spectra
TAG	Triglycerol
TBST	Tris Buffered Saline with Tween
TDP-43	Transactive response DNA-binding protein 43
TIA1	T cell internal antigen-1
TIAR	TIA-1-related
TNF-α	Tumour necrosis factor alpha
ug	microgram

Declaration

The work described here in this thesis was carried out at Durham University, Department of Biosciences between the period October 2015 and October 2021. All of the work is done by me unless it is stated. None of the work described in this thesis has been previously submitted for a degree at Durham University or other University.

Statement of Copyright

Publications arising from this work

1. Oral presentation “Role of Ras GTPase-activating protein-SH3-domain-binding protein (G3BP) in Cellular senescence”. Department of Biosciences/Durham University. 11th May 2018.

2. Poster “Role of Ras GTPase-activating protein-SH3-domain-binding protein (G3BP) in Cellular senescence”. Early Career Researcher Conference, Wolfson research institute for health and wellbeing, Calman learning center/Durham University. 11th June 2018.

3. Poster “Investigating the Role of Stress Granules in Senescence.” PG Conference, Department of Biosciences/Durham University. 12th May 2017.

4. Poster “Investigating the Role of Stress Granules in Senescence.” PG Conference, Department of Biosciences/Durham University. 13th May 2016.

Acknowledgments

This research was funded by the Ministry of Higher Education/Sultanate of Oman. I would like to thank Mrs Fatma Al-Mashaiki, Ministry of Higher Education/Oman and Yusra Al-Ismaily, Oman Embassy/UK for their help and continuous support.

I also would like to express my special thanks to my supervisor, Dr. Sushma Grellscheid for the guidance and support through my PhD journey. I'm grateful for the continuous help in improving research skills and encouragement of personal development.

I would like to thank Dr Nancy Kedersha for sharing G3BP U2OS cell lines and useful discussions. I would like to thank Dr. Martin Schroder for his guidance in the lab. I also would like to thank Max, Donata, Mike and Joy who were very welcoming when I first joined the department. I would like to thank Hanan and Amna for always being there whenever I need help and for being in the lab during the weekends.

I would like to thank Carl, Tom, Catherine, and Amy for being such great friends. Carl, thank you for your help in solving statistical problems. Tom and Catherine, thank you for helping me and making the long hours in the lab enjoyable. I would like to thank Franziska from the University of Bergen for her help.

Finally, I would like to give a special thanks to my husband Othman for supporting me and believing in me. Thank you to my mother, father and siblings for their support and being proud of my achievements. Special thanks to my kids Abdullah and Balqees who joined me in this journey lately.

Chapter 1

1 Introduction

1.1 Cellular Senescence

Mammalian cells are exposed to several external and internal stimuli that induce stress and damage to cells. Normal cells respond to stress or damage by activating signalling pathways responsible for damage repair. Nevertheless, if the stress or damage is prolonged and severe, mutation occurs and cells become dysfunctional. Hence, dysfunctional cells are either directed to apoptosis or cell-cycle arrest (Figure 1.1).

Cellular senescence was first described by Hayflick and colleagues five decades ago. They showed that normal fibroblast cells have a limited ability to proliferate in culture. Initially, the cells underwent continuous cell division. However, after a number of divisions, the cell growth declined gradually. Irreversibly, all cells stopped dividing in culture indicating that human cells have a finite lifetime in culture. The cells remained viable in culture although they ceased proliferation (Hayflick, 1965). This type of senescence is called replicative senescence and is induced by dysfunctional telomere (see section 1.1.1).

The limited cell divisions of cells in culture is known as cellular senescence. Therefore, cellular senescence is a phenotype of irreversible arrest of cell division. It has been observed in several kinds of cells including human fibroblasts (Hayflick, 1965), human skin (Dimri et al. 1995), primate retina (Mishima et al. 1999) and human liver (Paradis et al. 2001). Additionally, senescence has been observed in mouse embryonic fibroblast cells (Itahana et al., 2004).

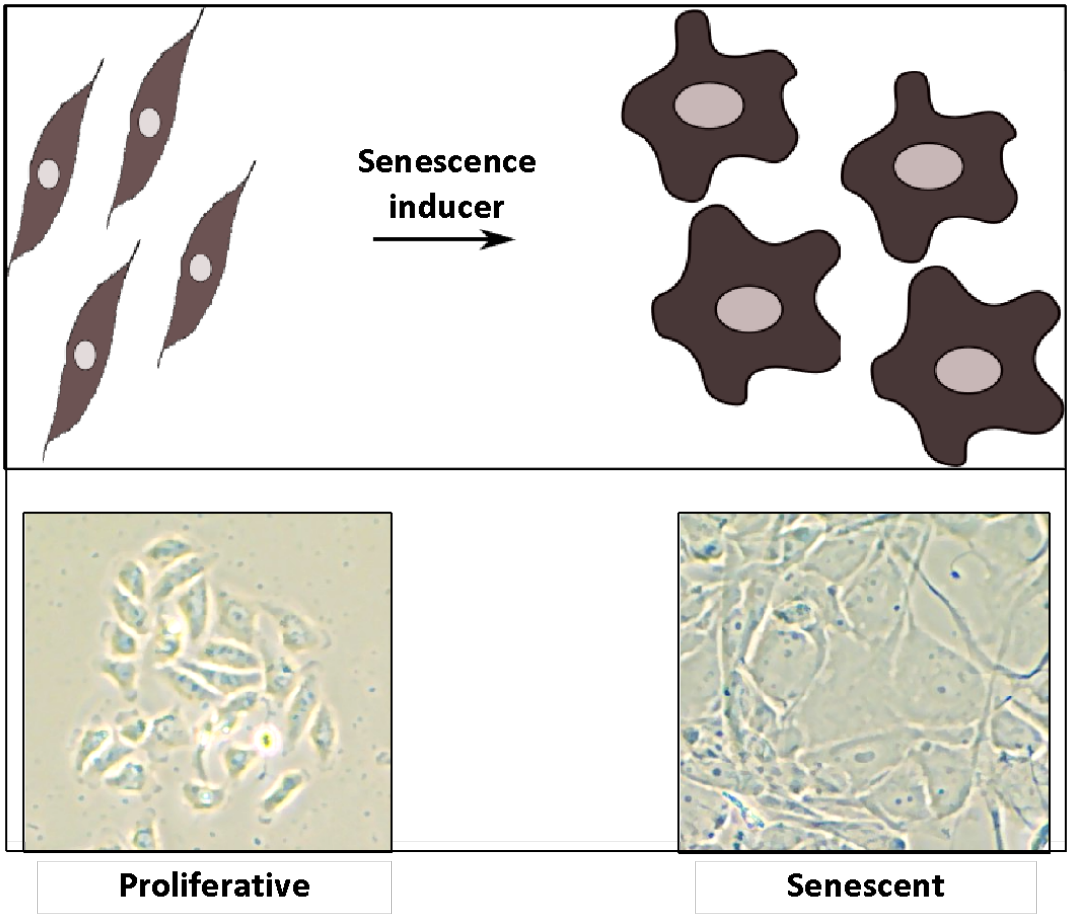

Figure 1.1 Schematic of senescence development.

When normal proliferative cells are exposed to senescence inducer, they undergo structural and morphological changes such as flattened cell shape. Images are of proliferative and senescent U2OS cells (cultured in our lab).

Senescent cells are cells that have lost their ability to proliferate. This process is induced by various factors including telomere shortening (replicative senescence) and exposure to DNA-damage agents such as ionizing radiation and oncogenes (stress-induced premature senescence). Several studies have revealed that senescent cells exist and accumulate at sites of age-related diseases such as benign hyperplastic prostate (Choi et al., 2000) and atherosclerotic lesions (Vasile et al., 2001). These observations indicate that senescent cells may contribute to aging and development of age-related diseases.

The senescence phenotype is stable and resistant to apoptosis (Campisi, J., 2005). It has been suggested that senescent cells remain persistent in tissues for years (Michaloglou et al., 2005). Although they are not functioning as dividing cells, senescent cells remain metabolically active (Roninson, 2003). Senescent cells and quiescent cells are distinct. Quiescent cells are responsive to mitogenic stimuli and resume proliferation. However, senescent cells are unresponsive to stimuli and the growth arrest phenotype is irreversible (Aravinthan, 2015). Additionally, the irreversible growth arrest phenotype of senescent cells acts as a program that prevents development of tumours. It prevents multiplication of cells with genetic mutations or functional defects. Hence, it prevents development of tumour cells.

Cellular senescence is known as the terminal phenotype that primary cells approach after undergoing a prolonged passage *in vitro* or multiple divisions *in vivo* (Schawrze et al., 2005). Senescent cells cease proliferation losing their ability to divide. Understanding senescence is crucial as it is implicated in tumour suppression and chronic diseases such as age-related diseases. Cellular senescence is triggered in response to various stresses including telomere shortening, DNA damage and oncogene activation leading to replicative senescence, stress-induced senescence and oncogene-induced senescence, respectively (Aravinthan, 2015).

1.1.1 Replicative Senescence

Replicative senescence is the phenotype of irreversible growth arrest that the cells reach after multiple passages in culture. This type of senescence is observed in different normal diploid human cells. Replicative senescence is induced by dysfunctional telomeres. After each cell division, telomere shortens leading to dysfunctional telomeres (Campisi, 1997). It was observed that human liver tissue loses 55 base pair of telomeric DNA per year (Takubo et al., 2000).

Telomeres are located at terminal regions of chromosomes. They are composed of telomeric DNA and associated telomeric proteins. The main function of telomeres is to maintain the stability of the cellular genome (Blackburn, 2001). However, replication of a linear DNA occurs with impossibility of full reproduction of previous length of DNA ends. Erosion of several telomere nucleotides (30-200 base pair/ cell division) after each cell division causes telomere length shortening in daughter cells (Lingner et al., 1995). Several studies have shown that telomere shortening is correlated to a cell's replicative potential. Following multiple cell divisions and when the telomere reaches a certain length, cells stop dividing leading to replicative senescence phenotype (Olovnikov, 1973; Whittemore et al., 2019).

Telomere length may act as a biological clock that determines life span of an organism. Length of telomeric DNA is affected by several factors including genetic make-up, environment and habits (smoking and diet). Cells undergo senescence after reaching below the critical limit of telomere length. Shortening of telomere length is recognised as DNA damage and triggers DNA damage responses which in turn leads to cell growth arrest and senescence (Figure 1.2). Furthermore, telomere shortening affects the health and lifespan of individuals. It is associated with age-related problems such as heart failure, diabetes and osteoporosis (Shammas, 2011).

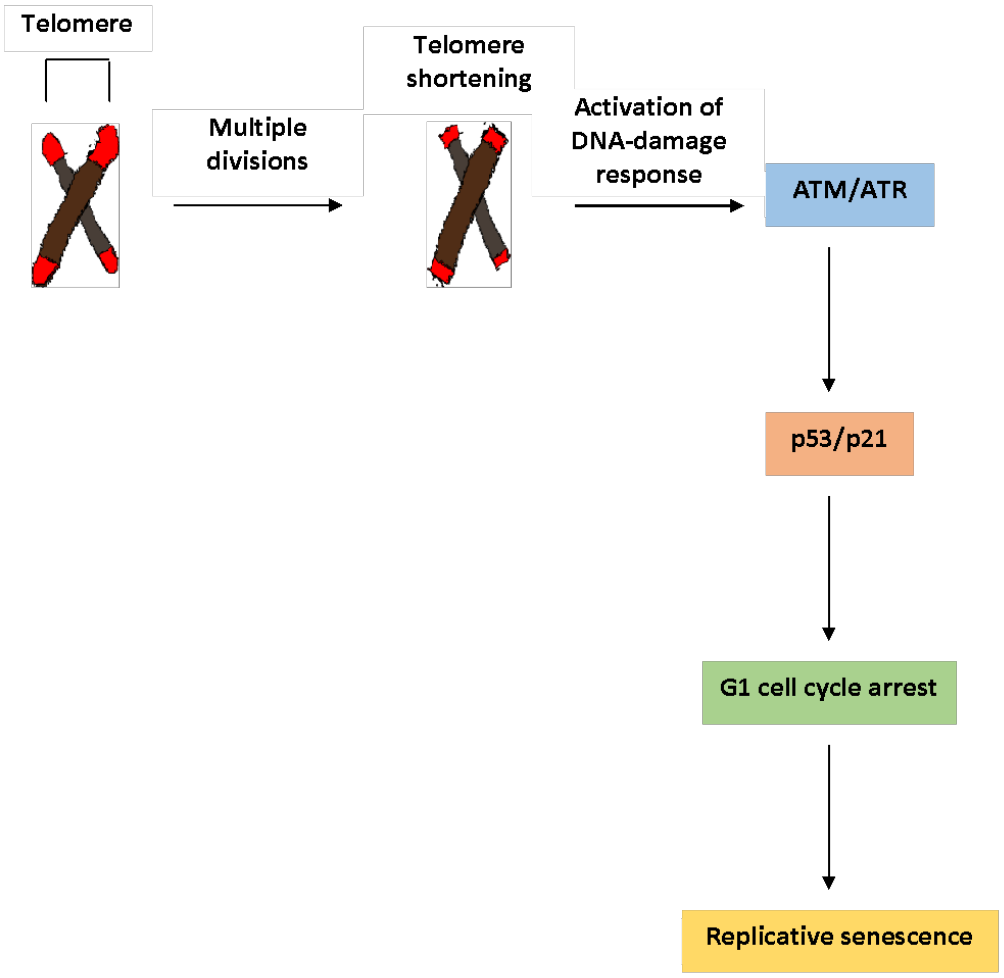

Figure 1.2 Schematic of replicative senescence.

Telomere shortening is the major driver of replicative senescence. Following multiple cell divisions, telomere length is shortened and recognised as DNA damage. DNA damage responses are triggered which activates p53/p21 pathways and thus cell cycle arrest.

Replicative senescence is characterized by cell growth arrest in response to serial passages in culture or multiple cell divisions *in vivo*. Replicative senescent cells exist in all tissues and organs. Changes associated with this sub-type of senescence includes morphological and molecular changes such as enlarged cell size and increased expression of tumour-suppressor proteins such as p21 and p16. However, the functional significance of the morphological changes of senescent cells is still unclear (Campisi, 2005; Herranz and Gil 2018).

Accumulation of senescent cells drives ageing and age-related diseases. The relation of senescent cells with ageing was originally based on observations of senescent cells accumulation in aged tissues. However, the development of transgenic models that allow detection of senescent cells helped in the identification of the role these cells play in ageing and age-related diseases. Additionally, development and use of genetic and drug strategies in selective elimination of senescent cells has shown that these cells can play a role in age-related pathologies (Muñoz-Espín and Serrano, 2014; Van Deursen, 2014).

1.1.2 Stress Induced Premature Senescence (SIPS)

Senescence is a cellular process, similar to replication and differentiation, that can occur at any time in life. It can occur in normal cells by repeated division cycles (replicative senescence) or can be accelerated and induced in response to various acute stress. This sub-type of senescence is known as stress induced premature senescence (SIPS). Under physiological stress, SIPS is induced to prevent further cell proliferation (Ben-Porath and Weinberg, 2004). Therefore, SIPS is a term that refers to a rapid senescence phenotype development stimulated by extrinsic stress.

It is well known that any unfavourable environmental factors affecting living organisms are considered a stress. Moreover, if the limit of stress tolerance exceeds the limit of cell adaptive capacity, it may lead to permanent damage or death. The first response of stress involves the decline of cells' energy and increase of catabolic over anabolic processes. Then cells enter a phase resistance which includes activation of adaptive and repair processes. However, if the stress intensity is too high and exposure is for long-term, the damage becomes irreparable leading to chronic diseases, senescence or even death (Lichtenthaler, 1998; Toussain et al., 2000).

SIPS is activated in cells relatively rapidly. It occurs in a manner of days following exposure to stimuli. An increased level of internal damage and low metabolic activity and adaptive capacity lead to SIPS. Hence, this accelerated senescence program is induced by multiple factors such as exposure to ionizing radiation, genotoxic drugs and oncogenes. It was observed that human fibroblast cells lose their ability to proliferate upon exposure to 20 Gy ionizing radiation (Cmielova et al., 2012) and high dose of hydrogen peroxide (H_2O_2) (Zdanov et al., 2006). Senescence is accelerated and SIPS phenotype is induced within hours or days upon the exposure to the stress (Fridlyanskaya et al., 2015).

Cells undergoing SIPS share similar features as those undergoing replicative senescence. However, they differ in the time at which these features start developing. While replicative senescence is regulated by progressive shortening of telomere, SIPS is driven by acute stress exposure. SIPS is not programmed at a specific time and therefore not triggered by telomere erosion (Frias et al., 2012; Raghuram, and Mishra, 2014).

Cells undergoing SIPS show irreversible senescence-like growth arrest. SIPS is triggered by activation of DNA-damage responses (DDR). Hence, exposure to a high intensity of a stressor (such as ionizing radiation) leads to formation of double-strand breaks (DSB) which in turn leads to activation of DDR. Consequently, ATM-p53-p21-pRb pathway is activated. Subsequently, p21-mediated G1 growth arrest is induced (Suzuki et al., 2001; Chainiaux et al., 2002) (Figure 1.3).

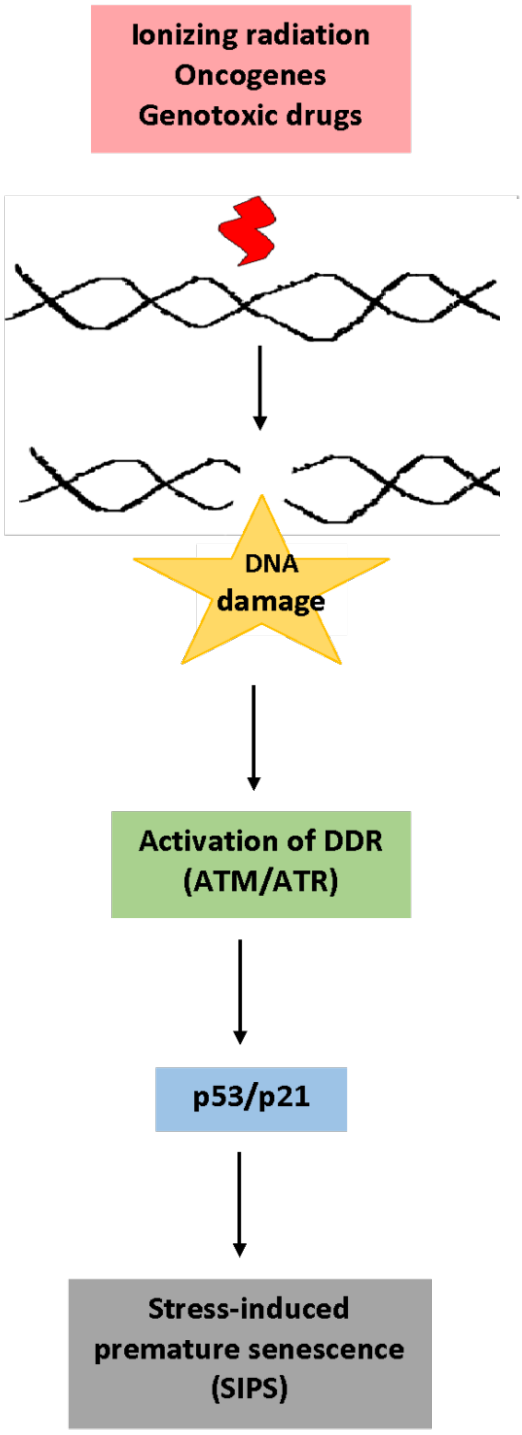

Figure 1.3 Schematic of stress-induced premature senescence (SIPS).
Exposure of proliferative cells to a high intensity of stressors such as ionizing radiation, oncogenes and genotoxic drugs leads to formation of double-strand breaks (DSB) which in turn leads to activation of DDR.

In most cells, DDR activates Ataxia telangiectasia mutated (ATM)/ Ataxia telangiectasia and Rad3-related (ATR), sensor kinases, that recognize and phosphorylate H2AX histone at sites of DNA breaks. The resulting γH2AX foci is needed for the recruitment of DDR players.

ATM/ATR phosphorylate p53 which stimulates transcription of p21, inhibitor of cyclin-dependent kinases. Furthermore, p16-pRB pathway is activated through involvement of p38/MAPK. p21 and p16 promote activation of RB which in turn binds to transcription factor E2F; a cell cycle progression regulator (Sherr and Roberts, 1999; Firsanov et al., 2011).

Drugs that induce senescence have shown significant effects against cancer development. Evidence has proven that senescence is a potent anticancer mechanism. Ionizing radiation and oncogenes have been observed to limit growth of unwanted cells. Therefore, SIPS could act as tumour suppressor mechanism (Herbig et al., 2004). However, accumulation of SIPS senescent cells may cause alteration in cell function and differentiation of neighbouring cells which may be responsible for the development of ageing and age-related diseases (Toussain et al., 2000).

1.1.3 Hallmarks of Senescence

Senescent cells share similar features including morphological changes and increased expression of certain proteins such as inhibitors of cyclin-dependent kinases p21 and p16. Moreover, it includes chromatin changes and secretion of different factors, a phenotype known as senescence-associated secretory phenotype (SASP) (Figure 1.4).

1.1.3.1 Growth Arrest

Cells respond to DNA damage induced by internal or external stress by preventing cell-cycle progression. Cell proliferation is only resumed when the DNA damage is repaired. The DNA damage generated by telomere shortening or exposure to stressors activates ATM/ATR pathway. Following that, the checkpoint kinase CHK2 is activated spreading the DDR signalling throughout the nucleus. DNA-damage triggers cell-division cycle 25 (CDC25) inactivation and p53 activation. Activation of p53 induces p21 which in turn induces rapid cell-

cycle arrest. Senescent cells show DNA content of G1 phase of cell cycle which indicates that G1/S transition is the site of cell-cycle arrest (Lukas et al., 2003; Bekker-Jensen et al., 2006; Mailand et al., 2000).

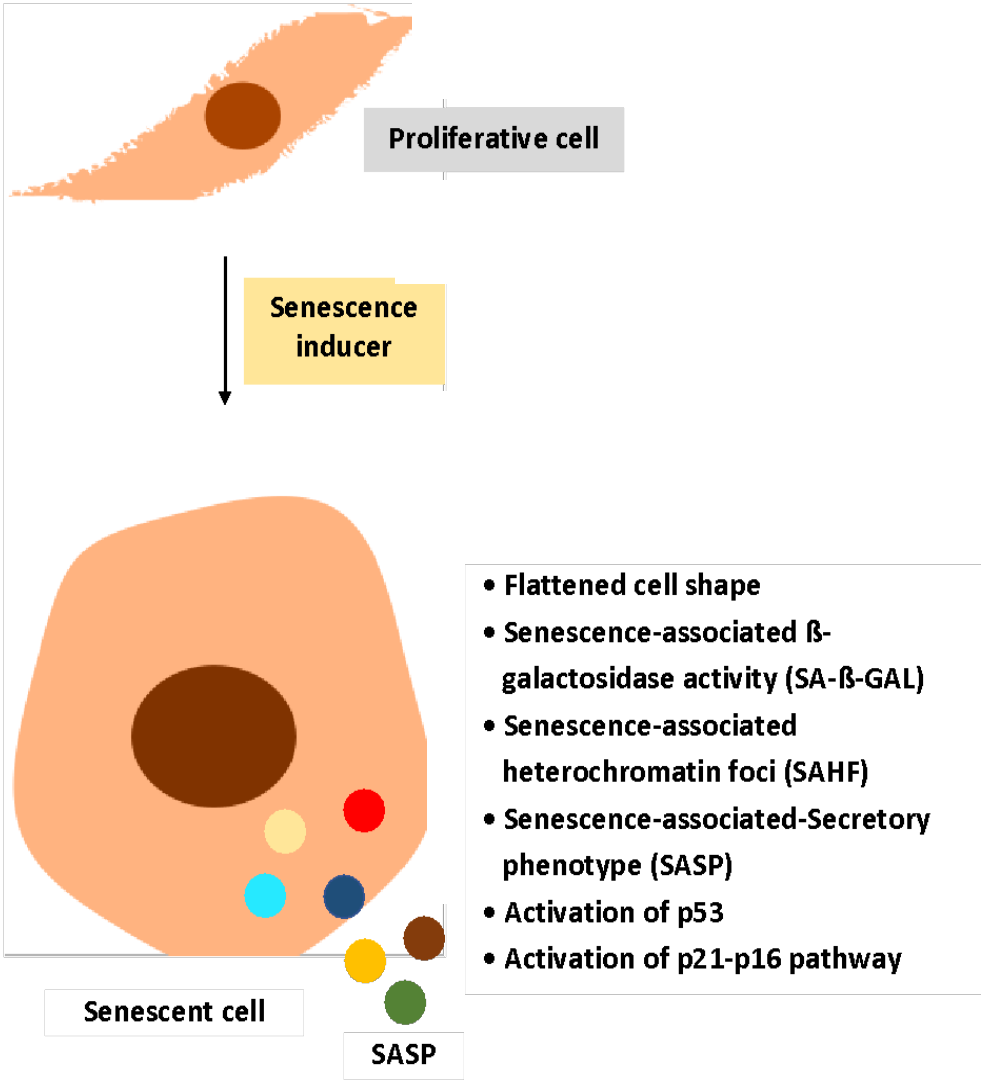

Figure 1.4 Senescence hallmarks.

Senescent cells are characterized by growth arrest and flattened cells shape. They also are characterized by increased SA-ß-Gal activity, SASP and formation of SAHF. Elevated levels of p53, p21 and p16 are required for the induction and maintenance of senescence phenotype.

1.1.3.2 Senescence-Associated ß-Galactosidase (SA-ß-Gal) Activity

Senescent cells are characterized by elevated senescence-associated ß-galactosidase (SA-ß-Gal) activity, permitting identification of senescent cells in mammalian tissues and in culture. In 1995, Dimri and his colleagues showed that senescent cells express ß-galactosidase activity at only pH 6.0. This activity is not similar to the enzymatic activity of the acidic ß-galactosidase that exists in all cells and is detectable at pH 4.0. SA-ß-Gal activity originates from the increase in the abundance of lysosomal enzymes. An increased expression of *GLB1*, a gene encoding the lysosomal enzyme, is responsible for the increased lysosomal enzyme and SA-ß-Gal activity (Lee et al., 2006). SA-ß-Gal activity is detected using chromogenic substrate 5-bromo-4-chloro-3-indoyl ß-D-galactopyranoside (X-gal). The hydrolysis process results in an insoluble blue compound (Dimri et al., 1995).

The increase in lysosomes and lysosomal enzyme activity have been associated with senescence. Therefore, SA-ß-Gal activity is strongly associated with senescent cells but not quiescent or fully differentiated cells. It can be used for determining abilities of drugs and genetic manipulation in inducing senescence. Moreover, SA-ß-Gal assay has been used extensively to examine senescence appearance after exposing cells to stressors. The limitation of this assay is that it is not completely specific. Hence, other senescence markers including SAHF and expression of p21 protein could be used alongside with SA-ß-Gal assay (Debacq-Chainiaux et al., 2005; Campisi, and Di Fagagna, 2007).

1.1.3.3 Senescence-Associated Heterochromatic Foci (SAHF)

Senescent cells undergo morphological and molecular changes including formation of senescence-associated heterochromatic foci (SAHF). SAHF are distinct structures that are formed in cells upon exposure to intrinsic (telomere dysfunction) or extrinsic (ionising

radiation) stresses. These stresses lead to a permanent cell-cycle arrest and ultimately senescence. Senescence is associated with global changes in nuclear structure. SAHF are heterochromatic structures that contain transcriptionally inactive regions packed together into highly dense chromatic fibres. SAHF sequester genes responsible for promoting proliferation. SAHF are detected by several molecular markers such as di- or tri-methylated lysine 9 histone H3 (H3K9Me2/3). (Narita et al., 2003; Aravinthan, 2015; Chandra, 2016).

1.1.3.4 Senescence-Associated Secretory Phenotype (SASP)

Senescent cells remain metabolically active and secrete several factors, a phenotype known as senescence-associated secretory phenotype (SASP). It is involved in inducing and maintaining senescence phenotype. Moreover, SASP includes cytokines, growth factors and extracellular proteins. It includes TNF-α, IL-6, IL-8, MMPs and IGF binding proteins. These proteins were observed to increase in tissues with chronological ageing. Furthermore, the expression of SASP components IL-6 and IGF binding protein-2 were observed to be elevated in p16-positive senescent cells isolated from older mice (Baker et al., 2011). Hence, it is suggested that SASP is the main driver of age-related inflammation. SASP cytokines such as IL-6 and IL-8 were observed to reinforce growth arrest and senescence (Kuilman et al., 2008; Tchkonia et al., 2013) (Figure 1.5).

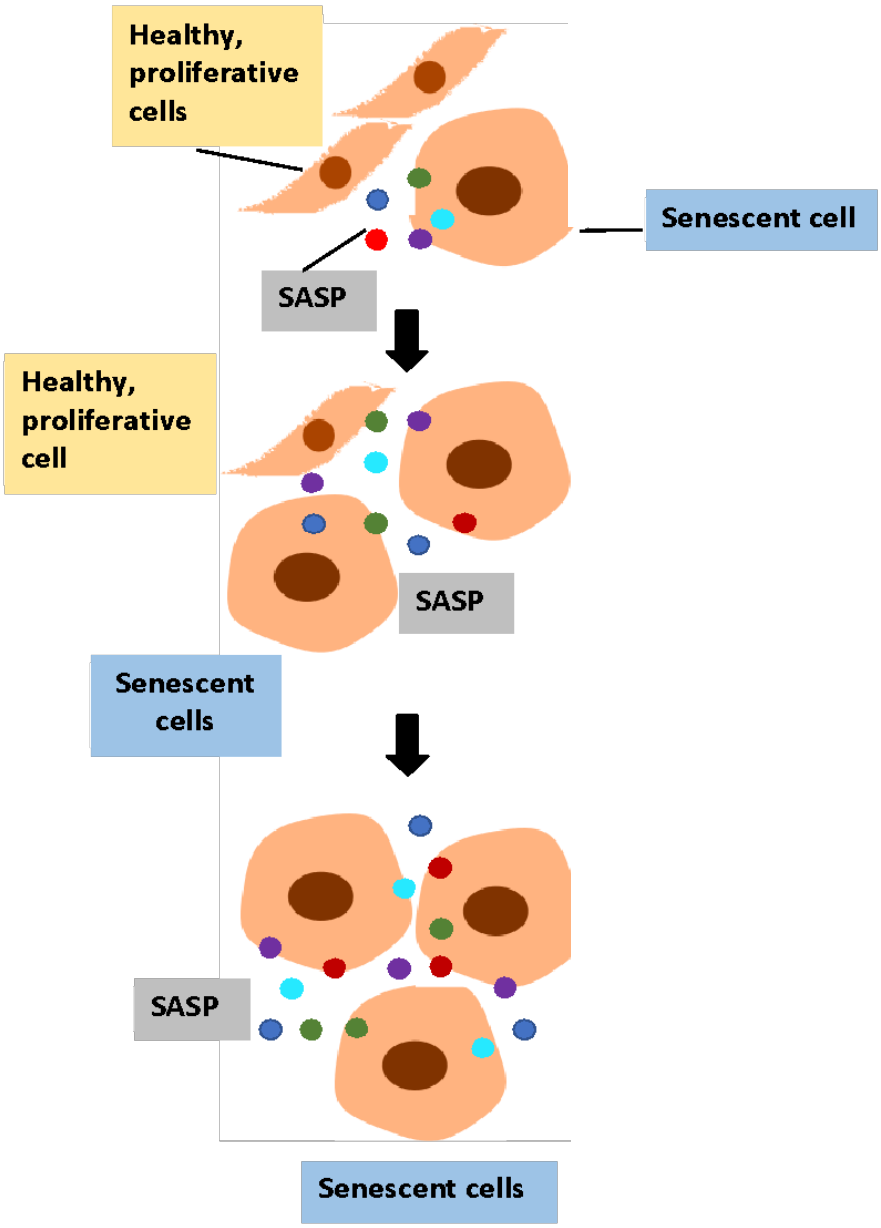

Figure 1.5 Schematic represents SASP phenotype in senescence.
Senescent cells secrete SASP which composed of cytokines that reinforce growth arrest in neighbouring proliferative cells and promote senescence.

1.1.3.5 Cyclin-Dependent Kinases

1.1.3.5.1 p53

Senescence phenotype is implemented by the activation of p53 pathway. Persistent DDR results in irreparable DNA damage which is associated with senescence. Hence, DDR involves phosphorylation of histone H2AX at Ser193 leading to deposition of γH2AX. Moreover, it involves an increased p53-binding protein 1 (53BP1) levels in the chromatin resulting in the activation of ataxia-telangiectasia mutated (ATM) and ataxia-telangiectasia and Rad3-related (ATR) followed by activation of CHK1 and CHK2. Eventually, it leads to activation of p53-p21 pathway (di Fagagna, 2008; Herranz and Gil, 2018) (Figure 1.6).

p53 is essential for a remarkable number of cellular processes such as senescence. It is a critical regulator of senescence phenotype. Inactivation of p53 was observed to be sufficient to increase the lifespan. Additionally, p53 inactivation is essential for reactivation of DNA synthesis (Shay et al., 1991; Itahana et al., 2001). Further studies showed that p53 plays a role in tumour suppression and apoptosis. Activation of p53 in mice was observed to promote cancer regression and eventually induced premature senescence in vivo (Xue et al., 2007; Ventura et al., 2007). The levels of p53 determine the programs that cells undergo such as senescence or apoptosis. It was observed that sublethal doses of hydrogen peroxide induced senescence while higher doses induced apoptosis. In the induced apoptosis program, the levels of p53 was 2-times higher than the p53 levels in senescence condition (Chen et al., 2000). Therefore, the threshold of intensity of stressor determines between senescence condition and apoptosis condition (Mijit et al., 2020).

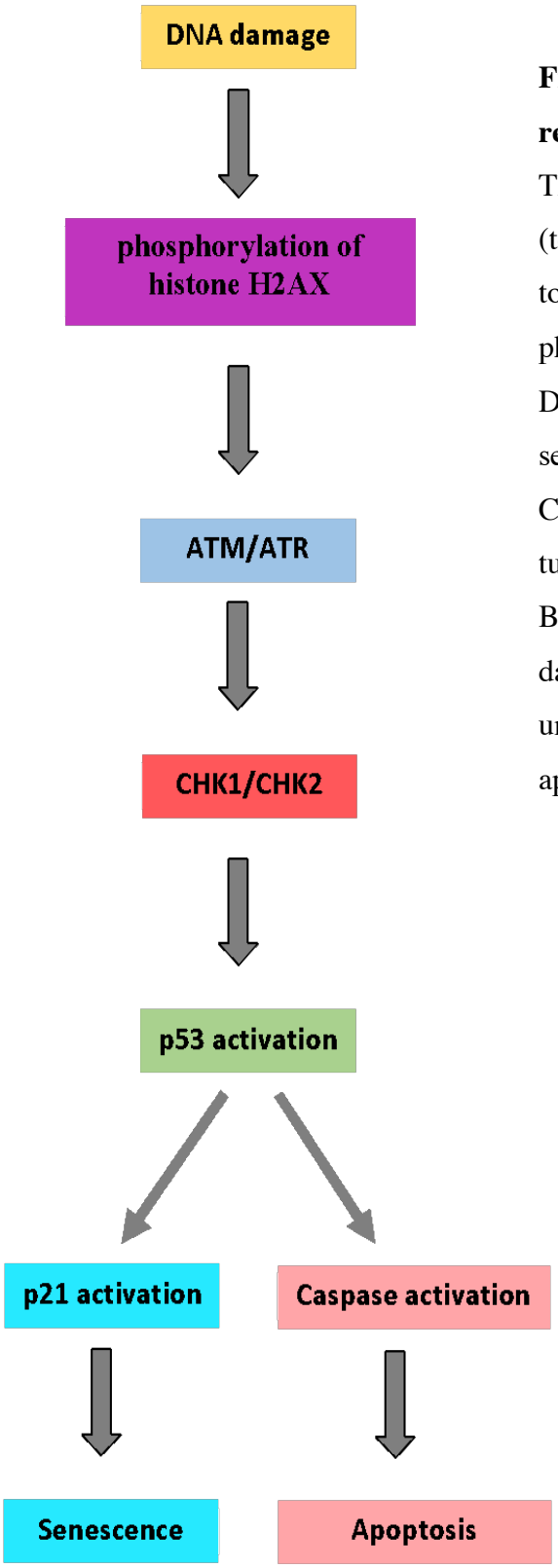

Figure 1.6 DNA damage response and p53 pathway. The induced DNA damage (telomere erosion or exposure to stressor) leads to phosphorylation of H2AX. Deposition of γH2AX is sensed by DDR and activates CHK1 and CHK2 which in turn leads to activation of p53. Based on the threshold of damage intensity, cells undergo senescence or apoptosis.

1.1.3.5.2 p21

Once p53 protein is stabilized, it proceeds to activate the downstream target; p21. P21 is known as cyclin-dependent kinase inhibitor 1 (CDKN1A) and encoded by *CDKN1A* gene. It binds to cyclin-dependent kinase (CDK) complex to inhibit CDK ability to form complex with cyclins, thus inhibiting CDK activation. CDK activation drives the transition of cell cycle from G1 to S phase (DNA synthesis). However, high levels of p21 protein stops cell division by preventing the cell cycle from entering S phase, arresting cell cycle at G1 phase. Consequently, senescence phenotype is induced (Xi et al., 2002; Georgakilas et al., 2017).

Elevated levels of p21 is a common feature of senescent cells. Upregulation of p21 is essential for inducing senescence, although its expression is not persistent (Sharpless and Sherr, 2015). Inactivation of p21 was observed to retain cells' ability to overcome cell cycle arrest in mammalian cells following a DNA damage (Chattopadhyay et al., 2001). P21 was suggested to play a role in regulating the viability of senescent cells following a DNA damage. Hence, in a p21-knockdown mouse, senescent cells were observed to be eliminated from fibrotic scars in the liver (Yosef et al., 2017). The activation of p21 and p53 in senescent cells is transient and lasts from hours to several weeks until growth arrest is established (Shtutman et al., 2017).

1.1.3.5.3 p16

Once p21 protein levels decline, p16 protein levels becomes upregulated, maintaining cell growth arrest (Shtutman et al., 2017). P16 is also known as CDKN2A and encoded by *CDKN2A* gene. P16 has been studied extensively as it plays a crucial role in senescence. It is one of the inhibitors of cyclin-dependent kinases that regulates cell growth by slowing cell cycle progression from G1 phase to S phase. Moreover, senescence is induced by activation of

p53-p21 pathway, however, the senescence phenotype is maintained by elevated expression of p16 (Rayess et al., 2012).

In senescent cells, p16 mediates senescence through retinoblastoma (Rb) pathway. P16 binds to CDK4/6 resulting in prevention of its kinase activity and therefore inhibiting phosphorylation of Rb. Consequently, Rb remains attached to transcription factor E2F1 preventing transcription of its target genes which is essential for G1/S transition. Inhibition of p16 through inactivation of Rb showed an increase in number of reprogrammed cells and de-differentiation in dividing cells (Li et al., 1994; Denchi et al., 2005; Li et al., 2009). P16 plays a critical role in in tumour suppression (Sen et al., 2017). In contrast, controlled expression of p16 is important for senescence suppression (Rayess et al., 2012).

1.1.3.6 Accumulation of Lipid Droplets

Cells contain diverse lipid molecules with distinct roles in cellular processes. In mammalian cells, the content of lipids is composed of fatty acids, phospholipids, sterols, glycerolipids and sphingolipids. Hence, lipids play a crucial role in cell survival and homeostasis such as structural, storage and signalling. Lipids are involved in the structure of the membrane, allowing compartmentalization of organelles. Moreover, lipid droplets are considered as storing sites of cholesterol esters and triacylglycerol which play a crucial role in lipid homeostasis in cells. Additionally, lipids can stimulate various cellular responses. They can bind to proteins, activating signalling pathways and thereby cellular processes. Binding of diacylglycerol to protein kinase C has been observed to affect adhesion, migration and proliferation of cells (Spitaler and Cantrell, 2004; Casares et al., 2019; Olzmann and Carvalho, 2019).

Lipids, including fatty acids, act as building blocks for cell membrane and signalling pathways mediators. Lipid droplets emerged as distinctive organelles that play a role in lipid homeostasis. They act as storage organelles of neutral lipids. Furthermore, they are dynamic organelles that are altered in structure and contents as they alternate between growth and consumption stages. Lipid droplets are synthesized and emerge from endoplasmic reticulum (ER). ER provides the constituent molecules needed for lipid droplet formation (Tauchi-Sato et al., 2002; Skinner et al., 2009).

Lipid droplet synthesis involves several steps including neutral lipids synthesis, formation of nascent lipid and lipid droplet budding and growth. Hence, lipid droplet structure is essentially composed of a core of neutral lipids enclosed by phospholipid monolayer. The first step in lipid droplet biogenesis involves triglycerol (TAG) and cholesterol ester synthesis which are the main components of neutral lipid. Then, lipid droplet biogenesis factors such as seipin facilitate the development of nascent lipid droplet. Lastly, lipid droplets emerge and bud from the ER. Lipid droplets grow and increase in size through fusion (Wang et al., 2016; Olzmann and Carvalho, 2019) (Figure 1.7). In senescence, several signalling pathways are altered leading to structural and molecular changes. Lipid regulation has been linked to cellular programs as they are required to control lipid synthesis and metabolism. Several studies have shown that lipids are required for fundamental cellular processes including cell division and apoptosis (Storck et al., 2018). Moreover, dysregulation of enzymes required for lipid metabolism has been linked to ageing and age-related diseases such as neurodegenerative diseases (Agmon, and Stockwell, 2017; Shaw et al., 2018).

Senescent cells are characterized by morphological changes including membrane remodelling. Lipids play a major role in the process of membrane remodelling. Transcriptomics and

lipidomics showed that lipid levels, lipid-regulating genes and lipid-related genes are highly regulated in senescent cells. Hence, it is suggested that lipid regulation plays a vital role in the process of senescence (Lizardo et al., 2017; Saitou et al., 2018; Millner et al., 2020).

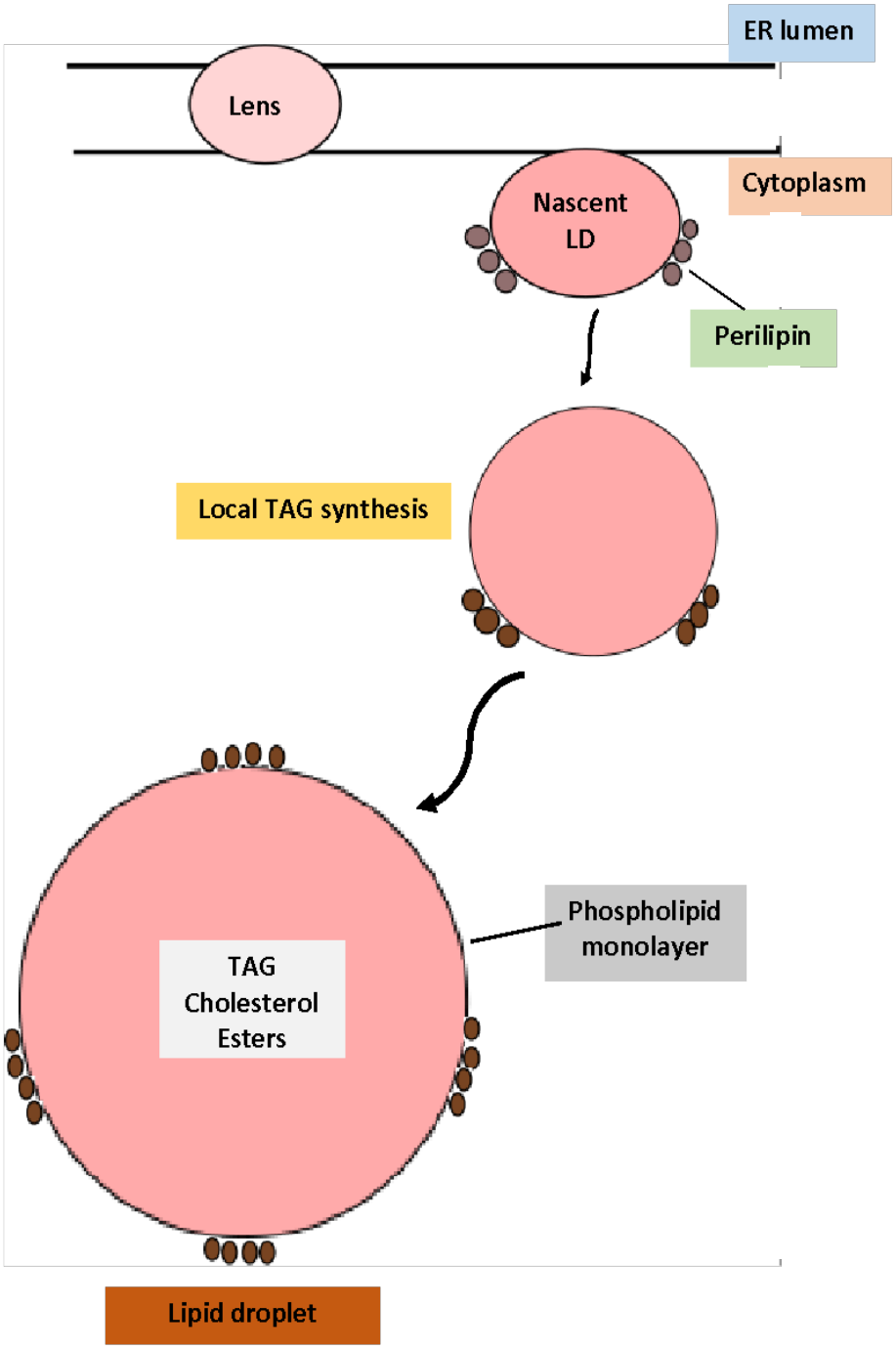

Figure 1.7 Lipid droplet synthesis.

Lipid droplet synthesis and emergence occur at ER. The synthesis process starts with formation of triglycerol (TAG) and cholesterol esters. Nascent lipids emerge first from ER which then increase in size to mature lipid droplet. Lipids droplets are enclosed by phospholipid monolayer. Perilipins are located on the surface of lipid droplets.

1.2 The Consequences of Senescence

Several studies have shown that senescent cells accumulate in tissues with age leading to ageing and age-related pathologies such as atherosclerosis. Age is known to be a risk factor for several diseases such as cardiovascular disease, osteoporosis, diabetes (type 2) and cancer (Matthews et al., 2006). Although the understanding of the process of ageing and development of age-related disease remains limited, it has helped in conceptualizing ageing and focus on age-related diseases (North and Sinclair, 2012).

1.2.1 Ageing

Ageing is a process that is characterised by a gradual decline in functions of body systems. It causes progressive deterioration in several organs that leads to tissue dysfunction. Subsequently, ageing increases the risk of diseases such as cardiovascular disease, osteoporosis and type 2 diabetes (Gunasekaran and Gannon, 2011; North and Sinclair, 2012; McHugh and Gil, 2018).

Senescence phenotype is the irreversible growth arrest that occurs in mitotic dividing cells. Hence, cells displaying altered phenotype could impair normal biological functions and is thought to contribute to ageing. Senescent cells could be detrimental to the tissue they reside in due to the secretion of extracellular matrix-degrading proteins and pro-inflammatory cytokines (SASP). Secretion of cytokines occurs in order to attract immune cells in order to remove senescent cells. However, in the ageing process, immune cell function and its ability to remove senescent cells are impaired. Elimination of senescent cells is effective in young organisms however, it gradually declines with age. Moreover, accumulation of senescent cells has been suggested to play a role in ageing process (Coppe et al., 2006; Burton, 2009).

Accumulation of senescent cells causes structural and functional alterations that result in ageing and age-related diseases. Senescent cells were observed to upregulate enzymes such as matrix metalloproteinases (MMPs) which are capable of degrading collagen and elastin. Secretion of MMPs by senescent cells was suggested to play a role in development of coronary heart disease (CAD) and progression of osteoporosis (Campisi, 2005; Nanni et al., 2007; Logar et al., 2007).

1.2.2 Cancer

Cellular senescence is a double-edged sword. It plays a role in suppressing cancer as it is controlled by multiple tumour suppressor genes such as *TP53* and *CDKN1A*. p53 and pRb pathways that control senescence phenotype, are commonly lost in cancer cells. The evidence from mice studies showed that inactivation of p53 protein led to failure of cells to respond to senescence signals. Senescence provides a major barrier that cells need to overcome in order to progress to malignancy. Thus, senescence is one of the cellular mechanisms that are involved in suppressing growth of cells at risk for tumorigenesis. As they alter the microenvironment of the tissue, they might stimulate tumorigenesis (Smith and Pereira-Smith, 1996; Campisi, 2000). Senescence stimuli such as telomere erosion and DNA damage lead to genomic instability, mutations and chromosomal aberrations. Hence, chromatin disruption such as silencing could disrupt normal cell differentiation which in turn might lead to unregulated growth of tumour cells. Furthermore, tumour cells are resistant to senescence signals and apoptosis. Therefore, senescence is considered as mechanism that irreversibly promotes cell growth arrest with a risk of inducing tumour (Campisi, 2001).

1.3 Cellular Response to Stress

Exposure of cells to stress leads to a range of responses varying from damage repair and cell survival to programmed cell death that eradicates damaged cells. The ability of cells in controlling the stress determines the fate of the cell. Depending on the type of stress and duration of exposure, cells mount protective or destructive response pathways.

1.3.1 Oxidative Stress

During stress, the homeostasis of a tissue is disrupted. Cells can cope with stress if it does not increase beyond a certain threshold. Hence, cells activate protective response pathways. However, a stress intensity above the threshold leads to activation of destructive (apoptosis) pathway. Of these stressors, oxidative stress and how cell respond to this stress have been studied extensively in the last few decades. In principle, introducing cells to oxidative stress causes accumulation of unfolded proteins. Consequently, it leads to activation of heat shock factor 1 (HSF1) which in turn promotes cells survival and inhibits apoptosis (Pirkkala et al., 2001; Fulda et al., 2010).

Exposure of cells to oxidative stress using sodium arsenite (NaAsO2) causes imbalance redox status and induces dysregulation of cellular metabolism. It has been observed to be associated with inhibition of cell proliferation and differentiation of certain types of cells (Dreval et al., 2018). Low doses of sodium arsenite induces stress response in various cell types. It showed an effect on mRNA and protein expression in cells such as keratinocytes (Sun et al., 2006). Additionally, oxidative stress activates the stress response signalling pathway which inhibits proliferation by promoting phosphorylation of eukaryotic initiator factor 2α (eIF2α) (Palangi et al., 2017).

Studies have shown that cells are exposed to oxidative stress endogenously. The endogenous oxidative stress is caused by the free radicals that are derived from mitochondria. The continuous generation of free radicals increases as an organism age leading to damage of macromolecules. Hence, calories restriction and a healthy diet have shown a decrease in free radicals and thus mitochondrial oxidative stress (Barja, 2002).

1.3.2 Stress Granules

Stressed cells undergo multiple changes that start with inhibition of mRNA translation through the disassembly of polysome-mRNAs complex. Subsequently, protein synthesis is prevented in order to save the cell's energy and maintain its homeostasis. Hence, granular bodies termed as stress granules are formed where the untranslated mRNAs are sequestered (Kedersha and Anderson, 2007).

Stress granules are non-membranous aggregations of mRNA and proteins (mRNPs) that are formed when the translation is reduced or inhibited. Inhibition of translation occurs when the cells are under stress and stress responses are activated. Stress granules are suggested to affect mRNA functions and localization. Moreover, they are thought to affect several cells signalling pathways. Thus, stress granules are dynamic structures as their formation process is reversible. The process of stress granule assembly and disassembly depends on the presence or absence of the stress (Anderson and Kedersha, 2009; Wheeler et al., 2016).

1.3.3 Formation of Stress Granules

Stress granules are membraneless structures. They undergo fusion forming larger and mature assemblies. The structure of stress granules is composed of an inner core and a surrounding shell. The core is highly concentrated with proteins and mRNAs compared to the shell, making

the shell more dynamic than the core. Moreover, stress granules flow in the cytosol and continually exchange components with the cytoplasm. Stress granule assembly lasts for minutes to hours fusing with each other forming larger granules (Kedersha et al., 2005; Protter and Parker, 2016; Wheeler et al., 2016).

Stress granules are involved in several stress-induced signalling cascades. Hence, under stress conditions, stress granules are formed which selectively downregulate proteins involved in translation and cell proliferation and upregulate proteins involved in stress-induced response. Once the stress is removed, stress granules disassemble and the sequestered mRNAs are released to resume translation and normal cell processes (Anderson and Kedersha, 2009; Chen and Liu, 2017).

Under stress exposure, stress-sensing kinases such as heme-regulated eIF2α kinase (HRI), protein kinase R (PKR), PKR-like ER kinase (PERK) or general control nonderepressible 2 (GCN2) are activated and lead to phosphorylation of eIF2α at serine 51. Phosphorylation of eIF2α inhibits translation and protein synthesis by reducing levels of the ternary complex eIF2-GTP-$tRNA_i^{Met}$ which is essential in the translation initiation process. Inhibition of translation leads to run off of translating mRNA preventing polysome elongation and thus resulting in polysome disassembly. Free 48S-mRNA-polysomes are crucial for the assembly of stress granules. Primary aggregation of stress granules is mediated by proteins that mediates mRNP assembly and nucleates stress granule formation. Secondary aggregation is promoted by protein-protein interactions forming larger and fewer assemblies (Anderson and Kedersha, 2007; 2009) (Figure 1.8).

Additionally, stress granules are formed when cell is undergoing Endoplasmic Reticulum (ER) stress, which is the imbalance between protein folding capacity and the demand that is placed on ER. To restore homeostasis of ER, stress responses are activated, including PERK, which induces the phosphorylation of eIF2α, thereby limiting protein synthesis (Cnop et al., 2017).

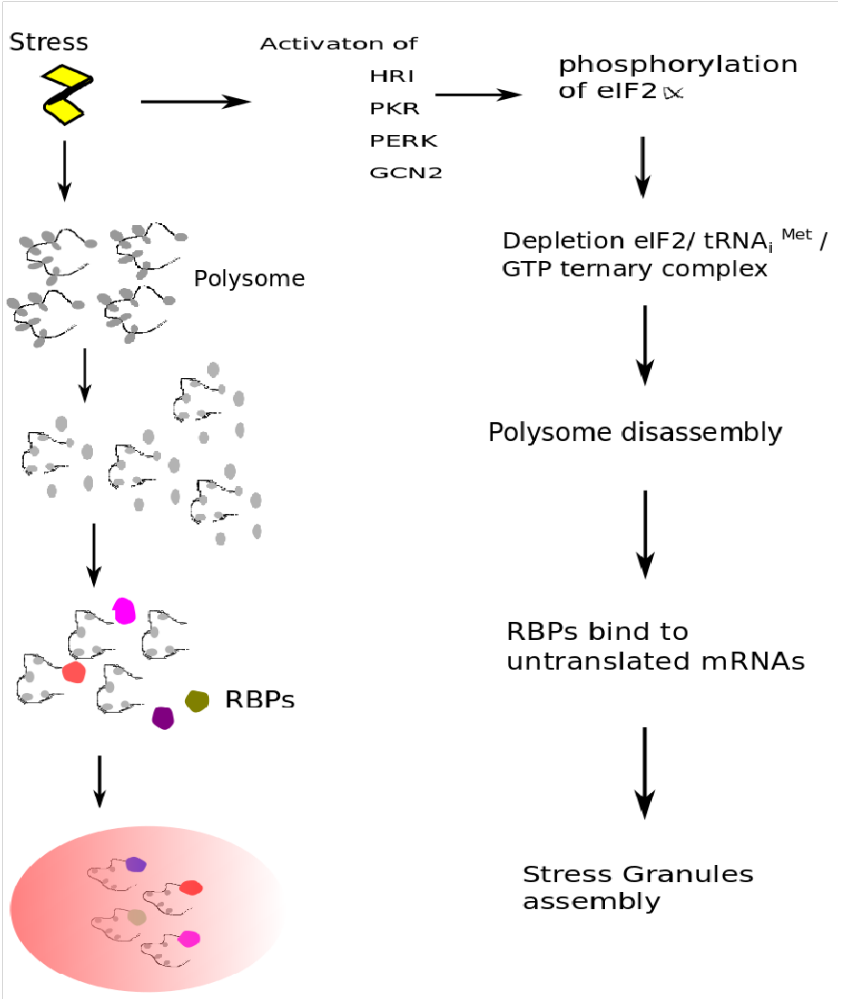

Figure 1.8 Stress granule formation.

Stress granules are structures that are formed in response to stress such as oxidative stress. Activation of stress-sensing kinases sense results in phosphorylation of eIF2α inhibiting translation and protein synthesis by reducing levels of the ternary complex eIF2-GTP-tRNAi^{Met}. Release of untranslated mRNAs promotes mRNA-RBP binding thereby stress granule formation.

1.3.3.1 RNA Component

The two main components of stress granules are RNAs and RNA-binding proteins. Stress granules contain a diverse group of mRNAs. Cytoplasmic poly(A) RNA and poly(A)-binding protein-1 are recruited to stress granules. Moreover, mRNAs encoding B-actin, insulin-like growth factor II (IGF-II) and glyceraldehyde-3-phosphate dehydrogenase (GAPDH) are detected in stress granules (Anderson and Kedersha, 2002; Stöhr et al., 2006). Furthermore, Stalled initiation complexes which are still bound to mRNAs were observed to be recruited to stress granules. Moreover, RNA-RNA interaction was suggested to help in the process of stress granule assembly. High availability of RNAs could nucleate interaction between several mRNAs thereby contribute to stress granule assembly (Van Treeck et al., 2018).

1.3.3.2 Protein Component

A second component of stress granules is RNA-binding proteins which bind to the free untranslated mRNAs. A class of RNA-binding proteins are linked to mRNA stability and translational inhibition. T cell internal antigen-1 (TIA1), TIA-1-related (TIAR) and fragile X mental retardation-related protein1 (FXR1) are involved in translational silencing (Kedersha et al., 1999; Mazroui et al., 2002). The second class of stress granules-associated RNA-binding proteins regulates RNA editing, localization and splicing. Moreover, these proteins are known to nucleate stress granule assembly. Ras-GTPase-activating protein SH3-domain-binding protein (G3BP), Caprin and survival of motor neurons (SMN) are involved in RNA metabolism and nucleates stress granule formation when overexpressed (Tourrière et al., 2003; Hua and Zhou, 2004; Solomon et al., 2007).

1.3.4 Detection of Stress Granules

RNA-binding proteins provide reliable markers for stress granule detection. G3BP is the commonly used stress granule marker as it is suggested to nucleate stress granule assembly. Moreover, TIA1 has been detected in stress granules induced by heat shock and oxidative stress. Overexpression of these RNA-binding proteins promotes stress granule formation. FXR1 is another marker of stress granules. It has been observed to be recruited to stress granules induced by stressors such as oxidative stress (Anderson and Kedersha, 2002; Protter and Parker, 2016).

Eukaryotic translation initiation factors are proteins that bind to the small ribosomal subunit during translation initiation. Hence, they are involved in the process of protein biosynthesis. Stress response in mammalian cells prevents translation initiation and involves stress granule formation. Translation initiation factors, untranslated mRNAs and proteins regulating mRNA functions are sequestered in the stress granules. Therefore, translation initiation factors such as eIF3 and eIF4G were observed to be recruited to stress granules thereby used as stress granule markers (Mazroui et al., 2002).

1.4 Conclusion

Cellular senescence is a phenotype of cell growth arrest. It occurs in response to internal or external stimuli that cause DNA damage. Consequently, DNA-damage repair signalling pathways are activated. However, if the damage is irreparable, cells are either directed to cell-cycle arrest (senescence) or apoptosis. Senescence prevents growth of cells with mutations or functional defects.

Cellular senescence is a phenotype that causes several molecular and structural changes. Senescent cells are characterized with flattened shape and enlarged size. Moreover, senescent cells show elevated ß-galactosidase activity which is detected at pH 6.0. Increased lysosomal enzyme activity has been detected to be associated with senescence. Additionally, senescence is associated with global changes in nuclear structure and formation of senescence-associated heterochromatin foci (SAHF). The elevated senescence-associated secretory phenotype (SASP) in senescent cells is involved in inducing and maintaining senescence phenotype. Increased expression of cyclin-dependent kinases including p53, p21 and p16 is crucial for initiation and maintenance of senescence phenotype. Senescence phenotype occurs following a finite number of cell divisions, this type of senescence is termed as replicative senescence. It occurs due to the telomere shortening which occurs after multiple cell divisions. Furthermore, senescence is induced when cells are exposed to a stress that causes irreparable DNA damage such as ionizing radiation and genotoxic drugs, termed as stress-induced premature senescence (SIPS). Senescence program provides a useful system to study alterations associated with senescence and investigate the role of senescence in ageing and age-related pathologies. Cells' response to stress such as heat shock and oxidative stress involves formation of stress granules. Stress granules play a role in maintaining the cell's energy when the cell is under stress by inhibiting translation and protein synthesis. G3BP is RNA-binding protein that nucleates the process of stress granule formation. The role of stress granules in senescence and disease development have been studied extensively.

Senescence involves changes in intracellular process and cell environment. Stress granules are proposed to play a role in senescence phenotype. The process of stress granule formation involves regulation of post-transcriptional modification. Hence, there is a need for developing

more models of human cells that incorporate both stress response and senescence phenotype and investigate the changes in senescence phenotype.

1.5 Project Aims and Objectives

1.5.1 Project Aims

The project aims to develop senescence programs in HDF and U2OS cells by multiple means (replicative or SIPS) and compare senescence-associated changes.

We will study primary human diploid fibroblast (HDF) cells through multiple passages (replicative senescence) and ionizing radiation-induced damage (SIPS). Population doublings of HDF will be monitored after each passage. Senescence phenotype will be examined using senescence markers.

Proliferative and senescent HDF cells will be subjected to oxidative stress to examine stress granule formation. We hypothesise that targeting the stress granule nucleating protein; G3BP, will provide a model to understand the role of stress granules in senescence phenotype progression. Due to the reliability and availability of U2OS cells with G3BP gene modifications, U2OS cells will be used to set up and optimize the senescence and stress granule studies including examining senescence progression, lipid accumulation and molecular alterations associated with senescence and G3BP variants. This study will provide a platform for many future stress granules and senescence studies.

1.5.2 Project Objectives

- Develop and characterise senescent HDF cells including characterisation of stress granules.
- Develop and characterize senescence in WT and G3BP modified U2OS cells.
- Investigate whether stress granules play a role in senescence phenotype progression.

Chapter 2

2 Materials and Methods

This chapter lists all materials used for experimental work. Solutions were prepared in type I laboratory H_2O generated by NANOpure Diamond UV/UF TOC water purification system. If needed, water was sterilized by autoclaving (121 °C, 30 min).

2.1 Materials

2.1.1 Cell Lines

Table 2.1: List of cell lines

Name	Description	Reference
HDF	Human Dermal Fibroblasts	Cells were kindly provided by a colleague at Durham University.
U2OS WT	Human osteosarcoma cell line	Kedersha et al., 2016
GFP-G3BP1	U2OS expressing GFP-G3BP1	Kedersha et al., 2005
ΔΔG3BP1/2	U2OS cells lacking G3BP1 and G3BP2 (ΔΔG3BP1/2 cells) expressing GFP	Kedersha et al., 2016
ΔΔG3BP1/2-GFP-G3BP1	ΔΔG3BP1/2 cells expressing GFP-G3BP1	Kedersha et al., 2016
ΔΔG3BP1/2-GFP-G3BP2a	ΔΔG3BP1/2 cells expressing GFP-G3BP2a	Kedersha et al., 2016
ΔΔG3BP1/2-GFP-G3BP2b	ΔΔG3BP1/2 cells expressing GFP-G3BP2b	Kedersha et al., 2016

2.1.2 Antibodies

Table 2.2: List of antibodies

Name	Primary / Secondary	Host	Supplier	Dilution	Use	Product Number
G3BP1	Primary	mouse	Santa Cruz	1:500	IF	SC-365338
G3PB1	Primary	rabbit	Proteintech	1:250	IF	13057-2-AP
CAPRIN	Primary	rabbit	Proteintech	1:200	IF	15112-1-AP
TIA-1	Primary	rabbit	Proteintech	1:250	IF	12133-2-AP
TDP-43	Primary	rabbit	Proteintech	1:250	IF	10782-2-AP
HUR	Primary	rabbit	Proteintech	1:250	IF	11910-1-AP
FXR1	Primary	rabbit	Bethyl	1:500	IF	A303-892A
EIF4G	Primary	rabbit	Bethyl	1:500	IF	A300-502A
SAHF	Primary	rabbit	Abcam	1:200	IF	AB8898
CDKN1A	Primary	rabbit	Proteintech	1:1000	WB	10355-1-AP
GAPDH	Primary	mouse	Sigma	1:2000	WB	G8795
Cy3	Secondary	rabbit	Jackson ImmunoResearch	1:500	IF	711-165-152
AF488	Secondary	mouse	Jackson ImmunoResearch	1:500	IF	115-545-205
Anti-rabbit IgG HRP-linked	Secondary	rabbit	Proteintech	1:2000	WB	SA00001-1

2.1.3 Cell Culture Reagents

Table 2.3: List of cell culture reagents

Name	Supplier	Product number
Dulbecco's modified Eagle's medium	Sigma	D5671
Fetal bovine serum	Sigma	F7524
200 mM L-Glutamine	Sigma	P4707
Penicillin (10000 U/ml)/ Streptomycin (10 mg/ml)	Sigma	P4333
Trypan blue solution 0.4 (w/v) in 0.81% sodium chloride and 0.06% potassium phosphate	Sigma	T8154
Trypsin-EDTA	Sigma	T3924
Phosphate-buffered saline (PBS)	Sigma	D8537
Dimethylsulphoxide (DMSO)	Sigma	D2650
Recovery cell culture freezing medium	Gibco	12648-010

2.1.4 Reagents

Table 2.4: List of reagents

Name	Supplier	Product number
Albumin bovine fraction V	Melford	A30075

B-Mercaptoethanol	Sigma	M3148
Glycerol	Sigma	G5516
Glycine	Sigma	G8790
Methanol	Sigma	322415
Magnesium chloride	Sigma	M8266
Propan-2-ol	Sigma	278475
Sodium chloride	Sigma	S7653
Sodium deoxycholate	Sigma	D6750
Sodium dodecyl sulphate (SDS)	Sigma	71725
Tris(hydroxymethyl) methylamine	Sigma	252859
Triton X-100	Sigma	X100
Tween-20	Sigma	85114
paraformaldehyde	Sigma	158127
Sodium Arsenite ($NaAsO_2$)	Fluka	7784-46-5
Vectashield mounting medium	Vector labs	H-1900
Doxorubicin	Sigma	D1515

2.1.5 Cell Culture Consumables

All cell culture consumables were supplied by Sarstedt unless it is specified.

2.1.6 Lipid Staining Reagents

Table 2.5: List of lipid staining reagents

Name	Supplier	Product number
Oil Red O	Sigma	O0625
Oleate	Sigma	O7501

2.1.7 Solutions for Protein Work

Table 2.6: List of solutions used for protein work

Solution	Protocol
RIPA buffer	0.3 ml 5 M NaCl, 0.5 ml 1 M Tris-HCl pH 8.0, 0.1 ml Triton X-100, 0.1 ml 10% sodium dodecyl sulphate (SDS), 0.5 ml 10% deoxycholate were added. Deionized H2O was added to 10 ml. Store at 4 C. Complete protease inhibitor was added. Once the protease inhibitor has been added, it was stored at -20 C.
Electrotransfer buffer	1.59 g Na2CO3 and 4.40 g NaHCO3 were dissolved in 5 L deionised water
Semi-dry transfer buffer, 10x	60.6 g Tris-base and 73.19 g Glycine were dissolved in 300 ml deionized H2O.

	Deionized H2O was added to 500 ml
Semi-dry transfer buffer, 1x	50 ml 10x semi-dry transfer buffer and 25 ml Methanol were added to 425 ml deionized H2O
TBST	80 g NaCl, 24.2 g Tris-base, and 1 ml Tween 20 were dissolved in 900 ml of deionized H2O. pH was adjusted to 7.6. Deionized H2O was added to 1 L.
SDS-PAGE sample buffer, 6x	3.78 g glycerol, 1.00 g SDS, 3.50 ml 1 M Tris-HCl, 500 ul 10 g/l bromophenol blue and 200 ul B-mercaptoethanol were dissolved in 10 ml deionized H2O
SDS-PAGE running buffer, 10x	30.03 g Tris, 10.00 g SDS and 144.13 g glycine were added to 800 ml deionized H2O. It was stirred until completely dissolved. Deionized H2O was added to 1 L.
5% milk powder + TBST	5 g milk powder was dissolved in 80 ml TBST. Stirred until it completely dissolved. TBST was added to 100 ml.
Stripping solution	350 ul B-mercaptoethanol and 1 g SDS was dissolved in 50 ml deionized H2O.

2.1.8 Senescence Associated ß-Galactosidase Reagents

Table 2.7: List of senescence associated ß-galactosidase reagents

Solution	**Supplier**	**Product number**
Citric acid	Sigma	C0759

Sodium phosphate	Sigma	S9763
Potassium ferrocyanide	Sigma	P3289
Potassium ferricyanide	Sigma	244023
5-bromo-4-chloro-3-indolyl-βD-galactopyranoside	Sigma	B4252

2.2 Methodology

2.2.1 Mammalian Cell Culture

2.2.1.1 Culture Conditions

Cells were cultured at 37°C under the following conditions: 95% (v/v) air, 5.0% (v/v) CO_2 and 95% humidity. All cell culture incubations were performed under these conditions unless otherwise specified. Cells were maintained by leaving them to grow to >90% confluency and splitting them afterwards. All cell culture work was performed in a sterile tissue culture flow hood. All equipment used for cell culture were sterilised with 70% (v/v) Ethanol. Tissue culture grade plastics were used to grow primary fibroblast cells and U2OS cells.

2.2.1.1.1 Primary Cells

Primary fibroblasts HDF cells were cultured in Dulbecco's Modified Eagle's Medium with 10% foetal bovine serum, 2 mM L-glutamine, 100 U/ml penicillin and 100 ug/ml streptomycin.

2.2.1.1.2 Osteosarcoma U2OS Cells

U2OS cells were cultured in Dulbecco's Modified Eagle's Medium supplemented with 10% foetal bovine serum, 2 mM L-glutamine, 100 U/ml penicillin and 100 ug/ml streptomycin (Kedersha et. al., 2016).

2.2.1.2 Reviving Cells

The cryovial was removed from the -80°C freezer and gently placed in a 37°C water bath and once the vial content defrosted, the vial was sterilised by spraying it with 70% (v/v) Ethanol and the cells were transferred from the vial to the prewarmed medium in a 25 cm^2 culture flask using a 5-ml serological pipette. The flask was then placed in a 37°C cell culture incubator (Gibco Opti-MEM, ThermoFisher Cat No. 31985062). Cells were left for approximately 5 hours to enhance cell adherence to the culture flask's floor. Flasks were examined under the microscope for cell adherence. Once the majority of the cells had settled on the floor of the flask, medium was replaced with a new fresh warm growth medium and placed back to the 37°C cell culture incubator.

2.2.1.3 Subculturing Cells

Cells were left to grow to a high confluency before splitting. Cells were fed every 2-3 days until the culture is confluent. Medium was aspirated from the flask using 10 ml serological pipette. Enough pre-warmed PBS was added to the cells (~0.1 ml/cm^2) to cover the surface of the culture flask. 10 ml and 2.5 ml PBS was added to 75 and 25 cm^2 flasks, respectively. The flask was gently rocked to remove the residual FBS that might inhibit the activity of trypsin. Cell washing was repeated twice, one minute each. Trypsin was then added to the culture flask to cover the adhering cell monolayer. The culture flask was placed in a humidified 37°C cell culture incubator for 2-5 min depending on cell confluency and cell line. During the incubation

period, the cells were regularly checked if a short or longer incubation period is needed. Once the cells had detached, warm fresh medium was added and pipetted many times to ensure detachment of the majority of the cells. Cells were re-suspended in a fresh medium and transferred to a new culture flask depending on the splitting ratio required. In case of HDF cells, a 5:10 ratio of cells: fresh medium was required whereas 1:10 was used for U2OS cells. Cell counting was performed using a cell haemocytometer.

2.2.1.4 Freezing Cells

Cells were cultured until they reached 70-80% confluency. Cells were trypsinized. Fresh medium was added to the cells. Then cells were transferred to a 15-ml falcon tube and centrifuged for 5 min at 1000 rcf/4°C. The supernatant was discarded. Freezing mix was added to the pellet. Freezing mix contained 50% (v/v) FBS, 40% (v/v) DMED, and 10% (v/v) DMSO. The volume of freezing mix used to suspend the pellet was dependent on cell confluency. In case of 70-80% cells confluency cultured on 75 cm^2 flask, 3 ml freezing mix was used to resuspend the cells. 1 ml of freezing mix was added to each new cryovial. Cryovials were then placed in a Mr Frosty (Thermo Fisher Scientific) which slows freezing in -80°C freezer at a rate of 1°C/min to reduce ice crystal formation and cell damage. The container was then placed in the -80°C freezer. Backup cryovials were stored in -140°C freezer for long term storage.

2.2.1.5 Cell Counting

Cells were cultured in the culture flask to reach confluency. After trypsinizing the cells, fresh medium was added. The fresh medium was pipetted several times to disperse any cell clumps and obtain a uniform suspension. Haemocytometer slide and coverslip was cleaned with 70% ethanol. A drop of cell suspension was transferred to the edge of the haemocytometer counting champers and then covered by the coverslip. Cells were allowed to settle for a few minutes

before counting. The Haemocytometer slide was observed under the microscope with 10X magnification. Cells in the four chambers were counted using a hand-held counter. The following calculations were used to determine the number of cells/ml:

Cells/ml = average count/square*dilution factor*10^4

Total number of cells = cells/ml*total volume of original cell suspension

2.2.2 Induction of Senescence

Senescence was induced in primary fibroblast and U2OS cells using ionizing radiation and doxorubicin; a DNA damaging agent.

2.2.2.1 Ionizing Radiation-Induced Senescence

Cells were cultured in a 75 cm^2 culture flask to reach ~70% confluency. Then cells were trypsinized and diluted to the desired dilution by adding fresh medium. Coverslips were sterilised by autoclave (121 °C, 30 min). They were left to dry in a 37 °C incubator for ~48 hrs. Coverslips were placed in each well of the 12-well plate. 1 ml of cell suspension (contains ~0.1 x 10^6 cells/cm^2) was added to each well. 24 hrs after seeding, cells were exposed to X-Ray ionizing radiation. 10 Gy (320 kV, 9 mA, 4 min) was used to induce senescence in primary fibroblast cells. 4 Gy (320 kV, 8 mA, 110 seconds) was used to induce senescence in U2OS cells. After irradiation, pre-warmed growth medium was added to cells before they were transferred to the 37 °C tissue culture incubator. Media was changed every 2-3 days. Cells were harvested 9 days after irradiation exposure.

2.2.2.2 DNA Damage-Induced Senescence

Cells were cultured in a 75 cm^2 culture flask before they were trypsinized. Sterilised coverslips were added to each well of 12-well plate. 1 ml of cells was added to each well. 12-well plate was transferred to 37 °C tissue culture incubator for 24 hrs before they were treated with Doxorubicin. Cells were treated with 200 nM Doxorubicin for 48 hrs in 37 °C tissue culture incubator. Then Doxorubicin was removed. Pre-warmed PBS was added to the cells for 1 min with gentle rocking. 1ml fresh growth medium was added per well and the 12-well plate was placed in 37 °C tissue culture incubator. Medium was changed every 2-3 days. Cells were harvested 7 days after first medium change.

2.2.3 Senescence Associated *B*-Galactosidase Detection

Cells were cultured in 75 cm^2 culture flask to 70% confluency. 24-well plate was prepared and sterilised coverslips were added to wells. Cells were trypsinized and diluted before they were transferred to 24-well plate adding 1ml (contains ~0.05 x 10^6 cells/cm^2) to each well. After 24 hrs, cells were exposed to senescence inducing treatment and kept in 37 °C tissue culture incubator for 7-9 days depending on the senescence induction method. Medium was then removed and PBS was added twice for 1 min with rocking. Cells were fixed with 4% paraformaldehyde for 15 min at room temperature. Fresh SA B-Gal staining solution was made consisting of 150 mM NaCl, 200 mM MgCl2, 40 mM citric acid, 12 mM sodium phosphate, adjusted to pH 6.4, 1 ml Potassium Solution (5 mM potassium ferrocyanide and 5 mM potassium ferricyanide) and 0.2ml 5-bromo-4-chloro-3-indolyl-βD-galactopyranoside (X-gal) 20 mg/ml stock solution). Fixed cells were incubated with senescence associated B-Galactosidase staining solution overnight at 37 °C. The fixed cells were checked for blue staining before removing the staining solution. SA-B-Gal staining solution was removed and

PBS was added to fixed cells twice before they were mounted in Vectashield mounting medium. Cells were imaged using a bright field Evos XL Core Cell Imaging microscope.

2.2.4 Induction of Oxidative Stress

Oxidative stress was induced in primary fibroblast cells and U2OS cells through incubating them with sodium arsenite ($NaAsO_2$). Cells were seeded in 12-well plate for 24 hrs before sodium arsenite treatment. 0.5 mM – 1.0 mM sodium arenite was added to fresh medium and mixed thoroughly. Old media was removed from the cells and replaced with sodium arsenite medium. Fibroblast cells were incubated with 1.0 mM sodium arsenite for 45 min in 37 °C tissue culture incubator. U2OS cells were incubated with 0.5 mM sodium arsenite for 30 min in 37 °C tissue culture incubator. Sodium arsenite was removed and PBS was added to cells twice 3 min each. Cells were fixed in 4% paraformaldehyde for 15 min at room temperature. Fixed cells were stained and imaged for oxidative stress markers.

2.2.5 Cell Treatment with Puromycin and Cycloheximide

Cells that were grown on coverslips in a 12-well plate were treated with Puromycin or Cycloheximide. 20 ug/ml Cycloheximide was used to prevent polysome dissociation and inhibit stress granule assembly. 5 ug/ml puromycin was used to promote polysome dissociation and stress granule assembly. Following cycloheximide or puromycin treatment cells were exposed to oxidative stress as described in 2.2.4.

2.2.6 Immunofluorescence

Cells were cultured on sterilised coverslips in 12-well plate until they reach 70-80% confluency. After cells were exposed to the required treatment, cells were washed twice with PBS. Cells were then fixed in 4% paraformaldehyde for 15 min at room temperature and

washed twice in PBS. Cells were permeabilized in 0.5% Triton X-100 for 20 min at room temperature. Coverslips were washed twice with 0.01% Tween-20 PBS. Coverslips were then blocked by incubating them in 3% BSA dissolved in PBS for 30 min. Primary antibodies were diluted in 3% BSA added to PBS (see table 2.) and coverslips were incubated in primary antibodies 1-2 hrs depending on the recommended incubation time of each antibody. Coverslips were washed with 0.01% Tween-20 PBS for 15 min before incubation in secondary antibodies. 15 min of 0.01% Tween-20 PBS washing was performed after secondary antibody incubation.

2.2.7 DAPI Staining

DAPI (4′,6-diamidino-2-phenylindole) staining solution was made consisting of 40 ng/ml DAPI in PBS and 0.02% sodium azide. Following the secondary antibody incubation and PBS washes, coverslips were incubated with DAPI staining for 10 min. Coverslips were then washed twice with PBS and mounted in Vectashield mounting medium.

2.2.8 Mitotracker

Live cells were cultured on coverslips in 12-well plate until they reach 70-80% confluency. Cells were then exposed to growth medium mixed carefully with 0.02% mitotracker. Then, coverslips were washed in PBS for 15 min before they were used for immunofluorescence labelling or mounted in Vectashield mounting medium.

2.2.9 Oleate Medium Preparation

1.5 mg of oleate was weighed on a piece of parafilm to avoid sticking of oleate in weighing boat. Oleate was added to 50 ml DMEM growth medium. Medium was mixed carefully with oleate by pipetting several times using P1000 pipette. Oleate medium was then filter sterilised

in a sterile flow hood. It was stored at 4 °C and left for 24 hrs before being used. 24 hrs after cell incubation on coverslips in growth medium, pre-warmed oleate medium was added to coverslips. Coverslips were then placed in a 37 °C tissue culture incubator overnight. Oleate medium was removed and coverslips were washed twice with PBS before they were fixed with 4% paraformaldehyde for 15 min at room temperature.

2.2.10 Oil Red O Staining

After cells were fixed and permeabilized with 0.5% Triton X-100, they were incubated in 60% isopropanol for 20 min. Isopropanol was removed. Oil Red O was diluted to 2:3 ratio and was added to coverslips for 20 min. Then, coverslips were washed in PBS for 15 min before they were used for immunofluorescence labelling or mounted in Vectashield mounting medium.

2.2.11 Western Blotting

2.2.11.1 Protein Extraction

Cells were cultured in 25 cm^2 culture flask to 70% confluency. Media was removed from cells. Ice-cold PBS was prepared and was used to wash cells three times. The washing was done with extra care to avoid disturbing the cells. Lysis RIPA buffer containing complete protease inhibitors was added to cells. Cells were scraped and lysate was collected in 1.5 ml falcon tube. Lysates were then centrifuged at 20,000 g for 20 min at 4 °C. Supernatant containing proteins was collected to a new falcon tube and pellet (cell debris) was discarded. Protein lysates were quantified or stored at -20 °C until quantification.

2.2.11.2 Protein Quantification

Protein lysates were quantified using the DC Protein Assay following the manufacturer's guide. BSA protein standards were used for protein quantification. 2 mg/ml BSA was dissolved

in water. A serial 1:2 dilution of BSA protein standards was made to make a standard curve range from 2 to 0.0625 mg/ml. BSA protein standards were stored at -20 °C. After quantifying protein samples, they were all diluted to the same concentration.

2.2.11.3 SDS-PAGE

SDS-PAGE was used to separate proteins. SDS-PAGE gels were prepared and electrophoresis unit was assembled according to manufacturer's instructions. The gel was prepared and injected into the gap between the glass sheets. Once the gel had polymerized, tanks were filled with 1x SDS-PAGE running buffer. 6x SDS-PAGE sample buffer was added to protein samples so each protein sample contained 5-fold diluted SDS-PAGE sample buffer. Samples were then incubated at 100 °C for 5 min. Following boiling, samples were spun for a short time at room temperature to collect all of the sample at the bottom of the tube. Samples were then loaded onto SDS-PAGE gel and run at a voltage appropriate for gel concentration. Running off of bromophenol blue dye front was always used as an indicator to stop gel running.

2.2.11.4 Semi-Dry Electro-Transfer

SDS-PAGE gel was removed from the two glass sheets of the electrophoresis unit. It was incubated in a container containing semi-dry transfer buffer for 15 min at room temperature with gentle rocking. PVDF membrane and Whatman 3 MM filter papers were cut to the size of the gel. PVDF membrane was incubated in 100% methanol for 5 min with rocking before it was transferred to semi-dry transfer buffer. Whatman filter papers were also soaked in semi-dry transfer buffer for 15 min with gentle rocking. Four pieces of Whatman filter paper were placed on the semi-dry transfer apparatus. The PVDF membrane was then placed on top of the filter papers. Then the gel was placed and finally the four filter papers were stacked on top of the gel. A small tube was used to remove bubbles by rolling it over the stack. The transfer

apparatus was then set transferring 2mA/cm^2 for ~75- 90 min. PVDF membrane was then transferred to tray containing 5% (w/v) milk powder in TBST overnight at 4 °C with shaking.

2.2.11.5 Antibody Staining

After blocking the membranes, they were placed into a 50-ml falcon tube. Primary antibodies were prepared in 5% milk powder in TBST. Membranes were incubated with primary antibodies on a roller overnight at 4 °C. Membranes were then washed for 15 min in TBST with gentle agitation. Secondary antibodies were prepared in 5% milk powder in TBST and incubated for 1-2 hrs at room temperature on a roller. Membranes were then washed in TBST for 15 min at room temperature.

2.2.11.6 Detection

Pierce ECL Plus Western Blotting Substrate was used for signal detection of the proteins. CL-XPosure ™ film was used to expose the membranes to. Exposure time was adjusted for each antibody and films were developed (Xograph imaging systems, Compact X4, Model: X4A). ImageJ was used to quantify the signals.

2.2.11.7 Blot Stripping

The blots were re-probed to detect non-phosphorylated proteins. They were washed in TBST for 10 min before being stripped with stripping buffer for 20 min at 65 °C with agitation. Blots were then incubated with primary and secondary antibodies as in 2.2.10.5.

2.2.12 Microscopy

2.2.12.1 Senescence Associated *B*-Galactosidase

Bright field microscopy of primary and U2OS cells was used to monitor B-galactosidase activity as a marker for senescence. Cells grown on sterilised coverslips were treated with senescence inducing agents before being incubated with SA-B-Gal staining solution. SA-B-Gal staining was detected using 20X objective lense.

2.2.12.2 Stress Granules and Senescence-Associated Heterochromatin Foci

Confocal microscopy of cells treated with sodium arsenite was used to detect G3BP1, eIF4G and FXR1 as markers of stress granules. SAHF was used as a marker of senescence. Zeiss 880 confocal microscope was used in this experiment. Alexa flour 844 secondary antibody was used and a green fluorescence was excited at 488 nm with 10% laser power. Green fluorescence between 500-550 nm was collected. Cy3 secondary antibody was used and orange fluorescence between 590-620 nm was collected.

2.2.12.3 Lipid Droplets

Cells incubated with oleate medium and stained with Oil Red-O was used to detect lipid droplet accumulation in proliferative and senescent U2OS cells. Zeiss 880 confocal microscope was used in this experiment. Red fluorescence between 650-670 nm was collected with HyD 5 detector.

2.2.13 Quantification and Statistical Analysis

To quantify stress granule markers, SAHF and lipid droplets, images were processed and analysed using ImageJ software. The average and standard error are used to present the data of

the experiments. For multiple comparisons, two-way analysis of variance (ANOVA) and t-test were used.

2.2.14 Proteomics Analysis

Cells were lysed and the protein was extracted and quantified as in 2.2.10.1 and 2.2.10.2. Protein samples have been run and data was processed against the 10,000-human protein SWATH library made available by Aebersold and co-workers (DOI:10.1038/sdata.2014.31). Data was processed using Sciex software: PeakView with the SWATH MicroApp plugin and MarkerView for data manipulation/output. R was used to perform FDR correction of t-test and for generation of graphics. Enrichment of GO terms was performed using tools available on pantherdb.org.

Chapter 3

3 Senescence in Primary Cells and Cancer Cell Lines

3.1 Cellular Senescence in Primary Cells

3.1.1 Introduction

Replicative senescence has been reported in many cell types including liver cells (Aikata et al., 2000), skin cells (Lindsey et al., 1991), lymphocytes (Pan et al., 1997) and colona mucosa (Hastie et al., 1990). Hence, several studies have investigated the mechanism behind replicative senescence and techniques to delay/prevent senescence and aging-associated disorders (Baker et al., 2011, 2016; Munoz-Espin & Serrano, 2014; Xu et al., 2015). In addition to replicative senescence, stress-induced premature senescence (SIPS) is induced by exposing cells to multiple factors including ionizing radiation, drug treatments and overexpression of activated oncogenes (such as RAS) (Chen et al., 1995; Toussaint et al., 2000; Dumont et al., 2001; Schauble et al., 2012) (Figure 3.1).

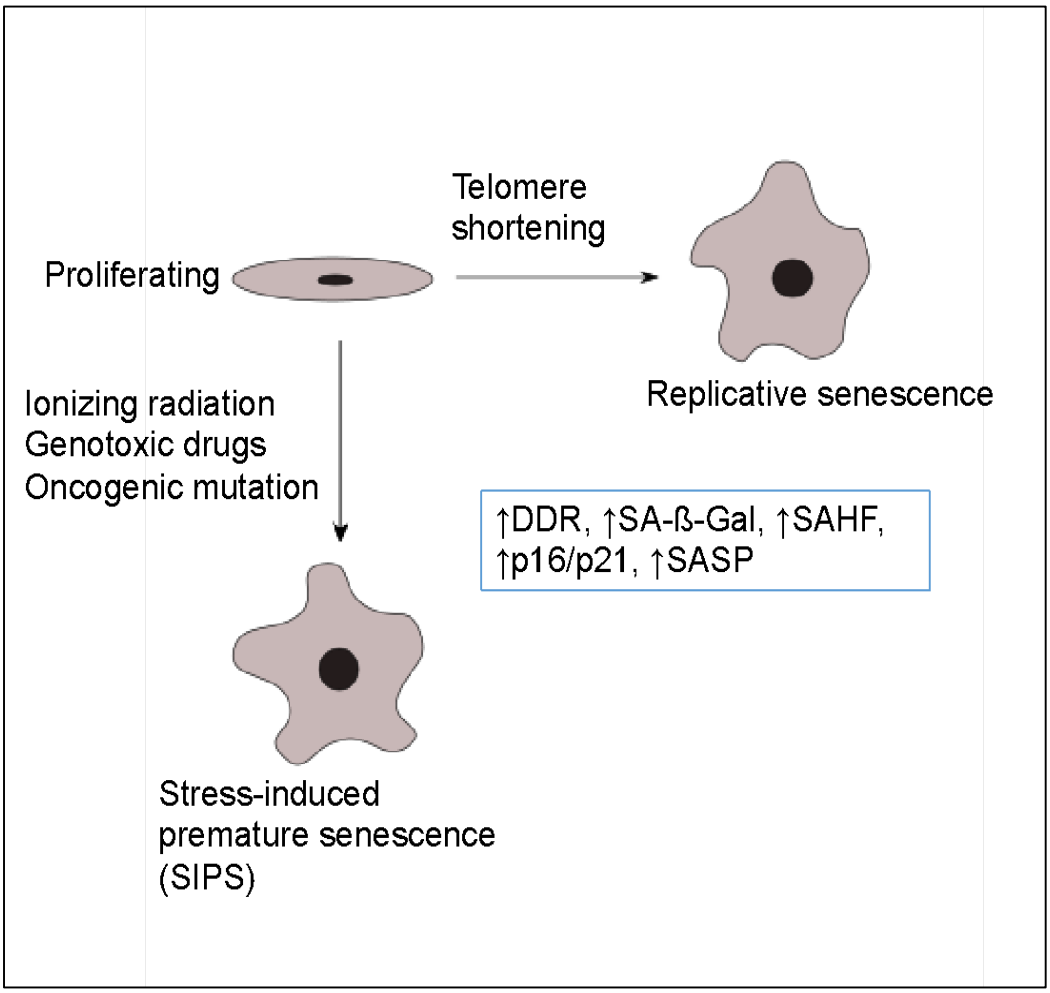

Figure 3.1. Senescence inducing factors and cell response.

Senescence phenotype is induced in proliferative cells when they undergo telomere shortening or are exposed to exogenous factors such as ionizing radiation and genotoxic drugs leading to replicative senescence and SIPS, respectively.

It has been previously shown that exposure to ionizing radiation induces damage to the DNA resulting in DNA lesions. In mammalian cells, ionizing radiation induces ~1000 single-stranded breaks and ~20-40 double-stranded breaks (Lomax et al., 2013). The formation of double-stranded breaks increases linearly with the dose of the radiation. They are considered the most deleterious lesions induced by ionizing radiation. In response to the DNA damage induced by the radiation, the DNA damage repair mechanisms (non-homologous end joining) are activated. However, when the damage is irreparable, cells either undergo apoptosis or

senescence, which is partly decided by the magnitude of stress (Noda et al., 2012; Sabin and Anderson, 2011; Lomax et al., 2013) (Figure 3.2).

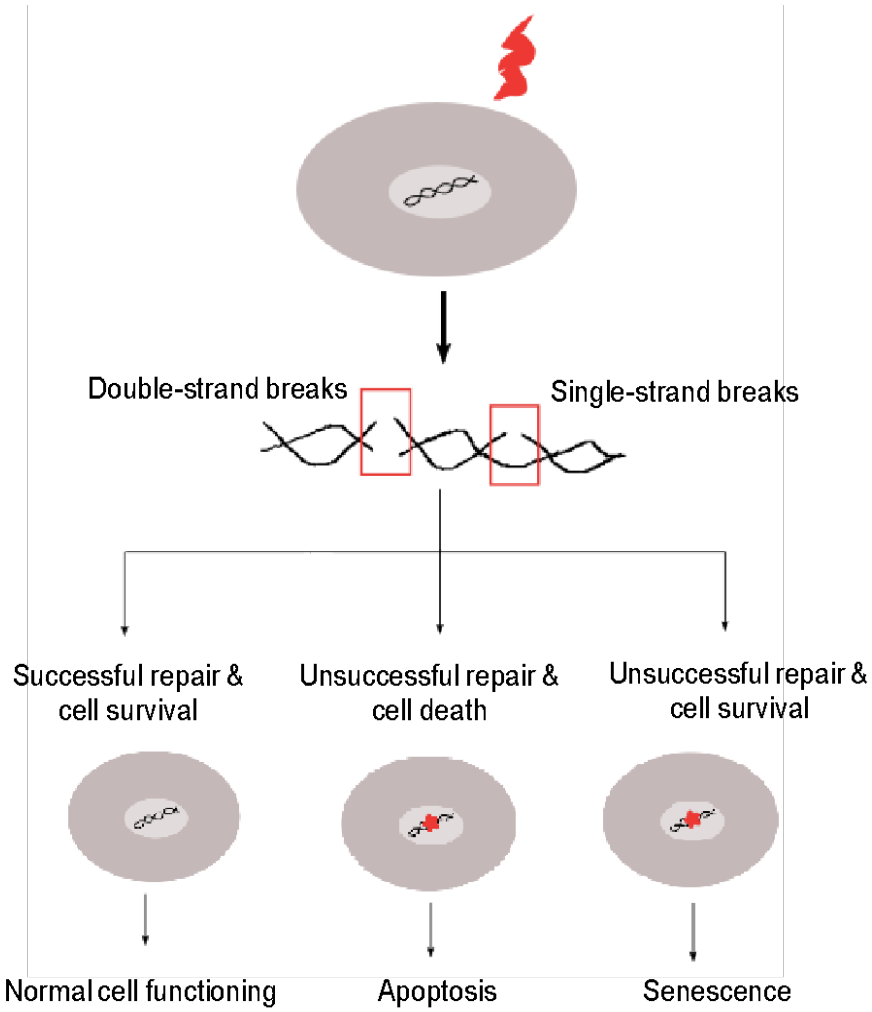

Figure 3.2 Ionizing radiation promotes senescence.
When cells are exposed to ionizing radiation, they activate DNA damage repair pathway. If the damage is irreparable, cells undergo apoptosis or senescence.

In addition to the ionizing radiation, senescence could be induced in cells by DNA-damaging drugs such as doxorubicin, etoposide and cisplatin. Doxorubicin is a chemotherapy drug known as anthracycline (Figure 3.3) which has been used as an anticancer drug for the last four decades. It acts by slowing/preventing the growth of cells. Thus, it is used to induce senescence in cultured cells. Furthermore, it is believed that doxorubicin induces senescence via several mechanisms including: DNA intercalation which leads to inhibition of macromolecules synthesis, free radical generation leading to DNA damage and lipid peroxidation, DNA cross-linking, separation of DNA strand, alteration of helicase activity and inhibition of Topoisomerase II (Gewirtz, 1999; Bielak-Zmijewska et al., 2014; Goodnow, 2017; Nair et al., 2017).

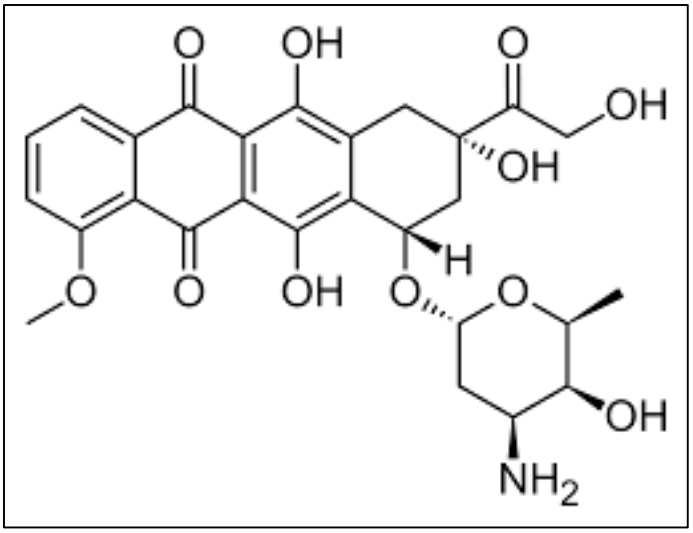

Figure 3.3 Chemical structure of (N-(5,5-Diacetoxypent-1-yl)) doxorubicin.

This compound shows anti-tumour activity by stabilizing DNA-topoisomerase II complex and thereby preventing cell growth (Lyu et al., 2012).

In addition to the irreversible growth arrest, senescent cells are characterized as giant, flattened, and multinucleate cells. Moreover, they show high activity of ß-galactosidase at pH. 6.0 (Campisi, 2005; Lee et al., 2005; Dimri et al., 1996). *GLB1,* a gene encoding lysosomal ß-D

galactosidase, is the gene that express senescence associated ß-galactosidase (SA-ß-Gal) activity (Lee at al., 2006; Schauble et al., 2012). SA-ß-Gal activity is detectable in young proliferative cells and senescent cells at pH 4.0 and pH 6.0, respectively. Furthermore, SA-ß-Gal activity has been detected in replicative and stressed induced senescent cells (Dimri et al., 1995). It also has been detected in organs of old humans and animals (Melk et al., 2003; Mishima et al., 1999).

The activity of SA-ß-Gal is measured by staining cells with X-gal (5- bromo-4-chloro-3-indolyl-β-D-galactopyranoside), a chromogenic substrate. X-gal is hydrolysed by ß-*D galactosidase* to galactose and 5- bromo-4-chloro-3-hydroxyindole forming blue precipitate 5,5'-dibromo-4,4'-dichloro-indigo (Figure 3.4). The positive cells develop blue stain which can be observed and quantified under a bright-field microscope (Lumba et al., 2017).

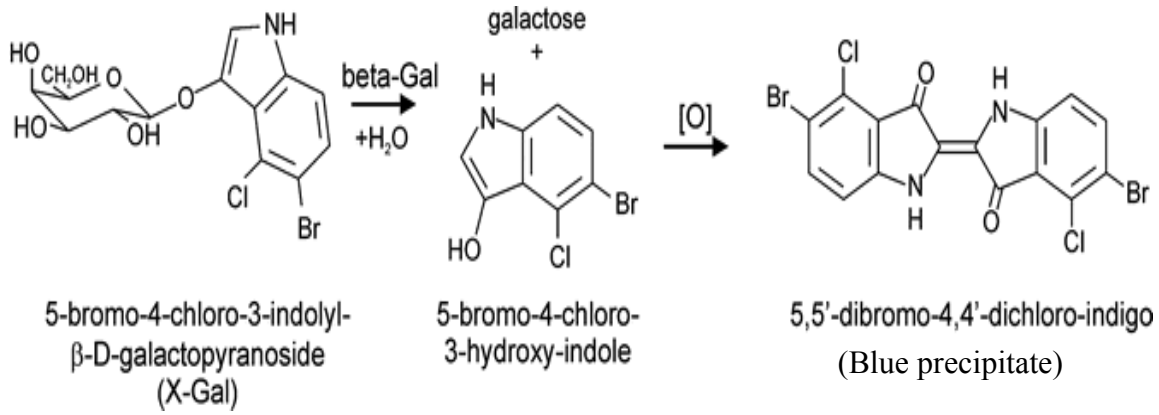

Figure 3.4 X-gal is used for in situ staining to measure activity of SA-ß-Gal. Senescent cells express ß-*galactosidase* activity which is detected by X-gal. X-gal forms a blue precipitate upon cleavage at pH. 6.0 (Dimri et al., 1996).

In addition to the morphological and structural features, senescent cells exhibit mitochondrial changes including impaired biogenesis and metabolic shifts (Correia-Melo et al., 2016; Vasileiou et al., 2019). At cellular level, mitochondrial dysfunction has been observed to be associated with senescence and aging (Correia-Melo et al., 2016). Kinetic studies showed that the increase of the mitochondrial mass occurs within 2-3 days after the peak of DNA damage (Passos et al., 2010). In senescence, the increased mass of mitochondria is reflected by a higher oxygen consumption per cell. Furthermore, Mitochondrial dysfunction has been observed to drive and maintain cellular senescence (Passos et al., 2007; Correia-Melo et al., 2016; Wiley et al., 2016).

Human fibroblast cells provide a good experimental model to study the mechanism and markers of senescence. Senescence features are well-expressed in fibroblast cells within a well-defined time course. Most fibroblast cells develop senescence features 7-14 days' post treatment (Stanulis-Praeger, 1987; Muñoz-Espín and Serrano, 2014; Jun and Lau, 2017). IMR90, HDF and MRC5 are the most commonly used fibroblast cells in experiments as they have shown detectable and defined senescence features (Chen et al., 2004).

3.1.1.1 Population Doubling

Cell replication is controlled by the cell cycle. Cell cycle provides a regulatory mechanism to protect the organism from any mutation development or growth of unwanted cells. Furthermore, cell cycle is divided into four individual phases (Figure 3.5). Synthesis (S) phase is the phase during which DNA is replicated. Mitosis (M) phase where DNA is packed and distributed to two daughter cells. To ensure transfer of the appropriate DNA copy to daughter cells, Gap phases (G) separate S phase and M phase providing cells with a proofreading time. G1 phase separates M phase from S phase whereas G2 phase separates S phase from M phase.

Gap 0 (G0) phase is the phase where no cell division is occurring and cell exit the growth cycle due to absence of growth factors or presence of pro-differentiation factors (Kastan and Bartek, 2004; Barbash and Diehl, 2008).

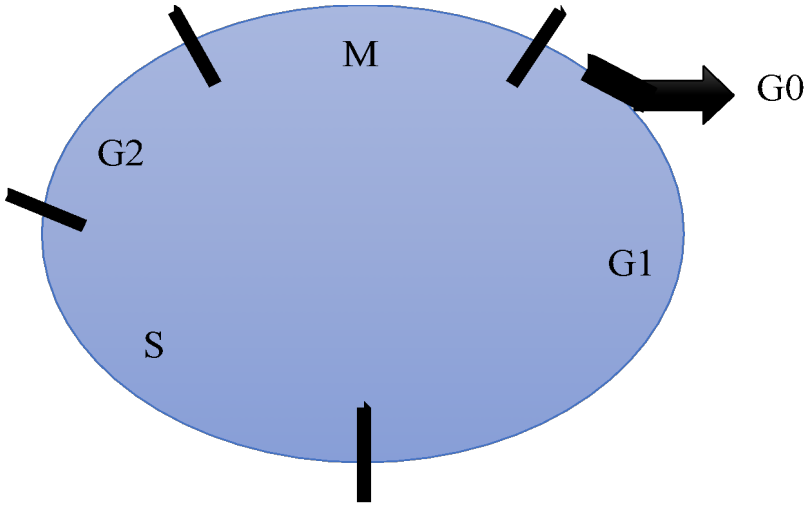

Figure 3.5 A simplified scheme of cell cycle.
The phases and duration of cell cycle are controlled by presence/absence of growth factors. Cell cycle is regulated by checkpoints leading to cell cycle progression or cell cycle arrest (G0).

As cells grow and divide, they follow a growth pattern that is composed of three phases. It includes lag phase, exponential phase, and stationary phase. During the lag phase, cells show little or no division as they recover from sub-culturing stress. Hence, cells are not dormant at this phase. At the exponential stage, the cells start growing and keep dividing until the surface of the vessel is occupied. During exponential growth, cell mass increases over time. Following the exponential cell growth, cells enter the stationary phase where they slow or stop dividing. To ensure viability and genetic stability, cells need to be maintained in the exponential phase (Assanga et al., 2013; Freshney, 2006).

A proliferating cell population grows exponentially and cell growth time is estimated at population level by counting cell number and measuring the growth curve. Thus, the cell population doubles in number during the exponential phase. The number of times the cell population has doubled since their primary isolation is known as population doubling. Therefore, population doubling is determined using the following formula:

$$PD = 3.32 (\log UCY - \log l) + X$$

Where UCY = the cell yield at that point, l = the cell number used as inoculum to begin that subculture, and X = the doubling level of the inoculum used to initiate the subculture being quantitated (Hayflick, 1973).

3.1.2 Aims and Objectives

3.1.2.1 Aims

The chapter aims to develop an understanding of the changes in HDF and U2OS cells when induced to senescence. Hence, HDF cells will be cultured in vitro in a growth chamber. Cell growth will be monitored and cell number will be counted. The population doubling will be calculated using the formula described earlier. Thus, cells reaching replicative senescence will be tested using senescence markers: structural changes and SA-ß-Gal activity. Therefore, senescence phenotype associated with replicative senescence in HDF cells will be detected. SIPS will be studied in HDF by exposing cells to high doses of ionizing radiation. Cell growth will be tracked over 21 days. Cells will be collected at several time points and tested for senescence markers: structural changes and SA-ß-Gal activity. Thus, replicative senescence and SIPS in HDF cells will be compared.

We hypothesize that HDF cells reach senescence following continual passaging in culture. Moreover, senescence phenotype can be induced in HDF cells by exposing them to ionizing radiation which causes DNA breaks and eventually activates pathways leading to cell growth arrest.

3.1.2.2 Objectives

1. Induce senescence in HDF cells replicatively and by SIPS.
2. Characterize the changes associated with replicative senescence and SIPS.

3.1.3 Materials and Method

3.1.3.1 Materials

All chemicals were purchased from Sigma unless stated otherwise.

3.1.3.2 Method

As described in chapter 2.

3.1.4 Results

3.1.4.1 Replicative Senescence in Primary Human Fibroblast Cells

In the current study, we investigated cellular senescence in primary human fibroblast cells (HDF). During cell culture, it is necessary to keep track of cellular growth and age. Therefore, a starting cell density of ~1*10^4 cells/ml of young HDF cells were seeded in a T75 tissue culture flask. During cell culturing, cell number was counted before seeding and after harvesting at ~80% confluency. Subsequently, population doubling was measured using the above PD formula. Figure 3.6(A) shows the cell growth curve of HDF cells which manifest all the cellular growth phases. It clearly shows that the pattern of cell growth is exponential. The behaviour of the curve is as follows: lag phase (0-~50 days), exponential phase (~50–75 days) and stationary phase (~75–250 days). Day 0 is the time of cell splitting.

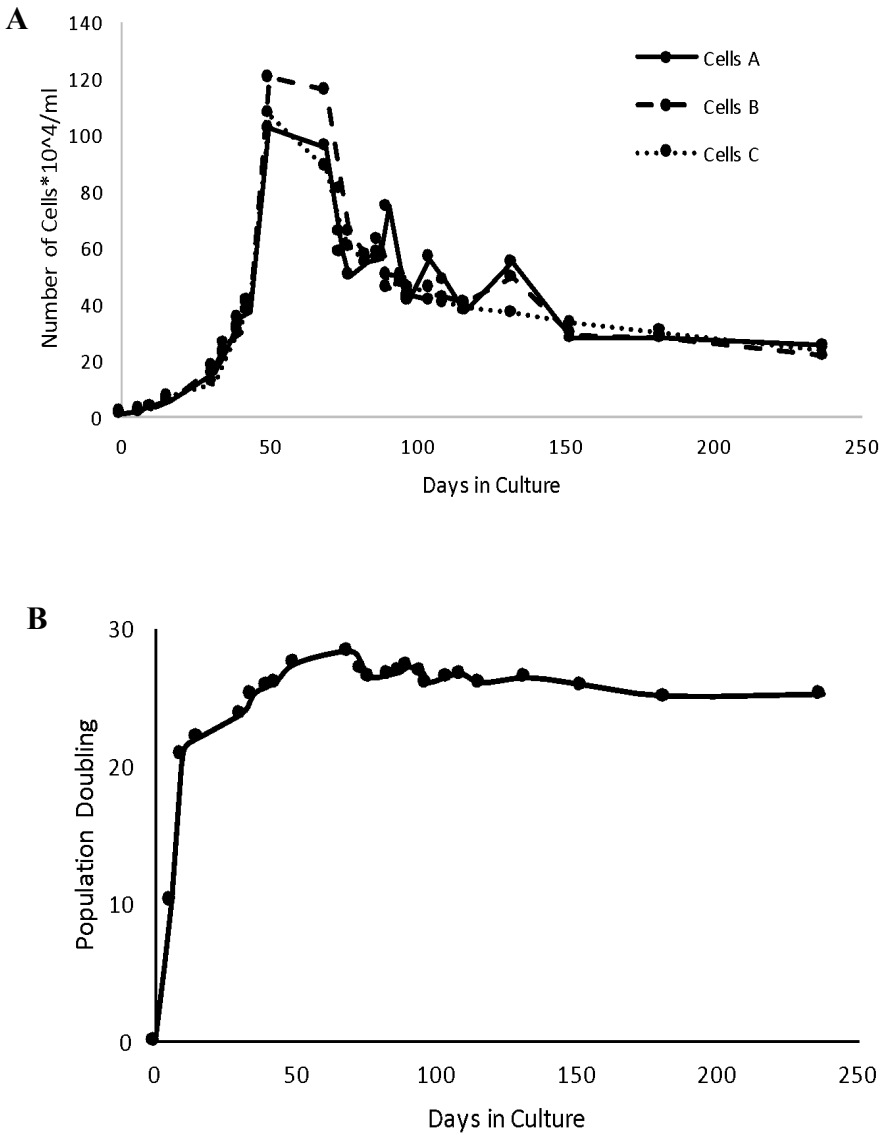

Figure 3.6 Cell growth pattern and population doubling curves of human fibroblast (HDF) cells.

At ~50 days, cells start exponential phase. At ~75 days, cells show a steady growth known as stationary phase (A). At PD= 21 cellular growth starts an exponential pattern. Cells stops dividing (early senescence) at PD=28. The flat line is a state of late senescence (B). Cells were cultured and monitored in triplicates (Cells A, B, C).

Following cell seeding, cells take up to 48 hrs to adhere to the culture vessel and start dividing (lag phase). As cells grow, more cytoplasmic mass is produced resulting in cell division and continuous increase of cell number (exponential phase). It is shown in figure 3.6(B) that after the first 50 days of incubation (PD= 21), cellular growth starts an exponential pattern. However, as human primary cells have shown limited proliferation capacity (Hayflick limit), HDF cells showed a steady cell growth after ~75 days of incubation, where the input (number of cells at seeding) and output (number of cells at harvesting) of cells is maintained (stationary phase). Figure 3.6(B) shows that cells reach early senescence at PD=28. Furthermore, at higher population doublings (flat line), cells showed no increase in cell number which is a state of late senescence (G0 phase). This is happening due telomere shortening after every cell division (Uzbecov, 2003).

3.1.4.2 Senescence Hallmarks

3.1.4.2.1 Replicative Senescence

Primary cells are known to initially proliferate but irreversibly enter senescence. Senescence phenotype includes more than irreversible cell division arrest. In addition to the growth arrest, it comprises morphological and metabolic changes (Campisi, 2005; Nakagawa and Opitz, 2007; Rodier and Campisi, 2011).

Thus, in the current study, cells' progression towards senescence was monitored and senescence phenotype was studied. SA-ß-Gal assay was used to examine senescence phenotype in HDF cells. Therefore, cells were collected and fixed at early passage (PD= 10) and late passage (PD= 28). Then, cells were stained with SA-ß-Gal staining. As expected, cells of late passage developed a blue stain at pH. 6.0 which indicates an increase in SA-ß-Gal activity. Accordingly, SA-ß-Gal positive cells are considered as fully-developed senescent cells. In

contrast, cells of early passage did not develop blue staining, indicating that cells are young and still proliferating (Figure 3.7A). The dark blue staining of SA-ß-Gal positive cells express the highest activity of lysosomal ß-Galactosidase hydrolase which express the late senescence state of cells (Lee et al., 2006).

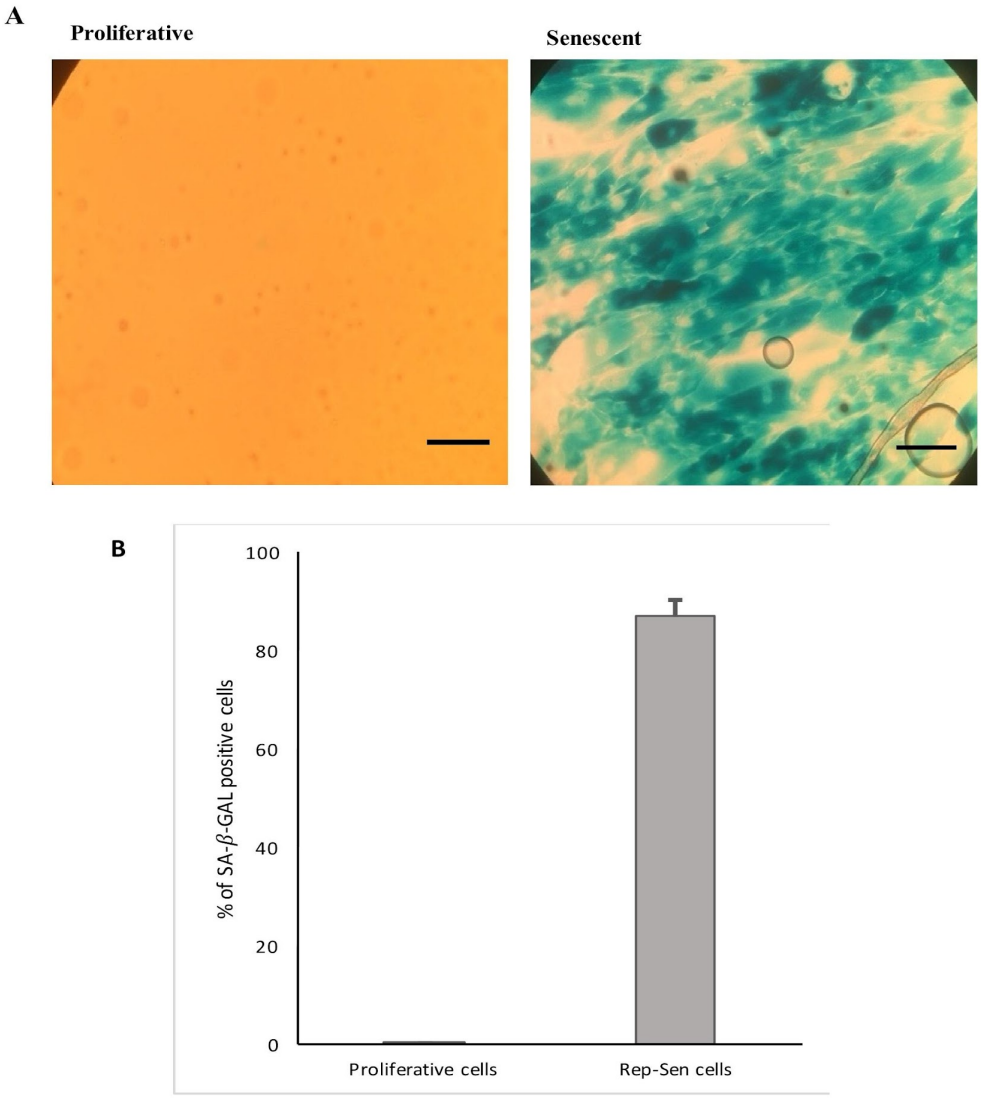

Figure 3.7 Human fibroblast cells developed senescence-associated phenotypes by continual passaging.

Cells were passaged until they stop proliferating, developing a state replicative senescence. Cells were tested for SA-ß-Gal activity. ~90% of senescent cells were positive to the staining. Scale bar= 100 um. Data represents mean ± SEM n=3, statistical significance was assessed using ANOVA t-test.

Furthermore, the positive cells were scored and data was analysed using ImageJ. Approximately, 90% of late passage cells were positive to SA-ß-Gal staining. Whereas, cells of early passage did not show any blue staining indicating that cells are proliferating (Figure 3.7B).

In addition to molecular changes (at levels of proteins including p21), senescence phenotype encompasses structural changes such as enlarged cell size. While running an experiment for other studies in the lab where J2 (a double-stranded RNA antibody) was used, we observed the structural difference between senescent and proliferative cells. The experiment involved staining late passage cells (PD= 28) and early passage cells (PD= 10) with J2 antibody. Cells were imaged using a confocal microscope. The size difference was clearly detected between proliferative and senescent cells. Proliferative cells were detected to have elongated and spindle shape. However, senescent cells were flattened and enlarged (Figure 3.8A). Size of proliferative cells was measured to range from 100-300 um^2 (Figure 3.8B). In contrast, the size of replicative senescent cells range between 3000-5000 um^2 (Figure 3.8C). Therefore, our observations are consistent with observations of studies carried by other research groups (Rodier and Campisi, 2011).

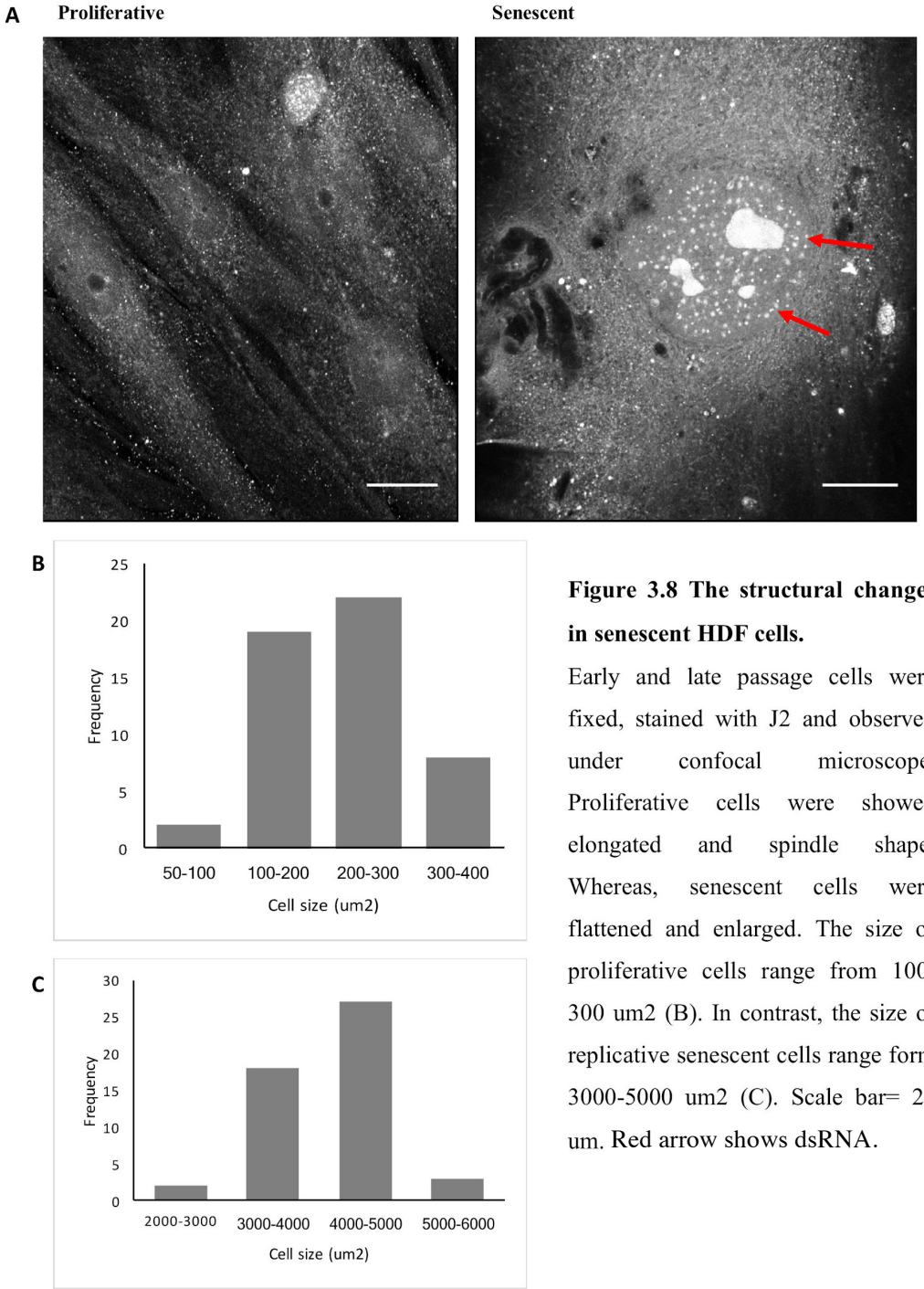

Figure 3.8 The structural changes in senescent HDF cells.

Early and late passage cells were fixed, stained with J2 and observed under confocal microscope. Proliferative cells were showed elongated and spindle shape. Whereas, senescent cells were flattened and enlarged. The size of proliferative cells range from 100-300 um2 (B). In contrast, the size of replicative senescent cells range form 3000-5000 um2 (C). Scale bar= 20 um. Red arrow shows dsRNA.

In addition to the increased cell size, senescent cells display other structural changes including expanded mitochondria. Using a mitochondrial marker (mitotracker) alongside double stranded RNA (J2) antibody, which was used for other studies in the lab, showed interesting changes in senescent HDF cells. Mitotracker is a stain specified for the mitochondria. Early and late passages of HDF cells were stained with mitotracker and J2 antibody. A difference in the appearance of the mitochondria was noticeably detected between proliferative and senescent cells (Figure 3.9). An increase in the size of mitochondria was detected in senescent cells. The change in mitochondrial size and shape is suggested to be due to the higher oxygen consumption per senescent cell (Passos et al., 2010). Surprisingly, dsRNAs were observed to be located in the nuclei of senescent cells (red arrow) (Figure 3.8, 3.9). Hence, we propose that dsRNAs could be used as a marker for senescent cells.

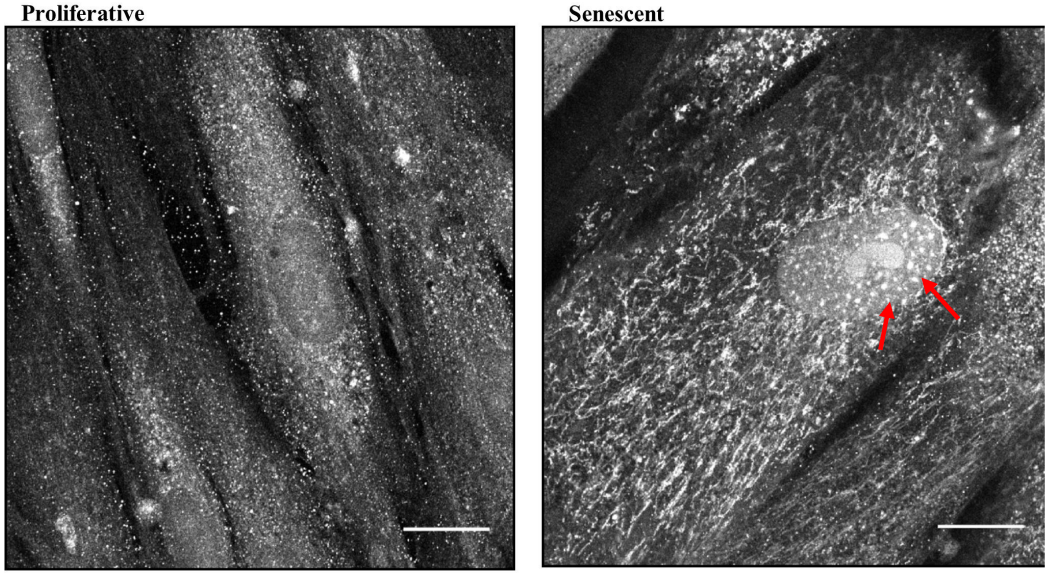

Figure 3.9 Mitochondrial mass in proliferative and senescent cells.

HDF cells developed senescence-associated phenotypes by continual passaging including mitochondrial mass increase. Mitotracker was used stain mitochondria and J2 was used to stain dsRNAs. Senescent cells showed an increase in the mass of mitochondria and assembly of dsRNAs in the nuclei. Scale bar= 20 um. Red arrow shows dsRNA.

3.1.4.2.2 Stress-Induced Premature Senescence

As we discussed previously, when cells reach senescence, they develop senescence-associated phenotype such as structural changes and elevated SA-ß-Gal activity. Stress-induced premature senescence (SIPS) is a distinct senescence program through which cells become senescent by exposing them to DNA-damage inducing agents including ionizing radiation and mitogenic drugs (Schauble et al., 2012). High doses of ionizing radiation are known to inhibit unwanted growth of cells (Moding et al., 2013). Hence, SIPS senescent cells stop dividing after a limited time following irradiation. Thus, in this study, senescence phenotype was monitored in HDF cells following their exposure to ionizing radiation.

Prior to exposing cells to IR, cells were cultured in culture vessels to ~90% confluency. Media was frequently changed to provide cells with required nutrients and minimize culturing stress. Subsequently, cells were exposed to 10 Gy ionizing radiation followed by adding fresh media and placing cells in a cell growth incubator. Thus, cells were grown and monitored for 21 days. Samples were collected every 7 days and stained with SA-ß-Gal staining.

SA-ß-Gal activity has not been detected in proliferative (Day 0) cells. However, as cells progress towards senescence, they showed an increase in the activity of SA-ß-Gal (Figure 3.10A). The number of SA-ß-Gal positive cells started to increase from Day 7 post-irradiation. Hence, at 7 days post-IR exposure, 15% of the population was senescent. Whereas, 35% of the population were detected to be positive to SA-ß-Gal by Day 14 post-irradiation. As we expected, an increase in SA-ß-Gal positive cells was observed 21 days post-IR exposure. It rose to 65% (Figure 3.8B).

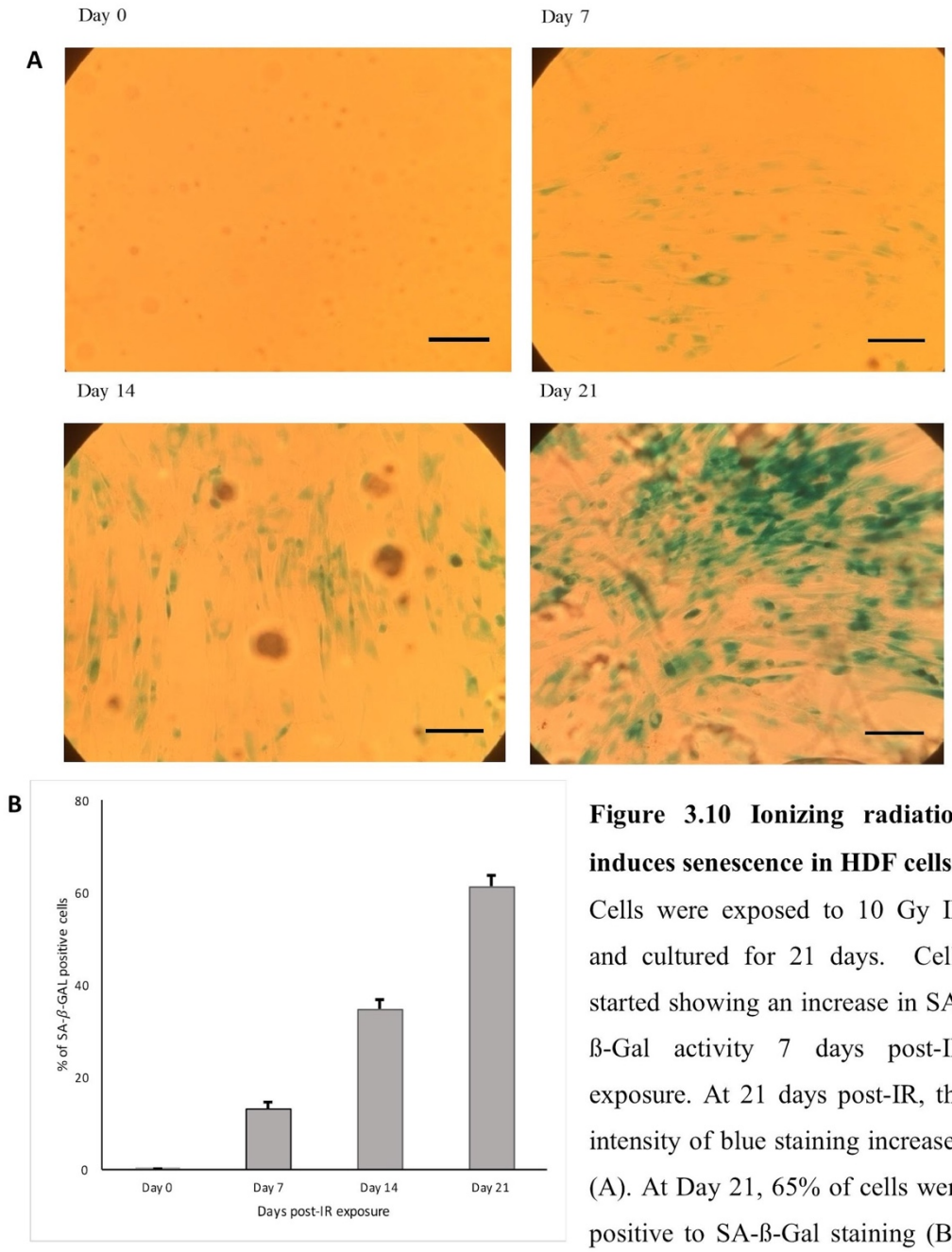

Figure 3.10 Ionizing radiation induces senescence in HDF cells. Cells were exposed to 10 Gy IR and cultured for 21 days. Cells started showing an increase in SA-ß-Gal activity 7 days post-IR exposure. At 21 days post-IR, the intensity of blue staining increased (A). At Day 21, 65% of cells were positive to SA-ß-Gal staining (B). Scale bar = 100 um. Data represents mean ± SEM n=3, statistical significance was assessed using ANOVA t-test.

Similar to replicative senescent cells, SIPS cells showed structural changes including enlarged cell shape and expanding mitochondria (Figure 3.11A). Hence, cells of Day 0 and Day 21 post-IR were stained with J2 antibody and mitotracker. SIPS senescent cells were flattened. An

increase in mitochondrial mass was detected in these cells. In contrast, Day 0 cells (proliferative) were showing elongated spindle structure. Our observations suggest that Day 21 cells are well-developed senescent cells.

The size of SIPS senescent cells was detected to be bigger than proliferative cells. The area of Day 0 and Day 21 cells was measured in ImageJ. The size of SIPS senescent cells was measured to range from 3000-4000 um2. Whereas, Day 0 (proliferative) cell size was detected to be from 100-300 um2 (Figure 3.11B). This data indicates that Day 21 cells are senescent cells that harbour senescence phenotypes such as increased cell size and mitochondrial mass.

Furthermore, both replicative and SIPS senescent cells exhibited senescence markers. However, the intensity of the markers differs between the two systems. The time required for the cells to reach senescence is significantly different. SIPS cells require weeks to reach senescence. Whereas, replicative senescent cells require 6-7 months to become fully senescent. Moreover, replicative senescent cells showed a higher SA-ß-Gal activity (80%) compared to IR-induced senescent cells (65%). Collectively, our data indicates that both senescence programs lead to fully-developed senescent cells exhibiting senescence associated phenotypes.

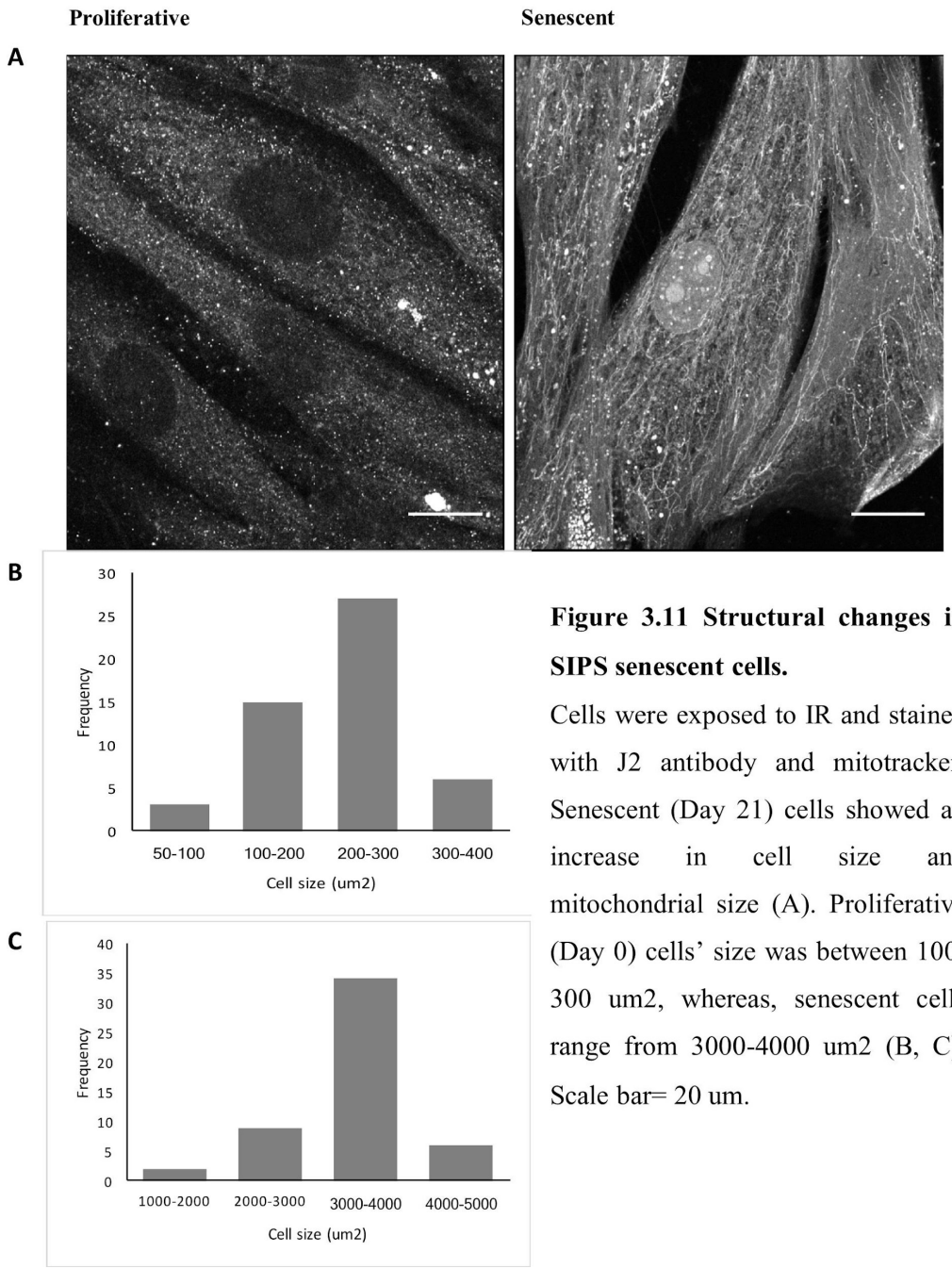

Figure 3.11 Structural changes in SIPS senescent cells.

Cells were exposed to IR and stained with J2 antibody and mitotracker. Senescent (Day 21) cells showed an increase in cell size and mitochondrial size (A). Proliferative (Day 0) cells' size was between 100-300 um2, whereas, senescent cells range from 3000-4000 um2 (B, C). Scale bar= 20 um.

3.2 Induction of Cellular Senescence in Osteosarcoma Cells (U2OS)

3.2.1 Introduction

In contrast to normal human fibroblast cells, cancer cells possess an indefinite ability to proliferate. Until recently, cancer cells were believed to have lost their ability to senesce. Senescence has been induced in cancer cells using several stimuli including oxidative stress, DNA damage, and DNA methylation alteration. Senescence phenotype in cancer cells is known as stress-induced premature senescence. Thus, therapy-induced senescence in cancer cells *in vitro* and *in vivo* has been considered as one of the possible responses to anticancer treatments (Collado et al., 2007; Lee and Lee, 2019). Moreover, it has been reported that Oncogene induced senescence was triggered by expressing oncogenes RAS^{G12V} or $BRAF^{V600E}$ (Acosta and Gil, 2012).

Radiation and chemotherapy are of the possible anticancer treatments that are widely used to treat cancerous cell growth. Furthermore, using low doses of radiation and DNA-damaging drugs have been observed to induce senescence *in vitro* (Kahlem et al., 2004; Schawrze et al., 2005). Senescent cells originated from cancer cells showed structural and molecular changes including increased cell size and high SA-ß-Gal activity at pH. 6.0 (Campisi, 2013; Kim and Park, 2019).

3.2.2 Aims and Objectives

3.2.2.1 Aims

The chapter aims to develop an understanding of the changes in HDF cells and U2OS when induced to senescence. To determine senescence phenotype in U2OS cells, cells will be induced to senescence using ionizing radiation and the DNA-damage inducing agent: Doxorubicin. The optimal dose of ionizing radiation and doxorubicin that are required to induce senescence will be examined. Therefore, cells will be exposed to ionizing radiation or doxorubicin and monitored for 14 days. Senescence phenotype will be tracked using SA-ß-Gal assay. Percentage of SA-ß-Gal positive cells will be counted using ImageJ.

We hypothesize that senescence phenotype could be induced in the cancerous U2OS cells and provide a reliable system to study senescence and stress granules.

3.2.2.2 Objectives

3. Induce senescence in U2OS cells by testing the optimal dose of ionizing radiation and doxorubicin.

3. Determine the changes associated with senescence in HDF and U2OS cells

3.2.3 Materials and Method

3.2.3.1 Materials

All chemicals were purchased from Sigma unless stated otherwise.

3.2.3.2 Method

As discussed in chapter 2.

3.3 Results

3.3.1 Ionizing Radiation-Induced Senescence

Ionizing radiation has been widely used to induce senescence and stop growth of cancer cells (Bentzen, 2006; Durante and Loeffler, 2010; Baskar et al., 2012). Cancerous cells are known to be more sensitive to DNA damage caused by ionizing radiation than normal cells. High dose of ionizing radiation induces DNA damage and subsequently cell death (Baskar et al., 2014).

Hence, in this study, the cancerous U2OS cells were exposed to low doses of ionizing radiation in order to optimize senescence induction. Therefore, U2OS cells were cultured in a culture vessel to ~90% confluency. Subsequently, cells were exposed to variable doses of ionizing radiation: 0 Gy, 2 Gy, 4 Gy, 6 Gy, and 8 Gy. Cells were then monitored for 14 days' post-irradiation to examine cell growth and senescence phenotype. Cells were then collected at Day 0, 3, 5, 7, 10 and 14 and examined for SA-ß-Gal activity (Figure 3.12A). Hence, low SA-ß-Gal activity was detected using 2 Gy dose. A 2 Gy dose is low and insufficient to induce senescence within 14 days. It might need a longer time to develop senescence phenotype. Additionally, 8 Gy was detected to induce senescence however, U2OS cells are sensitive to irradiation and thus cell number was observed to decline. Furthermore, cells exposed to 4 Gy and 6 Gy showed elevated SA-ß-Gal activity by Day 14 post-IR while maintaining cell number.

A percentage of ~10%, 27%, 12%, and 5% of SA-ß-Gal activity was detected in cells exposed to 2 Gy, 4 Gy, 6 Gy, and 8 Gy, respectively (Figure 3.12B). The highest activity of SA-ß-Gal was detected in cells exposed to 4 Gy. Moreover, 2 Gy is a very low dose and induced senescence phenotype in only 10% of the cells. Whereas, 8 Gy is an extremely high dose that might lead to low cell survival. 4 Gy was shown to induce senescence phenotype while

maintaining cell number. Therefore, for future experiments with U2OS cells, 4 Gy ionizing radiation was considered as the optimal dose.

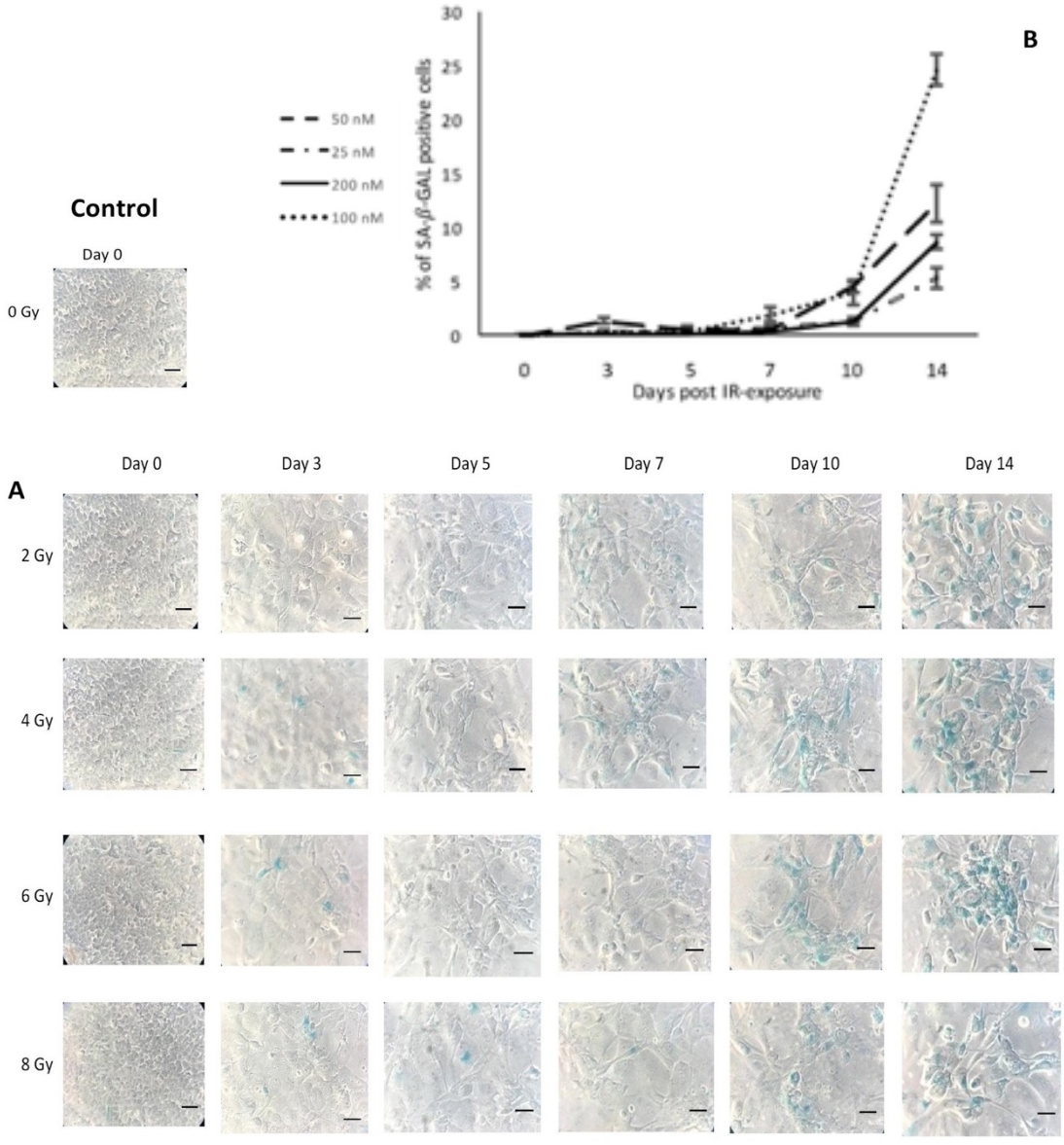

Figure 3.12 Stress-induced premature senescence in U2OS cells using ionizing radiation.

U2OS cells were treated with different doses of ionizing radiation and were monitored for 14 days. Cells were stained for SA-ß-Gal activity (A). Cells exposed to 0 Gy continued to grow and the culture vessel was confluent after few days (Control). 4 Gy showed high SA-ß-Gal activity (B). Scale bar= 100 um . Data represents mean ± SEM n=3, statistical significance was assessed using ANOVA t-test.

3.3.1.1 DNA Damage-Induced Senescence

Doxorubicin is a DNA-damaging chemotherapy agent. It has been used in cellular senescence and cancer research. Doxorubicin slows or stops cell growth by blocking the enzyme topoisomerase 2 (Jackson and Pereira-Smith, 2006). Doxorubicin can induce three different cell responses depending on the dose. In addition to apoptosis and necrosis, cells acquire senescence phenotype when exposed to low doses of doxorubicin (Zhang et al., 2011).

Therefore, in our study, U2OS cells were treated with different doses of doxorubicin: 0 nM, 25 nM, 50 nM, 100 nM and 200 nM for 48 hrs. Doxorubicin was removed and replaced with a fresh media. Cells were then monitored for 7 days subsequent to the treatment. Cells showed elevated activity of SA-ß-Gal. However, the number of SA-ß-Gal positive cells varied when applying different doses of doxorubicin. Hence, cells started showing blue staining 5 days' post-treatment. When using 25 and 50 nM doxorubicin, few cells developed blue staining and were positive to SA-ß-Gal staining. However, the number of SA-ß-Gal positive cells increased when using 100 and 200 nM (Figure 3.13A).

Furthermore, at 200 nM, 45% of cells were positive to SA-ß-Gal staining. Moreover, a percentage of 22%, 15% and 11% of cells were positive to SA-ß-Gal staining at 100 nM, 50 nM and 25 nM, respectively (Figure 3.13B). Thus, the following doxorubicin concentrations: 25 and 50 nM were not sufficient to induce senescence in all cells. However, 200 nM induced the highest number of senescent cells: 45%. Therefore, 200 nM doxorubicin was used as the optimal dose to induce senescence in U2OS in the following experiments.

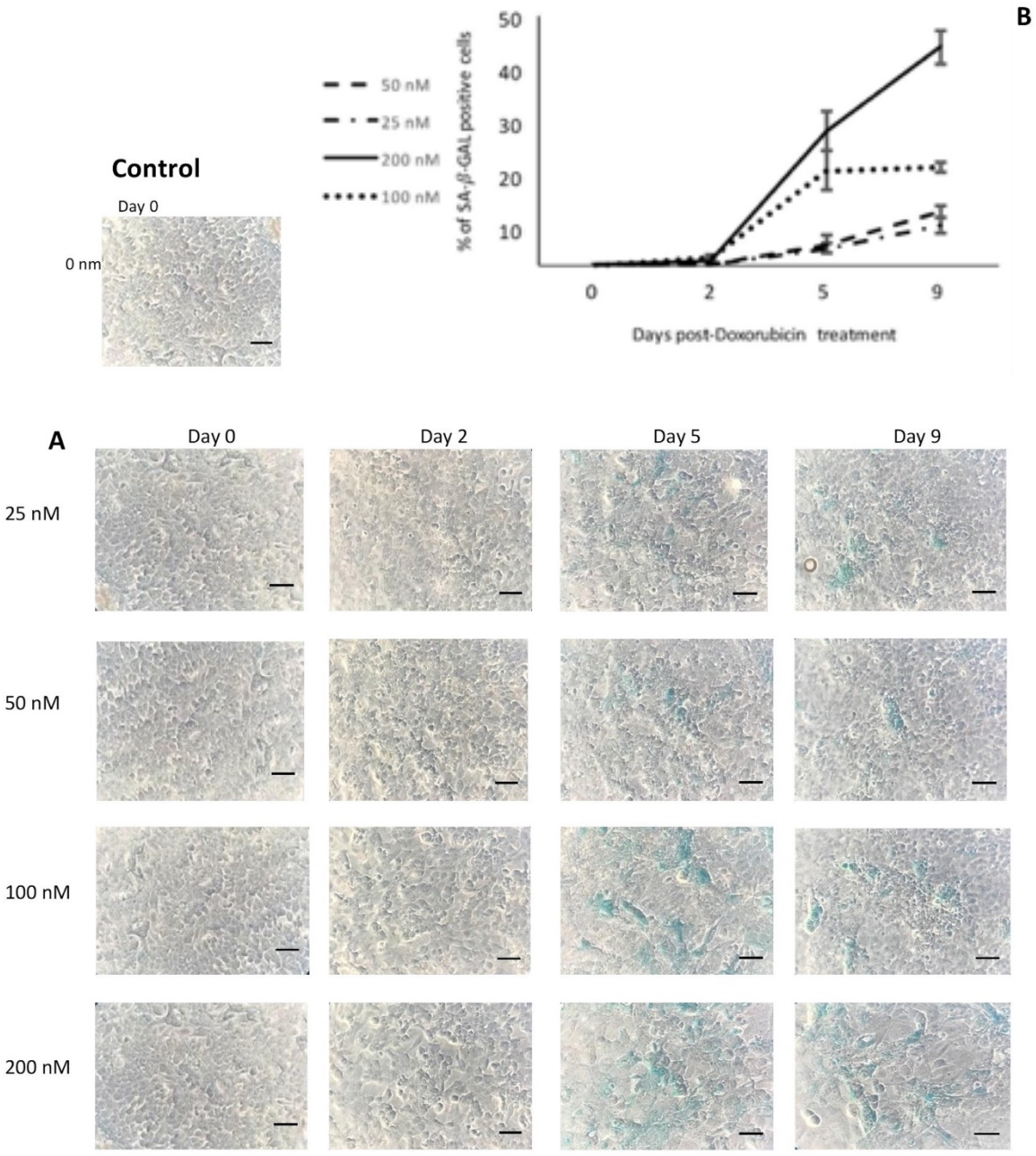

Figure 3.13 Doxorubicin-induced senescence in U2OS cells.

Cells were treated by a series of four exposures to doxorubicin. Senescent cells were positive to SA-ß-Gal staining and stained blue (A). 200 nm doxorubicin induced senescence in 45% of the population (B). Scale bar= 100 um. Data represents mean ± SEM n=3, statistical significance was assessed using ANOVA t-test.

3.4 Conclusion

Senescence is a state during which cells lose their ability to proliferate. Senescent cells show multiple senescence phenotypes including growth arrest, increased size of cell and mitochondria and high activity of SA-ß-Gal (Campisi, 2005). Hence, SA-ß-Gal staining has been used widely as a marker for senescent cells. Hydrolysis of X-gal results in synthesis of galactose and 5- bromo-4-chloro-3-hydroxyindole forming blue precipitate 5,5'-dibromo-4,4'-dichloro-indigo (Lumba et al., 2017).

Primary human fibroblast (HDF) cells reach senescence by multiple divisions *in vivo* or by continual passaging *in vitro*. The resulting state is known as replicative senescence. Population doubling reflects the total number of times the cells in a population have doubled. Cells growth curve represents three phases including lag phase, exponential phase and stationary phase. During the stationary phase, cells stop dividing and become senescent.

In this study, HDF cells were cultured and cell number was counted before and after passaging. Cells proliferation was terminated at PD= 28 (early senescence). Furthermore, at this PD, cells number dropped as cells stopped dividing. Therefore, cells replicatively senesce at ~75 of continual passaging. IMR90 (Marthandan et al., 2014) and MRC-5 (Lambert and Pirt, 1979; Ma et al., 2015) cells showed similar growth pattern (log, exponential and stationary phases) to HDF cells. The population doubling curve and cell growth curve are reliable indications of cells steady state of division (cellular senescence).

Moreover, SA-ß-Gal staining provides an indication of cells' growth status. Formation of blue precipitate that results from X-Gal hydrolysis in a cell population indicates that cells are senescent. Thus, HDF cells that were stained blue at pH. 6.0 indicates that cells are senescent.

Replicative and IR-induced premature senescent cells showed similar structural changes such as increase of cell size and mitochondria while proliferative cells show elongated spindle-like shape. Continual passaging of cells for ~75 days, resulted in 80% SA-ß-Gal positive cells (replicative senescent) while exposing cells to 10 Gy ionizing radiation resulted in 65% SA-ß-Gal positive cells (stress-induced premature senescence).

Previous studies showed that although stress-induced premature senescence displays similar senescence features to those in replicative senescence, they are not alike. Stress induced premature senescence showed differential expression of genes coding for proteins implicated in growth arrest (PTEN, IGFBP-3 and LRP-1) and senescent morphogenesis (TGF- b1 and LOXL2) (Doggett et al., 1992; Debacq-Chainiaux et al., 2005; Pascal et al., 2005). Thus, whether senescence is induced replicatively or prematurely, it is complex and many cellular functions are affected through multiple signalling pathways.

U2OS cancer cells have been used extensively in senescence studies (Bihani et al., 2004; Lin et al., 2014; Nakano et al., 2013). Therefore, senescence has been induced in these cells through H-ras-oncogene (Bihani et al., 2004), etoposide (Nagano et al., 2016), and doxorubicin (Anwar et al., 2016). In the recent study, senescence was induced in U2OS cells through ionizing radiation and doxorubicin treatment. IR-induced DNA damage resulted in senescence of 27% of the population. However, exposure to doxorubicin resulted in development of senescence phenotype (high SA-ß-Gal activity) in 45% of the population. Cell survival improved in Doxorubicin-induced senescence in relative to IR-induced senescence. Nevertheless, the percentage of SA-B-Gal positive cells is low and this is due to the loss of cells during the process of becoming senescent.

Chapter 4

4 Stress Granules in Senescence

4.1 Introduction

As discussed previously, senescent cells display structural and molecular changes in comparison to proliferative cells. Hence, senescent and proliferative cells respond differently to stressors. Constitutive exposure to stress leads to assemblies of granular structures known as stress granules. Moreover, aging, of which senescence is one characteristic, impairs cellular homeostasis, limiting their response to internal and external stressors (Liu et al., 2011; López-Otín et al., 2013; Moujaber et al., 2017).

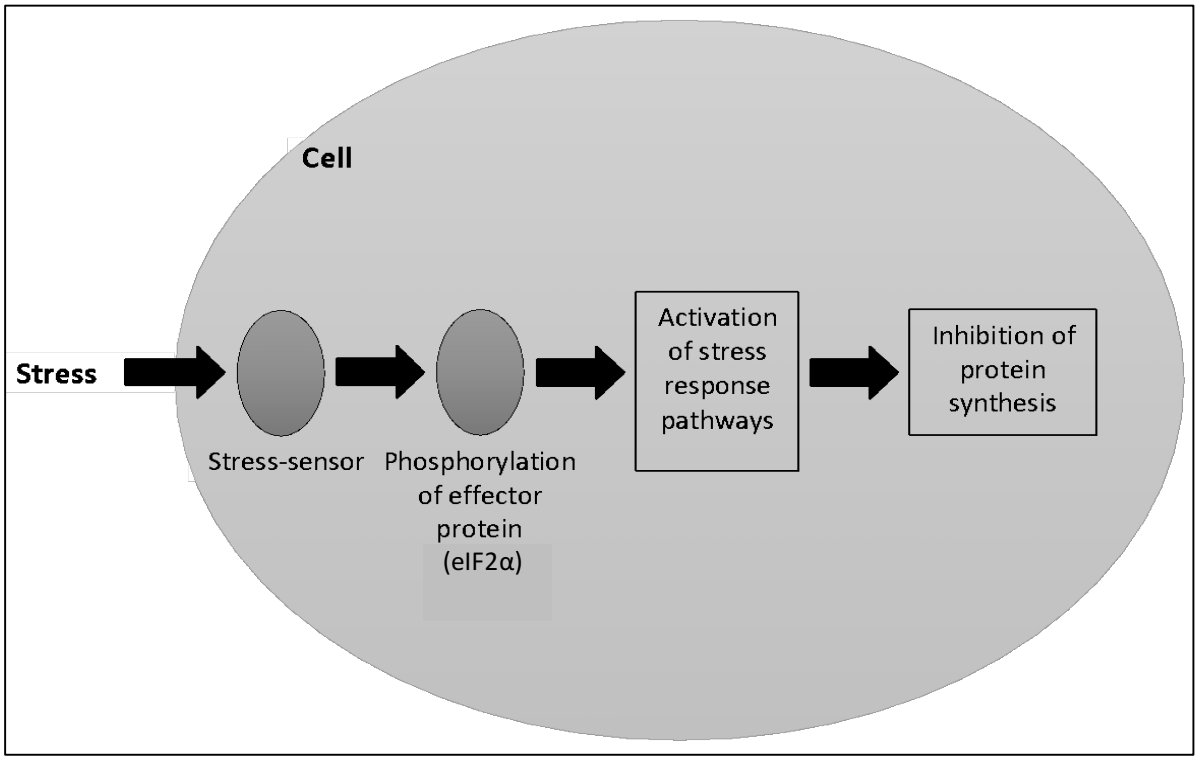

Figure 4.1 Schematic of cell response to stress.

Exposure of cells to stress results in detection of stress by stress-sensors. It then leads to activation of stress response pathways and consequently inhibition of protein synthesis.

Stress granules are non-membranous compartments that are formed upon exposure to stress. They are transient as they assemble in the presence of stress and disassemble when the stress diminishes (Anderson and Kedersha, 2008; Bounedjah et al., 2014; Protter and Parker, 2016; Wheeler et al., 2016). Stress granules are formed when translation initiation is prevented due to stress exposure (Kedersha et al., 1999). In contrast, they fail to form when untranslated mRNAs are associated with ribosomes (Buchan and Parker, 2009).

Stress granules are dynamic structures, showing liquid-like behaviour and are dependent on RNA and proteins for their assembly (Spector, 2006). They contain various RNA-binding proteins, non-RNA-binding proteins and translation initiation factors (Jain et al., 2016). During stress, such as oxidative stress, heat shock, nutrient starvation and osmotic stress, translation initiation is inhibited through phosphorylation of translation initiation factor eIF2α leading to the reduction of availability of eIF2–GTP–$tRNA^{Met}$ ternary complex. In the absence of the ternary complex, formation of 48S preinitiation complex is disrupted producing translationally stalled 48S complex. Subsequently, translating ribosomes run-off polysomes converting them to mRNPs which therefore lead to stress granule assembly (Bordeleau et al., 2005; Anderson and Kedersha, 2009; Kedersha et al., 2013; Van Treeck et al., 2018).

Furthermore, RNA-binding proteins control the localization of untranslated mRNPs to stress granules. G3BP is one of several RNA-binding proteins that regulate stress granule assembly. G3PB plays a major role in the assembly of stress granules when cells are exposed to stress such as oxidative stress. Phosphorylation of G3BP at serine 149 (amino acids 142-205) impairs its ability to nucleate stress granule assembly (Tourrière et al., 2003) suggesting that G3BP is a crucial element in the process of stress granule assembly. In addition to translationally stalled

48S complex that contains untranslated mRNAs, stress granules are composed of poly-A RNA bound to initiation factors (including eIF4A, eIF4G, eIF3, eIF4E), small ribosomal subunits, transcription factors, nucleases, RNA helicases, kinases and molecules involved in signalling (Anderson and Kedersha, 2009; Jain et al., 2016; Moujaber et al., 2017, Youn et al., 2019).

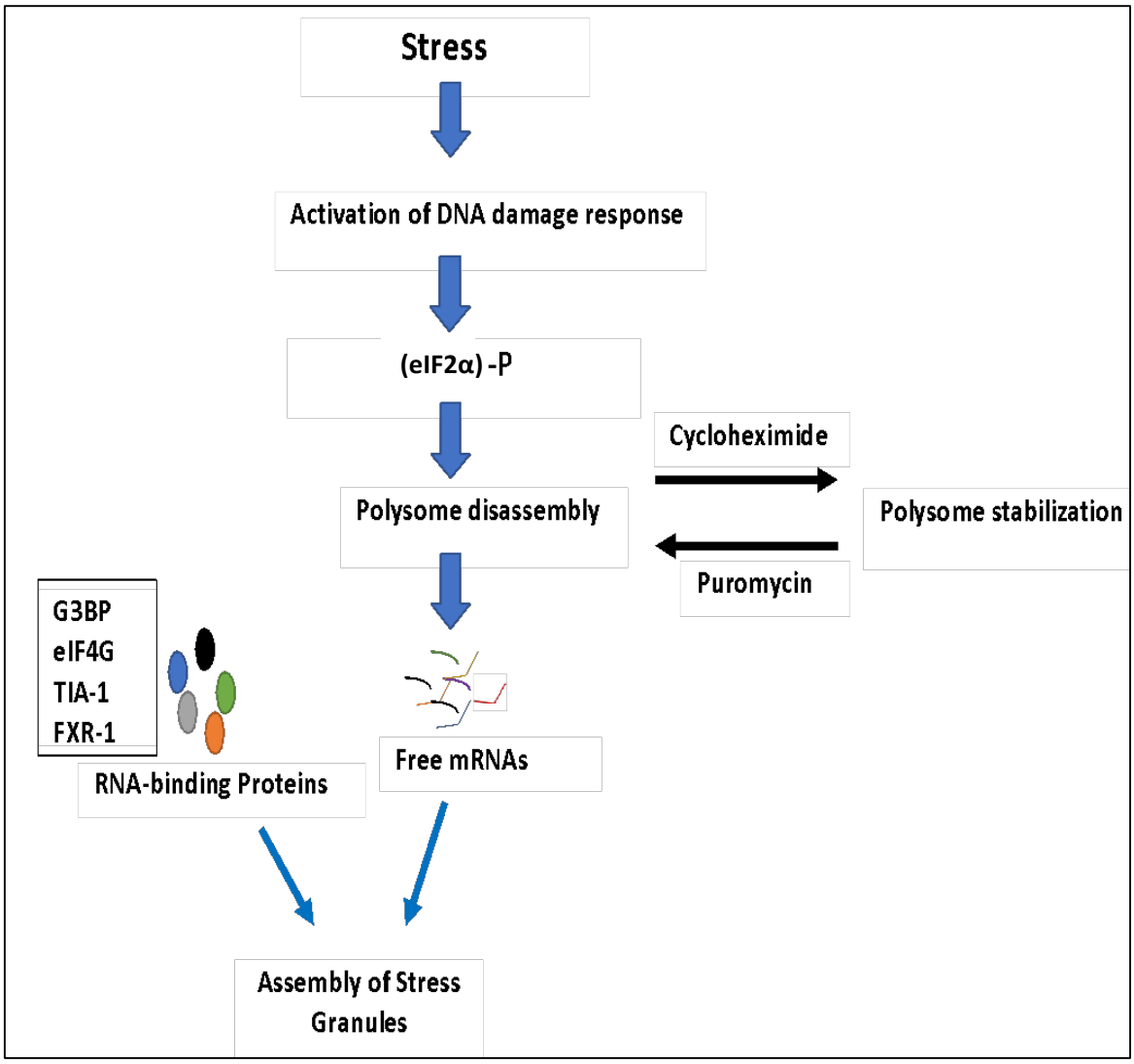

Figure 4.2 Schematic of regulatory components of stress granule assembly.
The untranslated free mRNAs and RNA binding proteins are the essential components of stress granule formation.

Stress granules are important and of interest for many reasons including: 1) their assemblies and dynamics can affect mRNAs translation, localization and degeneration, 2) they share similar mechanism of mRNP compartmentalization as they show similar components to neuronal granules and maternal mRNP, mutations in stress granules, 3) either increase or limit their formation, are causative of some neurodegenerative diseases 4) understanding their assemblies and role represent an exciting and new area to be investigated (Barbee et al., 2006; Li et al., 2013; Ramaswami et al., 2013). Hence, stress granules are formed as a cellular response to environmental stressors including oxidative stress, cold shock, amino acid starvation, heat shock, viral infection, and UV irradiation. However, exposure to X-irradiation or DNA-damaging agents do not promote stress granule assembly (Anderson and Kedersha, 2009).

Senescent cells are persistent and escape elimination. They showed many intracellular bioprocesses disruption such as changes of cellular environment, mitochondrial dysfunction and reduction in protein quality (Cao et al., 2020). These changes affect stress granule formation, explaining the significant reduction in stress granules as cells reach senescence (Moujaber et al., 2017). Senescent cells respond to stressors, however, their response showed impaired stress granule biogenesis (Lian and Gallouzi, 2009; Omer et al., 2018). Loss of proper stress granule formation in senescent kidney cells was suggested to be used as a marker for evaluation of age-related decline of cell function (Moujaber et al., 2017).

4.2 Aims and Objectives

4.2.1 Aims

The chapter aims to examine the response of proliferative and senescent HDF cells to oxidative stress. Hence, the optimal dose and exposure time of cells to the stressor was investigated. To obtain the knowledge on this topic, HDF cells will be cultured in vitro in a growth chamber. Cells reaching 90% confluency will be exposed to different doses of Sodium Arsenite (SA). Moreover, they will be treated for different time lengths. Next, cells will be stained with a stress granule marker: G3BP to count the number of stress granules per cell. Furthermore, recruitment of other RNA-binding proteins to SA-induced stress granules will be examined. Additionally, IR-senescent HDF cells will be treated in a way similar to proliferative cells. However, higher doses and longer exposure time will be applied as senescent cells are persistent and suggested to form improper stress granules. Hence, two stress granule markers: G3BP and eIF4G will be used to detect and count stress granules per cell. Moreover, recruitment of other RNA-binding proteins to SA-induced stress granules in senescent cells will be examined.

Furthermore, response of U2OS cells to SA will be examined. The optimal dose and exposure time of cells to SA will be tested. Stress granule marker: G3BP will be used to detect and count the number of stress granules per cell. Moreover, recruitment of RNA-binding proteins: eIF4G and FXR1 will be investigated.

We hypothesize that proliferative HDF cells form stress granules in response to SA exposure. Moreover, senescent HDF cells form stress granules at higher dose and longer exposure time. SA-induced stress granules showed different composition of RNA-binding proteins.

Additionally, U2OS cells form stress granules in response to oxidative stress. RNA-binding proteins are recruited to the sites of stress granules.

4.2.2 Objectives

1. Induce stress granule formation in HDF cells through using sodium arsenite (SA).

2. Characterize SA-induced stress granules and detect the RNA-binding proteins recruited to stress granules.

3. Induce stress granule formation in U2OS cells.

4. Examine the RNA-binding proteins recruited to SA-induced stress granules.

4.3 Materials and Methods

4.3.1 Materials

All chemicals were purchased from Sigma unless stated otherwise.

4.3.2 Methods

As described in chapter 2.

4.4 Results

4.4.1 Stress Granules in Proliferative and Senescent HDF Cells

4.4.1.1 Optimal Dose and Exposure Time of SA in Proliferative HDF Cells

4.4.1.1.1 Dose

Stress granules are formed when cells are exposed to stressors such as viral infection, oxidative, heat and starvation stress (Anderson and Kedersha, 2002, 2006, 2009; Buchan and Parker, 2009; White and Lloyd, 2012). To investigate the response of HDF cells to oxidative stress, sodium arsenite (SA) was introduced to proliferative HDF cells. Several concentrations of SA were used to monitor the optimal dose for stress granule assembly. Therefore, the following SA concentrations: 0 (control), 0.5, 1.0, 2.0, 4.0, and 6.0 mM were used. Subsequently, cells were fixed and stained with a stress granule marker: G3BP1 which is the commonly used marker for stress granules as it plays a critical role in stress granule assembly. Hence, control cells (0 mM SA) showed no aggregation of stress granules. Furthermore, cells started showing formation of stress granules at dose 0.5 mM SA. Number of stress granules increased at 1.0 mM SA. However, when the dose was increased (2.0-6.0 mM), the number of stress granules decreased gradually. At 6.0 mM SA, stress granules started to disassemble in most cells (Figure 4.3).

Number of observed stress granules per cell was counted using ImageJ. Thus, proliferative HDF cells showed an average of 9 and 10 SGs/cell when exposed to 0.5 and 1.0 mM SA, respectively, for 30 min. However, cells showed a decrease in the number of stress granules as SA dose increased. An average of 6, 5, and 4 SGs/cell was detected in cells when exposed to 2.0, 4.0, and 6.0 mM, respectively, for 30 min (Figure 4.4). Therefore, 1.0 mM SA will be used as the optimal dose for studying stress granules in proliferative HDF cells.

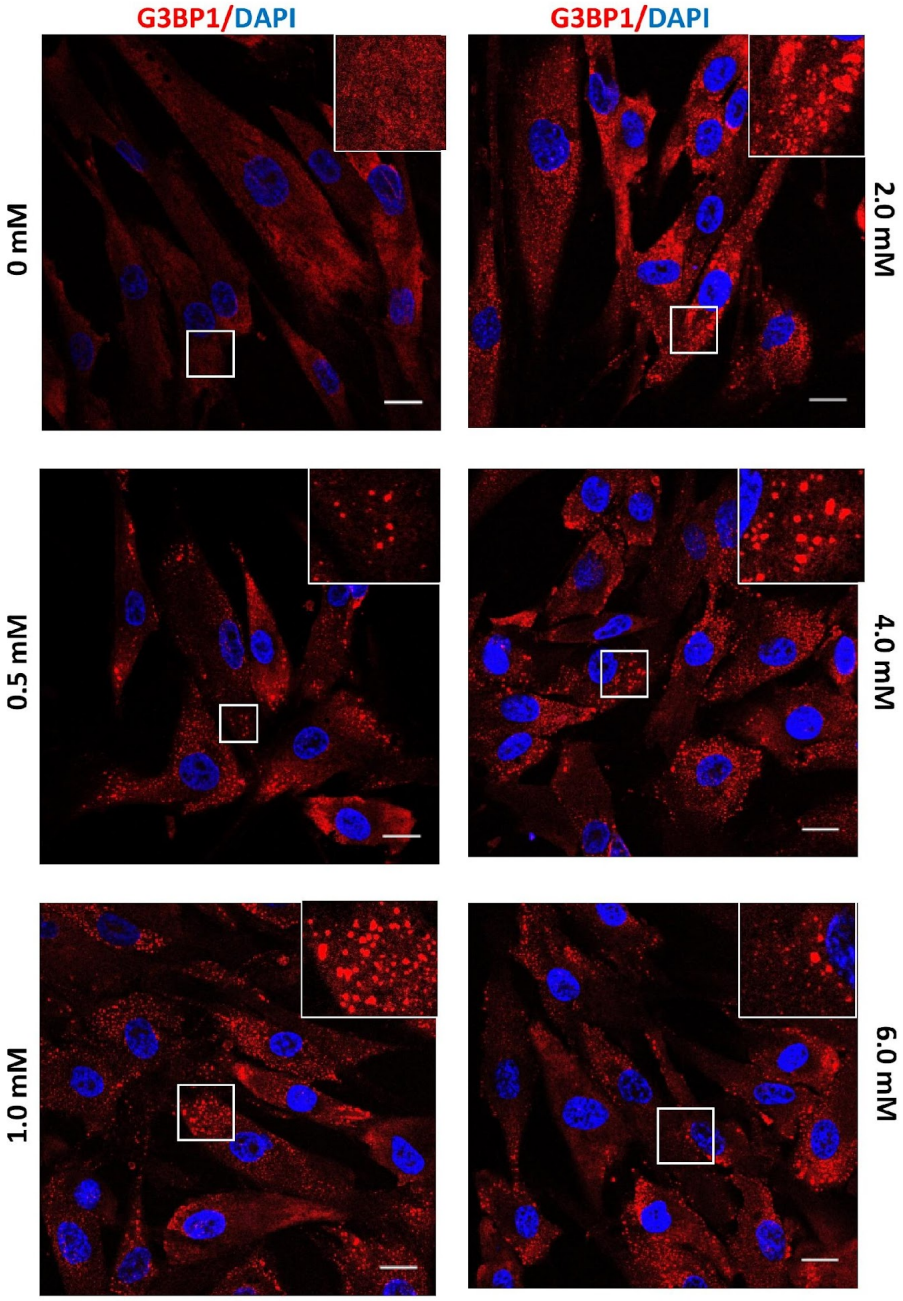

Figure 4.3 Sodium arsenite optimal dose to induce stress granules in proliferative HDF cells.

HDF cells were treated with different SA doses. Cells exposed to 1.0 mM SA showed the highest aggregation of G3BP1 granules. The number of granules decreased as SA concentration increased to 2.0-6.0 mM. 1.0 mM SA was used as the optimal dose for SG induction in proliferative HDF cells. Scale bar= 20 um.

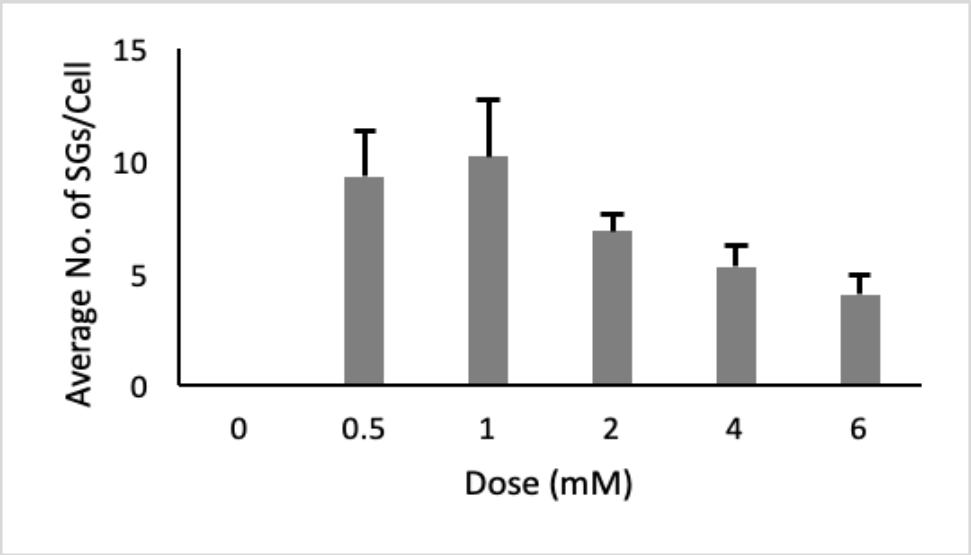

Figure 4.4 1.0 mM SA induces the highest number of stress granule aggregation in proliferative HDF cells.

A range of SA concentrations (0-6 mM) was used to test stress granule formation. Cells started forming stress granules at dose 0.5 mM, however, 1.0 mM showed the highest aggregation of stress granules. Data represents mean ± SEM n=3, statistical significance was assessed using ANOVA t-test.

4.4.1.1.2 Exposure Time

To test the optimal exposure time, proliferative HDF cells were treated with the optimal SA dose 1.0 mM (see section 4.4.1.1.1**)** for the following time periods: 0 (control), 10, 15, 30, 45, 60, 90 and 120 min. Cells were then fixed and stained with G3BP1 antibody. Hence, control cells did not show any aggregation of stress granules. At 10 and 15 min following SA treatment, cells did not show formation of stress granules. 30 min post-SA exposure, mature well-defined stress granules were detected in the cytoplasm of cells. Under long exposure to stress, cells are suggested to lose their ability to form/maintain stress granules. Therefore, at 45 and 60 min of SA exposure, the number of stress granules decreased significantly. Unexpectedly, 90 min of SA exposure showed an increase in the number of stress granules. However, they were detected to disassemble at 120 min in most cells (Figure 4.5).

Number of stress granules per cell was counted using ImageJ. Therefore, no stress granules were formed at 0, 10 and 15 min of SA exposure. At 30 min of SA exposure, an average of 11 SGs/cell were detected. However, the number of stress granules were observed to reduce to 8 SGs/cell and 3 SGs/cell at 45 and 60 min, respectively. Moreover, at 90 min post-SA exposure, a slight increase in stress granules was detected (4 SGs/cell) which then decreased significantly to ~1 SGs/cell. G3BP1 was used as a marker for stress granules in treated cells (Figure 4.6). Considering the above results, 30 min is used as the optimal exposure time to SA. Thus, in proliferative HDF cells, stress granules require 30 min of SA exposure to be formed and detected.

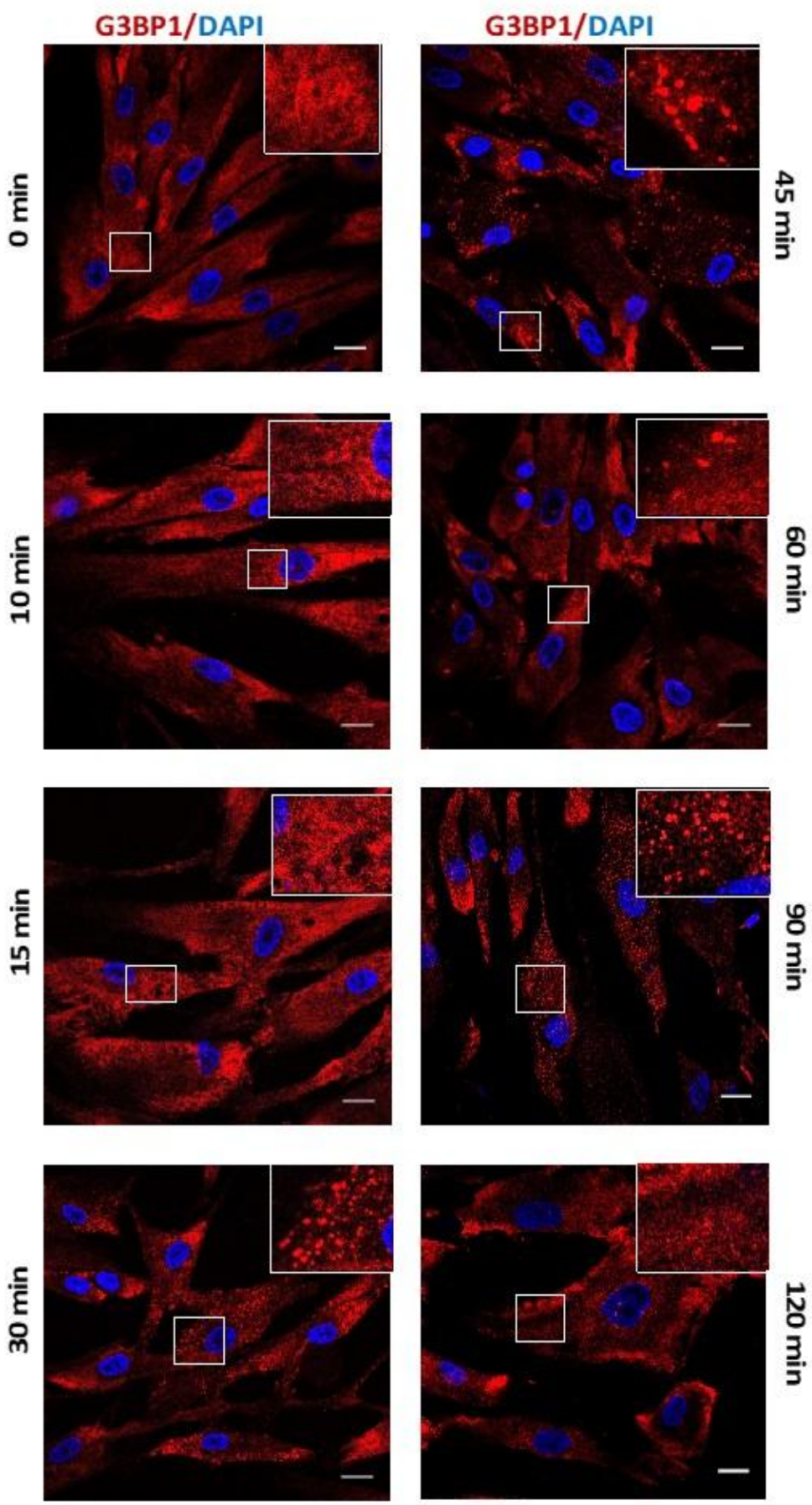
G3BP1/DAPI
G3BP1/DAPI
0 min
45 min
10 min
60 min
15 min
90 min
30 min
120 min

Figure 4.5 Proliferative HDF cells exposed to 1.0 mM SA for different time periods. HDF cells were exposed to 1.0 mM SA for 0, 10, 15, 30, 45, 60, 90 and 120 min. G3BP1 (red) was used as a marker for stress granules. Cells showed the highest assembly of stress granules after 30 min of SA exposure. Whereas, the lowest number of stress granules was detected at 120 min. 30 min was used as the optimal time of SA exposure in HDF cells. Scale bar= 20 um.

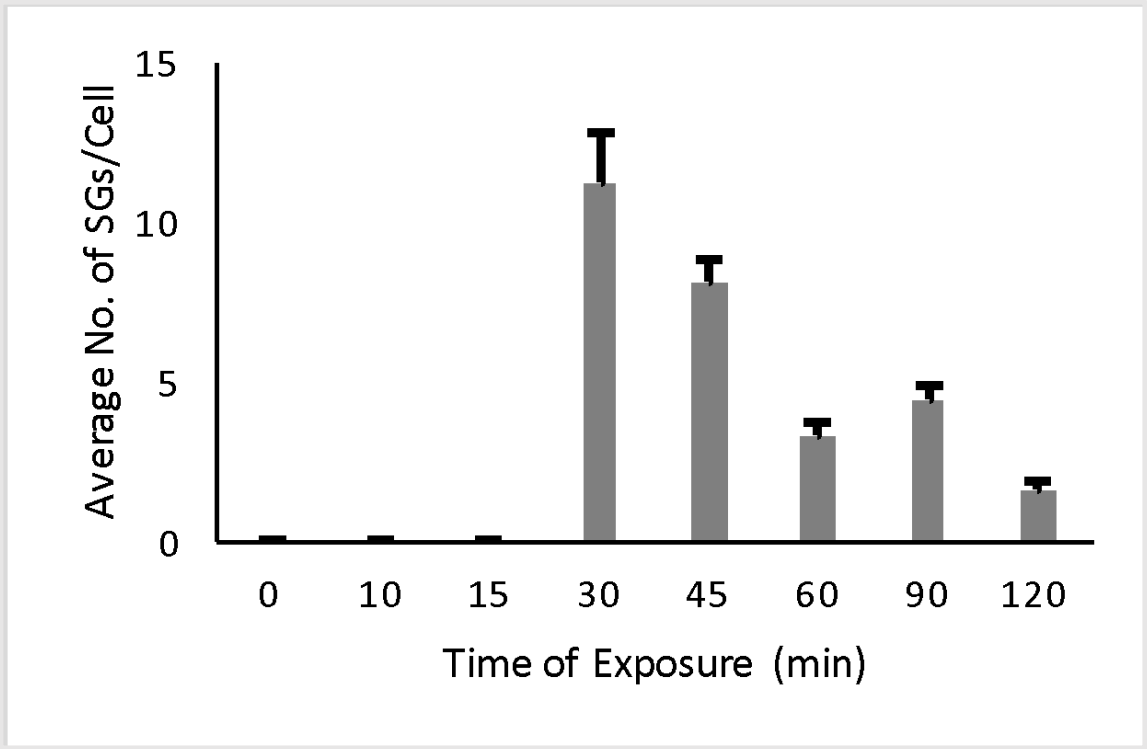

Figure 4.6 Proliferative HDF cells treated with SA at different exposure time. 30 min of SA exposure (1.0 mM) showed the highest assembly of stress granules. Whereas at 120 min most of cells lost their ability to form/maintain stress granules. Data represents mean ± SEM n=3, statistical significance was assessed using ANOVA t-test.

4.4.1.2 Optimal Dose and Exposure Time of SA in IR-Senescent HDF Cells

4.4.1.2.1 Dose

Several studies have detected that proliferative and senescent cells respond differently to stress (Lian and Gallouzi, 2009). Hence, to investigate the response of senescent HDF cells to oxidative stress, cells were treated with SA. First, to examine the required SA dose, senescent HDF cells were exposed to the following concentrations: 0 (control), 0.5, 1.0 and 2.0 mM for 40 min (Figure 4.7). G3BP1 was used as a marker for stress granules (Red). Thus, G3BP1 was detected to be diffused in the cytoplasm at 0 mM SA while a partial aggregation was detected at 0.5 mM SA. Moreover, aggregation of stress granules was detected at 1.0 and 2.0 mM SA. However, the highest aggregation was observed when using 1.0 mM SA suggesting that 1.0 mM SA is sufficient to induce formation of stress granules in senescent HDF cells (Figure 4.7A).

Furthermore, the number of stress granules was counted using ImageJ. Thus, control cells (0 mM SA) showed no assembly of stress granules. The G3BP1 protein was observed to be diffuse in the cytoplasm. Hence, when cells were exposed to 0.5 mM, few aggregates of stress granules (~3 SGs/cell) were detected. This observation shows that upon exposure to 0.5 mM SA, senescent HDF cells start to show assembly of stress granules. Additionally, exposure of senescent cells to higher doses: 1.0 and 2.0 mM showed assembly of an average of ~9 SGs/cell and 3 SGs/cell, respectively (Figure 4.7B). Thus, G3BP1 is still observed diffused in the cytoplasm at 1.0 and 2.0 mM. It indicates that stress granules are not properly formed in senescent cells. Indeed, as the higher aggregation of stress granules was detected at 1.0 mM, it was considered as the optimal dose for the induction stress granules in IR-induced senescent HDF cells.

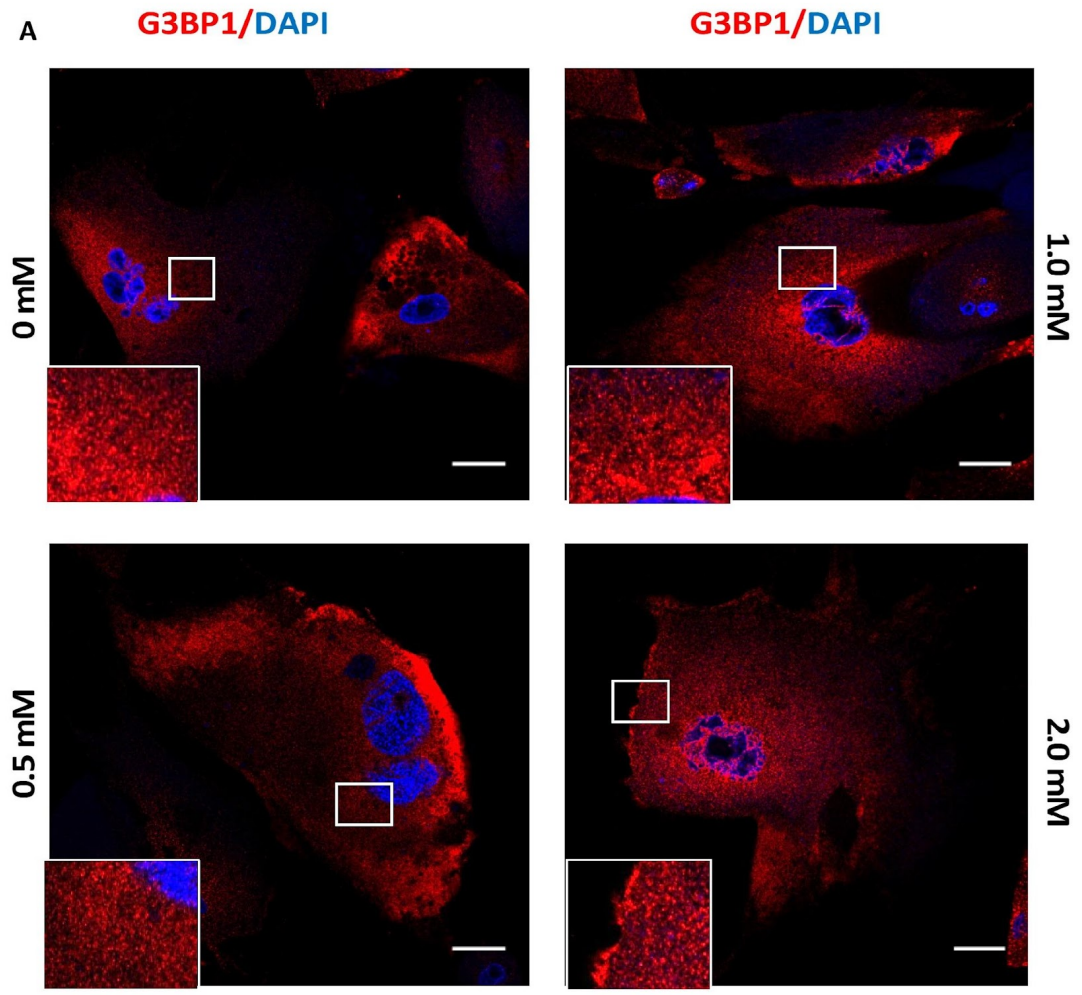

B

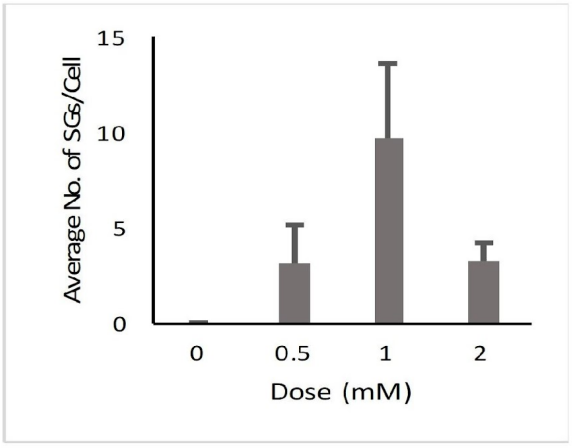

Figure 4.7 1.0 mM SA Induces stress granules in senescent fibroblast cells.

Cells were exposed to SA for 40 min. They were then stained with G3BP1 antibody (red) (A). 1.0 mM showed the highest assembly of stress granules in senescent HDF cells. While 0.5 and 2.0 mM showed almost similar number of SGs/cell (B). Scale bar= 20 um. Data represents mean ± SEM n=3, statistical significance was assessed using ANOVA t-test.

4.4.1.2.2 Exposure Time

To test the optimal time of SA exposure required to induce stress granule formation in IR-induced senescent HDF, cells were exposed to SA for different time intervals. Therefore, cells were exposed to 1.0 mM SA for the following time periods: 0, 30, 45, 60, 90 and 120 min. Cells were then stained with G3BP1 (Green) and eIF4G (Red) (Figure 4.8). eIF4G has been used as a marker for stress granules induced by oxidative stress. It is eukaryotic translation initiation factor 4 G which is involved in translation initiation. Thus, eIF4G has been detected to localize to stress granules when exposed to oxidative stress (Kedersha et al., 2016). Therefore, in addition to G3BP1, eIF4G is used in our study as a marker for stress granules in senescent HDF. Therefore, assembly of G3BP1 was first detected in cells following 30 min of SA exposure. However, after 45, 60, 90 and 120 min, assembly of G3BP1 was detected. Localization of eIF4G was also observed following 45, 60, 90 and 120 min of SA exposure. Hence, this explains the main role of G3BP1 in the assembly of stress granules in cells as it was detected as soon as the stress granules started to form. Moreover, the recruitment of eIF4G to stress granules was observed 15 min following the formation of stress granules. This indicates that mature stress granules which involve G3BP1 and eIF4G, form in senescent HDF cells 45 min following SA exposure.

Moreover, 45 min post SA exposure, cells showed the highest assembly of stress granules: ~10 SGs/cell. However, they showed ~4, 3, 3, and 5 SGs/cell after 30, 60, 90 and 120 min of exposure to 1.0 mM SA (Figure 4.9). Therefore, 45 min is used as the optimal exposure time of SA in senescent HDF cells.

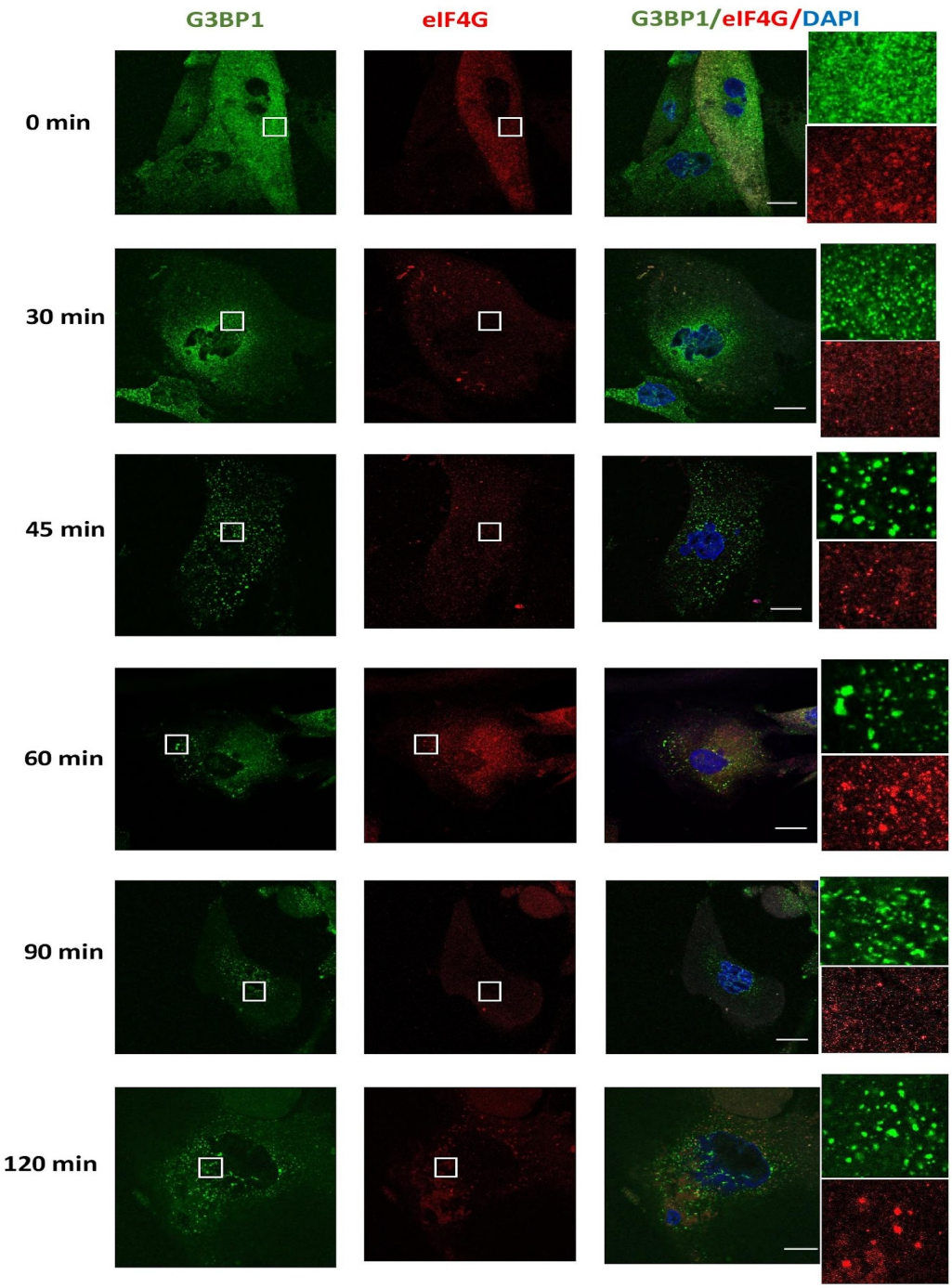

Figure 4.8 Senescent HDF cells were exposed to SA at different exposure time.

Cells were exposed to SA at different time periods and then stained with G3BP1 and eIF4G. It was observed that after 45 min of SA exposure, G3BP1 and eIF4G were observed to locate at sites of stress granules. Scale bar= 20 um.

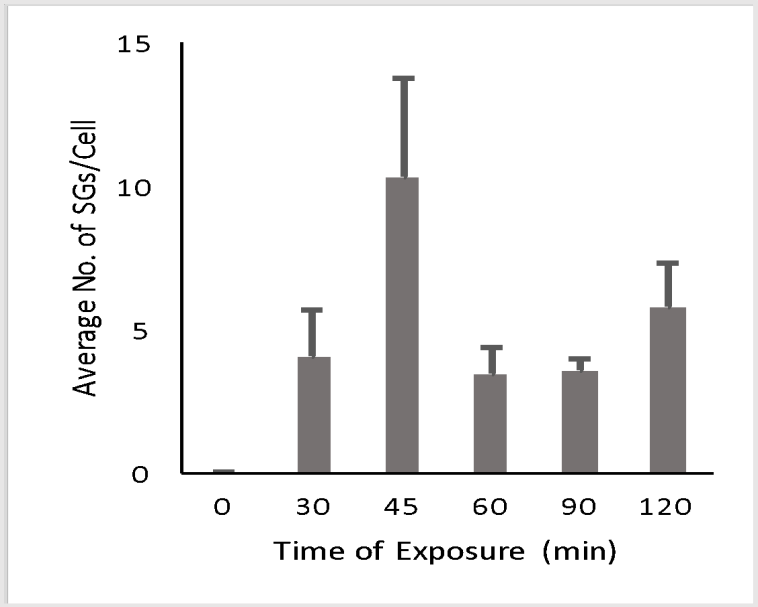

Figure 4.9 Senescent HDF cells were exposed to SA at different time length. Cells stained with G3BP1 and eIF4G showed that after 45 min of SA exposure, G3BP1 and eIF4G SGs were observed. An average of 10 SGs/cell were formed after 45 min. Therefore, 45 min was used as the optimal exposure time in senescent cells. Data represents mean ± SEM n=3, statistical significance was assessed using ANOVA t-test.

4.4.2 Stress Granules in U2OS Cells

4.4.2.1 SA Optimal Dose and Exposure Time in U2OS Cells

4.4.2.1.1 Dose

Response of cells to stress depends on the type of cell (primary cells or cancerous cell lines) and stressor (such as oxidative stress and heat shock) (Anderson and Kedersha, 2002; White and Lloyd, 2012). U2OS cells have been used widely in stress granules studies as they provide a good system in culture. They are easy to grow and harvest. The doubling time of U2OS cells is ~24 hours (Russo et al., 2006). Moreover, U2OS cells are reliable and have been introduced to different stimuli (oxidative stress, viral infection and heat shock). Additionally, changes at gene level have been introduced in U2OS cells in order to examine the role of certain gene/protein (Kedersha et al., 2008; 2016). Hence, in this study U2OS cells are used as they provide a reliable system to study stress granules and role of G3BP in stress response and senescence mechanism.

Therefore, in the recent study, U2OS cells were used to provide a clear understanding of stress granules and their role in senescence. To start this study, the optimal dose of SA was examined. Hence, U2OS cells were exposed to the following concentrations of SA: 0, 0.1, 0.2, 0.5, 1.0 and 2.0 mM SA for 30 min. The cancerous U2OS cells are delicate and therefore we used less concentrated SA (Kedersha et al., 2005). Cells were then stained with G3BP1 antibody (Green) (Figure 4.10A). Control (0 mM) cells did not show any formation of stress granules. Moreover, stress granules were first detected in few cells when they were exposed to 0.2 mM SA. When 0.5 mM SA was applied to cells, the number of stress granules increased significantly. However, stress granule number decreased at 1.0 and 2.0 mM SA. This indicates that 0.5 mM SA is the optimal dose for the induction of stress granules in U2OS cells.

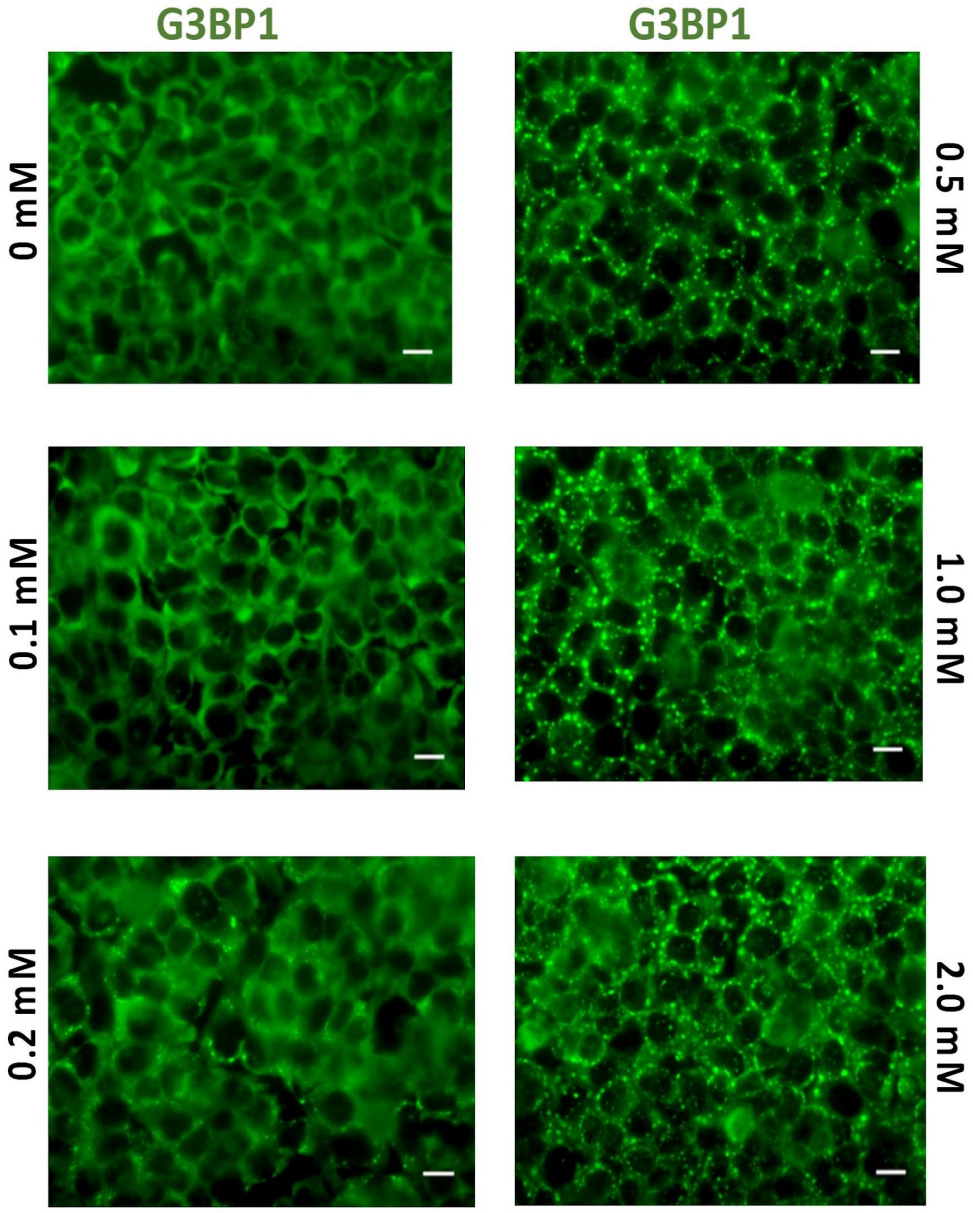

Figure 4.10 WT U2OS cells treated with different concentrations of SA.
WT U2OS cells were treated with 0, 0.1, 0.2, 0.5, 1.0 and 2.0 mM SA. Cells were stained with G3BP1 (Green). The first detection of stress granules was at 0.2 mM SA. At 0.5 mM SA, number of stress granules increased significantly. The number of stress granules reduced at 1.0 and 2.0 mM SA. Scale bar=20 um.

To count the number of stress granules per cell, ImageJ was used. The average number of stress granules per cell (SGs/cell) was calculated. Hence, control cells (0 mM SA) and cells treated

with 0.1 mM SA showed no formation of stress granules. Moreover, an average of ~1, 18, 10 and 7 SGs/cell were detected in cells when exposed to 0.2, 0.5, 1.0 and 2.0 mM SA, respectively (Figure 4.11). Thus, 0.5 mM SA induced the highest assembly of stress granules. Furthermore, the decrease in number of stress granules at 1.0 and 2.0 mM SA is suggested to result from fusion of smaller granules forming bigger ones. Therefore, 0.5 mM SA was used as the optimal dose of SA to induce SGs assembly in U2OS cells.

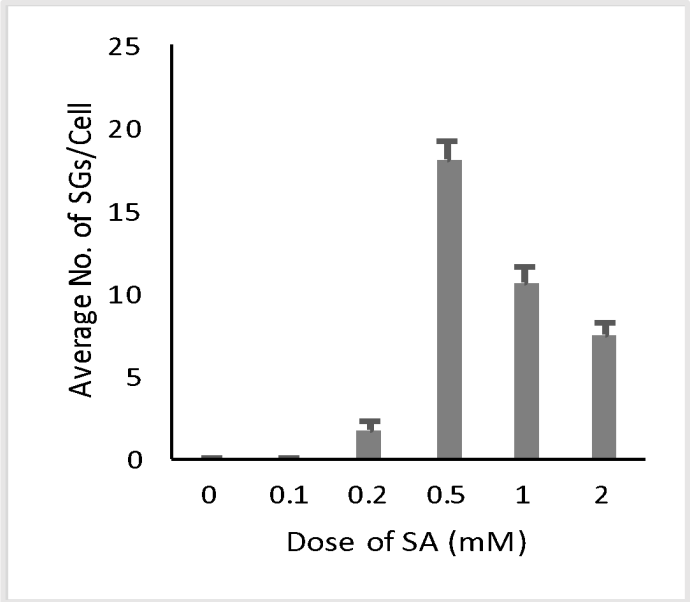

Figure 4.11 The optimal dose of SA to induce stress granule assembly in U2OS cells.

The following concentrations: 0, 0.1, 0.2, 0.5, 1.0 and 2.0 mM of SA were used to test the optimal dose of SA for the induction of stress granule formation in U2OS cells. Cells exposed at 0.5 mM SA showed the highest number of stress granule assembly (18 SGs/cell). The number of stress granules reduced at 1.0 and 2.0 mM SA to 10 and 7 SGs/cell, respectively. Data represents mean ± SEM n=3, statistical significance was assessed using ANOVA t-test.

4.4.2.1.2 Exposure Time

Following the determination of the optimal SA dose, time length of SA exposure was examined. Thus, U2OS cells were treated with 0.5 mM SA (section 4.4.2.1.1) for: 0 (control), 15, 30, 45, 60, 90 and 120 min. Cells were then stained with G3BP1 (Green) and eIF4G (Red) antibodies (Figure 4.12). G3BP1 is known to nucleate stress granules and thus it is used as a marker for stress granules. Therefore, in addition to G3BP1, eIF4G was used in this experiment as a second marker for stress granules. Control (0 min of SA exposure) cells did not show assembly of stress granules. G3BP1 and eIF4G were observed diffused in the cytoplasm. Hence, after 15 min of SA exposure, cells showed no/few assembly of stress granules. Following 30 min of SA exposure, cells showed a significant increase in the number of stress granules. Both G3BP1 and eIF4G showed localization to the site of stress granule assembly. Surprisingly, the number of stress granules decreased after 45 min of SA exposure. Furthermore, the number of stress granules was detected to rise after 60 min of SA exposure. At 90 and 120 min of SA exposure, cells showed a consistent number of stress granules. G3BP1 and eIF4G showed localization to the sites of stress granule assembly.

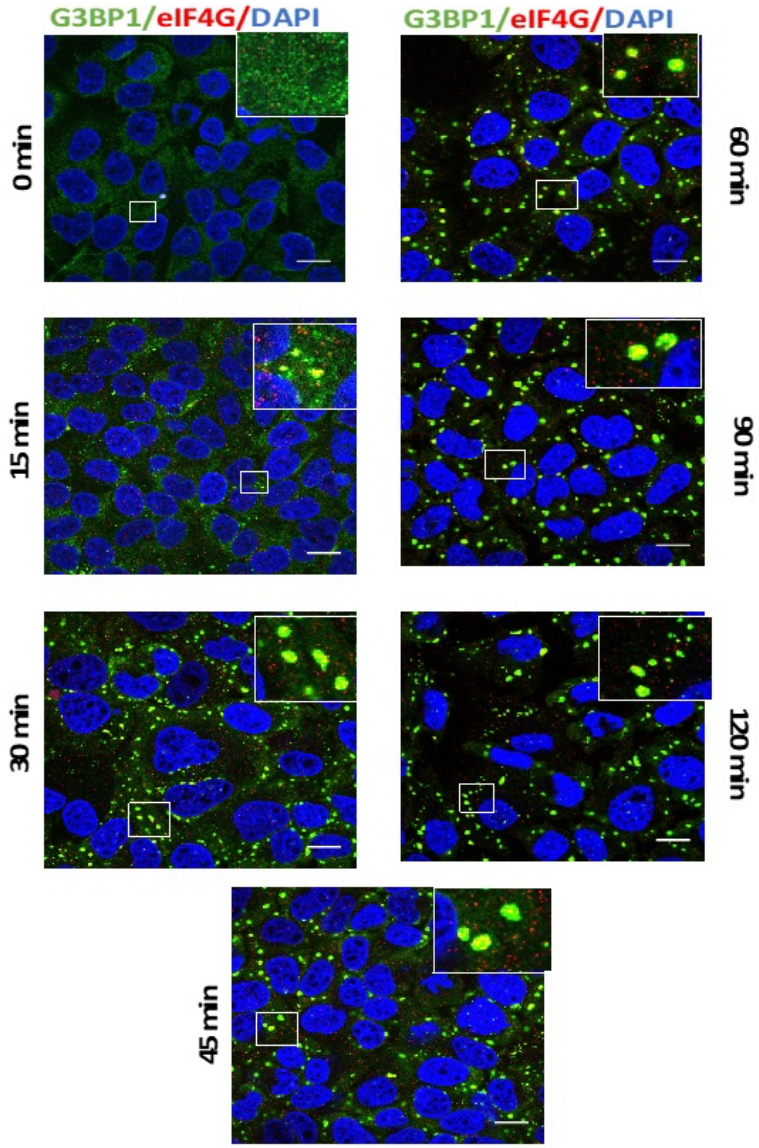

Figure 4.12 Determination of the optimal time length of SA exposure in U2OS cells. U2OS cells were exposed to 0.5 mM SA for different time periods: 0, 15, 30, 45, 60, 90 and 120 min. Cells were harvested and stained with stress granules markers G3BP1 (Green) and eIF4G (Red). Control cells (0 min) showed no assembly of stress granules. Number of stress granules increased significantly after 30 min of SA exposure. The number of stress granules decreased at 45 min following SA exposure. The number of stress granules increased after 60 min and remained consistent at 90 and 120 min. Scale bar= 20 um.

Furthermore, the number of stress granules formed upon exposure to 0.5 mM at different time periods was counted using ImageJ. Hence, control cells (0 min) showed no formation of stress granules. At 15 min after SA exposure, an average of ~2 SGs/cell was detected. The highest assembly of stress granules was observed after 30 min of SA treatment. An average of ~26 SGs/cell was detected. Unexpectedly, a reduction in stress granule number was observed at 45 min of SA exposure. The number declined to ~11 SGs/cell. Thus, at 60 min, the number of stress granules rose to 22 SGs/cell. Moreover, at 90 and 120 min, an increase in stress granules was counted. Exposure of cells to SA for 90 and 120 min was observed to induce formation of 24 SGs/cell (Figure 4.13). Therefore, exposure time of 30 min was used as the optimal SA exposure time required for the induction of stress granules in U2OS cells.

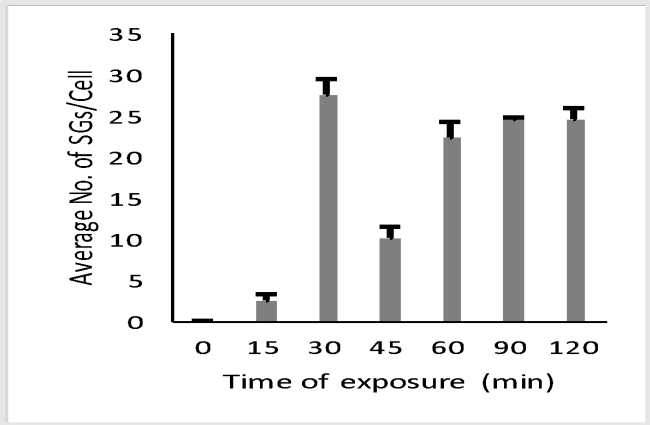

Figure 4.13 WT U2OS cells exposed to 0.5 mM SA for different time periods. Cells exposed to SA for 0, 15, 30, 45, 60, 90 and 120 min. Control cells (0 min) showed no assembly of stress granules. ~2 SGs/cell was detected in cells at 15 min of SA exposure. SA exposure for 30 min showed the highest assembly of 27 SGs/cell. After 45 min, stress granule number reduced to 10 SGs/cell. The number of stress increased to 22 SGs/cell after 60 min of SA exposure. Stress granule number rose at 90 min to 24 SG/cell and remained consistent at 120 min. Data represents mean ± SEM n=3, statistical significance was assessed using ANOVA t-test.

4.4.2.2 Stress Granule Factors in HDF Cells

4.4.2.2.1 G3BP1

The RNA-binding protein G3BP1 is one of the main components of stress granules. It is essential for the assembly process of stress granules. Hence, studies have shown that knockdown of G3BP1 reduced the assembly of stress granules in differentiating erythroid cells (Ghisolfi et al., 2012). Furthermore, knockout of G3BP1 and G3BP2 prevents the assembly events of stress granules (Kedersha et al., 2016).

In this study, we investigate the assembly of stress granules in HDF cells and the recruitment of different RNA-binding proteins to stress granules. Hence, proliferative HDF cells were treated/untreated with 1.0 mM SA for 30 min. Additionally, IR-induced senescent HDF cells and replicative senescent HDF cells were treated/untreated with 1.0 mM SA for 45 min. Cells were then fixed and stained with G3BP1 antibody (Figure 4.14, 4.15). In the untreated proliferative (Day 0) cells, G3BP1 was detected diffused in cytoplasm. Treated cells showed assembly of stress granules and recruitment of G3BP1 to sites of stress granules. Moreover, untreated Day 7, Day 14 and Day 21 (post-IR exposure) cells did not show assembly of stress granules. G3BP1 was observed diffused in the cytoplasm. Thus, SA-treated Day 7, Day 14 and Day 21 cells showed formation of stress granules and localization of G3BP1 at sites of stress granule assembly. However, Day 14 and 21 cells showed reduction in number and size of stress granules (Figure 4.14). Therefore, stress granule assembly is suggested to be impaired in IR-induced senescent cells and consequently G3BP1 recruitment to stress granules.

Furthermore, replicative senescent HDF cells were treated/untreated with SA. They were then stained with G3BP1 antibody (Figure 4.15). Untreated cells did not show formation of stress granules. G3BP1 was observed diffused in the cytoplasm. Hence, SA-treated replicative

senescent cells showed reduced assembly of stress granules and thus localization of G3BP1 to stress granule sites. It is suggested that the stress granule formation process is impaired in senescent cells. The improper size and number of stress granules is suggested to be a feature of the persistent senescent cells.

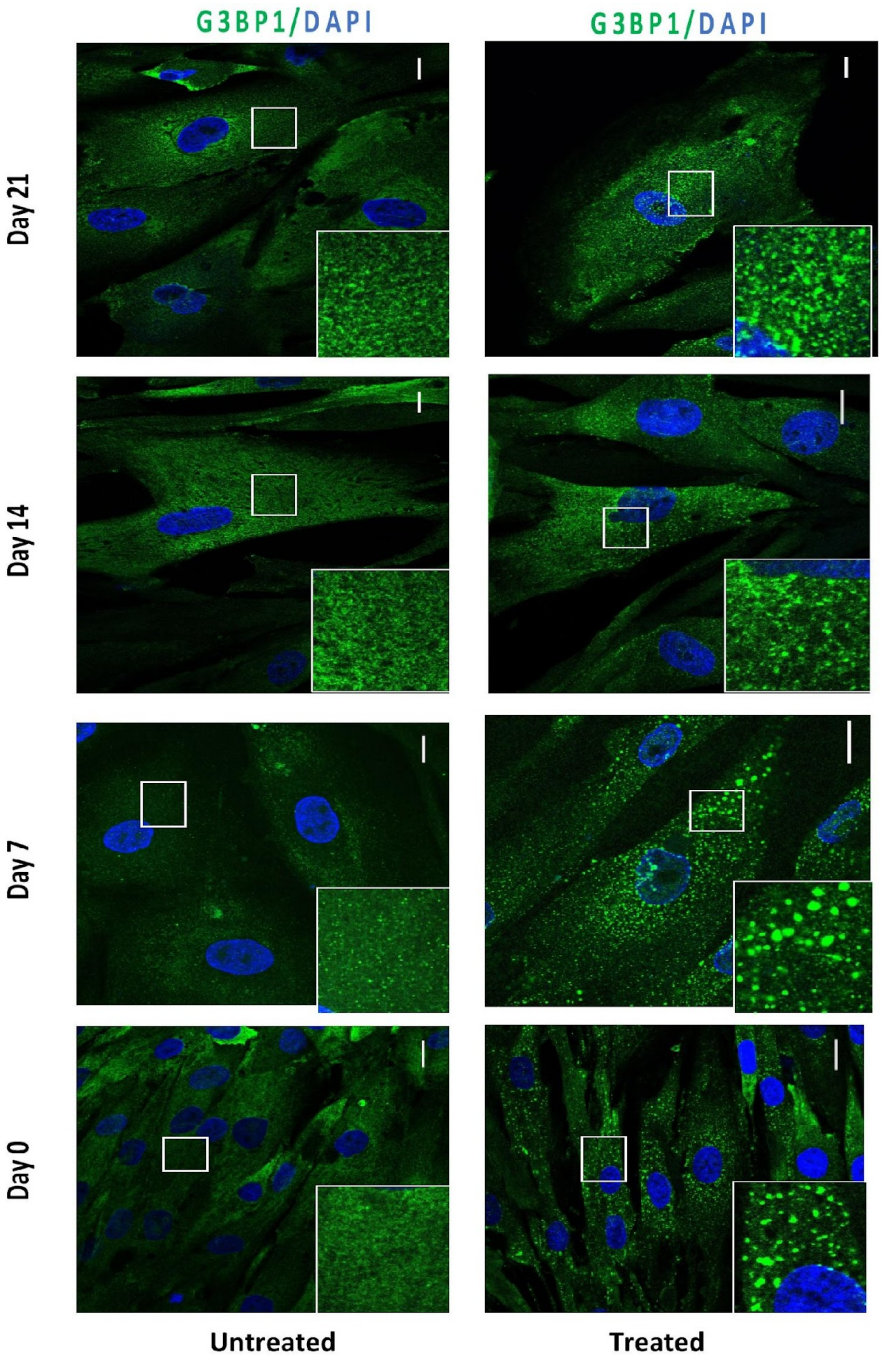

Figure 4.14 G3BP1 recruitment to SA-induced stress granules in HDF proliferative and IR-induced senescent cells.

Proliferative and IR-induced senescent cells were treated/untreated with 1.0 mM SA and stained with G3BP1 antibody (Green). G3BP1 was observed diffused in untreated cells. Stressed cells showed formation of stress granules. Day 0 (proliferative) cells showed formation of stress granules. At Day 7, 14, and 21 post IR exposure, number of stress granules reduced. Scale bar= 20 um.

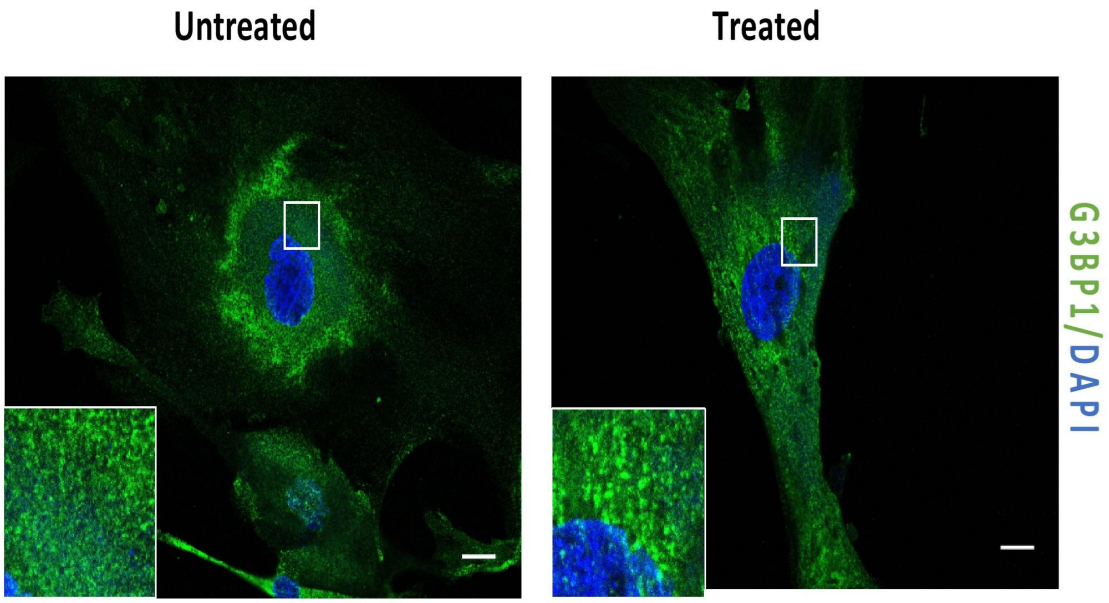

Figure 4.15 Stress granule formation and recruitment of G3BP1 in replicative senescent HDF cells.

Replicative senescent cells were treated/untreated with 1.0 mM SA for 45 min. Cells were stained with G3BP1 antibody (Green). G3BP1 was detected diffused in untreated cells. Treated cells showed formation of small stress granules. G3BP1 was detected to be localized to stress granules sites. Scale bar= 20 um.

Furthermore, the number of stress granules in proliferative, IR-induced senescent and replicative senescent HDF cells was counted and compared using ImageJ. The number of stress granules per cell (SGs/cell) was used as representative of SA-induced stress assemblies in each cell group (Figure 4.16). Accordingly, SA-treated proliferative (Day 0) cells showed an average of ~26 SGs/cell. Moreover, treated Day 7 cells showed a reduced stress granule number: ~17 SG/cell. At Day 14 and Day 21 post-IR exposure, ~15 and 12 SGs/cell were detected, respectively. Thus, a reduction in the number of stress granules was detected as cells progress to senescence. Additionally, replicative senescent cells showed a significant reduction in the number of stress granules: ~6 SGs/cell. Therefore, the impaired stress granule assembly

and thus recruitment of G3BP1 to stress granules was observed in IR-induced and replicative senescent cells. This data suggests that as cells progress to senescence, their ability to form stress granules is impaired and hence the recruitment of RNA-binding proteins such as G3BP1 to the locations of stress granule assembly.

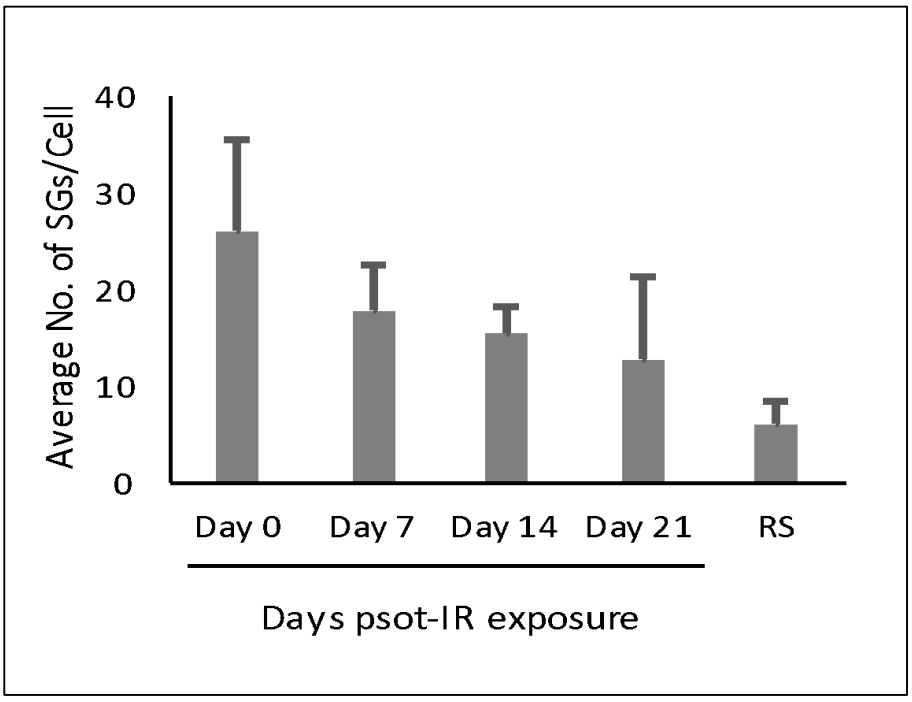

Figure 4.16 Stress granule number in SA-treated proliferative, IR-induced and replicative senescent cells.

The number of stress granules per cell was counted using ImageJ. Proliferative (Day 0) cells showed ~26 SGs/cell. IR-treated cells showed a reduction of stress granule number as they progress towards senescence (Day 14 and 21). They showed ~17, 15 and 12 SGs/cell at Day 7, 14 and 21, respectively. Replicative senescent cells showed ~6 SGs/cell. Data represents mean ± SEM n=3, statistical significance was assessed using ANOVA t-test.

4.4.2.2.2 Stress Granule Factors Other Than G3BP1

4.4.2.2.2.1 TIA-1

Several RNA-binding proteins have been studied and observed to play a crucial role in the initiation process of stress granule assembly. Hence, components such as T-cell intracellular antigen-1 (TIA-1), Caprin and fragile X mental retardation syndrome-related protein 1 (FXR1) can also initiate stress granule assembly depending on the type of the cells and stressor. Thus, TIA-1 is known to promote translation arrest when cells are exposed to an assault. TIA-1 is an RNA-binding protein that has been detected at sites of stress granules. It consists of three domains that are required for the assembly of stress granules (Dember et al., 1996). Hence, lacking of RNA-binding domains (TIA-1ΔRRM) but Overexpression of a mutant encoding PRD domain which is essential for the assembly of stress granules prevents the assembly process of stress granules in COS transfectants (Kedersha et al., 1999).

Hence, in our study, we investigate the stress granule assembly and recruitment of TIA-1 to SA-induced stress granules. Therefore, proliferative (Day 0), IR-induced senescent and replicative senescent cells were treated with/without 1.0 mM SA for 30 (replicative cells) and 45 (senescent cells) min. Cells were then fixed and stained with TIA-1 antibody (Figure 4.17). In SA-untreated proliferative cells, TIA-1 was observed to locate at the nuclei (Figure 4.17A). Moreover, in treated proliferative cells, TIA-1 remained at the nuclei. Additionally, when IR-induced senescent cells were untreated with SA, TIA-1 was detected at the nuclei. Similarly, SA-treated IR-induced senescent cells (Day 7 and Day 14 post-IR exposure) did not show localization of TIA-1 to sites of stress granule assembly. Replicative senescent cells were observed to form stress granules but did not show recruitment of TIA-1 at sites of stress granule assembly. The SA-untreated replicative HDF cells showed localization of TIA-1 at the nuclei of cells (Figure 4.17B). This data might indicate that TIA-1 has no observed role in stress-

induced translational arrest, stress granule assembly in proliferative, IR-induced and replicative senescent cells.

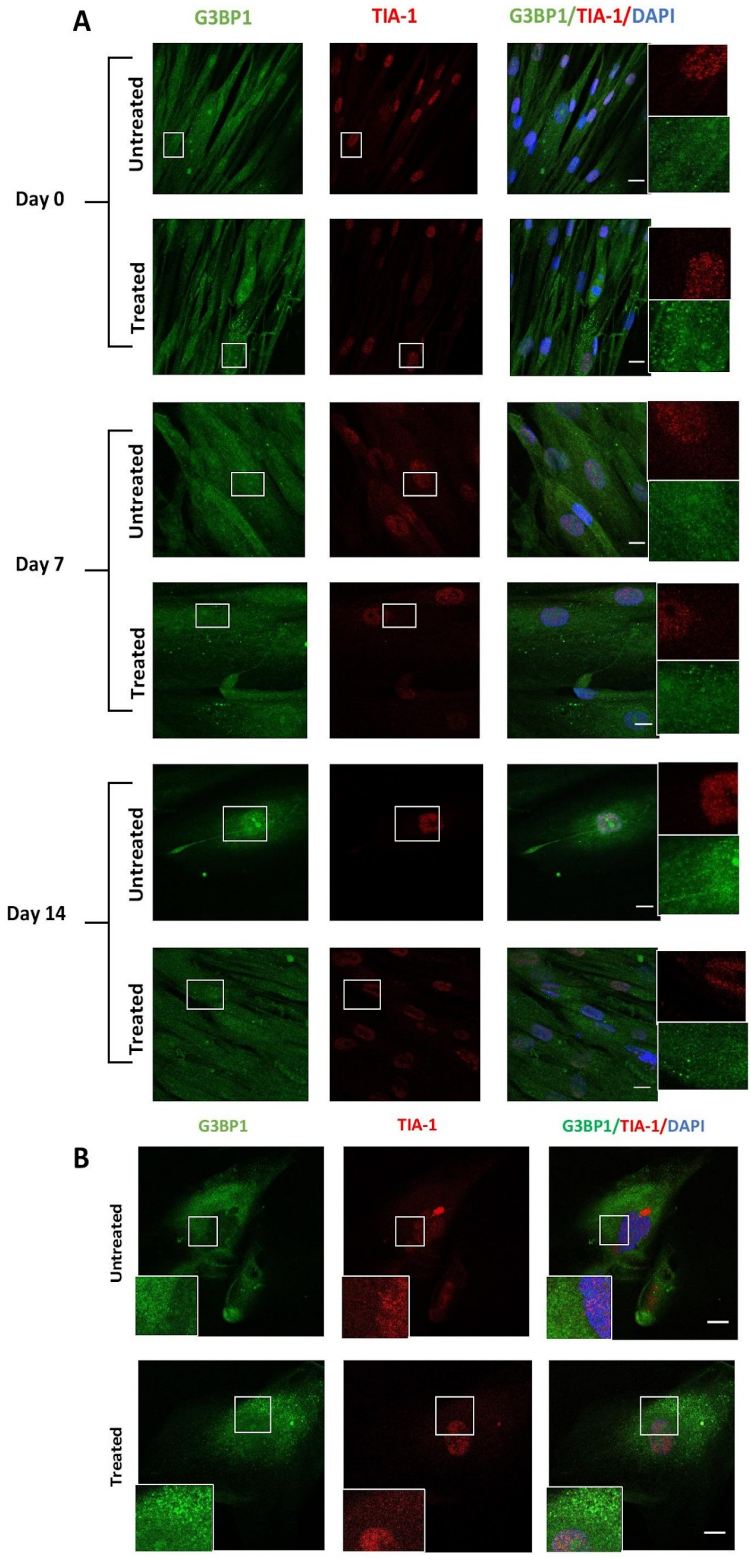

Figure 4.17 TIA-1 recruitment to SA-induced stress granules in HDF proliferative, IR-induced senescent cells and replicative senescent cells. Proliferative and IR-induced senescent cells (A) were treated/untreated with 1.0 mM SA and stained with G3BP1 (Green) and TIA-1 (Red) antibodies. TIA-1 was observed at nuclei of untreated cells. Stressed cells showed formation of stress granules. Day 0 (proliferative) cells showed formation of stress granules. TIA-1 was still located at the nuclei. At Day 7 and 14 post IR exposure, TIA-1 was observed at the nuclei. Replicative senescent cells were treated with 1.0 mM SA for 45 min. Cells stained with TIA-1 showed localization of TIA-1 at the nuclei. Scale bar= 20 um.

4.4.2.2.2.2 Caprin-1

Of the RNA-binding proteins that has been detected in stress granules is Caprin-1. The cytoplasmic activation/proliferation-associated protein-1 (Caprin-1) is suggested to be involved in cell cycle regulation as it is required for progression of cell from G1 phase to S phase (Wang et al., 2005). Moreover, Caprin-1 has been observed to play a role in stress granule assembly either by self-interaction or by interaction with other RNA-binding proteins depending on the type of stimulus. Hence, under oxidative stress, interaction of Caprin-1 with G3BP1 was observed in cells. Overexpression of Caprin-1 induced phosphorylation of eIF-2∂ and therefore inhibition of protein synthesis resulting in formation of stress granules (Solomon et al., 2007). Collectively, Caprin-1 involvement in stress granule assembly varies depending on type of stress.

In the current study, we investigate the involvement of Caprin-1 protein in stress granules in HDF cells. Hence, the proliferative (Day 0) and IR-induced senescent (Day 7 and 14) cells were treated/untreated with 1.0 mM SA for 30 and 45 min, respectively. Cells were then fixed and stained with Caprin-1 antibody (Figure 4.18). In the untreated cells, Caprin-1 was observed diffused in the cytoplasm. However, the treated proliferative cells showed assembly of Caprin-1 at sites of stress granules. Moreover, Day 7 and Day 14 (IR-induced senescent) cells showed assembly of Caprin-1 at sites of stress granules. These observations indicate that under oxidative stress, Caprin-1 is involved in the assembly of stress granules in proliferative and IR-induced senescent HDF cells.

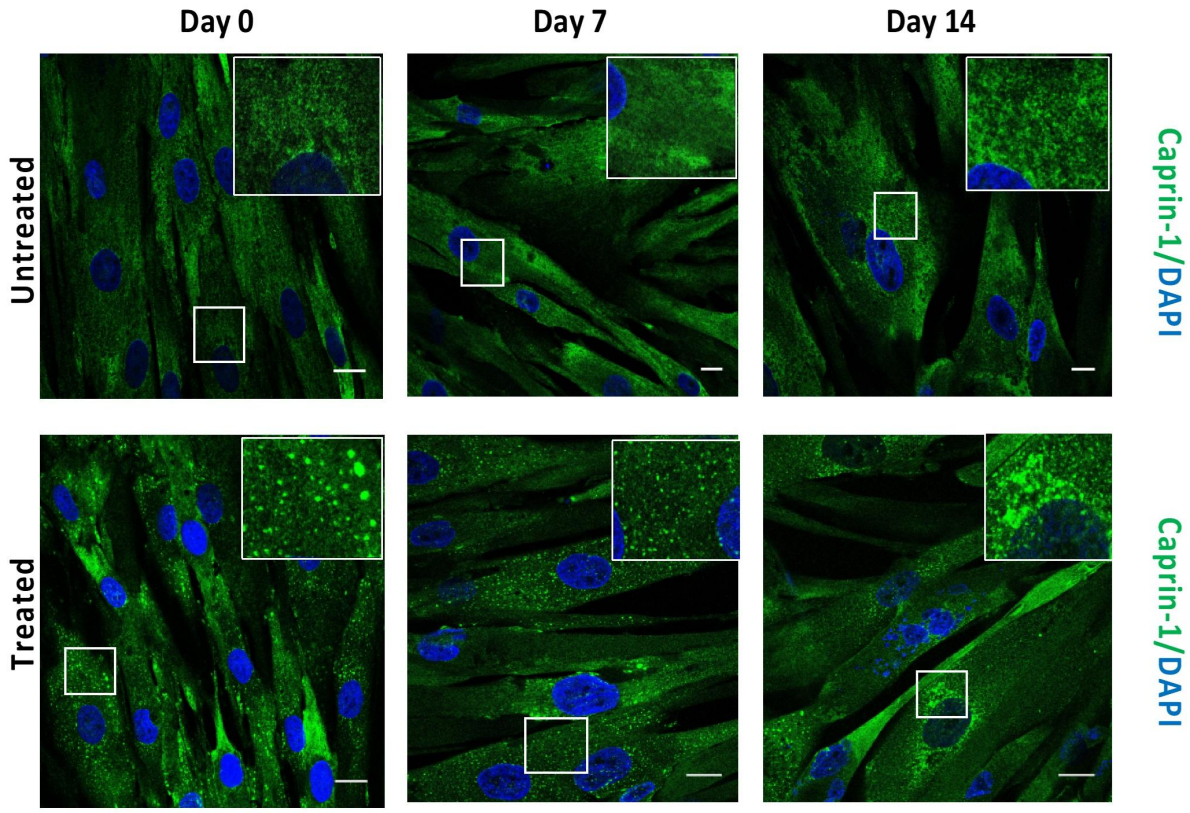

Figure 4.18 Caprin-1 recruitment to sites of stress granule assembly in proliferative and IR-induced senescent HDF cells.

Proliferative and IR-induced senescent HDF cells were treated with/out 1.0 mM SA for 30 and 45 min, respectively. Cells were stained with Caprin-1 antibody (Green). SA-untreated cells showed Caprin-1 diffused in the cytoplasm. Treated proliferative (Day 0) cells showed involvement of Caprin-1 at sites of stress granules. IR-induced senescent (Day 7 and 14) cells showed localization of Caprin-1 at sites of stress granules. Scale bar= 20 um.

Additionally, replicative senescent HDF cells were examined for the recruitment of Caprin-1 at sites of stress granules. Hence, cells were treated/untreated with 1.0 mM SA for 45 min. Cells were then fixed and stained with Caprin-1 antibody (Figure 4.19). SA-untreated cells showed Caprin-1 diffused in the cytoplasm. Nevertheless, SA-treated cells showed formation of few and small stress granules and recruitment of Caprin-1 to sites to stress granule assembly.

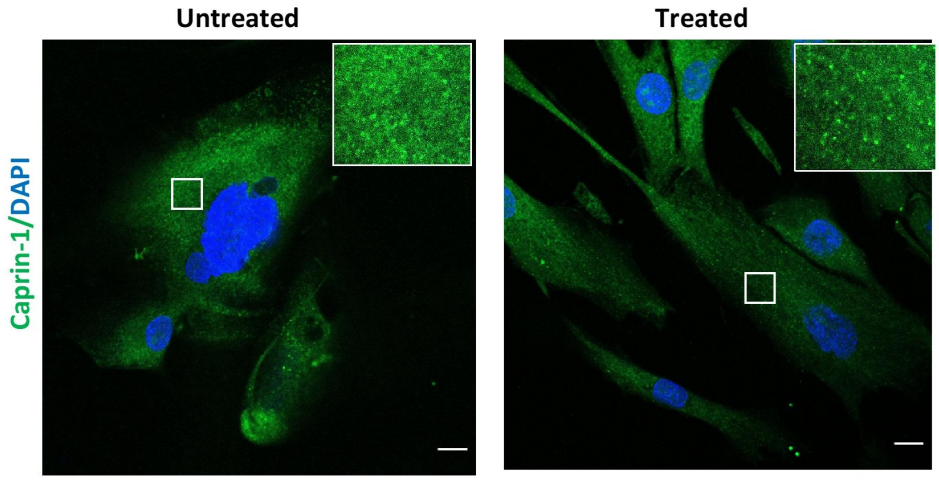

Figure 4.19 Replicative senescent HDF cells showed formation of few small stress granules and localization of Caprin-1 at sites of stress granule assembly. Replicative senescent cells were treated with/out 1.0 mM SA for 45 min. Cells were then stained with Caprin-1 antibody (Green). SA-untreated cells showed Caprin-1 diffused in the cytoplasm. SA-treated cells showed formation of few stress granules and involvement of Caprin-1 at sites of stress granules. Scale bar= 20 um.

Figure 4.20 shows that young cells formed ~29 Caprin-1 positive granules/cell. Day 7, Day 14 and Rep-senescent cells showed assembly of 26, 18 and 6 Caprin-1 positive granules/cell. Day 14 cells and Rep-senescent cells show significant reduction in Caprin-1 positive granules. Day 14 and Rep-senescent cells lose their ability to form Caprin-1 positive granules compared to Day 0 and 7.

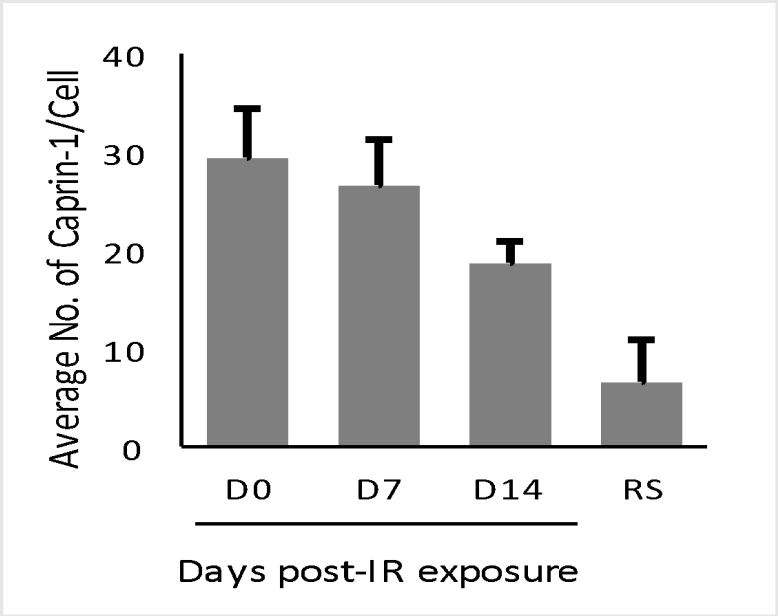

Figure 4.20 Count of Caprin-1 in HDF cells.

Proliferative (Day 0), IR-induced senescent (Day 7 and 14) and replicative senescent (RS) cells were treated with SA. Number of Caprin-1 was counted using ImageJ software. Day 0 cells showed the highest assembly of stress granules and localization of Caprin-1 at sites of stress granules. Day 7, 14 and RS cells showed a gradual decrease in number of stress granules and number of Caprin-1 localized to sites of stress granules. Day 0 cells showed formation and localization of ~29 Caprin-1/cell. Day 7 and 14 showed formation and localization ~25 and 19 Caprin-1/cell. An average of ~6 Caprin-1/cell was detected in SA-treated RS cells. Data represents mean ± SEM n=3, statistical significance was assessed using ANOVA t-test.

4.4.2.2.2.3 TDP-43

Transactive response DNA-binding protein 43 (TDP-43) is a DNA/RNA binding protein involved in RNA processing (Colombrita et al., 2009). It is a multifunctional protein that regulates gene expression in nucleus and cytoplasm (Dewey et al., 2011). Several studies have indicated that TDP-43 localizes to stress granules in response to heat shock and oxidative stress (Colombrita et al., 2009; Freibaum et al., 2010). Thus, the stress granule composition is known to depend on the cell type and stressor (Guil et al., 2006; Anderson and Kedersha, 2008).

Hence, in response to sorbitol stress, TDP-43 has been suggested to be associated with cytoplasmic stress granules. Moreover, WT and mutant TDP-43 showed different responses to oxidative stress and heat shock. Furthermore, mutant TDP-43 was detected to form fewer and bigger stress granules compared to WT TDP-43 (Dewey et al., 2011).

In our study, we investigate the involvement of TDP-43 to stress granules which are induced by SA. Therefore, proliferative (Day 0), IR-induced (Day 7 and 14) senescent and replicative senescent cells were exposed to 1.0 mM SA for 30 min (Day 0) and 45 min (Day 7, 14, and replicative senescent). Cells were then fixed and stained with TDP-43 antibody (Figure 4.21). SA-untreated proliferative cells (Day 0) showed TDP-43 diffused in the cytoplasm. Surprisingly, SA-treated cells showed similar behaviour as untreated cells. No assembly of TDP-43 was detected upon SA exposure. IR-induced senescent (Day 7 and 14) cells (Figure 4.21A) and replicative senescent cells (Figure 4.21B) did not show assembly of TDP-43 following SA treatment. Hence, it is suggested that TDP-43 is not recruited to stress granules following SA treatment in HDF cells.

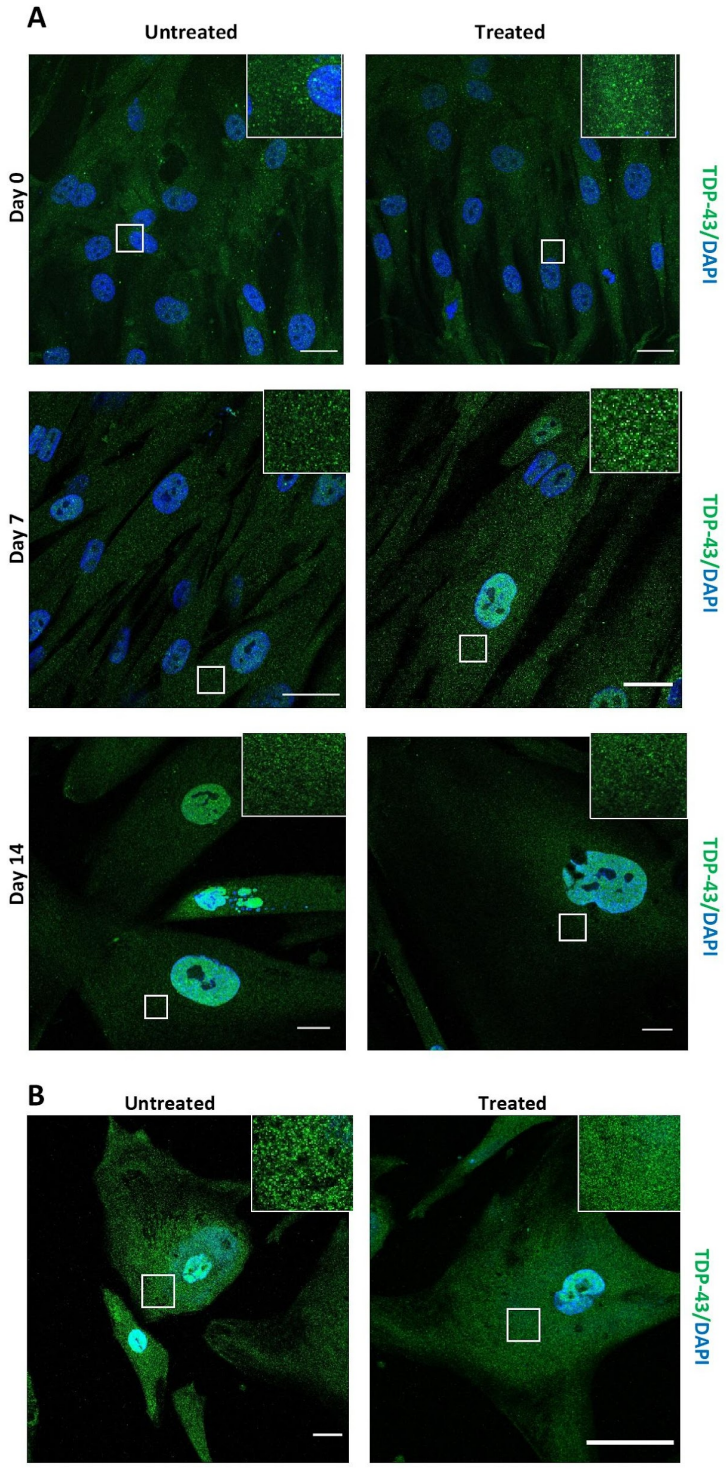

Figure 4.21 Assembly of TDP-43 in proliferative, IR induced senescent and replicative senescent cells.

Proliferative (Day 0), IR-induced senescent (Day 7 and 14) (A) and Replicative senescent (B) cells were untreated/treated with 1.0 mM SA for 30 min (proliferative) and 45 min (senescent). Cells were fixed and stained with TDP-43 antibody (Green). Cells did not show assembly of TDP-43 upon SA treatment. Scale bar= 20 um.

4.4.2.3 Stress Granule Factors in U2OS Cells

4.4.2.3.1 G3BP1

It has been shown by many studies that G3BP1 is crucial for stress granule assembly. Moreover, it has been shown that knockdown of G3BP1 reduces/stops the formation of stress granules (Ghisolfi et al., 2012; Kedersha et al., 2016). Cells lacking G3BP1 lose their ability to form stress granules when exposed to stressors. Additionally, Tourrière et al (2003) showed that exposure of cells to oxidative stress induces dephosphorylation of G3BP1 at Ser-149 leading to multimerization of G3BP1 and initiation of SGs assembly.

Following examination of stress granules in HDF cells, we asked a question of the response of U2OS cells to oxidative stress. Hence, the ability of U2OS cells to form stress granules was examined in proliferative U2OS cells. Therefore, U2OS cells were treated with 0.5 mM SA for 30 min. Cells were then fixed and stained with G3BP1 antibody (Figure 4.22). SA-untreated cells showed G3BP1 diffused in the cytoplasm. Whereas, SA-treated cells displayed assembly of stress granules. This data indicates that the dividing U2OS cells are capable of forming stress granules upon exposure to oxidative stress. G3BP1 is suggested to play a role in stress granule assembly.

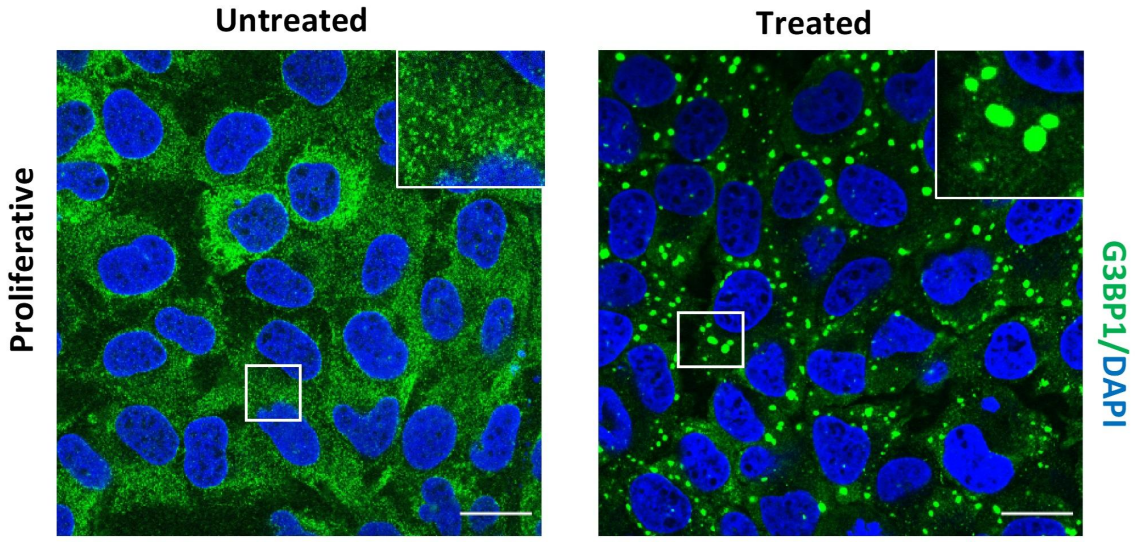

Figure 4.22 Assembly of stress granules in U2OS cells.

Cells were treated/untreated with 0.5 mM SA for 30 min. Cells were then fixed and stained with G3BP1 antibody (Green). G3BP1 was observed diffused in the cytoplasm of untreated cells. Treated cells showed assembly of stress granules. Scale bar= 20 um.

Furthermore, response of senescent U2OS cells to oxidative stress was explained previously. Hence, here we compare the response of proliferative and senescent U2OS cells to oxidative stress. Ability of senescent cells to form stress granules was examined. Thus, doxorubicin-induced senescent cells were exposed to 0.5 mM SA for 30 min. This was followed by cell fixation and G3BP1 immunostaining (Green). Untreated senescent cells did not show assembly of stress granules. Moreover, treated senescent cells showed no/few stress granules (Figure 4.23). Our data suggests that assembly of proper stress granules is impaired in senescent cells.

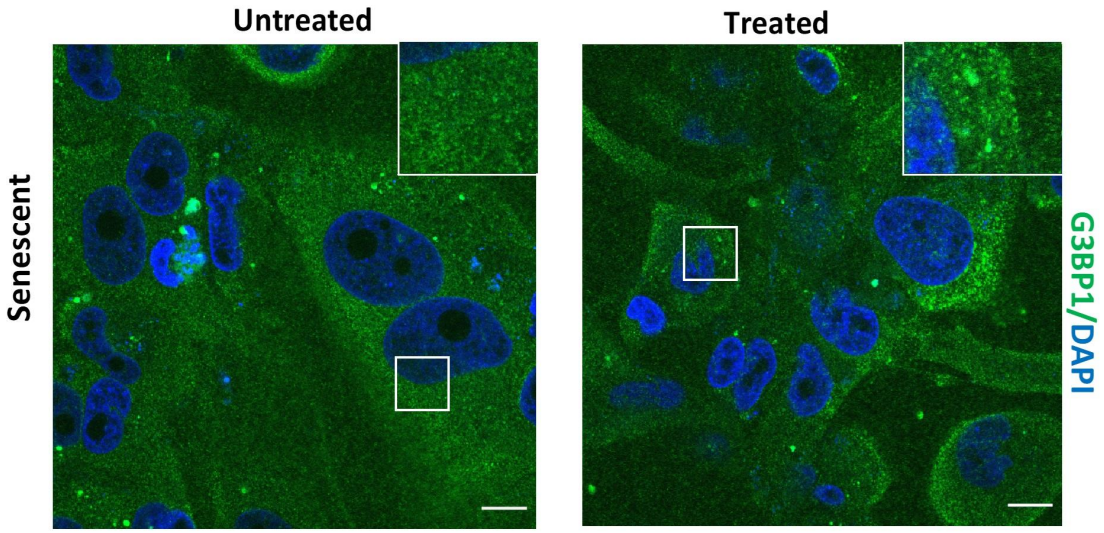

Figure 4.23 G3BP1 in senescent U2OS.

Senescence was induced in U2OS cells using 200 nM Doxorubicin. Senescent cells were treated/untreated with 0.5 mM SA for 30 min. Cells were than fixed and stained with G3BP1 (Green). Untreated cells showed no assembly of stress granules. Treated cells showed no/few stress granules. Scale bar= 20 um.

Furthermore, the number of stress granules between treated/untreated proliferative and senescent cells was compared. ImageJ was used to quantify the number of stress granules. The data was then analysed and plotted using Excel (Figure 4.24). Untreated proliferative U2OS cells showed no assembly of stress granules (Figure 4.22) and thus 0 SGs/cell was obtained. Nevertheless, treated proliferative cells showed assembly of stress granules (Figure 4.22). An average of 17 SGs/cell was counted. Moreover, senescent U2OS cells was observed to form no/few stress granules upon SA exposure (Figure 4.23). An average of 4 SGs/cell was detected in treated senescent cells (Figure 4.24). Therefore, our data shows that senescent U2OS form less stress granules compared to proliferative cells. It is suggested that senescent cells lose their ability to form stress granules and thus form small impaired stress granules.

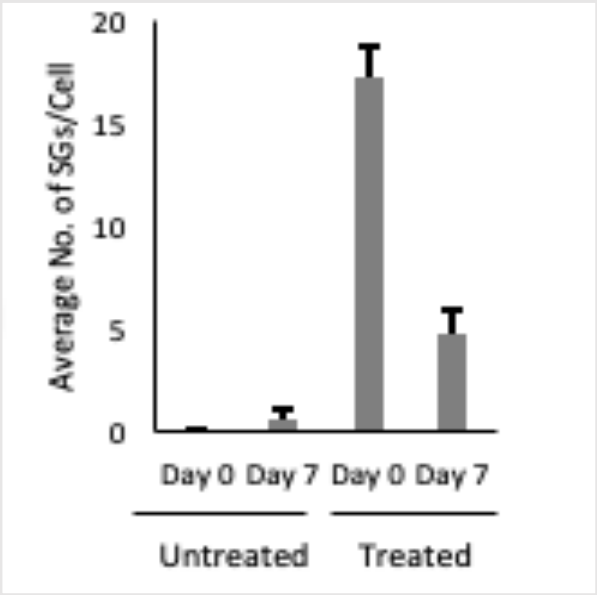

Figure 4.24 Number of stress granules in proliferative and senescent U2OS cells.

Number of stress granules was quantified using ImageJ. In SA-untreated cells, 0 SGs/cell was detected. SA-treated proliferative (Day 0) cells showed assembly of 17 SGs/cells. In SA-treated senescent cells, an average of 4 SGs/cell were detected. Data represents mean ± SEM n=3, statistical significance was assessed using ANOVA t-test.

4.4.2.3.2 Stress Granule Factors Other Than G3BP1

4.4.2.3.2.1 EIF4G

Formation of stress granules is considered as a protective response during which translation and protein synthesis are inhibited (Kedersha et al., 2002). Moreover, several eukaryotic translation initiation factors are involved in process of translation initiation. Of these translation initiation factors, the eukaryotic initiation factor eIF4G, is an essential scaffold protein which facilitates ribosome binding to mRNA (Gingras et al., 1999; Kahvejian et al., 2005). Many studies have shown that stress granules contain most translation regulation proteins and mRNA including 48S complex and eIF4G (Kedersha et al., 2002).

In our study, we examine the recruitment of eIF4G to stress granules in U2OS cells. Therefore, proliferative U2OS cells were treated/untreated with 0.5 mM SA for 30 min. Cells were then fixed and stained with G3BP1 (Green) and eIF4G (Red) (Figure 4.25). Untreated cells did not show assembly of stress granules. G3BP1 and eIF4G were observed diffused in the cytoplasm.

Additionally, treated cells showed assembly of stress granules. eIF4G was observed to be colocalized with G3BP1.The colocalization of G3BP1 and eIF4G was mostly detected at sites of the mature stress granules. At sites of no colocalization, G3BP1 is detected but not eIF4G. This observation suggests that G3BP1 is essential in stress granule assembly. Subsequent to the aggregation of stress granules, eIF4G is translocated to the sites of stress granules.

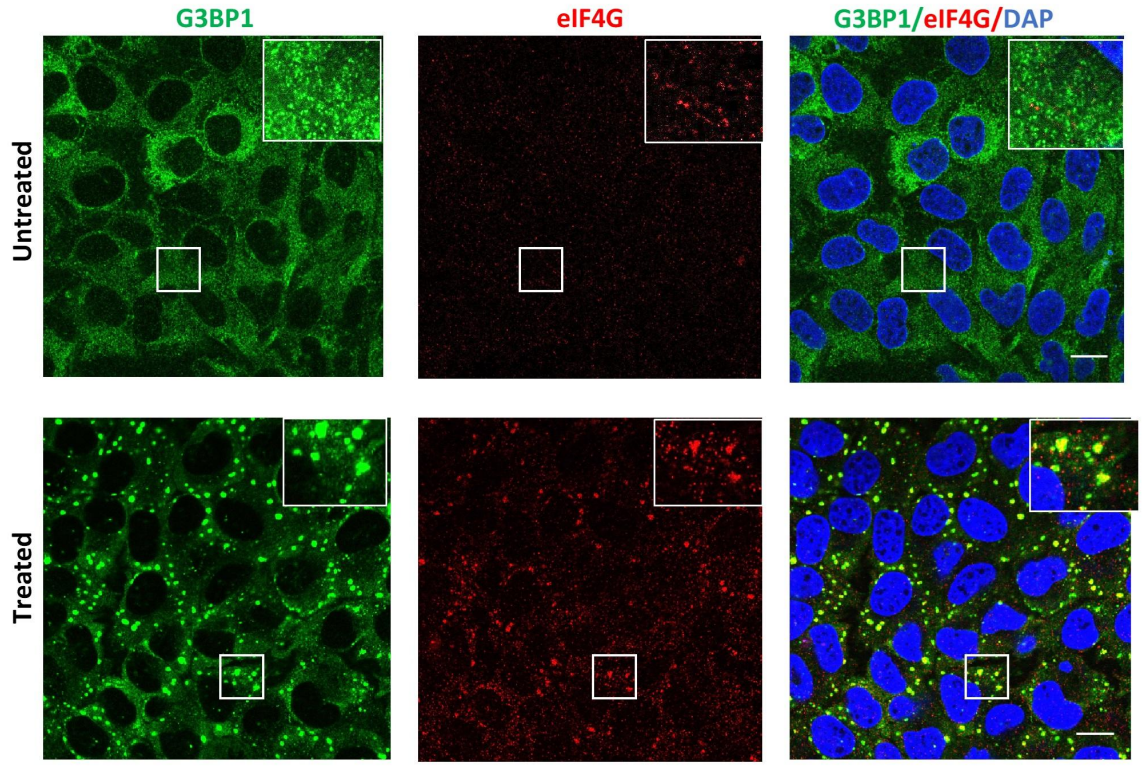

Figure 4.25 eIF4G in proliferative U2OS cells.

Cells were treated/untreated with 0.5 mM SA for 30 min. Cells were then fixed and stained with G3BP1 (Green) and eIF4G (Red). Untreated cells did not assembly of stress granules. Treated cells showed assembly of stress granules and colocalization of G3BP1 and eIF4G. Scale bar= 20 um.

To count the number of stress granules in proliferative U2OS cells, ImageJ was used. Furthermore, a quantitative comparison of the number of G3BP1 and eIF4G was performed.

The average number of stress granules per cell (SGs/cell) was calculated (Figure 4.26). Untreated cells showed 0 SGs/cell. They did not show assembly of G3BP1 or eIF4G. On the other hand, the treated cells showed assembly of stress granules. This was detected using the stress granules nucleating protein: G3BP1. Thus, an average of 8 SGs/cell were counted. The number of eIF4G was counted separately. The detected number of eIF4G was 6 SGs/cell. G3BP1 and eIF4G showed a colocalization of 75%. This data suggests that eIF4G is recruited to stress granules, however, its translocation is a subsequent event to G3BP1 assembly.

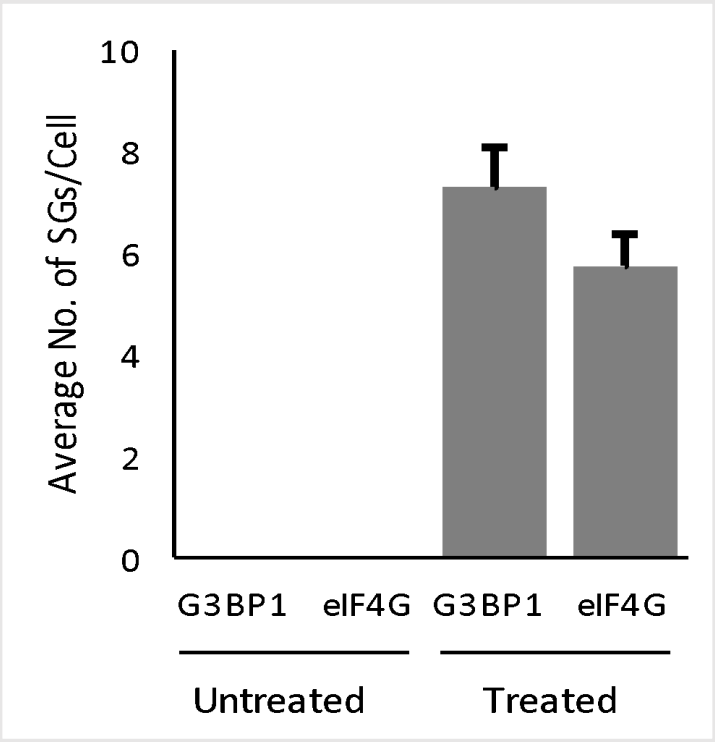

Figure 4.26 Quantitative representation of eIF4G and G3BP1 in proliferative U2OS cells.

SA-untreated cells showed assembly of no G3BP1 and eIF4G. Under SA treatment, an average of 8 G3BP1 and 6 eIF4G per cell were detected. A colocalization of 75% was detected between G3BP1 and eIF4G. Data represents mean ± SEM n=3, statistical significance was assessed using ANOVA t-test.

4.4.2.3.2.2 FXR1

Fragile X retardation factor 1 (FXR1) is mRNA binding protein encoded by FMR gene. Lack of FXR1 protein is known to cause fragile X syndrome, a genetic condition causing developmental disorders (Turner et al., 1996). Moreover, FXR1 has been observed to locate at sites of stress granule assembly. Mazouri et al (2002) has shown that FMRP (FXR1 is homologue gene of FMRP) moves into stress granules during heat stress in cultured fibroblast cells. Additionally, FXR1 was detected to assemble in IDH4 when exposed to oxidative stress (Lian and Gallouzi, 2009). Thus, it has been suggested that FXR1 is recruited to stress granules when cells are exposed to stress such as heat shock and sodium arsenite.

Hence, in our study, we examine the localization of FXR1 to stress granules in proliferative U2OS cells when treated with SA. Therefore, U2OS cells were treated/untreated with 0.5 mM SA for 30 min. Cells were then fixed and stained with G3BP1 (Green) and FXR1 (Red) antibodies (Figure 4.27). Untreated cells did not show assembly of stress granules. G3BP1 and FXR1 were observed diffused in the cytoplasm. Moreover, assembly of stress granules was observed in the treated cells. FXR1 was observed to colocalize with G3BP1 at sites of mature stress granules. G3BP1 was only observed at sites of no colocalization. This observation suggests that G3BP1 nucleates stress granule assembly. Moreover, FXR1 translocation is a subsequent event to stress granule aggregation.

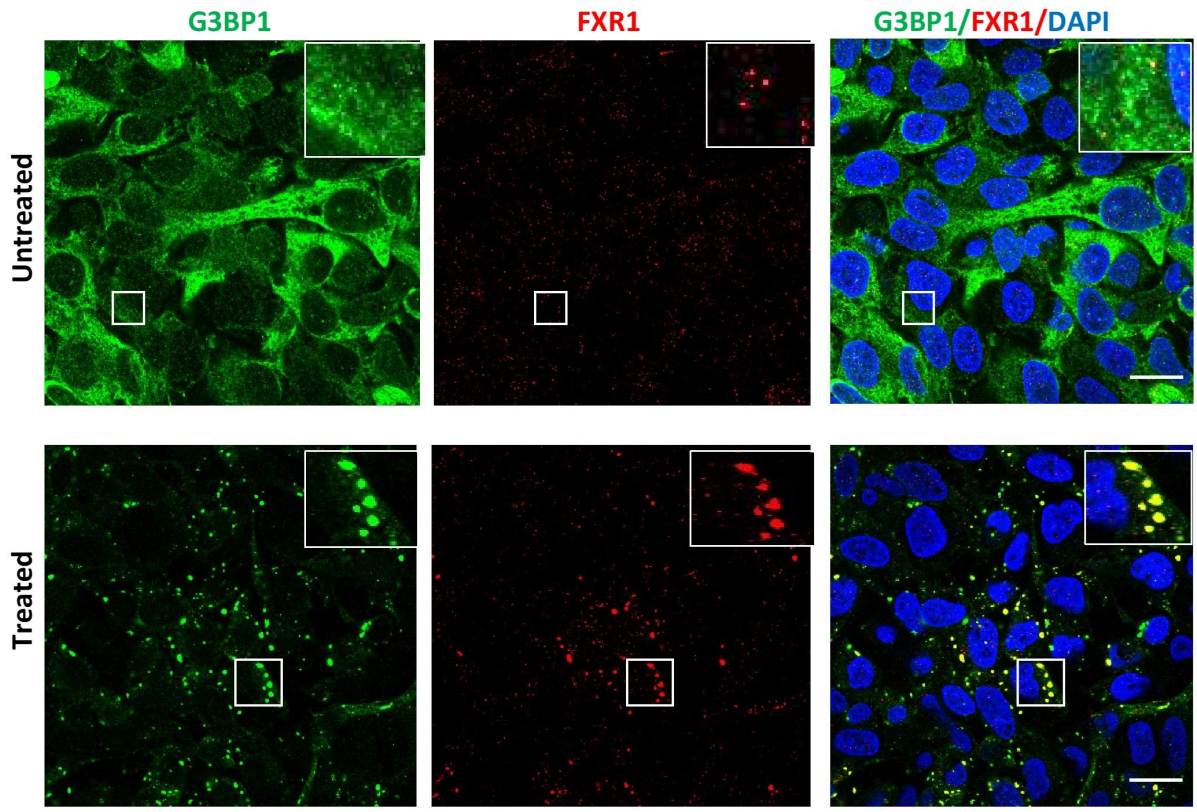

Figure 4.27 FXR1 in proliferative U2OS cells.

Cells were un/treated with 0.5 mM SA for 30 min. Cells were then fixed and stained with G3BP1 (Green) and FXR1 (Red). Untreated cells did not show assembly of stress granules. Treated cells showed assembly of stress granules and colocalization of G3BP1 and FXR1. Scale bar= 20 um.

To count the number of FXR1 in proliferative U2OS cells, ImageJ was used. A quantitative comparison of the number of FXR1 and G3BP1 was performed. The average number of stress granules per cell (SGs/cell) was counted using Excel (Figure 4.28). Untreated cells showed 0 SGs/cell. They did not show assembly of FXR1 or G3BP1. As shown previously, SA-treated cells show assembly of stress granules. This was detected using the stress granule nucleating protein: G3BP1. Thus, an average of 9 SGs/cell were counted. The number of FXR1 was counted individually. An average of 5 SGs/cell was detected. Seemingly, G3BP1 and FXR1

shows a colocalization of 55%. Therefore, our observations suggest that FXR1 is recruited to stress granules. Nevertheless, its translocation is a subsequent event to G3BP1 assembly.

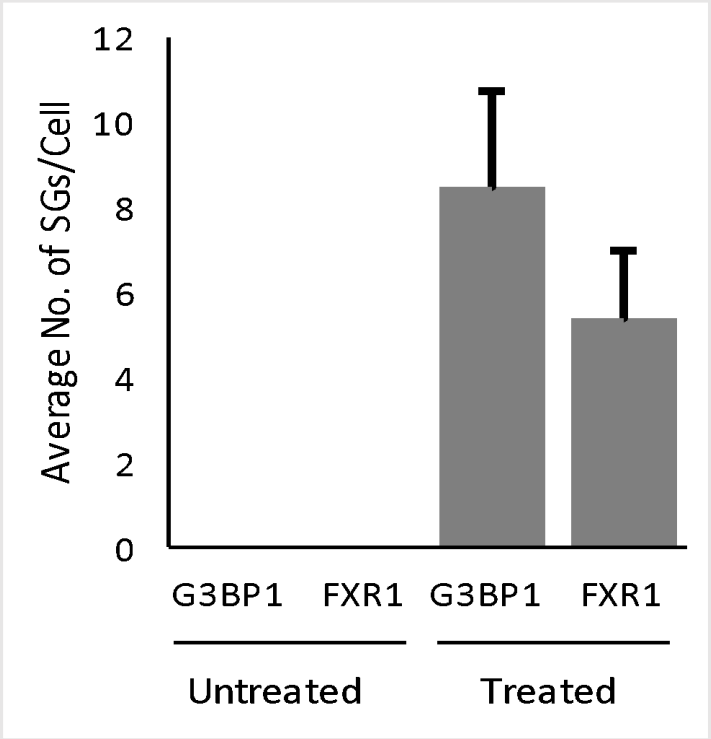

Figure 4.28 Quantitative representation of FXR1 and G3BP1 in proliferative U2OS cells.

SA-untreated cells did not show assembly of FXR1 and G3BP1. Under SA treatment, an average of 9 G3BP1 and 5 FXR1 per cell were counted. A colocalization of 55% was detected between G3BP1 and FXR1. Data represents mean ± SEM n=3, statistical significance was assessed using ANOVA t-test.

4.4.3 Puromycin and Cycloheximide Treatment

Cycloheximide is known as a protein biosynthesis inhibitor in eukaryotic cells. It has been used widely in studies of mRNA and stress granules as it leads to polysome stabilization. Cycloheximide traps mRNAs in polysomes preventing stress granule assembly (Mollet et al., 2008). Hence, under cold shock, cycloheximide was observed to block stress granule assembly. It was also detected to disassemble the pre-formed stress granules (Hofmann et al., 2012). Puromycin is a translational inhibitor in both prokaryotic and eukaryotic cells. It inhibits protein synthesis by destabilizing polysomes and releasing mRNAs from polysomes. Therefore, puromycin promotes stress granule assembly by making free mRNAs available (Kedersha et al., 2000; Basu et al., 2017). Hence, cycloheximide and puromycin are used to classify stress granules from other granular structures in the cells (Kedersha et al., 2000).

4.4.3.1 HDF Cells

In our recent study, we examine the response of proliferative and senescent HDF cells to cycloheximide and puromycin. Therefore, proliferative HDF cells were exposed to 1.0 mM SA for 30 min. It was then followed by cycloheximide or puromycin treatments. Cells were fixed and stained with G3BP1 antibody (Red) (Figure 4.29). SA-untreated cells did not show assembly of stress granules. Hence, when SA-treated cells were exposed to cycloheximide, stress granule formation was prevented. This was expected as cycloheximide acts as stress granule assembly inhibitor (Kedersha et al., 2013). Furthermore, puromycin treatment was detected to promote stress granule assembly in SA-treated cells. It was observed to form proper mature stress granules. This data indicates that stress granules are prevented/disassembled by cycloheximide and promoted by puromycin treatment.

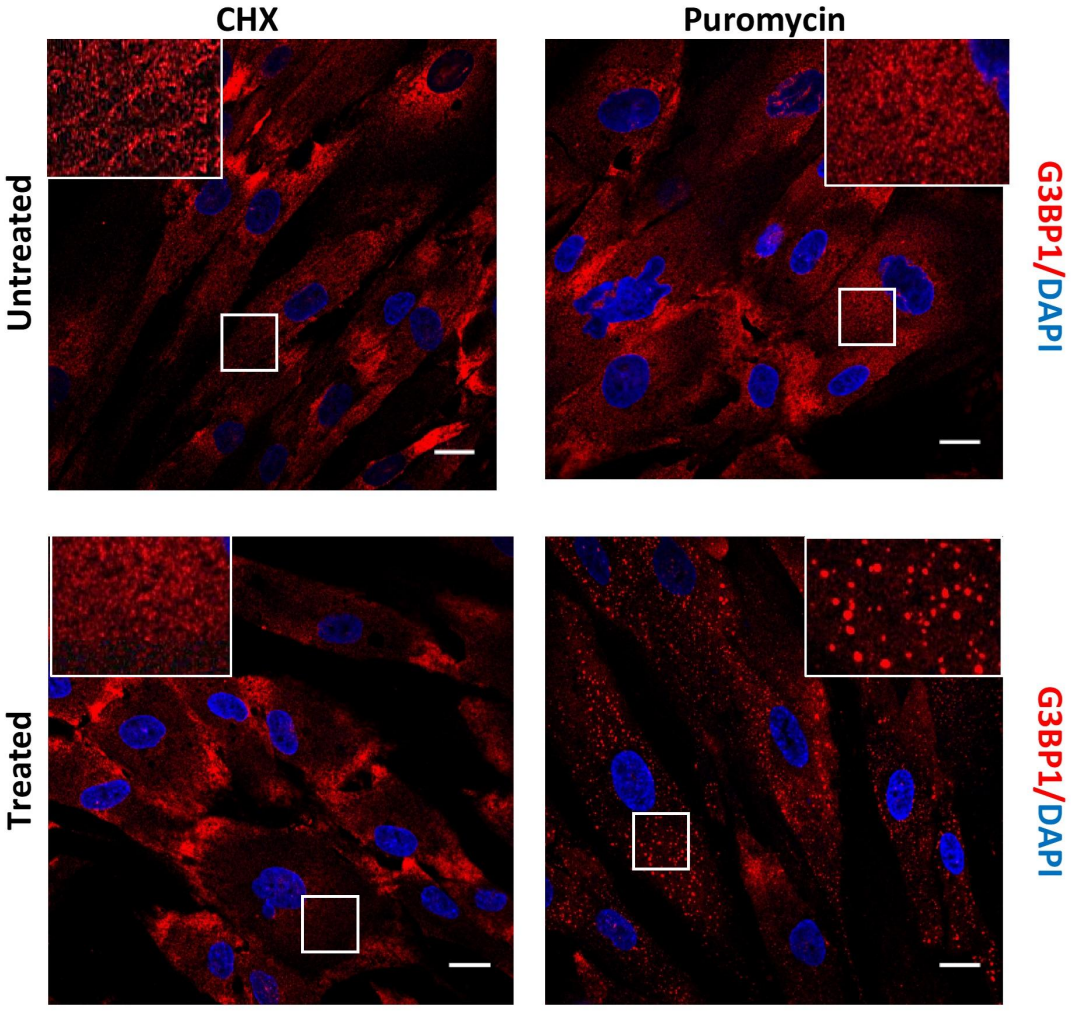

Figure 4.29 Cycloheximide (CHX) and puromycin shows counteract effect on stress granulrs in proliferative HDF cells.

HDF cells were treated/untreated with 1.0 mM SA for 30 min. CHX or puromycin was added to cells. SA-untreated cells did show assembly of stress granules. CHX was observed to inhibit stress granule assembly. Puromycin was detected to promote stress granules formation. Scale bar= 20 um.

Furthermore, the effect of cycloheximide and puromycin on the formation of stress granules was then examined in senescent HDF cells. Therefore, senescent HDF cells were treated/untreated with 1.0 mM SA for 45 min. Subsequently, cycloheximide or puromycin was added to cells. Cells were then fixed and stained with G3BP1 (Red) (Figure 4.30). SA-untreated

cells did not show assembly of stress granules. Expectedly, cycloheximide was detected to inhibit stress granule formation. On the other hand, puromycin promotes stress granule formation in SA-treated cells. However, the formed stress granules in senescent cells are smaller than stress granules in proliferative cells. This observation indicates that under oxidative stress and puromycin treatments, formation of stress granules is impaired in senescent cells.

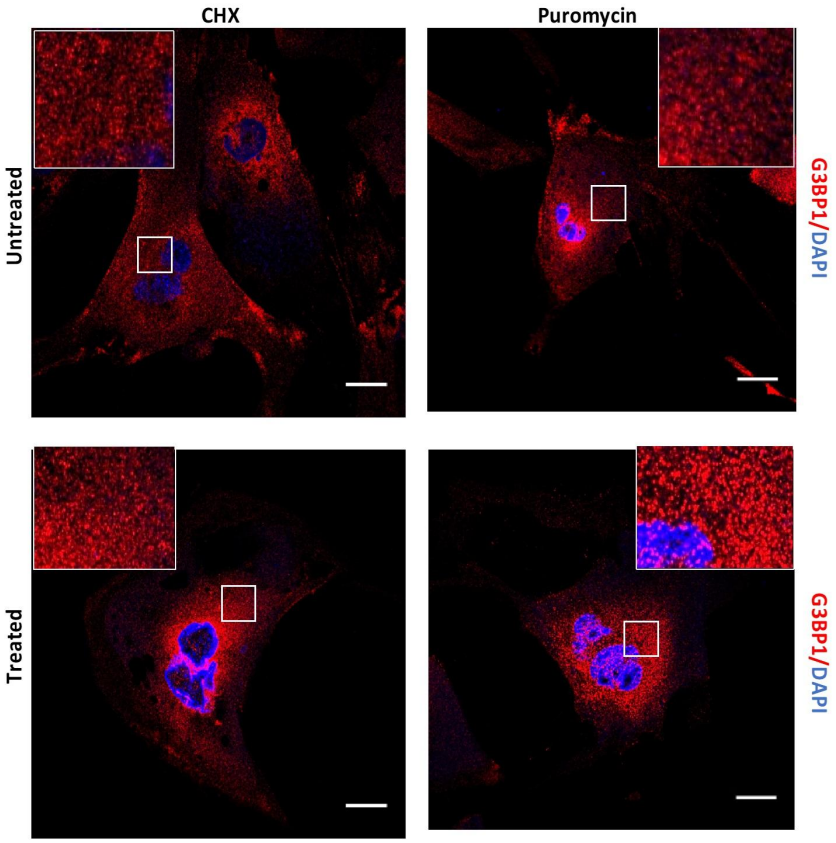

Figure 4.30 Cycloheximide (CHX) and puromycin treatments in senescent HDF cells. Cells were treated/untreated with 1.0 SA for 45 min. This was followed by CHX or puromycin treatments. Cells were fixed and stained with G3BP1 (Red).SA-untreated cells did not show assembly of stress granules. Upon SA exposure, CHX was observed to inhibit stress granules formation while puromycin was detected to induce stress granules assembly. Scale bar= 20 um.

Cycloheximide and puromycin effect on stress granules was observed in proliferative and senescent cells. Thus, cycloheximide inhibited stress granule assembly by trapping mRNAs in polysomes. On the other hand, puromycin promoted stress granule formation by releasing mRNAs from polysomes and making them available to start the events of stress granule formation. Hence, to quantitatively compare the number of stress granules in stressed/unstressed proliferative and senescent HDF cells treated with cycloheximide or puromycin, ImageJ was used. Images were processed using ImageJ to count the number of stress granules. The obtained data was then analysed and plotted in Excel. SA-untreated cells showed no formation of stress granules. Hence, this data was not involved in the comparison plot below. Moreover, SA/CHX-treated proliferative HDF cells showed 0 SGs/cell. Whereas, SA/Puromycin-treated proliferative cells showed formation of 20 SGs/cells. SA/CHX treatment inhibited stress granule formation in senescent cells. 0 SGs/cell was obtained. Thus, SA/Puromycin treatment promoted stress granules in senescent cells. An average of 6 SGs/cell was counted (Figure 4.31). Therefore, our data suggests that upon oxidative stress, cycloheximide inhibits stress granule assembly while puromycin promotes stress granule assembly in proliferative and senescent HDF cells.

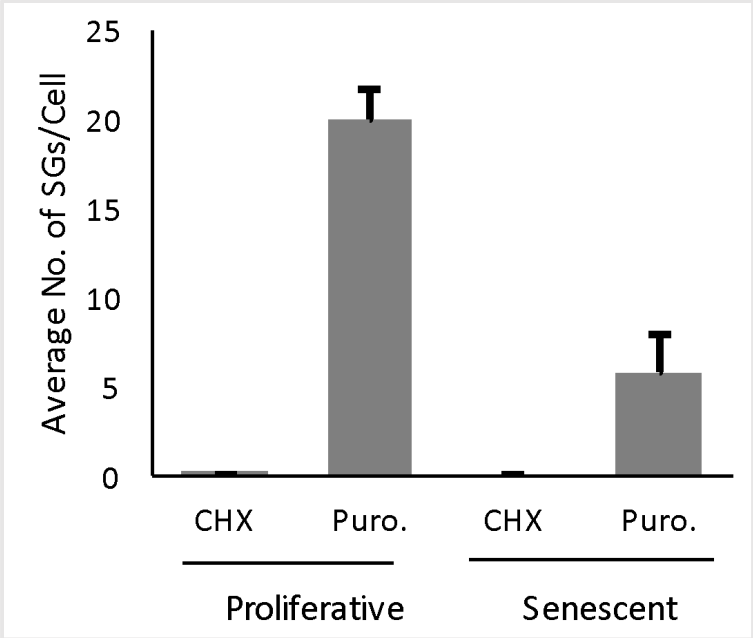

Figure 4.31 Quantitative comparison of stress granules in HDF cells treated with Cycloheximide (CHX) and puromycin (Puro.).

Upon SA exposure, CHX inhibits stress granule assembly while Puro. induces stress granule assembly in proliferative and senescent HDF cells. In SA/CHX-treated cells, 0 SGs/cell was counted. Under SA/Puro-treatment, an average of 20 SGs/cell was detected in proliferative cells, while only 6 SGs/cell were detected in senescent cells. Data represents mean ± SEM n=3, statistical significance was assessed using ANOVA t-test.

4.4.3.2 U2OS Cells

In order to examine the effect of cycloheximide and puromycin on stress granule formation in U2OS cells, proliferative U2OS cells were treated with cycloheximide or puromycin. Cells were exposed to 0.5 mM SA for 30 min. SA treatment was then followed by cycloheximide or puromycin. Cells were then fixed and stained with G3BP1 (Green) and eIF4G (Red) antibodies (Figure 4.32). As expected, SA/CHX treatment was observed to inhibit stress granule assembly. It is also suggested to disassemble the pre-formed stress granules. SA/puromycin treatment was observed to promote the assembly of stress granules.

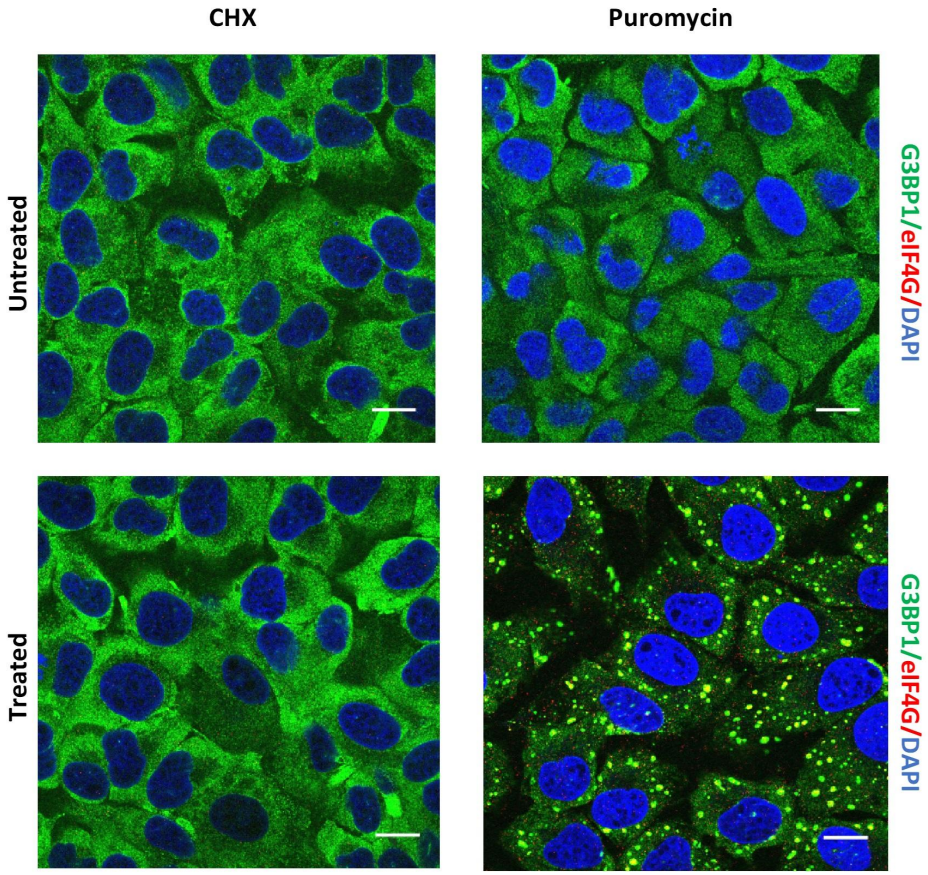

Figure 4.32 Treatment of proliferative U2OS cells with Cychloheximide (CHX) and Puromycin.

Cells were treated/untreated with 0.5 mM SA for 30 min. This was followed by Cycloheximide (CHX) or puromycin treatment. Cells were than fixed and stained with G3BP1 (Green) and eIF4G (Red). SA-untreated cells did not assembly of stress granules. SA/CHX treatment was observed to inhibit assembly of stress granules. SA/puromycin treatment was detected to promote stress granule assembly. Scale bar= 20 um

Furthermore, the number of stress granules formed under oxidative stress and cycloheximide or puromycin treatments was counted using ImageJ and plotted using Excel. As described before, cycloheximide inhibits stress granule assembly and disassembles the pre-formed stress granules. We detected 0 SGs/cell under SA/CHX treatments. An average of 14 SGs/cell was detected in cells upon SA/puromycin treatment (Figure 4.33). Therefore, our data is consistent

with previous studies (Kedersha et al., 2000). Cycloheximide inhibits stress granule formation while puromycin promotes their formation.

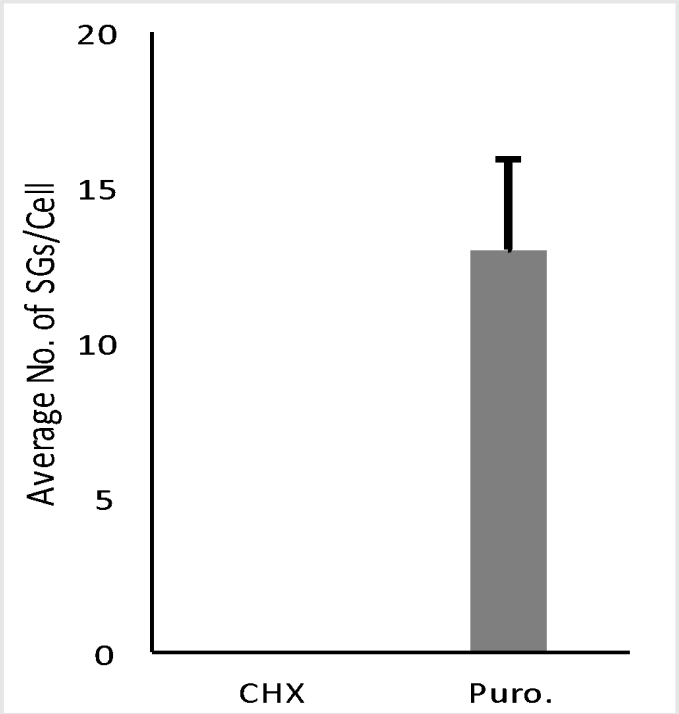

Figure 4.33 Quantitative representation of stress granules in U2OS under Cycloheximide (CHX) and Puromycin (Puro.) treatments.
Number of stress granules was quantified using ImageJ. An average of 14 cells were counted in cells treated with SA/puromycin. Cells that were treated with SA/CHX showed 0 SGs/cell. An average of 13 SGs/cells were counted. Data represents mean ± SEM n=3, statistical significance was assessed using ANOVA t-test.

4.5 Comparison of Different Routes to Senescence in HDF Cells

Stress granules are cytoplasmic entities that are formed upon exposure to environmental stressors such as oxidative stress, heat and cold shock. Stress granules play a protective role as it stops translation and protein synthesis by relocating untranslated mRNAs to their assembly sites (Kedersha et al., 1999; Anderson and Kedersha, 2008). They are composed of translationally stalled 48S complex, free untranslated mRNAs and RNA-binding proteins. RNA-binding proteins are essential in the process of stress granule assembly such as G3BP1, TIA-1, eIF4G and FXR1. It has been suggested that the recruitment of RNA-binding proteins to stress granules is dependent on the cell type and stress (Buchan and Parker, 2009; Bounedjah et al., 2014).

Proliferative and senescent cells were observed to respond distinctly to stress (Lian and Gallouzi, 2009; Omer et al., 2018). Senescent cells' response showed formation of impaired stress granules. Loss of proper stress granule formation in senescent cells was considered as a marker for evaluation of age-related diseases (Moujaber et al., 2017). In our study, the difference in stress response between proliferative and senescent cells was studied. Under oxidative stress, proliferative HDF cells were observed to form stress granules. It was detected by staining them with G3BP1 antibody which is an essential component of stress granules. Replicative senescent cells showed few/no stress granule assembly suggesting that senescent cells lose their ability to form stress granules. Other stress granule components: TIA-1 and TDP-43 were observed not to be recruited to stress granules in both proliferative and senescent cells. However, Caprin-1 was observed to be recruited to stress granules in proliferative cells but no/few Caprin-1 were observed in senescent cells. This data suggests that G3BP1 is essential in promoting stress granule assembly in HDF cells under oxidative stress.

Replicative senescent cells and IR-induced senescent cells show similar senescence markers (discussed in chapter 3). However, their response to stress is different. IR-induced senescent cells (Day 14) maintain their ability of stress granule formation, although the number of stress granules is few compared to proliferative cells (Day 0). G3BP1 was detected in IR-induced senescent cells suggesting its importance in stress granule formation when exposed to oxidative stress. Moreover, Caprin-1 was observed to be recruited to stress granules in IR-induced senescent cells. There was no difference observed in the recruitment of TIA-1 and TDP-43 in replicative and IR-induced senescent cells. Therefore, this data suggests that replicative senescent cells lost their ability of forming stress granules, while it is maintained in IR-induced senescent cells. Additionally; Caprin-1 is suggested to be a component of stress granules in HDF cells.

4.6 Conclusion

Stress granule assembly is induced by exposure to stressors such as oxidative stress. G3BP1, TIA-1 and FXR-1 are of the stress granule components that are essential/recruited to stress granules. The conditions required for induction of stress granules differ depending on the type of the cell. In our study, we examined stress granules induction in primary fibroblast (HDF) cells and U2OS cells. Both systems are distinct and therefore stress granule stimulation conditions were different.

To induce stress granule assembly in HDF cells, a range of SA concentrations (0-6.0 mM) were used for 30 min. Proliferative and senescent HDF cells showed an increase in stress granule assembly when exposed to 1.0 mM SA. However, the optimal exposure time was observed to be 30 min and 45 min for proliferative and senescent cells, respectively. In the case of U2OS cells, the working conditions were detected as following: 0.5 mM SA for 30 min. Under these

conditions, the translation was ceased and the highest aggregation of stress granules was observed. Several studies have used variable concentrations and exposure time depending on cell type and research purpose (Lian and Gallouzi, 2009; Kedersha et al., 2013).

RNA-binding proteins are essential components of stress granules. They promote assembly of stress granules as they bind to untranslated mRNAs and translocate to stress granule sites. Therefore, it is a protective mechanism to save cells energy until the insult is removed. Of the RNA-binding proteins, G3BP1 is suggested to be an essential stress granule component that initiates the assembly events (Matsuki et al., 2013). Hence, in our recent study, G3BP1 was studied in proliferative and senescent HDF cells. G3BP1 was detected in proliferative cells. No/few G3BP1 was observed in senescent cells suggesting the impaired ability of stress granule formation in senescent cells. Moreover, U2OS cells showed recruitment of G3BP1 to stress granules suggesting its crucial role in stress granule formation. Collectively, under oxidative stress, proliferative HDF and U2OS cells showed assembly of stress granules and recruitment of G3BP1 to stress granule sites. However, senescent HDF cells showed no/few G3BP1 located at stress granules as stress granule assembly is impaired.

Stress granules contain multiple factors that are involved in the process of their assembly. TIA-1, FXR-1 and Caprin-1 are of the stress granule components that were observed to locate to stress granules under variable stressors. In our study, TIA-1 and TDP-43 were not detected to locate to stress granules under oxidative stress in proliferative and senescent HDF cells. Whereas, Caprin-1 was detected at sites of stress granule assembly in proliferative cells and no/few in senescent cells. FXR-1 and eIF4G were examined in U2OS cells and observed to locate to stress granule sites under oxidative stress suggesting their involvement in stress

granule assembly. As G3BP is known to nucleate stress granule assembly, it could be used as a control for future studies in HDF cells.

Additionally, the effect of cycloheximide and puromycin was investigated in HDF and U2OS cells. Both drugs are inhibitors of protein synthesis, however, cycloheximide prevents stress granule assembly by stabilizing polysomes while puromycin induces stress granule assembly by destabilizing polysomes and release of untranslated mRNAs. Cycloheximide showed inhibition of stress granules in proliferative and senescent cells. Whereas, puromycin induced stress granule assembly in cells. Therefore, these results provide a framework for future studies of stress granules in HDF and U2OS cells.

Chapter 5

5 Senescence in WT U2OS and G3BP Knock-out Cells

5.1 Introduction

Mammalian stress granules are assemblies of mRNAs and proteins. They are formed through interactions of RNA binding proteins with the free untranslated mRNAs (Protter and Parker, 2016). Stress granules are known to contain a large population of proteins. Of these proteins, G3BP is an essential protein that is recruited to stress granules. It is known to initiate the process of stress granule assembly in presence of stress (Tourriere et al., 2003).

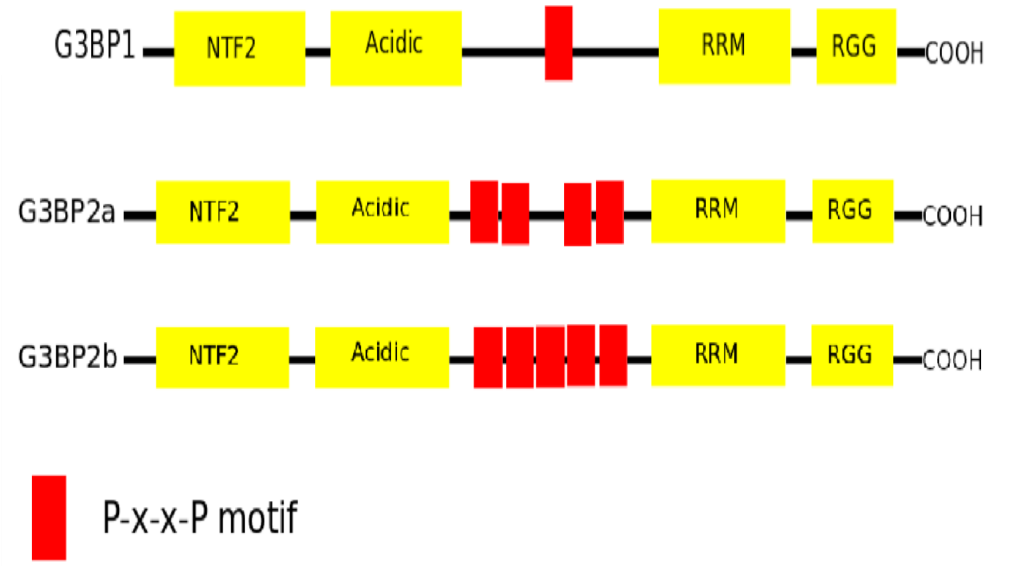

Figure 5.1 Schematic representation of G3BP domains.

G3BP1 and G3BP2 are homologous proteins. G3BP1 and G3BP2 share common domains: NTF2 domain, RRM and RRG domains. G3BP2 is alternatively spliced to G3BP2a and 2b.

The two forms of G3BP: G3BP1 and G3BP2 are homologous proteins that were observed to play an essential role in stress granule assembly (Tourriere et al., 2003; Götte et al., 2019). G3BP1 contains five regions: N-terminal NTF2-like domain, the acidic region, the PXXP motif, RRMs domain and C-terminal RGG domain. RGG and NTF2-like domains are required for SGs assembly (Tourriere et al., 2003; Matsuki et al., 2012; Kedersha et al., 2016). G3BP2 has similar domains as G3BP1 including NTF2-like domain, RRMs and RGG domains (Irvine et al., 2004) (Figure 5.1).

Both G3BP1 and G3BP2 are essential for stress granule formation. Knockdown of G3BP1 and/or G3BP2 in HeLa cells showed a reduction in stress granule number. Thus, double knockdown (G3BP1 and G3BP2) showed a much more significantly reduced number of stress granules compared to single knockdown (G3BP1 or G3BP2) (Matsuki et al., 2012). These observations indicate that G3BP1 and G3BP2 are required for stress granule formation under oxidative stress (Matsuki et al., 2012). Additionally, Kobayashi et al. (2012) showed that endogenous G3BP2 is recruited to stress granules when cells are exposed to sodium arsenite or heat shock. Furthermore, stress granule formation can be induced by overexpression of G3BP1 (Tourriere et al., 2003).

5.2 Aims and Objectives

5.2.1 Aims

This chapter aims to examine the role of G3BP1/2 in stress granule formation and development of senescence phenotype. Thus, WT U2OS cells, where G3BP1/2 exists, will be used as a control for this study. Double-knockout (hereafter referred as ΔΔG3BP1/2) cells were developed (and provided to us by Dr. Nancy Kedersha, Boston, US) to study cells' processes such as stress response and senescence in absence of G3BP1/2. To obtain the knowledge on this topic, WT U2OS and ΔΔG3BP1/2 cells will be cultured in vitro in a growth chamber. Cells reaching 90% confluency will be exposed to 0.5 mM SA for 30 min. Next, cells will be stained with stress granule markers: G3BP1 or G3BP2, EIF4G and FXR1 to count the number of stress granules per cell. Furthermore, senescence phenotype is monitored in WT U2OS and ΔΔG3BP1/2 cells upon doxorubicin (200 nM) treatment. doxorubicin-treated cells will be stained with senescence markers: SA-ß-Gal, SAHF and p21 to compare progression of cells towards senescence.

Furthermore, the role of each form of G3BP (G3BP1, G3BP2a and G3BP2b) on stress granule formation and senescence is examined. Thus, GFP-tagged-G3BP1, GFP-tagged-G3BP2a, GFP-tagged-G3BP2b were genetically reconstituted to ΔΔG3BP1/2 cells individually through transient transfection forming GFP-G3BP1, GFP-G3BP2a, GFP-G3BP2b cells (provided to us by Dr. Nancy Kedersha, Boston, US). Hence, these cells will be treated in a way similar to WT U2OS cells to develop an understanding of the role G3BP1, G3BP2a and G3BP2b in stress response and senescence. Stress granule markers: G3BP1 or G3BP2, EIF4G and FXR1 will be used to count the number of stress granules per cell. Senescence markers: SA-ß-Gal, SAHF and p21 will be used to compare progression of cells towards senescence.

We hypothesize that ΔΔG3BP1/2 lose their ability to form stress granules due to absence of G3BP1/2. Moreover, they show accelerated progression towards senescence. Re-constitution of cells with G3BP1, G3BP2a or G3BP2b individually rescue cells' ability of stress granule formation. It also slows cells' progression to senescence.

5.2.2 Objectives

1. Investigate stress granule formation in double-knockout (ΔΔG3BP1/2) cells.
2. Examine senescence markers: SA-ß-Gal, SAHF and p21 in ΔΔG3BP1/2 cells.
3. Compare stress granules and senescence phenotype in WT U2OS and ΔΔG3BP1/2 cells.
4. Examine stress granule formation in GFP-G3BP1, GFP-G3BP2a, and GFP-G3BP2b cells.
5. Observe senescence phenotype in GFP-G3BP1, GFP-G3BP2a, and GFP-G3BP2b cells using senescence markers: SA-ß-Gal, SAHF and p21.

5.3 Materials and Methods

5.3.1 Materials

All chemicals were purchased from Sigma unless stated otherwise.

5.3.2 Methods

As described in chapter 2.

5.4 Results

5.4.1 Loss of G3BP1/2 Significantly Reduced Stress Granule Formation

G3PB is known to nucleate stress granule assembly when cells are exposed to stressor such as oxidative stress (Kedersha et al., 2016). The two forms of G3BP: G3BP1 and G3BP2 coexist as they are expressed in most cells (Matsuki et al., 2013). Phosphorylation of G3BP1 at Serine149 impairs its ability to nucleate stress granules and therefore stress granule formation (Tourrière et al., 2003). Moreover, it has been shown that G3BP interacts with other RBPs such as FXR1 and Caprin-1 promoting stress granule assembly (Soloman et al., 2007; Kedersha et al., 2016). Hence, these studies have suggested that G3BP1/2 plays a crucial role in stress response and stress granule formation. Therefore, in our study, we show that knockout of G3BP1 and G3BP2 (ΔΔG3BP1/2) inhibits stress granule assembly in proliferative and senescent cells. Additionally, ΔΔG3BP1/2 cells showed an increased number of senescent cells (Day 9) when compared to WT U2OS cells.

In our recent study, we used genetically modified U2OS cells developed based on CRISPR/Cas9 technology. The developed cells were genetically ablated for the RNA binding proteins G3BP1 and G3BP2 (Kedersha et al., 2016). The resulting cells were then tagged with Green Fluorescent Protein (GFP) to enable visualization of any assembly of stress granules (Figure 5.2).

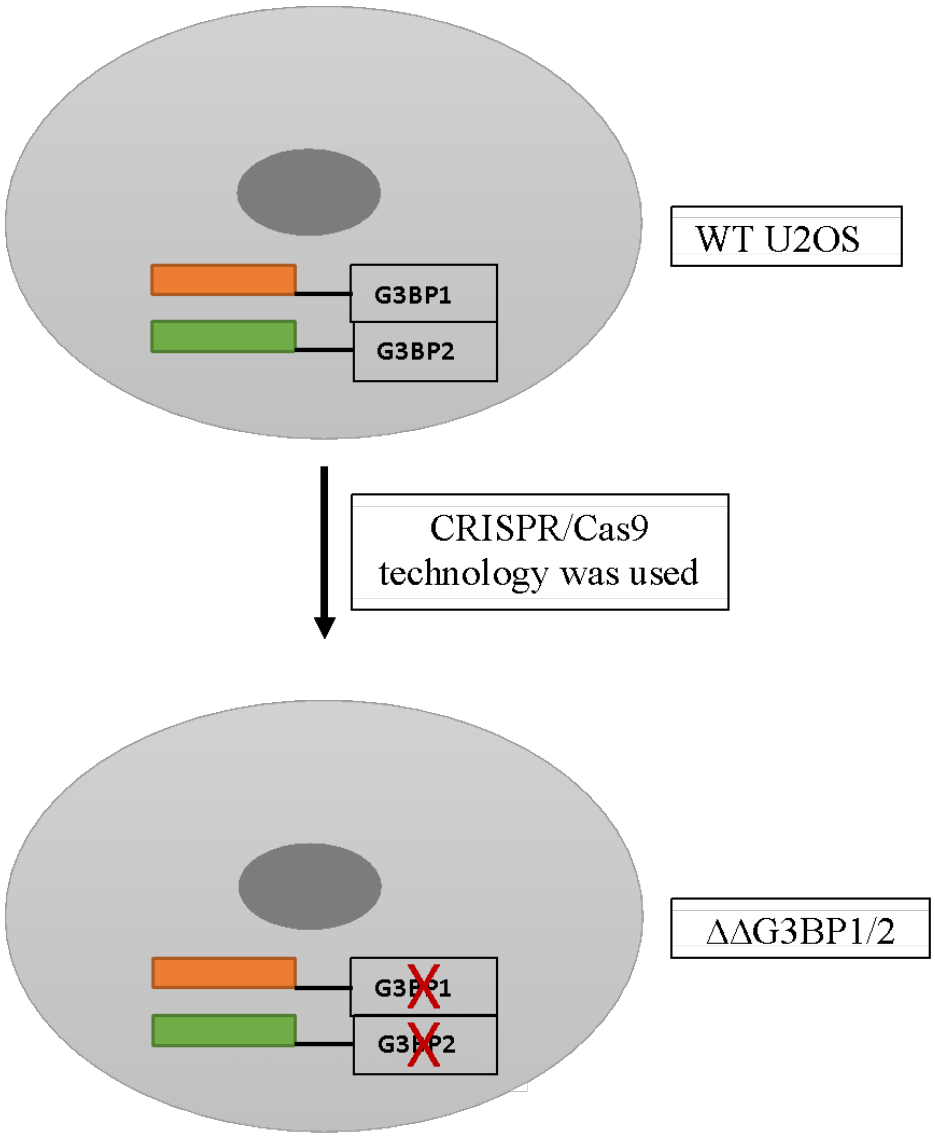

Figure 5.2 WT U2OS were used to generate cells lacking G3BP1 and G3BP2 (ΔΔG3BP1/2).

Endogenous G3BP1 and G3BP2 play a role in stress granule formation. CRISPR/Cas9 technology was used to develop cells lacking G3BP1 and G3BP2 (ΔΔG3BP1/2). The double knockout cells were then tagged with GFP.

5.4.2 Stress Granule Markers

5.4.2.1 G3BP1

In our study, we investigate formation of stress granules in WT U2OS and ΔΔG3BP1/2 cells under oxidative stress. Therefore, cells were exposed to 0.5 mM SA for 30 min. WT U2OS were then stained with G3BP1. ΔΔG3BP1/2 cells are tagged with GFP protein, a fluorescence marker used for visualization of cells. Expectedly, WT U2OS that were untreated with SA showed no formation of stress granules. Exposure of WT U2OS cells to SA stimulated formation of stress granules. G3BP1 was detected to be recruited to sites of stress granules (Figure 5.3). On the other hand, SA-untreated ΔΔG3BP1/2 showed no formation of stress granules. When ΔΔG3BP1/2 cells were treated with SA, they also did not show formation of stress granules (Figure 5.3). Our data showed that stress granules are stimulated upon SA exposure in WT U2OS. It also showed that knockout of G3BP1/2 inhibits stress granule formation in ΔΔG3BP1/2 cells which is consistent with other studies (Kedersha et al., 2016).

A quantitative comparison of stress granule number per cell was performed in WT U2OS and ΔΔG3BP1/2 cells. Hence, SA-untreated WT U2OS cells showed no stress granules (0 SGs/cell). However, when WT U2OS cells were treated with SA, they showed formation of stress granules. They showed formation of an average 8 SGs/cell. In contrast, SA-untreated ΔΔG3BP1/2 cells revealed no formation of stress granules. Exposure of ΔΔG3BP1/2 cells with SA did not stimulate stress granules. Thus, 0 SGs/cell were detected (Figure 5.4).

Collectively, our data shows that SA promoted stress granule formation in WT U2OS cells. G3BP1 was observed to be recruited to the sites of stress granule assembly. Additionally, knockout of G3BP1 and G3BP2 significantly reduced stress granule formation. Therefore, it is suggested that G3BP1 and G3BP2 play an essential role in stress granule formation.

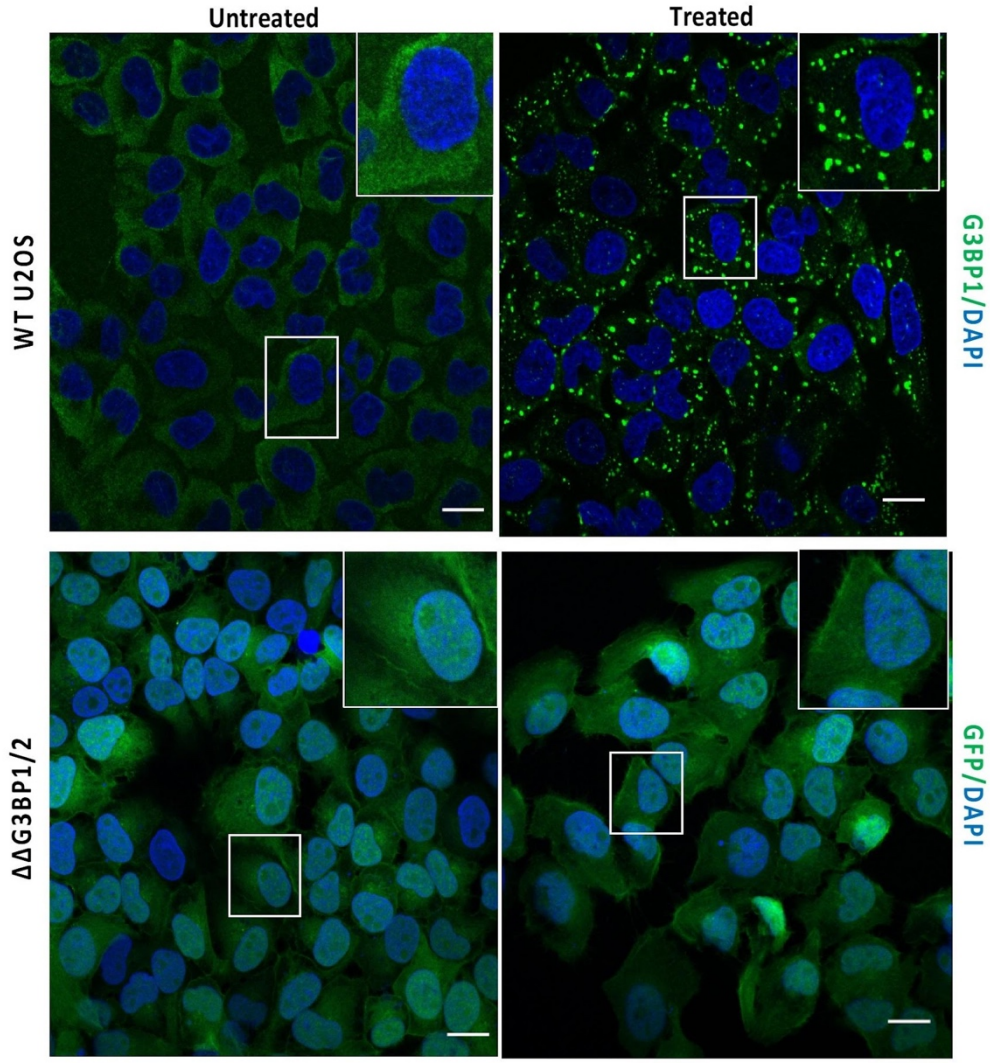

Figure 5.3 Knockout of G3BP1 and G3BP2 inhibited stress granules formation in ΔΔG3BP1/2 cells.

WT U2OS and ΔΔG3BP1/2 cells were treated/untreated with 0.5 mM SA for 30 min. G3BP1 was used as a marker for stress granules formation. WT U2OS cells showed assembly of stress granules under SA treatment. While ΔΔG3BP1/2 did not show formation of stress granules. Scale bar= 20 um.

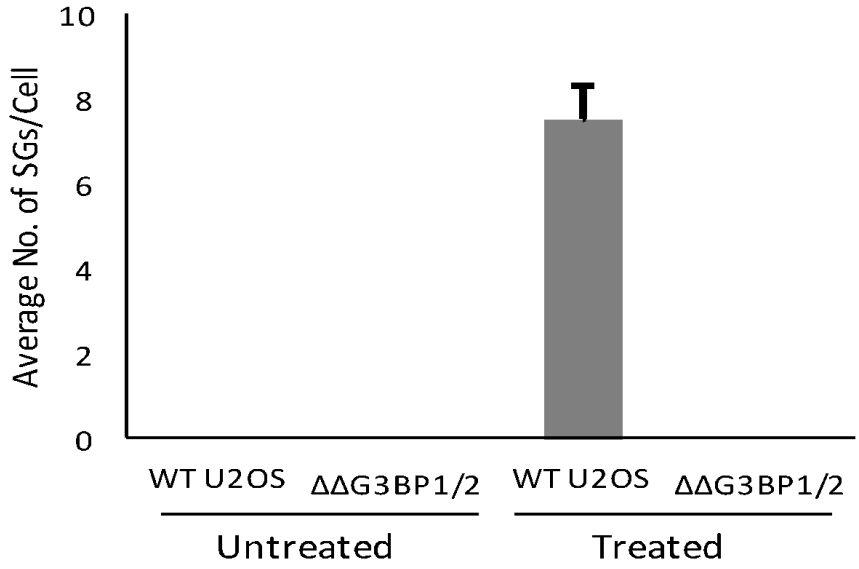

Figure 5.4 Sodium arsenite induced formation of stress granules in WT U2OS but not ΔΔG3BP1/2 cells.

SA-treated WT U2OS showed formation of 8 SGs/cell, whereas the untreated cells did not show stress granule formation. ΔΔG3BP1/2 cells showed 0 SGs/cells when treated with SA. Data represents mean ± SEM n=3, statistical significance was assessed using ANOVA t-test.

5.4.2.2 FXR1

It has been reported previously that several RNA-binding proteins locate to the sites of stress granule assembly. Of these RNA-binding proteins, FXR1 and eIF4G which are suggested to bind to the free mRNAs and translocate them to stress granules. Therefore, in our recent study, WT U2OS and ΔΔG3BP1/2 cells were treated/untreated with 0.5 mM SA for 30 min. Cells were then fixed and stained with G3BP1 and FXR1 antibodies to observe FXR1 recruitment to stress granules. Hence, SA-untreated WT U2OS cells were not observed to form stress granules. FXR1 was observed to be diffused in the cytoplasm. On the other hand, SA-treated cells showed formation of stress granules. FXR1 was detected to be recruited to stress granules. Co-localization of G3BP1 and FXR1 was seen at sites of mature stress granules (Figure 5.5).

Thus, this data suggests involvement of FXR1 is stress granule formation in WT U2OS cells upon exposure to oxidative stress.

Furthermore, ΔΔG3BP1/2 cells did not show formation of stress granules when they were untreated with SA. FXR1 was observed to be diffused in the cytoplasm. Similarly, SA-treated ΔΔG3BP1/2 cells did not show formation of stress granules. FXR1 was detected diffused in the cytoplasm (Figure 5.5). Thus, our data shows that exposure of ΔΔG3BP1/2 cells to SA did not stimulate FXR1 assembly suggesting the essential role of G3BP1 and G3BP2 in stress granule formation and recruitment of FXR1 to stress granules.

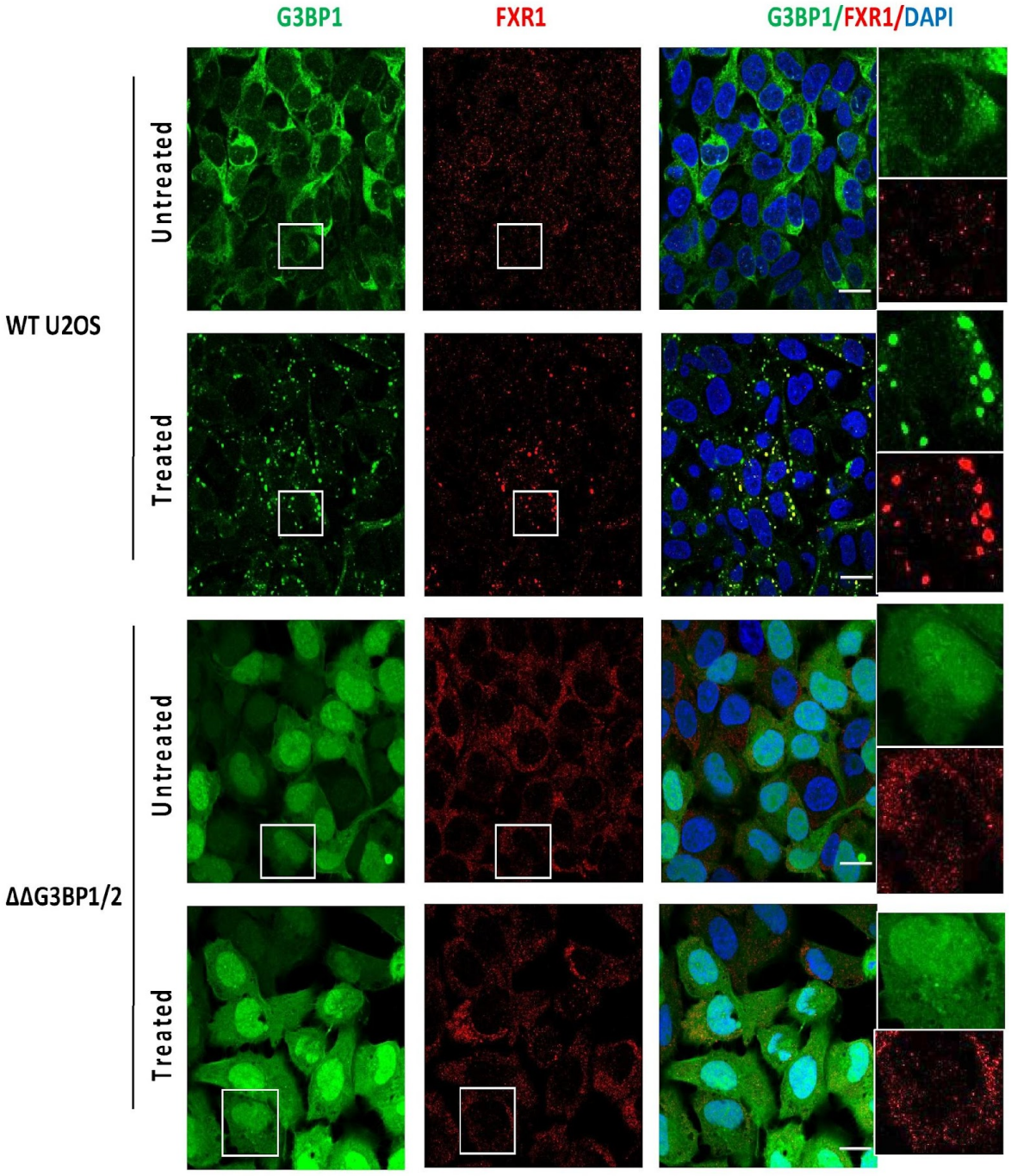

Figure 5.5 FXR1 is recruited to stress granules in WT U2OS cells and detected to be diffused in ΔΔG3BP1/2 cells.

WT U2OS and ΔΔG3BP1/2 were treated/untreated with 0.5 mM SA for 30 min and stained with FXR1 (Red) and G3BP1 (Green). WT U2OS cells showed assembly of stress granules. G3BP1 and FXR1showed co-localization at sites of stress granules. SA-treated and untreated ΔΔG3BP1/2 did not show formation of stress granules. FXR1 was detected to be diffused in the cytoplasm. Scale bar= 20 um.

Furthermore, a quantitative comparison of G3BP1 and FXR1 localized to stress granules was performed. ImageJ was used to count G3BP1 and FXR1 per cell separately. SA-treated WT U2OS cells showed formation of stress granules. G3BP1 and FXR1 were detected at sites of stress granule assembly. Hence, the number of G3BP1 recruited to stress granule sites was higher than FXR1. G3BP1 showed an increase of 2.6-fold change compared to FXR1. Thus, the percentage of G3BP1 and FXR1 that showed co-localization at sites of stress granules was 40%. This observation indicates that G3BP1 is first recruited to stress granules followed by FXR1. In contrast to WT U2OS, ΔΔG3BP1/2 cells did not show formation of stress granules under oxidative stress. G3BP1 and FXR1 were not detected to aggregate (Figure 5.6).

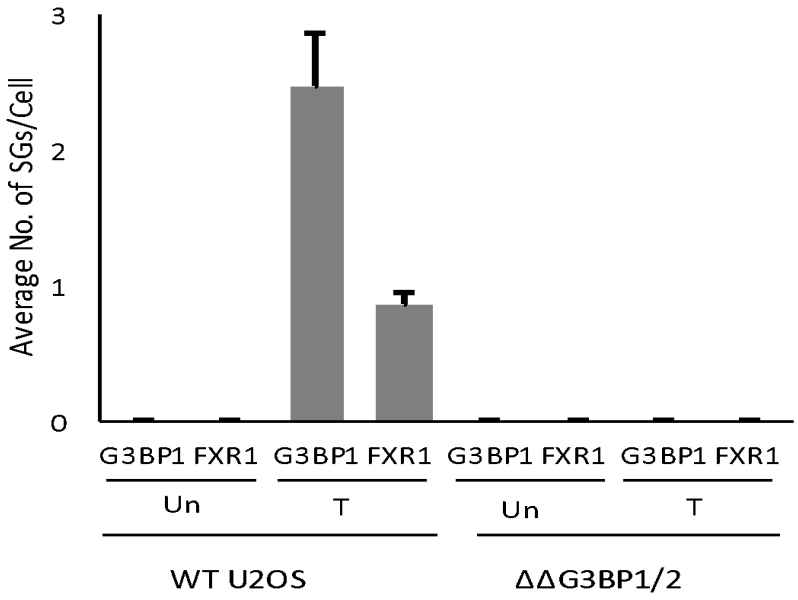

Figure 5.6 G3BP1 and FXR1 were detected at sites of stress granule assembly in WT U2OS cells.

WT U2OS cells showed assembly of stress granules and recruitment of G3BP1 and FXR1 to sites of stress granules. Whereas, ΔΔG3BP1/2 cells did not show formation of stress granules under SA exposure. G3BP1 recruited to stress granules was observed to increase (2.6-fold change) compared to FXR1in WT U2OS cells. Data represents mean ± SEM n=3, statistical significance was assessed using ANOVA t-test.

5.4.2.3 EIF4G

EIF4G is a translation initiation factor that has been observed to be recruited to stress granules under oxidative stress (Kedersha et al., 2016). Therefore, in our study, WT U2OS and ΔΔG3BP1/2 cells were treated/untreated with 0.5 mM SA for 30 min. Cells were then fixed and stained with G3BP1 and EIF4G antibodies to observe EIF4G recruitment to stress granules. Hence, SA-untreated WT U2OS cells were not detected to form stress granules. EIF4G was observed to be diffused in the cytoplasm. Nevertheless, SA-treated cells showed formation of stress granules. EIF4G was detected to be recruited to stress granules. Co-localization of G3BP1 and eIF4G was observed at sites of fully-developed stress granules (Figure 5.7). Thus, this data suggests involvement of eIF4G is stress granule formation in WT U2OS cells upon SA exposure.

Furthermore, ΔΔG3BP1/2 cells did not show formation of stress granules upon SA treatment. EIF4G was detected to be diffused in the cytoplasm. Similarly, SA-treated ΔΔG3BP1/2 cells did not show formation of stress granules and thus eIF4G was observed to be diffused in the cytoplasm (Figure 5.7). Therefore, our data indicates that exposure of ΔΔG3BP1/2 cells to SA do not stimulate eIF4G assembly suggesting the essential role of G3BP1 and G3BP2 in stress granule formation and recruitment of eIF4G to the sites of stress granule assembly.

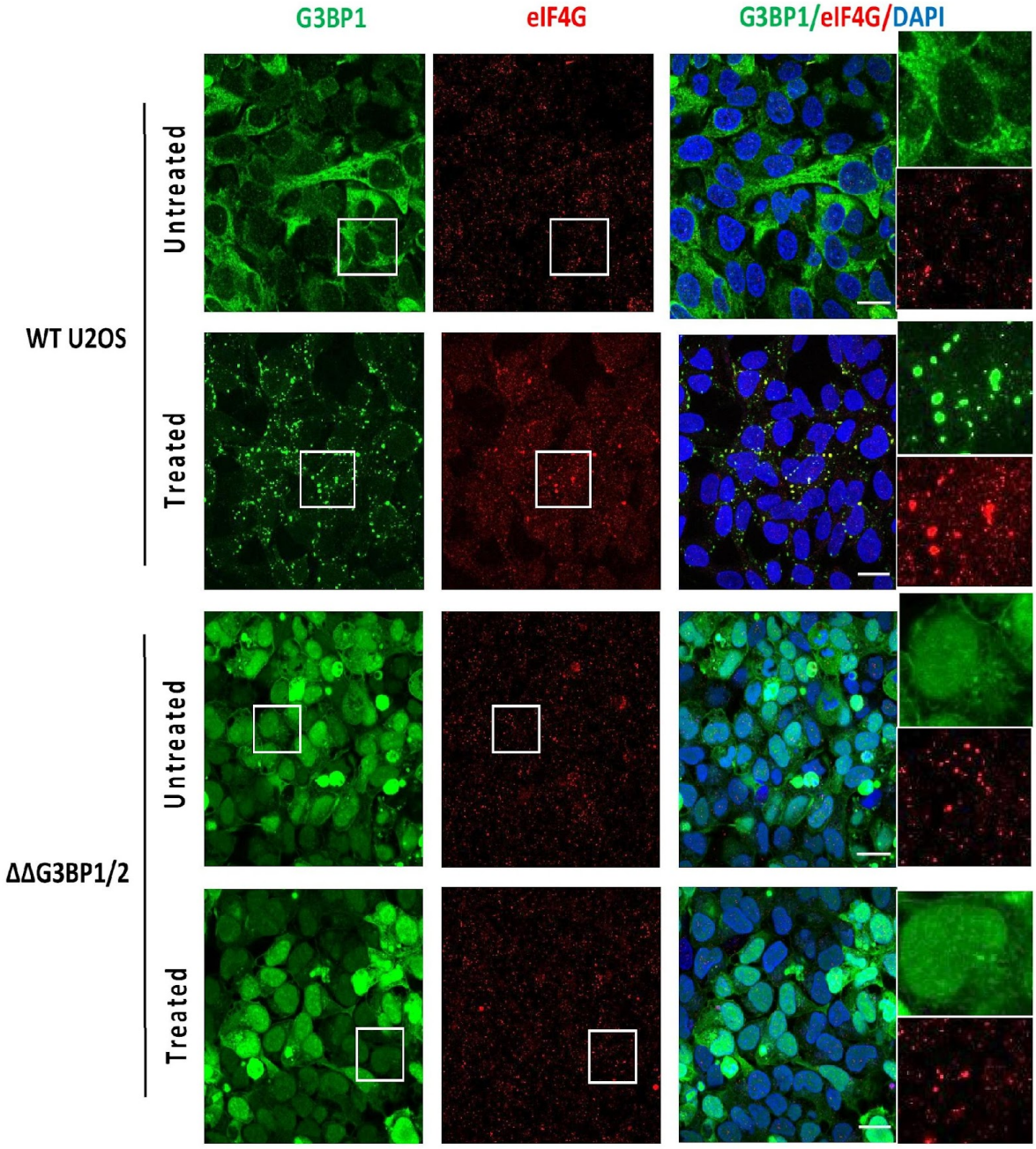

Figure 5.7 EIF4G is involved in stress granule formation in WT U2OS cells and detected to be diffused in ΔΔG3BP1/2 cells.

WT U2OS and ΔΔG3BP1/2 cells were treated/untreated with 0.5 mM SA for 30 min and stained with EIF4G (Red) and G3BP1 (Green). WT U2OS cells showed assembly of stress granules. Co-localization G3BP1 and EIF4G was observed at sites of stress granule. assembly. SA-treated and untreated ΔΔG3BP1/2 did not show formation of stress granules. EIF4G was detected to be diffused in the cytoplasm. Scale bar= 20 um.

Additionally, a quantitative comparison of G3BP1 and eIF4G recruitment to stress granules was performed. ImageJ was used to count G3BP1 and eIF4G per cell distinctly. Formation of stress granules was observed in SA-treated WT U2OS cells. G3BP1 and eIF4G were localized at sites of stress granules. Thus, the number G3BP1 recruited to stress granules was higher than eIF4G. G3BP1 showed an increase of 3-fold change compared to eIF4G. Thus, the percentage of G3BP1 and eIF4G that showed co-localization at sites of stress granules was 33%. Similar to FXR1, G3BP1 is suggested to first be recruited to stress granules and then followed by eIF4G. Furthermore, ΔΔG3BP1/2 cells did not show formation of stress granules when treated with SA. G3BP1 and eIF4G were not observed to aggregate in ΔΔG3BP1/2 cells (Figure 5.8). Thus, this finding indicates the crucial role of G3BP1 and G3BP2 in nucleating stress granule assembly and the recruitment of eIF4G to the sites of stress granules.

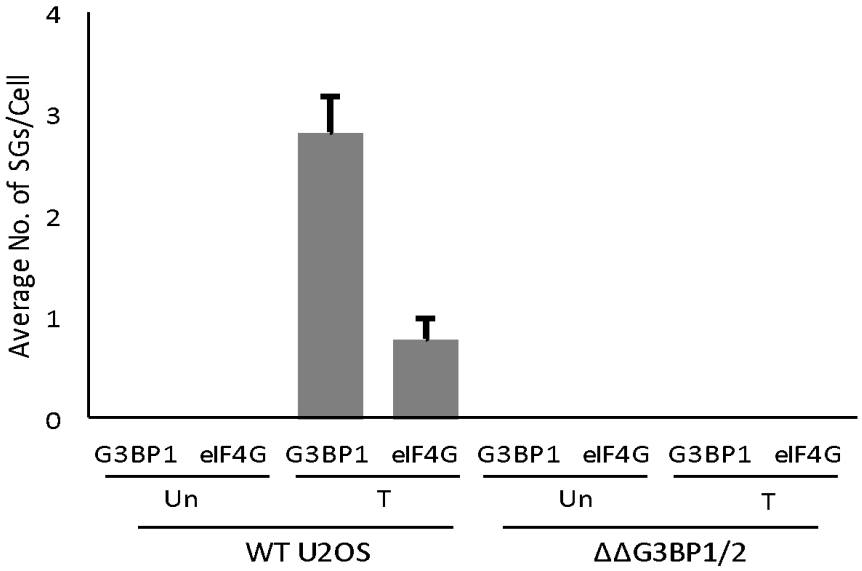

Figure 5.8 EIF4G was detected at sites of stress granule assembly in WT U2OS cells.

WT U2OS cells showed formation of stress granules and recruitment of G3BP1 and eIF4G to stress granules. In WT U2OS cells, G3BP1 recruited to stress granules was observed to increase (3-fold change) compared to eIF4G. ΔΔG3BP1/2 cells did not show formation of stress granules upon SA treatment. Data represents mean ± SEM n=3, statistical significance was assessed using ANOVA t-test.

5.4.3 G3BP Knockout Promotes Senescence in Most of the Population

Senescence, the irreversible cell-cycle arrest, acts as a safeguard to prevent the growth of unwanted or sick cells which are then eliminated by the immune system (Dimri, 2005; Campisi, 2007). Several studies have suggested that, in aged individuals, senescent cells escape the immune system and accumulate in different tissues for a long time causing age-related diseases such as cancer (Campisi and d'Adda di Fagagna, 2007; Campisi and Yaswen, 2009). This functional duality of senescent cells raises questions that are still unanswered. Frequent exposure of senescent cells to stress has been observed to make changes in expression of key genes involved in the anti-proliferative effect of senescent cells towards unwanted/sick cells (Campisi, 2005).

Repeated exposure of senescent cells to external assaults causes changes in genes involved in promoting and maintaining senescence and therefore, preventing tumour cells growth (Gallouzi, 2009; Lian and Gallouzi, 2009). Stress granules are protective bodies that are formed in stressed cells to enhance cells' viability (Kedersha and Anderson, 2002; Lavut and Raveh, 2012). Stress granules help cells to cope with external stressors and reprogram RNA metabolism and protein synthesis (Kedersha et al., 1999). Senescent cells were observed to form stress granules when exposed to oxidative stress (SA) or heat shock (Lian and Gallouzi, 2009). However, senescent cells' capacity of forming stress granules was observed to decrease compared to exponentially growing cells. The impaired ability of stress granule formation and slow recovery from stress were detected in senescent cells. This could indicate the impaired protective mechanism and delay in the synthesis of proteins required for the maintenance of senescence phenotype (Gallouzi, 2009; Lian and Gallouzi, 2009).

G3BP is essentially required for stress granule formation in proliferative cells. G3BP has been detected in stressed proliferative and senescent cells with a significant reduction in senescent cells (Omer et al., 2018). Stress granules are important for the pro-survival of senescent cells. However, whether G3BP plays a role in senescence by modulating signalling pathways that enhance cell proliferation and delay senescence is still unclear.

Several senescence promoting proteins such as p21 and plasminogen activator inhibitor-1 (PAI-1) were observed to be recruited to stress granules (Lian and Gallouzi, 2009; Omer et al., 2018). It was suggested that localization of senescence proteins to these entities maintains cell proliferation state (Omer et al., 2018). Therefore, in our study, we examine the role of G3BP (G3BP1 and G3BP2) in modulating senescence signalling pathways in U2OS cells. We investigate the consequences of disrupted stress granule assembly on delaying, maintaining or accelerating senescence phenotype.

Thus, in this study, we induced senescence in WT U2OS and ΔΔG3BP1/2 cells through using doxorubicin; a DNA-damage inducing drug. Therefore, cells were treated with 200 nM doxorubicin for 48 hours. Cells were then monitored for 7 days and tested using senescence markers: SA-ß-Gal staining, SAHF and p21antibodies.

5.4.3.1 Senescence Associated ß Galactosidase Activity (SA-ß-Gal)

SA-ß-Gal activity is a commonly used marker of senescence. Senescent cells stain blue at pH 6.0. The blue stain is produced due to the activity of ß-Galactosidase enzyme that catalyses the hydrolysis of β-galactosides into monosaccharides (Dimri et al., 1995; Morgunova et al., 2015).

In our study, SA-ß-Gal assay was used to examine senescence in WT U2OS and ΔΔG3BP1/2 cells. Therefore, cells were cultured until they reached 90% confluency. Then, cells were treated with 200 nM doxorubicin for 48 hours. Cells were collected at Day 0 (when Doxorubicin was added), Day 2 (when Doxorubicin was removed), Day 5, Day 7 and Day 9. SA-ß-Gal assay was performed through incubating the fixed cells with staining solution overnight at 37°C. Cells were observed under the bright microscope. WT U2OS cells showed development of blue stain at Day 2 post-doxorubicin treatment. An increased intensity of blue stain was observed at Day 7 and 9. SA-ß-Gal positive cells (blue) are senescent cells. Hence, senescent cells were detected at Day 2. The intensity of the stain increased at Day 7 and 9 indicating that most cells are senescent by Day 7 (Figure 5.9). Furthermore, ΔΔG3BP1/2 cells showed production of blue stain at Day 2 post-doxorubicin treatment. A gradual increase in the intensity of blue stain was detected in cells from Day 2 to Day 9 (Figure 5.9). This observation indicates that the number of senescent cells (blue stain) increases following doxorubicin treatment.

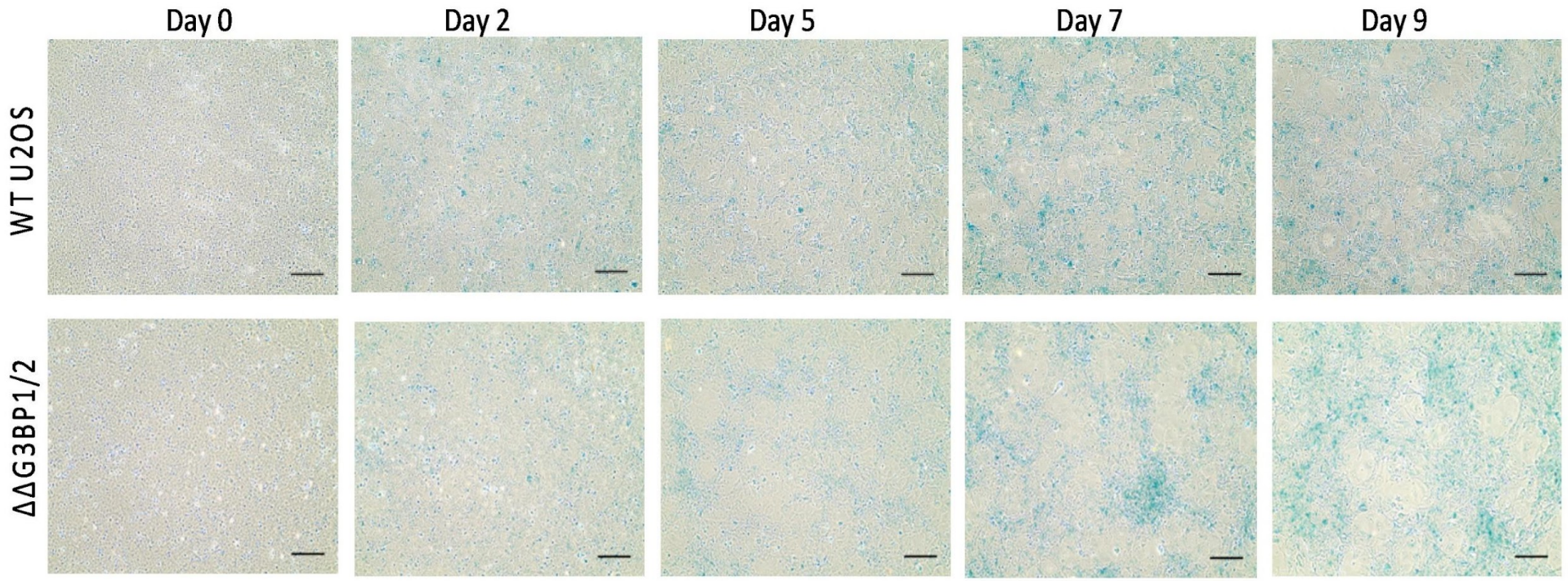

Figure 5.9 SA-ß-Gal positive cells were detected in WT U2OS and ΔΔG3BP1/2 cells. 200 nM Doxorubicin was used to induce senescence in WT U2OS and ΔΔG3BP1/2 cells. Cells were fixed and incubated with SA-ß-Gal staining solution overnight at 37ºC. Blue stain was detected in WT U2OS and ΔΔG3BP1/2 cells at Day 2 post-doxorubicin treatment. Gradual increase in the intensity of blue stain was observed in WT U2OS and ΔΔG3BP1/2 cells. The blue stain indicates SA-ß-Gal positive (senescent) cells. Scale bar= 100 um.

The percentage of SA-ß-Gal positive cells was counted in WT U2OS and ΔΔG3BP1/2 cells using ImageJ. The development of blue staining was monitored. WT U2OS cells showed a gradual increase in the intensity of blue staining. Hence, at Day 0, cells did not show production of blue stain which indicates that they are not yet senescent. At Day 2, cells showed the development of blue SA-ß-Gal positive staining. At Day 5, an increase of 2.5-fold change was detected in SA-ß-Gal positive cells. Moreover, cells showed a significant increase in SA-ß-Gal staining at Day 7. They showed a fold change of 4 compared to Day 5. A decline of 1.25-fold in the SA-ß-Gal positive cells was detected in Day 9 cells compared to Day 7. This might be due the loss of positive cells that underwent apoptosis (Figure 5.10).

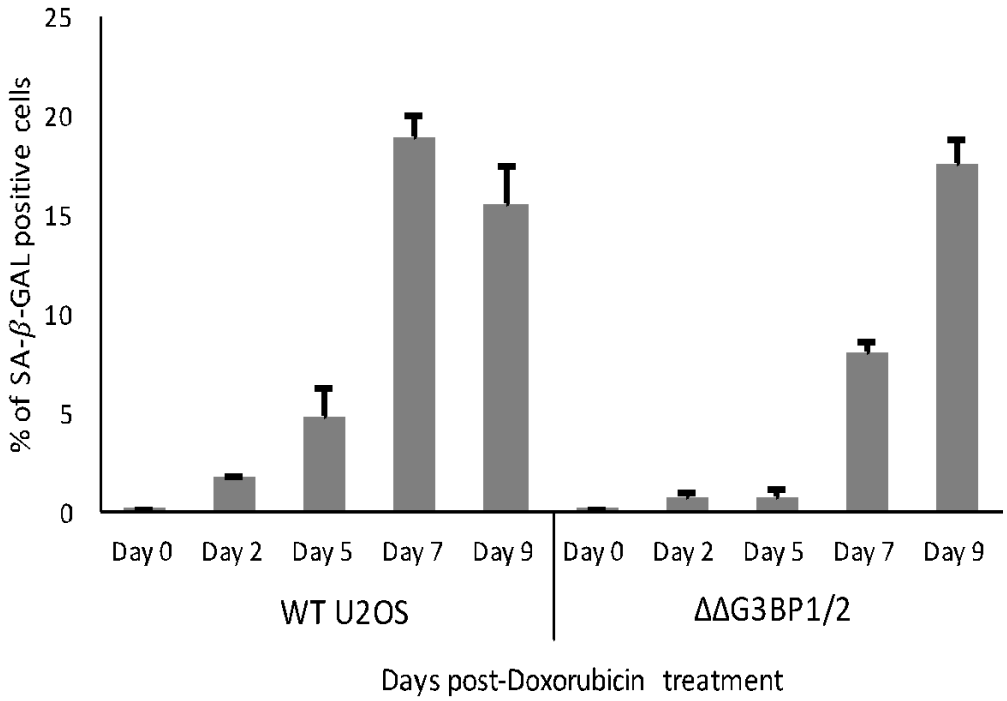

Figure 5.10 Knockout of G3BP1/2 accelerates development of senescence phenotype in ΔΔG3BP1/2 cells.

WT U2OS and ΔΔG3BP1/2 cells showed development of blue stain at Day 2 post-doxorubicin treatment. At Day 9, ΔΔG3BP1/2 showed an increase in SA-ß-Gal positive cells compared to WT U2OS. Data represents mean ± SEM n=3, statistical significance was assessed using ANOVA t-test.

Furthermore, ΔΔG3BP1/2 cells showed development of blue stain at Day 2 post-doxorubicin treatment. At Day 5, a minor increase was observed. Thus, a significant increase in SA-ß-Gal positive cells was observed at Day 7 compared to Day 5. An increase of 8-fold change was observed at Day 7. Moreover, at Day 9, ΔΔG3BP1/2 cells showed an increase of 2.4-fold change compared to Day 7 cells (Figure 5.10). Thus, SA-ß-Gal staining showed that at Day 9, ΔΔG3BP1/2 cell cultures are enriched in SA-ß-Gal positive cells compared to WT U2OS cells. Therefore, our data suggests that WT U2OS cells reach senescence faster (Day 5) compared to ΔΔG3BP1/2 cells; however, knockout of G3BP1/2 promotes senescence in most of the population by Day 9.

5.4.3.2 Senescence-Associated Heterochromatin Foci (SAHF)

In addition to the expression of SA-ß-Gal activity, formation of SAHF is one of the characteristic of senescent cells. SAHF are formed when the chromatin in the nucleus of senescent cells undergoes remodelling by forming domains of heterochromatin (Zhang et al., 2007). In our recent study, we examined SAHF formation in WT U2OS and ΔΔG3BP1/2 cells following their treatment with doxorubicin. SAHF formation was monitored at Day 0, Day 2, Day 5, Day 7 and Day 9 post-doxorubicin treatment. Cells forming 5 or more SAHF were considered to be senescent cells. WT U2OS cells showed few (less than 5) granular structures at Day 0, 2 and 5. At Day 7 and 9, WT cells showed an increased number of SAHF (more than 5). On the other hand, ΔΔG3BP1/2 cells showed few foci at Day 0 and 2. At Day 5, they showed high formation of the foci (more than 5) with a dramatic increase at Day 7 and 9 (Figure 5.11). Thus, our data suggests that ΔΔG3BP1/2 cells are displaying increased formation of senescence-associated phenotype: SAHF compared to WT U2OS cells.

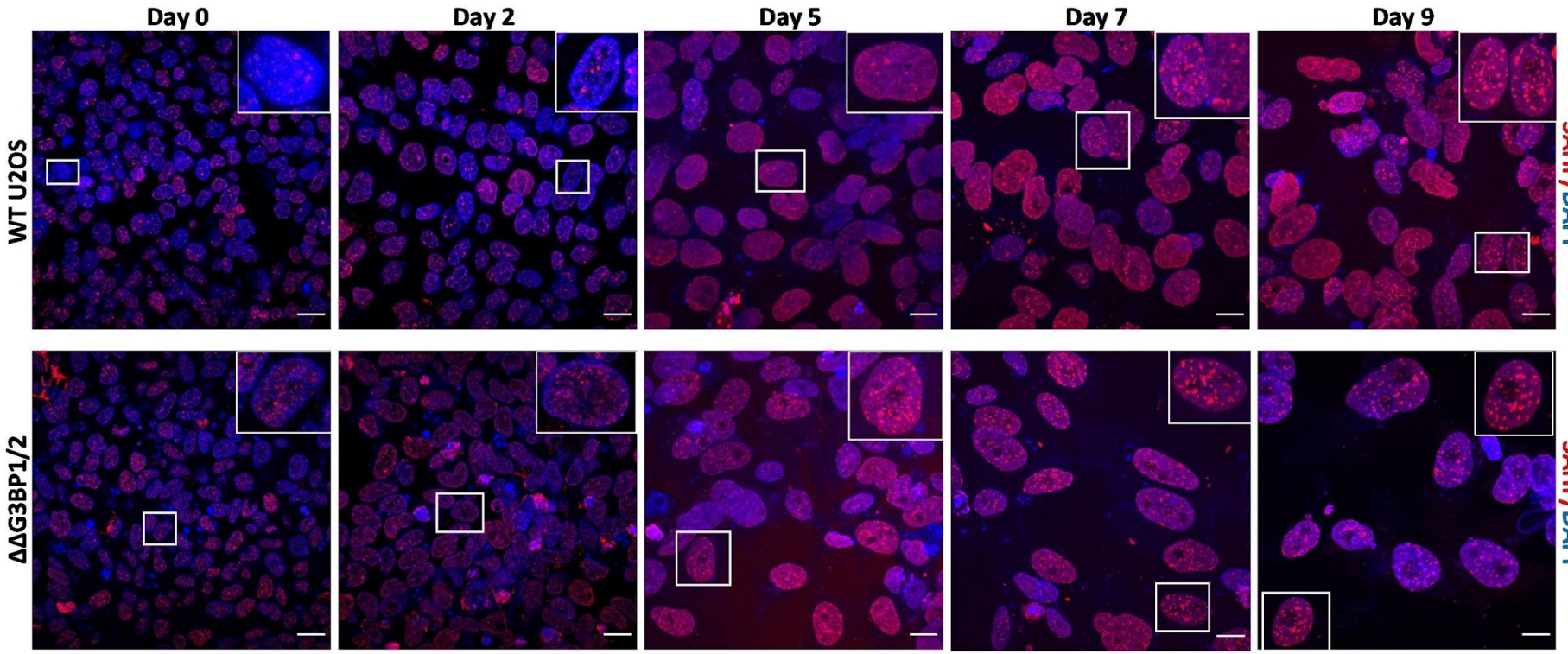

Figure 5.11 WT U2OS and ΔΔG3BP1/2 cells showed gradual formation of SAHF. WT U2OS and ΔΔG3BP1/2 cells were treated with 200 nM doxorubicin for 48 hours. Cells were collected at Day 0, 2, 5, 7 and 9, fixed and stained with SAHF antibody (Red). WT U2OS cells showed no/few SAHF (less than 5 foci per cell) at Day 0, 2 and 5. At Day 7 and 9, they showed increased number of SAHF. ΔΔG3BP1/2 cells showed few SAHF (less than 5 foci per cell) at Day 0 and 2. At Day 5, they showed high formation of the SAHF (more than 5 foci per cell) which then showed a dramatic increase at Day 7 and 9. Scale bar= 20 um.

Furthermore, ImageJ was used to perform quantitative comparison of SAHF formation in WT U2OS and ΔΔG3BP1/2 cells. In WT U2OS cells, SAHF staining showed formation of no/few SAHF at Day 0, 2 and 5. At Day 7, cells showed an increase in the number of SAHF-forming cells of a 3.75-fold change compared to Day 5 cells. Moreover, at Day 9, cells revealed elevated formation of SAHF. An increase of 2.5-fold change was detected in SAHF-forming cells at Day 9 compared to Day 7. In contrast, ΔΔG3BP1/2 cells did not show formation of >5 SAHF per cell at Day 0 and 2. Therefore, the percentage of SAHF-forming cells was counted to be 0%. At Day 5, cells showed a significant increase in SAHF formation. By Day 7, cells showed an increase in SAHF-forming cells. They revealed an increase of 2.6-fold change compared to Day 5 cells. At Day 9, cells showed an increased number of SAHF-forming cells compared to Day 7. They showed an increase of 1.2-fold change (Figure 5.12).

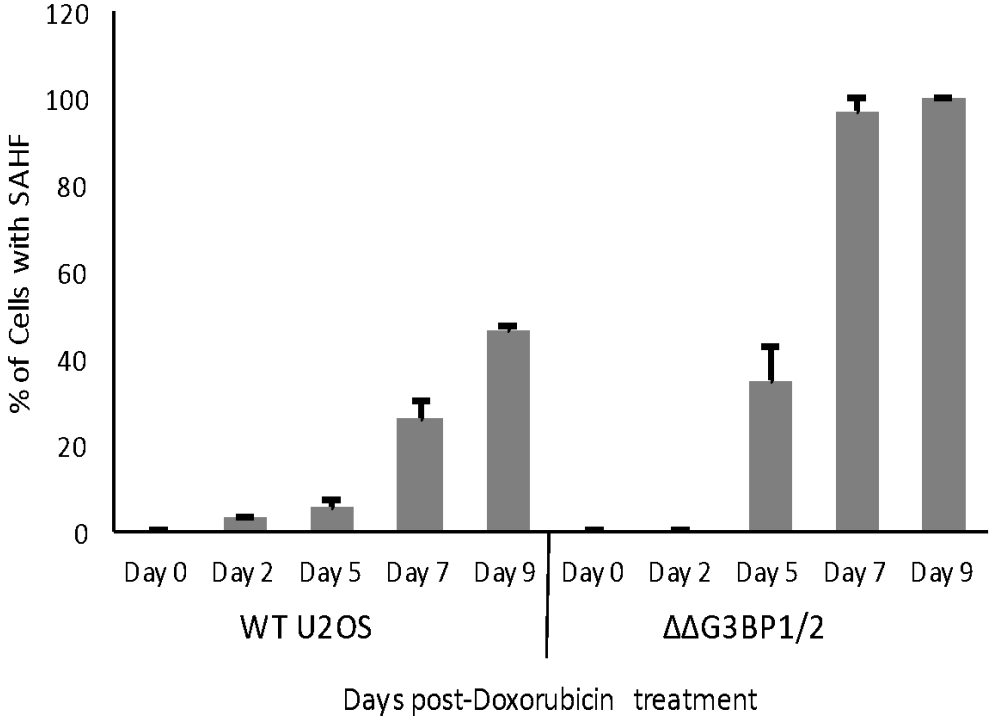

Figure 5.12 Absence of G3BP1/2 promotes senescence phenotype in mostly all ΔΔG3BP1/2 cells.

WT U2OS and ΔΔG3BP1/2 cells showed gradual increase in the SAHF foci. WT U2OS cells showed formation of SAHF by Day 2 whereas, ΔΔG3BP1/2 cells showed FAHF formation by Day 5. At Day 9, approximately 100% of ΔΔG3BP1/2 cells showed formation of SAHF. However, only 47% of WT U2OS cells were detected to form SAHF. Data represents mean ± SEM n=3, statistical significance was assessed using ANOVA t-test.

Collectively, WT U2OS and ΔΔG3BP1/2 cells showed gradual increase in SAHF foci. However, the number of SAHF varied between the two cell types. WT U2OS cells showed formation of SAHF by Day 2 whereas, ΔΔG3BP1/2 cells showed SAHF formation by Day 5. By Day 9, approximately 100% of ΔΔG3BP1/2 cells showed formation of SAHF. However, only 47% of WT U2OS cells were detected to form SAHF (Figure 5.12). Thus, our data suggests that absence of G3BP1/2 promotes senescence phenotype.

5.4.3.3 P21

Senescence phenotype is associated with high expression of p21 protein which is known to promote senescence in cells. The transcriptional activation of p21, a cyclin-dependent kinase induces cell cycle arrest (Shtutman et al., 2017). p21 mRNA was observed to be localized to stress granules, which in turn interferes with its translation in senescent IDH4 cells (Lian and Gallouzi, 2009). Therefore, in our study we tested expression of p21 protein in WT U2OS and ΔΔG3BP1/2 cells.

Thus, cells were induced to senescence through incubating them with 200 nM doxorubicin for 48 hours. Cells were then collected at Day 0 and Day 9. Following protein extraction, protein samples were incubated with p21 antibody. At Day 9, WT U2OS and ΔΔG3BP1/2 cells showed an increase in the expression of p21 protein compared to Day 0 (control) (Figure 5.13). The levels of p21 protein is studied and quantified in chapter 7.

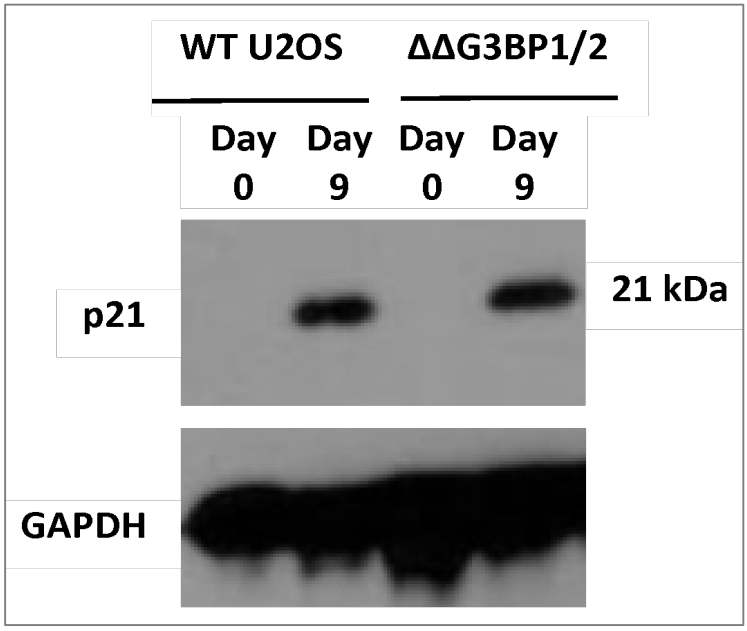

Figure 5.13 High p21 protein level was detected in ΔΔG3BP1/2 cells.
Senescence was induced in WT U2OS and ΔΔG3BP1/2 cells through incubating cells with 200 nM doxorubicin for 48 hours. Western blots were performed using cell extracts from cells at Day 0 (control) and Day 9 post-doxorubicin treatment. p21 and GAPDH (loading control) antibodies were used.

5.4.4 Stress in Cells Re-Constituted with G3BP1

The importance of G3BP, an essential driver of stress granule formation has been studied in the development of senescence phenotype (Omer et al., 2018). It was shown that repeated exposure to SA stress in the presence of G3BP delays senescence. Additionally, knockdown of G3BP1 in IDH4 cells through using G3BP1-specific siRNA increased the percentage of SA-ß-Gal positive cells compared to the control cells (Omer et al., 2018). Therefore, it has been suggested that G3BP plays a role in senescence phenotype development (Omer et al., 2018).

As we have shown previously that knockout of G3BP1/2 (ΔΔG3BP1/2) increased the percentage of senescence markers (SA-ß-Gal, SAHF and p21)-positive cells compared to WT U2OS (where endogenous G3BP1 and G3BP2 are present). This finding indicates that depletion of G3BP1/2 accelerates the development of senescence phenotype suggesting the importance of G3BP1/2 in senescence and the signalling pathways that lead to senescence. To address the role of G3BP1 on stress granule formation and senescence, we assessed whether adding G3BP1 to the double-knockout cells (ΔΔG3BP1/2) rescues stress granule competence and effects senescence phenotype development (see section 5.7).

In order to answer the questions asked above, GFP-tagged G3BP1 was genetically re-constituted to ΔΔG3BP1/2 cells through transient transfection of cells with GFP-G3BP1 protein (Kedersha et al., 2016) (Figure 5.14). ΔΔG3BP1/2+GFP-G3BP1 (hereafter referred as GFP-G3BP1) cells were developed and tested for stress granule assembly and senescence phenotype development.

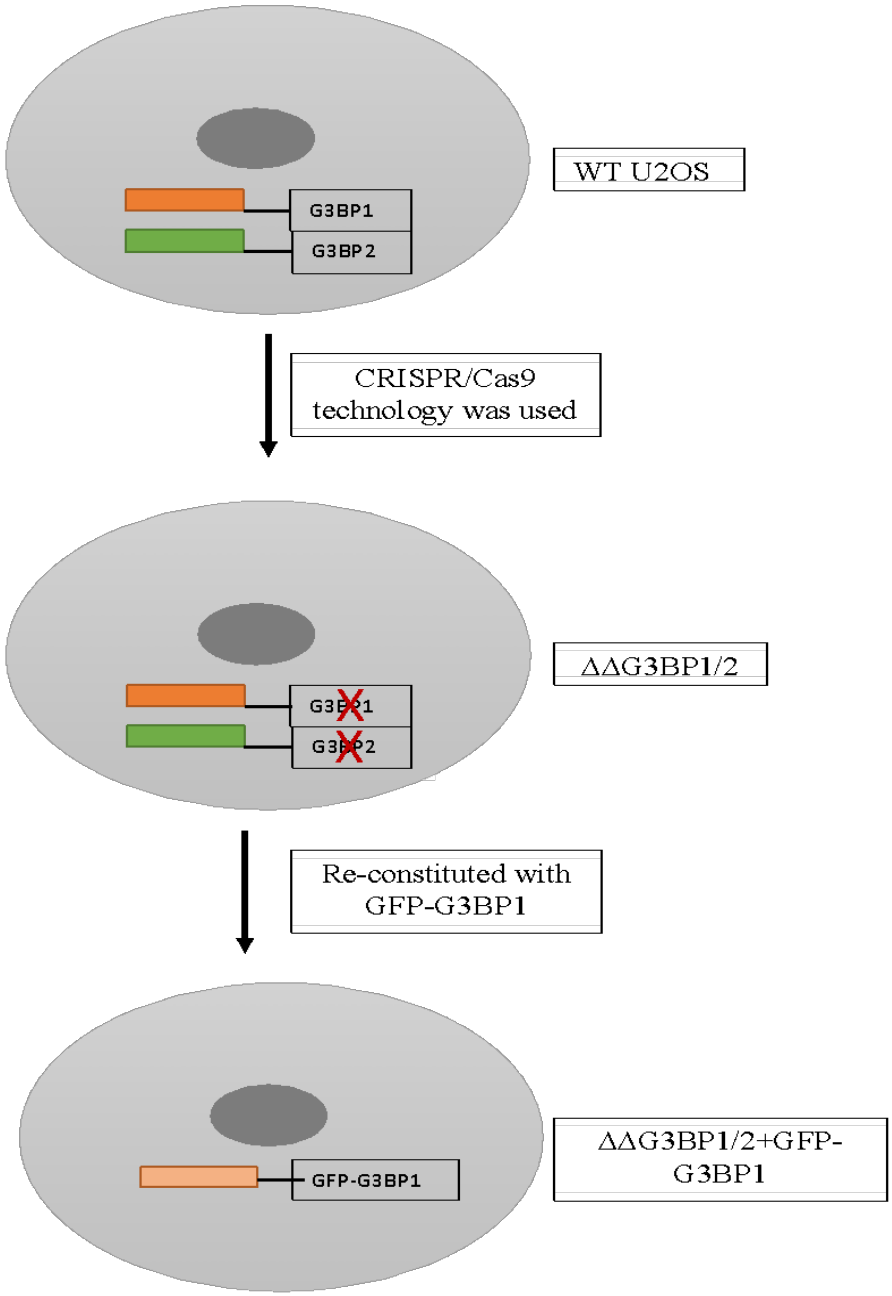

Figure 5.14 Schematic diagram shows the development of ΔΔG3BP1/2+GFP-G3BP1 through transient transfection of ΔΔG3BP1/2 with GFP-G3BP1.

To test the effect of G3BP1 on stress granule competence and senescence phenotype development, G3BP1/2 knockout cells (ΔΔG3BP1/2) were transiently transfected with GFP-tagged G3BP1 forming ΔΔG3BP1/2+GFP-G3BP1 cells.

5.4.4.1 Stress Granule Markers

5.4.4.1.1 G3BP1

The process of stress granule formation in knockout cells (ΔΔG3BP1/2) was observed to be depleted due to the ablation of G3BP1 and G3BP2. Hence, ΔΔG3BP1/2 cells were incapable of stress granule formation under oxidative stress (see section 5.4). Therefore, we examine here whether stress granule formation is rescued in transfectant GFP-G3BP1 cells.

Therefore, GFP-G3BP1 cells were treated with/out 0.5 mM SA for 30 min. GFP-G3BP1 cells are tagged with GFP protein, a fluorescence marker used for visualization of G3BP1 and stress granule assembly. Expectedly, GFP-G3BP1 cells that were untreated with SA showed no formation of stress granules. Exposure of GFP-G3BP1 cells to SA stimulated formation of stress granules. G3BP1 was detected to be recruited to sites of stress granules (Figure 5.15). On the other hand, exposure of WT U2OS cells to SA stimulated formation of stress granules. G3BP1 was detected to be recruited to sites of stress granules. Moreover, when ΔΔG3BP1/2 cells were treated with SA, they did not show formation of stress granules (Figure 5.15). Thus, our observations indicate that re-constitution of cells with G3BP1 rescues stress granule formation. G3BP1 is recruited to sites of stress granules. Our data is consistent with other studies (Kedersha et al., 2016) where it has been shown that double knockout of G3BP1/2 inhibited stress granules, however, presence of G3BP1 only promoted stress granule formation.

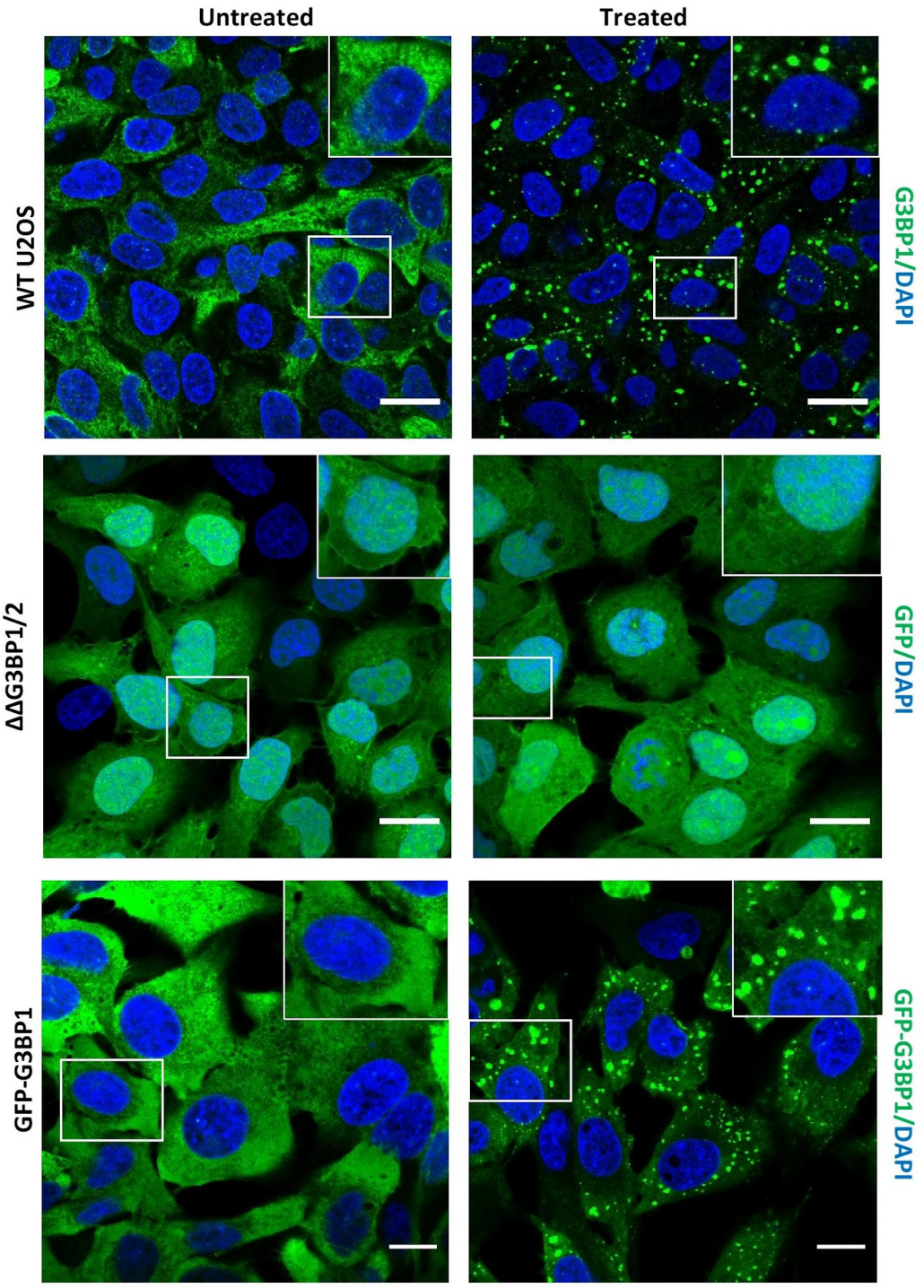

Figure 5.15 Stress granule formation is rescued in GFP-G3BP1 cells. WT U2OS, ΔΔG3BP1/2 and GFP-G3BP1 cells were treated with 0.5 mM SA for 30 min. WT U2OS and GFP-G3BP1 showed assembly of stress granules while ΔΔG3BP1/2 did not show formation stress granules. Scale bar= 20 um.

A quantitative comparison of stress granule number per cell was performed in SA-treated GFP-G3BP1, WT U2OS and ΔΔG3BP1/2 cells. Hence, SA-treated WT U2OS cells showed formation of stress granules. They showed formation of an average 8 SGs/cell. In contrast, SA-treated ΔΔG3BP1/2 cells revealed no formation of stress granules. Exposure of ΔΔG3BP1/2 cells with SA did not stimulate stress granules. Thus, 0 SGs/cell were detected. Moreover, SA-treated GFP-G3BP1 cells showed formation of stress granules. SA stimulated formation of 5 SGs/cells in GFP-G3BP1 cells (Figure 5.16). Hence, the number of stress granules was observed to decline in GFP-G3BP1 when compared to WT U2OS. They showed a decrease of 1.6-fold change. Our observation suggests that presence of only one form of G3BP: G3BP1 rescues formation of 62.5% of stress granules.

Collectively, our data shows that SA promoted stress granule formation in WT U2OS cells. G3BP1 was observed to be recruited to the sites of stress granule assembly. Additionally, knockout of G3BP1 and G3BP2 significantly reduced stress granule formation. Re-constitution of cells with G3BP1 rescues formation of stress granules in GFP-G3BP1 cells. It promoted formation of 62.5% of stress granules. Therefore, it is suggested that G3BP1 plays an essential role in stress granule formation.

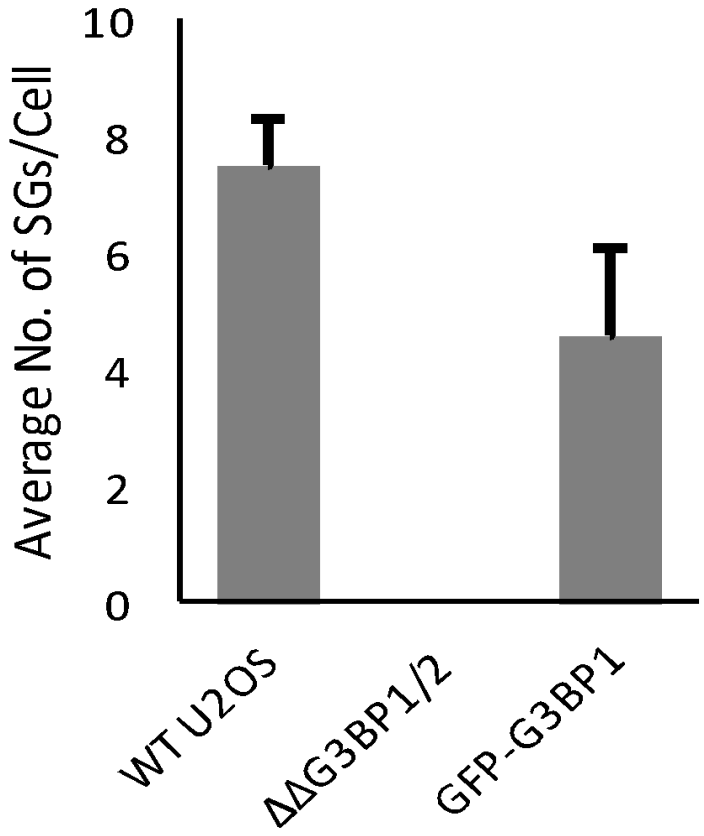

Figure 5.16 G3BP1 promotes formation of stress granules in GFP-G3BP1 under oxidative stress.

WT U2OS, ΔΔG3BP1/2 and GFP-G3BP1 cells were treated with 0.5 mM SA for 30 min. WT U2OS showed assembly of stress granules while ΔΔG3BP1/2 did not show stress granule formation Re-constitution of cells with G3BP1 promoted formation of stress granules in GFP-G3BP1 cells under oxidative stress. It promoted formation of 62.5% of stress granules. Data represents mean ± SEM n=3, statistical significance was assessed using ANOVA t-test.

5.4.4.1.2 FXR1

The RNA-binding proteins FXR1 and eIF4G were detected to localize at stress granules in WT U2OS cells (see section 5.4). Therefore, in our recent study, WT U2OS and ΔΔG3BP1/2 cells were treated/untreated with 0.5 mM SA for 30 min. Cells were then fixed and stained with FXR1 antibody to observe FXR1 recruitment to stress granules. Hence, SA-untreated GFP-G3BP1 cells were not observed to form stress granules. FXR1 was observed to be diffused in the cytoplasm. On the other hand, SA-treated cells showed formation of stress granules. FXR1 was detected to be recruited to stress granules. Co-localization of G3BP1 and FXR1 was seen at sites of mature stress granules (Figure 5.17A). Thus, this data suggests that FXR1 is recruited to stress granules upon oxidative stress exposure.

Furthermore, a quantitative comparison of G3BP1 and FXR1 that were localized at stress granule sites was performed. ImageJ was used to count G3BP1 and FXR1 per cell separately. SA-treated GFP-G3BP1 cells showed formation of stress granules. G3BP1 and FXR1 were detected at sites of stress granule assembly. Hence, the number G3BP1 recruited to stress granule sites was higher than FXR1. G3BP1 showed an increase of 1.3-fold change compared to FXR1. The percentage of G3BP1 and FXR1 co-localization was detected as 67% (Figure 7.17B). This observation indicates that G3BP1 is first recruited to stress granules followed by FXR1. It also indicates that presence of G3BP1 only promotes FXR1 assembly under oxidative stress.

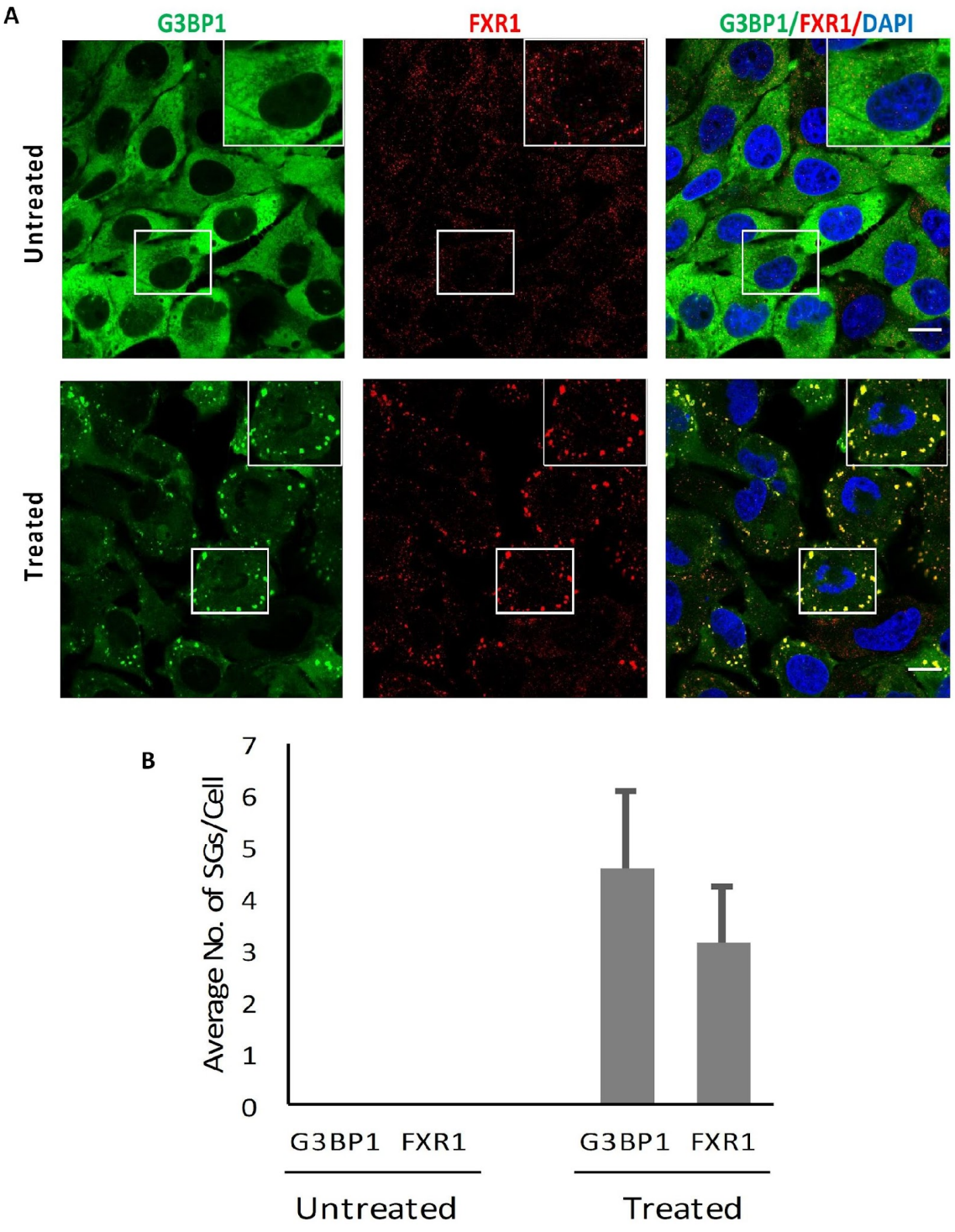

Figure 5.17 FXR1 is recruited to stress granules in GFP-G3BP1 cells.

GFP-G3BP1 cells were treated/untreated with 0.5 mM SA for 30 min and stained with FXR1 antibody. Cells showed assembly of stress granules (A). The percentage of G3BP1 and FXR1 that showed co-localization at sites of stress granules was 67% (B). Scale bar= 20 um. Data represents mean ± SEM n=3, statistical significance was assessed using ANOVA t-test.

5.4.4.1.3 EIF4G

The translation initiation factor EIF4G has been detected to localize at stress granule sites under oxidative stress (Kedersha et al., 2016). Therefore, in our study, GFP-G3BP1 cells were treated/untreated with 0.5 mM SA for 30 min. Cells were then fixed and stained with eIF4G antibody to observe eIF4G recruitment to stress granules. Hence, SA-untreated GFP-G3BP1 cells were not detected to form stress granules. eIF4G was observed to be diffused in the cytoplasm. Nevertheless, SA-treated cells showed formation of stress granules. EIF4G was detected to be recruited to stress granules. Co-localization of G3BP1 and eIF4G was observed at sites of fully-developed stress granules (Figure 5.18A). Thus, this data suggests involvement of eIF4G in stress granule formation in WT U2OS cells upon SA exposure.

Additionally, a quantitative comparison of G3BP1 and eIF4G recruitment to stress granules was performed. ImageJ was used to count G3BP1 and eIF4G per cell distinctly. Formation of stress granules was observed in SA-treated GFP-G3BP1 cells. G3BP1 and eIF4G were observed to localize at sites of stress granules. Thus, the number G3BP1 recruited to stress granules was higher than eIF4G. G3BP1 showed an increase of 4-fold change compared to eIF4G (Figure 5.18B). Thus, the percentage of G3BP1 and eIF4G that showed co-localization at sites of stress granules was 25%. Therefore, it is suggested that presence of only one form of G3BP reduces the recruitment of eIF4G to stress granules.

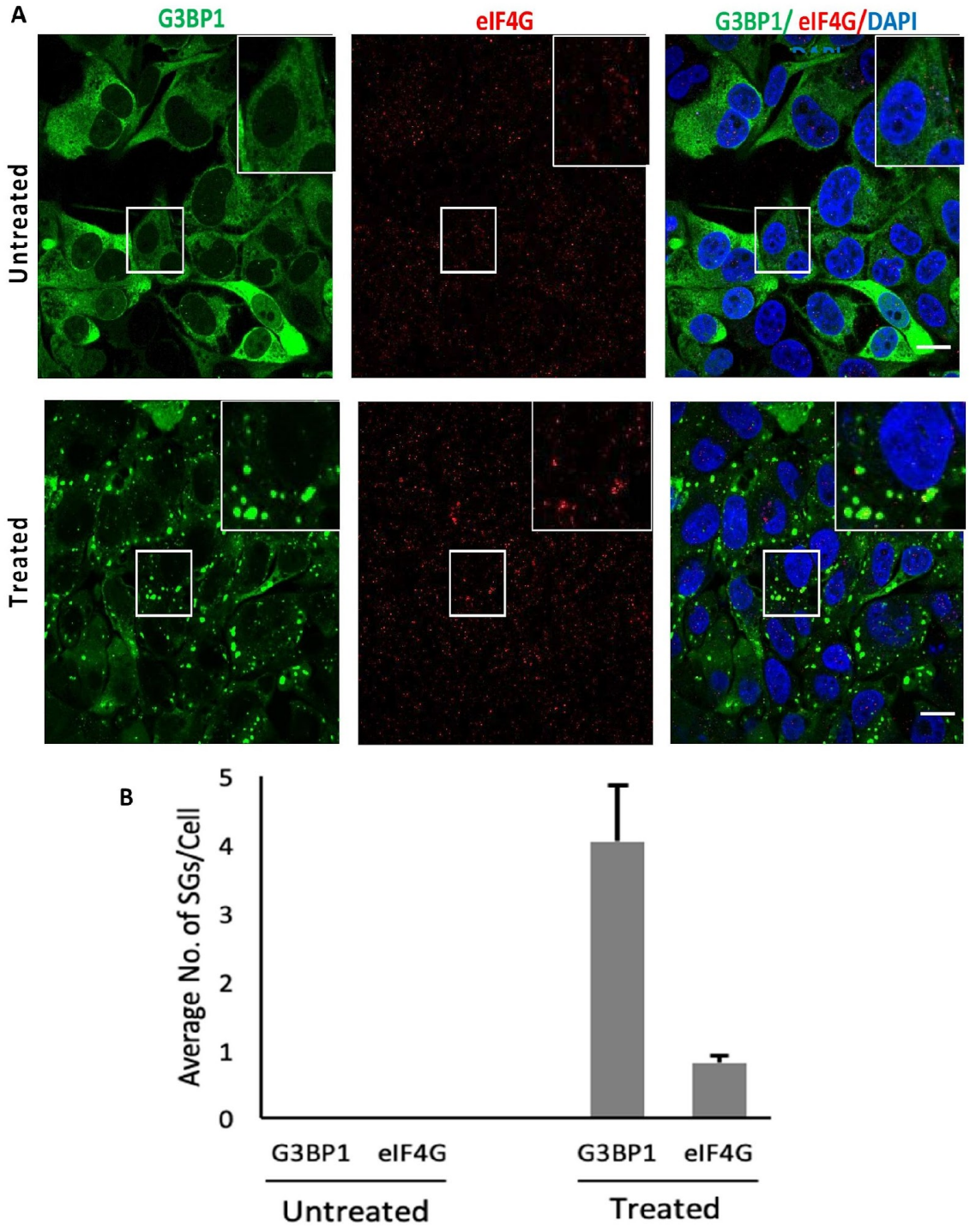

Figure 5.18 EIF4G is recruited to stress granules in GFP-G3BP1 cells.

GFP-G3BP1 cells were treated/untreated with 0.5 mM SA for 30 min and stained with EIF4G antibody. Cells showed assembly of stress granules (A). The percentage of G3BP1 and EIF4G that showed co-localization at sites of stress granules was 25% (B). Scale bar= 20 um. Data represents mean ± SEM n=3, statistical significance was assessed using ANOVA t-test.

5.4.5 Senescence in GFP-G3BP1 Cells

5.4.5.1 Senescence Associated ß-Galactosidase Activity (SA-ß-Gal)

SA-ß-Gal activity is used as a marker for senescence. Senescent cells stain blue at pH 6.0. The blue stain is produced due to the activity of ß-Galactosidase enzyme that catalyses the hydrolysis of β-galactosides into monosaccharides (Dimri et al., 1995; Morgunova et al., 2015).

Thus, in our study, SA-ß-Gal assay was used to examine senescence phenotype in GFP-G3BP1 cells. Therefore, cells were cultured until they reached 90% confluency. Then, cells were treated with 200 nM doxorubicin for 48 hours. Cells were collected at Day, Day 2, Day 5, Day 7 and Day 9. SA-ß-Gal assay was performed through incubating the fixed cells with staining solution overnight at 37°C. Cells were observed under the bright microscope. GFP-G3BP1 cells showed development of blue stain at Day 2 post-doxorubicin treatment. An increased intensity of blue stain was observed at Day 5 and 7. SA-ß-Gal positive cells (blue) are senescent cells. However, SA-ß-Gal positive cells in GFP-G3BP1 were significantly low compared to WT U2OS cells indicating that G3BP1 only does not promote senescence phenotype (Figure 5.19).

The percentage of SA-ß-Gal positive cells was counted in GFP-G3BP1 cells using ImageJ. The production of blue stain was monitored. GFP-G3BP1 cells showed a gradual increase in the intensity of blue stain. Hence, at Day 0, cells did not show production of blue stain which indicates that cells are still proliferating. At Day 2, cells showed development of blue stain. This observation indicates that cells possess senescence associated changes; SA-ß-Gal positive staining. At Day 5, an increase of 1.6-fold change was detected in SA-ß-Gal positive cells. The

percentage of SA-ß-Gal positive cells was maintained at Day 7. A decline of 3-fold change in the SA-ß-Gal positive cells was detected in Day 9 cells compared to Day 7. This might be due to the loss of SA-ß-Gal positive cells that underwent apoptosis (Figure 5.20A). When we compare GFP-G3BP1 cells to WT U2OS cells, SA-ß-Gal positive GFP-G3BP1 cells was significantly reduced. It showed a decline of 16-fold change (Figure 5.20A). This data indicates that presence of only one form of G3BP reduces cells' progression towards senescence.

5.4.5.1.1 Senescence-Associated Heterochromatin Foci (SAHF)

Moreover, we examined SAHF formation in GFP-G3BP1 cells following doxorubicin treatment. SAHF formation was monitored at Day 0, Day 2, Day 5, Day 7 and Day 9 post-doxorubicin treatment. Cells that are forming 5 or more SAHF are counted and considered as senescent cells. Therefore, GFP-G3BP1 cells showed few (less than 5) granular structures at Day 0 and 2. Thus, at Day 5, 7 and 9, they showed increased number of SAHF (more than 5) (Figure 5.19). Furthermore, ImageJ was used to quantify SAHF formation in GFP-G3BP1 cells. Cells showed formation of no/few SAHF at Day 0 and 2. At Day 5, cells revealed an increase of 5-fold change in SAHF-forming cells. At Day 7, cells showed an increase in the number of SAHF-forming cells of a 1.5-fold change compared to Day 5 cells. Moreover, cells maintained a similar number of SAHF-forming cells at Day 9 compared to Day 7 (Figure 5.20B). When we compare GFP-G3BP1 cells to WT U2OS cells, SAHF-forming cells in GFP-G3BP1 cells were significantly reduced. It showed a decline of 2-fold change (Figure 5.20B).

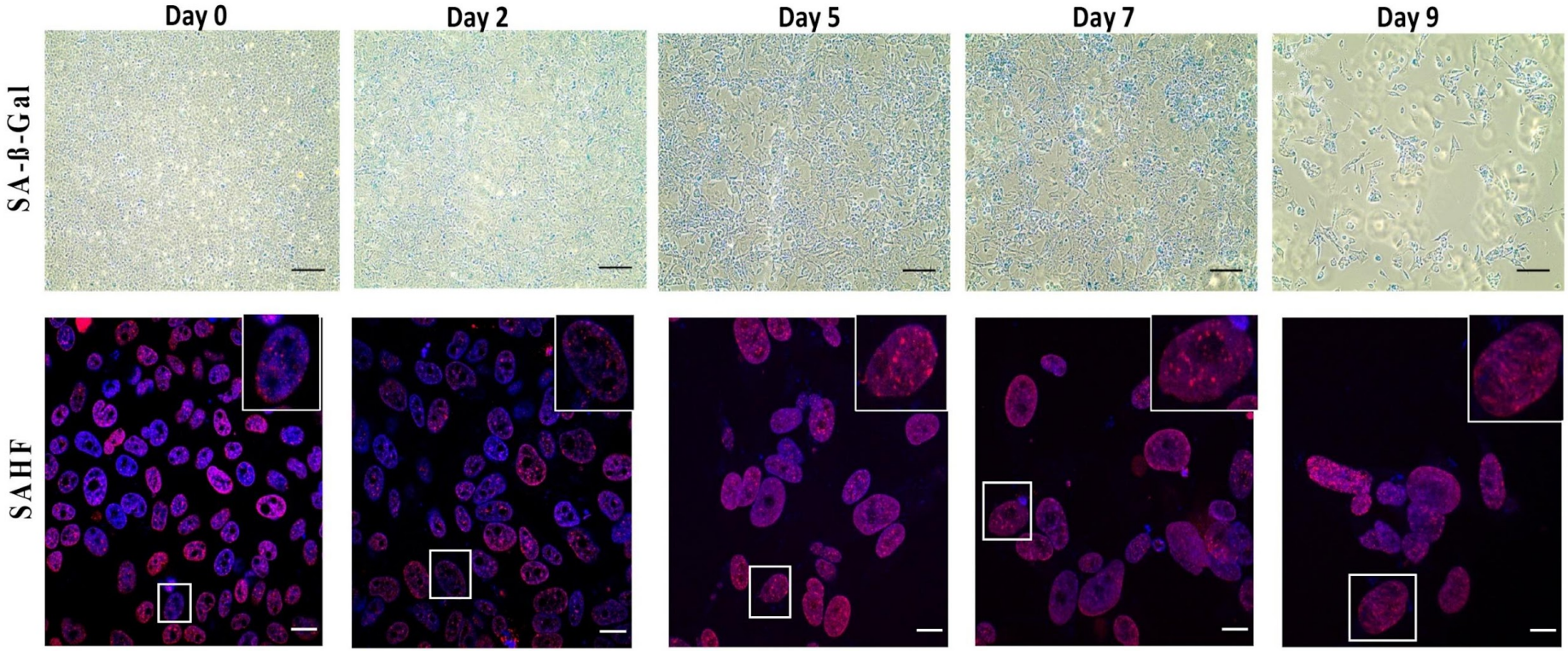

Figure 5.19 GFP-G3BP1 cells showed gradual formation of SA-ß-Gal and SAHF. GFP-G3BP1 cells were treated with 200 nM doxorubicin for 48 hours. Cells were collected at Day 0, 2, 5, 7 and 9, fixed and stained with SA-ß-Gal staining or SAHF antibody (Red). GFP-G3BP1 cells showed development of blue stain at Day 2 post-doxorubicin treatment. An increased intensity of blue stain was observed at Day 5 and 7. Cells showed no/few SAHF (less than 5 foci per cell) at Day 0 and 2. At Day 5, 7 and 9, they showed increased number of SAHF. Scale bar = 20 um. SA-ß-Gal (scale bar= 100 um). SAHF (scale bar= 20 um).

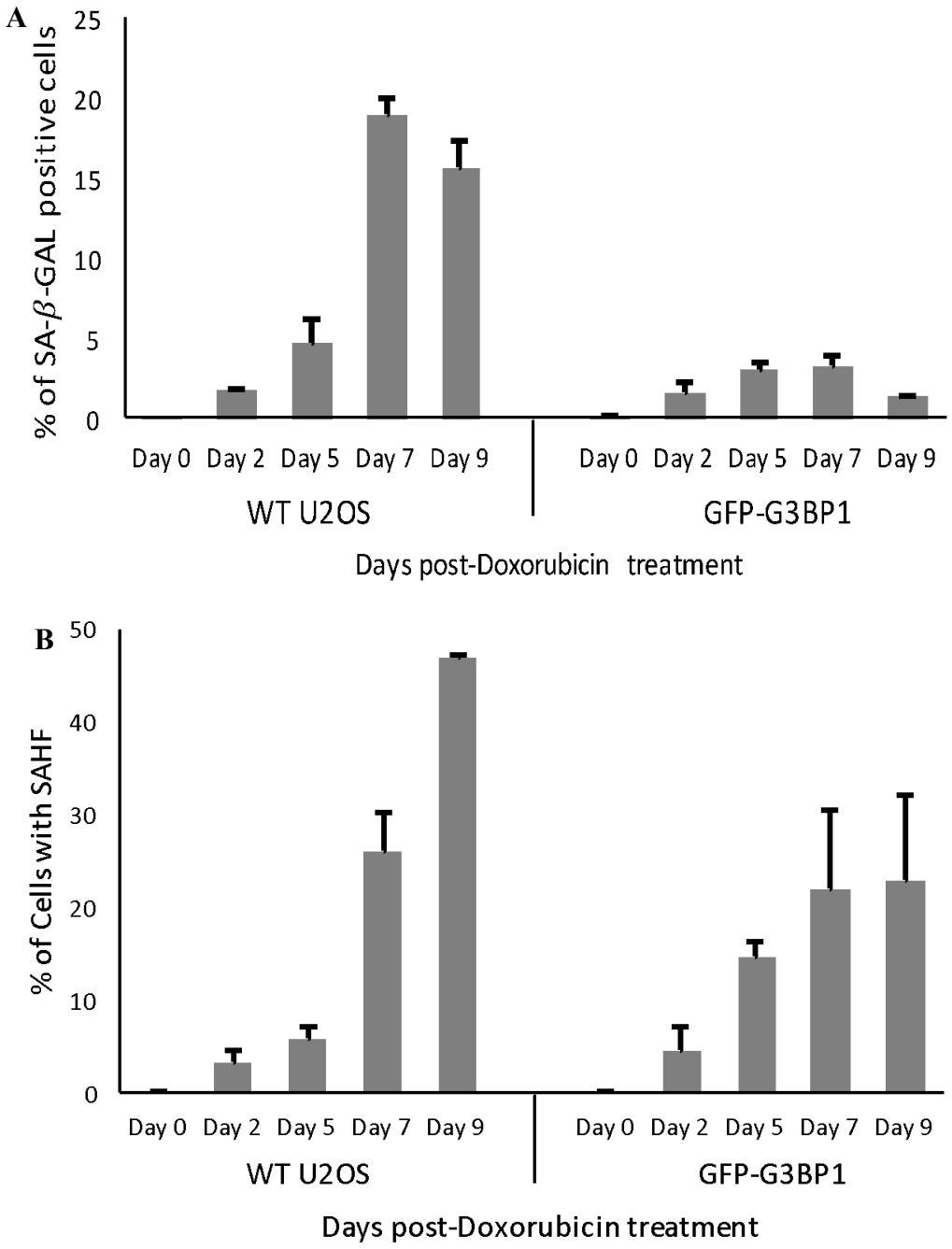

Figure 5.20 G3BP1 slows cells' progression towards senescence.

SA-ß-Gal positive cells in GFP-G3BP1 cells was significantly reduced (16-fold change) compared to WT U2OS cells (A). When we compare GFP-G3BP1 cells to WT U2OS cells, SAHF-forming cells in GFP-G3BP1 cells was reduced. It showed a decline of 2-fold change (B). Data represents mean ± SEM n=3, statistical significance was assessed using ANOVA t-test.

5.4.5.1.2 P21

Senescence phenotype is associated with increased expression of p21 protein which is known to promote senescence in cells. The transcriptional activation of p21, a cyclin-dependent kinase induces cell cycle arrest (Shtutman et al., 2017).

Thus, GFP-G3BP1 cells were induced to senescence through incubating them with 200 nM doxorubicin for 48 hours. Cells were then collected at Day 0 and Day 9. Following protein extraction, protein samples were incubated with p21 antibody. At Day 9, GFP-G3BP1 cells showed an increase in the expression of p21 protein compared to Day 0 (control) (Figure 5.21). Presence of G3BP1 resulted in a decline in p21 protein when compared to WT U2OS cells of Day 9. Hence, our observations indicate that presence of only one form of G3BP, i.e. G3BP1, potentially slows development of senescence phenotype in GFP-G3BP1 cells.

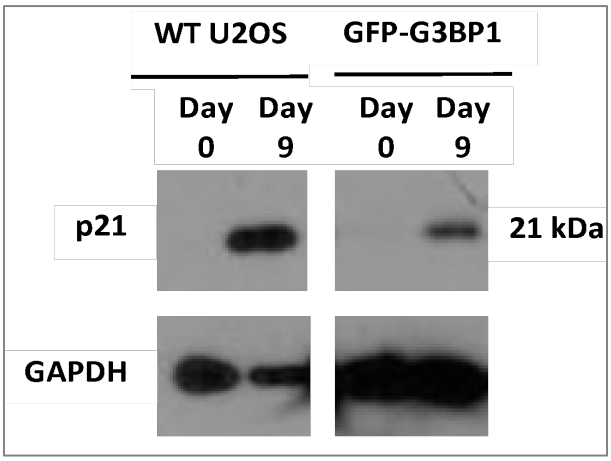

Figure 5.21 Low p21 protein level was detected in GFP-G3BP1 cells.
Senescence was induced in GFP-G3BP1 cells through incubating cells with 200 nM doxorubicin for 48 hours. Western blots were performed using cell extracts from cells at Day 0 (control) and Day 9 post-doxorubicin treatment. p21 and GAPDH (loading control) antibodies were used.

5.4.6 Stress Granules in GFP-G3BP2a and GFP-G3BP2b Cells

As explained previously, G3BP plays a crucial role in stress granule formation (see section 5.4). Double-knockout cells (ΔΔG3BP1/2) did not show formation of stress granules when treated with SA. However, re-constitution of cells with G3BP1 promoted stress granule formation under oxidative stress (see section 5.6). Thus, in addition to G3BP1, G3BP2 is also required for stress granule formation. Endogenous G3BP2 was observed to be recruited to stress granules in response to oxidative stress and heat shock (Kobayashi et al. 2012; Kedersha et al., 2016). Therefore, to address the role of G3BP2 on stress granule formation, we assessed whether adding G3BP2a or G3BP2b to the double-knockout cells (ΔΔG3BP1/2) rescues stress granules competence.

In our study, we investigate the role of G3BP2a and G3BP2b in stress granule formation and development of senescence phenotype. Therefore, exogenous G3BP2a and G3BP2b were genetically re-constituted individually to G3BP knockout (ΔΔG3BP1/2) cells through transient transfection of cells with GFP-G3BP2a or GFP-G3BP2b (Figure 5.22). Then, ΔΔG3BP1/2+GFP-G3BP2a (hereafter referred as GFP-G3BP2a) and ΔΔG3BP1/2+GFP-G3BP2b (hereafter referred as GFP-G3BP2b) cells were tested for stress granule formation and senescence phenotype development (see section 5.9).

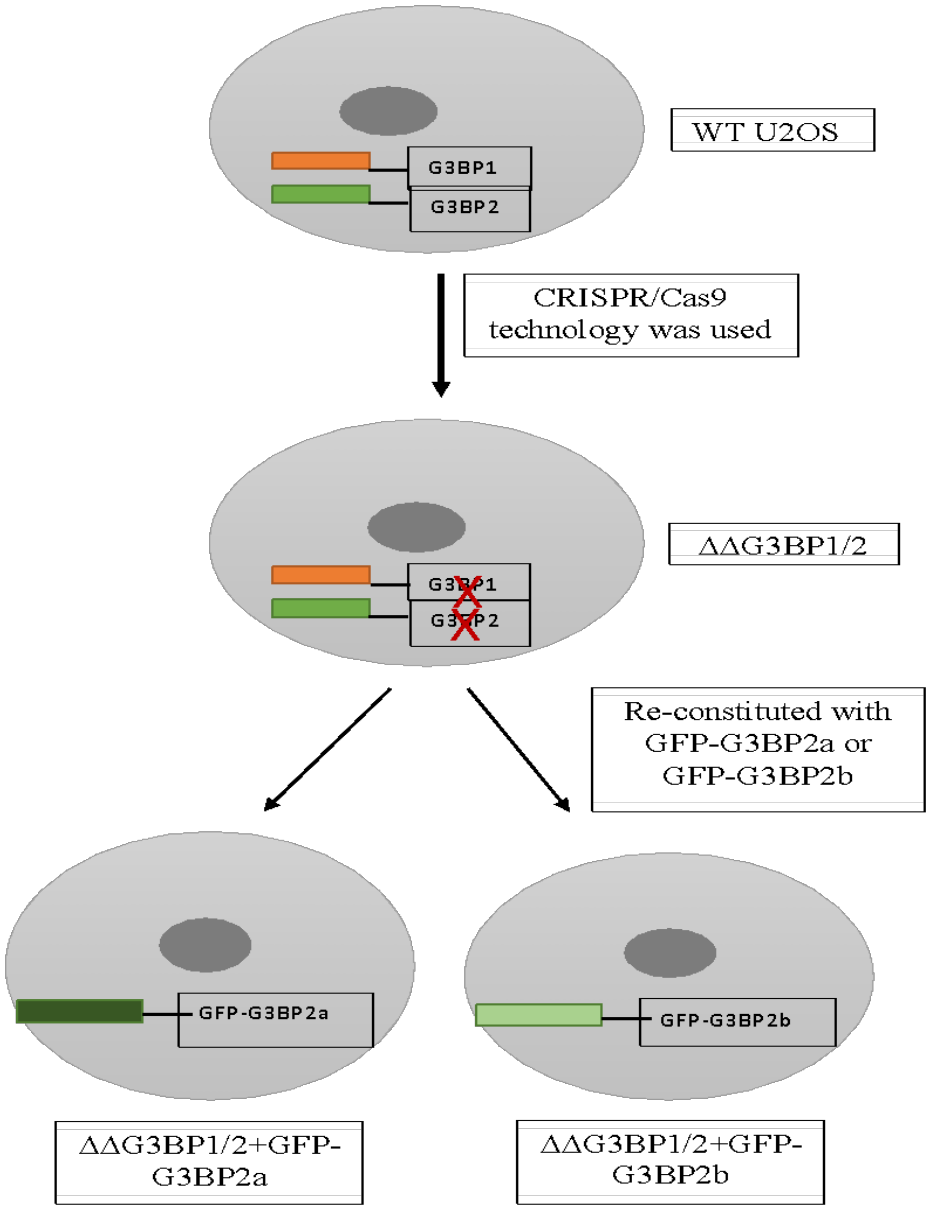

Figure 5.22 Schematic diagram shows the development of ΔΔG3BP1/2+GFP-G3BP2a and ΔΔG3BP1/2+GFP-G3BP2b cells.

To test the effect of G3BP2a and G3BP2b on SGs competence and senescence phenotype development, G3BP1 and G3BP2 knockout cells (ΔΔG3BP1/2) were transiently transfected with GFP-tagged G3BP2a or GFP-tagged G3BP2b forming ΔΔG3BP1/2+GFP-G3BP2a or ΔΔG3BP1/2+GFP-G3BP2b cells.

5.4.6.1 Stress Granule Formation

5.4.6.1.1 G3BP2a or G3BP2b

The formation of stress granules in the double-knockout cells (ΔΔG3BP1/2) was observed to be inhibited due to the lack of G3BP1 and G3BP2a/b. Hence, ΔΔG3BP1/2 cells were incapable of stress granule formation under oxidative stress (see section 5.4). To address the role of G3BP2a/b in stress granule formation, cells transfected with G3BP2 or G3BP2b are exposed to oxidative stress and examined whether stress granule formation is rescued.

Therefore, GFP-G3BP2a and GFP-G3BP2b cells were treated with/out 0.5 mM SA for 30 min. GFP-G3BP2a and GFP-G3BP2b cells are tagged with GFP protein, a fluorescence marker used for visualization of G3BP2a and G3BP2b. Thus, SA-untreated GFP-G3BP2a cells did not show formation of stress granules. Exposure of GFP-G3BP2a cells to SA stimulated formation of stress granules. G3BP2a was detected to be recruited to sites of stress granules (Figure 5.23).

On the other hand, exposure of GFP-G3BP2b cells to SA stimulated formation of stress granules. G3BP2b was also detected to be recruited to sites of stress granules. SA-untreated cells showed no formation of stress granules (Figure 5.23). Thus, our observations indicate that re-constitution of cells with G3BP2a or G3BP2b rescues stress granule formation. Both G3BP2a and G3BP2b are recruited to sites of stress granules which indicates that they play a major role in stress granule formation.

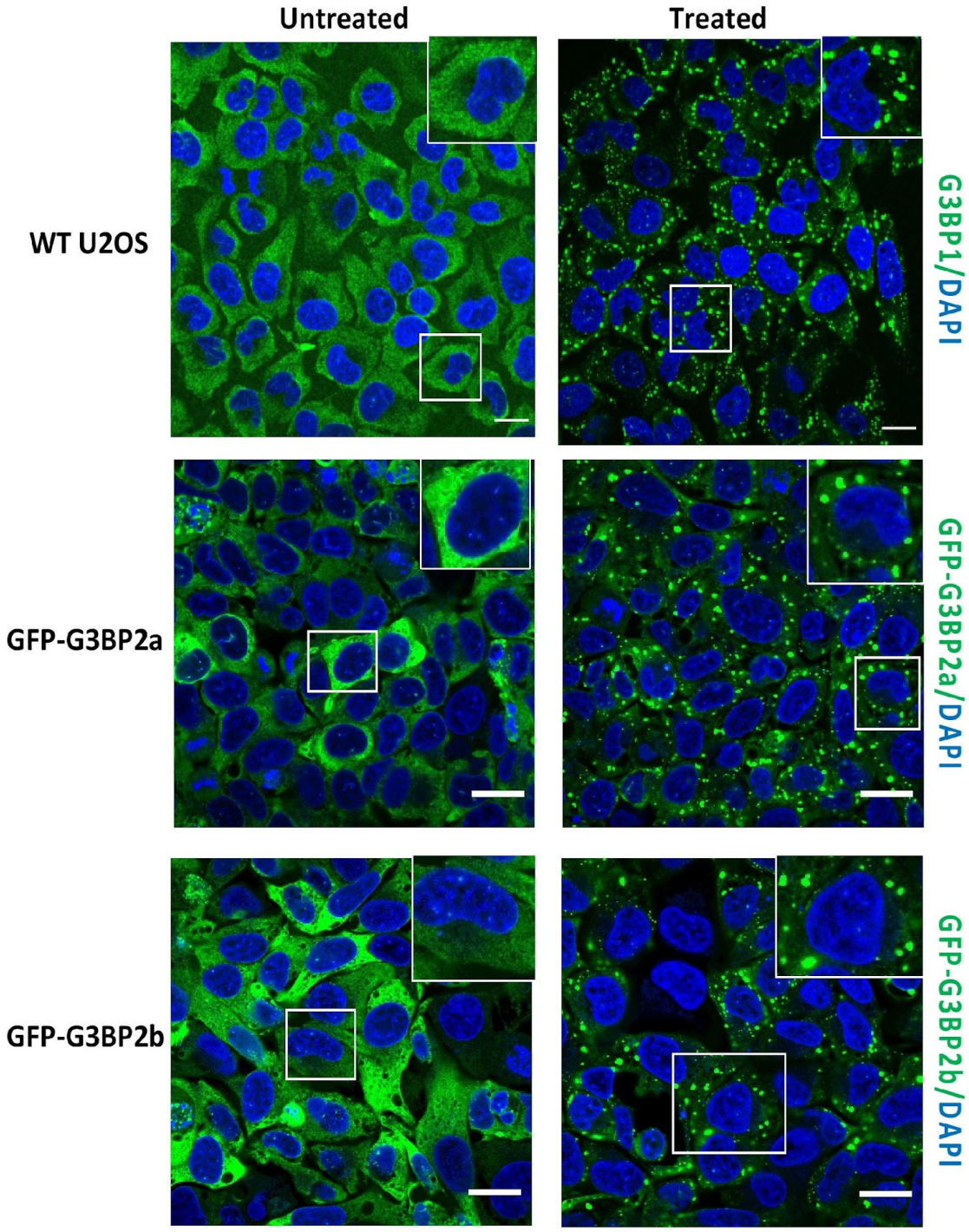

Figure 5.23 Stress granule formation is rescued in GFP-G3BP2a and GFP-G3BP2b cells.

WT U2OS, GFP-G3BP2a and GFP-G3BP2b cells were treated with/out 0.5 mM SA for 30 min. WT U2OS, GFP-G3BP2a and GFP-G3BP2b cells showed assembly of stress granules under SA treatment. Scale bar= 20 um.

A quantitative comparison of stress granule formation was performed in GFP-G3BP2a, GFP-G3BP2b and WT U2OS cells. Hence, cells that were not treated with SA did not show formation of stress granules. On the other hand, SA-treated WT U2OS cells showed formation of an average 8 SGs/cell. When GFP-G3BP2a cells were treated with SA, they showed formation of an average 3 SGs/cell. SA-treated GFP-G3BP2b cells revealed formation of 3.8 SGs/cell (Figure 5.24). Thus, GFP-G3BP2a cells showed a significant decline (2.6-fold change) in stress granule formation. Additionally, GFP-G3BP2b cells revealed a reduction of 2-fold change in the number of stress granules. Therefore, our observations suggest that presence of G3BP2a or G3BP2b promotes stress granule formation. The number of the assembled stress granules in GFP-G3BP2a and GFP-G3BP2b cells is lower than in WT U2OS cells.

Therefore, re-constitution of cells with G3BP2a rescued the formation of 37.8% of stress granules when compared to WT U2OS cells. Moreover, presence of G3BP2b induced formation of 47.5% of stress granules. Hence, G3BP2b is suggested to play an important role in stress granule formation as it showed increased stress granule formation (1.3-fold change) in GFP-G3BP2b cells compared to GFP-G3BP2a cells.

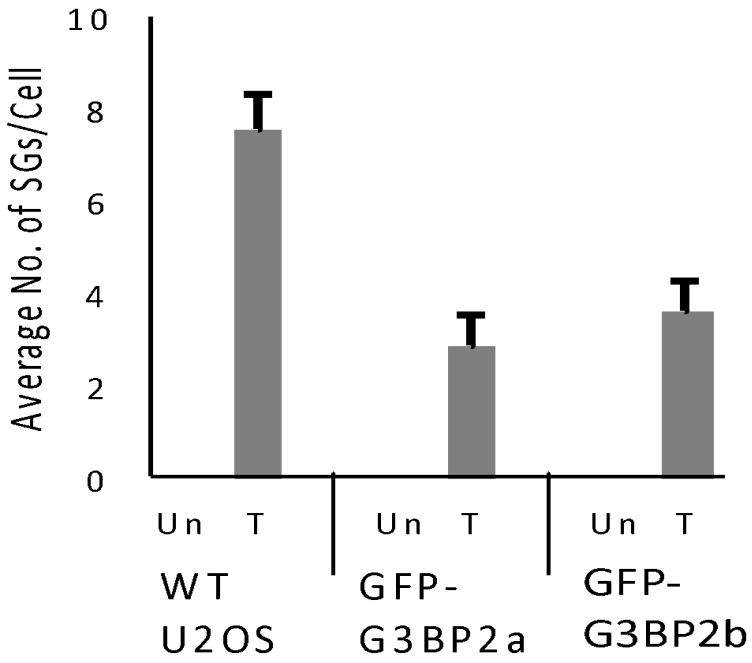

Figure 5.24 G3BP2a and G3BP2b promotes formation of stress granules. WT U2OS, GFP-G3BP2a and GFP-G3BP2b cells were treated with 0.5 mM SA for 30 min. Re-constitution of cells with G3BP2a rescued formation of 37.8% of stress granules when compared to WT U2OS cells. Presence of G3BP2b induced formation of 47.5% of stress granules. Data represents mean ± SEM n=3, statistical significance was assessed using ANOVA t-test.

5.4.6.1.2 FXR1

We have shown previously that stress granule formation was depleted in ΔΔG3BP1/2 cells and therefore FXR1 was observed to be diffused in the cytoplasm. Here we examine the recruitment of FXR1 to stress granules in GFP-G3BP2a and GFP-G3BP2b cells. Therefore, in our recent study, GFP-G3BP2a and GFP-G3BP2b cells were treated/untreated with 0.5 mM SA for 30 min. Cells were then fixed and stained with FXR1 antibody to observe FXR1 recruitment to stress granules.

Hence, SA-untreated GFP-G3BP2a and GFP-G3BP2b cells did not show formation of stress granules. FXR1 was observed diffused in the cytoplasm. On the other hand, SA-treated GFP-G3BP2a cells showed formation of stress granules. FXR1 was detected to be recruited to stress granules. Co-localization of G3BP2a and FXR1 was seen at sites of mature stress granules (Figure 5.25A). Thus, this data suggests that FXR1 is recruited to stress granules upon oxidative stress exposure in GFP-G3BP2a cells.

In contrast, GFP-G3BP2b cells showed formation of stress granules upon SA exposure. G3BP2b was observed to be recruited to stress granule sites. Additionally, FXR1 was detected at sites of stress granule assembly (Figure 5.26A). G3BP2b and FXR1 were observed to co-localize at sites of mature stress granules. This data indicates that FXR1 is involved in stress granules in GFP-G3BP2b cells upon oxidative stress.

Furthermore, a quantitative comparison of G3BP2a or G3BP2b and FXR1 that were localized at stress granule sites was performed. ImageJ was used to count G3BP2a or G3BP2b and FXR1 per cell separately. G3BP2a and FXR1 were detected at sites of stress granule assembly. Hence, the number G3BP2a recruited to stress granule sites was higher than FXR1. G3BP2a showed

an increase of 1.2-fold change compared to FXR1. The percentage of G3BP2a and FXR1 co-localization was detected as 86.2% (Figure 5.25B). This observation indicates that G3BP2a is first recruited to stress granules followed by FXR1. It also indicates that presence of only one from of G3BP: G3BP2a promotes assembly of FXR1 under oxidative stress.

On the other hand, G3BP2b promoted formation of stress granules. Both G3BP2b and FXR1 were detected at sites of stress granule assembly. Thus, the detected G3BP2b recruited to stress granule sites was higher than FXR1. G3BP2b revealed an increase of 2-fold change compared to FXR1. Consequently, 50% of G3BP2b and FXR1 showed co-localization at sites of stress granules (Figure 5.26B). This observation indicates that G3BP2b is required to promote assembly of FXR1. It also indicates that presence of G3BP2b induces FXR1 assembly under oxidative stress.

Collectively, FXR1 was observed to be recruited to stress granules in GFP-G3BP2a and GFP-G3BP2b cells. G3BP2a and G3BP2b showed an increase of 1.2 and 2-fold change compared to FXR1 in GFP-G3BP2a and GFP-G3BP2b, respectively. 86.2% of G3BP2a and FXR1 revealed co-localization, whereas 50% of G3BP2b and FXR1 showed co-localization at sites of stress granules. Hence, GFP-G3BP2a cells showed a decrease of 1.7-fold change in FXR1 compared to GFP-G3BP2b cells.

5.4.6.1.3 EIF4G

The recruitment of translation initiation factor eIF4G has been studied in cells exposed to oxidative stress (Kedersha et al., 2016). Therefore, we examined eIF4G recruitment to stress granules in GFP-G3BP2a and GFP-G3BP2b cells. Thus, cells were treated/untreated with 0.5 mM SA for 30 min. Cells were then fixed and stained with eIF4G antibody.

Thus, SA-untreated GFP-G3BP2a and GFP-G3BP2b showed no formation of stress granules. FXR1 was observed to be diffused in the cytoplasm. Nevertheless, SA-treated GFP-G3BP2a and GFP-G3BP2b cells showed formation of stress granules. However, few/no EIF4G was detected to assemble. Co-localization of G3BP2a or G3BP2b and eIF4G was not observed at sites of stress granules (Figure 5.25A, 5.26A). Thus, this data suggests that eIF4G is not recruited to stress granules upon oxidative stress exposure in GFP-G3BP2a and GFP-G3BP2b cells.

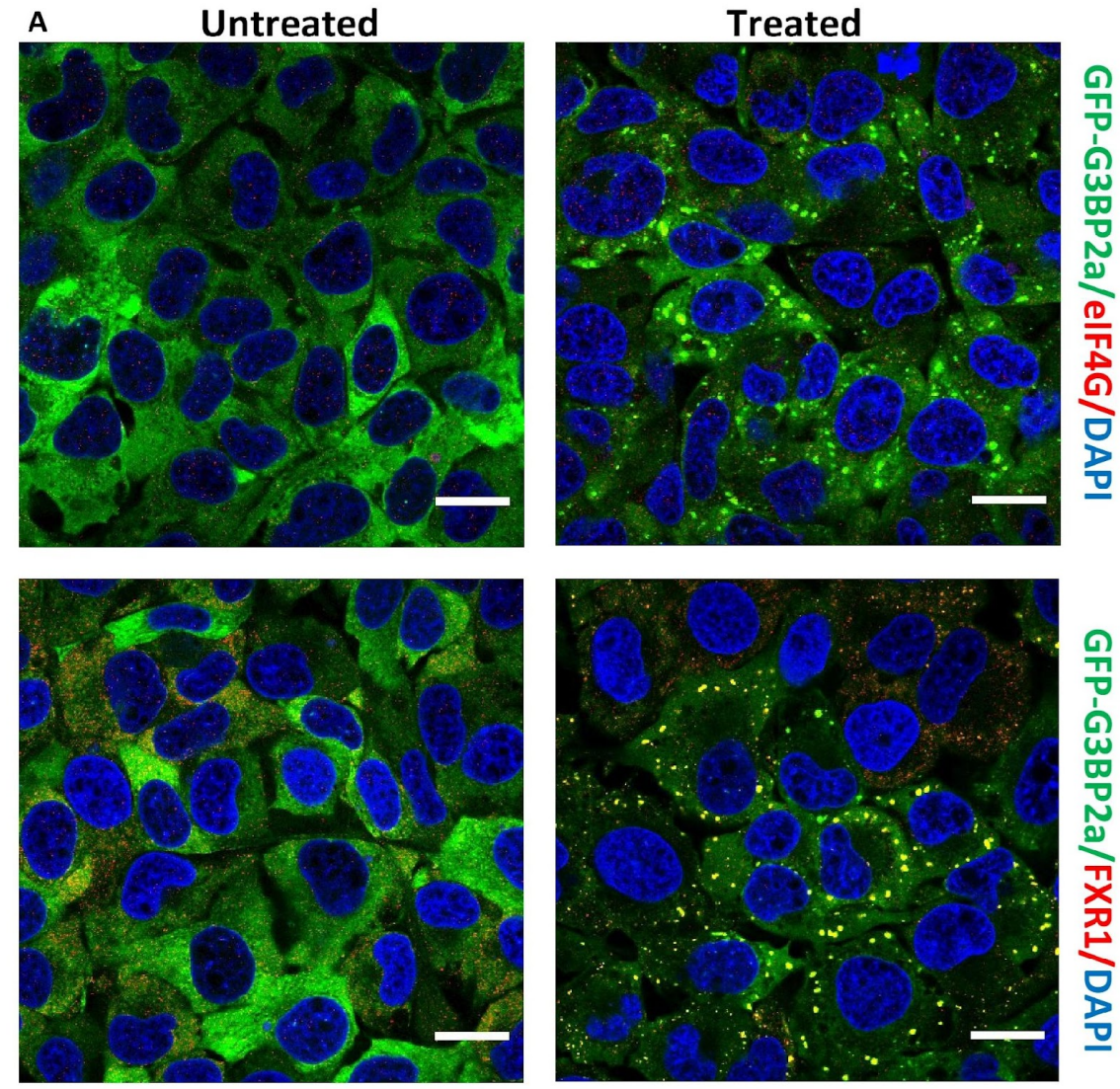

Figure 5.25 FXR1 is recruited to stress granules in GFP-G3BP2a cells. GFP-G3BP2a cells were un/treated with 0.5 mM SA for 30 min and stained with FXR1 and EIF4G antibodies. Cells showed assembly of stress granules (A). G3BP2a showed an increase of 1.2-fold change compared to FXR1. Few/no EIF4G was detected in cells (B). Data represents mean ± SEM n=3, statistical significance was assessed using ANOVA t-test. Scale bar= 20 um.

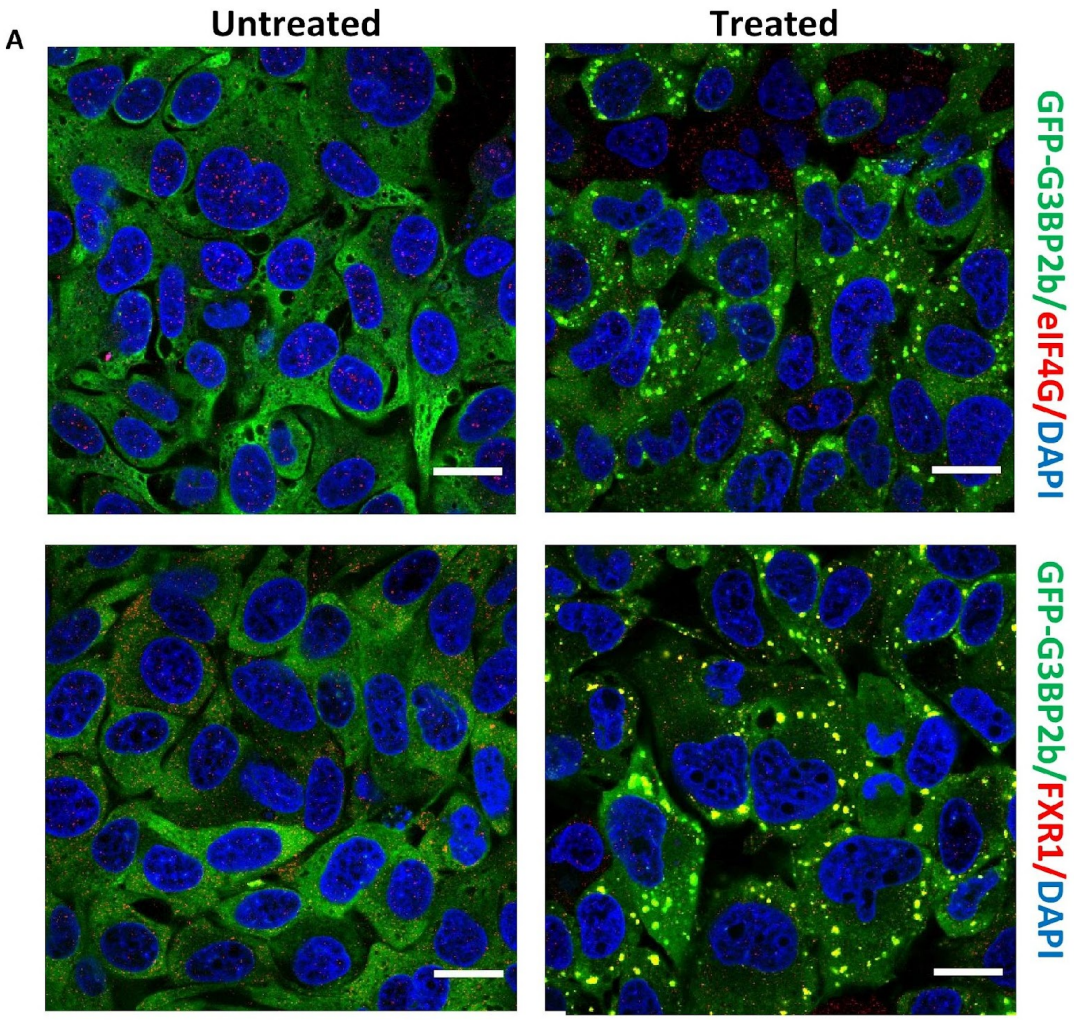

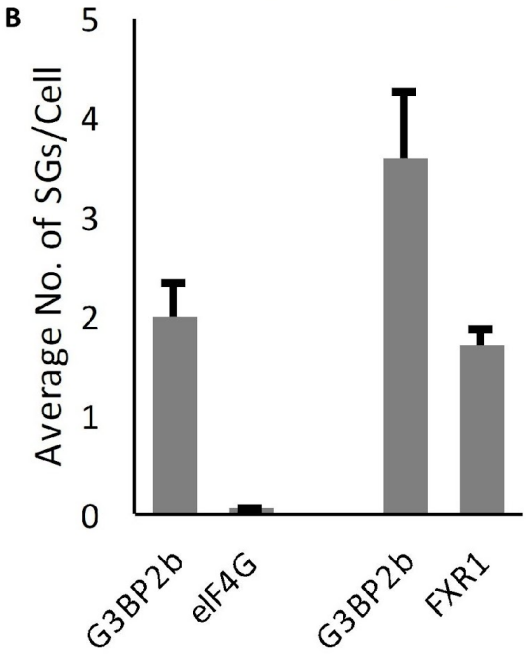

Figure 5.26 FXR1 but not EIF4G is recruited to stress granules in GFP-G3BP2b cells. GFP-G3BP2b cells were un/treated with 0.5 mM SA for 30 min and stained with FXR1 and EIF4G antibodies. Cells showed assembly of stress granules (A). G3BP2b revealed an increase of 2-fold change compared to FXR1. 50% of G3BP2b and FXR1 showed co-localization at sites of stress granules. Few/no EIF4G was detected in cells (B). Data represents mean ± SEM n=3, statistical significance was assessed using ANOVA t-test. Scale bar= 20 um.

5.4.7 Senescence in GFP-G3BP2a and GFP-G3BP2b Cells

5.4.7.1 Senescence Associated ß-Galactosidase Activity (SA-ß-Gal)

The role of G3BP2a and G3BP2b in senescence was investigated in GFP-G3BP2a and GFP-G3BP2b cells. Hence, in our study, SA-ß-Gal assay was used to examine senescence phenotype in GFP-G3BP2a and GFP-G3BP2b cells. Therefore, cells were cultured until they reached 90% confluency. Then, cells were treated with 200 nM doxorubicin for 48 hours. Cells were collected at Day 0, Day 2, Day 5, Day 7 and Day 9. SA-ß-Gal assay was performed through incubating cells with staining solution overnight at 37°C. Cells were then observed under the bright microscope. GFP-G3BP2a cells showed development of blue stain at Day 5 post-doxorubicin treatment. A gradual increase in the intensity of blue stain was observed at Day 7 and 9. On the other hand, GFP-G3BP2b cells showed development of SA-ß-Gal positive cells at Day 2. Cells then showed a gradual increase in the intensity of blue stain. Hence, GFP-G3BP2a and GFP-G3BP2b cells showed low percentage of SA-ß-Gal positive cells compared to WT U2OS cells indicating that G3BP2a or G3BP2b only slows development of senescence phenotype (Figure 5.27A).

The percentage of SA-ß-Gal positive cells was counted in GFP-G3BP2a and GFP-G3BP2b cells using ImageJ. GFP-G3BP2a cells showed a gradual increase in the intensity of blue stain. Hence, at Day 0 and 2, cells did not show production of blue stain which indicates that cells are still proliferating. At Day 5, cells showed development of blue stain. This observation indicates that cells possess senescence associated changes; SA-ß-Gal positive staining. At Day 7, an increase of 2.4-fold change was detected in SA-ß-Gal positive cells. The percentage of SA-ß-Gal positive cells was nearly maintained at Day 9. In contrast, GFP-G3BP2b cells showed development of blue stain at Day 2. It showed an increase of 4.7-fold change in SA-ß-Gal positive cells at Day 5 compared to Day 2. At Day 7, cells showed increased (1.2-fold

change) SA-ß-Gal positive cells. An increase of 1.2-fold change was detected at Day 9 (Figure 5.27B).

Collectively, SA-ß-Gal positive cells showed a gradual increase in GFP-G3BP2a and GFP-G3BP2b cells. Hence, GFP-G3BP2a showed a slow progression towards senescence when compared to GFP-G3BP2b cells. At Day 9, GFP-G3BP2a cells showed a decrease of 1.7-fold change in SA-ß-Gal positive cells compared to GFP-G3BP2b cells. Nevertheless, WT U2OS cells revealed the highest percentage of SA-ß-Gal positive cells. Thus, our observation indicates that presence of one form of G3BP: G3BP2a or G3BP2b slows cells' progression towards senescence.

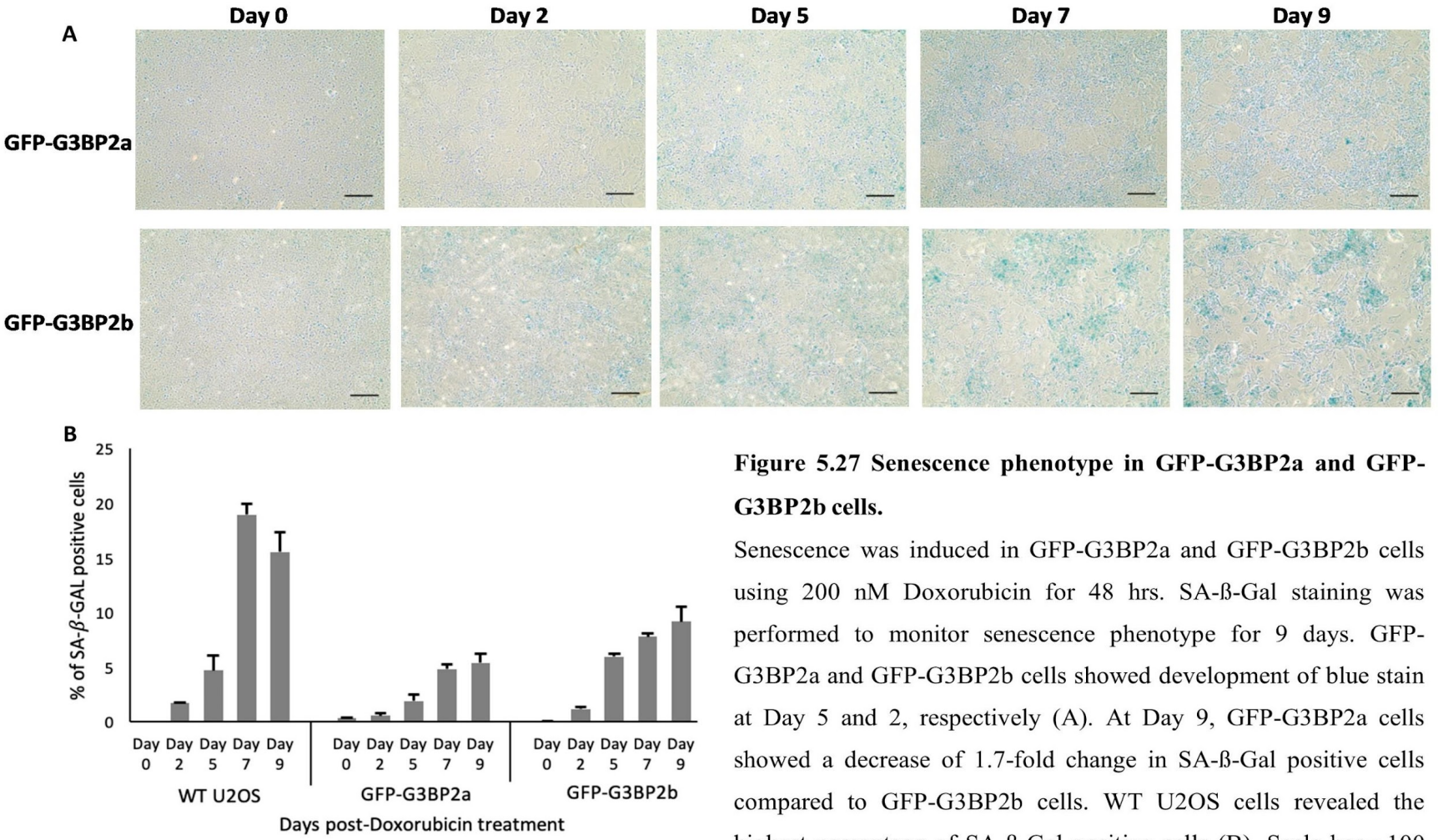

Figure 5.27 Senescence phenotype in GFP-G3BP2a and GFP-G3BP2b cells.

Senescence was induced in GFP-G3BP2a and GFP-G3BP2b cells using 200 nM Doxorubicin for 48 hrs. SA-ß-Gal staining was performed to monitor senescence phenotype for 9 days. GFP-G3BP2a and GFP-G3BP2b cells showed development of blue stain at Day 5 and 2, respectively (A). At Day 9, GFP-G3BP2a cells showed a decrease of 1.7-fold change in SA-ß-Gal positive cells compared to GFP-G3BP2b cells. WT U2OS cells revealed the highest percentage of SA-ß-Gal positive cells (B). Scale bar= 100 um. Data represents mean ± SEM n=3, statistical significance was assessed using ANOVA t-test.

5.4.7.2 SAHF

Furthermore, we examined SAHF formation in GFP-G3BP2a and GFP-G3BP2b cells following doxorubicin treatment. SAHF formation was monitored at Day 0, Day 2, Day 5, Day 7 and Day 9 post-doxorubicin treatment. Cells that are forming 5 or more SAHF are counted and considered as senescent cells. Therefore, GFP-G3BP2a cells showed few (less than 5) granular structures at Day 0 and 2. Thus, at Day 5, 7 and 9, they showed an increased number of SAHF (more than 5). In contrast, GFP-G3BP2b showed formation of SAHF at Day 5. The number of SAHF was detected to increase at Day 7 and 9 (Figure 5.28A).

Hence, ImageJ was used to quantify SAHF formation in GFP-G3BP2a and GFP-G3BP2b cells. GFP-G3BP2a cells showed formation of no/few SAHF at Day 0 and 2. At Day 5, cells revealed an increase of 10-fold change in SAHF-forming cells. At Day 7, cells showed an increase in the number of SAHF-forming cells of a 3-fold change compared to Day 5 cells. Moreover, cells showed a minor decrease in the number of SAHF-forming cells at Day 9 compared to Day 7 (Figure 5.28B). On the other hand, GFP-G3BP2b cells showed an increase of 2-fold change at Day 2. Hence, cells showed a gradual increase of 7.5, 10 and 17.5-fold change at Day 5, 7, and 9, respectively. When we compare GFP-G3BP2a to GFP-G3BP2b cells, SAHF-forming cells in GFP-G3BP2b cells were increased. It showed a rise of 1.4-fold change (Figure 5.28B).

Collectively, SAHF-forming cells revealed an increase in GFP-G3BP2a and GFP-G3BP2b cells. Thus, GFP-G3BP2b showed an increased cells' progression towards senescence when compared to GFP-G3BP2a cells. At Day 9, GFP-G3BP2b cells showed an increase of 1.4-fold change in SAHF-forming cells compared to GFP-G3BP2a cells. However, WT U2OS cells revealed the highest number of SAHF-forming cells compared to GFP-G3BP2a and GFP-

G3BP2b cells. Thus, our observation indicates that G3BP2a or G3BP2b slows cells' progression towards senescence.

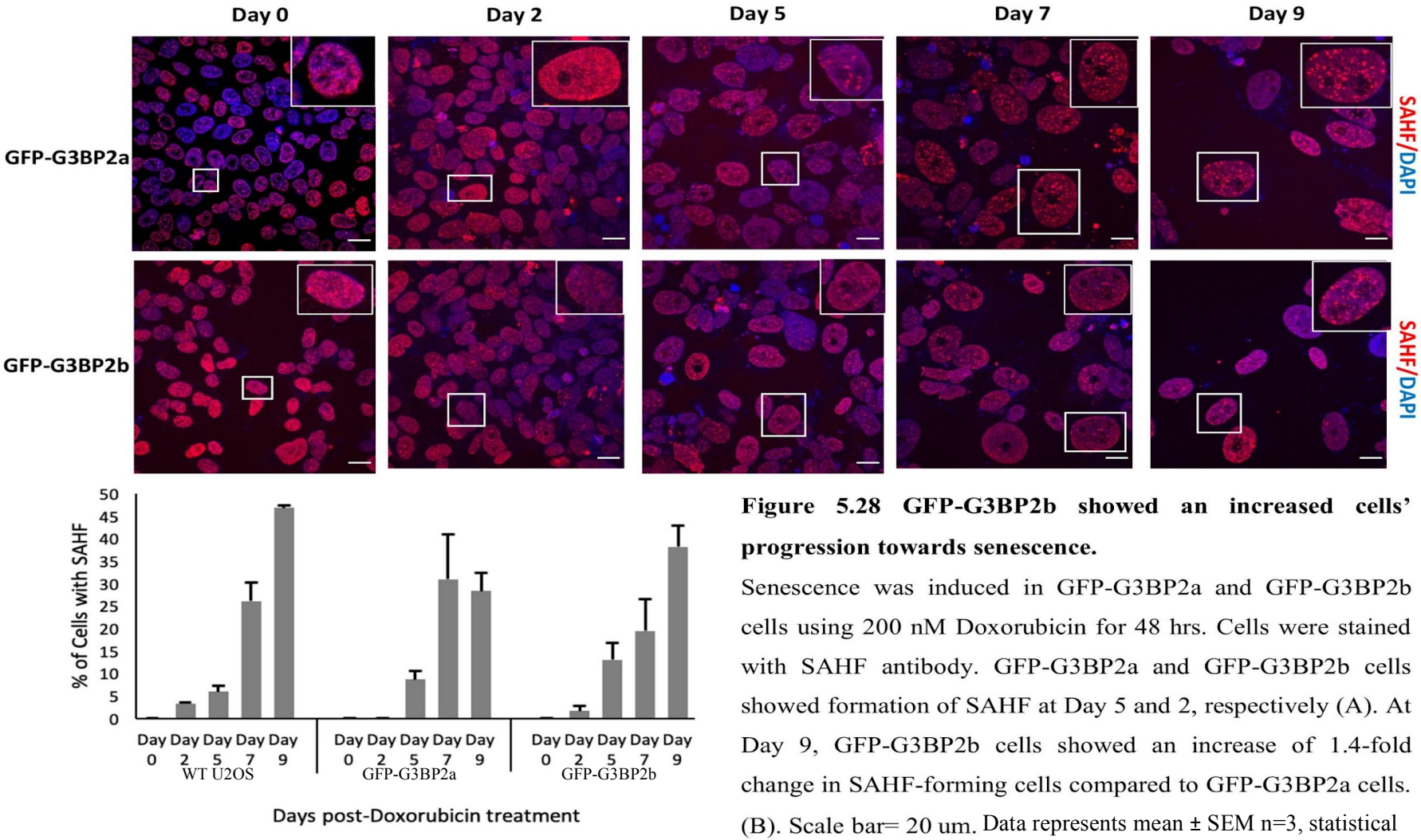

Figure 5.28 GFP-G3BP2b showed an increased cells' progression towards senescence.

Senescence was induced in GFP-G3BP2a and GFP-G3BP2b cells using 200 nM Doxorubicin for 48 hrs. Cells were stained with SAHF antibody. GFP-G3BP2a and GFP-G3BP2b cells showed formation of SAHF at Day 5 and 2, respectively (A). At Day 9, GFP-G3BP2b cells showed an increase of 1.4-fold change in SAHF-forming cells compared to GFP-G3BP2a cells. (B). Scale bar= 20 um. Data represents mean ± SEM n=3, statistical significance was assessed using ANOVA t-test.

5.4.7.3 P21

GFP-G3BP2a and GFP-G3BP2b cells were induced to senescence through incubating them with 200 nM doxorubicin for 48 hours. Cells were then collected at Day 0 and Day 9. Following protein extraction, protein samples were incubated with p21 antibody. At Day 9, GFP-G3BP2a cells showed an increase in the expression of p21 protein compared to Day 0 (control). Moreover, GFP-G3BP2b cells revealed increased p21 levels at Day 9 compared to Day 0 (Figure 5.29). G3BP2b showed a decline in p21 protein compared to G3BP2a. However, WT U2OS cells showed an increased p21 levels compared to GFP-G3BP2a and GFP-G3BP2b cells. Thus, our observations indicate that G3BP2a or G3BP2b slows cells' progression towards senescence, but G3BP2b cells are slightly faster than G3BP2a.

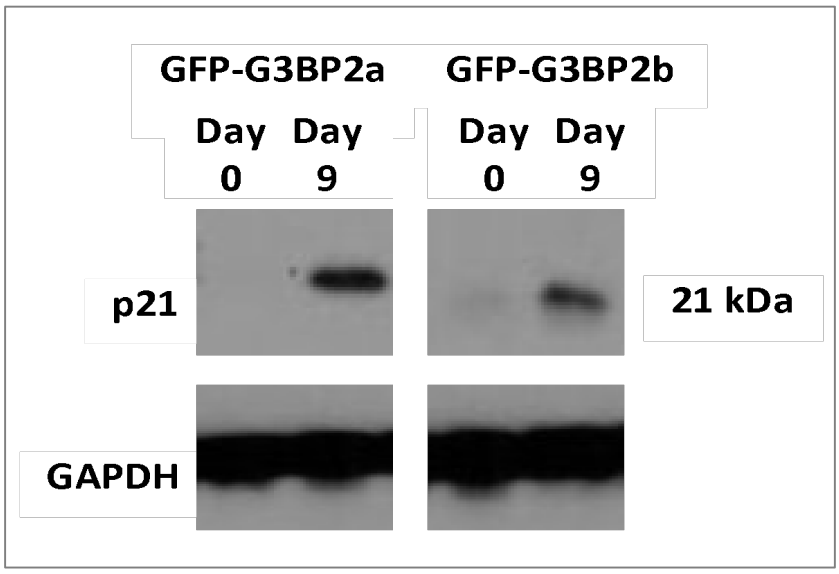

Figure 5.29 Low p21 protein level was detected in GFP-G3BP2b cells. Senescence was induced in GFP-G3BP2a and GFP-G3BP2b cells through incubating cells with 200 nM doxorubicin for 48 hours. Western blots were performed using cell extracts from cells at Day 0 (control) and Day 9 post-doxorubicin treatment. p21 and GAPDH (loading control) antibodies were used.

5.5 Conclusion

Cellular senescence is a state of cell cycle arrest that is activated in response to a cell's exposure to external stimuli. Senescence has been studied extensively during the last decades with the discoverer of senescence in 1965 Dr. Leonard Hayflick (and Moorhead, 1961; He and Sharpless, 2017). It has been established that cellular senescence is involved in certain physiological and pathological states (Sharpless and Sherr, 2015). Repeated exposure of cells to external assaults was observed to cause changes in genes involved in promoting and maintaining senescence (Gallouzi, 2009; Lian and Gallouzi, 2009). Senescent cells are characterized with changes in cellular structures and protein expression. They exhibit increased cell size, increased SA-ß-Gal activity, and increased p21 protein expression. Other markers involve increased SAHF and SASP markers (Campisi, 2007; Campisi and d'Adda di Fagagna, 2007; He and Sharpless, 2017).

In mammalian cells, RNA-binding proteins including G3BP are involved in translation repression during stress. It is associated with the assembly of stress granules that contain free untranslated mRNAs. During stress exposure, translation inhibition occurs as a result of phosphorylation of initiation factor eIF2-α (Kedersha and Anderson, 2002; Wek et al., 2006). G3BP is an important component of stress granules that is conserved in eukaryotes. Presence of G3BP are essential for stress granule formation. However, overexpression of G3BP is sufficient for stress granule assembly in absence of stress (Tourrière et al., 2003). G3BP interacts with several protein partners under stress conditions such as Caprin-1 and FXR1 (Lian and Gallouzi, 2009; Kedersha et al., 2016). The three forms of G3BP: G3BP1, G3BP2a and G3BP2b were detected in stressed cells. They are required to nucleate the formation and condensation of stress granules (Tourrière et al., 2003; Götte et al., 2019).

G3BP was observed in proliferative and senescent cells that underwent stress such as oxidative stress and heat shock. G3BP expression was significantly reduced in senescent cells (Omer et al., 2018). Stress granules are protective structures but whether they are involved in senescence, either progression or inhibition; is still unclear. To understand the function of G3BP in senescence, we performed several experiments that involved SA-ß-Gal, SAHF staining and quantification of p21 protein expression in WT U2OS and stably transfected cells with different GFP-fused G3BP genes. The resulting cells are: ΔΔG3BP1/2 (knockout of both G3BP1 and G3BP2). GFP-G3BP1 (transient transfection with exogenous G3BP1), GFP-G3BP2a (transient transfection with exogenous G3BP2a) and GFP-G3BP2b (transient transfection with exogenous G3BP2b) cells.

To investigate WT U2OS (control) cells' response to oxidative stress, cells were treated with SA. Thus, SA exposure induced stress granule assembly in WT cells. Other stress granule markers such as eIF4G and FXR1 were also detected to be recruited to stress granules. As a result of G3BP1/2 knockout, ΔΔG3BP1/2 cells were incapable of stress granule formation under SA exposure. Stressed GFP-G3BP1 cells showed a decrease in stress granule assembly compared to WT U2OS. Additionally, they showed few/no recruitment of eIF4G to stress granules. In contrast, FXR1 localization to stress granule sites was observed to increase compared to eIF4G. Moreover, stressed GFP-G3BP2a and GFP-G3BP2b showed decrease in stress granules compared to WT U2OS cells. eIF4G assembly decreased significantly in both GFP-G3BP2a and GFP-G3BP2b cells. Whereas, FXR1 showed localisation to sites of stress granule assembly.

Senescence phenotype was studied in cells using doxorubicin, a DNA-damage inducing agent. Senescence was induced in WT U2OS and ΔΔG3BP1/2 cells. ΔΔG3BP1/2 cells showed an

increase (4-fold) in senescent cells compared to WT U2OS cells. When GFP-G3BP1 cells were induced to senescence, they showed a decrease of 3-fold change in senescent cells compared to WT U2OS cells. GFP-G3BP2a and GFP-G3BP2b cells showed a decrease of 1-fold and 1.5-fold change, respectively, in senescent cells compared to the WT cells

Taken together, our data confirm that loss of G3BPs (G3BP1, G3BP2a, G3BP2b) accelerates senescence phenotype. Re-constitution of cells with G3BP1 solely, delayed senescence phenotype suggesting that G3BP1 plays a role in delaying senescence. Additionally, G3BP2a and G3BP2b individually reduced cells' progression to senescence. Briefly, knockout of G3BP accelerates senescence. It indicates that G3BP plays a major role in delaying senescence as it slows senescence progression significantly.

Chapter 6

6 Lipid Droplets in WT U2OS and Knockout Cells

6.1 Introduction

Lipid droplets are the main store of lipids in mammalian cells. Excessive fatty acid synthesis leads to a process of fatty acids conversion to neutral lipids and deposition of these lipids in cytoplasmic inclusions. Subsequently, neutral lipids are sequestered in lipid droplets (Martin and Parton, 2006). Lipid droplets consist of fatty acids and sterols. It has been conserved from prokaryotic to eukaryotic cells (Murphy, 2001). They have a crucial role in storing cholesterol to maintain intracellular lipid homeostasis (Martin and Parton, 2005).

Lipid droplets are formed due to the elevated levels of fatty acids and cholesterol. Maintenance of cholesterol levels in cells is essential for maintaining cell functions. The extra free cholesterol is converted to cholesterol esters and stored in lipid droplets (Kuerschner et al., 2008; Brasaemle and Wolins, 2012). Endoplasmic reticulum (ER) is the origin of nascent lipid droplets. Lipid droplet biogenesis is regulated by multiple enzymatic reactions. The enzymes required for the synthesis of neutral lipids reside in ER such as glycerol-3-phosphate acyltransferases, phosphatidic acid phosphohydrolase and diacylglycerol acyltransferase (Pol et al., 2014). In mammalian cells, once sufficient neutral lipid accumulates, lipid droplets dissociate from ER (Champan et al., 2012). It was observed that the protein composition of lipid droplets is distinct from proteins of ER membrane. The budding mechanism requires lipid droplets coat protein such as perilipins (Murphy, 2001; Martin and Parton, 2006; Yang et al., 2012).

Lipid droplets are organelles that are conserved in almost all organisms from prokaryotes to eukaryotes (Mak, 2012, Walther and Farese, 2012). They are inclusions that are surrounded by a phospholipids monolayer and associated proteins. They consist of neutral lipids, triacylglycerols or cholestryl esters. Lipid droplets are formed through two major pathways: the Kennedy pathway and the Lands cycle (Butler and Mallampalli, 2010; Krahmer et al., 2011). Proteins are involved in the synthesis of lipid droplets. ER proteins: seipin and fat-storage-inducing transmembrane protein, are suggested to play structural role in lipid droplet formation (Gross et al., 2010). Moreover, they contribute to loading lipid droplets with neutral lipids, phospholipids and proteins (Gross et al., 2011). Additionally, perilipins (termed as Plin) are a family of five related proteins that are involved in regulation of neutral lipid lipolysis (Kimmel et al., 2010). They regulate lipolysis by controlling access of lipases to lipid droplets (Bickel et al., 2009). Fully differentiated lipid droplets (10-100 um diameter) are associated with phospholipid monolayer membranes and Plin covering their surfaces (Fujimoto and Parton, 2011).

Lipid droplets are linked to many cellular processes including protein degradation, and are increased following cellular damage and lipid overload. The distribution and size of lipid droplets are linked to many cellular processes and served as biomarkers for metabolic responses and diseases such as obesity, non-alcoholic steatohepatitis and type 2 diabetes (Agarwal and Garg, 2006; Anderson and Borlak, 2008; Bostrom et al., 2009). Accumulation of lipid droplets could have implications and cause syndromes such as Chanarin-Dorfman syndrome, where triacylglycerol is stored in different tissues but not adipose tissue (Fujimoto et al., 2008; Rohwedder et al., 2014). A decrease in the average size of lipid droplets was observed in human cells following weight loss and physical activity (He et al., 2004). Additionally, lipid droplets are important for the replication of hepatitis type C virus (HCV).

The viral particles target lipid droplets resulting in HCV assembly in lipid droplets (Sato et al., 2006).

Human aging is associated with an increase of physical disability, loss of muscle strength due to decrease in muscle mass and accumulation of adipose tissue in muscles. PLIN2 has been observed to increase with age. It was reported that the expression of PLIN2 increases with age (Conte et al., 2013). The increased PLIN2 expression is associated with a decrease of muscle strength. Additionally, PLIN2 expression was observed to correlate with the activation of p53 (senescence promoter) (Conte et al., 2005; Conte et al., 2016; Kaushik and Cuervo, 2016). In humans, loss of muscle quality was associated with increased lipid droplet deposition in muscles (Goodpaster et al., 2008; Marcus et al., 2010).

To address the functional organization of lipid droplets in senescent cells, we performed microscopic analysis of lipid droplets in WT U2OS and G3BP knockout cells. Lipid droplets were induced by incubating cells with Oleate enriched cell culture medium for 24 hours. Cells were then fixed and stained with Oil Red O to visualise lipid droplets using fluorescent microscopy. Moreover, SA-stressed/unstressed cells were exposed to oleate media and stained with Oil Red O to observe the role of oxidative stress on lipid droplet accumulation.

6.2 Aims and Objectives

6.2.1 Aims

This chapter aims to examine the formation of lipid droplets in proliferative and senescent U2OS cells. Hence, the number of lipid droplets per cell was observed and counted under oleate and/or oxidative stress exposure. To obtain the knowledge on this topic, proliferative WT U2OS, ΔΔG3BP1/2, GFP-G3BP1, GFP-G3BP2a and GFP-G3BP2b cells will be cultured in vitro in a growth chamber. Cells reaching 90% confluency will be incubated with/out oleate (3%) overnight. Subsequently, they will be treated with/out 0.5 mM SA for 30 min. Then, cells will be stained with a lipid droplet marker: Oil Red O to count the number of lipid droplets per cell. Furthermore, to induce senescence phenotype, WT U2OS, ΔΔG3BP1/2, GFP-G3BP1, GFP-G3BP2a and GFP-G3BP2b cells with 90% confluency will be incubated with 200 nM Doxorubicin for 48 hours. Then, senescent (Day 9-post doxorubicin treatment) cells will be treated in a way similar to proliferative cells in order to induce and detect formation of lipid droplets. G3BP1 or G3BP2 will be used as a marker for stress granule formation in stressed cells. Number of small and large lipid droplets under oleate and/or SA will be counted using ImageJ and analysed using Excel.

Furthermore, response of WT U2OS, ΔΔG3BP1/2, GFP-G3BP1, GFP-G3BP2a and GFP-G3BP2b cells to oleate will be examined. Formation and accumulation of lipid droplets will be tested. Lipid droplet marker: Oil Red O will be used to detect and count the number of lipid droplets per cell. Moreover, formation of large and small lipid droplets and stress granules will be investigated.

6.2.2 Objectives

1. Induce lipid droplet formation in WT U2OS, ΔΔG3BP1/2, GFP-G3BP1, GFP-G3BP2a and GFP-G3BP2b cells through incubation with oleate.
2. Expose cells to SA stress.
3. Characterize and detect small and large lipid droplets based on their size.
4. Induce senescence phenotype in cells.
5. Examine lipid droplet formation in senescent cells.
6. Compare lipid droplet formation in proliferative and senescent cells under oleate and/or SA.

6.3 Materials and Methods

6.3.1 Materials

All chemicals were purchased from Sigma unless stated otherwise.

6.3.2 Methods

As described in chapter 2.

6.4 Results

6.4.1 Lipid Droplets in WT U2OS Cells

Lipid droplets are fat storage organelles that exist in most cells (Athenstaedt et al., 1999). Multiple staining methods have been used to visualise, localise and quantify lipid droplets in cells such as Perilipin2/ADRP staining (Londos et al., 1999; Ohsaki et al., 2005), Oil Red O (Koopman et al., 2001; Escorcia et al., 2018) and Nile Red (Greenspan et al., 1985; Deye et al., 1990). Oil Red O (1-([4-(Xylylazo)xylyl]azo)-2-naphthol) staining is a widely-used lipid droplet marker as it accumulates in lipid-containing compartments such as lipid droplets. It can be visualised under bright field and fluorescent microscopes.

Oleate (C18H33O2) (Figure 6.1) has been observed to induce the formation of lipid droplets in Huh-7 cells (Rohwedder et al., 2014). Following oleate treatment, the high amount of newly formed lipid droplets came from the increased synthesis of lipids from the existing cellular lipids rather than oleate incorporation (Rohwedder et al., 2014). Lipid generation is due to involvement of fatty-acid-stimulated signalling pathways including phosphoinositide 3-kinase (PI3-kinase). It is proposed that the PI3-kinase pathway is crucial for lipid droplet synthesis in oleate-stimulated cells. Inhibition of PI3-kinase inhibited lipid droplet synthesis (McDermott et al., 2004; Rohwedder et al., 2014). Therefore, in our study, oleate is used as an inducing agent for lipid droplet synthesis in WT U2OS and G3BP-knockout cells.

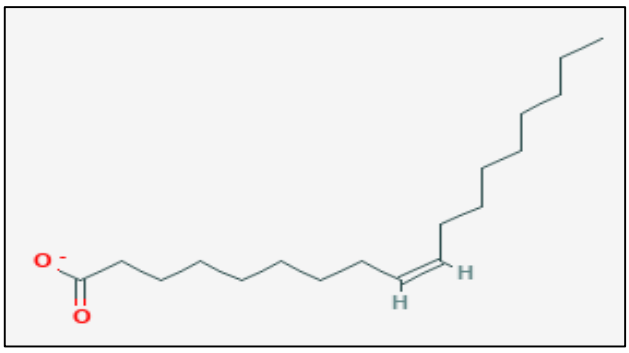

Figure 6.1 Oleate (C18H33O2). Oleate is used as a lipid droplet inducer in mammalian cells.

6.4.1.1 Lipid Droplets in Proliferative WT U2OS Cells

6.4.1.1.1 Oleate Induces Lipid Droplet Formation

To induce and visualise lipid droplet formation in WT U2OS cells, cells were treated with oleate (0.3%) and stained with Oil Red O. Cells were then visualized using fluorescent microscope. Oleate-treated cells showed an increase in the number of lipid droplets (LDs)/cell. Small (≤200 um2) and large (250-1000 um2) LDs were observed to increase in oleate-treated cells. On the other hand, oleate-untreated cells revealed accumulation of fewer LDs/cell. They showed accumulation of small LDs only (Figure 6.2).

To perform a quantitative comparison of the number and size of LDs under oleate treatment, ImageJ was used. Hence, Oleate-untreated cells showed accumulation of an average 12 LDs/cell. However, oleate-treated cells showed accumulation of 20 LDs/cell. The total number of LDs was observed to increase (2.2-fold) under oleate treatment. Moreover, the number of large LDs increased under oleate treatment (3-fold) compared to untreated cells (Figure 6.3). Therefore, our data suggests that oleate treatment induces accumulation of both small and large LDs in proliferative WT U2OS.

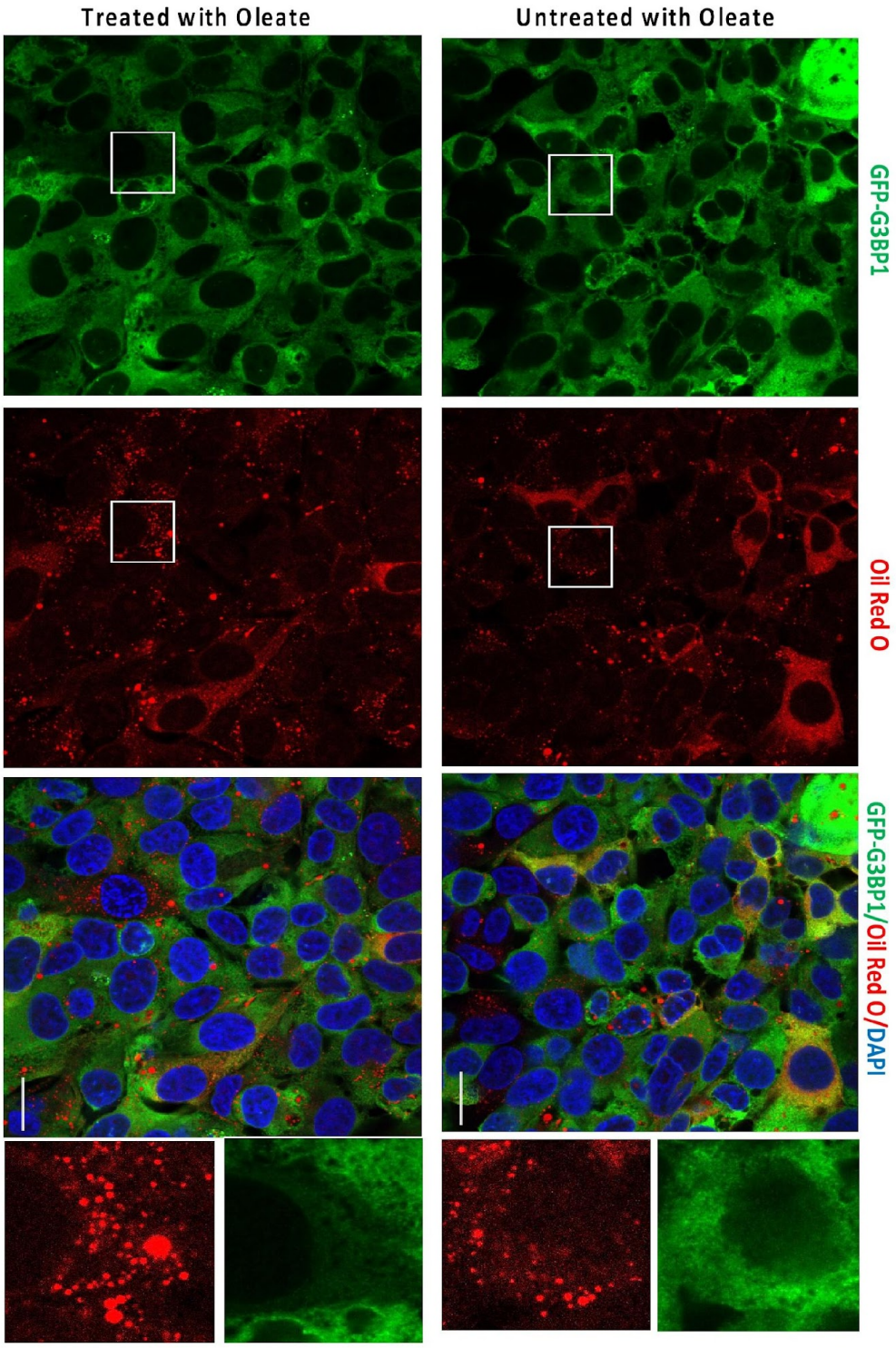

Figure 6.2 Oleat induced formation of lipid droplets in WT U2OS cells.

Cells were incubated with/out oleate (0.3%) for 24 hrs. Cells were then fixed and stained with Oil Red O. Lipid droplets (LDs) were detected in oleate-untreated cells. Oleate-treated cells accumulation of small and large LDs. Scale bar= 20 um.

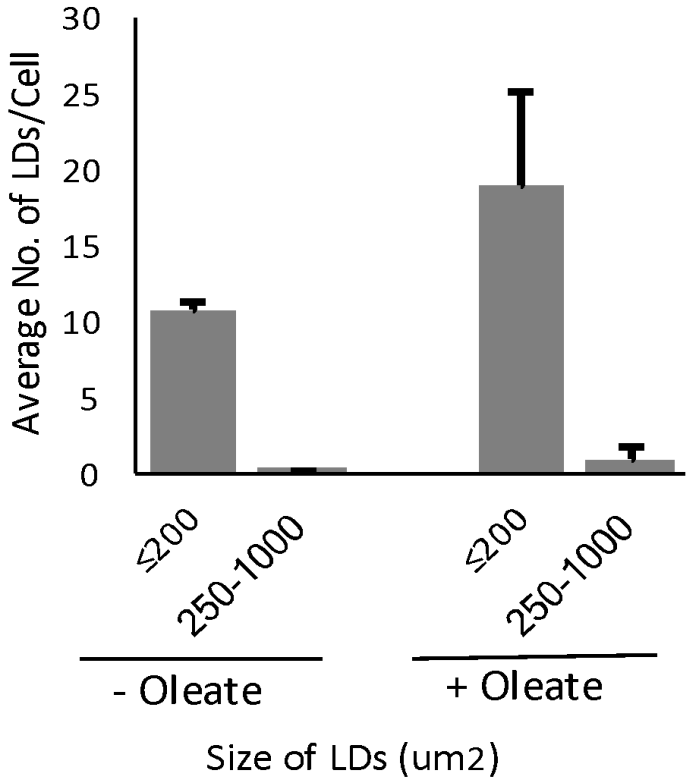

Figure 6.3 Oleate induced lipid droplet accumulation in WT U2OS cells.

Cells were incubated with/out oleate (0.3%) for 24 hrs. Oleate-untreated cells showed accumulation of small (<200 um2) LDs whereas large (250-1000 um2) LDs were not detected. Oleate was observed to induce accumulation of small and large LDs. The number of small LDs increased 2.2.-fold change. Large LDs increased 3-fold change compared to untreated cells. Data represents mean ± SEM n=3, statistical significance was assessed using ANOVA t-test.

6.4.1.1.2 Sodium Arsenite Induces Accumulation of Lipid Droplets

Lipid droplets act as energy storage organelles. They respond to cell stress such as starvation, viral infection and oxidative stress (Henne et al., 2018). Lipid droplets are suggested to contribute to stress response and cell survival. To investigate the effect of oxidative stress on lipid droplet formation in WT U2OS cells, cells were incubated with/out oleate overnight. Then, cells were treated with/out 0.5 mM SA for 30 min followed by fixation and Oil Red O staining. As expected, SA-treated cells showed assembly of stress granules. Moreover, under oxidative stress, lipid droplets were observed to locate at one side of the cell. This indicates that they are synthesized and generated from ER. Lipid droplets were observed to be connected to ER tubules forming ER/droplet bridges (Wilfling et al., 2014). Additionally, oleate-untreated/SA-treated cells revealed accumulation of lipid droplets. Hence, the number of lipid droplets increased under oleate/SA treatments (Figure 6.4). Thus, our data suggests that oxidative stress induces lipid droplet accumulation in WT U2OS which is consistent with observations of other studies (Amen and Kaganovich, 2021).

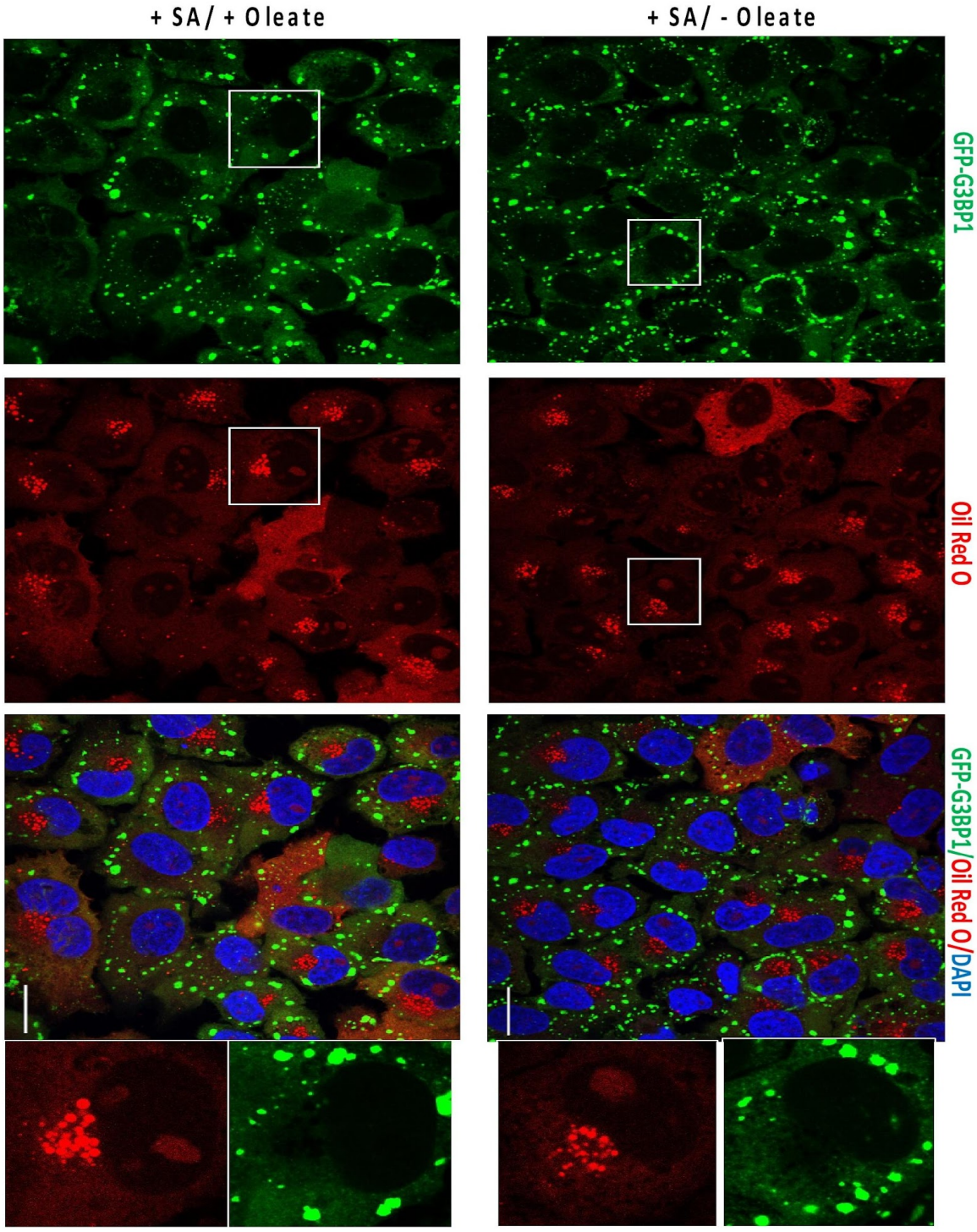

Figure 6.4 WT U2OS cells formed stress granules and lipid droplets under SA treatment. WT U2OS were incubated with/out oleate overnight and exposed to 0.5 mM SA for 30 min. Oil Red O was used to stain lipid droplets. SA-treated cells showed assembly of stress granules (GFP-G3BP1). Treatment with oleate showed an increase in LDs (Oil Red O). Scale bar= 20 um.

To address whether oleate affects the number of lipid droplets in stressed cells, we performed quantitative comparison of lipid droplet number using ImageJ. Hence, under SA exposure (+SA/-Oleate), small LDs (>200 um2) were detected. An average of 10 LDs/cell were counted. On the other hand, large LDs (250-1000 um2) were not observed to be formed, suggesting that small LDs are formed and utilised as energy reservoir rather than accumulating to form large LDs. Incubation of cells with oleate overnight followed by SA treatment (+SA/+Oleate) induced accumulation of small LDs but not large ones. An increase of 1.5-fold change was detected (Figure 6.5). Hence, our data reveals that oleate treatment induces lipid droplet formation in SA-treated WT U2OS cells.

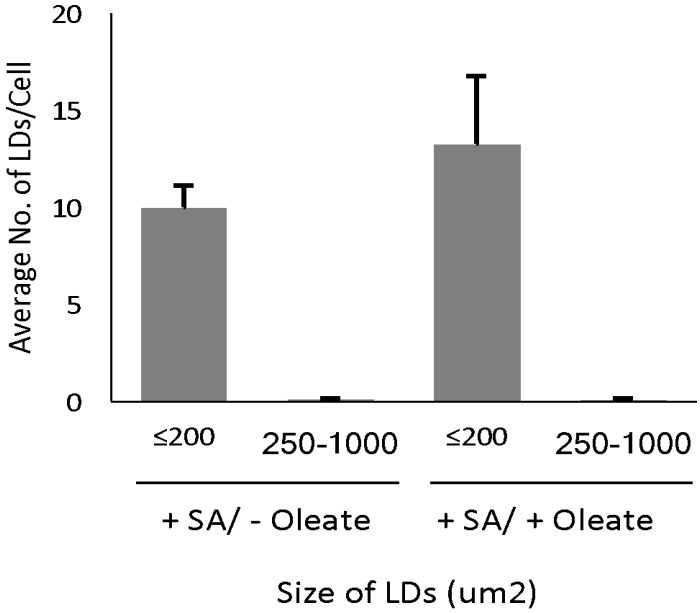

Figure 6.5 Oleate induced lipid droplet accumulation in SA-treated WT U2OS cells.

WT U2OS were incubated with/out oleate overnight and exposed to 0.5 mM SA for 30 min. SA induced formation of small LDs but not large LDs. Treatment of cells with oleate and SA (+SA/+Oleate) showed an increase (1.5 fold) in small LDs but not large LDs. Data represents mean ± SEM n=3, statistical significance was assessed using ANOVA t-test.

To quantitatively answer the question whether the number of lipid droplets increases upon SA exposure, lipid droplets in SA-treated and untreated cells were counted. As shown previously, oleate induces lipid droplet accumulation. Thus, when we compare lipid droplets in cell treated with (Figure 6.4) and without (Figure 6.2) SA, we observed a slight decrease (1.3-fold) in lipid droplets in SA-treated cells. Hence, our data suggests that lipid droplets are consumed as an energy source in stressed cells to maintain cell's homeostasis.

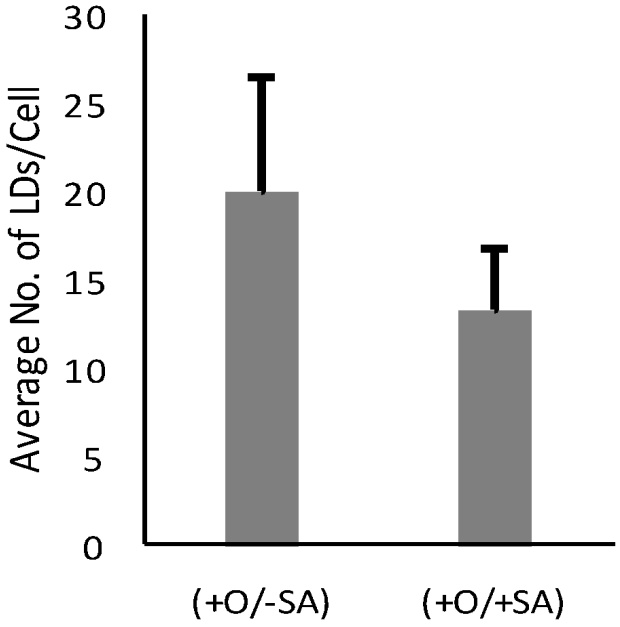

Figure 6.6 Oxidative stress reduced lipid droplet accumulation in WT U2OS cells.

WT U2OS were incubated with oleate overnight and treated with/out 0.5 mM SA for 30 min. SA-treated cells (+O/+SA) showed a reduction of 1.3-fold change in LDs number compared to SA-untreated cells (+O/-SA). Data represents mean ± SEM n=3, statistical significance was assessed using ANOVA t-test.

6.4.1.2 Lipid Droplets in Senescent WT U2OS Cells

Senescent cells are metabolically active cells in absence of cell division. Accumulation and modification of lipids were observed to be associated with aging and age-related diseases (Schroeder et al., 2015). Triglycerides were observed to accumulate in replicative senescent BJ fibroblast cells due to the active regulation of lipid-regulating genes and abundance of specific families of lipids (Lizardo et al., 2017). Moreover, senescent cells showed accumulation of lipid droplets due to activation of multiple lipid metabolic pathways. Proteomic analysis of therapy-induced senescent cells displayed an increase in annexin phospholipid binding protein, triglyceride synthesis enzyme and glycolipid processing enzymes (Flor et al., 2017). Therefore, we here investigate lipid droplet accumulation in senescent WT U2OS cells.

In our recent study, lipid droplet accumulation was examined in senescent WT U2OS. Therefore, cells were treated with doxorubicin (200 nM) for 48 hours to induce senescence phenotype. Senescent cells were then incubated with/out oleate for 24 hours. Subsequently, cells were treated with/out 0.5 mM SA for 30 min. Then, cells were fixed and stained with Oil Red O to visualize lipid droplets. Senescent cells are characterized as enlarged, multinucleate cells (Figure 6.7). Moreover, oleate-untreated senescent cells showed accumulation of small LDs. However, incubating cells overnight with oleate was observed to induce accumulation of small and large LDs. Small LDs showed a significant increase of 7-fold change. Whereas large LDs showed an increase of 9-fold change compared to oleate-untreated cells (Figure 6.7).

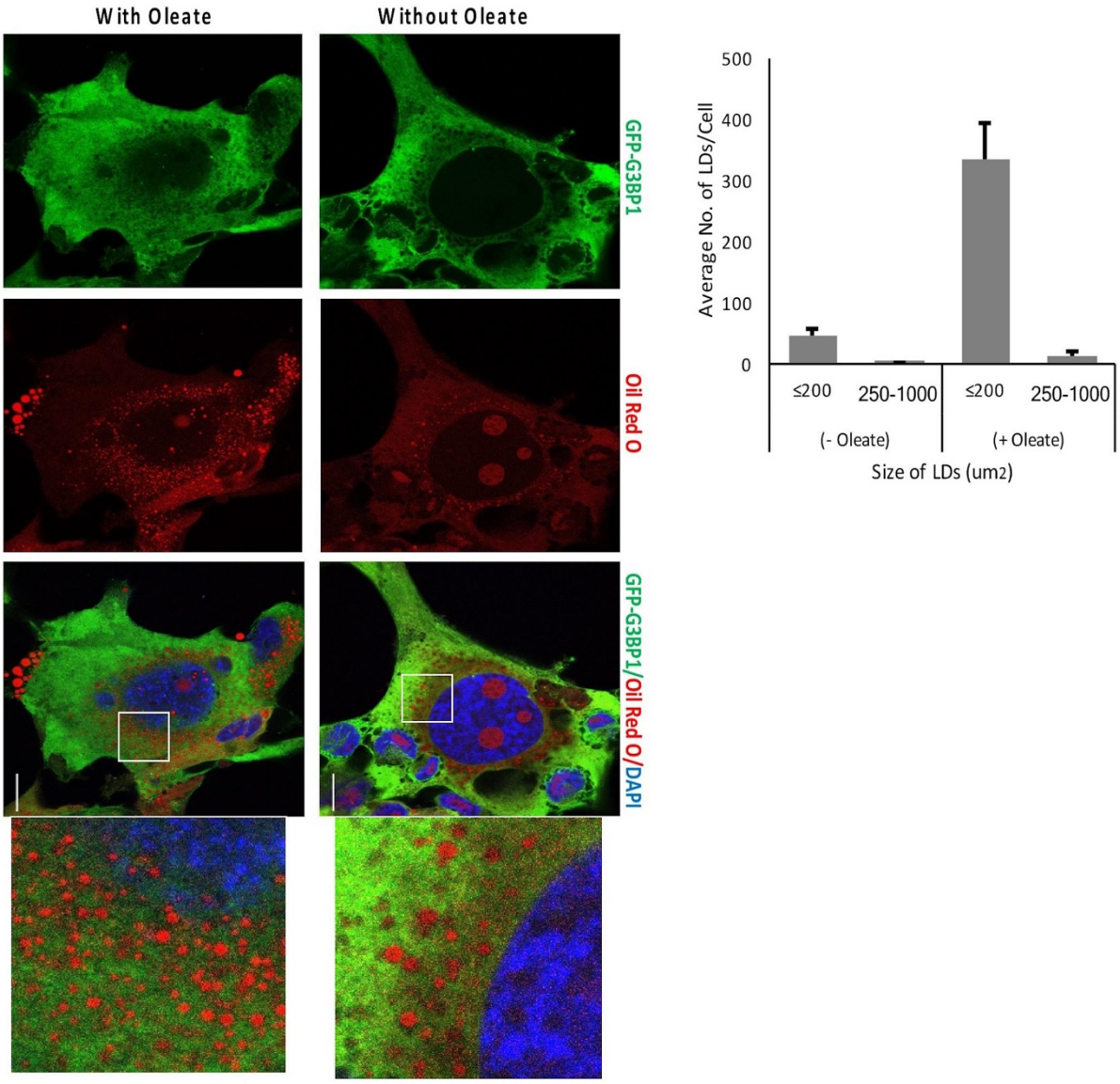

Figure 6.7 Oleate induced lipid droplet accumulation in senescent WT U2OS cells. Doxorubicin-induced senescent cells were treated with/out oleate for 24 hrs. Cells were fixed and stained with Oil Red O (red) to visualize lipid droplets. Oleate-untreated cells showed accumulation of lipid droplets. Oleate was observed to induce lipid droplet accumulation. Small LDs were observed to significantly increase (7-fold change) upon oleate treatment. Large LDs showed an increase of 9-fold change. Data represents mean ± SEM n=3, statistical significance was assessed using ANOVA t-test. Scale bar= 20 um.

Oxidative stress was observed to reduce accumulation of lipid droplets in proliferative WT U2OS cells (Figure 6.4). Hence, we examined lipid droplet accumulation in senescent cells under oxidative stress and oleate treatment. Senescent cells showed formation of small-size stress granules in response to SA exposure. As expected, it was observed that accumulation of small LDs is affected by oleate incubation. It showed an increase of 2-fold change compared to oleate-untreated cells (Figure 6.8). This data indicates oleate induced accumulation of lipid droplets in SA-treated senescent cells.

Moreover, senescent cells displayed an increase (6-fold) in lipid droplets compared to proliferative (Figure 6.4) WT U2OS cells. Under oxidative stress, proliferative and senescent cells showed a decrease in lipid droplet accumulation (Figure 6.9). Collectively, lipid droplet accumulation is suggested to increase in senescent WT U2OS compared to proliferative cells. Hence, our observations suggest that oxidative stress regulates lipid droplet accumulation in proliferative and senescent cells.

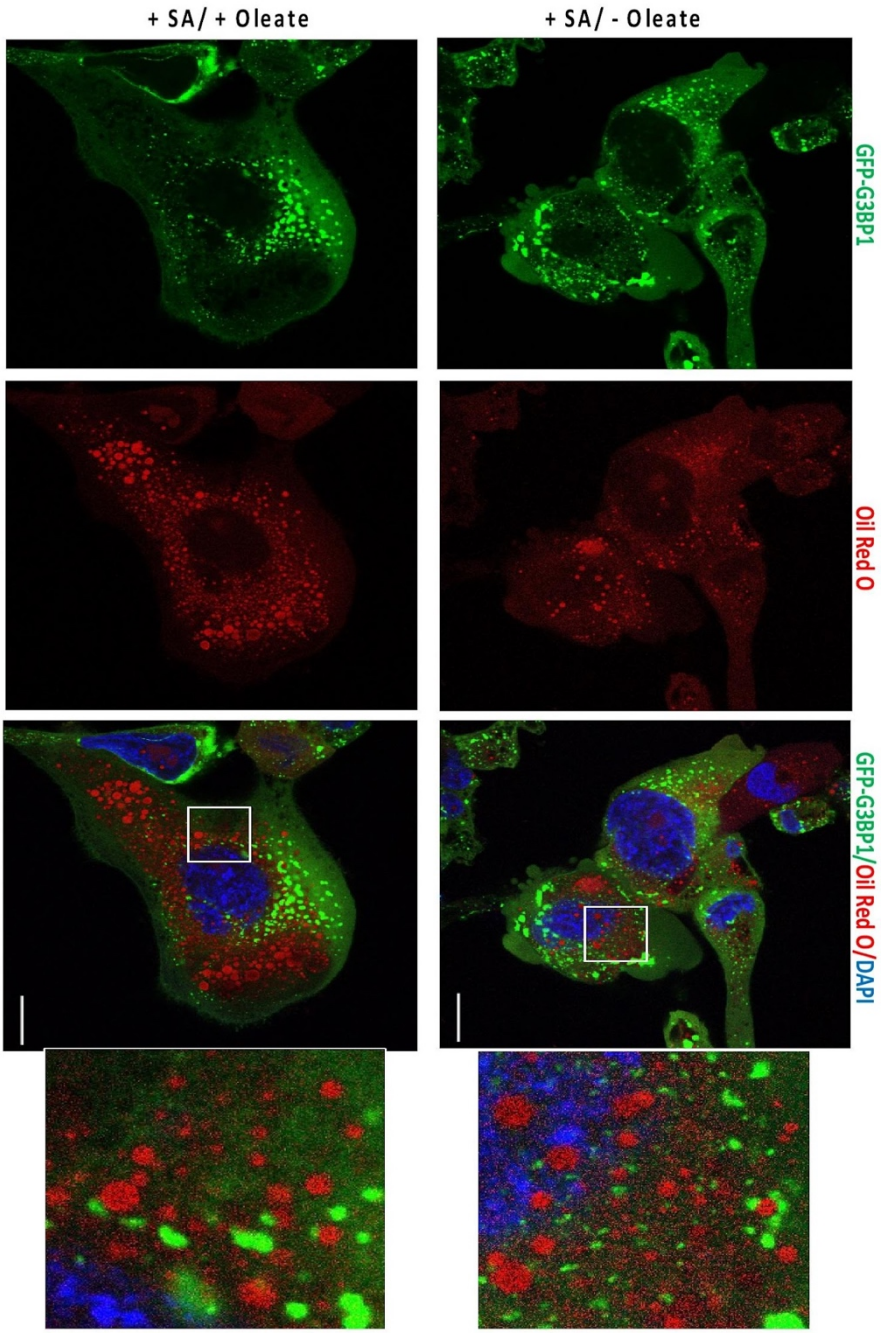

Figure 6.8 Oleate induced lipid droplet accumulation in SA-treated senescent WT U2OS cells.

Senescent cells were treated with/out oleate for 24 hrs and exposed to SA for 30 min. Cells were then fixed and stained with Oil Red O (red) to visualize lipid droplets. Stress granules were observed to aggregate in SA-treated cells. Oleate treatment induced lipid droplet accumulation in SA-treated cells. Scale bar= 20 um.

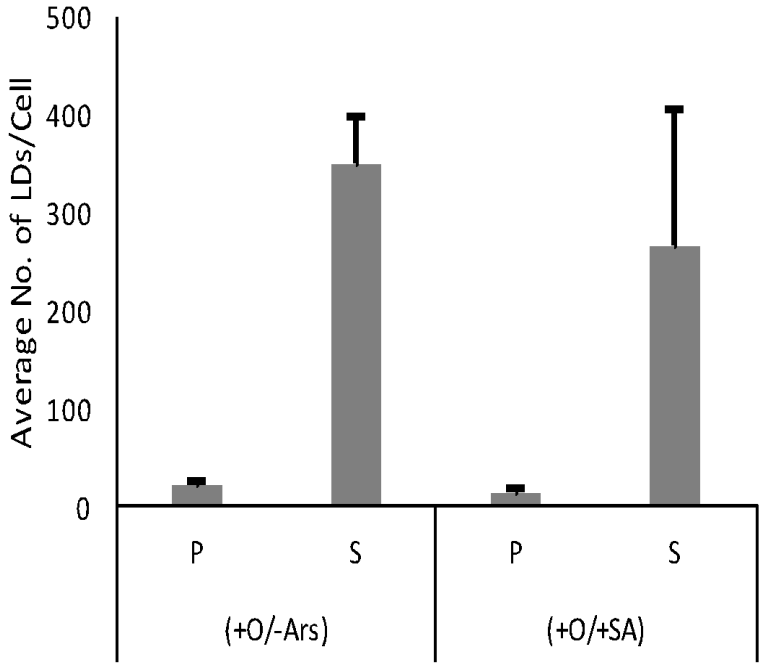

Figure 6.9 Lipid droplet accumulation is reduced in senescent and proliferative cells in response to oxidative stress.

WT U2OS were incubated with oleate overnight and treated with/out 0.5 mM SA for 30 min. Senescent cells showed an increase in LDs compared to proliferative cells. SA-treated proliferative and senescent cells (+O/+SA) showed a reduction in LDs number compared to SA-untreated cells (+O/-SA). Data represents mean ± SEM n=3, statistical significance was assessed using ANOVA t-test.

6.4.2 Lipid Droplets in G3BP Knockout (ΔΔG3BP1/2) Cells

6.4.2.1 Inhibition of Lipid Droplets in Proliferative ΔΔG3BP1/2 Cells

Our recent data showed that G3BP1/2 knockout (ΔΔG3BP1/2) cells display a significant decrease in stress granule formation (discussed in chapter 4). Additionally, they showed an increased progression towards senescence (discussed in chapter 5). Hence, it is suggested that G3BP plays a role in development of senescence phenotype in U2OS cells. Accumulation of lipids has been observed to increase in senescent cells. Thus, we here investigate whether lipid droplets increase in senescent ΔΔG3BP1/2 cells and whether it could be used as a senescence marker along with other markers.

We here investigate lipid droplet formation in G3BP1/2 knockout cells. ΔΔG3BP1/2 cells were incubated with/out oleate for 24 hours followed by SA exposure (0.5 mM for 30 min). Cells were then fixed and stained with Oil Red O to visualise lipid droplets. Thus, oleate-untreated (control) cells did not show formation of lipid droplets. Moreover, oleate treatment did not induce lipid droplet formation in ΔΔG3BP1/2 cells (Figure 6.10). This observation suggests that inhibition of stress granules by knocking out G3BP1/2 prevents lipid droplet formation. Oxidative stress is known to induce stress granule formation. However, in ΔΔG3BP1/2 cells and due to absence of G3BP1/2, stress granules were inhibited. On the other hand, few/no lipid droplets/cell were formed under SA stress. SA and oleate treatment induced formation of small lipid droplets (Figure 6.10). Our data shows that inhibition of stress granules inhibits lipid droplet formation suggesting that G3BP might play a role in lipid droplet formation. Additionally, oxidative stress induces formation of small lipid droplets in ΔΔG3BP1/2 cells.

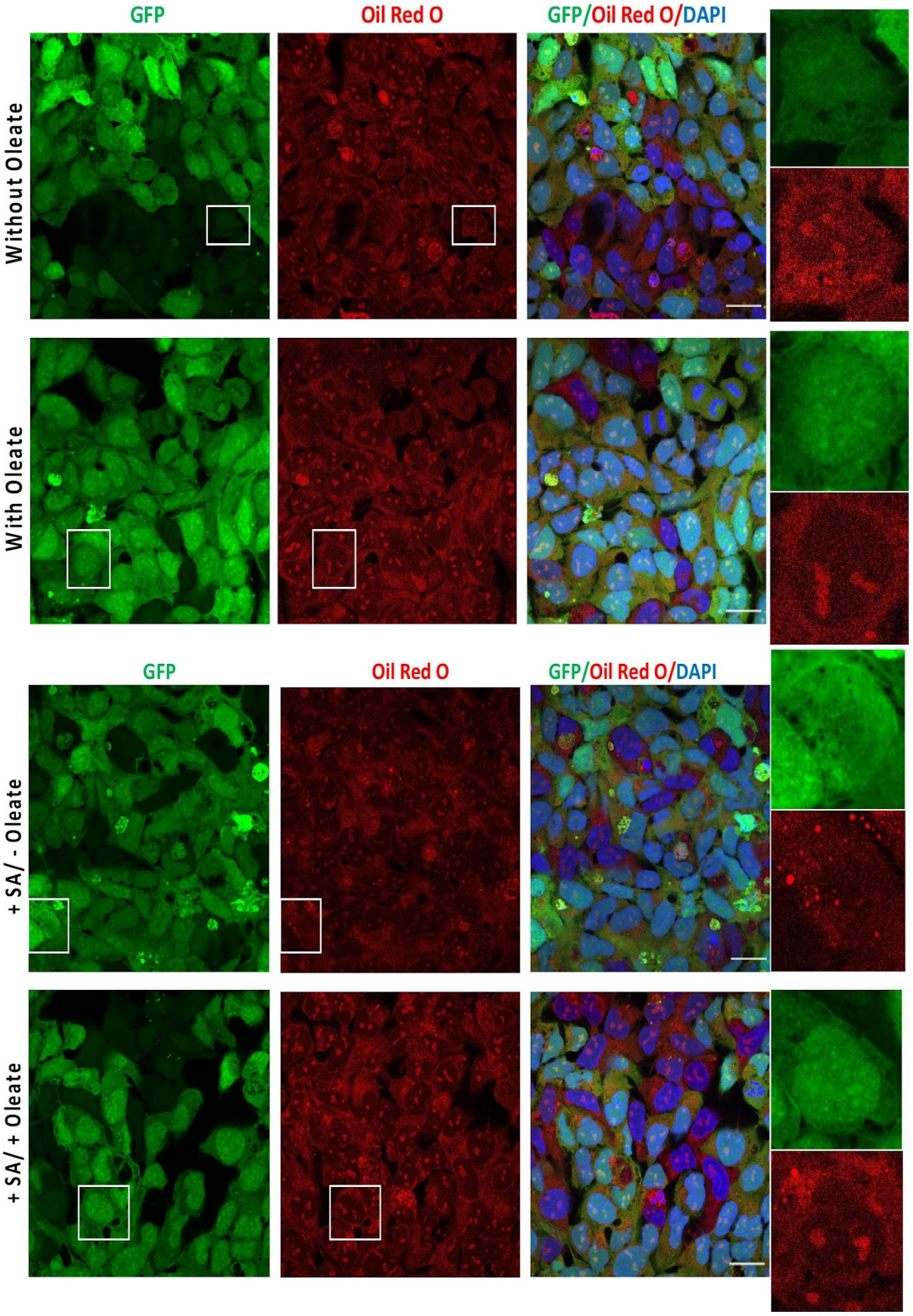
GFP
Oil Red O
GFP/Oil Red O/DAPI
Without Oleate
With Oleate
GFP
Oil Red O
GFP/Oil Red O/DAPI
+ SA/ - Oleate
+ SA/ + Oleate

Figure 6.10 Inhibition of stress granules inhibits lipid droplet formation in ΔΔG3BP1/2 cells.

Cells were incubated with/out 3% oleate overnight and then treated with 0.5 mM SA for 30 min. Cells were then fixed and stained with Oil Red O to visualize lipid droplets. Oleate did not induce lipid droplets in ΔΔG3BP1/2 cells. Cells exposed to SA showed no/few formation of lipid droplets/cell. Scale bar= 20 um.

To quantitatively compare lipid droplet formation under oleate and/or SA treatment in ΔΔG3BP1/2 cells, ImageJ was used to count lipid droplets/per cell. Hence, no lipid droplets were detected in control (-O/-SA) cells. Additionally, incubation of cells with oleate (+O/-SA) showed 0 LDs/cell. Exposure of ΔΔG3BP1/2 cells to SA showed an increase of 3-fold change in LDs/cell. However, the increase was observed in small LDs (>200 um2) but not large LDs (250-1000 um2). Moreover, incubation of cells with oleate followed by SA exposure (+O/+SA) induced formation of small LDs. An increase of 4-fold change was detected (Figure 6.11). Nevertheless, large LDs are suggested to form as a result of accumulation/fusion of small LDs under certain conditions. Hence, in ΔΔG3BP1/2 cells, large LDs were not detected and this could be due to the unavailability of small LDs originally in control (-O/-SA) cells.

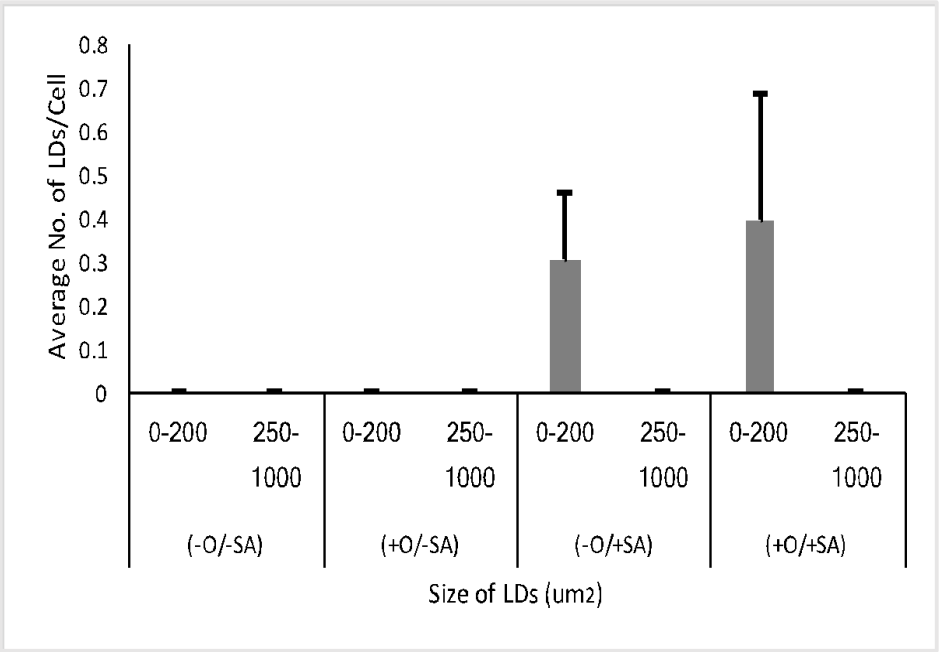

Figure 6.11 Oxidative stress induces formation of small lipid droplets in ΔΔG3BP1/2 cells.

Oleate-treated (+O/-SA) and -untreated (-O/-SA) cells showed no lipid droplet formation. SA (-O/+SA) exposure showed an increase of 3-fold change in small LDs number. SA and oleate (+O/+SA) treatment led an increase of 4-fold change. Data represents mean ± SEM n=3, statistical significance was assessed using ANOVA t-test.

6.4.2.2 Lipid Droplets in Senescent ΔΔG3BP1/2 Cells

Proliferative ΔΔG3BP1/2 cells showed inhibition of lipid droplet formation (see section 6.4.2.1) However, oxidative stress induced lipid droplet formation. Hence, we ask a question whether senescent ΔΔG3BP1/2 cells form lipid droplets under oleate and/or oxidative stress. Therefore, cells were treated with doxorubicin (200 nM) for 48 hours to induce senescence phenotype. Senescent cells were then incubated with/out oleate for 24 hours. Subsequently, cells were treated with/out 0.5 mM SA for 30 min. Then, cells were fixed and stained with Oil Red O to visualize lipid droplets. Senescent cells are characterized with the multinucleate and enlarged size (Figure 6.12). Moreover, oleate-untreated senescent cells showed formation of few LDs. However, incubating cells overnight with oleate was observed to induce formation of small LDs (Figure 6.12A). Hence, we examined lipid droplet accumulation in senescent cells under oxidative stress and oleate treatment. Senescent cells did not show formation of stress granules in response to SA exposure. This is due to absence of G3BP1/2. Moreover, accumulation of small LDs was observed to increase under oleate incubation (Figure 6.12B). Hence, our data indicates that oleate and/or SA induce accumulation of lipid droplets in senescent ΔΔG3BP1/2 cells.

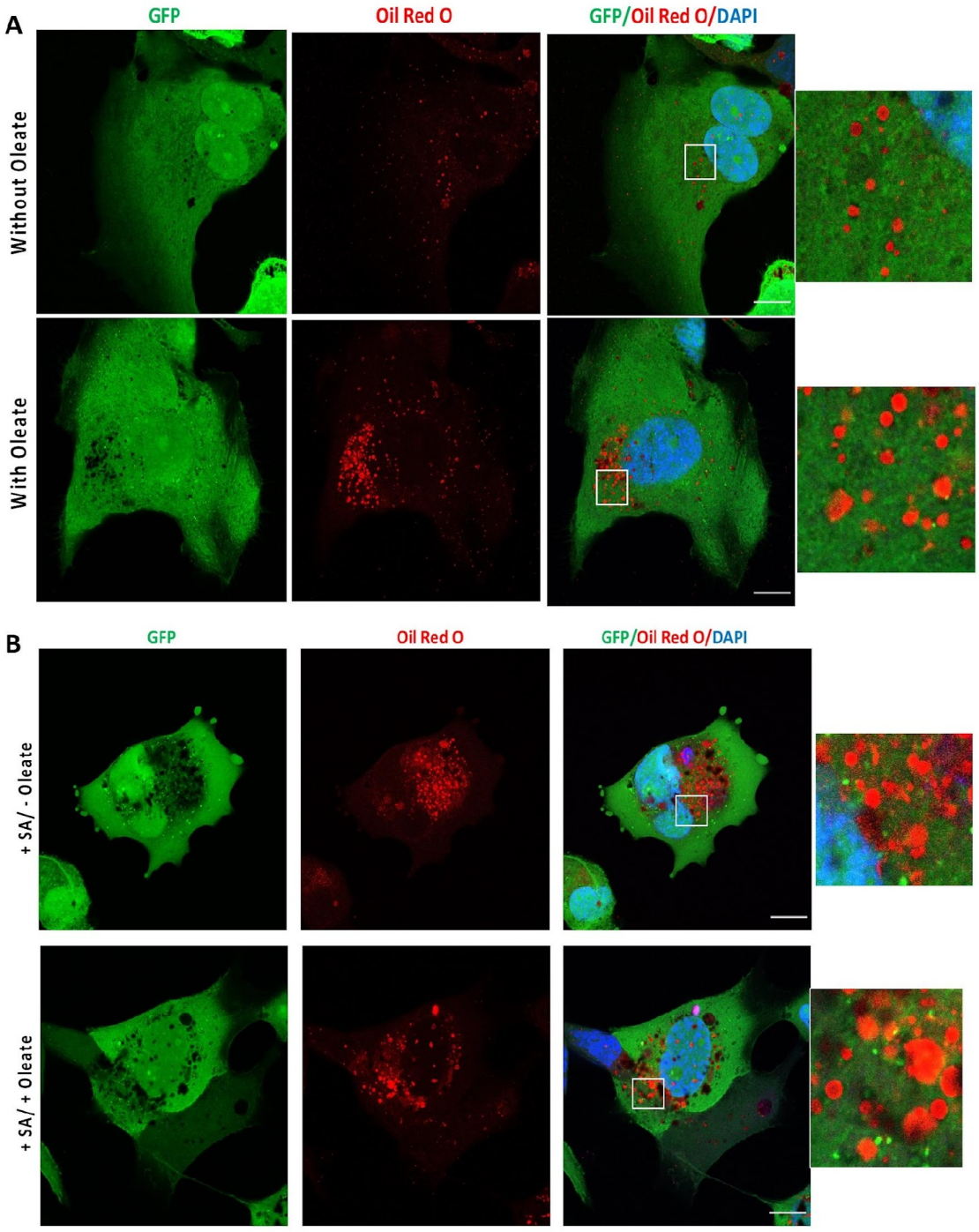

Figure 6.12 Formation of lipid droplets in senescent ΔΔG3BP1/2 cells. Cells were incubated with 3% oleate overnight and then treated with 0.5 mM SA for 30 min. Cells were then fixed and stained with Oil Red O to visualize lipid droplets. Oleate induced lipid droplets in senescent ΔΔG3BP1/2 cells (A). Cells exposed to SA showed formation of lipid droplets (B). Scale bar= 20 um.

To quantitatively compare lipid droplet formation in senescent ΔΔG3BP1/2 cells under oleate and/or SA treatment, ImageJ was used. Oleate-untreated cells (-O/-SA) showed formation of small LDs but not large LDs. An increase of 1.5-fold change was observed under oleate treatment (+O/-SA). Hence, it is suggested that oleate induces formation of lipid droplets. Under oxidative stress (-O/+SA), cells showed formation of small (<200 um2) and large (250-1000 um2) LDs. An increase of 1-fold change and 9-fold change was detected in small and large LDs, respectively. Furthermore, SA and oleate treatments (+O/+SA) induced formation of small LDs and large LDs. Small LDs showed an increase of 1.6-fold change while large LD revealed an increase of 5-fold change (Figure 6.13). Collectively, lipid droplet formation is suggested to be inhibited in proliferative ΔΔG3BP1/2 cells but increased in senescent ΔΔG3BP1/2 cells.

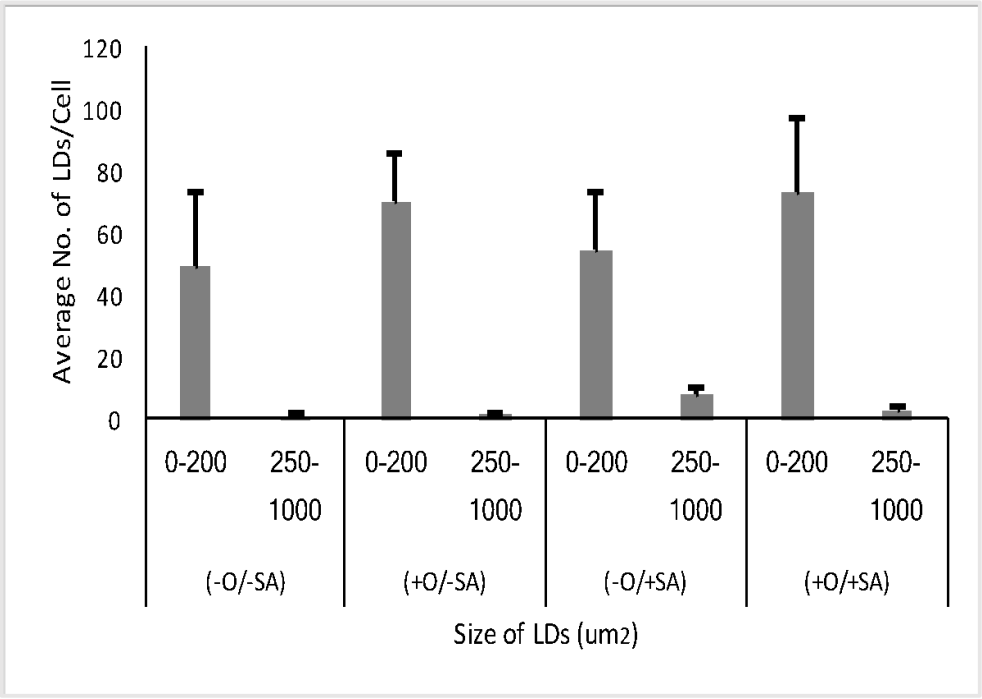

Figure 6.13 Oxidative stress induced formation of small and large lipid droplets in senescent ΔΔG3BP1/2 cells.

Oleate-treated (+O/-SA) and -untreated (-O/-SA) cells showed formation of small lipid droplets. An increase of 1.5-fold change was observed under oleate treatment (+O/-SA). SA (-O/+SA) exposure showed an increase of 1- and 9-fold change in small and large LDs, respectively. SA and oleate (+O/+SA) treatment induced formation of lipid droplets. Small LDs showed an increase of 1.6-fold change while large LD revealed an increase 5-fold change compared to control (-O/-SA) cells. Data represents mean ± SEM n=3, statistical significance was assessed using ANOVA t-test.

6.4.3 Lipid Droplets in GFP-G3BP1 Cells

6.4.3.1 Lipid Droplet Formation in Proliferative GFP-G3BP1 Cells

Absence of G3BP was observed to reduce stress granule formation (Kedersha et al., 2016). Previously, we detected the inability of ΔΔG3BP1/2 cells of forming stress granules when exposed to oxidative stress (discussed in chapter 4). Re-constitution of ΔΔG3BP1/2 cells with one form of G3BP; G3BP1 (GFP-G3BP1 cells), rescued cells' ability of stress granule formation (discussed in chapter 4). Our previous data revealed that proliferative ΔΔG3BP1/2 cells appeared to lose the ability of forming lipid droplets. Thus, this data suggests that G3BP is required for lipid droplet formation.

We here investigate the formation of lipid droplets in GFP-G3BP1 cells. Hence, we assessed G3BP1 role in lipid droplet formation in GFP-G3BP1 cells. Proliferative GFP-G3BP1 cells were incubated with/out oleate to for 24 hours followed by SA exposure (0.5 mM for 30 min). Then, cells were fixed and stained with Oil Red O to visualise lipid droplets. Hence, oleate-untreated (control cells) showed no/few lipid droplet formation. However, oleate-treated cells revealed formation of lipid droplets (Figure 6.14A). Thus, our observation suggests that presence of G3BP1 promotes formation of lipid droplets. Additionally, re-constitution of cells with G3BP1 was observed to rescue stress granule formation under oxidative stress. Thus, oxidative stress solely revealed formation of lipid droplets. Moreover, incubation of GFP-G3BP1 cells with oleate and SA exposure stimulated formation of lipid droplets (Figure 6.14B). ER-droplet bridges were observed in GFP-G3BP1 cells upon oleate and SA treatment indicating that lipid droplets remain in contact to their mother organelle; Endoplasmic Reticulum (ER). Nevertheless, our data shows that presence of G3BP1 rescues stress granules and lipid droplet formation in GFP-G3BP1 cells.

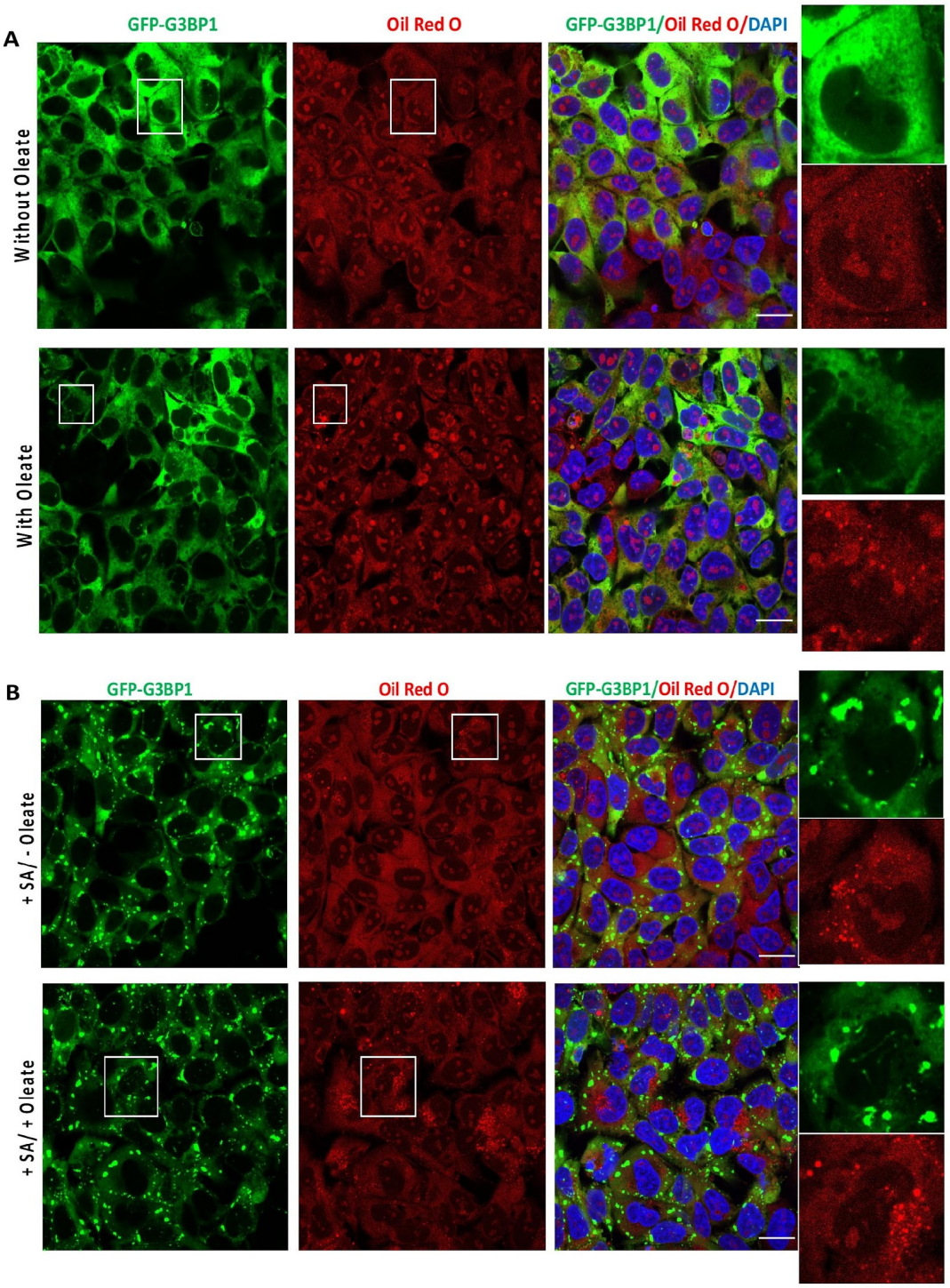

Figure 6.14 Re-constitution of cells with G3BP1 promotes lipid droplet formation. GFP-G3BP1 cells were incubated with/out 3% oleate for 24 hours and then un/treated with 0.5 mM SA for 30 min. Cells were stained with Oil Red O to visualize lipid droplets. Oleate was observed to induce lipid droplet formation in GFP-G3BP1 cells (A). Cells treated with SA showed formation of lipid droplets (B). Scale bar= 20 um.

To quantitatively compare lipid droplet formation under oleate and/or SA treatment in GFP-G3BP1 cells, ImageJ was used to count lipid droplets/per cell. Thus, few small LDs were detected in control (-O/-SA) cells, whereas, large LDs were not detected. Incubation of cells with oleate (+O/-SA) showed an increase of 3-fold change in small LDs but not large LDs. Exposure of GFP-G3BP1 cells to SA showed an increase of 4-fold change in LDs/cell compared to control cells. The increase was observed in small LDs but not large LDs. Moreover, incubation of cells with oleate followed by SA exposure (+O/+SA) induced formation of small LDs. An increase of 5.5-fold change was detected compared to -O/+SA cells. Small number of large LDs was detected under oleate/SA (+O/+SA) treatment (Figure 6.15).

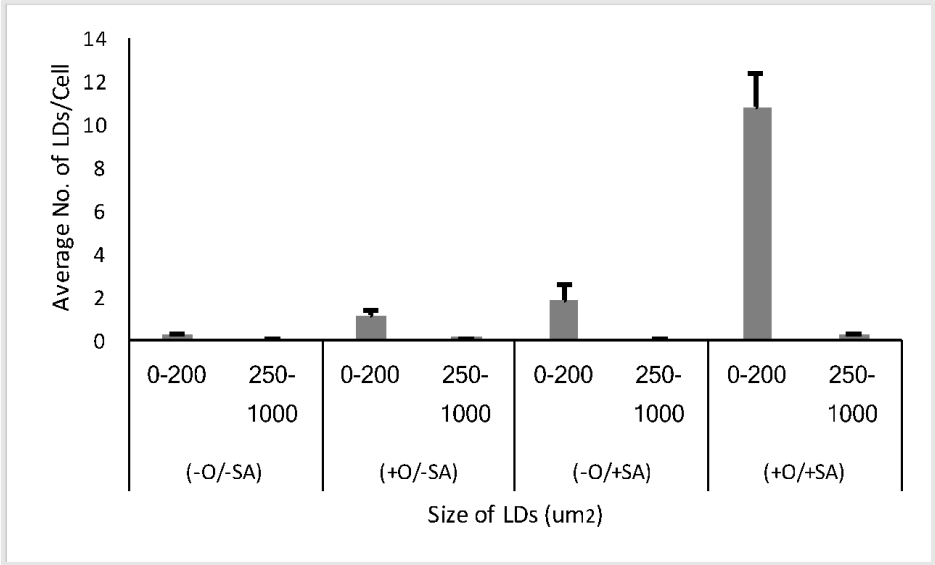

Figure 6.15 Formation of lipid droplets increased under oxidative stress in GFP-G3BP1.

Oleate-untreated (-O/-SA) cells showed formation of no/few lipid droplets. oleate-treated (+O/-SA) cells showed formation of small LDs (3-fold change). SA exposure (-O/+SA) showed an increase of 4-fold change in small LDs number. SA and oleate (+O/+SA) treatment led an increase of 5.5-fold change compared to -O/+SA cells. Data represents mean ± SEM n=3, statistical significance was assessed using ANOVA t-test.

6.4.3.2 Accumulation of Lipid Droplets in Senescent GFP-G3BP1 Cells

Proliferative GFP-G3BP1 cells showed formation of lipid droplets under oleate and/or SA treatment (see section 6.6.1). Thus, we ask the question whether senescent GFP-G3BP1 cells form lipid droplets under control, oleate and/or SA treatment. Therefore, cells were treated with doxorubicin (200 nM) for 48 hours to induce senescence phenotype. Senescent cells were then incubated with/out oleate for 24 hours. Subsequently, cells were treated with/out 0.5 mM SA for 30 min. Then, cells were fixed and stained with Oil Red O to visualize lipid droplets. The enlarged cells phenotype was detected in cells indicating that cells are senescent (Figure 6.16). Additionally, oleate-untreated cells showed formation of no/few lipid droplets. Incubation of cells with oleate stimulated lipid droplet formation (Figure 6.16A). We then examined lipid droplet formation under oxidative stress. Thus, treatment of cells with 0.5 mM SA induced formation of stress granules and lipid droplets. Moreover, Oleate and SA treatment led to an increased formation of lipid droplets (Figure 6.16B). Hence, our observations suggest that G3BP1 somewhat rescues stress granule formation in senescent GFP-G3BP1 cells, but not to WT U2OS levels. It also induces formation of lipid droplets under oleate and/or SA treatment.

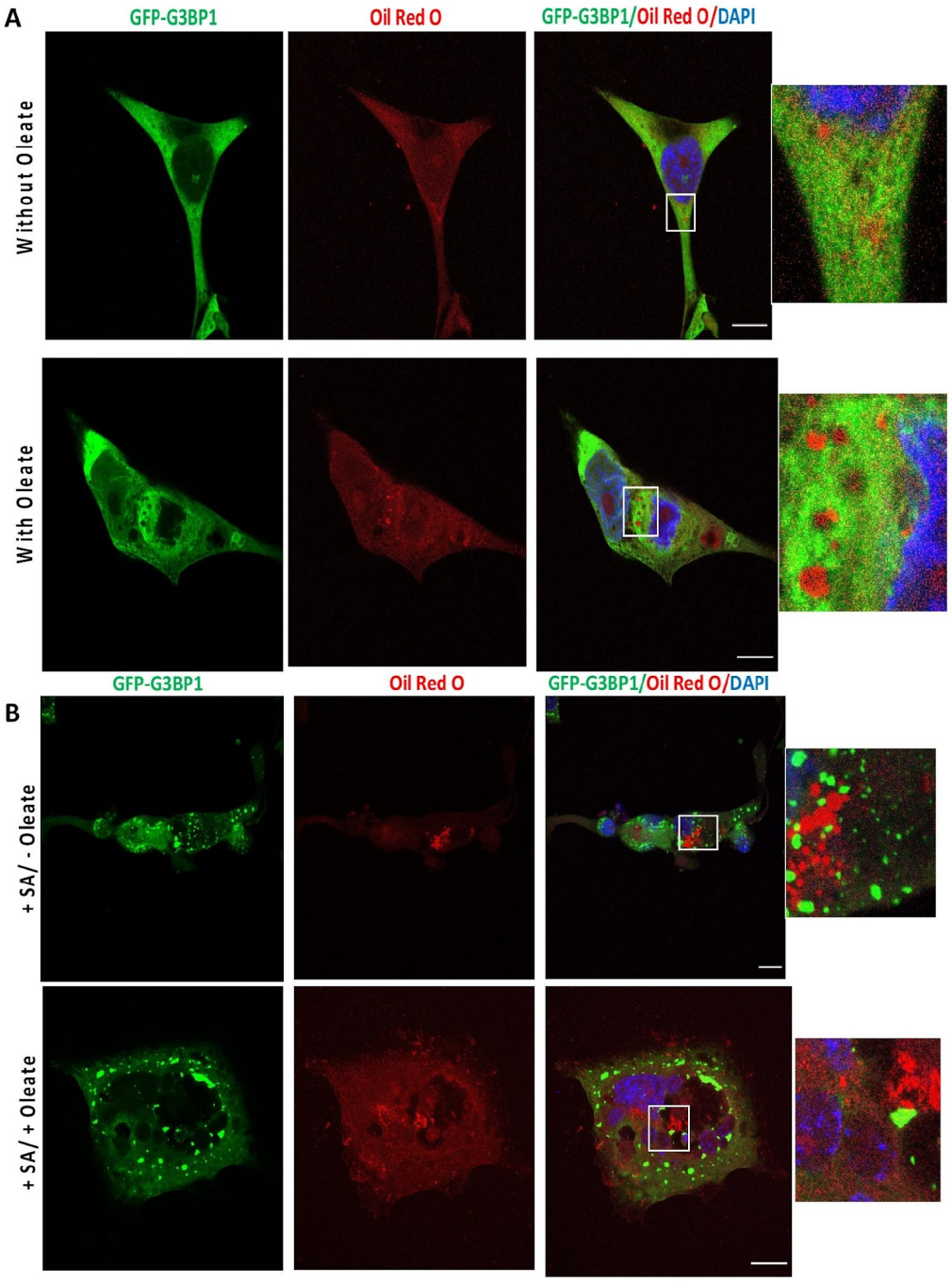

Figure 6.16 Formation of lipid droplets in senescent GFP-G3BP1 cells. Cells were incubated with 3% oleate overnight and then treated with 0.5 mM SA for 30 min. Cells were then fixed and stained with Oil Red O to visualize lipid droplets. Oleate induced lipid droplet formation in senescent GFP-G3BP1 cells (A). Cells exposed to SA showed increased formation of lipid droplets (B). Scale bar= 20 um.

To quantitatively compare lipid droplet formation in senescent GFP-G3BP1 cells under oleate and/or SA treatment, ImageJ was used. Oleate-untreated cells (-O/-SA) showed formation of small and large LDs. Under oleate incubation (+O/-SA), an increase of 3-fold change was observed in small LDs. A minor increase in large LDs number was detected. Thus, it indicates that oleate treatment induces lipid droplet formation. Oxidative stress was detected to induce lipid droplet formation. An increase of 4-fold change was detected in cells treated with SA (-O/+SA). This increase was observed in small LDs. Large LDs showed an increase of 2-fold change. Treatment of cells with SA and oleate (+O/+SA) induced lipid droplet formation. Small LDs showed an increase of 3-fold compared to -O/+SA cells (Figure 6.17).

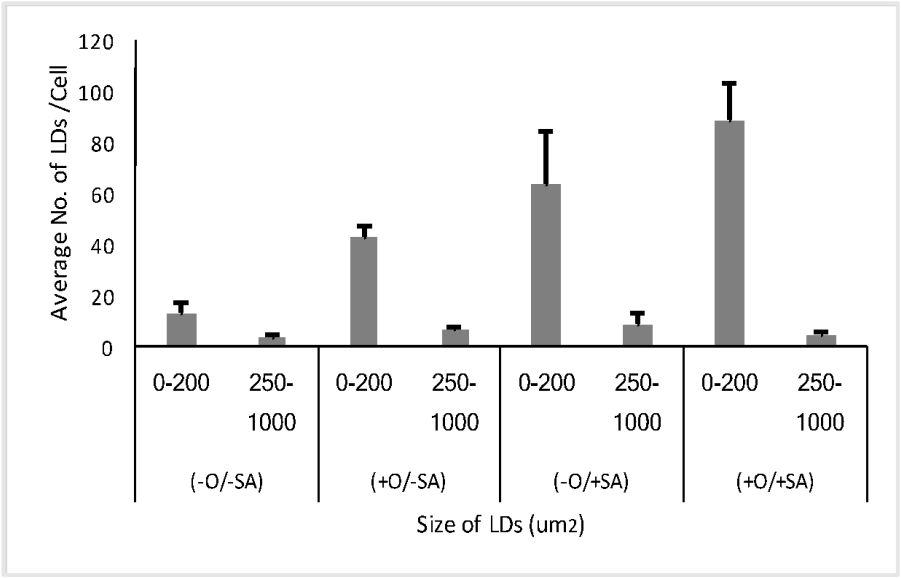

Figure 6.17 Oxidative stress induced formation of lipid droplets in senescent GFP-G3BP1 cells.

Oleate-untreated (-O/-SA) cells showed formation of small and large LDs. Oleate-treated (+O/-SA) cells showed increase in small lipid droplets. An increase of 3-fold change was observed under oleate treatment (+O/-SA). SA (-O/+SA) exposure showed an increase of 4- and 2-fold change in small and large LDs, respectively. SA and oleate (+O/+SA) treatment induced formation of small LDs. They showed an increase of 3-fold change compared to -O/+SA cells. Data represents mean ± SEM n=3, statistical significance was assessed using ANOVA t-test.

Collectively, our data suggests that G3BP1 somewhat restored cells' ability to form lipid droplets. Lipid droplets were observed to be formed in senescent GFP-G3BP1 cells. Moreover, oleate treatment induced formation of lipid droplets in senescent cells. Oxidative stress stimulated lipid droplet formation in senescent cells. Interestingly, stressed senescent cells revealed a significant increase in lipid droplets compared to proliferative cells, though these are still lower than the number previously observed in the WT senescent cells in figure 6.7.

6.4.4 Lipid Droplets in GFP-G3BP2a Cells

6.4.4.1 G3BP2a Somewhat Restore Cells' Ability of Forming Lipid Droplets in Proliferative GFP-G3BP2a Cells

In addition to G3BP1, G3BP2 is required for the formation of stress granules. G3BP2a and G3BP2b are two forms of G3BP2. They have been examined for their involvement in stress granule assembly. G3BP2a and G3BP2b have been observed to be recruited into stress granules (Kedersha et al., 2016; Matsuki et al., 2013). Thus, absence of G3BP2 alongside G3BP1 was observed to reduce stress granule formation in ΔΔG3BP1/2 (discussed in chapter 4). Nevertheless, re-constitution of G3BP knockout (ΔΔG3BP1/2) cells with one form of G3BP2: G3BP2a (GFP-G3BP2a cells) somewhat restored cells' ability of forming stress granules. However, the number of stress granules in GFP-G3BP2a cells was reduced compared to the WT cells (discussed in chapter 5). On the other hand, proliferative ΔΔG3BP1/2 cells were observed to lose the ability to form lipid droplets (see section 6.3). Thus, this data suggests that G3BP1/2 is required for lipid droplet formation.

We here examine the role of G3BP2a in lipid droplet formation by monitoring lipid droplets in GFP-G3BP2a cells. Proliferative GFP-G3BP2a cells were incubated with/out oleate to for 24 hours followed by SA exposure (0.5 mM for 30 min). Next, cells were fixed and stained with

Oil Red O for visualisation of lipid droplets. Oleate-untreated (control cells) showed no/few lipid droplet formation. Additionally, oleate-treated cells revealed formation of no/few lipid droplets per cell indicating that G3BP2a promotes formation of lipid droplets (Figure 6.18A). Oxidative stress was observed to induce stress granule formation in GFP-G3BP2a cells. Thus, oxidative stress solely induced formation of lipid droplets. Incubation of GFP-G3BP2a cells with oleate followed by SA exposure stimulated formation of lipid droplets (Figure 6.18B).

To quantitatively compare lipid droplet formation under oleate and/or SA treatment in GFP-G3BP2a cells, ImageJ was used. Thus, few small LDs were detected in control (-O/-SA) cells, whereas, large LDs were not detected. Incubation of cells with oleate (+O/-SA) showed no change in the number of small LDs. Large LDs were not detected. Exposure of GFP-G3BP2a cells to SA showed an increase of 3.5-fold change in LDs/cell compared to control cells. The increase was observed in small LDs but not large LDs. Moreover, incubation of cells with oleate followed by SA exposure (+O/+SA) induced formation of small LDs. An increase of 4-fold change was detected compared to -O/+SA cells. Small number of large LDs was detected under oleate/SA (+O/+SA) treatment (Figure 6.19).

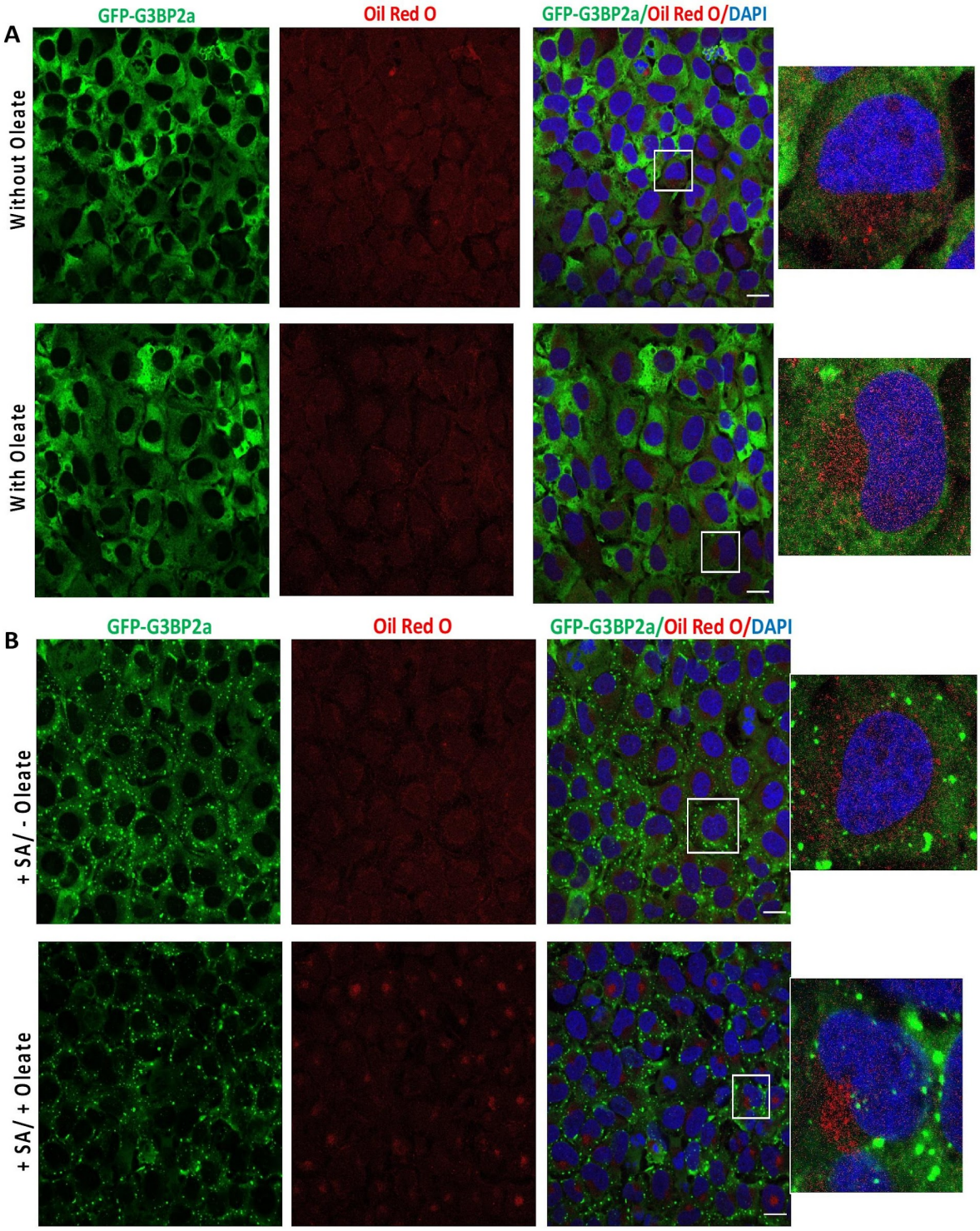

Figure 6.18 Re-constitution of cells with G3BP2a promotes lipid droplet formation. GFP-G3BP2a cells were incubated with/out 3% oleate for 24 hours and then un/treated with 0.5 mM SA for 30 min. Cells were stained with Oil Red O to visualize lipid droplets. Oleate was not observed to induce lipid droplet formation in GFP-G3BP2a cells (A). Cells treated with SA showed formation of lipid droplets (B). Scale bar= 20 um.

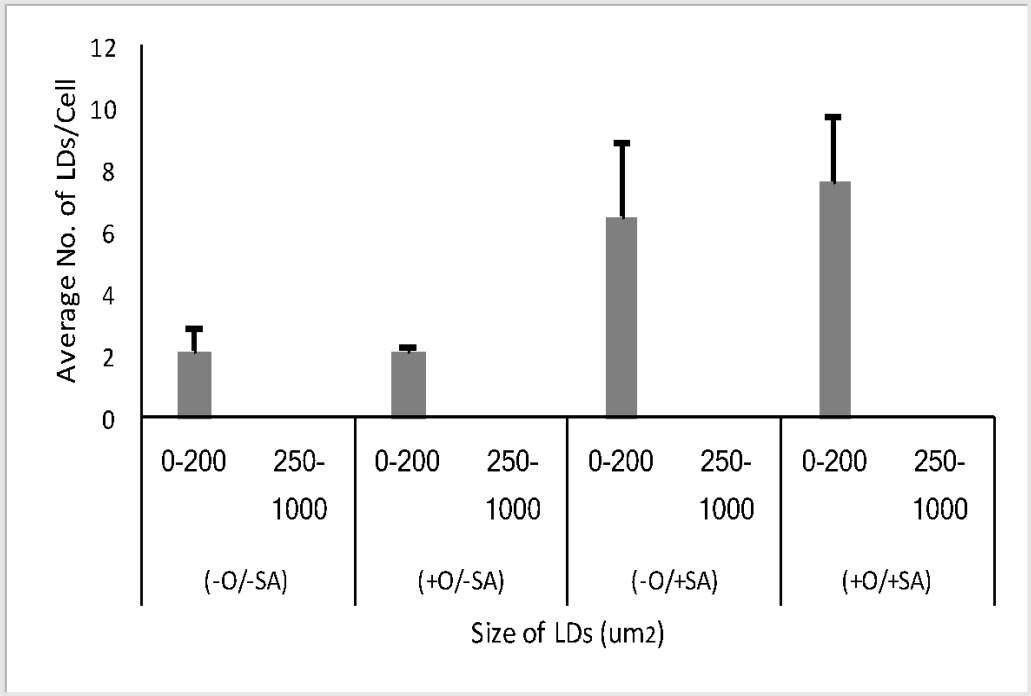

Figure 6.19 Formation of lipid droplets increased under oxidative stress in GFP-G3BP2a.

Oleate-untreated (-O/-SA) cells showed formation of no/few lipid droplets. oleate-treated (+O/-SA) cells showed formation of small LDs. SA exposure (-O/+SA) showed an increase of 3.5-fold change in small LDs number. SA and oleate (+O/+SA) treatment led an increase of 4-fold change compared to -O/+SA cells. Data represents mean ± SEM n=3, statistical significance was assessed using ANOVA t-test.

6.4.4.2 Oxidative Stress Reduced Lipid Droplets in Senescent GFP-G3BP2a Cells

Proliferative GFP-G3BP2a cells showed formation of lipid droplets under oleate and/or SA treatment (see section 6.4.4.1). We then ask the question whether senescent GFP-G3BP2a cells form lipid droplets under control, oleate and/or SA treatment. Therefore, cells were treated with doxorubicin (200 nM) for 48 hours to induce senescence. Senescent cells were then incubated with/out oleate for 24 hours. Subsequently, cells were treated with/out 0.5 mM SA for 30 min. Afterwards, cells were fixed and stained with Oil Red O to visualize lipid droplets.

The multinucleate, enlarged cell phenotype was detected in cells indicating that cells are senescent (Figure 6.20).

Furthermore, oleate-untreated cells showed formation of lipid droplets. Incubation of cells with oleate stimulated lipid droplet formation (Figure 6.20A). We then examined lipid droplet formation under oxidative stress. Thus, treatment of cells with 0.5 mM SA induced formation of stress granules but reduced formation of lipid droplets when compared to control cells. Moreover, Oleate and SA treatment led to an increased formation of lipid droplets (Figure 6.20B). Hence, our observations suggest that G3BP2a rescues stress granule formation in senescent GFP-G3BP2a cells. It also induces formation of lipid droplets under oleate and/or SA treatment.

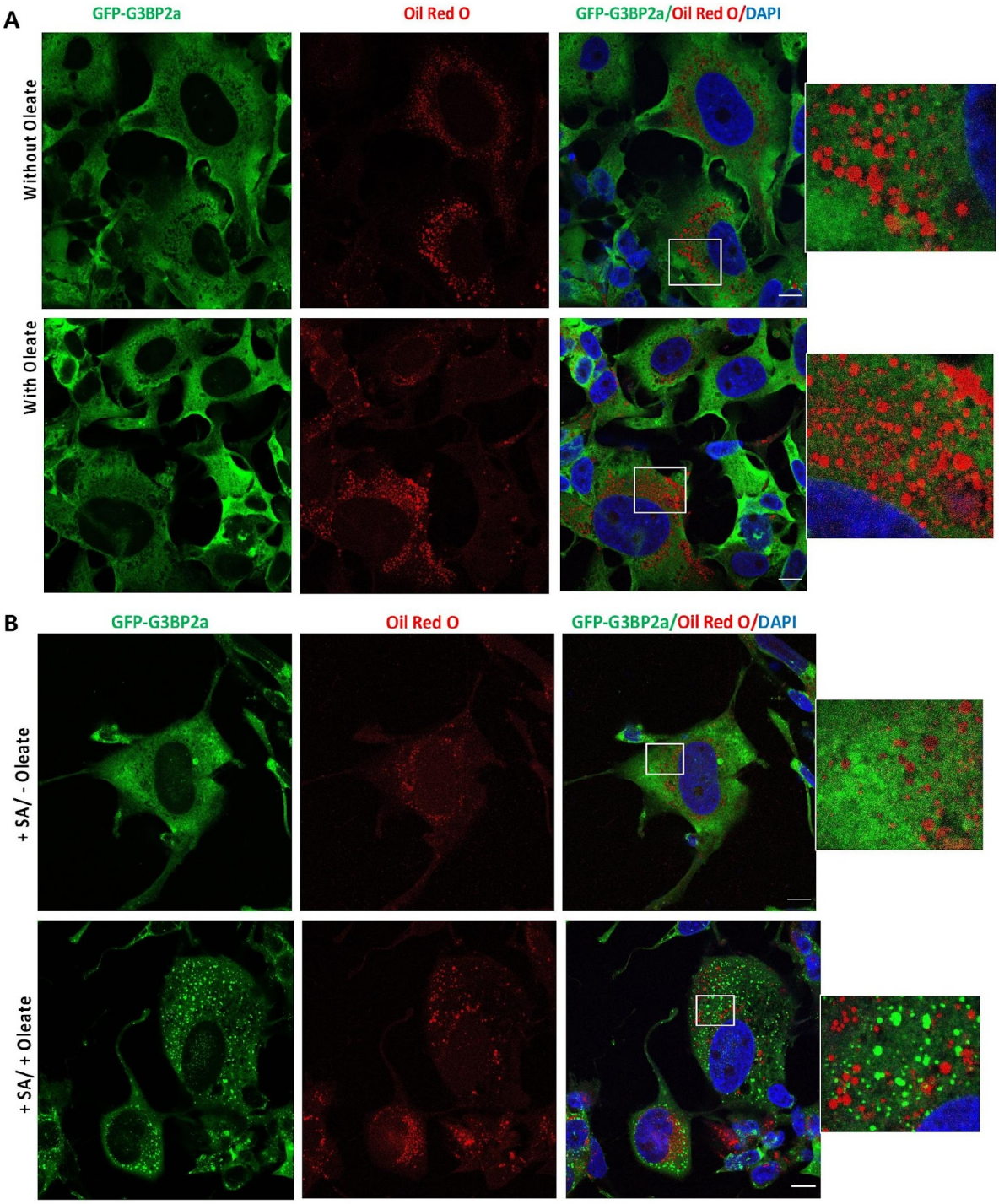

Figure 6.20 Formation of lipid droplets in senescent GFP-G3BP2a cells. Cells were incubated with/out 3% oleate overnight and then un/treated with 0.5 mM SA for 30 min. Cells were then fixed and stained with Oil Red O to visualize lipid droplets. Oleate induced lipid droplet formation in senescent GFP-G3BP2a cells (A). Cells exposed to SA/oleate showed formation of lipid droplets (B). Scale bar= 20 um.

To perform a quantitative comparison of lipid droplet formation in senescent GFP-G3BP2a cells under oleate and/or SA treatment, ImageJ was used. Oleate-untreated cells (-O/-SA) showed formation of small LDs. Under oleate incubation (+O/-SA), an increase of 1.6-fold change was observed in small LDs. Cells did not show formation of large LDs. Thus, it indicates that oleate treatment induces lipid droplet formation in senescent GFP-G3BP2a cells. Oxidative stress was detected to induce lipid droplet formation. Small LDs were detected but not large LDs. However, a decrease of 1-fold change was detected in cells treated with SA (-O/+SA) when compared to control (-O/-SA) cells. Moreover, treatment of cells with SA and oleate (+O/+SA) induced lipid droplet formation. Small LDs showed an increase of 1.6-fold compared to -O/+SA cells (Figure 6.21).

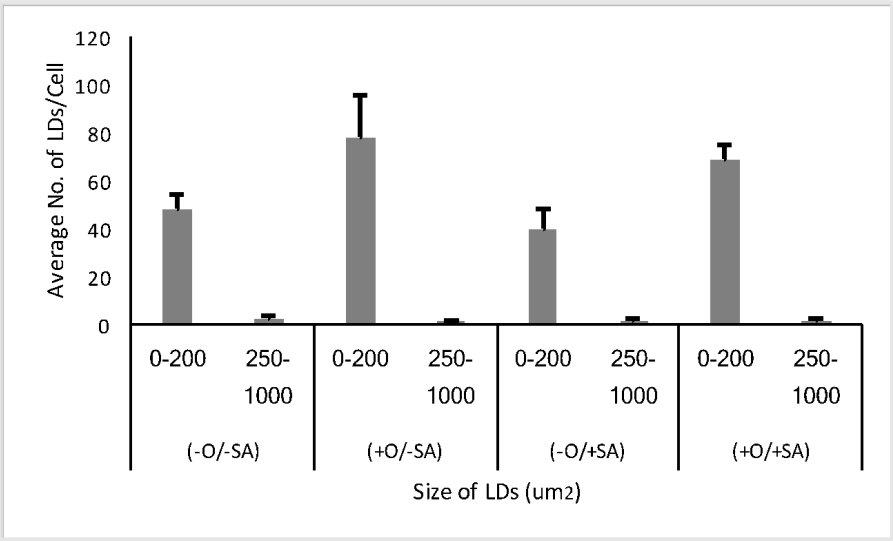

Figure 6.21 Oxidative stress reduced formation of lipid droplets in senescent GFP-G3BP2a cells.

Oleate-untreated (-O/-SA) cells showed formation of small LDs. Oleate-treated (+O/-SA) cells showed increase in small lipid droplets. An increase of 1.6-fold change was observed under oleate treatment (+O/-SA). SA (-O/+SA) exposure showed a decrease of 1-fold change in small LDs. SA and oleate (+O/+SA) treatment induced formation of small LDs. They showed an increase of 1.6-fold change compared to -O/+SA cells. Data represents mean ± SEM n=3, statistical significance was assessed using ANOVA t-test.

6.4.5 Lipid Droplets in GFP-G3BP2b Cells

6.4.5.1 Oxidative Stress Induced Lipid Droplet Formation in GFP-G3BP2b Cells

G3BP2b is one form of G3BP2 protein. It plays a role in stress granule formation. G3BP2b was observed to be recruited into stress granules under oxidative stress (Matsuki et al., 2013). Re-constitution of cells with G3BP2b restored cells' ability to form stress granules upon SA exposure. However, the number of stress granules in GFP-G3BP2b cells was observed to reduce when compared to the WT cells (discussed in chapter 5).

It was previously shown that lipid droplet formation is affected by presence or absence of G3BP (G3BP1 and G3BP2). Hence, ΔΔG3BP1/2 cells revealed a reduction in the cells' ability of forming lipid droplets (see section 6.4.2). However, presence of G3BP1 or G3BP2a individually promoted lipid droplet formation in proliferative and senescent cells (see sections 6.4.3 and 6.4.4). This data indicates that G3BP is required for the process of lipid droplet synthesis.

Therefore, we here examine the role of G3BP2b in lipid droplet formation by monitoring lipid droplet formation in GFP-G3BP2b cells. Proliferative GFP-G3BP2b cells were incubated with/out oleate to for 24 hours followed by SA exposure (0.5 mM for 30 min). Then, cells were fixed and stained with Oil Red O for visualisation of lipid droplets. Hence, oleate-untreated (control cells) showed no/few lipid droplet formation. Moreover, oleate-treated cells revealed elevated formation of lipid droplets per cell indicating that oleate promotes formation of lipid droplets in GFP-G3BP2b cells (Figure 6.22A). Oxidative stress was observed to induce stress granule formation in GFP-G3BP2b cells. However, the number of lipid droplets was observed to decrease when compared to control cells. Incubation of GFP-G3BP2b cells with oleate followed by SA exposure stimulated formation of lipid droplets. The number of lipid droplets

per cell showed a significant increase indicating that oleate alongside with oxidative stress exposure induced lipid droplet formation (Figure 6.22B).

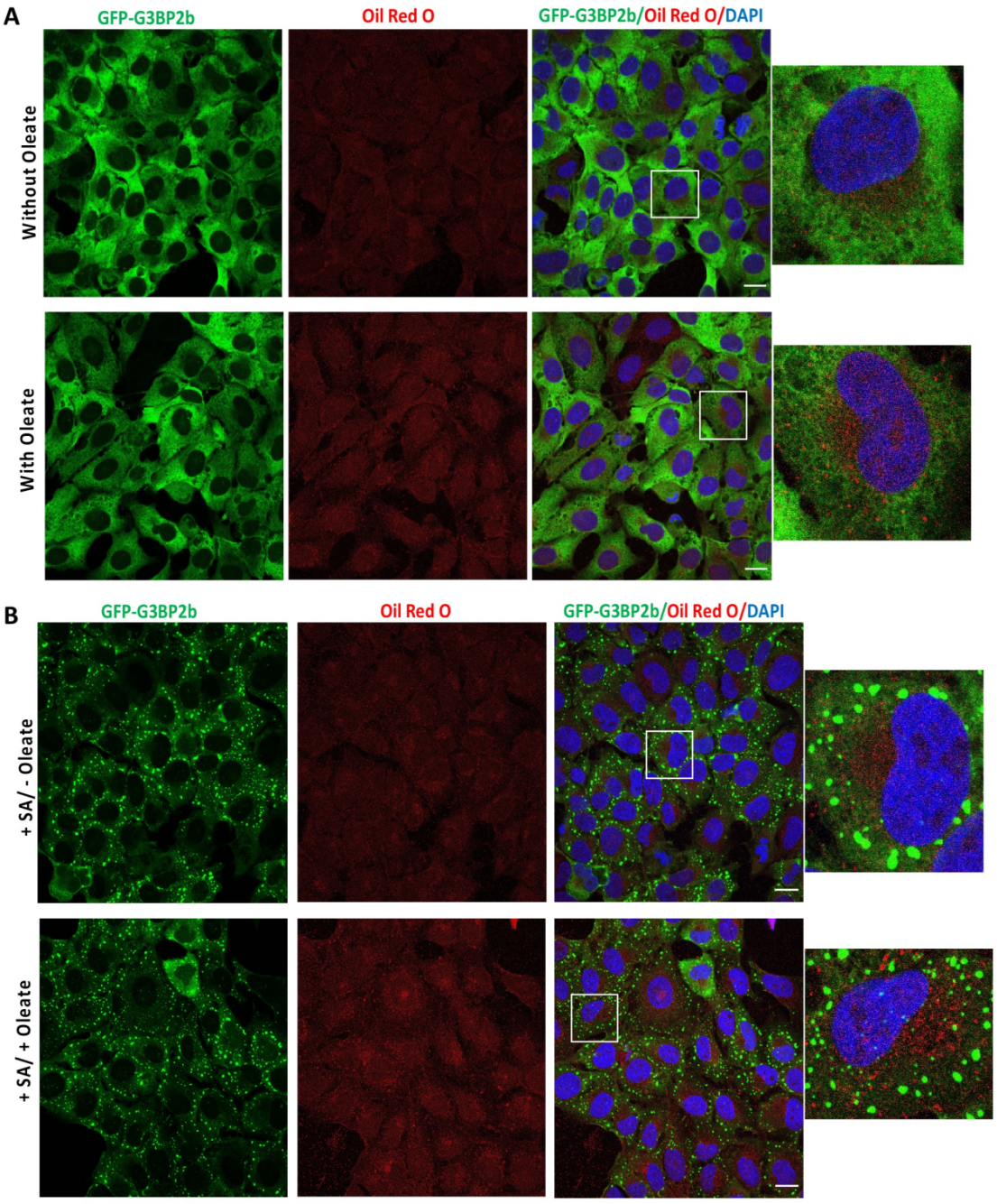

Figure 6.22 Re-constitution of cells with G3BP2b promotes lipid droplet formation. GFP-G3BP2b cells were incubated with/out 3% oleate for 24 hours and then un/treated with 0.5 mM SA for 30 min. Cells were stained with Oil Red O to visualize lipid droplets. Oleate was not observed to induce lipid droplet formation in GFP-G3BP2b cells (A). Cells treated with SA showed formation of lipid droplets (B). Scale bar= 20 um.

To quantitatively compare lipid droplet formation under oleate and/or SA treatment in GFP-G3BP2b cells, ImageJ was used to count lipid droplets per cell. Thus, few small LDs were detected in control (-O/-SA) cells, whereas, large LDs were not detected. Incubation of cells with oleate (+O/-SA) showed an increase of 1.6-fold change in the number of small LDs. Large lipid droplets were not detected. Exposure of GFP-G3BP2b cells to SA (-O/+SA) showed a decline of 2-fold change in small LDs compared to control cells. Large LDs were not detected under SA treatment. Moreover, incubation of cells with oleate followed by SA exposure (+O/+SA) induced formation of small LDs. An increase of 4.25-fold change was detected compared to -O/+SA cells. Large LDs were not detected under oleate/SA (+O/+SA) treatment (Figure 6.23).

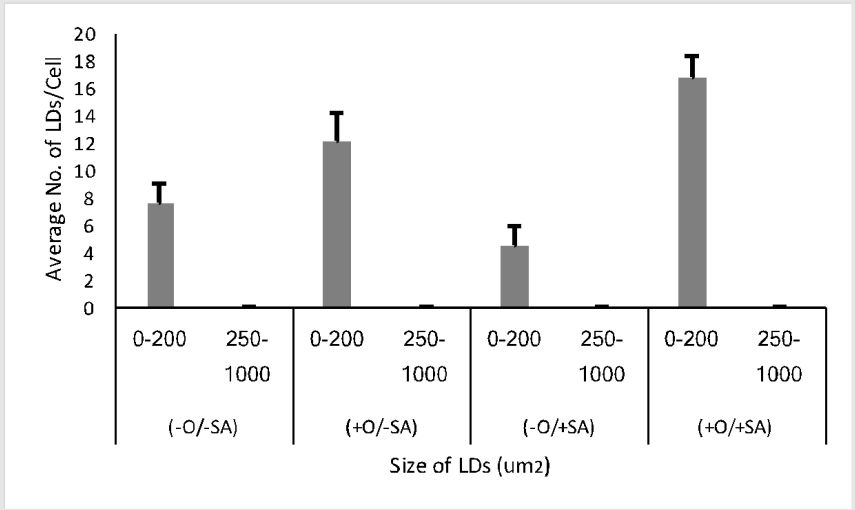

Figure 6.23 Formation of lipid droplets increased under oleate and oxidative stress in GFP-G3BP2b cells.

Oleate-untreated (-O/-SA) cells showed formation of few lipid droplets. oleate-treated (+O/-SA) cells showed formation of small LDs (1.6-fold change). SA exposure (-O/+SA) showed a decline of 2-fold change in small LDs number. SA and oleate (+O/+SA) treatment led an increase of 4.25-fold change compared to -O/+SA cells. Data represents mean ± SEM n=3, statistical significance was assessed using ANOVA t-test.

6.4.5.2 Oxidative Stress Reduced Lipid Droplet Formation in Senescent GFP-G3BP2b Cells

It was detected previously that presence of G3BP2b in proliferative cells promoted formation of lipid droplets under oleate and/or SA treatment (see section 6.4.5.1). We then ask the question whether senescent GFP-G3BP2b cells form lipid droplets under control, oleate and/or SA treatment. Therefore, cells were treated with doxorubicin (200 nM) for 48 hours to induce senescence phenotype. Senescent cells were then incubated with/out oleate for 24 hours. Subsequently, cells were treated with/out 0.5 mM SA for 30 min. Then, cells were fixed and stained with Oil Red O to visualize lipid droplets. The multinuclear, enlarged cells were detected indicating that cells are senescent (Figure 6.24).

Furthermore, oleate-untreated senescent cells showed formation of lipid droplets. Oleate-untreated cells showed formation of lipid droplets. Moreover, incubation of senescent cells with oleate induced formation of lipid droplets (Figure 6.24A). We then examined lipid droplet formation under oxidative stress. Thus, treatment of cells with 0.5 mM SA induced formation of stress granules but reduced formation of lipid droplets when compared to control cells. Moreover, Oleate and SA treatment led to an increased formation of lipid droplets (Figure 6.24B). Hence, our observations suggest that G3BP2b rescues stress granule formation in senescent GFP-G3BP2b cells. It also induces formation of lipid droplets under oleate and/or SA treatment.

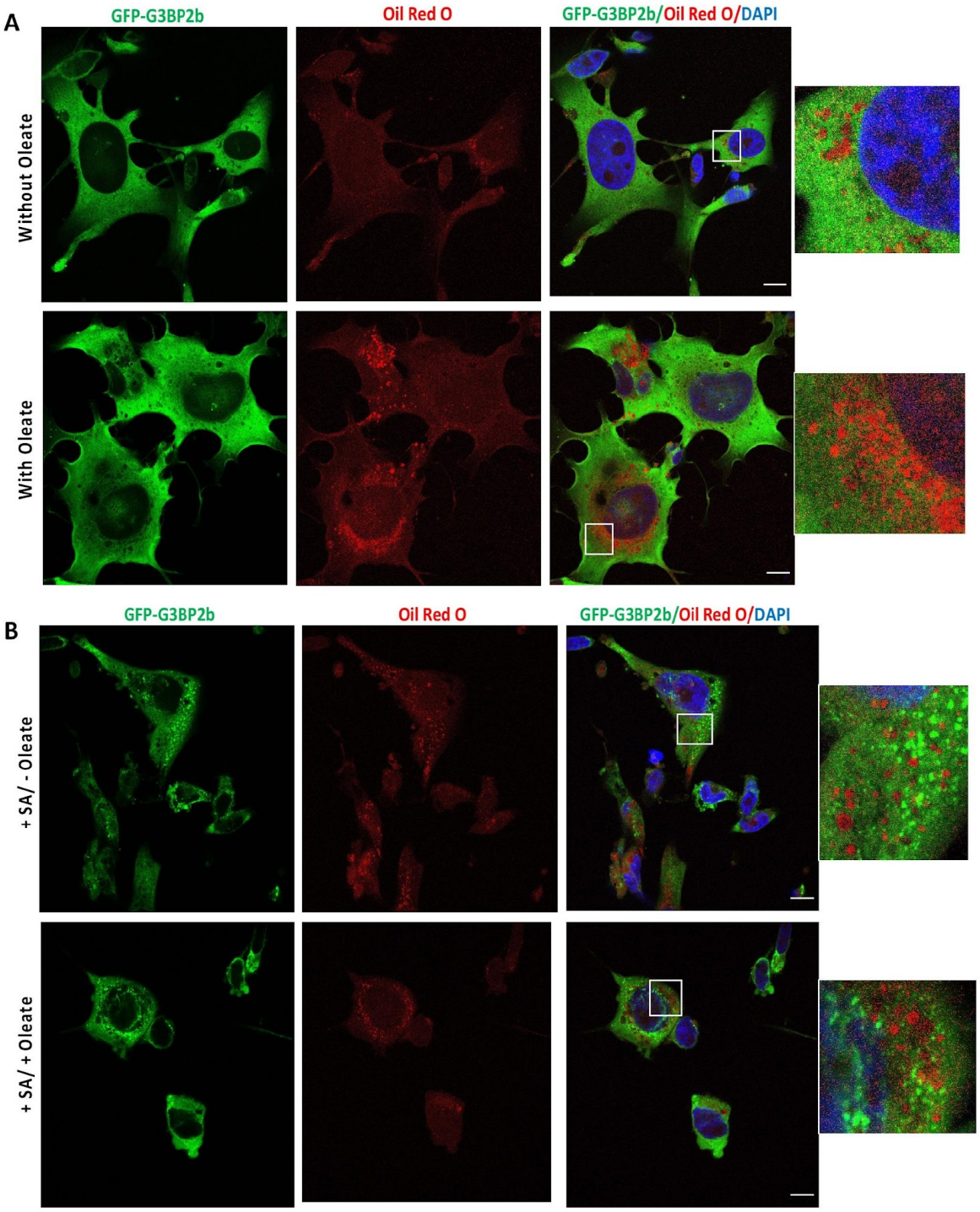

Figure 6.24 Formation of lipid droplets in senescent GFP-G3BP2b cells. Cells were incubated with/out 3% oleate overnight and then un/treated with 0.5 mM SA for 30 min. Cells were then fixed and stained with Oil Red O to visualize lipid droplets. Oleate induced lipid droplet formation in senescent GFP-G3BP2b cells (A). Cells exposed to SA/oleate showed a decline in lipid droplets (B). Scale bar= 20 um.

To perform quantitative comparison of lipid droplets in senescent GFP-G3BP2b cells under oleate and/or SA treatment, ImageJ was used. Oleate-untreated cells (-O/-SA) showed formation of small LDs. Large LDs were not detected indicating that under control conditions, cells only form small LDs. Under oleate treatment (+O/-SA), an increase of 2-fold change was observed in small LDs. Cells showed formation of large LDs. Hence, our observation indicates that oleate treatment induces lipid droplet formation in senescent GFP-G3BP2b cells. Furthermore, oxidative stress was detected to induce lipid droplet formation. Small LDs were observed to be formed but not large LDs. When cells treated with -O/+SA are compared to control (-O/-SA) cells, a decline of 3-fold change was. Moreover, treatment of cells with SA and oleate (+O/+SA) induced lipid droplet formation. Small LDs showed an increase of 4.8-fold compared to -O/+SA cells (Figure 6.25).

Collectively, our data suggests that G3BP2b somewhat restored cells' ability to form lipid droplets. Lipid droplets were observed to be formed in senescent GFP-G3BP2b cells. Moreover, Oleate treatment induced formation of lipid droplets in cells. Oxidative stress was observed to reduce formation of lipid droplets in senescent GFP-G3BP2b cells.

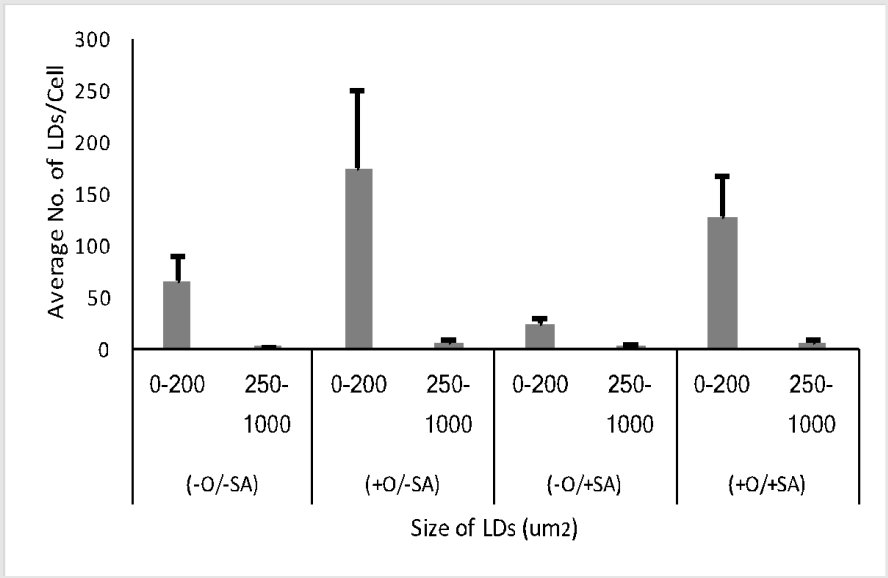

Figure 6.25 Oxidative stress reduced formation of lipid droplets in senescent GFP-G3BP2b cells.

Oleate-untreated (-O/-SA) cells showed formation of small LDs. Oleate-treated (+O/-SA) cells showed increase in small lipid droplets. An increase of 2-fold change was observed under oleate treatment (+O/-SA). SA (-O/+SA) exposure showed a decrease of 3-fold change in small LDs. SA and oleate (+O/+SA) treatment induced formation of small LDs. They showed an increase of 4.8-fold change compared to -O/+SA cells. Data represents mean ± SEM n=3, statistical significance was assessed using ANOVA t-test.

6.4.6 Proteomics Analysis of Lipid Proteins (Perilipin)

Mammalian cells produce and store lipids in cytosolic lipid droplets. Lipid droplets are coated with members of a family of protein known as Perilipin. Perilipin group is composed of multiple proteins including perilipin-1 (PLIN1), perilipin-2 (PLIN2), perilipin-3 (PLIN3) and perilipin-4 (PLIN4). Furthermore, PLIN proteins were detected to locate on the surface of lipid droplets. However, PLIN2 is the commonly used marker for lipid droplets and has been detected in several cell types (Blanchette-Mackie et al., 1995; Brasaemle, D., 2007;). In our current study, the proteomics data (shown in chapter 7) revealed a change in PLIN2, PLIN3 and PLIN4 from proliferative to senescent cells. PLIN2 showed an increase of 1.2(log2)-fold

change whereas the change in PLIN3 and PLIN4 was slight and insignificant (Figure 6.26). Previous studies have suggested that the increase in lipid droplet proteins such as PLIN2 associates with ageing and age-related disorders. Therefore, it is suggested that the rise in PLIN2 protein associates with senescence phenotype in WT U2OS cells.

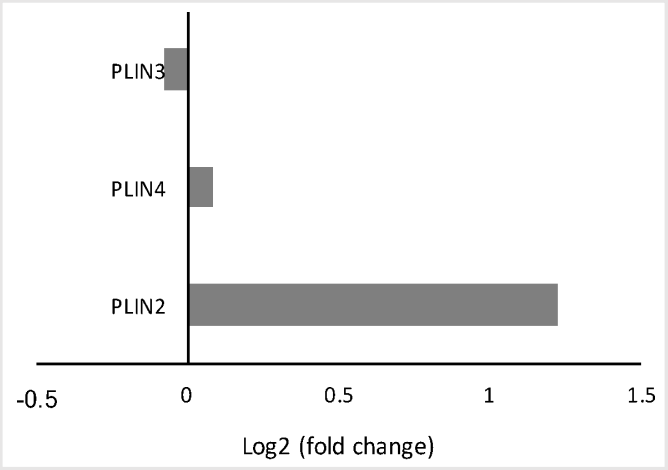

Figure 6.26 Levels of lipid proteins in WT U2OS cells.
PLIN2 protein was detected to significantly increase (1.2 (log2) fold change) in senescent cells compared to proliferative cells. The change in PLIN3 and PLIN4 between proliferative and senescent cells was insignificant.

The levels of PLIN2 and PLIN3 proteins were investigated in proliferative and senescent ΔΔG3BP1/2 cells. Proteomics analysis (shown in chapter 7) revealed an increase in levels PLIN2 (1.4-(log2) fold change) in senescent cells compared to proliferative ones. Level of PLIN3 protein was detected to increase slightly (0.6-(log2) fold change) from proliferative to senescent cells (Figure 6.27).

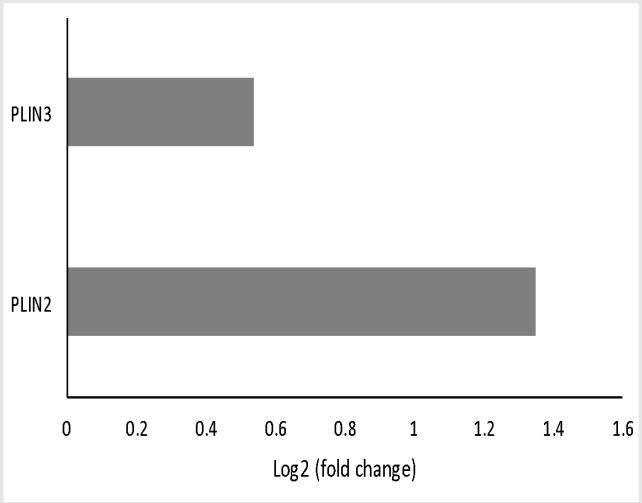

Figure 6.27 Levels of Perilipin proteins in proliferative and senescent ΔΔG3BP1/2 cells.

Level of PLIN2 protein was detected to rise (1.4(log2)-fold change) in senescent cells compared to proliferative cells. A slight change in the levels of PLIN3 protein was detected between proliferative and senescent cells.

The levels of PLIN2 and PLIN3 proteins were investigated in proliferative and senescent GFP-G3BP1 cells. Proteomics analysis (shown in chapter 7) revealed an increase in levels PLIN2 (1.2-(log2) fold change) in cells when becoming senescent. Levels of PLIN3 protein showed insignificant change (0.6-(log2) fold change) from proliferative to senescent cells (Figure 6.28).

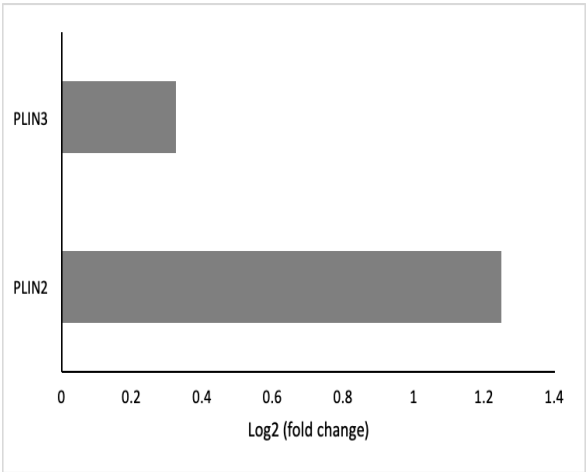

Figure 6.28 Levels of Perilipin proteins in proliferative and senescent GFP-G3BP1 cells.

Level of PLIN2 protein was detected to rise (1.2 (log2) fold change) in senescent cells when compared to proliferative cells. A minor change (0.3 (log2) fold change) in the levels of PLIN3 protein was detected between proliferative and senescent cells.

The levels of PLIN2 and PLIN3 proteins were investigated in proliferative and senescent GFP-G3BP2a cells. Proteomics analysis revealed an increase in levels PLIN2 (1 (log2) fold change) in senescent cells compared to proliferative ones. Level of PLIN3 protein was detected to increase from proliferative to senescent cells, however, the change was insignificant (Figure 6.29).

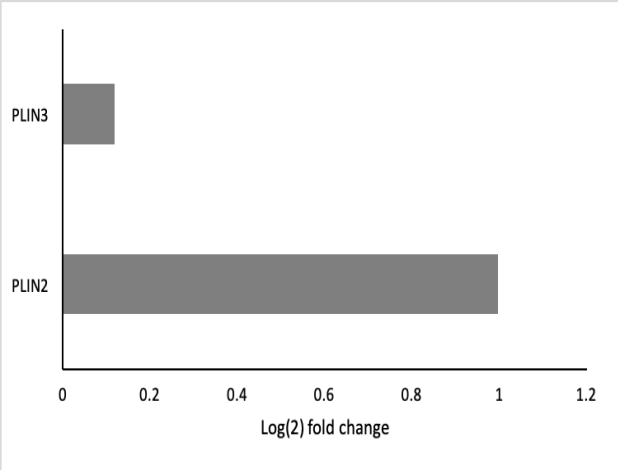

Figure 6.29 Levels of Perilipin proteins in proliferative and senescent GFP-G3BP2a cells.
Level of PLIN2 protein was detected to rise (1 (log2) fold change) in senescent cells compared to proliferative cells. A minor change in the levels of PLIN3 protein was detected between proliferative and senescent cells.

The levels of PLIN2 and PLIN3 proteins were investigated in proliferative and senescent GFP-G3BP2b cells. Proteomics analysis revealed an increase in levels PLIN2 (1.1 (log2) fold change) in senescent cells compared to proliferative ones. PLIN3 protein was not detected in the lysates of GFP-G3BP2b cells (Figure 6.30).

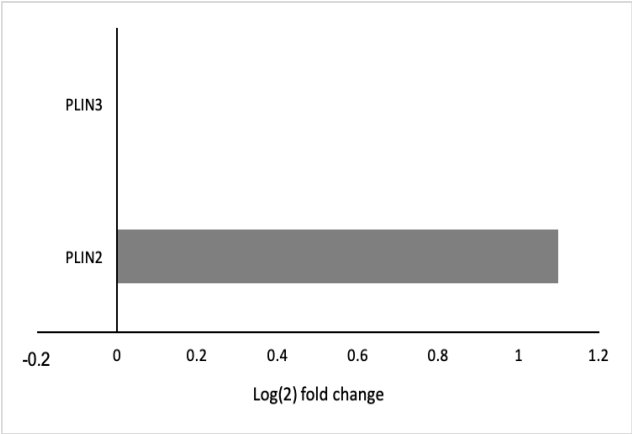

Figure 6.30 Levels of Perilipin proteins in GFP-G3BP2b cells.
Level of PLIN2 protein was detected to rise (1.1 (log2) fold change) in senescent cells. PLIN3 protein was not detected in the lysates.

Collectively, proteomics data revealed a change of 1.2(log2)-fold in PLIN2 from proliferative to senescent cells suggesting that the rise in PLIN2 protein associates with senescence phenotype in WT U2OS cells. ΔΔG3BP1/2 cells showed the increase of 1.2-fold in levels PLIN2 compared to WT U2OS cells. Change in PLIN2 was insignificant from proliferative to senescent GFP-G3BP1, GFP-G3BP2a and GFP-G3BP2b cells.

6.5 Conclusion

Lipid droplets are the main store of lipids in mammalian cells. They have a crucial role in storing cholesterol to maintain intracellular lipid homeostasis (Martin and Parton, 2005). Endoplasmic reticulum (ER) is the origin of nascent lipid droplets. Lipid droplet biogenesis is regulated by multiple enzymatic reactions. Moreover, Proteins are involved in the synthesis of lipid droplets. ER proteins: seipin and fat-storage-inducing transmembrane protein, are suggested to play a structural role in lipid droplet formation (Gross et al., 2010). perilipins (termed as Plin) are a family of five related proteins that are involved in regulation of neutral lipid lipolysis (Kimmel et al., 2010).

Lipid droplets are linked to many cellular processes including protein degradation, and are increased following cellular damage and lipid overload (Agarwal and Garg, 2006). Additionally, human aging is associated with an increase of physical disability, loss of muscle strength due to decrease in muscle mass and accumulation of adipose tissue in muscles. PLIN2 has been observed to increase with age. It was reported that the expression of PLIN2 increases with age (Conte et al., 2013).

Hence, in our study we examine the formation of lipid droplets in proliferative and senescent WT U2OS and G3BP knockout cells. Therefore, lipid droplet formation was observed and counted under oleate and/or oxidative stress exposure. Oleate is used as an inducing agent for lipid droplet synthesis. Oil Red O staining is a widely-used lipid droplet marker as it accumulates in lipid-containing compartments such as lipid droplets.

WT U2OS cells were treated with/out oleate and stained with Oil Red O staining to visualise lipid droplet formation. The number of LDs was observed to increase (2.2-fold) under oleate

treatment indicating that oleate induces lipid droplet formation. To investigate the effect of oxidative stress on lipid droplet formation in WT U2OS cells, cells were incubated with/out oleate followed by SA exposure. The number of lipid droplets increased under oleate/SA treatments. Thus, our data suggests that oxidative stress induced lipid droplet accumulation in WT U2OS cells which is consistent with observations of other studies (Amen and Kaganovich, 2021). Accumulation of lipid droplets was examined in senescent WT U2OS. Incubation of cells with oleate was observed to induce accumulation of LDs. Lipid droplets are suggested to increase in senescent WT U2OS compared to proliferative cells. Our observations suggest that oxidative stress regulates lipid droplet accumulation in proliferative and senescent cells.

We then investigated lipid droplet formation in ΔΔG3BP1/2 cells. Hence, proliferative cells did not show formation of lipid droplets suggesting that inhibition of stress granules by knocking out G3BP1/2 prevents lipid droplet formation. Moreover, oxidative stress was observed to induce lipid droplet formation in proliferative ΔΔG3BP1/2 cells. On the other hand, senescent cells showed formation of few LDs. Treatment of senescent ΔΔG3BP1/2 cells with Oleate and SA was detected to induce accumulation of lipid droplets. Collectively, lipid droplet formation is suggested to be inhibited in proliferative ΔΔG3BP1/2 cells but increased in senescent ΔΔG3BP1/2 cells.

Re-constitution of cells with one form of G3BP1 (GFP-G3BP1 cells) was observed to rescue cells' ability of stress granule formation. Presence of G3BP1 was detected to promote formation of lipid droplets. Oxidative stress was seen to stimulate formation of lipid droplets. Additionally, incubation of senescent cells with oleate stimulated lipid droplet formation. SA induced formation of stress granules and lipid droplets.

G3BP2 is required for the formation of stress granules. Proliferative GFP-G3BP2a cells that were incubated with oleate followed by SA treatment stimulated formation of lipid droplets. Additionally, oleate and SA treatment led to an increased formation of lipid droplets. On the other hand, incubation of GFP-G3BP2b cells with oleate followed by SA exposure stimulated formation of lipid droplets. The number of lipid droplets per cell showed a significant increase indicating that oleate alongside oxidative stress exposure induced lipid droplet formation. Moreover, Oleate and SA treatment led to an increased formation of lipid droplets in senescent GFP-G3BP2b cells.

Proteomics data showed the increase in levels of PLIN2 protein in senescent cells compared to proliferative ones. This observation is consistent with other studies that show an increase in lipid accumulation in senescence (Conte et al., 2013). Furthermore, the levels of PLIN2 vary depending on the presence and/or absence of G3BP. ΔΔG3BP1/2 cells showed the highest increase in PLIN2 levels compared to WT U2OS, GFP-G3BP1, GFP-G3BP2a and GFP-G3BP2b cells. This indicates that G3BP might play a role in the regulation of lipid synthesis and accumulation.

Collectively, lipid droplet formation is induced in proliferative and senescent WT U2OS cells under oxidative stress. Knockout of G3BP inhibits formation of lipid droplets as well as stress granules indicating that G3BP plays a role in lipid droplet formation. Re-constitution of knockout cells with G3BP1 rescues lipid droplet formation. G3BP2a or G3BP2b promotes lipid droplet formation. Hence, we suggest that G3BP is required for the process of lipid droplet formation.

Chapter 7

7 Proteomics Analysis of Stress Granules and Senescence Proteins in U2OS Cell Lines

7.1 Introduction

Living cells have several coordinated biological processes that occur simultaneously. These processes encompass different functions such as regulatory, catalytic and synthetic functions. Through biochemical and biophysical studies, it's well known that the biological process functions are carried out by proteins. However, protein and proteome properties and behaviour remained elusive until the development of mass spectrometry-based technologies which help provide a clear understanding of proteome function, composition and structure (Aebersold and Mann, 2016).

The proteins of the living cell collectively form the proteome; which is the full set of proteins expressed by the cell. The proteome network enables the cell to adapt to any internal or external perturbations. Therefore, it enables the cell to define the functional state and determines its phenotype (Feng et al., 2014; Aebersold and Mann, 2016).

Proteome of cells and the mediated molecular mechanisms have been studied by large-scale measurements of proteome that have become possible by development of mass spectrometry based methods such as LC-MS/MS and SWATH-MS.

To answer many research questions in fields such as drug screening and discovery, consistent and quantitatively accurate proteomics data from several samples are required. The mass

spectrometry-based method: Sequential Windowed Acquisition of All Theoretical Fragment Ion Mass Spectra (SWATH-MS) has been developed to address the need of delivering high quality and consistent quantification of large-scale projects (Ludwig et al., 2018). The major advantage of SWATH-MS is enabling the quantitative analysis of 1,000s of proteins with high accuracy and quantitative consistency. The research fields that require these properties include clinical drug studies (Tan et al, 2017) and genetic association studies (Williams et al, 2016).

To perform SWATH-MS analyses, protein samples that are non-labelled are digested with trypsin. The resulting peptides are processed and analysed by liquid chromatography coupled to a tandem mass spectrometer. The acquisition mode operated is called data-independent acquisition (DIA) where all ionized molecules that fall in a specified mass range are fragmented in a systematic style. The resulting multiplexed fragment spectrum is interpreted by

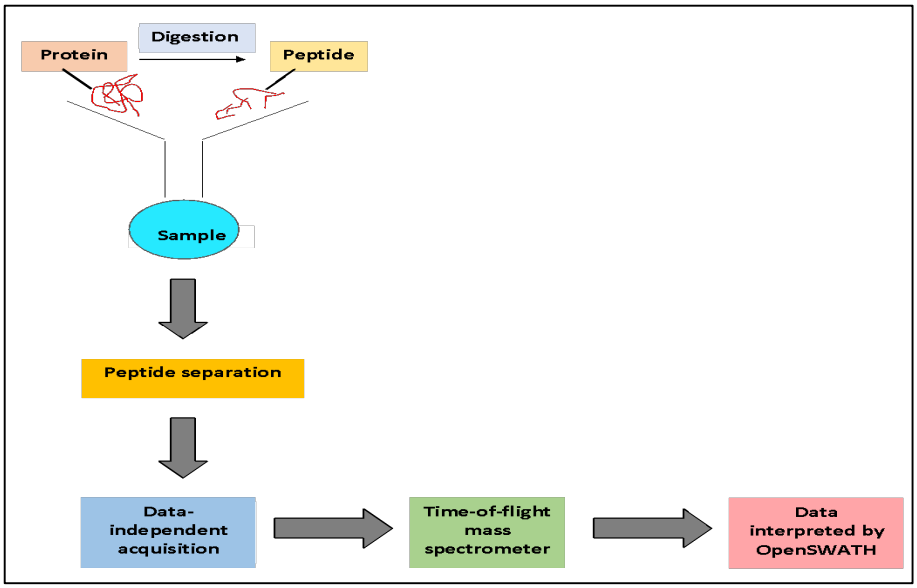

Figure 7.1 Schematic of SWATH-MS workflow.

SWATH-MS workflow starts by sample preparation where the proteins are extracted and digested. Peptides are then separated and introduced into mass spectrometer. In data-independent acquisition, a specific range of *m/z* values are selected for fragmentation. Fragments are acquisitioned in a time-of-flight mass spectrometer. The resulting fragment spectrum is interpreted by OpenSWATH software.

OpenSWATH software (Figure 7.1) (Aebersold and Mann, 2016; Ludwig et al., 2018).

Furthermore, multiple steps are involved in the preparation of samples for mass spectrometry analysis. It involves the following steps: proteins extraction, fractionation, digestion, separation and ionization. Consequently, it is well-suited for the detection of proteins in cells exposed to treatment or chemicals.

Preparation of samples for LC-MS based proteomic experiments requires multiple steps. The first step is cell collection which is performed by adding a lysis buffer to cells in order to break the cell membrane. Next, cells are homogenized and centrifuged to separate cell debris and membrane from cell lysate which contains the proteins. Then, proteins are chemically or enzymatically cleaved/digested into fragments to facilitate protein identification. Digestion of proteins results in peptide fragments that are reduced in size making them more tractable and amenable to mass spectrometry analysis. Moreover, separation techniques used in MS based proteomics analysis such as high-performance liquid chromatography, enables reducing the simultaneous introduction of identical/similar peptide masses into the mass spectrometer (see chapter 2) (Pitt, 2009; Karpievitch et al., 2010). Mass spectrometers contain ion source, mass analyser and ion detector. The charge of each peptide is assigned by ion source. Mass analyser is responsible for measuring the mass-to-charge (m/z) ratio of each ion which is then captured by an ion detector and the intensity of each ion is measured. In a mass spectrum, mass analyser generates m/z information on the x-axis and the detector generates peak intensity information on the y-axis (Ye e al., 2008; Karpievitch et al., 2010).

7.2 Aims and Objectives

7.2.1 Aims

The chapter aims to develop an understanding of the changes associated with senescence under different G3BP backgrounds. Hence, WT U2OS and ΔΔG3BP1/2 cells will be used to investigate the changes in protein levels following senescence induction. Proliferative (Day 0) cells will be used as control. To determine the role of each form of G3BP in senescence process, G3BP1-, G3BP2a- or G3BP2b-reconstituted cells will be induced to senescence and protein changes will be visualized using SWATH-MS, interpreted using OpenSWATH. RStudio software will be used to quantify and generate plots of protein changes.

We hypothesize that changes at the protein level will be associated with senescence in WT U2OS. Knockout of G3BP (ΔΔG3BP1/2) will cause changes in proteins thereby it will affect senescence phenotype development. Re-constitution of cells with G3BP forms individually will provide a clear view of how G3BP is affecting other proteins and hence the senescence process.

7.2.2 Objectives

1. Characterize the protein changes associated with senescence in WT U2OS and compare it with changes in ΔΔG3BP1/2 cells.
2. Determine the alterations of proteins associated with senescence (p21 and p16) and RNA-binding proteins involved in stress granule formation in control and G3BP mutant cell-lines.

7.3 Materials and Method

7.3.1 Materials

All chemicals were purchased from Sigma unless stated otherwise.

7.3.2 Methods

Preparation of peptide samples for proteomics analysis and mass spectrometry was performed by a department facility. Briefly, samples were prepared using FASP Protein Digestion Kit and sequencing grade-modified trypsin. Next, samples were freeze-dried and re-suspended in 3% acetonitrile, 0.1% TFA followed by de-salting step. Sample fractions (5 ug peptides) were analysed using ekspert TM nanoLC 425 coupled to a quadrupole Time-Of-Flight mass spectrometer. Subsequently, samples were filtered using TriArt C18 Capillary guard column with 5 um, 5 x 0.5 mm trap column. At separation step, samples were loaded on TriArt C18 Capillary column, 12 nm, S-3 um, 150 x 0.3 mm for 57 min at a flow rate 5 ul/min. Afterwards, SWATH acquisition was performed for 55 min. The time of each scan cycle was 3.2 second. Data acquired from each scan cycle (400-1250 m/z) were processed using SCIEX version 1.7.1 software.

7.4 Results

7.4.1 WT U2OS Cells

Senescence occurs when DNA damage response proteins are activated which in turn activate p53. Cyclin-dependent kinase inhibitors including p21 (CDKN1A) is a target for p53. Activation of p21 leads to the activation of p16 (CDKN2A) (Campisi, 2005). Furthermore, the altered pattern of gene expression and cell shape, high activity of ß-galactosidase, SASP, and secretion of factors such as growth factors and insoluble extracellular matrix components are the hallmarks of senescence phenotype (Cho and Hwang, 2012).

During senescence, cells irreversibly lose their ability to proliferate. Moreover, several proteins are known to regulate cell-cycle progression at G1-S phase promoting senescence phenotype (Fridlyanskaya et al., 2015). Hence, in our study, exposure of WT U2OS cells to 200 nM doxorubicin for 48 hours was observed to induce senescence phenotype (discussed in chapter 4). Cells were observed to display multiple senescence markers such as elevated SA-ß-Gal activity, formation of SAHF and high expression of p21 protein (discussed in chapter 5).

To investigate the molecular changes in senescent cells, a quantitative proteome analysis of day 0 (proliferative) and day 9 (senescent) WT U2OS cells was performed using SWATH-MS. A total of 5358 proteins were identified in WT U2OS lysates. Approximately 2715 proteins were identified at a rate of adjusted p-value < 0.05. Moreover, proteomics analysis revealed that 175 proteins were showing an absolute fold change higher than 2 and smaller than -2. Hence, I discuss these 175 significantly changing proteins with regard to senescence and stress granule formation (Figure 7.2). Hence, the role of the significantly changing proteins and proteins associated with senescence and stress granule formation are discussed here.

Figure 7.2 Proteomics analysis of proliferative (Day 0) and senescent (Day 9) WT U2OS cells.

The plot shows the distribution of proteins forming a volcano plot. The marks are showing the distribution of all 5358 proteins detected in lysates of WT U2OS. The grey marks are the proteins with no significant change. Green colour marks represent proteins with fold change >2 and <-2. Green marks are showing the highly-dysregulated proteins from proliferative to senescent cells>4 and <-4-fold change (adjusted p-value ≤ 0.05).

7.4.1.1 Most Highly Dysregulated Proteins

Among the 5358 proteins that were detected in lysates of WT U2OS, 175 proteins were detected to significantly change. The levels of EBI-3, KRT8, FDXR, KRT79, LCP1, KRT17, GPNMB, CDKN1A, KRT20, CES2, KRT81, DAB2IP, PSTPIP2, WRAP53 and GPT proteins were detected to change significantly from proliferative to senescent cells. They showed a significant increase in senescent cells with a fold change > 4-fold. On the other hand, the levels of H1-10, CA9, DHRS2, H1-5, ENPP1, RECQL4, EPX and CEP350 proteins were detected to decline significantly in senescent cells (fold change < -4) (Figure 7.2).

7.4.1.1.1 Upregulated Proteins

Several cytoskeletal proteins were identified to be increased in senescent cells such as KRT8, KRT79 and KRT20. These proteins showed an increase of 2 up to 5.5-fold change in senescent cells compared to proliferative cells (Figure 7.3). It is suggested that cytoskeletal proteins occur in more abundance in senescent cells. The overproduction of cytoskeletal proteins brings about the shape of senescent cells. Moreover, alterations in the cytoskeletal proteins are suggested to affect shape, adhesion and migration of cells (Gourlay and Ayscough, 2005). In human fibroblasts, cytoskeletal proteins such as vimentin and actin were observed to increase (3-fold change) compared to young proliferative cells. Additionally, the structural changes associated with senescence (changes in cell shape) was induced in young fibroblast cells after transfecting them with vimentin construct (Nishio et al., 2001).

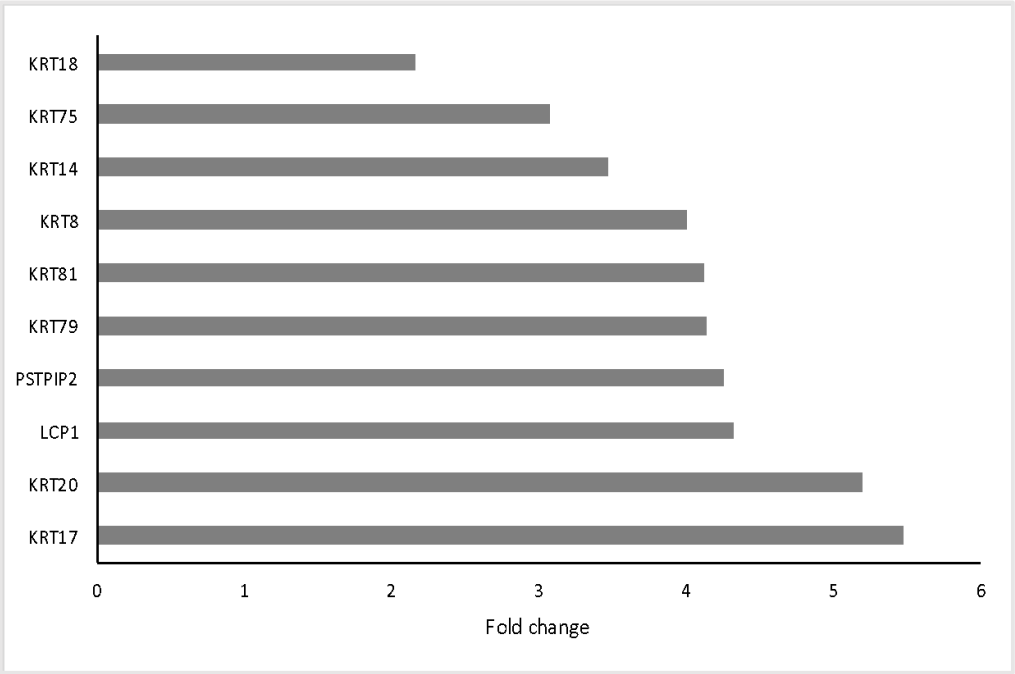

Figure 7.3 Level of cytoskeletal proteins in senescent WT U2OS cells.
Level of cytoskeletal proteins was observed to increase in senescent cells compared to proliferative cells.

Furthermore, the transmembrane glycoprotein NMB (GPNMB) protein has shown an increase in the fold change (4.5-fold change) (Figure 7.2). GPNMB protein is known to be involved in the negative regulation of cell proliferation and cytokine production (Uniprot.org). Hence, the elevated levels of GPNMB protein in senescent cells is suggested to negatively control cell proliferation and growth factor production.

Moreover, adrenodoxin oxidoreductase (FDXR) protein was detected to significantly increase from proliferative to senescent cells. It showed an increase of 4.5-fold change (Figure 7.2). FDXR is involved in cholesterol metabolism and steroid biosynthesis. Hence, the increase in the levels of FDXR correlates with the increase in lipids and lipid droplets (discussed in chapter 6). Moreover, previous studies have suggested that the increase in fat associates with ageing

and age-related disorders (Tchkonia et al., 2010). Therefore, it is suggested that the rise in FDXR protein associates with senescence phenotype in WT U2OS cells.

Disabled homolog 2-interacting protein (DAB2IP) protein acts as a scaffold protein that regulates several signalling pathways including cell growth inhibition, apoptosis and cell survival (Uniprot.org). Hence, it regulates cell cycle checkpoints by reducing G1 phase cyclin levels and thus resulting in cell cycle arrest. DAB2IP was found silenced in multiple cancer types such as prostate cancer leading to metastatic potential (Smits et al., 2012; Tsai et al., 2014).

Collectively, the increase in the levels of cytoskeletal proteins and proteins involved in regulation of cell proliferation and cell cycle is associated with senescence phenotype in WT U2OS cells.

7.4.1.1.2 Upregulated Pathways from Proliferative to Senescent WT U2OS Cells

The significantly changing proteins in response to senescence induction were tested for statistical underrepresentation using enrichGO after FDR control. Based on the GO enrichment, the significantly upregulated proteins from proliferative to senescent cells were enriched in 20 terms in the category biological processes. The proteins were enriched according to gene count which is the number of enriched genes in GO term (Figure 7.4).

GO enrichment uncovered that the highly-upregulated proteins in senescent cells were involved in establishment of protein localization to membrane, protein targeting, protein localization to endoplasmic reticulum, RNA catabolic process, small molecule catabolic process, protein-containing complex disassembly, extracellular structure organization, intrinsic

apoptotic signalling pathway, mitochondrial gene expression and membrane lipid catabolic process (Table 7.1).

Of the significantly changing proteins, ribosomal proteins (RP) are involved in protein establishment and localization to membrane, and RNA catabolic process. RPL4, RPL32, RPL14, RPL13A, RPL18, RPL17, RPL18A, RPL35A and RPL29 are suggested to be linked to the regulation of p53 and hence senescence induction in WT U2OS cells. RP proteins were identified to bind to Mdm2 leading to inhibition of its ubiquitin ligase activity. Therefore, it was suggested that RP proteins cause p53 upregulation and senescence induction (Bursać et al., 2012)

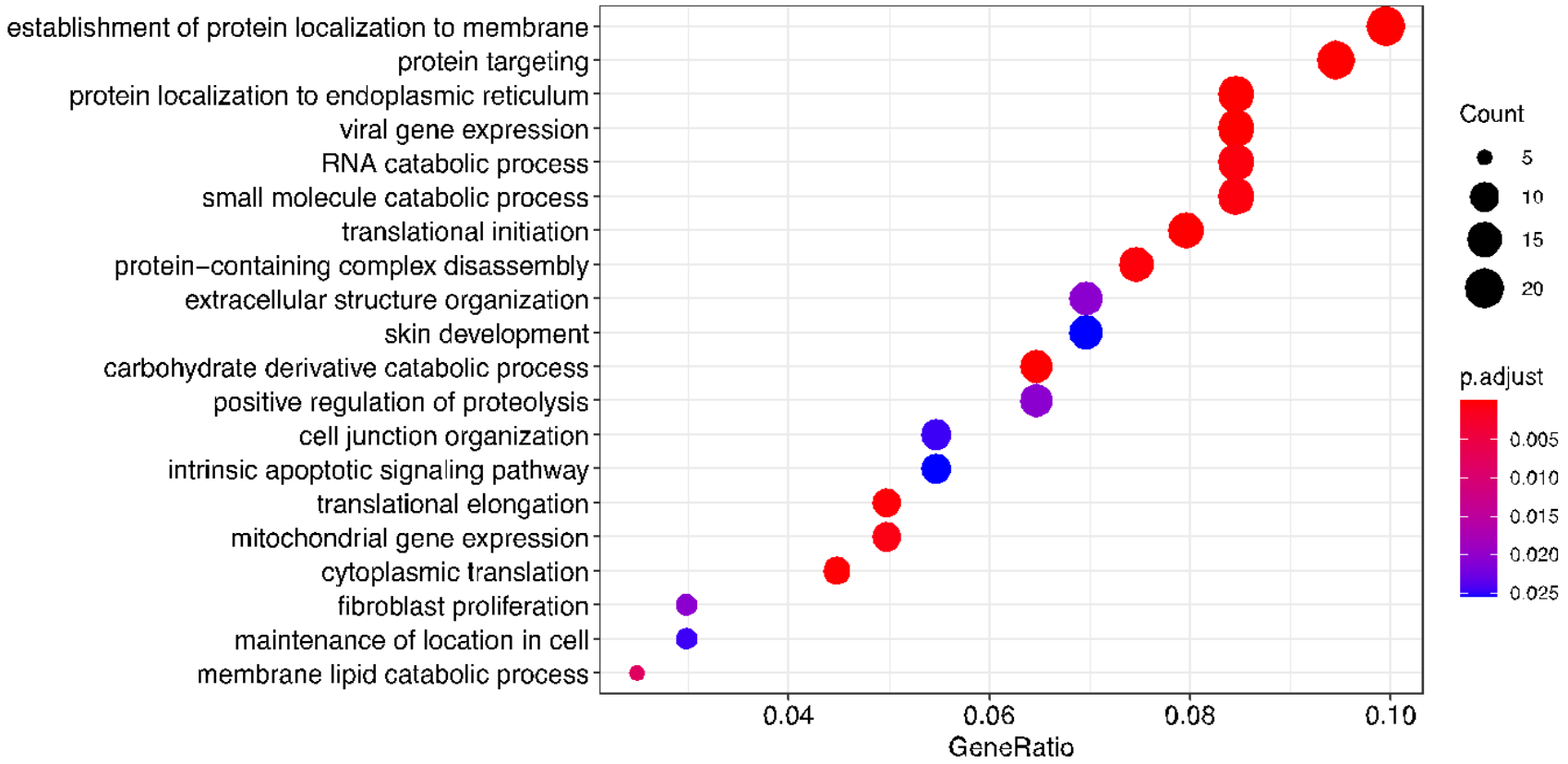

Figure 7.4 Overrepresentation of GO biological process terms in the upregulated proteins.

GO biological process terms found to be statistically overrepresented upon doxorubicin treatment (senescence induction). Proteins were tested against all detected proteins in the data set using enrichGO. Count is the number genes that are enriched in each GO term. Gene ratio is a percentage of differentially upregulated genes in each GO term.

7.4.1.1.3 Downregulated Proteins

In contrast to the upregulated proteins, there are proteins that showed a significant decrease in senescent cells including H1-10, CA9, DHRS2, H1-5, ENPP1, RECQL4, EPX and CEP350 proteins (Figure 7.6). The Histone H1 (H1-10, H1-5 and H1-1) proteins are involved in several pathways including double-strand DNA binding, chromatin remodelling, nucleosome spacing and DNA methylation (Uniprot.org). The levels of these proteins showed a decrease of 4.5 to 2.5-fold change in senescent cells (Figure 7.5).

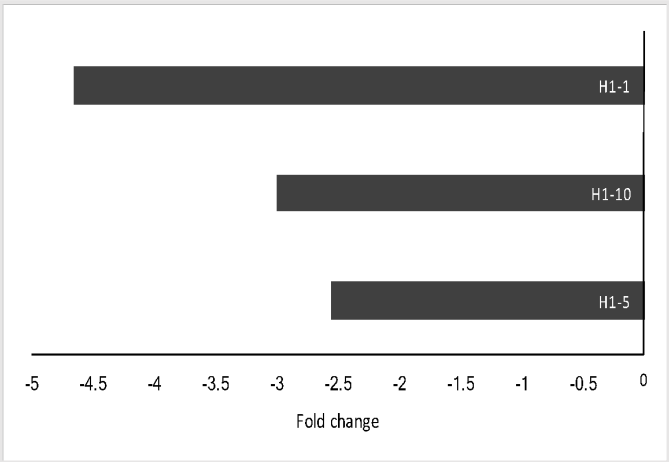

Figure 7.5 Level of H1 proteins in WT U2OS cells.
H1-1 protein was detected to decline significantly (4.5-fold change) from proliferative to senescent cells. Levels of H1-5 and H1-10 proteins were also reduced significantly in senescent cells.

Carbonic anhydrase 9 (CA9) is suggested to be involved in cell proliferation (Uniprot.org). It decreased (5-fold change) in senescent cells suggesting that it plays a role in cell proliferation control and thus senescence. Additionally, Ectonucleotide pyrophosphatase/phosphodiesterase family member 1 (ENPP1), ATP-dependent DNA helicase Q4 (RECQL4), Dehydrogenase/reductase SDR family member 2 (DHRS2), Eosinophil peroxidase (EPX) and Centrosome-associated protein 350 (CEP350) are downregulated in senescent cells (-2 to -4-fold change) (Figure 7.2). Accordingly, these proteins are involved in regulation of cell growth, DNA replication, telomere maintenance and cell replication (Uniprot.org). Hence, the downregulation of these proteins correlates with senescence.

7.4.1.1.4 Downregulated Pathways from Proliferative to Senescent WT U2OS Cells

Furthermore, in this study, the significantly changing proteins in response to senescence induction were tested for statistical overrepresentation using enrichGO after FDR control. Based on the GO enrichment, the significantly downregulated proteins from proliferative to senescent cells were enriched in 20 terms in the category biological processes. The proteins were enriched according to gene count which is the number of enriched genes in GO term (Figure 7.6).

GO enrichment uncovered that the highly-downregulated proteins in senescent cells were involved in DNA conformation change, DNA recombination, protein-DNA complex subunit organization, regulation of protein organization, regulation of DNA metabolic process, peptidyl-lysine modification and histone modification. The Histone H1 proteins were among the genes enriched in these signalling pathways (Table 7.2).

The regulation of macromolecule biosynthetic processes was underrepresented in significantly changing proteins from doxorubicin treatment (senescent cells). This reveals that proteins involved in the regulation of macromolecule biosynthetic are downregulated in comparison to the total quantifiable proteome detected. Macromolecule biosynthetic processes are known as the cascades and chemical reactions that result in formation of molecules and substances needed for cellular processes. Thus, the biosynthetic processes are energy-requiring processes through which simple substances are converted into more complex ones. It is well known that cells undergoing senescence are not dividing but remain metabolically active which suggests the downregulation of biosynthetic processes.

Of the significantly changing proteins, Histone H1 proteins are involved in DNA conformation and organization. H1-10, H1-2, H1-4, H1-5, H1-0 and H1-1 are linked to the regulation of DNA conformation, organization and metabolic process in senescent WT U2OS cells. Moreover, the proteins annotated to these terms are 10-11 proteins including PHF10, POLE3, DNMT1, DCAF1, H4C9, RECQL4, CTCF, UBTF, BRD4 and NCAPH, PAXIP1, UBE2V2 and PRD4. These annotated proteins are known to locate at the nuclei of cells suggesting that they play a crucial role in regulation of DNA processes.

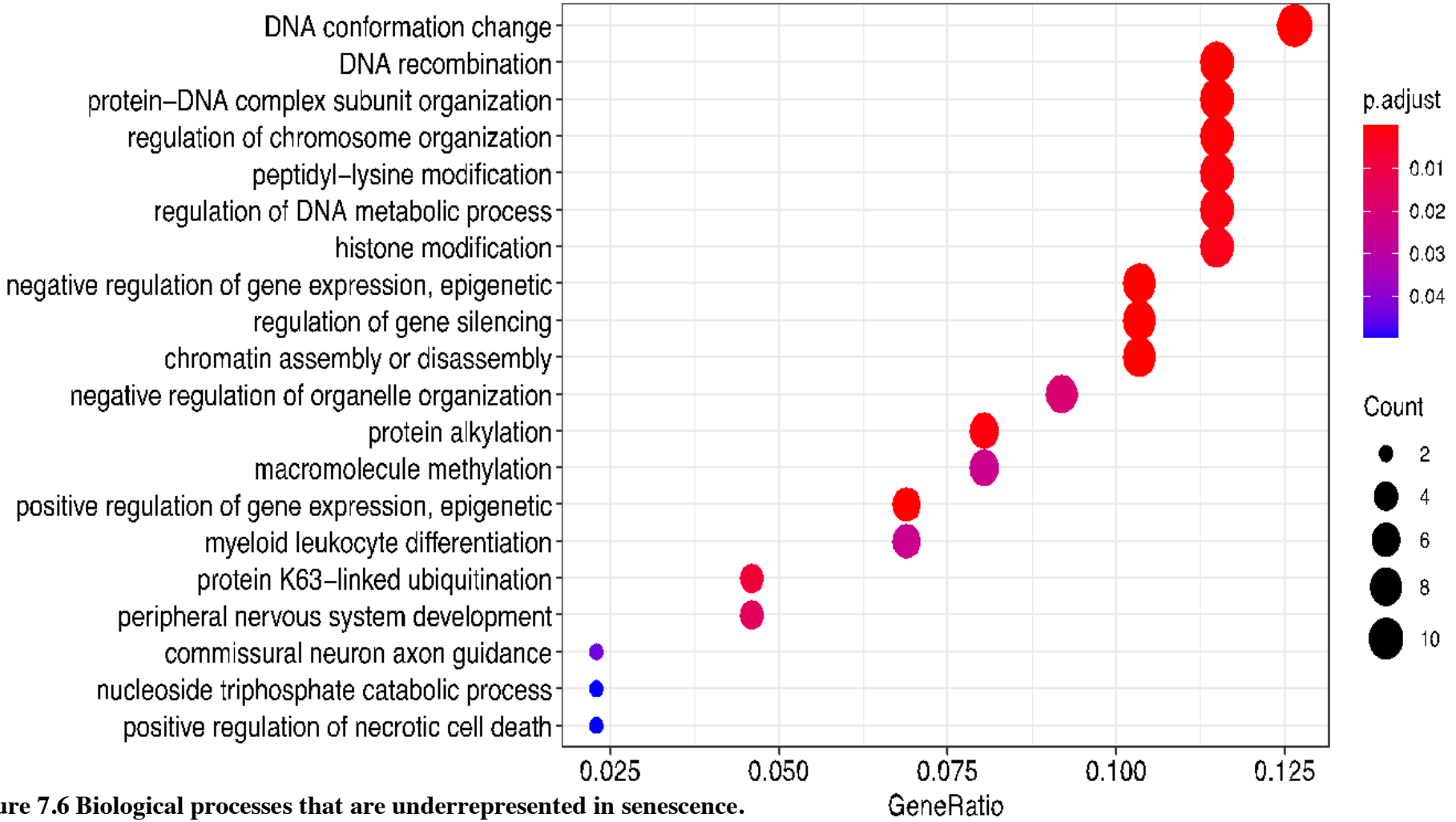

Figure 7.6 Biological processes that are underrepresented in senescence.

GO biological process terms that are found to be statistically underrepresented upon doxorubicin treatment (senescence induction). Proteins were tested against all detected proteins in the data set using enrichGO. Count is the number genes that are enriched in each GO term. Gene ratio is a percentage of differentially upregulated genes in each GO term.

7.4.1.2 Senescence Associated Proteins

Senescence phenotype is induced by several factors that lead to activation of certain proteins. These proteins are known to be associated with senescence (van Deursen, 2014; Gorgoulis et al., 2019; Nassrally et al., 2019). Cyclin-dependent kinase inhibitors including p53, p21 and p16 are known to regulate cell growth thereby promoting senescence phenotype (Puente et al., 2014; Aix et al., 2016). Hence, we here investigate the changes in the levels of kinase inhibitors between proliferative and senescent WT U2OS cells. Additionally, other senescence associated proteins such as PML and LMNB1 are investigated.

7.4.1.2.1 Cyclin-Dependent Kinase Inhibitors

P53 protein (encoded by TP53 gene) plays an essential role in senescence response. It senses the DNA-damage and activates the DDR pathway. However, if the damage is irreparable, proliferation is inhibited and senescence is induced. Proteomics analysis revealed insignificant change in tumour protein p53-inducible protein 11 (TP53I11) and tumour protein p53-binding protein 1 (TP53BP1) (Table 7.3) (Figure 7.7). It is suggested that p53 levels transiently increase during the stress leading to activation of p21 and eventually inducing senescence phenotype (Itahana et al., 2001; Herranz and Gil, 2018).

Senescent cells are characterized with an increase in the expression of p21. The proteomics analysis showed a significant increase in the expression of p21 protein from proliferative to senescent cells. An increase of ~5-fold change in p21 levels was detected in senescent cells (Figure 7.7). p21 is a target of p53. It is suggested that p21 is responsible for the functional changes in senescent cells. Sustained rise levels of p21 protein is required for long intervals after reaching senescence (Stein et al., 1999; Itahana et al., 2001).

CDKN2A (p16) protein is involved in senescence phenotype. It has been reported that p16 is activated by p21. The subsequent increase in p16 protein levels plays a role in maintaining senescence phenotype. Nevertheless, in our recent study, insignificant change in the levels of Cyclin Dependent Kinase Inhibitor 2A-interacting protein (CDKN2AIP) (Table 7.3) was detected (Figure 7.7). CDKN2A (p16) protein was not detected in the lysates of cells.

Table 7.3: List of proteins involved in DNA damage-repair and cell growth regulation pathway.

Protein	Function
TP53I11	Considered as a negative regulator of cell proliferation.
TP53BP1	Double-strand break (DSB) repair protein involved in response to DNA damage and telomere dynamics.
CDKN1A	Binds to and inhibits the activity of cyclin-cyclin-dependent kinase2 or -cyclin-dependent kinase4 complexes, and thus functions as a regulator of cell cycle progression at G1.
CDKN2AIP	Regulates DNA damage response in a dose-dependent manner through a number of signalling pathways involved in cell proliferation, apoptosis and senescence.

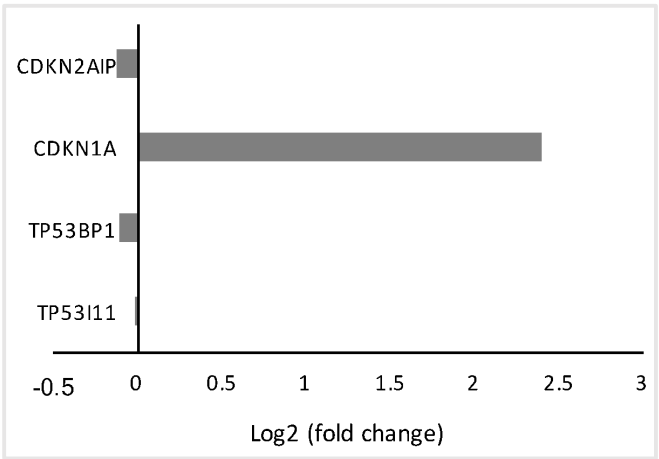

Figure 7.7 Change in cyclin-dependent kinase inhibitors level.
CDKN1A (p21) protein was detected to increase significantly (2.5- (log2) fold change) in senescent cells compared to proliferative cells. TP53I11, TP53BP1 and CDKN2AIP showed insignificant change between proliferative and senescent cells.

Our proteomics data reveals that the levels of cyclin-dependent kinase inhibitors varies depending on the stages of senescence induction. It has been observed by previous studies that p53 protein level is elevated during stress exposure whether it is telomere erosion or radiation exposure. Upon activation of p21, p53 levels decrease (Georgakilas et al., 2017). Moreover, sustained rise of p21 is required to promote phenotype changes associated with senescence. Once p21 levels decrease, p16 levels goes up to maintain senescence phenotype induced by p21 protein. Hence, our observations are confirming the findings of other studies. The significant increase in level of p21 protein but not p53 or p16 proteins indicates that cells are senescent. P21 protein is promoting senescence phenotype (Sharpless and Sherr, 2015). To observe the changes in p16 protein levels, cells are required to be kept for a longer time (day 14 or 21 post-doxorubicin exposure) to extract the lysates and run proteomics analysis.

7.4.1.2.2 PML and LMNB1

Other senescence associated proteins including Protein PML (PML) (Rokudai et al., 2013) and Lamin-B1 (LMNB1) (Freund et al., 2012) have been used as markers for senescence by several research groups. It has been observed that LMNB1 declines in senescent cells compared to proliferative cells (Freund et al., 2012). This loss has been associated with senescence and has been used as a marker of senescence. Hence, our data shows that LMNB1 protein levels declined from proliferative to senescent cells. Its level showed a change of -1.6 (log2) fold change (Figure 7.8).

Furthermore, PML protein is of the several proteins that are differentially regulated during senescence. It is suggested that PML plays a role in various cellular processes such as DNA damage response, tumour suppression and senescence (Uniprot.org). Thus, it plays a role in DNA damage response by positively regulating p53 protein which in turn results in cell cycle

arrest. Moreover, PML has been detected to dramatically increase in ras-arrested fibroblast cells (Rokudai et al., 2013). Consistent with previous reports (Ferbeyre et al., 2000; Rokudai et al., 2013), the levels of PML in senescent WT U2OS was more pronounced than in proliferative cells. The levels of PML protein showed a log2 fold change of 1.2 from proliferative to senescent cells (Figure 7.8).

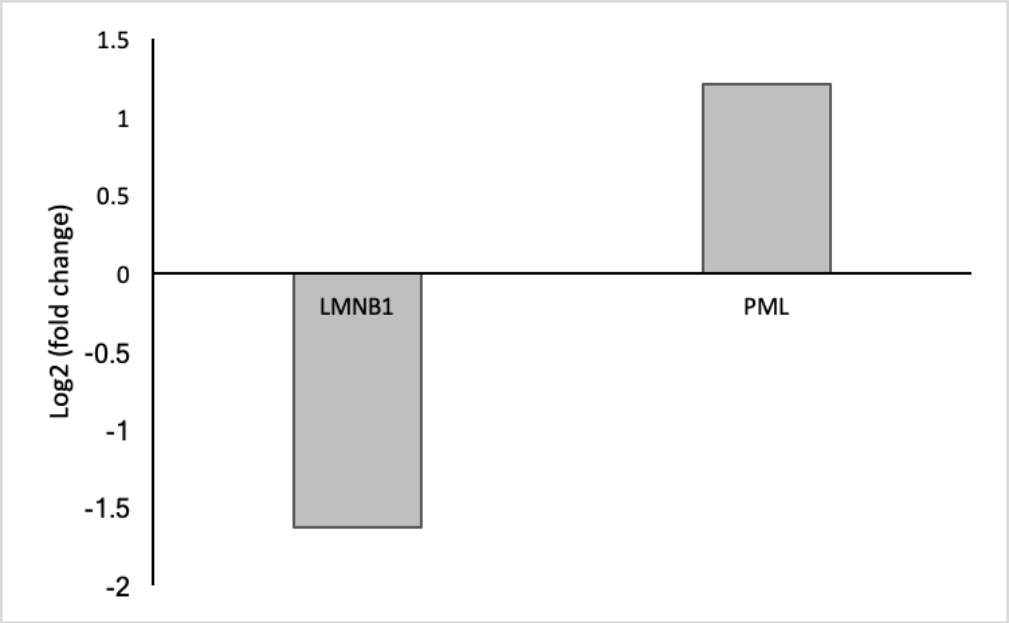

Figure 7.8 Change in the level of LMNB1 and PML proteins.
Level of LMNB1 and PML proteins was investigated in WT U2OS cells. LMNB1 was detected to decrease significantly (-1.6 (log2) fold change) from proliferative to senescent cells. PML was observed to increase (1.2 (log2) fold change) from proliferative to senescent cells.

7.4.1.3 Stress Granule Proteins

Following the proteome analysis of proliferative and senescent WT U2OS cells, the change in the levels of stress granule proteins was investigated. Expectation that stress granule proteins will decline in level in senescent cells, especially those that drive stress granule formation including G3BP1, G3BP2 or Caprin-1. Stress granule contains several proteins such as TIA1, TIAR, EIF4G, Caprin-1, USP10, HUR and TDP-43 but a few of them are drivers of stress granules and others are stress granule resident proteins that are recruited to stress granules. In addition to proteins, stress granules are composed of free untranslated mRNAs (Wheeler et al., 2016).

G3BP is one of the crucial RNA-binding proteins that plays an essential role in nucleating stress granule formation (Kedersha et al., 2016). In our current study, G3BP1 protein levels were observed to slightly decline from young to senescent cells while G3BP2 protein levels were detected to slightly rise in senescent cells (Figure 7.9).

Change in other stress granule residues such as eIF4G, FXR1, USP10, CAPRIN1, TDP43 (TAR DNA-binding protein 43) and HUR (known as ELAVL1: ELAV-like protein 1) protein levels was investigated. Insignificant change was detected in these proteins (Figure 7.9). Our observation suggests that the protein residues of stress granules might not be involved in the process of stress granule formation in senescent cells.

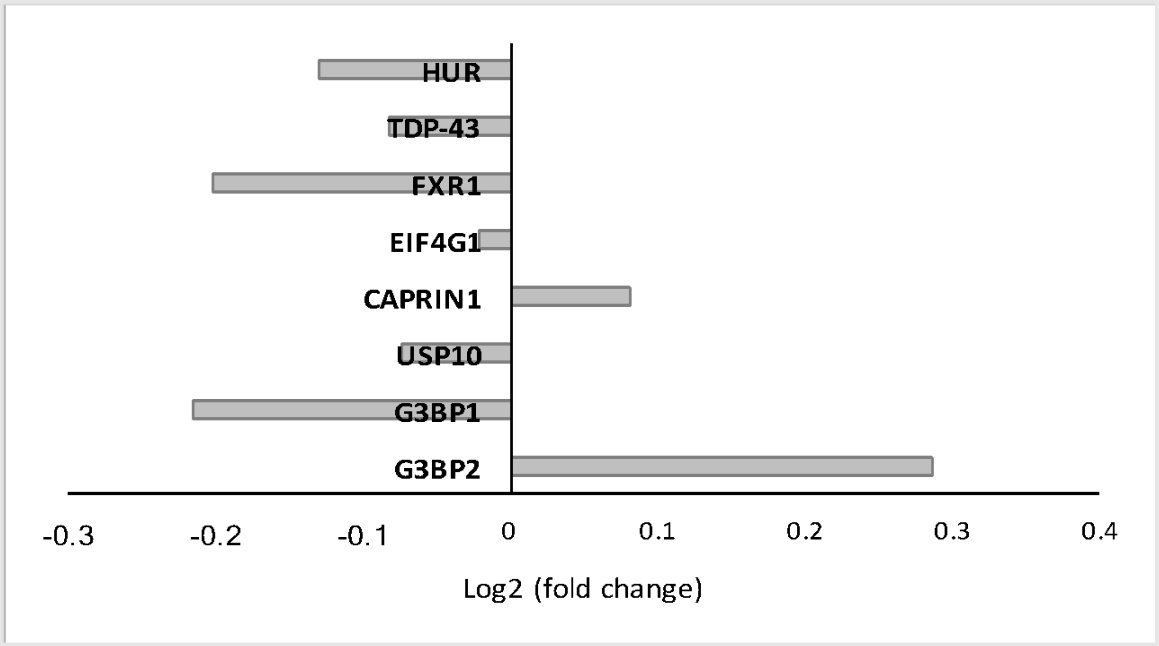

Figure 7.9 level of stress granule proteins in WT U2OS cells.

The level of G3BP1, USP10, EIF4G, FXR1, TDP-43 and HUR proteins was observed to slightly decline from proliferative to senescent cells. Whereas, G3BP2 and CAPRIN1 proteins levels were observed to slightly rise from proliferative to senescent cells.

7.4.2 ΔΔG3BP1/2 Cells

As shown previously, treatment of ΔΔG3BP1/2 cells with doxorubicin (200 nM) for 48 hrs induces senescence phenotype (discussed in chapter 5). Alterations associated with senescence involve morphological and molecular changes (Campisi, 2005). Change in the shape of senescent cells was associated with an elevation in the levels of cytoskeletal proteins (Gourlay and Ayscough, 2005). Moreover, increased p53 levels upon activation of DDR leads to activation of p21 (Campisi, 2005). High levels of p21 protein are required to be maintained in cells for several weeks in order to inhibit cell growth and induce changes associated with senescence. Subsequently, reduction in p21 protein levels is followed by an increased p16 protein level. p16 protein is required to maintain senescence phenotype (Itahana et al., 2001; Campisi, 2005).

Following the investigation of the effect of senescence induction on protein levels in WT U2OS cells, we then ask the question whether absence of G3BP1/2 affects senescence progression and the molecular changes associated with senescence. Therefore, lysates were collected from proliferative (day 0) and senescent (day 9) ΔΔG3BP1/2 cells. Quantitative proteomics analysis was performed using SWATH-MS. A total of 5791 proteins were identified in the lysates of ΔΔG3BP1/2 cells. Approximately 2714 proteins were identified at a rate of adjusted p-value < 0.05. Proteomics analysis showed that 299 proteins were showing an absolute fold change higher than 2 or smaller than -2. I discuss these 299 significantly changing proteins with regard to senescence and stress granule formation. The role of the significantly changing proteins and proteins associated with senescence and stress granule formation are discussed here.

7.4.2.1 Most Highly Dysregulated Proteins

Among the 2714 proteins that were detected in lysates of ΔΔG3BP1/2 cells, 299 proteins were detected to significantly change. The proteins that are coloured in grey are not showing a significant change (< 2 and > -2-fold change, adjusted p-value > 0.05). Nevertheless, the proteins that are marked as green are significantly changing (>2 and <-2-fold change, adjusted p-value < 0.05). The highly changing proteins (> 4 and < -4-fold change) are coloured as red. It is not possible to label all significantly changing proteins, therefore, proteins higher than 4 and less than -4 are labelled (Figure 7.10).

The levels of LAMB3, TIMP1, RRM2B, SOD2, FLNC, ABAT, CRYAB, APOE, SERPINE1, CD68, CLIC2, OASL, CHKB, ARSA, CDKN1A, CXCL8, CYFIP2, GNG4, SYP, GPS2 and RND3 proteins were detected to significantly increase in senescent ΔΔG3BP1/2 cells with a fold change higher than 4. In contrast, the levels of PHGDH, TYMS, DUT, ANXA2, NCAPD2, RRM2, NCAPH, L1CAM, SMC4, TK1, UBE2T, DHFR, SNRPD3, PBK, NUF2, KIFC1, STMN1, UBE2V1, GPA33, OSTC, ANXA4, SPC25, CDCA3, GINS4, HACD2 and SCAF8 proteins were detected to decline significantly in senescent ΔΔG3BP1/2 cells with a fold change smaller than -4 (Figure 7.10).

Figure 7.10 Proteomics analysis of proliferative (Day 0) compared to senescent (Day 9) ΔΔG3BP1/2 cells.

The plot shows the distribution of proteins forming a volcano plot. The marks are showing the distribution of all 5358 proteins detected in lysates of ΔΔG3BP1/2 cells. The grey marks are the proteins with no significant change. Green colour marks represent proteins with fold change >2 and <-2. Green marks are showing the highly-dysregulated proteins from proliferative to senescent cells >4 and <-4-fold change (adjusted p-value ≤ 0.05).

7.4.2.1.1 Upregulated Proteins

Of these proteins, several nuclear and mitochondrial proteins showed significant decline from proliferative to senescent cells. These proteins are suggested to be involved in several biological processes such as regulation of transcription, DNA replication, translation, cell cycle, DNA-damage response, activation of MAPK activity, G1/S transition of mitotic cell cycle and cell division. Additionally, the mitochondrial protein TYMS regulates the biosynthesis pathway: mitochondrial thymidylate pathway (Table 7.4).

Table 7.4 Nuclear and mitochondrial proteins that are significantly down-regulated from proliferative to senescent ΔΔG3BP1/2 cells.

Label	Name	Location
H1-1	Histone H1.1	Nuclear
SPC24	Kinetochore protein Spc24	Nuclear
PCLAF	PCNA-associated factor	Nuclear
H1-5	Histone H1.5	Nuclear
RFC2	Replication factor C subunit 2	Nuclear
UBE2V1	Ubiquitin-conjugating enzyme E2 variant 1	Nuclear
RECQL4	ATP-dependent DNA helicase Q4	Nuclear
MCM6	DNA replication licensing factor MCM6	Nuclear
SNRPD3	Small nuclear ribonucleoprotein Sm D3	Nuclear
TYMS	Thymidylate synthase	Mitochondrial

Proteomics analysis revealed an increase in the levels of lysosomal proteins from proliferative to senescent cells (Table 7.5). Lysosome is essential for the remodelling of cells. It is suggested that chromatin of senescent cells is processed via lysosomal pathway which in turn contributes to senescence phenotype stability (Ivanov et al., 2013).

Table 7.5 Lysosomal proteins that are significantly up-regulated from proliferative to senescent ΔΔG3BP1/2 cells.

Label	Name	Location
ARSA	Arylsulfatase A	Lysosomal
CD68	Macrosialin	Lysosomal
CTSS	Cathepsin S	Lysosomal

Superoxide dismutase [Mn] protein (SOD2) was observed to rise in levels in senescent cells. It showed an increase of 2.2-fold change from proliferative to senescent cells. SOD2 is a mitochondrial protein. It is involved in destroying superoxide radicals generated in stressed cells or cells that are toxic and could cause damage to other cells (MacMillan-Crow and Thompson, 1999). SOD2 is also suggested to be involved in age-dependent response to reactive oxygen species (ROS) (Uniprot.org).

Of the highly-increased protein levels in ΔΔG3BP1/2 senescent cells, PH domain leucine-rich repeat-containing protein phosphatase 1 (PHLPP1) showed an increased protein levels (3.1-fold change). PHLPP1 is a nuclear protein and is suggested to play a role in inhibiting cancer cell proliferation by acting as a tumour suppressor (Uniprot.org). It regulates Akt signalling

pathways by dephosphorylation of Ser-473 which triggers suppression of tumour growth (Gao et al., 2005).

7.4.2.1.2 Upregulated Pathways from Proliferative to Senescent ΔΔG3BP1/2 Cells

The significantly changing proteins in response to senescence induction were tested for statistical underrepresentation using enrichGO after FDR control. Based on the GO enrichment, the significantly upregulated proteins from proliferative to senescent ΔΔG3BP1/2 cells were enriched in 20 terms in the category biological processes. The proteins were enriched according to gene count which is the number of enriched genes in GO term (Figure 7.11).

GO enrichment uncovered that the highly-upregulated proteins in senescent cells were involved in small molecule catabolic process, extracellular structure organization, regulation of endopeptidase activity, fatty acid metabolic process, regulation of apoptotic signalling pathway, cellular response to external stimulus, cellular amino acid metabolic process, lipid catabolic process, lipid modification and regulation of mitochondrion organization (Table 7.6).

The proteomics analysis of lysates from proliferative and senescent ΔΔG3BP1/2 cells revealed that the overrepresentation of regulation of apoptotic signalling pathway. A total of 18 proteins were annotated to this term including SOD2, CD44, CAV1, FAS, GPX1, RRM2B, ATP5IF1 and SERPINE1. Apoptotic signalling pathway involves a series of signals that stimulates apoptotic cell death. Hence, senescent cells are known to resist apoptosis. They are persistent and live for a long time in the tissue/organ. Therefore, it is suggested here that apoptotic signalling pathway is regulated in senescent ΔΔG3BP1/2 cells which is a known feature of senescence phenotype.

Fatty acid metabolic process was observed to be overrepresented in senescent ΔΔG3BP1/2 cells. Proteomics analysis and statistical overrepresentation test revealed that 19 proteins are involved in the process of fatty acid metabolic. Of the proteins involved in the fatty acid metabolic process: MYO5A, ERLIN2, CES2, CAV1 and GPX1 are significantly changing proteins (fold-change higher 2). Fatty acid metabolic process involves any synthesis and degradation of fatty acid. Hence, it involves the degradation of stored fats and synthesis of structural lipids. Those fatty acids and lipids are involved in the building of membranes of cells. The increased size of senescent cells increases the demand for structural lipids that are required for the construction process of cell membrane. Hence, our observations suggest that lack of G3BP1/2 promotes senescence and increases the fatty acid and lipid metabolism in order to synthesize structural lipids.

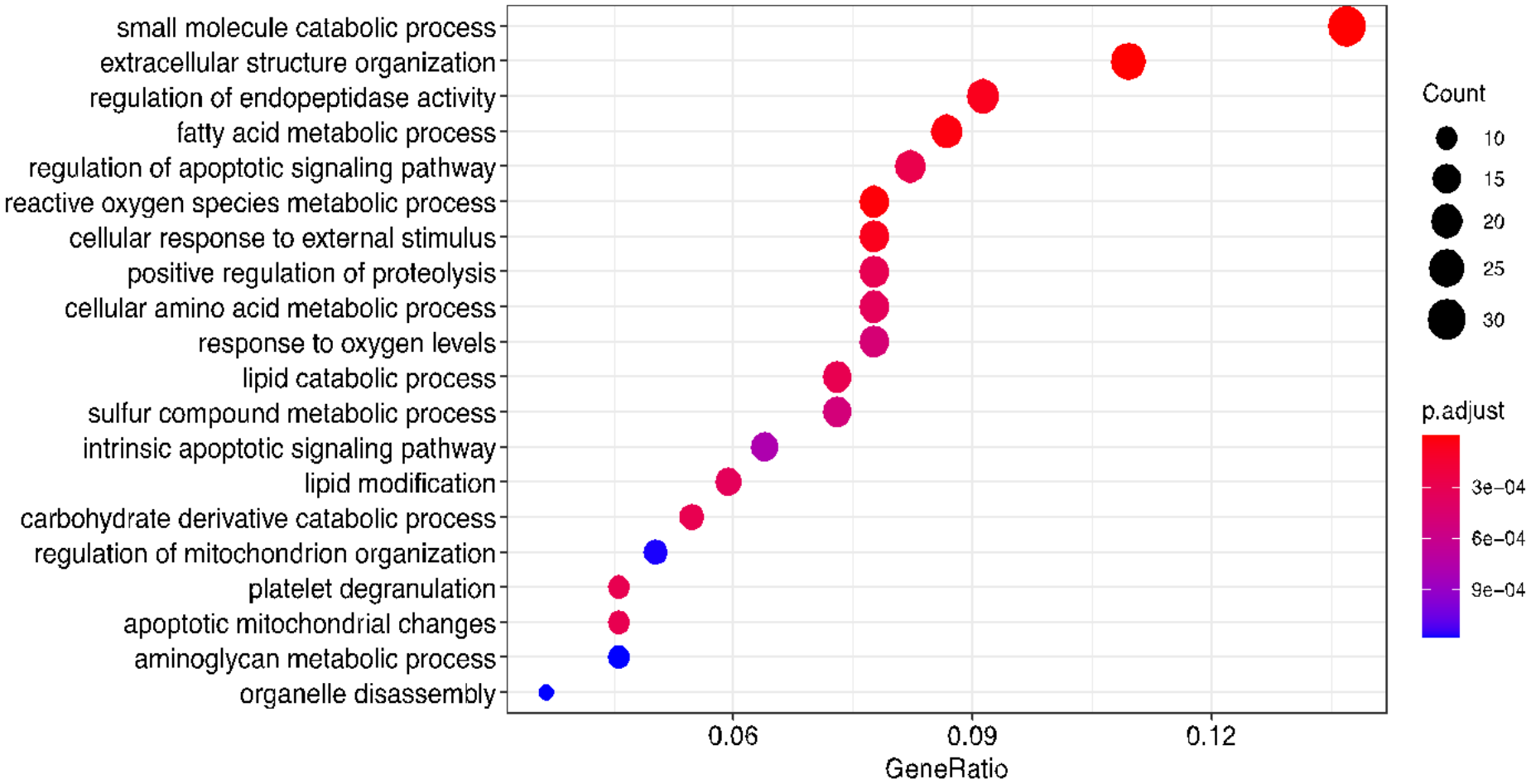

Figure 7.11 Overrepresentation of GO biological process terms.

GO biological process terms found to be statistically overrepresented upon doxorubicin treatment (senescence induction). Proteins were tested against all detected proteins in the data set using enrichGO. Count is the number genes that are enriched in each GO term. Gene ratio is a percentage of differentially upregulated genes in each GO term.

7.4.2.1.3 Downregulated Proteins

Several proteins that are involved in DNA synthesis and cell cycle progression were observed to reduce significantly in senescent cells. The levels of Histone H1.1 (H1-1) protein were reduced significantly (4.3-fold change) from proliferative to senescent cells. H1-1 protein is a nuclear protein and involved in chromosome condensation and chromatin DNA binding. Moreover, it plays a role in gene transcription by regulating chromatin modelling, nucleosome spacing and DNA methylation (Uniprot. org).

The proteomics data revealed a decrease in Annexin A2 (ANXA2) protein levels from proliferative to senescent cells. It showed a decrease of 3-fold change. ANXA2 plays a role in regulating cell growth. It has been detected in several cancer types. Knockdown of ANXA2 gene lead to reduced DNA synthesis and cell division. Therefore, it is suggested that ANXA2 protein is an essential regulator of cell proliferation. Moreover, ANXA2 plays a role in p53-mediated apoptosis and inhibits damage-induced apoptosis by activating pro-survival signals (Chiang et al., 1999; Huang et a., 2005; Wang and Lin 2014).

Histone 4C proteins showed a significant decrease in senescent ΔΔG3BP1/2 cells. The proteomics analysis revealed a decrease of ~2.6-fold change in H4C proteins including H4C2, H4C8, H4C6, H4C5, H4C4, H4C3, H4C12, H4C15, H4C14, H4C13, H4C1, H4C11 and H4C9. Histone 4C proteins are involved in regulation of DNA replication and nucleosome remodelling (Uniprot. org).

Nucleosome is the central unit of eukaryotic chromatin. It promotes condensation of DNA into a smaller volume limiting accessibility of DNA to several cellular machineries. Hence,

nucleosome is a DNA segment that is wrapped around a core of proteins called histones. Nucleosome consists of four core histones: Histone H4, Histone H2A, Histone H2B, Histone H3 (Figure 7.15). Histones H3 and H4 are known to bind to terminal parts of DNA. They are the most highly conserved histones. Moreover, they are suggested to play a role in regulating chromatin formation (Hyland et al., 2005).

7.4.2.1.4 Downregulated Pathways from Proliferative to Senescent ΔΔG3BP1/2 Cells

Furthermore, in this study, the significantly changing proteins in response to senescence induction were tested for statistical underrepresentation using enrichGO after FDR control. Gene ontology enrichment showed that the significantly downregulated proteins from proliferative to senescent cells were enriched in 20 terms in the category biological processes. The proteins were enriched according to the number of enriched genes in GO term which is known as gene count (Figure 7.12).

GO enrichment revealed that the highly-downregulated proteins in senescent cells were involved in the following biological processes: DNA replication, DNA conformation change, chromosome segregation, positive regulation of cell cycle, regulation of DNA metabolic process, DNA recombination, protein-DNA complex subunit organization, cell cycle G1/S phase transition, DNA biosynthetic process, microtubule cytoskeleton organization involved in mitosis, telomere organization and DNA strand remodelling (Table 7.7).

The downregulation of proteins involved in DNA synthesis and replication, and cell cycle regulation indicates that cells are not dividing and the process of cell growth is ceased. The downregulation is pronounced in cells of day 9 post-doxorubicin treatment which suggests that cells are senescent. Thus, we suggest that the loss of G3BP1/2 promotes senescence. Our

proteomics data is consistent with other markers of senescence (chapter 5) that were used to indicate the stage of the cells whether actively-dividing or senescent.

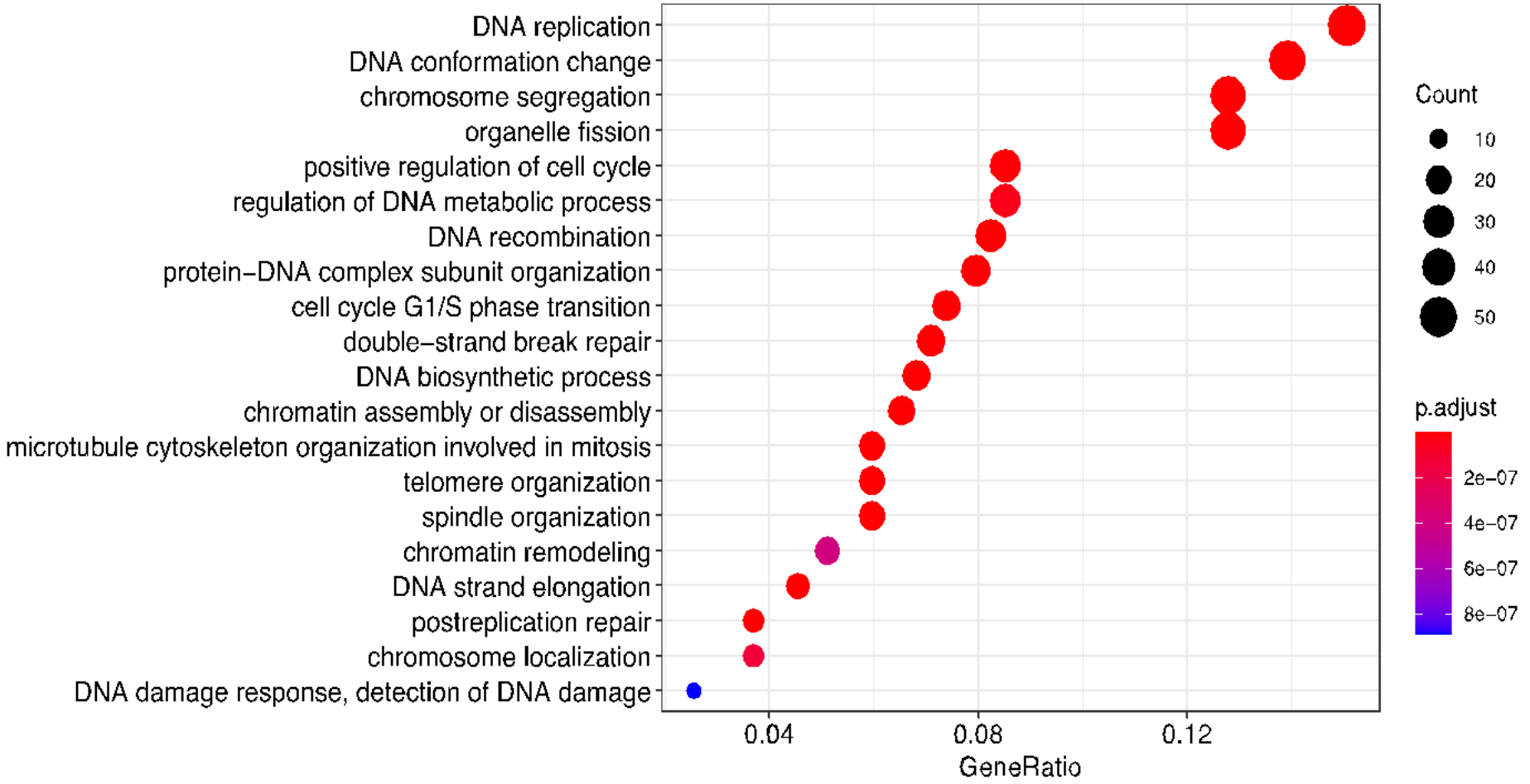

Figure 7.12 Biological processes that are underrepresented in senescence.

GO biological process terms that are found to be statistically underrepresented upon doxorubicin treatment (senescence induction). Proteins were tested against all detected proteins in the data set using enrichGO. Count is the number genes that are enriched in each GO term. Gene ratio is a percentage of differentially downregulated genes in each GO term.

7.4.2.2 Senescence Associated Proteins

To induce senescence phenotype, activation of certain proteins is required. These proteins are known to be associated with senescence including cyclin-dependent kinase inhibitors: p53, p21 and p16 (van Deursen, 2014; Gorgoulis et al., 2019; Nassrally et al., 2019). We here investigate the changes in the levels of kinase inhibitors between proliferative and senescent ΔΔG3BP1/2 cells.

7.4.2.2.1 Cyclin-Dependent Kinase Inhibitors

Senescence is initiated by activating p53 (TP53) which senses the irreparable DNA-damage. Proteomics analysis revealed a minor increase in Tumour protein p53-inducible protein 11 (TP53I11) and Tumour protein p53-binding protein 1 (TP53BP1) in senescent ΔΔG3BP1/2 cells compared to proliferative cells. Thus, a significant increase (2.8 log (2) fold change) in p21 protein levels was detected in senescent ΔΔG3BP1/2 cells (Figure 7.20). Levels of p16 protein rise following the decline in p21 protein levels. The proteomics data revealed no change in the levels of CDKN2AIP between proliferative and senescent ΔΔG3BP1/2 cells (Figure 7.13).

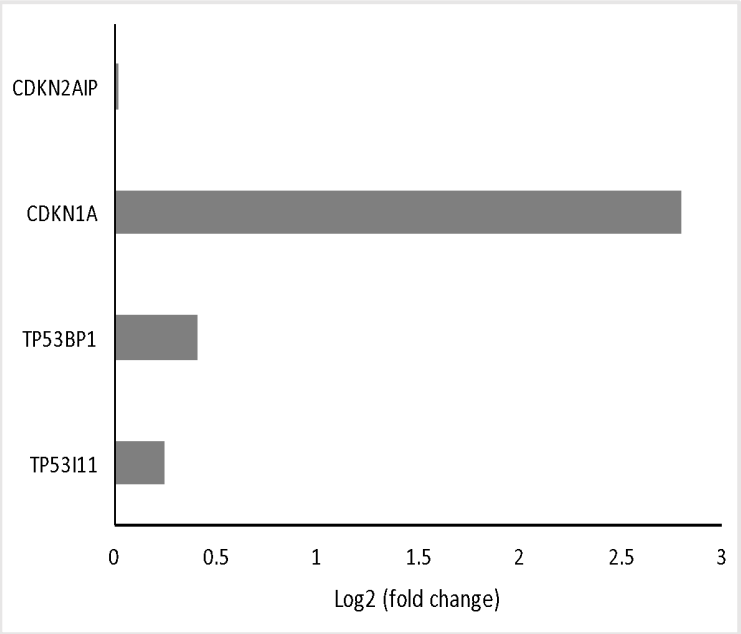

Figure 7.13 Level of cyclin-dependent kinase inhibiting proteins in ΔΔG3BP1/2 cells. CDKN1A protein was detected to increase significantly (2.8 (log2)-fold change) from proliferative to senescent cells. TP53I11 and TP53BP1 proteins showed a slight increase in senescent cells which is not significant.

Thus, our proteomics data showed that the level of cyclin-dependent kinase inhibitors: p53, p21 and p16 varies. It depends on the stage of senescence. It has been detected by several studies that p53 protein level is elevated during exposure to a DNA-damaging stressor. P53 induces activation of p21. Once p21 is activated, p53 levels decline (Georgakilas et al., 2017). Sustained rise of p21 is required to induce changes associated with senescence. P21 activates p16 which is required to maintain senescence phenotype induced by p21 protein. Therefore, our observations are confirming the findings of other studies. The significant increase in of p21 levels but not p53 or p16 proteins suggests that cells are senescent. In order to observe the changes in p16 protein levels, cells are required to be kept for a longer time (day 14 or 21 post-doxorubicin exposure) to extract lysates from cells and perform proteomics analysis.

7.4.2.2.2 PML and LMNB1

Protein PML (PML) (Rokudai et al., 2013) and Lamin-B1 (LMNB1) (Freund et al., 2012) are considered as senescence associated proteins and have been used as markers for senescence.

LMNB1 has been observed to decline in senescent cells compared to proliferative cells (Freund et al., 2012). This decline has been detected to be associated with senescence and therefore LMNB1 has been used as a marker of senescence. Hence, our data shows that LMNB1 protein levels declined from proliferative to senescent ΔΔG3BP1/2 cells. Its level showed a change of -2.02 (log2) fold change (Figure 7.14).

Furthermore, PML protein is of the several proteins that are dysregulated during senescence. Of the cellular processes that PML is suggested to be involved in DNA damage response, tumour suppression and senescence (Uniprot.org). Thus, it plays a role in DNA damage response by positively regulating p53 protein which in turn results in cell cycle arrest. Moreover, PML has been detected to dramatically increase in ras-arrested fibroblast cells (Rokudai et al., 2013). Consistent with previous reports (Ferbeyre et al., 2000; Rokudai et al., 2013), the levels of PML in senescent ΔΔG3BP1/2 cells was more pronounced than in proliferative cells. The levels of PML protein showed a log2 fold change of 1 from proliferative to senescent cells (Figure 7.14).

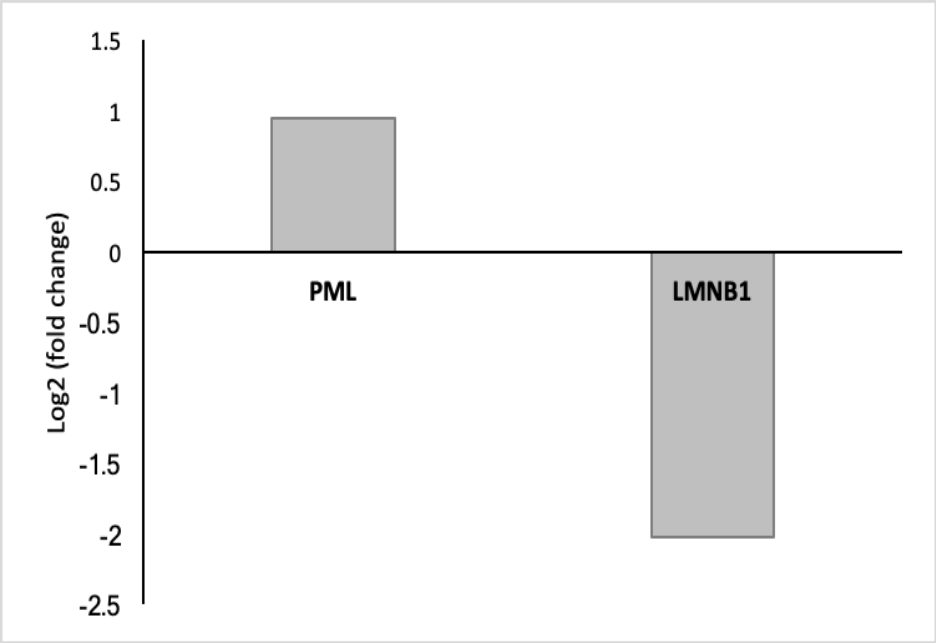

Figure 7.14 Change in the level of LMNB1 and PML proteins.

Level of LMNB1 and PML proteins was investigated in ΔΔG3BP1/2 cells. LMNB1 was detected to decrease significantly (-2.02 (log2) fold change) from proliferative to senescent cells. PML was observed to increase (1 (log2) fold change) from proliferative to senescent cells.

7.4.2.3 Stress Granule Proteins

Following the protein and proteome analysis of proliferative and senescent ΔΔG3BP1/2 cells, the change in RNA-binding proteins levels was investigated (Figure 7.15). G3BP plays a crucial role in stress granule formation upon exposure to a stress. Knockout of G3BP1/2 inhibited stress granule formation in ΔΔG3BP1/2 cells (discussed in chapter 4). Proteomics analysis showed no change in most stress granule proteins USP10, CAPRIN1, eIF4G, FXR1, TDP43 and HUR. Expectedly, endogenous G3BP1 and G3BP2 were not detected in the lysate of ΔΔG3BP1/2 cells.

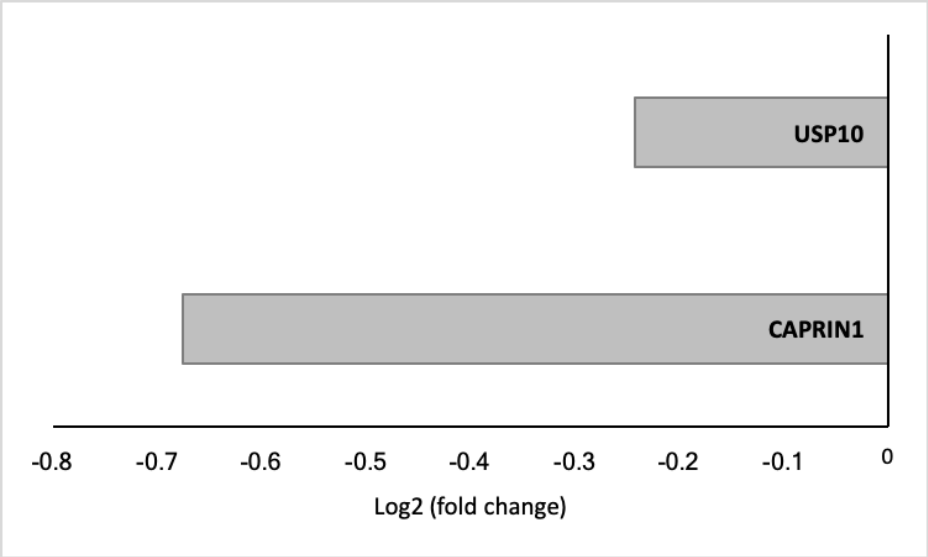

Figure 7.15 Change in the level of RNA-binding proteins from proliferative to senescent ΔΔG3BP1/2 cells.

The level of USP10 and Caprin1 proteins were observed to decline from proliferative to senescent cells. Caprin1 showed a decrease of 0.7-(log2) fold change in senescent cells.

7.4.3 GFP-G3BP1 Cells

As shown in chapter 5, senescence phenotype is observed in GFP-G3BP1 cells upon exposure to doxorubicin (200 nM) for 48 hours. Certain morphological and molecular alterations are associated with senescence (Campisi, 2005). Change in the shape of senescent cells was observed to be associated with a rise in the levels of cytoskeletal proteins (Gourlay and Ayscough, 2005). In addition to morphological changes, levels of p53, p21 and p16 were observed to increase in senescent cells (Campisi, 2005). Elevated levels of p21 protein is needed in order to inhibit cell growth and induce changes associated with senescence phenotype. Moreover, p16 protein is required to maintain senescence phenotype (Itahana et al., 2001; Campisi, 2005).

Following the investigation of the effect of senescence on proteins levels in WT U2OS cells and ΔΔG3BP1/2 cells, we then investigate whether re-constitution of ΔΔG3BP1/2 cells with G3BP1 (GFP-G3BP1 cells) slows senescence progression and the molecular changes associated senescence. Therefore, lysates were collected from proliferative (day 0) and senescent (day 9) GFP-G3BP1 cells. Quantitative proteomics analysis was performed using SWATH-MS. A total of 5428 proteins were identified in the lysates of GFP-G3BP1 cells. Approximately 2869 proteins were identified at a rate of adjusted p-value < 0.05. Proteomics analysis showed that 415 proteins were showing an absolute fold change higher than 2 or smaller than -2. I discuss these 415 significantly changing proteins with regard to senescence and stress granule formation. The role of the significantly changing proteins and proteins associated with senescence and stress granule formation are discussed here.

7.4.3.1 Most Highly Dysregulated Proteins

Among the 2869 proteins that were detected in lysates of GFP-G3BP1 cells, 415 proteins were detected to significantly change. The proteins that are coloured in grey are not showing a significant change (< 2 and > -2-fold change, adjusted p-value > 0.05). Nevertheless, the proteins that are marked as green are significantly changing (>2 and <-2-fold change, adjusted p-value < 0.05). The highly changing proteins (> 4 and < -4-fold change) are coloured as red. It is not possible to label all significantly changing proteins, therefore, proteins higher than 4 and less than -4 are labelled (Figure 7.16).

The levels of RRM2B, IFIT1, CDKN1A, FAS, OAS2, CPA4, PHLPP1, SYP, CHKB, SYK and HAUS6 proteins were detected to significantly increase in senescent GFP-G3BP1 cells with a fold change higher than 4. In contrast, the levels of PHGDH, SMC4, TK1, MCM3, PBK, NCAPH, RRM2, NDC80, H1-5, UBE2T, TMPO, AURKB, NUF2, UBE2V1, ANXA2, CKS2, CDC20, SPC24, LMCD1, SLC1A4, GPT and TRAIP proteins were detected to decrease significantly in senescent GFP-G3BP1 cells with a fold change smaller than -4 (Figure 7.16).

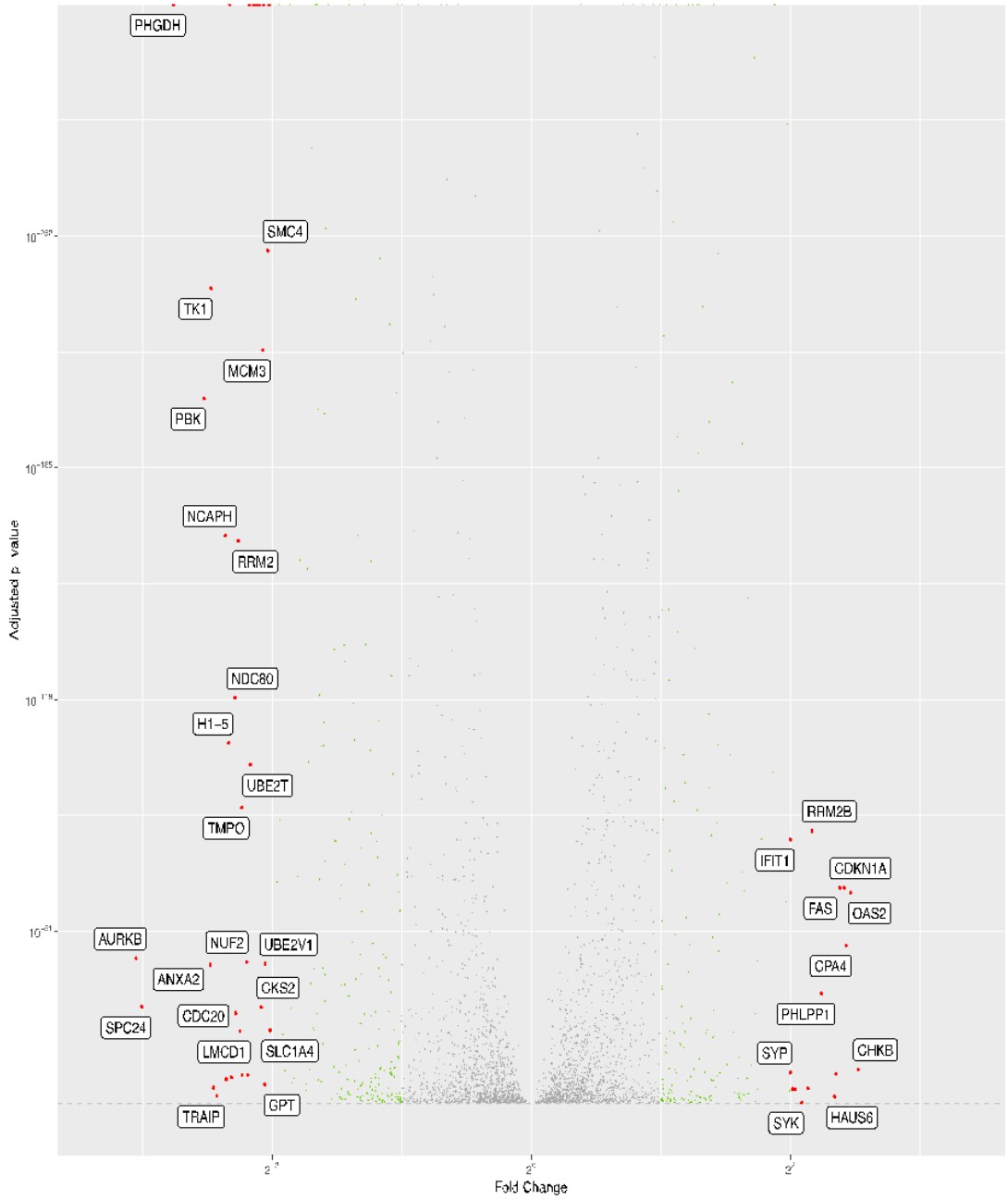

Figure 7.16 Proteomics analysis of proliferative (Day 0) and senescent (Day 9) GFP-G3BP1 cells.

The plot shows the distribution of proteins forming a volcano plot. The marks are showing the distribution of all 5428 proteins detected in lysates of GFP-G3BP1 cells. The grey marks are the proteins with no significant change. Green colour marks represent proteins with fold change bigger than 2 and smaller than -2. Green marks are the highly-dysregulated proteins from proliferative to senescent cells with a fold change >4 and <-4 (adjusted p-value ≤ 0.05).

7.4.3.1.1 Upregulated Proteins

Of the significantly changing proteins, Ribonucleoside-diphosphate reductase subunit M2 B (RRM2B) which showed an increase in senescent cells of 4.5-fold change. RRM2B is suggested to play an essential role in cell survival. It is suggested to repair DNA damage in a p53/TP53-dependent manner during senescence (Cho et al., 2015). RRM2B was observed to be expressed at high levels in senescence primary human fibroblast IMR90 cells (Kuo et al., 2012). It acts as a supplier of deoxyribonucleotides for the process of DNA repair in cells arrested at G1 or G2 phase of cell cycle (Uniprot.org). RRM2B exists in nucleus and cytoplasm as it translocates from cytoplasm to nucleus during exposure to DNA damage-inducing agents (Uniprot. org).

PH domain leucine-rich repeat-containing protein phosphatase 1 (PHLPP1) proteins was observed to increase significantly in senescent GFP-G3BP1 cells when compared to proliferative cells. It is involved in the regulation of Akt signalling pathway which in turn promotes cell cycle, cell survival, growth and proliferation in response to external stimuli (Shi et al., 2019). Hence, upregulation of PHLPP1 protein in senescent GFP-G3BP1 cells is suggested to control cells' growth and proliferation.

7.4.3.1.2 Upregulated Pathways from Proliferative to Senescent GFP-G3BP1 Cells

The significantly changing proteins in response to senescence induction were tested for statistical overrepresentation using enrichGO after FDR control. Based on the GO enrichment, the significantly upregulated proteins from proliferative to senescent GFP-G3BP1 cells were enriched in 20 terms in the category of biological processes. The proteins were enriched according to gene count which is the number of enriched genes in GO term (Figure 7.17).

GO enrichment uncovered that the highly-upregulated proteins in senescent cells were involved in small molecule catabolic process, regulation of endopeptidase activity, positive regulation of proteolysis, coenzyme metabolic process, regulation of multi-organism process, carbohydrate derivative catabolic process, response to endoplasmic reticulum stress, intrinsic apoptotic signalling pathway, cellular ketone metabolic process and lipoprotein catabolic process (Table 7.8).

The proteomics analysis of lysates from proliferative and senescent GFP-G3BP1 cells revealed that the overrepresentation of small molecule catabolic process. A total of 19 proteins were annotated to this term including ALDH2, HADHB, TIGAR, APOE, ACOT8, MLYCD, IL4I1, ACAA1, CD44 and ABAT. These proteins are significantly changing proteins (fold-change higher than 2). Moreover, small molecule metabolic process (GO:0044281) is defined as the pathways and chemical reactions that involve small molecules or any low molecular weight molecule (Uniprot. org). This data suggests that the molecular changes of small molecules increases with senescence in GFP-G3BP1 cells.

Moreover, regulation of endopeptidase activity was observed to be overrepresented in senescent GFP-G3BP1 cells. Hence, regulation of endopeptidase activity (GO:0052548) involves any processes that modulate endopeptidase activity which is the endohydrolysis of protein bonds (Uniprot. org; Weiss et al., 2020). Proteomics analysis and statistical overrepresentation test revealed that 18 proteins are involved in the process of endoplasmic activity regulation. Of the proteins involved in of fatty acid metabolic process: AHSG, SERPINB5, PML, FAS, CST3 and CRADD are significantly changing proteins (fold-change higher than 2). Hence, our observation suggests the differences in the endopeptidase activity which is associated with senescence in GFP-G3BP1 cells.

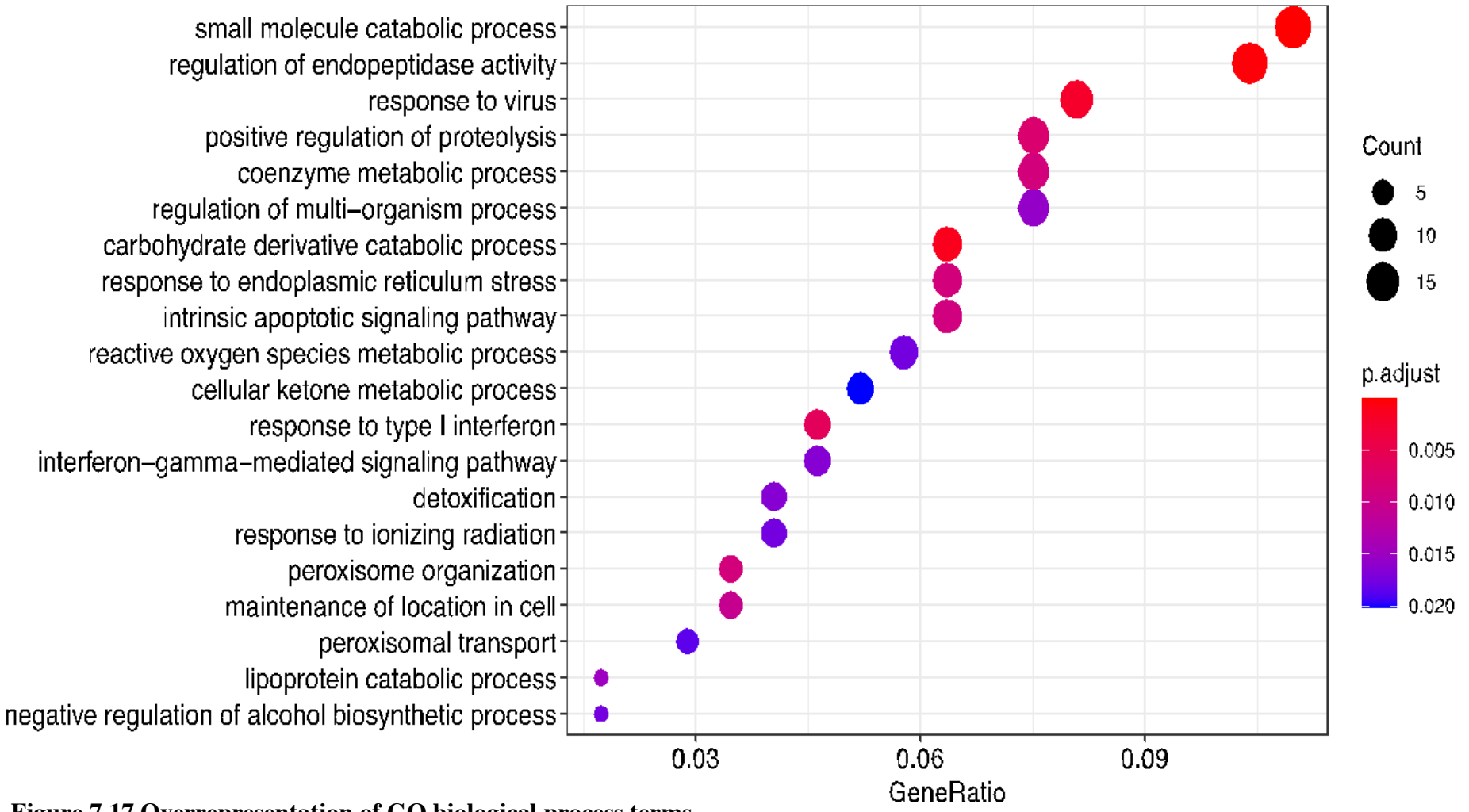

Figure 7.17 Overrepresentation of GO biological process terms.

GO biological process terms found to be statistically overrepresented upon doxorubicin treatment (senescence induction). Proteins were tested against all detected proteins in the data set using enrichGO. Count is the number genes that are enriched in each GO term. Gene ratio is a percentage of differentially upregulated genes in each GO term.

7.4.3.1.3 Downregulated Proteins

Of the significantly downregulated proteins is the minichromosome maintenance (MCM) proteins including DNA replication licensing factor MCM3 (MCM3), DNA replication licensing factor MCM2 (MCM2), DNA replication licensing factor MCM4 (MCM4), DNA replication licensing factor MCM5 (MCM4), DNA replication licensing factor MCM5 (MCM5), DNA replication licensing factor MCM6 (MCM6) and DNA replication licensing factor MCM7 (MCM7) (Forsburg, 2004; Meagher et al., 2019). The proteins of this family showed a significant reduction in GFP-G3BP1 cells when becoming senescent. They showed a change of -2.01 to -2.2 log (2) fold change (Figure 7.18). MCM proteins plays a role in several processes including DNA replication, replication initiation, DNA strand elongation and pre-replicative complex assembly (Meagher et al., 2019). Hence, the significant downregulation of these proteins indicates that cells are not dividing; senescent.

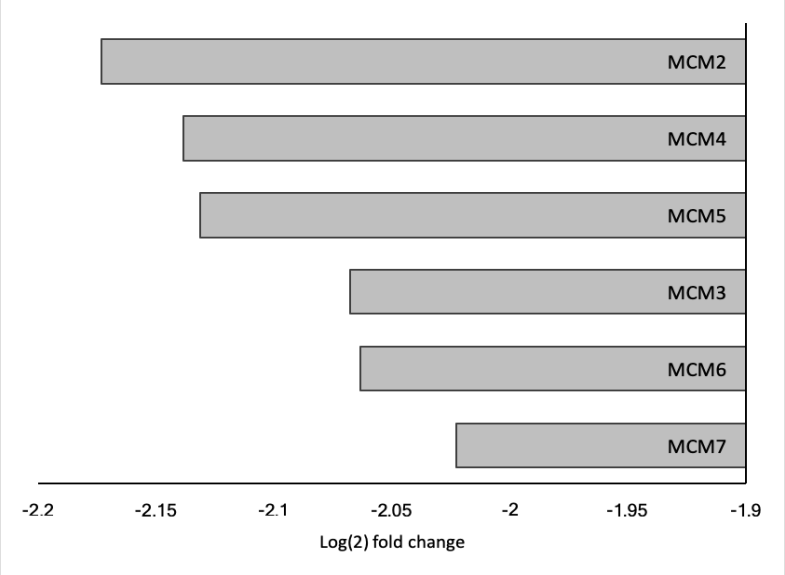

Figure 7.18 Level of minichromosome maintenance proteins varies from proliferative to senescent GFP-G3BP1 cells.

MCM proteins were detected to decrease significantly from proliferative to senescent cells. They showed a change of -2.01 to -2.2 log (2) fold change. The reduction was observed in senescent cells indicating that DNA replication is reduced.

Additionally, proteomics analysis revealed that condensin complex subunit 2 (NCAPH) was significantly downregulated in GFP-G3BP1 cells when becoming senescent. It showed a decrease of 2.3 log (2) fold change. NCAPH protein was detected to locate in nucleus. It plays a role in cellular processes including cell division and mitotic chromosome condensation (Uniprot.org). Moreover, NCAPH is known as the regulatory subunit of the condensin complex. Condensin complex is required for the process of interphase chromatin conversion into mitotic-like condensed chromosome (Kimura et al., 2001).

7.4.3.1.4 Downregulated Pathways from Proliferative to Senescent GFP-G3BP1 Cells

Furthermore, in this study, the significantly changing proteins in response to senescence induction were tested for statistical underrepresentation using enrichGO after FDR control. Gene ontology enrichment showed that the significantly downregulated proteins from proliferative to senescent cells were enriched in 20 terms in the category biological processes. The proteins were enriched according to the number of enriched genes in GO term which is known as gene count (Figure 7.19).

GO enrichment revealed that the highly-downregulated proteins in senescent cells were involved in the following biological processes: DNA replication, DNA conformation change, chromosome segregation, DNA recombination, regulation of chromosome organization, regulation of DNA metabolic process, protein-DNA complex subunit organization, cell cycle G1/S phase transition, DNA biosynthetic process, double-strand break repair, microtubule cytoskeleton organization involved in mitosis and DNA strand elongation, (Table 7.9).

The downregulation of proteins involved in DNA synthesis and replication, and cell cycle regulation indicates that cells are not dividing and the process of cell growth is ceased. The

downregulation is pronounced in cells of day 9 post-doxorubicin treatment which suggests that cells are senescent. Thus, we suggest that presence of G3BP1 but loss of G3BP2 promotes senescence. Hence, our proteomics data is consistent with other markers of senescence (discussed in chapter 5) that were used to indicate the stage of the cells whether actively-dividing or senescent.

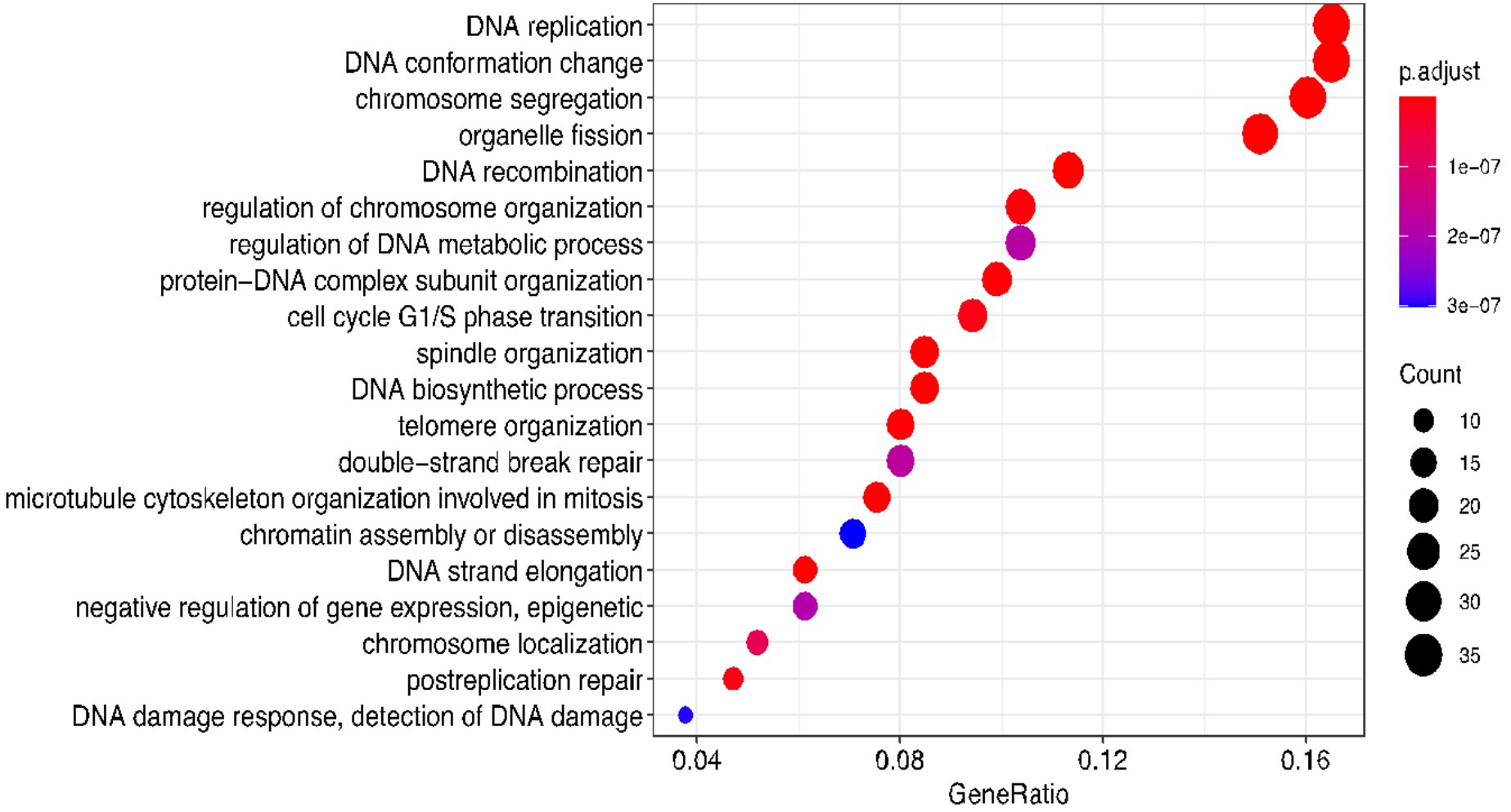

Figure 7.19 Biological processes that are underrepresented in senescence.

GO biological process terms that are found to be statistically underrepresented upon doxorubicin treatment (senescence induction) in GFP-G3BP1 cells. Proteins were tested against all detected proteins in the data set using enrichGO. Count is the number of genes that are enriched in each GO term. Gene ratio is a percentage of differentially downregulated genes in each GO term.

7.4.3.2 Senescence Associated Proteins

To induce senescence phenotype, activation of certain proteins is required. These proteins are known to be associated with senescence including cyclin-dependent kinase inhibitors: p53, p21 and p16 (van Deursen, 2014; Gorgoulis et al., 2019; Nassrally et al., 2019). Hence, cyclin-dependent kinase inhibitors are known to promote senescence phenotype by regulating cell growth (Aix et al., 2016; Puente et al., 2014). We here investigate the changes in the levels of kinase inhibitors between proliferative and senescent GFP-G3BP1 cells. Moreover, other senescence associated proteins such as PML and LMNB1 are investigated.

7.4.3.2.1 Cyclin-Dependent Kinase Inhibitors

Proteomics analysis revealed an increase of 1.4-fold change in p53 protein in senescent (day 9) GFP-G3BP1 cells compared to proliferative (day 0) cells. Furthermore, an increase of 5.3-fold change was detected in p21 protein levels in GFP-G3BP1 cells (Figure 7.20).

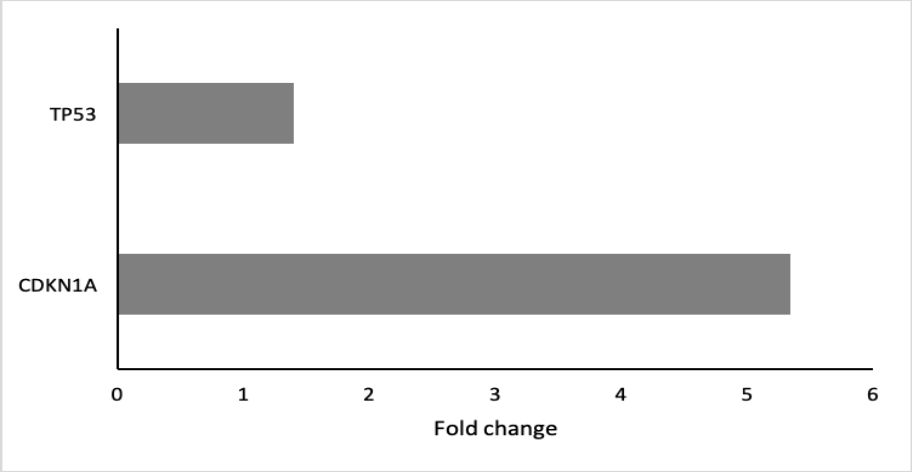

Figure 7.20 Level of cyclin-dependent kinase inhibiting proteins varies from proliferative to senescent cells.

CDKN1A (p21) protein was detected to increase significantly (5.3-fold change) from proliferative to senescent cells. TP53 (p53) showed an increase of 1.4-fold change from proliferative to senescent GFP-G3BP1 cells.

7.4.3.2.2 PML and LMNB1

Protein PML (PML) (Rokudai et al., 2013) and Lamin-B1 (LMNB1) (Freund et al., 2012) are considered as senescence associated proteins and have been used as markers for senescence. LMNB1 has been observed to decline in senescent cells compared to proliferative cells (Freund et al., 2012). Thus, our proteomics analysis shows that LMNB1 protein levels declined from proliferative to senescent GFP-G3BP1 cells. Its level showed a change of -1.6 (log2) fold change (Figure 7.21).

Furthermore, PML protein is of the several proteins that are dysregulated during senescence. Of the cellular processes that PML is suggested to regulate are DNA damage response, tumour suppression and senescence (Uniprot.org). Moreover, PML has been detected to dramatically increase in ras-arrested fibroblast cells (Rokudai et al., 2013). Consistent with previous reports (Ferbeyre et al., 2000; Rokudai et al., 2013), the levels of PML in senescent GFP-G3BP1 cells was observed to increase compared to proliferative cells. The levels of PML protein showed a log2 fold change of 1.2 from proliferative to senescent cells (Figure 7.21).

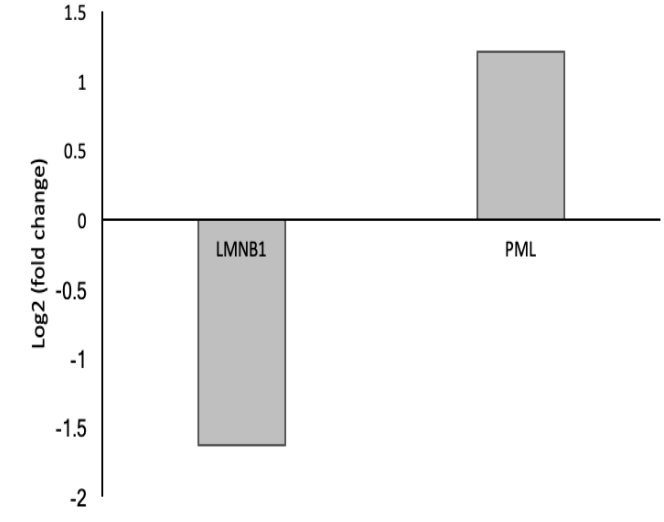

Figure 7.21 Change in the level of LMNB1 and PML proteins.
Level of LMNB1 and PML proteins was investigated in GFP-G3BP1 cells. LMNB1 was detected to decrease significantly (-1.6 (log2) fold change) from proliferative to senescent cells. PML was observed to increase (1.2 (log2) fold change) from proliferative to senescent cells.

7.4.3.3 Stress Granule Proteins

Following the protein and proteome analysis of proliferative and senescent GFP-G3BP1 cells, the change in stress granule proteins levels was investigated. G3BP1 is crucial for the process of stress granule formation. In our current study, G3BP1 protein levels was observed to decline from young to senescent GFP-G3BP1 cell. However, the detected change was insignificant (smaller than 2 and bigger than -2). Other RBPs including FXR1 and TDP43 did not show significant change (Figure 7.22).

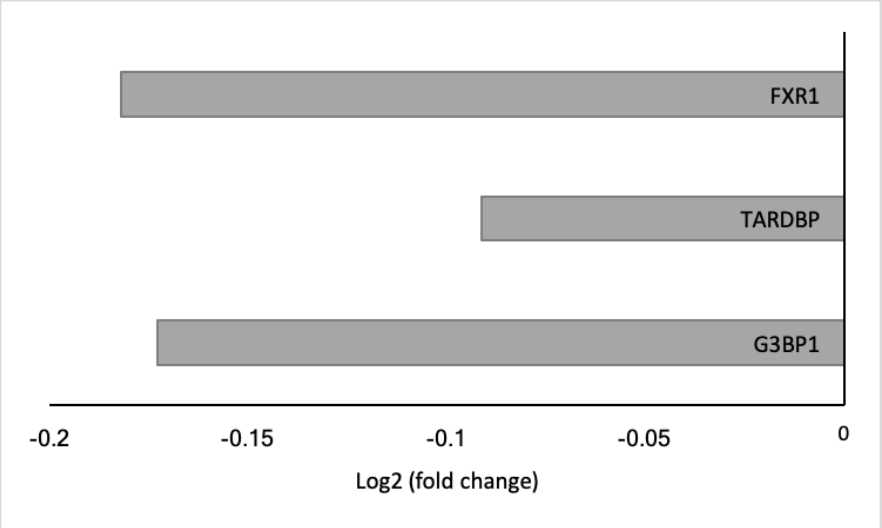

Figure 7.22 Change in the level of RNA-binding proteins from proliferative to senescent GFP-G3BP1 cells.

The level of G3BP1, TARDBP and FXR1 proteins were observed to decline from proliferative to senescent cells. They showed insignificant change.

7.4.4 GFP-G3BP2a Cells

As shown in chapter 5, senescence phenotype was observed in GFP-G3BP2a cells upon exposure to doxorubicin (200 nM) for 48 hours. Certain morphological and molecular alterations are associated with senescence (Campisi, 2005). In addition to morphological changes, levels of cyclin-dependent kinase inhibitors: p53, p21 and p16 were observed to increase in senescent cells (Campisi, 2005). Hence, the intensity of senescence markers in GFP-G3BP2a cells was observed to be lower than WT U2OS and ΔΔG3BP1/2 cells (discussed in chapter 5).

Following the investigation of the effect of senescence on proteins levels in WT U2OS cells and ΔΔG3BP1/2 cells, we then investigate whether re-constitution of ΔΔG3BP1/2 cells with G3BP2a (GFP-G3BP2a cells) slows senescence progression and the molecular changes associated senescence. Therefore, lysates were collected from proliferative (day 0) and senescent (day 9) GFP-G3BP2a cells. Quantitative proteomics analysis was performed using SWATH-MS. A total of 5689 proteins were identified in the lysates of GFP-G3BP2a cells. Approximately 2958 proteins were identified at a rate of adjusted p-value < 0.05. Proteomics analysis showed that 406 proteins were showing an absolute fold change higher than 2 or smaller than -2. I discuss these 406 significantly changing proteins with regard to senescence and stress granule formation. The role of the significantly changing proteins and proteins associated with senescence and stress granule formation are discussed here.

7.4.4.1 Most Highly Dysregulated Proteins

The proteins detected in the lysates of the cells were plotted in a volcano plot (Figure 7.23). The proteins that are coloured in grey are not showing a significant change (< 2 and > -2-fold change, adjusted p-value > 0.05). Nevertheless, the proteins that are marked as green are

significantly changing (>2 and <-2-fold change, adjusted p-value < 0.05). The highly changing proteins (> 4 and < -4-fold change) are coloured as red. It is not possible to label all significantly changing proteins, therefore, proteins higher than 4 and less than -4 are labelled (Figure 7.23).

Among the 2958 proteins that were detected in lysates of GFP-G3BP2a cells, 406 proteins were detected to significantly change. However, the levels of HBA1, SOD2, LAMB3, CDKN1A, CASP1, SYP, PCLO, OAS2, RRM2B, RND3, RRAD, APOC3, HBB, CEPT1 and THAP12 proteins were detected to significantly increase in senescent GFP-G3BP2a cells with a fold change higher than 4. In contrast, the levels of H1-1, H1-5, DUT, DHRS2, CDK1, TYMS, NCAPH, PRIM1, SPC24, UBE2T, TK1, UBE2V2, NUF2, DHFR, ANXA2, CHMP3, CIAO2A, RIOK2, COMMD8, GINS3, EPX and AP2S1 proteins were detected to significantly decrease in senescent GFP-G3BP2a cells with a fold change smaller than -4 (Figure 7.23).

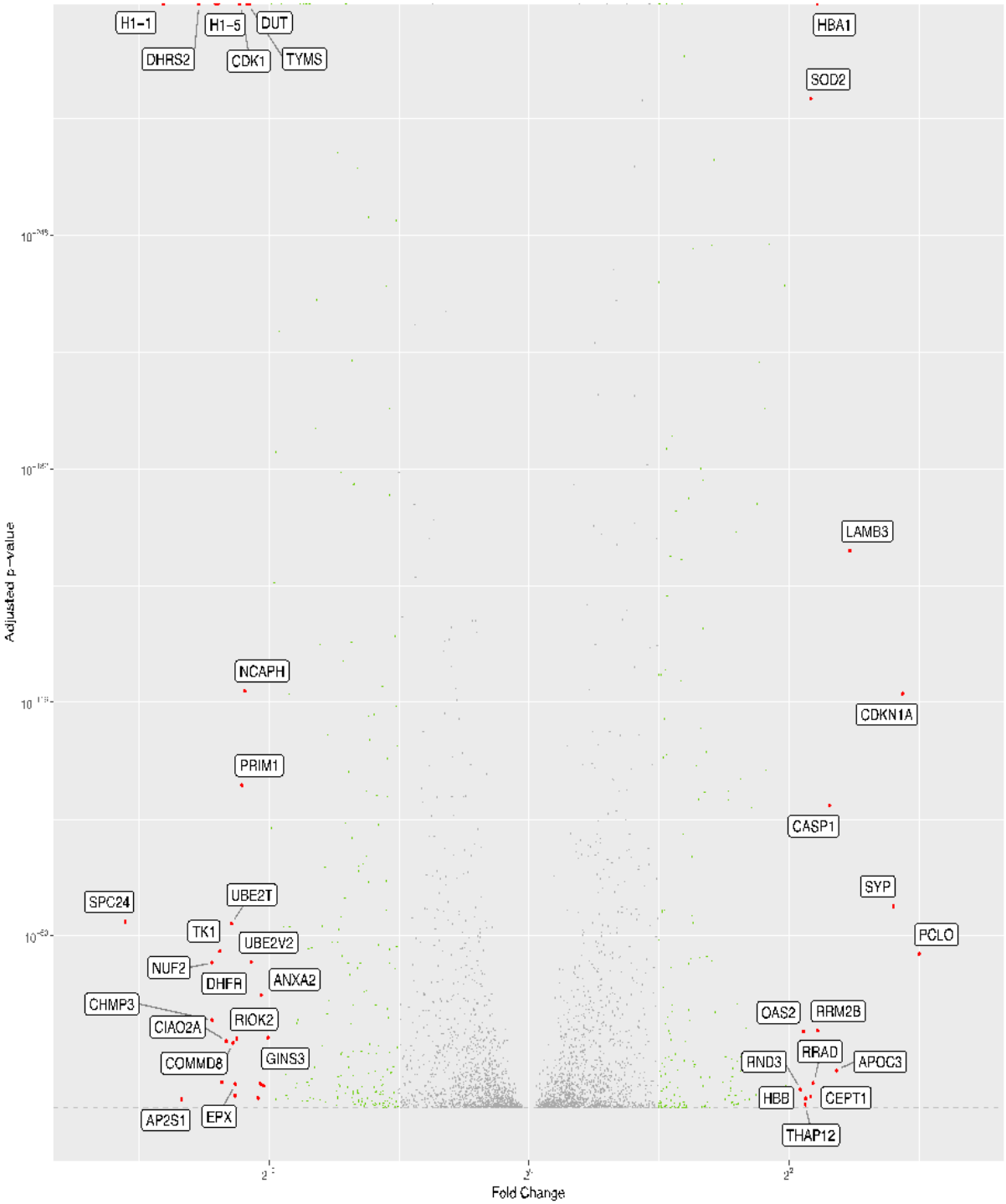

Figure 7.23 Proteomics analysis of proliferative (Day 0) and senescent (Day 9) GFP-G3BP2a cells.

The plot shows the distribution of proteins forming a volcano plot. The marks are showing the distribution of all 5689 proteins detected in lysates of GFP-G3BP2a cells. The grey marks are the proteins with no significant change. Green colour marks represent proteins with fold change bigger than 2 and smaller than -2. Green marks are the highly-dysregulated proteins from proliferative to senescent cells with a fold change >4 and <-4 (adjusted p-value ≤ 0.05).

7.4.4.1.1 Upregulated Proteins

Caspase-1 (CASP1) proteins are the significantly changing proteins in GFP-G3BP2a cells. Caspase proteins belong to protease enzymes family. They play a critical role in apoptosis and cell immunity inducing formation of canonical inflammasomes or pyroptosis (Uniprot.org). Hence, they are involved in cleaving proteins into mature peptides (Feng et al., 2004; Ball et al., 2020).

Caspase proteins are proteases that are linked to cellular networks involved in cell death and inflammation. Caspases are classified according to their involvement in pathways apoptosis or inflammation. Accordingly, casapase-3, caspase-6, caspase-7, caspase-8 and caspase-9 are involved in apoptosis. Whereas, caspase-1, caspase-4, caspase-5, and caspase-12 have been detected to play a role in inflammation (McIlwain et al., 2013). The caspases that are involved in inflammation play an essential role in mediating innate system responses. When these caspases are formed, they are inactive. However, they become active when they are engaged to recognition receptors forming inflammasome (Martinon et al., 2002; McIlwain et al., 2013).

Furthermore, our proteomics analysis showed significant increase in the levels of CASP1 and CASP4 proteins in cells when becoming senescent. CASP1 showed an increase of 2.3 (log2) fold change while an increase of 1.3 (log2) fold change was detected in levels of CASP4 protein. Other Caspase proteins including CASP3, CASP6, CASP7 and CASP8 showed a minor change from proliferative to senescent cells (Figure 7.24). Activation of CASP1 and CASP4 were observed to induce inflammation (Ball et al., 2020). CASP1 and CASP4 are classified as inflammatory caspases as they recruit immune cells to the sites of defected cells (McIlwain et al., 2013). Therefore, our data suggests that the upregulation of Caspase proteins 1 and 4 promotes cleavage of inflammatory cytokines, inducing inflammation.

Of the significantly changing proteins, Ribonucleoside-diphosphate reductase subunit M2 B (RRM2B) which showed an increase in senescent cells of 4.7-fold change. RRM2B is suggested to play an essential role in cell survival. It is suggested to repair DNA damage in a p53/TP53-dependent manner during senescence (Cho et al., 2015). Moreover, it acts as a supplier of deoxyribonucleotides for the process of DNA repair in cells arrested at G1 or G2 phase of cell cycle (Uniprot.org). RRM2B exists in nucleus and cytoplasm as it translocates from cytoplasm to nucleus during exposure to DNA damage-inducing agents (Uniprot. org). Therefore, the upregulation of RRM2B in senescent GFP-G3BP2a cells suggests the involvement of this protein to repair the damage in DNA caused by doxorubicin treatment.

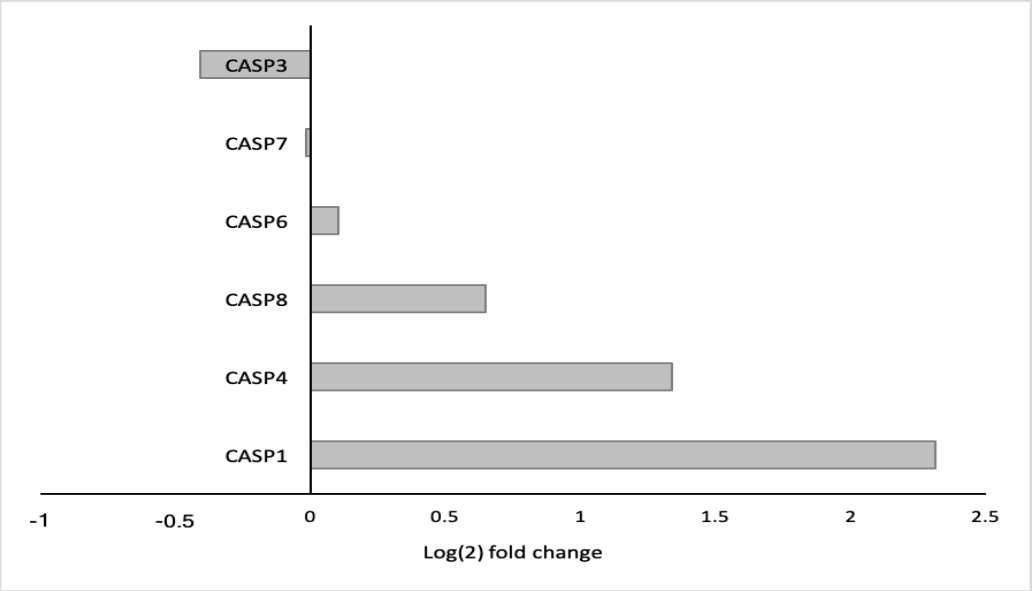

Figure 7.24 Level of Caspase proteins varies from proliferative to senescent GFP-G3BP2a cells.

Caspase-1 (CASP1) and Caspase-4 (CASP4) proteins were detected to increase significantly from proliferative to senescent GFP-G3BP2a cells. CASP1 and CASP4 showed a change of 2.3 and 1.3 log (2) fold change, respectively. CASP3, CASP6, CASP7 and CASP8 showed insignificant change between proliferative and senescent cells.

7.4.4.1.2 Upregulated Pathways from Proliferative to Senescent GFP-G3BP2a Cells

The significantly changing proteins in response to senescence induction were tested for statistical overrepresentation using enrichGO after FDR control. Based on the GO enrichment, the significantly upregulated proteins from proliferative to senescent GFP-G3BP2a cells were enriched in 20 terms in the category biological processes. The proteins were enriched according to gene count which is the number of enriched genes in GO term (Figure 7.25).

GO enrichment showed that the highly-upregulated proteins in senescent GFP-G3BP2a cells were involved in regulation of endopeptidase activity, small molecule catabolic process, regulation of multi-organism process, negative regulation of proteolysis, extracellular structure organization, intrinsic apoptotic signalling pathway, steroid metabolic process, aging, fatty acid metabolic process, secondary alcohol metabolic process, pyridine-containing compound metabolic process, carbohydrate derivative catabolic process, oxidoreduction coenzyme metabolic process and regulation of myeloid leukocyte mediated immunity (Table 7.10).

The proteomics analysis of lysates from proliferative and senescent GFP-G3BP2a cells showed that the overrepresentation of the biological process term: regulation of endopeptidase activity (GO:0052548). Hence, it involves any processes that regulate endopeptidase activity. Endopeptidase is known to catalyse the break of peptide bonds within a protein (Uniprot. org; Weiss et al., 2020). Proteomics analysis and statistical overrepresentation test revealed that 15 proteins are involved in the process of endoplasmic activity regulation. Of the proteins involved in the fatty acid metabolic process: SERBINA1, SERPINB5, PML, FAS, CASP4 and CASP1 are significantly changing proteins (fold-change higher than 2). Hence, our observation suggests the differences in the endopeptidase activity is associated with senescence in GFP-G3BP2a cells.

Moreover, the small molecule catabolic process was observed to be overrepresented in senescent GFP-G3BP2a cells. Small molecule metabolic process (GO:0044281) is known as the pathways and chemical reactions that involve small molecules or any low molecular weight molecule (Uniprot. org). Thus, a total of 14 proteins were annotated to this term including RBKS, ACAD11, TIGAR, APOE, ACOT8, PNP, IL4I1, ACAA1, CD44 and ABAT. These proteins are significantly changing proteins (fold-change higher than 2). This data suggests that the molecular changes of small molecules increases with senescence in GFP-G3BP2a cells.

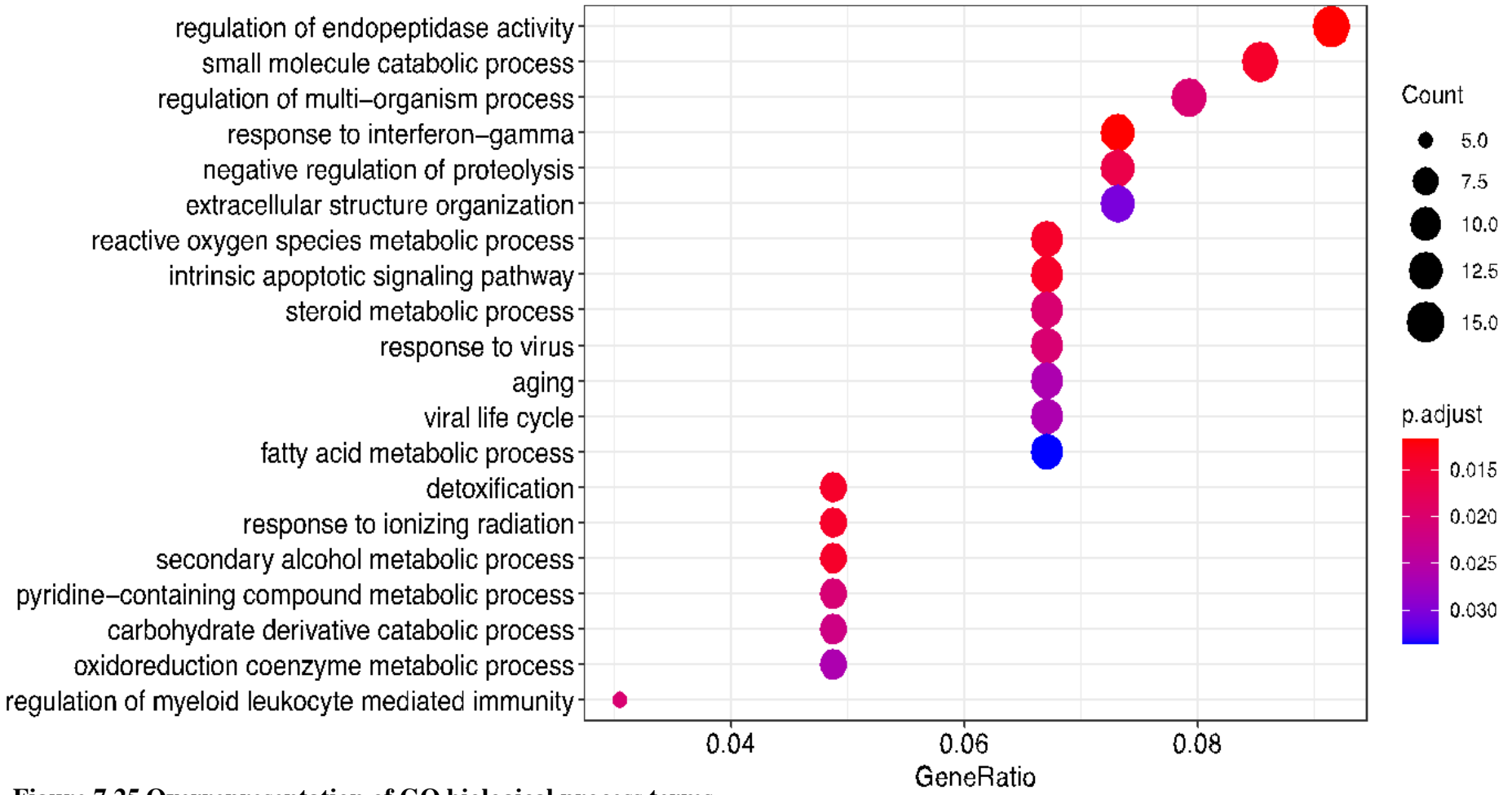

Figure 7.25 Overrepresentation of GO biological process terms.

GO biological process terms found to be statistically overrepresented upon doxorubicin treatment (senescence induction). Proteins were tested against all detected proteins in the data set using enrichGO. Count is the number genes that are enriched in each GO term. Gene ratio is a percentage of differentially upregulated genes in each GO term.

7.4.4.1.3 Downregulated Proteins

The Histone H1 (H1-1 and H1-5) proteins are involved in several pathways including chromatin remodelling, double-strand DNA binding, DNA methylation and nucleosome spacing (Uniprot.org). The levels of these proteins showed a decrease of -3.1 to -1.4 (log2) fold change in senescent cells (Figure 7.26). Hence, the decrease in the levels of these proteins results in negative regulation of DNA replication and thus inhibition of cell division. The downregulation of Histone H1 proteins is suggested to correlate with senescence process.

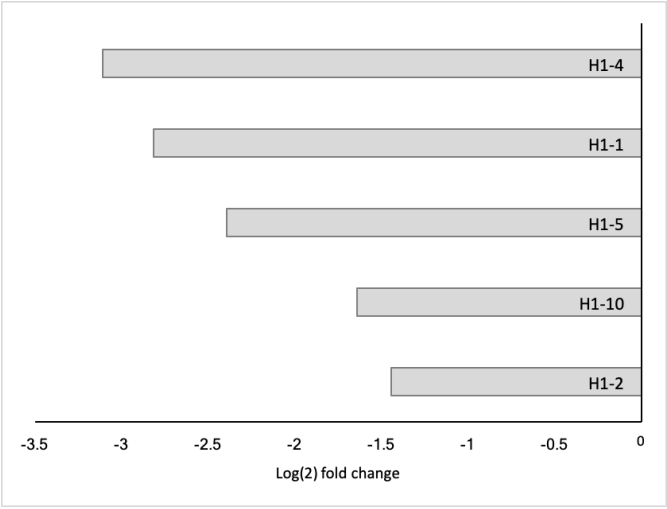

Figure 7.26 Level of Histone H1 proteins in GFP-G3BP2a cells. H1-4 protein was detected to decline significantly (-3.1 (log2) fold change) from proliferative to senescent cells. Levels of H1-1, H1-5, H1-10 and H1-2 proteins were also reduced significantly in senescent cells.

The proteomics data revealed a decrease in Annexin A2 (ANXA2) protein levels in cells when becoming senescent. It showed a decrease of 2.1 (log2) fold change. ANXA2 is known to play a role in regulating cell growth. It has been detected in several cancer types. Knockdown of ANXA2 gene led to reduced DNA synthesis and cell division. Therefore, it is suggested that ANXA2 protein is an essential regulator of cell proliferation (Huang et a., 2005; Wang and Lin 2014). Our observation suggests that downregulation of ANXA2 is correlated with senescence in GFP-G3BP2a cells.

7.4.4.1.4 Downregulated Pathways from Proliferative to Senescent GFP-G3BP2a Cells

Furthermore, the significantly changing proteins in response to senescence induction were tested for statistical underrepresentation using enrichGO after FDR control. Gene ontology enrichment showed that the significantly downregulated proteins from proliferative to senescent GFP-G3BP2a cells were enriched in 20 terms in the category biological processes. The proteins were enriched according to the number of enriched genes in GO term which is known as gene count (Figure 7.27).

GO enrichment revealed that the highly-downregulated proteins in senescent GFP-G3BP2a cells were involved in the following biological processes: chromosome segregation, organelle fission, DNA replication, DNA conformation change, regulation of chromosome organization, DNA recombination, cell cycle G1/S phase transition, positive regulation of cell cycle, protein-DNA complex subunit organization, regulation of DNA metabolic process, DNA biosynthetic process, microtubule cytoskeleton organization involved in mitosis, spindle organization, cell cycle checkpoint and DNA damage response (Table 7.11).

Most of the pathways that were observed to be downregulated in senescent GFP-G3BP2a cells are involved in DNA synthesis and replication, and cell cycle regulation. It indicates that DNA replication and processes required for cell division are inhibited. The downregulation is pronounced in cells of day 9 post-doxorubicin treatment which suggests that cells are senescent.

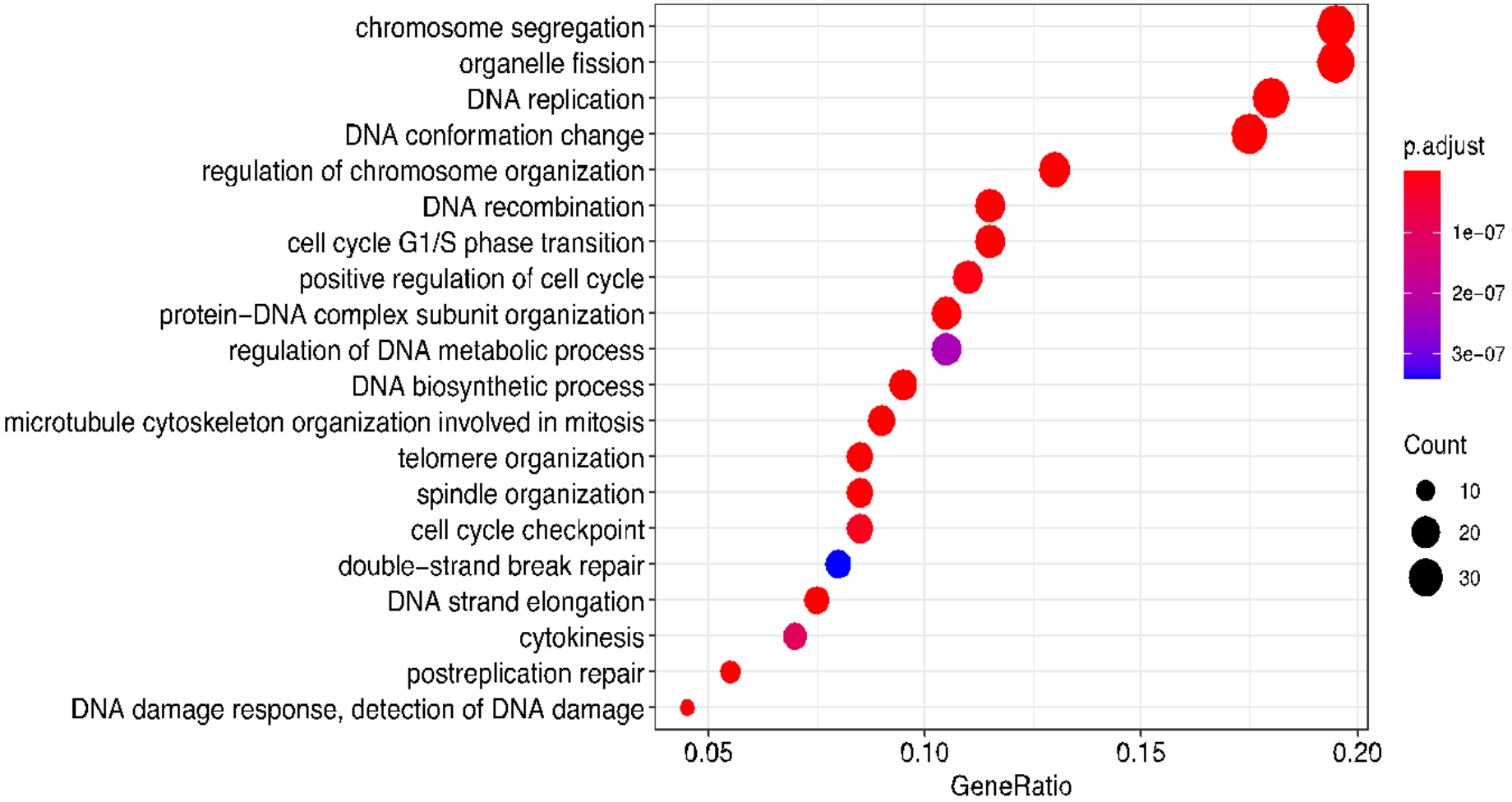

Figure 7.27 Biological processes that are underrepresented in senescence.

GO biological process terms that are found to be statistically underrepresented upon doxorubicin treatment (senescence induction) in GFP-G3BP2a cells. Proteins were tested against all detected proteins in the data set using enrichGO. Count is the number of genes that are enriched in each GO term. Gene ratio is a percentage of differentially downregulated genes in each GO term.

7.4.4.2 Senescence Associated Proteins

To induce senescence phenotype, activation of certain proteins is required. These proteins are known to be associated with senescence including cyclin-dependent kinase inhibitors: p53, p21 and p16 (van Deursen, 2014; Gorgoulis et al., 2019; Nassrally et al., 2019). Thus, cyclin-dependent kinase inhibitors are known to regulate cell growth and promote senescence phenotype (Puente et al., 2014; Aix et al., 2016). We here investigate the changes in the levels of kinase inhibitors between proliferative and senescent GFP-G3BP2a cells.

7.4.4.2.1 Cyclin-Dependent Kinase Inhibitors

Proteomics analysis revealed a significant increase (2.9 log (2) fold change) in p21 protein levels was detected in senescent GFP-G3BP2a cells. However, insignificant change in TP53, TP53BP1 and CDKN2AIP in GFP-G3BP2a cells when becoming senescent (Figure 7.28).

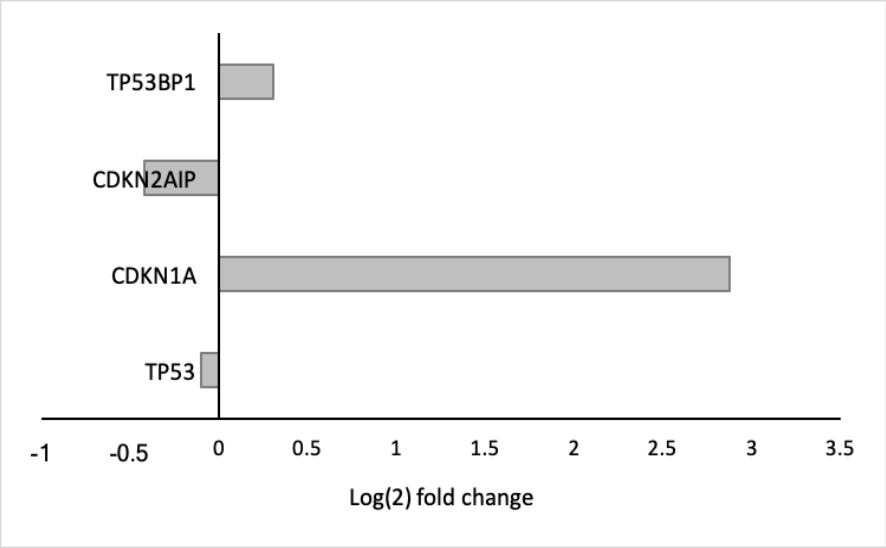

Figure 7.28 Level of cyclin-dependent kinase inhibitors varies from proliferative to senescent GFP-G3BP2a cells.

CDKN1A (p21) protein was detected to increase significantly (2.9 (log2) fold change) from proliferative to senescent cells. TP53, TP53BP1 and CDKN2AIP proteins showed insignificant change in cells when becoming senescent.

Thus, our proteomics data showed that the levels of cyclin-dependent kinase inhibitors: p53, p21 and p16 varies. It depends on the stage of senescence. It has been detected by several studies that high levels of p53 protein induces activation of p21. Following activation of p21, p53 levels decline (Georgakilas et al., 2017). Sustained rise of p21 is required to induce changes associated with senescence. P21 activates p16 which is required to maintain senescence phenotype induced by p21 protein (Campisi, 2005). Therefore, our observations are confirming the findings of other studies. The significant increase in p21 levels but not p53 or p16 proteins suggests that cells are senescent. In order to observe the changes in p16 protein levels, cells are required to be kept for a longer time (day 14 or 21 post-doxorubicin exposure) to extract lysates from cells and perform proteomics analysis.

7.4.4.2.2 PML and LMNB1

Protein PML (PML) (Rokudai et al., 2013) and Lamin-B1 (LMNB1) (Freund et al., 2012) are considered as senescence associated proteins. They have been used as markers for senescence. LMNB1 has been observed to decline in senescent cells when compared to proliferative cells (Freund et al., 2012). Hence, our data revealed that the levels of LMNB1 protein show insignificant change from proliferative to senescent GFP-G3BP2a cells (Figure 7.29).

Furthermore, PML protein is of the several proteins that are dysregulated during senescence. Of the cellular processes that PML is suggested to be involved in are DNA damage response, tumour suppression and senescence (Uniprot.org). It plays a role in DNA damage response by positively regulating p53 protein which in turn results in cell cycle arrest. Moreover, PML has been detected to dramatically increase in ras-arrested fibroblast cells (Rokudai et al., 2013). Consistent with previous reports (Ferbeyre et al., 2000; Rokudai et al., 2013), senescent GFP-G3BP2a cells showed a significant increase in the levels of PML protein compared to

proliferative cells. The levels of PML protein showed a log2 fold change of 1.4 from proliferative to senescent cells (Figure 7.29).

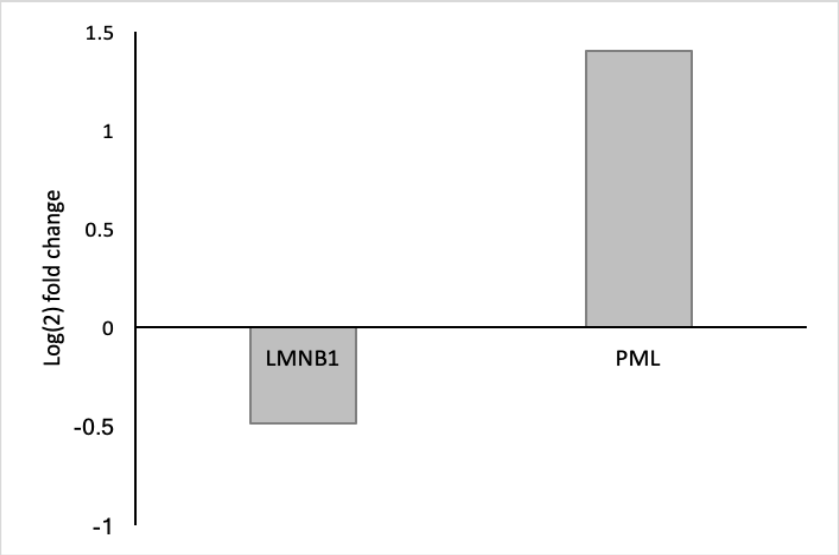

Figure 7.29 Change in the level of LMNB1 and PML proteins in GFP-G3BP2a cells. Level of LMNB1 and PML proteins was investigated in GFP-G3BP2a cells. LMNB1 showed insignificant change from proliferative to senescent cells. PML was observed to increase (1.4 (log2) fold change) from proliferative to senescent cells.

7.4.4.3 Stress Granule Proteins

Following the protein and proteome analysis of proliferative and senescent GFP-G3BP2a cells, the change in stress granule protein levels was investigated. G3BP plays a crucial role in stress granule formation upon exposure to stress. In our current study, G3BP2 protein levels was observed to increase from proliferative to senescent GFP-G3BP2a cells. However, the detected change was insignificant (smaller than 2 and bigger than -2) (Figure 7.30). Levels of other RBPs including USP10, CAPRIN1 and FXR1 showed insignificant change.

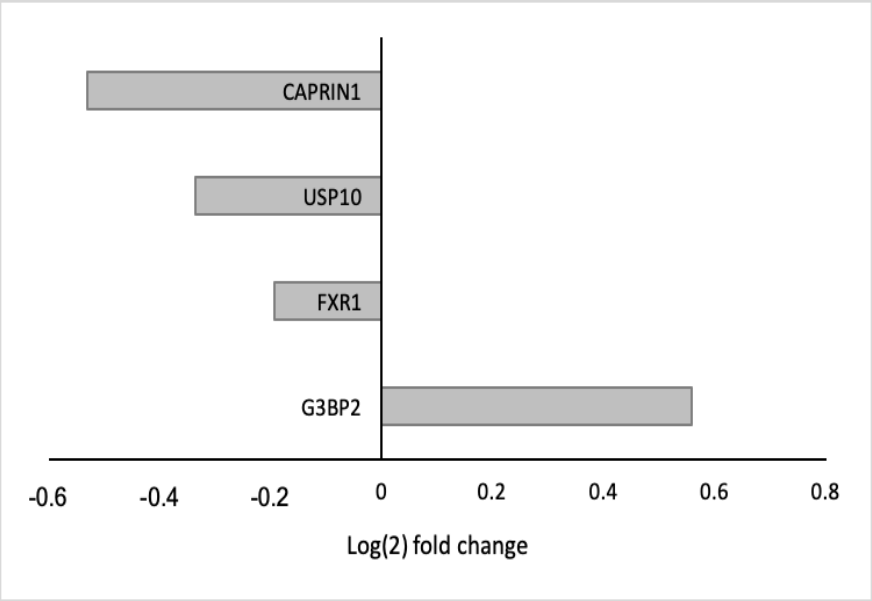

Figure 7.30 Change in the level of RNA-binding proteins from proliferative to senescent GFP-G3BP2a cells.

The level of G3BP2, FXR1, USP10 and Caprin1 proteins was observed to show minor changes from proliferative to senescent cells. G3BP2 showed an increase of 0.6-(log2) fold change in senescent cells. While CAPRIN1 showed a decrease of 0.5-(log2) fold change.

7.4.5 GFP-G3BP2b Cells

Senescence phenotype was induced in GFP-G3BP2b cells upon exposure to doxorubicin (200 nM) for 48 hours (discussed in chapter 5). Certain morphological and molecular changes are associated with senescence (Campisi, 2005). In addition to enlarged cell size and fragmented nuclei, levels of cyclin-dependent kinase inhibitors: p53, p21 and p16 have been observed to increase in senescent cells (Campisi, 2005). Hence, we here investigate the changes of proteins associated with senescence and stress granules between proliferative and senescent GFP-G3BP2b cells.

Following the investigation of the effect of senescence on proteins levels in WT U2OS cells and ΔΔG3BP1/2 cells, we then investigate whether re-constitution of ΔΔG3BP1/2 cells with G3BP2b (GFP-G3BP2b cells) slows/accelerates senescence progression and occurrence of the molecular changes associated with senescence. Therefore, lysates were collected from proliferative (day 0) and senescent (day 9) GFP-G3BP2b cells. Quantitative proteomics analysis was performed using SWATH-MS. A total of 5687 proteins were identified in the lysates of GFP-G3BP2b cells. Approximately 2859 proteins were identified at a rate of adjusted p-value < 0.05. Proteomics analysis showed that 250 proteins were showing an absolute fold change higher than 2 or smaller than -2. I discuss these 250 significantly changing proteins with regard to senescence and stress granule formation. Moreover, the role of the significantly changing proteins are discussed here.

7.4.5.1 Most Highly Dysregulated Proteins

The proteins detected in the lysates of the cells were plotted in a volcano plot (Figure 7.31). The proteins that are coloured in grey are not showing a significant change (< 2 and > -2-fold change, adjusted p-value > 0.05). Nevertheless, the proteins that are marked as green are

significantly changing (>2 and <-2-fold change, adjusted p-value < 0.05). The highly changing proteins (> 4 and < -4-fold change) are coloured as red. It is not possible to label all significantly changing proteins, therefore, proteins higher than 4 and less than -4 are labelled (Figure 7.31).

Among the 2859 proteins that were detected in lysates of GFP-G3BP2a cells, 250 proteins were detected to significantly change. However, the levels of GDF15, APOC3, MMP1, CD68, NR0B1, FTL, TBR1 and PTK2B proteins were detected to be significantly upregulated in senescent GFP-G3BP2b cells with a fold change higher than 4. In contrast, the levels of H1-1, L1CAM, PHGDH, CDK1, H1-5, TK1, TYMS, PBK, RRM2, GPA33, UBE2V1, SPC24, VMA21, FGFR1OP and A1BG proteins were detected to significantly decrease in senescent GFP-G3BP2b cells with a fold change smaller than -4 (Figure 7.31).

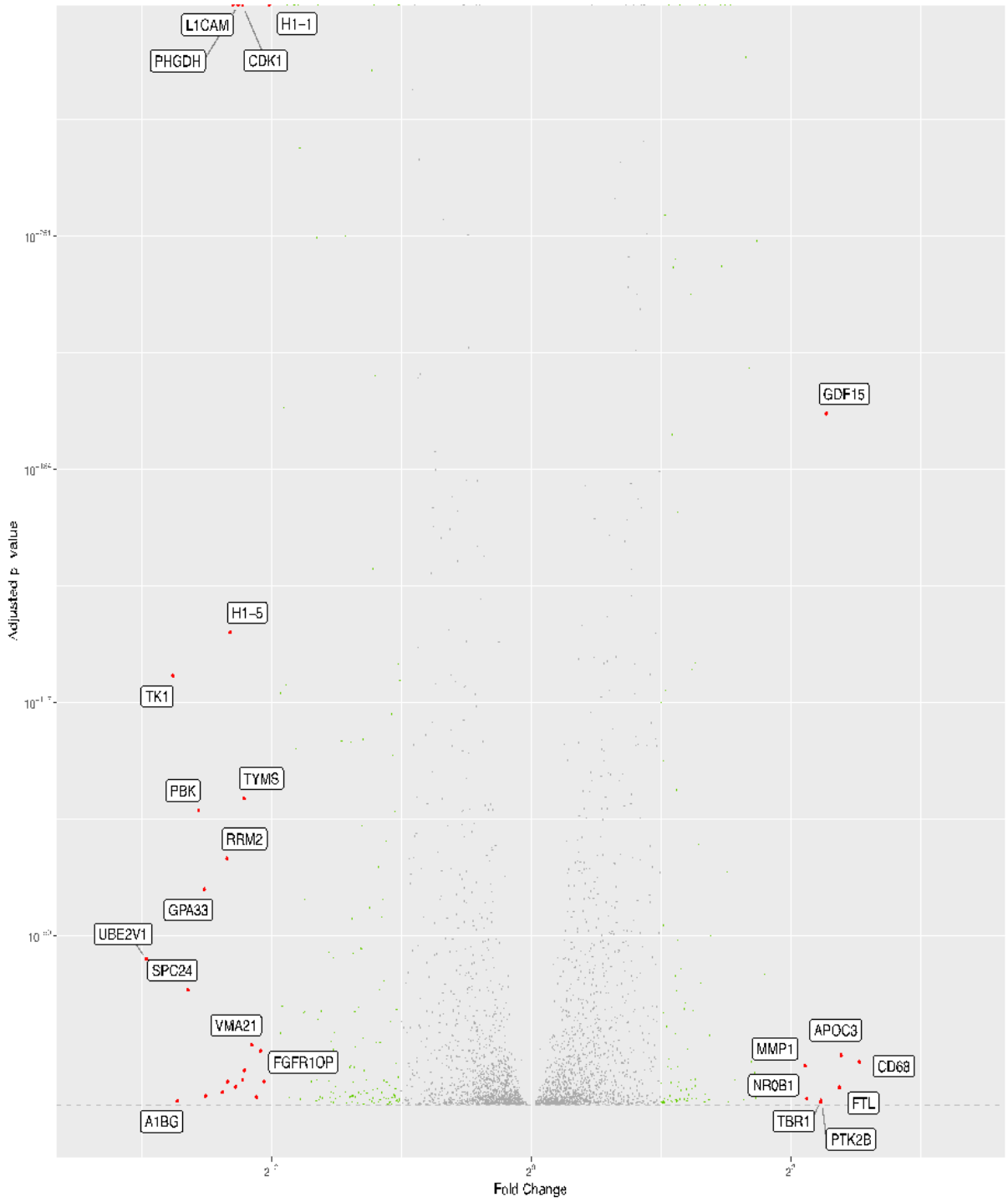

Figure 7.31 Proteomics analysis of proliferative (Day 0) and senescent (Day 9) GFP-G3BP2b cells.

The plot shows the distribution of proteins forming a volcano plot. The marks are showing the distribution of all 5687 proteins detected in lysates of GFP-G3BP2b cells. The grey marks are the proteins with no significant change. Green colour marks represent proteins with fold change bigger than 2 and smaller than -2. Red marks are the highly-dysregulated proteins from proliferative to senescent cells with a fold change >4 and <-4 (adjusted p-value ≤ 0.05).

7.4.5.1.1 Upregulated Proteins

Of the significantly changing proteins in cells is growth/differentiation factor-15 (GDF15). Our proteomics analysis showed significant increase in the levels of GDF15 protein in GFP-G3BP2b cells when becoming senescent. GDF15 showed an increase of 2.3 (log2) fold change (Figure 7.48). Hence, GDF15 protein is also known as macrophage inhibitory cytokine-1. It has been observed to be induced when cells are exposed to stressors, to maintain cellular homeostasis. Additionally, it was suggested that GDF15 plays a role in immune responses and acts as an immune checkpoint (Wischhusen et al., 2020). Therefore, our data suggests that GDF15 upregulation is required in order to maintain cellular homeostasis.

Of the significantly changing proteins, Apolipoprotein C-III (APOC3) which showed an increase in senescent cells of 2.4 (log2) fold change. APOC3 is suggested to play an essential role in fatty acid homeostasis in the cell. It is suggested to be involved in cholesterol homeostasis, lipoprotein metabolic process, regulation of lipid metabolic/catabolic processes and regulation of receptor-mediated endocytosis (Uniprot. org). Additionally, changes in the levels of APOC3 have been observed in aged mice (Araki et al., 2004). The increased expression of APOC3 has been associated with cardiovascular disorders, lipoprotein profile and longevity (Atzmon et al., 2006). Therefore, the upregulation of APOC3 in senescent GFP-G3BP2b cells suggests the association of APOC3 to senescence phenotype.

7.4.5.1.2 Upregulated Pathways from Proliferative to Senescent GFP-G3BP2b Cells

The significantly changing proteins in response to senescence induction were tested for statistical overrepresentation using enrichGO after FDR control. Based on the GO enrichment, the significantly upregulated proteins from proliferative to senescent GFP-G3BP2b cells were

enriched in 20 terms in the category biological processes. The proteins were enriched according to gene count which is the number of enriched genes in GO term (Figure 7.32).

GO enrichment showed that the highly-upregulated proteins in senescent GFP-G3BP2b cells were involved in regulation of endopeptidase activity, response to interferon-gamma, regulation of multi-organism process, lipid catabolic process, regulation of proteolysis, fatty acid metabolic process, small molecule catabolic process, response to reactive oxygen species, response to type I interferon, secondary alcohol metabolic process, sterol metabolic process, response to dietary access, negative regulation of signal transduction by p53 class mediator and acylglycerol homeostasis (Table 7.12).

The proteomics analysis of lysates from proliferative and senescent GFP-G3BP2b cells showed that the overrepresentation of the biological process term: regulation of endopeptidase activity (GO:0052548). Hence, it involves any processes that regulate endopeptidase activity. Endopeptidase is known to catalyse the break of peptide bonds within a protein (Uniprot. org; Weiss et al., 2020). Proteomics analysis and statistical overrepresentation test revealed that 11 proteins are involved in the process of endoplasmic activity regulation. Of the proteins involved in the fatty acid metabolic process: CD44, CRYAB, GPX1, FAS, CASP1 and TIMP1 are significantly changing proteins (fold-change higher than 2). Hence, our observation suggests the differences in the endopeptidase activity is associated with senescence in GFP-G3BP2b cells.

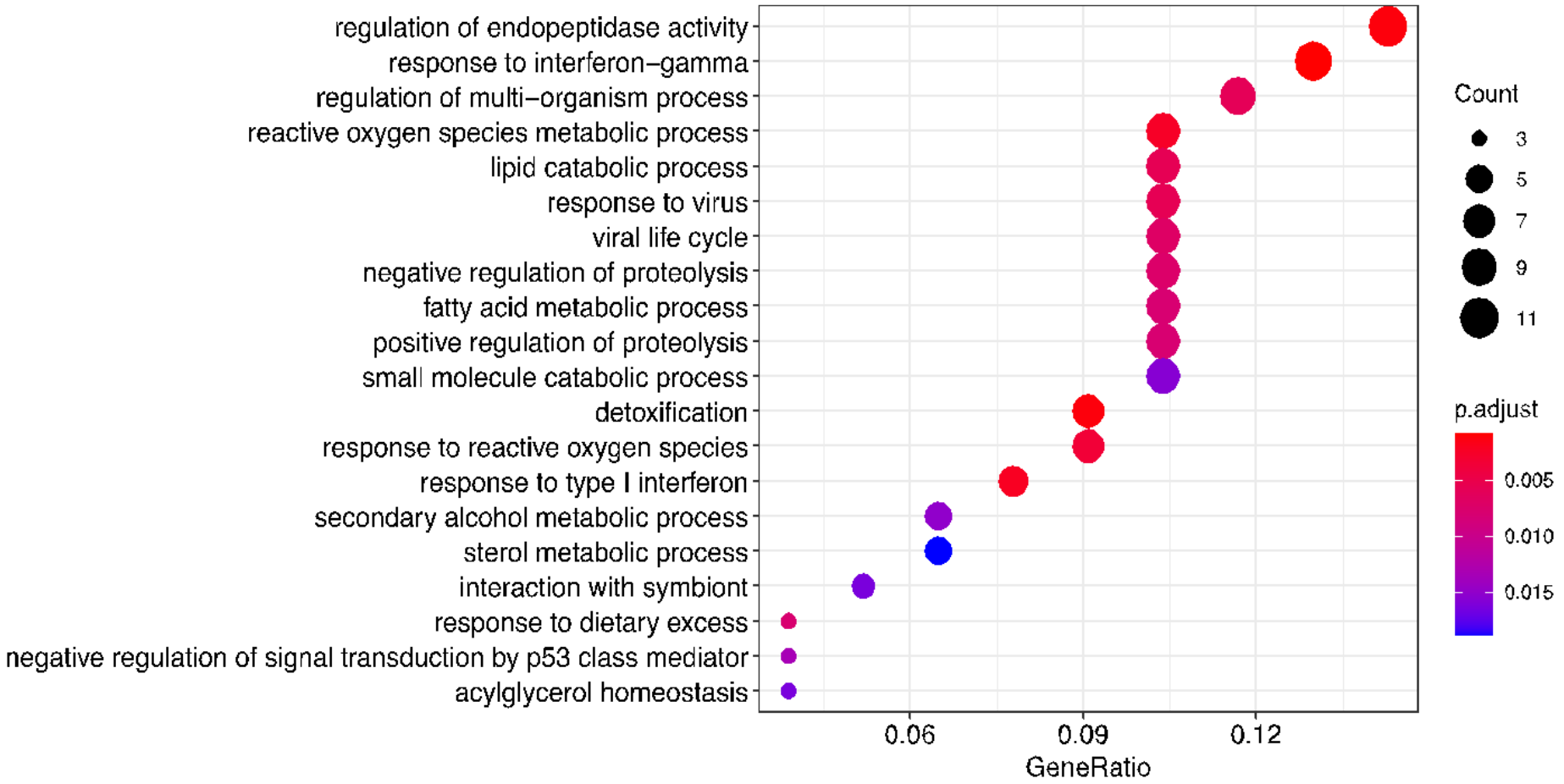

Figure 7.32 Overrepresentation of GO biological process terms.

GO biological process terms found to be statistically overrepresented upon doxorubicin treatment (senescence induction). Proteins were tested against all detected proteins in the data set using enrichGO. Count is the number genes that are enriched in each GO term. Gene ratio is a percentage of differentially upregulated genes in each GO term.

7.4.5.1.3 Downregulated Proteins

The Histone H1 (H1-5, H1-1 and H1-10) proteins are involved in several pathways including chromatin remodelling, double-strand DNA binding, DNA methylation and nucleosome spacing (Uniprot.org). The levels of these proteins showed a decrease of -2.3 to -1.3 (log2) fold change in senescent cells (Figure 7.33). Hence, the decrease in the levels of these proteins results in negative regulation of DNA replication and thus inhibition of cell division. The downregulation of Histone H1 proteins is suggested to correlate with senescence process.

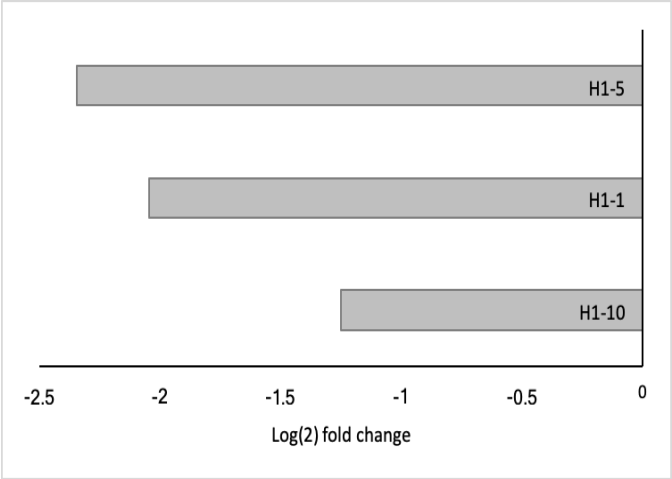

Figure 7.33 Level of Histone H1 proteins in GFP-G3BP2b cells. H1-5 protein was detected to decline significantly (-3.1 (log2) fold change) from proliferative to senescent cells. Levels of H1-1, H1-5, H1-10 and H1-2 proteins were also reduced significantly in senescent cells.

The proteomics data revealed decrease in Cyclin-dependent kinase 1 (CDK1) and Cyclin-dependent kinase 6 (CDK6) proteins' levels in cells when becoming senescent. A decrease of -2.1 and -1.4 (log2) fold change in CDK1 and CDK6, respectively (Figure 7.34). CDK is known to play a role in regulating the cell cycle. It modulates the centrosome cycle, regulating G1 progress and G1-S transition (Uniprot.org). They are essential for cell differentiation, cell proliferation, cell cycle arrest and G1/S transition of mitotic cell cycle (Uniprot. org). Our observation suggests that downregulation of CDK1 and CDK6 is correlated with senescence in GFP-G3BP2b cells.

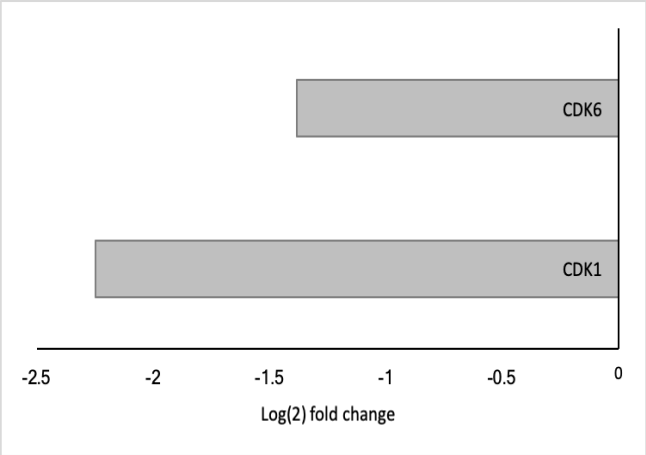

Figure 7.34 Level of CDK proteins in GFP-G3BP2b cells.
CDK1 protein was detected to decline significantly (-2.2 (log2) fold change) from proliferative to senescent cells. Levels of CDK6 protein was also reduced significantly (-1.4 (log2) fold change in senescent cells.

7.4.5.1.4 Downregulated Pathways from Proliferative to Senescent GFP-G3BP2b Cells

The significantly changing proteins in response to senescence induction were tested for statistical underrepresentation using enrichGO after FDR control. Gene ontology enrichment showed that the significantly downregulated proteins from proliferative to senescent GFP-G3BP2b cells were enriched in 20 terms in the category of biological processes. The proteins were enriched according to the number of enriched genes in the GO term which is known as gene count (Figure 7.35).

GO enrichment revealed that the highly-downregulated proteins in senescent GFP-G3BP2b cells were involved in the following biological processes: organelle fission, DNA replication, chromosome segregation, DNA conformation change, cell cycle G1/S phase transition, regulation of chromosome organization, negative regulation of organelle organization, anatomical structure homeostasis, microtubule cytoskeleton organization involved in mitosis, DNA biosynthetic process, DNA recombination, protein-DNA complex subunit organization, positive regulation of cell cycle, spindle organization, DNA strand elongation, chromosome localization and deoxyribonucleotide metabolic process (Table 7.13).

Most of the pathways that were observed to be downregulated in senescent GFP-G3BP2b cells are involved in DNA synthesis and replication, and cell cycle regulation. It indicates that DNA replication and processes required for cell division are inhibited. The downregulation is pronounced in cells of day 9 post-doxorubicin treatment which suggests that cells are senescent.

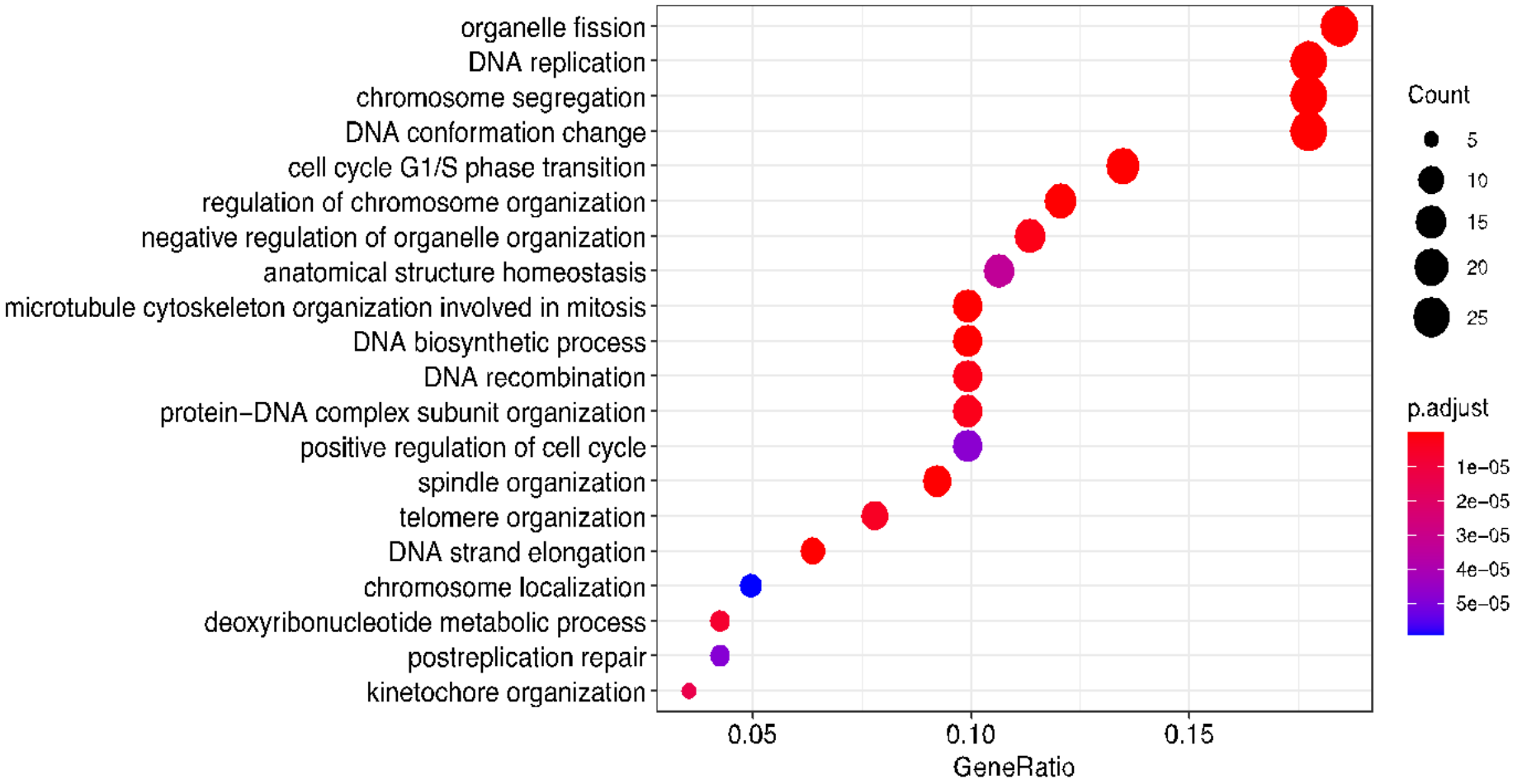

Figure 7.35 Biological processes that are underrepresented in senescence.

GO biological process terms that are found to be statistically underrepresented upon doxorubicin treatment (senescence induction) in GFP-G3BP2b cells. Proteins were tested against all detected proteins in the data set using enrichGO. Count is the number of genes that are enriched in each GO term. Gene ratio is a percentage of differentially downregulated genes in each GO term.

7.4.5.2 Senescence Associated Proteins

To induce senescence phenotype, activation of certain proteins is required. These proteins are known to be associated with senescence including cyclin-dependent kinase inhibitors: p53, p21 and p16 (van Deursen, 2014; Gorgoulis et al., 2019; Nassrally et al., 2019). Thus, cyclin-dependent kinase inhibitors are known to regulate cell growth and promote senescence phenotype (Aix et al., 2016; Puente et al., 2014). We here investigate the changes in the levels of kinase inhibitors between proliferative and senescent GFP-G3BP2b cells. Moreover, other senescence associated proteins such as PML and LMNB1 are investigated.

7.4.5.2.1 Cyclin-Dependent Kinase Inhibitors

Proteomics analysis revealed insignificant change in Tumour protein p53-inducible protein 11 (TP53I11) and Tumour protein p53-binding protein 1 (TP53BP1) in GFP-G3BP2b cells when becoming senescent. Nevertheless, a significant increase (1.4 log (2) fold change) in p21 protein levels was detected in senescent GFP-G3BP2b cells. The change in the levels of Cyclin Dependent Kinase Inhibitor 2A-interacting protein (CDKN2AIP) was detected to be insignificant from proliferative to senescent GFP-G3BP2b cells (Figure 7.36).

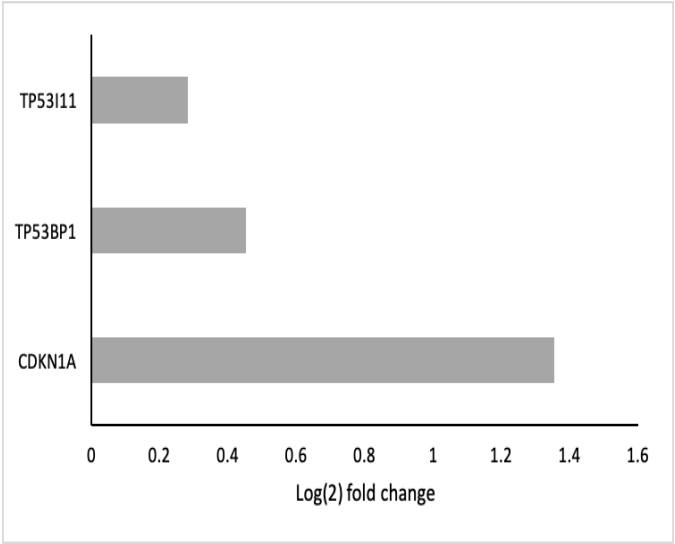

Figure 7.36 Level of cyclin-dependent kinase inhibitors in GFP-G3BP2b cells.

CDKN1A (p21) protein was detected to increase significantly (1.4 (log2) fold change) from proliferative to senescent cells. TP53I11 and TP53BP1 proteins showed insignificant change in cells when becoming senescent.

7.4.5.2.2 PML and LMNB1

Protein PML (PML) (Rokudai et al., 2013) and Lamin-B1 (LMNB1) (Freund et al., 2012) are considered as senescence associated proteins. They have been used as markers for senescence. LMNB1 has been observed to decline in senescent cells when compared to proliferative cells (Freund et al., 2012). Hence, our data revealed that the levels of LMNB1 protein show insignificant change from proliferative to senescent GFP-G3BP2b cells (Figure 7.37).

Furthermore, PML protein is of the several proteins that are dysregulated during senescence. Of the cellular processes that PML is suggested to be involved in are DNA damage response, tumour suppression and senescence (Uniprot.org). It plays a role in DNA damage response by positively regulating p53 protein which in turn results in cell cycle arrest. Moreover, PML has been detected to dramatically increase in ras-arrested fibroblast cells (Rokudai et al., 2013). Consistent with previous reports (Ferbeyre et al., 2000; Rokudai et al., 2013), senescent GFP-G3BP2b cells showed a significant increase in the levels of PML protein compared to proliferative cells. The levels of PML protein showed a log2 fold change of 1 from proliferative to senescent cells (Figure 7.37).

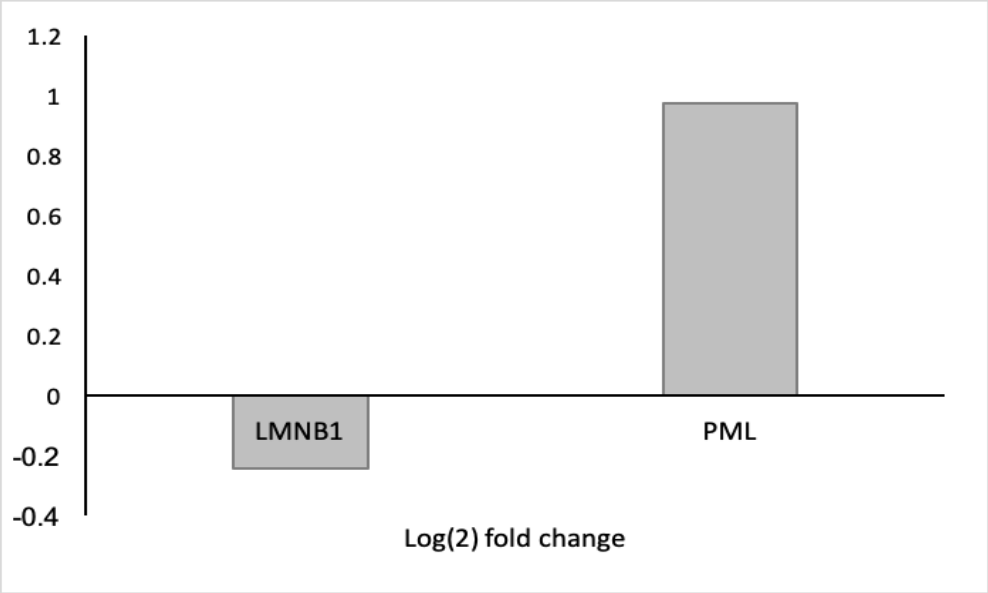

Figure 7.37 Change in the level of LMNB1 and PML proteins in GFP-G3BP2b cells.

Level of LMNB1 and PML proteins was investigated in GFP-G3BP2b cells. LMNB1 showed insignificant change from proliferative to senescent cells. PML was observed to increase (1 (log2) fold change) from proliferative to senescent cells.

7.4.5.3 Stress Granule Proteins

Following the protein and proteome analysis of proliferative and senescent GFP-G3BP2b cells, the change in stress granule protein levels was investigated. G3BP plays a crucial role in stress granule formation upon exposure to stress. Knockout of G3BP1/2 inhibited stress granule formation. However, re-constitution of cells with G3BP2b solely rescued formation of stress granules in GFP-G3BP2b cells (discussed in chapter 4). In our current study, G3BP2 protein levels were observed to decrease from proliferative to senescent GFP-G3BP2a cell. However, the detected change was insignificant (smaller than 2 and bigger than -2). Other RBPs including USP10, CAPRIN1 and HUR showed insignificant change (Figure 7.38).

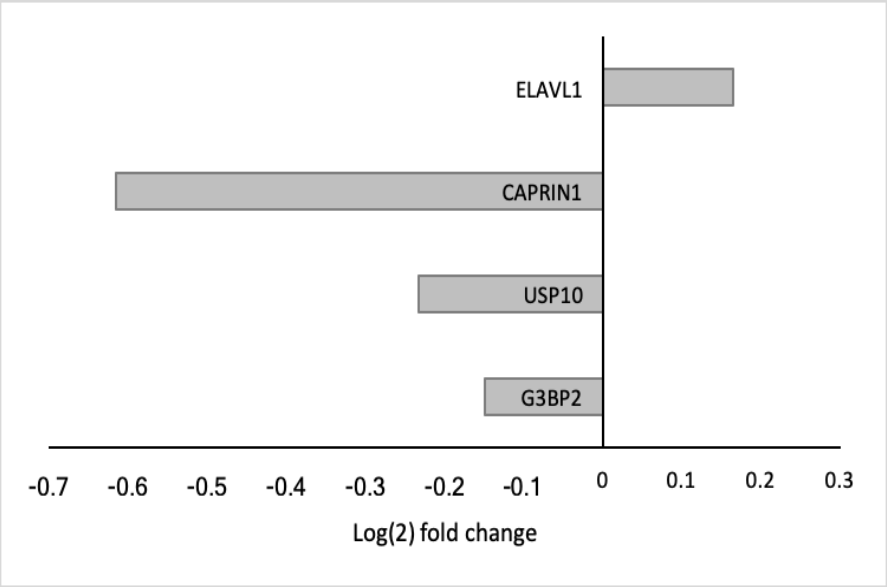

Figure 7.38 Change in the level of RNA-binding proteins from proliferative to senescent GFP-G3BP2b cells.

The level of G3BP2, ELAVL1, USP10 and Caprin1 proteins were observed to show minor changes from proliferative to senescent cells. G3BP2 showed insignificant change in senescent cells. While CAPRIN1 showed a decrease of -0.5-(log2) fold change.

7.5 Conclusion

The proteins of the living cell form the proteome; which is the full set of proteins expressed by the cell. Thus, the proteome network enables the cell to adapt to any internal or external perturbations (Aebersold and Mann, 2016). In order to address the need of delivering high quality and consistent quantification of large-scale studies, Sequential Windowed Acquisition of All Theoretical Fragment Ion Mass Spectra (SWATH-MS) has been developed (Ludwig et al., 2018).

Therefore, a quantitative proteome analysis of proliferative and senescent WT U2OS cells was performed using SWATH-MS. Proteomics analysis revealed that 175 proteins were showing a significant change higher than 2 and smaller than -2. Cytoskeletal proteins were identified to increase significantly in senescent cells. Alterations in the cytoskeletal proteins were suggested to affect shape, adhesion and migration of cells (Gourlay and Ayscough, 2005). Furthermore, CDKN1A showed a significant increase in the expression of p21 protein from proliferative to senescent cells. Sustained rise levels of p21 protein is required for long intervals after reaching senescence (Itahana et al., 2001). In contrast, RNA-binding proteins associated with stress granules did not reveal significant changes from proliferative to senescent cells. Moreover, Furthermore, GO enrichment uncovered that the highly-downregulated proteins in senescent cells were involved in DNA replication and cell proliferation while the highly-upregulated protein were involved in extracellular structure organization, intrinsic apoptotic signalling pathway, mitochondrial gene expression and membrane lipid catabolic process. Collectively, senescence is associated with changes in proteins such as p21, PLIN2 but not stress granule proteins.

Furthermore, the role of G3BP1/2 on senescence progression and the molecular changes associated with senescence was investigated. Quantitative proteomics analysis revealed 299 proteins were showing significant change (higher than 2 or smaller than -2). Of the significantly changing proteins, several nuclear and mitochondrial proteins showed significant decline from proliferative to senescent cells. These proteins are involved in regulation of transcription, DNA replication, translation and other biological processes. CDKN1A showed a significant increase in senescent ΔΔG3BP1/2 cells compared to proliferative cells. Moreover, LMNB1 showed a significant decline in senescent cells. In contrast, RNA-binding proteins did not show significant change between proliferative and senescent ΔΔG3BP1/2 cells. GO enrichment analysis revealed the highly-downregulated proteins are involved in processes including DNA replication and conformation, and cell cycle regulation. In contrast, the proteomics analysis of lysates from proliferative and senescent ΔΔG3BP1/2 cells revealed the overrepresentation of regulation of apoptotic signalling pathway and fatty acid metabolic process.

Lysates of proliferative and senescent GFP-G3BP1 cells were examined. Proteomics analysis revealed 415 proteins that are showing an absolute fold change higher than 2 or smaller than -2. CDKN1A showed a significant increase from proliferative to senescent cells. Moreover, LMNB1 protein levels declined significantly from proliferative to senescent GFP-G3BP1 cells. RNA-binding proteins associated with stress granules did not show significant change between proliferative and senescent GFP-G3BP1 cells. GO enrichment analysis revealed the highly-downregulated proteins to be involved in biological processes including DNA regulation and cell cycle G1/S phase transition. Thus, the highly-upregulated proteins are involved in processes including regulation of endopeptidase activity and regulation of proteolysis.

Analysis of lysates of proliferative and senescent GFP-G3BP2a cells showed 406 proteins with significant fold change (higher than 2 or smaller than -2). CDKN1A showed a significant increase from proliferative to senescent GFP-G3BP2a cells. LMNB1 protein did not show significant change whereas PML showed significant increase in senescent cells compared to proliferative cells. RNA-binding proteins were not detected to significantly change between proliferative and senescent GFP-G3BP2a cells. Furthermore, GO enrichment analysis revealed the highly-downregulated proteins to be involved in processes including DNA replication and DNA biosynthetic process. On the other hand, the highly-upregulated proteins in senescent GFP-G3BP2a cells were involved in processes such as regulation of endopeptidase activity and fatty acid metabolic process.

GFP-G3BP2b cells were investigated for the molecular changes associated with senescence. Hence, proteomics analysis showed that 250 proteins were showing an absolute fold change higher than 2 or smaller than -2. CDKN1A protein levels was detected to significantly increase from proliferative to senescent GFP-G3BP2b cells. LMNB1and PML proteins showed insignificant change in senescent GFP-G3BP2b cells. Furthermore, RNA-binding proteins associated with stress granules showed insignificant change from proliferative to senescent cells. GO enrichment revealed that the highly-downregulated proteins in senescent GFP-G3BP2b cells are involved in biological processes including DNA replication and cell cycle G1/S phase transition. Hence, the highly-upregulated proteins in senescent GFP-G3BP2b cells were detected to be involved in processes including lipid catabolic process and fatty acid metabolic process.

The senescence markers: p21, LMNB1 and PML alongside SAHF, SA-ß-Gal are commonly used to detect senescence phenotype in cells. SAHF and SA-ß-Gal staining showed that most

of ΔΔG3BP1/2 cells are showing senescence phenotype. Adding to that ΔΔG3BP1/2 cells showed the highest percentage of SAHF and SA-ß-Gal positive test compared to WT U2OS, GFP-G3BP1, GFP-G3BP2a and GFP-G3BP2b cells (discussed in chapter 5). Proteomics analysis of senescence proteins in WT U2OS, ΔΔG3BP1/2, GFP-G3BP1, GFP-G3BP2a and GFP-G3BP2b cells revealed the increased levels of p21 in senescent cells compared to proliferative cells. ΔΔG3BP1/2 and GFP-G3BP2a cells showed the highest levels of p21 compared to WT U2OS, GFP-G3BP1, and GFP-G3BP2b cells (Figure 7.39). This observation, alongside with SAHF and SA-ß-Gal staining observations, we suggest that ΔΔG3BP1/2 cells are reaching senescence faster than other cell types. Moreover, out of these staining tests and proteomics analysis we observe that GFP-G3BP2b cells are showing lowest levels of senescence proteins and staining positive cells, suggesting that G3BP2b play contribute to signalling pathways that delay senescence phenotype.

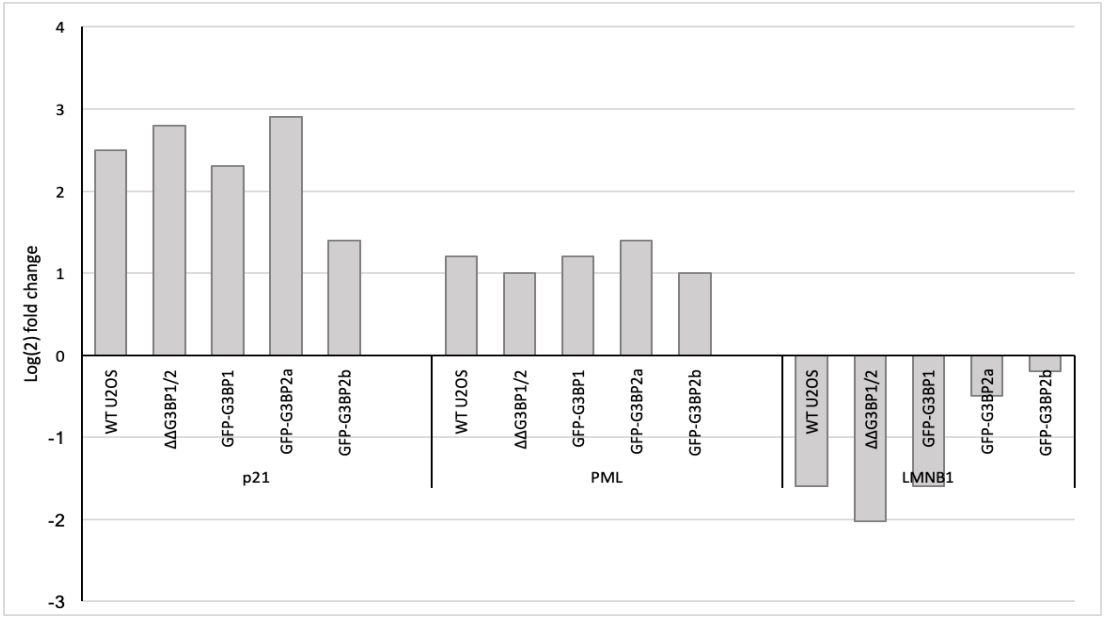

Figure 7.39 Level of senescence proteins in WT U2OS, ΔΔG3BP1/2, GFP-G3BP1, GFP-G3BP2a and GFP-G3BP2b cells.

The level of senescence proteins: p21, PML and LMNB1 in cells. The expression of these proteins varies depending on cell type.

Chapter 8

8 Discussion and Conclusion

Cellular senescence has been observed in several kinds of cells including human fibroblasts (Hayflick, 1965), human skin (Dimri et al. 1995), primate retina (Mishima et al. 1999) and human and mouse liver (Paradis et al. 2001). The irreversible growth arrest phenotype of senescent cells acts as a program that prevents development of tumours as it prevents multiplication of cells with genetic mutations or functional defects. Understanding senescence is crucial as it is implicated in tumour suppression and chronic age-related diseases.

Cellular senescence is triggered in response to various stresses including telomere shortening, DNA damage and oncogene activation leading to replicative senescence, stress-induced senescence and oncogene-induced senescence, respectively (Aravinthan, 2015). Replicative senescence is induced by dysfunctional telomeres (Campisi, 1997). Stress induced pre-mature senescence (SIPS) refers to a rapid senescence phenotype development stimulated by extrinsic stress. Cells undergoing SIPS share similar features as those undergoing replicative senescence. However, they differ in the time at which these features start developing.

Senescent cells share similar features including morphological changes and increased expression of certain proteins such as inhibitors of cyclin-dependent kinases p53, p21 and p16. Moreover, it includes chromatin changes and secretion of different factors, a phenotype known as senescence-associated secretory phenotype (SASP). Hence, the DNA damage generated by telomere shortening or exposure to stressors activate p53. Activation of p53 induces p21 which in turn induces rapid cell-cycle arrest. Senescent cells are characterized by elevated Senescence-associated ß-galactosidase (SA-ß-Gal) activity. Additionally, formation of

senescence-associated heterochromatic foci (SAHF) in senescent cells lead to sequestering genes responsible for promoting proliferation (Chandra, 2016).

Lipids play a crucial role in cell survival and homeostasis such as structural, storage and signalling. Lipid droplets emerged as distinctive organelles that play a role in lipid homeostasis. Lipids are required for fundamental cellular processes including cell division and apoptosis (Storck et al., 2018). dysregulation of enzymes required for lipid metabolism has been linked to ageing and age-related diseases such as neurodegenerative diseases (Agmon and Stockwell, 2017). It is suggested that lipid regulation plays a vital role in the process of senescence (Saitou et al., 2018; Millner et al., 2020).

Exposure of cells to stress leads to a range of responses varying from damage repair and cell survival to programmed cell death that eradicates damaged cells. Depending on the type of stress and duration of exposure, cells mount protective or destructive response pathways. During stress, the homeostasis of a tissue is disrupted. Subsequently, protein synthesis is prevented in order to save the cell's energy and maintain its homeostasis. Stress granules are non-membranous aggregations of mRNA and proteins (mRNPs) that are formed when the translation is reduced or inhibited. The two main components of stress granules are RNAs and RNA-binding proteins. Ras-GTPase-activating protein SH3-domain-binding protein (G3BP) is involved in RNA metabolism and nucleates stress granule formation (Kedersha et al., 2016).

Thus, senescence involves changes in intracellular processes. Stress granules are proposed to play a role in senescence phenotype. Hence, there is a need for developing more models of human cells that incorporate both stress response and senescence phenotype and investigate the changes in senescence phenotype.

8.1 Senescence Phenotype in HDF and U2OS Cells

Primary human fibroblast cells reach replicative senescence by multiple divisions *in vivo* or by continual passaging *in vitro*. Population doubling (PD) is the term for the total number of times the cells in a population have doubled. Thus, in our study, cell proliferation was terminated at PD= 28 (early senescence) where the cell number declined as cells stopped dividing. Therefore, fibroblast cells replicatively senesce at ~75 of continual passaging. This observation is consistent with work of other groups (Lambert and Pirt, 1979; Marthandan et al., 2014; Ma et al., 2015). They showed similar growth pattern to HDF cells: log, exponential and stationary phases.

Furthermore, SA-ß-Gal staining provides an indication of cells' growth status. Continual passaging of cells for ~75 days, resulted in 80% SA-ß-Gal positive cells (replicative senescent) while exposing cells to 10 Gy ionizing radiation resulted in 65% SA-ß-Gal positive cells (SIPS). Senescence was induced in U2OS cells through exposure to ionizing radiation (10 Gy) and doxorubicin treatment. IR-induced DNA damage resulted in senescence of 27% of the population and extensive cell death. Exposing U2OS cells to doxorubicin (200 nM) resulted in development of senescence phenotype in 45% of the population.

8.2 Stress Granule Formation in HDF and U2OS Cells

Stress granules are non-membranous compartments that are formed upon exposure to stress (Protter and Parker, 2016; Wheeler et al., 2016). Hence, they are formed when translation initiation is prevented due to stress exposure (Kedersha et al., 1999). Additionally, they contain various RNA-binding proteins, non-RNA-binding proteins and translation initiation factors (Jain et al., 2016). G3BP is one of several RNA-binding proteins that regulate stress granule assembly.

Stress granule formation was induced in HDF cells by exposing cells to a range of SA concentrations (0-6.0 mM). Proliferative and senescent HDF cells showed an increase in the assembly of stress granules when they were treated to 1.0 mM SA. However, the optimal exposure time was observed to be 30 min for proliferative cells and 45 min for senescent cells. The working conditions for U2OS cells were detected to be: 0.5 mM SA for 30 min. Thus, the concentrations and exposure time observed here are in line with several studies to depend on the cell type and research purpose (Lian and Gallouzi, 2009; Kedersha et al., 2013).

G3BP1 was used as a marker to study stress granules in proliferative and senescent HDF cells. G3BP1 granules were detected in proliferative but not senescent HDF cells suggesting the impaired ability of stress granule formation in senescent cells. In contrast, WT U2OS cells showed recruitment of G3BP1 to stress granules and cells lacking G3BP1/2 showed a total absence of stress granules confirming its crucial role in stress granule formation (Kedersha et al, 2016).

Several RNA-binding proteins including TIA-1, FXR-1 and Caprin-1 are stress granule components. Caprin-1 was detected at sites of stress granule assembly in proliferative HDF cells but rarely in senescent HDF cells. However, TIA-1 and TDP-43 were not observed in stress granules under oxidative stress in proliferative or senescent HDF cells. On the other hand, FXR-1 and eIF4G were examined in U2OS cells and observed to locate to stress granule sites under oxidative stress.

Cycloheximide and puromycin are inhibitors of protein synthesis. Cycloheximide prevents stress granule assembly by stabilizing polysomes whereas puromycin induces stress granule assembly by destabilizing polysomes. As expected, in our study, cycloheximide showed

inhibition of stress granules in proliferative and senescent cells. Whereas, puromycin induced stress granule assembly in proliferative cells. This data provides a framework for future studies of stress granules in HDF and U2OS cells.

8.3 Knockout of G3BP Increases Number of Senescent Cells

Stress granules are known to contain a large population of proteins. G3BP is an essential RNA-binding protein that is recruited to stress granules. It is known to initiate the process of stress granule formation in presence of stress (Tourriere et al., 2003). G3BP1 and G3BP2 are homologous proteins that were observed to play an essential role in stress granule assembly (Tourriere et al., 2003; Götte et al., 2019).

To understand the function of G3BP in senescence, we performed several experiments that involved SA-ß-Gal, SAHF staining and quantification of p21 protein expression in WT U2OS and stably transfected cells with different GFP-fused G3BP genes. Hence, SA exposure was observed to induce stress granule assembly in WT U2OS cells. G3BP1 or G3BP2, eIF4G and FXR1 were detected to be recruited to stress granules. In contrast, ΔΔG3BP1/2 cells were incapable of stress granule formation under SA exposure. GFP-G3BP1 cells showed a decrease in stress granule assembly compared to WT U2OS. Moreover, stressed GFP-G3BP2a and GFP-G3BP2b showed decrease in stress granule formation. eIF4G assembly decreased significantly in GFP-G3BP1, GFP-G3BP2a and GFP-G3BP2b cells. FXR1 showed localisation to sites of stress granule assembly.

WT U2OS and ΔΔG3BP1/2 cells displayed senescence phenotype upon doxorubicin treatment. Hence, ΔΔG3BP1/2 cells showed an increase of 4-fold change in senescent cells compared to WT U2OS cells. On the other hand, GFP-G3BP1 cells revealed a decrease of 3-fold change in

senescent cells when compared to WT U2OS cells. G3BP2a and G3BP2b proteins led to a decrease of 1-fold and 1.5-fold change in senescent cells compared to WT U2OS cells. Collectively, knockout of G3BP accelerates development of senescence phenotype. On the other hand, G3BP slows senescence progression significantly. Hence, it indicates that G3BP plays a major role in delaying senescence.

8.4 Knockout of G3BP Inhibits Lipid Droplet Formation

In addition to structural changes, senescence is associated with changes in accumulation of lipids. PLIN2; a protein involved in regulation of lipid lipolysis, was observed to increase with age (Kimmel et al., 2010). Hence, we examined formation of lipid droplets in proliferative and senescent WT U2OS and G3BP knockout cells. Oleate was used as an inducer for lipid droplet synthesis. Hence, oxidative stress induced lipid droplet formation in proliferative WT U2OS cells which is consistent with observations of other studies (Amen and Kaganovich, 2021). Senescent cells showed an increase in lipid droplets. Moreover, oxidative stress stimulated formation of lipid droplets in proliferative and senescent cells. On the other hand, formation of lipid droplets was inhibited in proliferative ΔΔG3BP1/2 cells. However, oxidative stress was observed to induce lipid droplet formation in proliferative cells. Senescent ΔΔG3BP1/2 cells showed formation of few LDs. Under oxidative stress, lipid droplets were detected in senescent cells.

Re-constitution of cells with G3BP1 led to formation of lipid droplets. Oxidative stress was detected to promote formation of lipid droplets. Moreover, SA treatment stimulated formation of lipid droplets in GFP-G3BP2a and GFP-G3BP2b cells. SA led to an increased formation of lipid droplets in senescent GFP-G3BP2b cells compared to GFP-G3BP2a cells. Hence, we suggest that G3BP plays a role in the process of lipid droplet formation.

8.5 Elevated CDKN1A and PLIN2 Protein Levels in ΔΔG3BP1/2 Cells

Quantitative proteome analysis of proliferative and senescent cells was required to develop an understanding of molecular changes associated with senescence in WT U2OS and G3BP-knockout cells. Hence, Sequential Windowed Acquisition of All Theoretical Fragment Ion Mass Spectra (SWATH-MS) was used to perform this study. The number of significantly changing protein detected in WT U2OS and ΔΔG3BP1/2 cells was 175 and 299 protein, respectively. Levels of CDKN1A protein showed significant change from proliferative to senescent cells in both cell types. However, ΔΔG3BP1/2 cells showed a rise of 1.2-fold change in CDKN1A levels compared to WT U2OS cells. Moreover, RNA-binding proteins associated with stress granules did not show significant change in WT U2OS and ΔΔG3BP1/2 cells. PLIN2 showed an increase from proliferative to senescent cells in WT U2OS and ΔΔG3BP1/2 cells. Hence, the levels of PLIN2 showed an increase of 1.2-fold change in ΔΔG3BP1/2 cells compared to WT U2OS cells. GO enrichment analysis revealed that the highly-downregulated proteins in senescent WT U2OS and ΔΔG3BP1/2 cells are involved in processes including DNA replication and cell proliferation.

Re-constitution of cells with G3BP1 protein rescues stress granules and lipid droplet formation. Hence, proteomics analysis revealed 415 proteins that are showing significant change (higher than 2 or smaller than -2). Levels of CDKN1A and PLIN2 proteins showed significant change from proliferative to senescent cells. However, GFP-G3BP1 cells showed similar levels of CDKN1A and PLIN2 proteins to WT U2OS cells. Furthermore, RNA-binding proteins associated with stress granules did not show significant change in GFP-G3BP1 cells. Of the biological processes that are underrepresented in senescent GFP-G3BP1 cells are DNA regulation and cell cycle G1/S phase transition.

G3BP2a and G3BP2b proteins were shown previously to play a role in stress granule formation and lipid droplet synthesis. Hence. Proteomics analysis showed that 406 and 250 proteins are showing significant changes (higher than 2 or smaller than -2). Levels of CDKN1A and PLIN2 proteins showed significant change from proliferative to senescent GFP-G3BP2a and GFP-G3BP2b cells. Hence, CDKN1A protein revealed an increase of 2-fold change in GFP-G3BP2a cells compared to GFP-G3BP2b cells. However, PLIN2 protein levels is similar in both cell types. GO enrichment analysis revealed that the highly-downregulated proteins in senescent GFP-G3BP2a and GFP-G3BP2b cells are involved in processes including DNA replication, DNA biosynthetic process and cell cycle G1/S phase transition.

In conclusion, this thesis establishes the framework for inducing senescence and stress granules in a primary cell type as well as a cancer cell line, as presented in chapter 3 and 4 that can be used for various studies. The senescence phenotype involves changes in cellular processes and cell environment. In our study, senescence was induced in HDF cells replicatively and by stress-induced premature senescence, SIPS, which display similar senescence features to those replicative senescent cells. Furthermore, senescence was induced in U2OS cancer cells through ionizing radiation and doxorubicin treatment.

Stress granules are an important component of the cellular stress response machinery. G3BP is suggested to be an essential stress granule component that initiates the assembly events. Loss of both G3BP1 and 2 in U2OS cells, ΔΔG3BP1/2, showed loss of stress granule formation in proliferating and senescent cells, suggesting its crucial role in stress granule formation. Furthermore, loss of G3BP promotes early induction of the senescence phenotype in ΔΔG3BP1/2 cells. Re-constitution of cells with G3BP1, G3BP2a or G3BP2b, delayed cells'

progression to senescence. Thus, it indicates that G3BP plays a major role in senescence as shown in chapters 4 and 5.

Lipid droplets have a crucial role in storing cholesterol to maintain intracellular lipid homeostasis (Martin and Parton, 2005). They are linked to many cellular processes including protein degradation, and are increased following cellular damage and lipid overload (Agarwal and Garg, 2006). Thus, formation of lipid droplets was studied as described in chapter 6 in proliferative and senescent U2OS cells under oxidative stress. Formation of lipid droplets was inhibited in ΔΔG3BP1/2 cells, indicating that G3BP plays a role in lipid droplet formation. Re-constitution of knockout cells with G3BP1 partially restores cells' ability of lipid droplet formation. Hence, we suggest that G3BP might regulate the process of lipid droplet formation and accumulation. These results are further supported by proteomics studies presented in Chapter 7 showing significant changes in levels of lipid metabolism proteins in ΔΔG3BP1/2 senescent cells.

9 Bibliography

1. Acosta, J.C. and Gil, J., 2012. Senescence: a new weapon for cancer therapy. Trends in cell biology, 22(4), pp.211-219.
2. Aebersold, R. and Mann, M., 2016. Mass-spectrometric exploration of proteome structure and function. Nature, 537(7620), pp.347-355.
3. Agarwal, A. K. and Garg, A., 2006. Genetic disorders of adipose tissue development, differentiation, and death. Annu. Rev. Genomics Hum. Genet. 7, 175-199.
4. Agmon, E. and Stockwell, B.R., 2017. Lipid homeostasis and regulated cell death. Current opinion in chemical biology, 39, pp.83-89.
5. Aikata, H., Takaishi, H., Kawakami, Y., Takahashi, S., Kitamoto, M., Nakanishi, T., Nakamura, Y., Shimamoto, F., Kajiyama, G., Ide, T., 2000. Telomere reduction in human liver tissues with age and chronic inflammation. Exp. Cell Res. 256, 578–582.
6. Amen, T. and Kaganovich, D., 2021. Small molecule screen reveals joint regulation of Stress Granule formation and Lipid Droplet biogenesis. Frontiers in cell and developmental biology, 8, p.1843.
7. Anderson, N. and Borlak, J., 2008. Molecular mechanisms and therapeutic targets in steatosis and steatohepatitis. Pharmacol. Rev. 60, 311-357.
8. Anderson, P. and Kedersha, N., 2002. Stressful initiations. Journal of cell science, 115(16), pp.3227-3234.
9. Anderson, P. and Kedersha, N., 2006. RNA granules. Journal of Cell Biology, 172(6), pp.803-808.
10. Anderson, P. and Kedersha, N., 2008. Stress granules: the Tao of RNA triage. Trends in biochemical sciences, 33(3), pp.141-150.
11. Anderson, P. and Kedersha, N., 2009. Stress granules. Current biology, 19(10), pp. R397-R398.
12. Antar, L.N., Dictenberg, J.B., Plociniak, M., Afroz, R. and Bassell, G.J., 2005. Localization of FMRP- associated mRNA granules and requirement of microtubules for activity- dependent trafficking in hippocampal neurons. Genes, Brain and Behavior, 4(6), pp.350-359.

13. Anwar, T., Khosla, S. and Ramakrishna, G., 2016. Increased expression of SIRT2 is a novel marker of cellular senescence and is dependent on wild type p53 status. Cell Cycle, 15(14), pp.1883-1897.
14. Araki, S., Okazaki, M. and Goto, S., 2004. Impaired lipid metabolism in aged mice as revealed by fasting-induced expression of apolipoprotein mRNAs in the liver and changes in serum lipids. Gerontology, 50(4), pp.206-215.
15. Aravinthan, A., 2015. Cellular senescence: a hitchhiker's guide. Human cell, 28(2), pp.51-64.
16. Athenstaedt, K., Zweytick, D., Jandrositz, A., Kohlwein, S. D. and Daum, G. (1999). Identification and characterization of major lipid particle proteins of the yeast Saccharomyces cerevisiae. J. Bacteriol. 181, 6441-6448.
17. Atzmon, G., Rincon, M., Schechter, C.B., Shuldiner, A.R., Lipton, R.B., Bergman, A. and Barzilai, N., 2006. Lipoprotein genotype and conserved pathway for exceptional longevity in humans. PLoS biology, 4(4), p. e113.
18. Baker, D.J., Childs, B.G., Durik, M., Wijers, M.E., Sieben, C.J., Zhong, J.A., Saltness, R., Jeganathan, K.B., Verzosa, G.C., Pezeshki, A., Khazaie, K., Miller, J.D., van Deursen, J.M., 2016. Naturally occurring p16Ink4a-positive cells shorten healthy lifespan. Nature 530, 184–189.
19. Baker, D.J., Wijshake, T., Tchkonia, T., LeBrasseur, N.K., Childs, B.G., Van De Sluis, B., Kirkland, J.L. and van Deursen, J.M., 2011. Clearance of p16 Ink4a-positive senescent cells delays ageing-associated disorders. Nature, 479(7372), pp.232-236.
20. Ball, D.P., Taabazuing, C.Y., Griswold, A.R., Orth, E.L., Rao, S.D., Kotliar, I.B., Vostal, L.E., Johnson, D.C. and Bachovchin, D.A., 2020. Caspase-1 interdomain linker cleavage is required for pyroptosis. Life science alliance, 3(3).
21. Barbee, S.A., Estes, P.S., Cziko, A.M., Hillebrand, J., Luedeman, R.A., Coller, J.M., Johnson, N., Howlett, I.C., Geng, C., Ueda, R. and Brand, A.H., 2006. Staufen-and FMRP-containing neuronal RNPs are structurally and functionally related to somatic P bodies. Neuron, 52(6), pp.997-1009.
22. Barja, G., 2002. Endogenous oxidative stress: relationship to aging, longevity and caloric restriction. Ageing research reviews, 1(3), pp.397-411.
23. Baskar R., Lee K. A., Yeo R., Yeoh K.-W., 2012. Cancer and radiation therapy: current advances and future directions. Int. J. Med. Sci. 9, 193–199. 10.7150/ijms.3635

24. Baskar, R., Dai, J., Wenlong, N., Yeo, R. and Yeoh, K.W., 2014. Biological response of cancer cells to radiation treatment. Frontiers in molecular biosciences, 1, p.24.
25. Basu, M., Courtney, S.C. and Brinton, M.A., 2017. Arsenite-induced stress granule formation is inhibited by elevated levels of reduced glutathione in West Nile virus-infected cells. PLoS pathogens, 13(2), p.e1006240.
26. Bekker-Jensen, S., Lukas, C., Kitagawa, R., Melander, F., Kastan, M.B., Bartek, J. and Lukas, J., 2006. Spatial organization of the mammalian genome surveillance machinery in response to DNA strand breaks. The Journal of cell biology, 173(2), pp.195-206.
27. Ben-Porath, I. and Weinberg, R.A., 2004. When cells get stressed: an integrative view of cellular senescence. The Journal of clinical investigation, 113(1), pp.8-13.
28. Bentzen S. M., 2006. Preventing or reducing late side effects of radiation therapy: radiobiology meets molecular pathology. Nat. Rev. Cancer 6, 702–713. 10.1038/nrc1950
29. Bickel, P.E., J.T. Tansey, and M.A. Welte. 2009. PAT proteins, an ancient family of lipid droplet proteins that regulate cellular lipid stores. Biochim. Biophys. Acta. 1791:419–440. http://dx.doi.org/10.1016/j.bbalip.2009.04.002
30. Bielak-Zmijewska, A., Wnuk, M., Przybylska, D., Grabowska, W., Lewinska, A., Alster, O., Korwek, Z., Cmoch, A., Myszka, A., Pikula, S. and Mosieniak, G., 2014. A comparison of replicative senescence and doxorubicin-induced premature senescence of vascular smooth muscle cells isolated from human aorta. Biogerontology, 15(1), pp.47-64.
31. Bihani, T., Mason, D.X., Jackson, T., Chen, S.C., Boettner, B. and Lin, A.W., 2004. Differential oncogenic Ras signaling and senescence in tumor cells. Cell Cycle, 3(9), pp.1199-1205.
32. Blackburn, E.H., 2001. Switching and signaling at the telomere. Cell, 106(6), pp.661-673.
33. Blanchette-Mackie, E.J., Dwyer, N.K., Barber, T., Coxey, R.A., Takeda, T., Rondinone, C.M., Theodorakis, J.L., Greenberg, A.S. and Londos, C., 1995. Perilipin is located on the surface layer of intracellular lipid droplets in adipocytes. Journal of lipid research, 36(6), pp.1211-1226.
34. Bondarenko PV, Chelius D, Shaler TA., 2002. Identification and relative quantitation of protein mixtures by enzymatic digestion followed by capillary reversed-phase liquid chromatography- tandem mass spectrometry. Anal Chem.; 74:4741–4749.
35. Bordeleau, M.E., Matthews, J., Wojnar, J.M., Lindqvist, L., Novac, O., Jankowsky, E., Sonenberg, N., Northcote, P., Teesdale-Spittle, P. and Pelletier, J., 2005. Stimulation of mammalian translation initiation factor eIF4A activity by a small molecule inhibitor of

eukaryotic translation. Proceedings of the National Academy of Sciences, 102(30), pp.10460-10465.

36. Borghesan, M. and O'Loghlen, A., 2017. Integrins in senescence and aging. Cell Cycle, 16(10), p.909.
37. Bostro ¨m, P., Andersson, L., Li, L., Perkins, R., Højlund, K., Bore ´n, J. and Olofsson, S.-O., 2009. The assembly of lipid droplets and its relation to cellular insulin sensitivity. Biochem. Soc. Trans. 37, 981-985.
38. Bounedjah, O., Desforges, B., Wu, T.D., Pioche-Durieu, C., Marco, S., Hamon, L., Curmi, P.A., Guerquin-Kern, J.L., Piétrement, O. and Pastré, D., 2014. Free mRNA in excess upon polysome dissociation is a scaffold for protein multimerization to form stress granules. Nucleic acids research, 42(13), pp.8678-8691.
39. Brasaemle, D., 2007. The perilipin family of structural lipid droplet proteins: stabilization of lipid droplets and control of lipolysis. Journal of Lipid Research, 48(12), pp.2547-2559.
40. Brasaemle, D.L. and Wolins, N.E., 2012. Packaging of fat: an evolving model of lipid droplet assembly and expansion. Journal of Biological Chemistry, 287(4), pp.2273-2279.
41. Buchan, J.R. and Parker, R., 2009. Eukaryotic stress granules: the ins and outs of translation. Molecular cell, 36(6), pp.932-941.
42. Bursać, S., Brdovčak, M.C., Pfannkuchen, M., Orsolić, I., Golomb, L., Zhu, Y., Katz, C., Daftuar, L., Grabušić, K., Vukelić, I. and Filić, V., 2012. Mutual protection of ribosomal proteins L5 and L11 from degradation is essential for p53 activation upon ribosomal biogenesis stress. Proceedings of the National Academy of Sciences, 109(50), pp.20467-20472.
43. Burton, D.G.A., 2009. Cellular senescence, ageing and disease. Age, 31(1), pp.1-9.
44. Butler, P.L., and R.K. Mallampalli. 2010. Cross-talk between remodeling and de novo pathways maintains phospholipid balance through ubiquitination. J. Biol. Chem. 285:6246–6258. http://dx.doi.org/10.1074/jbc.M109.017350
45. Caciotti, A., Donati, M.A., Boneh, A., d'Azzo, A., Federico, A., Parini, R., Antuzzi, D., Bardelli, T., Nosi, D., Kimonis, V. and Zammarchi, E., 2005. Role of β- galactosidase and elastin binding protein in lysosomal and nonlysosomal complexes of patients with GM1-gangliosidosis. Human mutation, 25(3), pp.285-292.
46. Campisi, J. and Di Fagagna, F.D.A., 2007. Cellular senescence: when bad things happen to good cells. Nature reviews Molecular cell biology, 8(9), pp.729-740.

47. Campisi, J. and Yaswen, P., 2009. Aging and cancer cell biology, 2009. Aging cell, 8(3), pp.221-225.
48. Campisi, J., 1997. The biology of replicative senescence.
49. Campisi, J., 2000. Cancer, aging and cellular senescence. In vivo (Athens, Greece), 14(1), pp.183-188.
50. Campisi, J., 2001. Cellular senescence as a tumor-suppressor mechanism. Trends in cell biology, 11(11), pp.S27-S31.
51. Campisi, J., 2005. Senescent cells, tumor suppression, and organismal aging: good citizens, bad neighbors. Cell, 120(4), pp.513-522.
52. Campisi, J., 2007. Aging and cancer cell biology. Aging cell, 6(3), pp.261-263.
53. Campisi, J., 2013. Aging, cellular senescence, and cancer. Annual review of physiology, 75, pp.685-705.
54. Cao, X., Jin, X. and Liu, B., 2020. The involvement of stress granules in aging and aging-associated diseases. Aging Cell, p.e13136.
55. Casares, D., Escribá, P.V. and Rosselló, C.A., 2019. Membrane lipid composition: effect on membrane and organelle structure, function and compartmentalization and therapeutic avenues. International journal of molecular sciences, 20(9), p.2167.
56. Chainiaux, F., Magalhaes, J.P., Eliaers, F., Remacle, J. and Toussaint, O., 2002. UVB-induced premature senescence of human diploid skin fibroblasts. The international journal of biochemistry & cell biology, 34(11), pp.1331-1339.
57. Chandra, T., 2016. Senescence Associated Heterochromatic Foci: SAHF. In The Functional Nucleus (pp. 205-218). Springer, Cham.
58. Chapman, K.D., Dyer, J.M. and Mullen, R.T., 2012. Biogenesis and functions of lipid droplets in plants thematic review series: lipid droplet synthesis and metabolism: from yeast to man. Journal of lipid research, 53(2), pp.215-226.
59. Chattopadhyay, D., Ghosh, M.K., Mal, A. and Harter, M.L., 2001. Inactivation of p21 by E1A leads to the induction of apoptosis in DNA-damaged cells. Journal of virology, 75(20), pp.9844-9856.
60. Chen, L. and Liu, B., 2017. Relationships between stress granules, oxidative stress, and neurodegenerative diseases. Oxidative medicine and cellular longevity, 2017.
61. Chen, Q., Fischer, A., Reagan, J.D., Yan, L.J., and Ames, B.N., 1995. Oxidative DNA damage and senescence of human diploid fibroblast cells. Proc. Natl. Acad. Sci. U. S. A.

92, 4337-4341.

62. Chen, Q.M., Liu, J. and Merrett, J.B., 2000. Apoptosis or senescence-like growth arrest: influence of cell-cycle position, p53, p21 and bax in H2O2 response of normal human fibroblasts. Biochemical Journal, 347(2), pp.543-551.
63. Chiang, Y., Rizzino, A., Sibenaller, Z.A., Wold, M.S. and Vishwanatha, J.K., 1999. Specific down-regulation of annexin II expression in human cells interferes with cell proliferation. Molecular and cellular biochemistry, 199(1-2), pp.139-147.
64. Cho, E.C., Kuo, M.L., Cheng, J.H., Cheng, Y.C., Hsieh, Y.C., Liu, Y.R., Hsieh, R.H. and Yen, Y., 2015. RRM2B-mediated regulation of mitochondrial activity and inflammation under oxidative stress. Mediators of inflammation, 2015.
65. Cho, S. and Hwang, E.S., 2012. Status of mTOR activity may phenotypically differentiate senescence and quiescence. Molecules and cells, 33(6), pp.597-604.
66. Choi J, Shendrik I, Peacocke M, Peehl D, Buttyan R, Ikeguchi EF, Katz AE and Benson MC., 2000. Expression of senescence- associated beta-galactosidase in enlarged prostates from men with benign prostatic hyperplasia. Urology 56: 160–166
67. Cmielova, J., Havelek, R., Soukup, T., Jiroutová, A., Visek, B., Suchánek, J., Vavrova, J., Mokry, J., Muthna, D., Bruckova, L. and Filip, S., 2012. Gamma radiation induces senescence in human adult mesenchymal stem cells from bone marrow and periodontal ligaments. International journal of radiation biology, 88(5), pp.393-404.
68. Cnop, M., Toivonen, S., Igoillo-Esteve, M. and Salpea, P., 2017. Endoplasmic reticulum stress and eIF2α phosphorylation: the Achilles heel of pancreatic β cells. Molecular metabolism, 6(9), pp.1024-1039.
69. Collado, M., Blasco, M.A. and Serrano, M., 2007. Cellular senescence in cancer and aging. Cell, 130(2), pp.223-233.
70. Colombrita, C., Zennaro, E., Fallini, C., Weber, M., Sommacal, A., Buratti, E., Silani, V. and Ratti, A., 2009. TDP- 43 is recruited to stress granules in conditions of oxidative insult. Journal of neurochemistry, 111(4), pp.1051-1061.
71. Colombrita, C., Zennaro, E., Fallini, C., Weber, M., Sommacal, A., Buratti, E., Silani, V. and Ratti, A., 2009. TDP- 43 is recruited to stress granules in conditions of oxidative insult. Journal of neurochemistry, 111(4), pp.1051-1061.
72. Conte, M., Franceschi, C., Sandri, M. and Salvioli, S., 2016. Perilipin 2 and age-related metabolic diseases: a new perspective. Trends in Endocrinology & Metabolism, 27(12), pp.893-903.

73. Conte, M., Vasuri, F., Bertaggia, E., Armani, A., Santoro, A., Bellavista, E., Degiovanni, A., D'Errico-Grigioni, A., Trisolino, G., Capri, M. and Franchi, M.V., 2015. Differential expression of perilipin 2 and 5 in human skeletal muscle during aging and their association with atrophy-related genes. Biogerontology, 16(3), pp.329-340.
74. Conte, M., Vasuri, F., Trisolino, G., Bellavista, E., Santoro, A., Degiovanni, A., Martucci, E., D'Errico-Grigioni, A., Caporossi, D., Capri, M. and Maier, A.B., 2013. Increased Plin2 expression in human skeletal muscle is associated with sarcopenia and muscle weakness. PLoS One, 8(8), p.e73709.
75. Coppé, J.P., Kauser, K., Campisi, J. and Beauséjour, C.M., 2006. Secretion of vascular endothelial growth factor by primary human fibroblasts at senescence. Journal of Biological Chemistry, 281(40), pp.29568-29574.
76. Correia- Melo, C., Marques, F.D., Anderson, R., Hewitt, G., Hewitt, R., Cole, J., Carroll, B.M., Miwa, S., Birch, J., Merz, A. and Rushton, M.D., 2016. Mitochondria are required for pro- ageing features of the senescent phenotype. The EMBO journal, 35(7), pp.724-742.
77. de Magalhães, J.P. and Passos, J.F., 2018. Stress, cell senescence and organismal ageing. Mechanisms of ageing and development, 170, pp.2-9.
78. de Magalhaes, J.P., Toussaint, O., 2004c. Telomeres and telomerase: a modern fountain of youth? Rejuvenation Res. 7, 126–133.
79. Debacq-Chainiaux, F., Borlon, C., Pascal, T., Royer, V., Eliaers, F., Ninane, N., Carrard, G., Friguet, B., de Longueville, F., Boffe, S., Remacle, J. and Toussaint, O., 2005. Repeated exposure of human skin fibroblasts to UVB at subcytotoxic level triggers premature senescence through the TGF-beta1 signaling pathway. J. Cell Sci. 118, 743–758.
80. Dember, L.M., Kim, N.D., Liu, K.Q. and Anderson, P., 1996. Individual RNA recognition motifs of TIA-1 and TIAR have different RNA binding specificities. Journal of Biological Chemistry, 271(5), pp.2783-2788.
81. Denchi, E.L., Attwooll, C., Pasini, D. and Helin, K., 2005. Deregulated E2F activity induces hyperplasia and senescence-like features in the mouse pituitary gland. Molecular and cellular biology, 25(7), pp.2660-2672.
82. Dewey, C.M., Cenik, B., Sephton, C.F., Dries, D.R., Mayer, P., Good, S.K., Johnson, B.A., Herz, J. and Yu, G., 2011. TDP-43 is directed to stress granules by sorbitol, a novel physiological osmotic and oxidative stressor. Molecular and cellular biology, 31(5), pp.1098-1108.

83. Deye, J. F., Berger, T. A., and Anderson, A. G. 1990. Nile red as a solvatochromic dye for measuring solvent strength in normal liquids and mixtures of normal liquids with supercritical and near critical fluids. Anal Chem. 62:615-622.
84. di Fagagna, F.D.A., 2008. Living on a break: cellular senescence as a DNA-damage response. Nature Reviews Cancer, 8(7), pp.512-522.
85. Dimri GP, Lee X, Basile G, Acosta M, Scott G, Roskelley C, Medrano EE, Linskens M, Rubelj I, Pereira-Smith OM et al., 1995. A novel biomarker identifies senescent human cells in culture and in aging skin in vivo. Proc Natl Acad Sci USA 92: 9363–9367
86. Dimri, G.P., 2005. What has senescence got to do with cancer?. Cancer cell, 7(6), pp.505-512.
87. Dimri, G.P., Lee, X., Basile, G., Acosta, M., Scott, G., Roskelley, C., Medrano, E.E., LINskENs, M.A.A.R.T.E.N., Rubelj, I. and Pereira-Smith, O., 1995. A biomarker that identifies senescent human cells in culture and in aging skin in vivo. Proceedings of the National Academy of Sciences, 92(20), pp.9363-9367.
88. Dirac, A.M. and Bernards, R., 2003. Reversal of senescence in mouse fibroblasts through lentiviral suppression of p53. Journal of Biological Chemistry, 278(14), pp.11731-11734.
89. Doggett, D.L., Rotenberg, M.O., Pignolo, R.J., Phillips, P.D. and Cristofalo, V.J., 1992. Differential gene expression between young and senescent, quiescent WI-38 cells. Mech. Ageing Dev. 65, 239– 255.
90. Dreval, K., Tryndyak, V., Kindrat, I., Twaddle, N.C., Orisakwe, O.E., Mudalige, T.K., Beland, F.A., Doerge, D.R. and Pogribny, I.P., 2018. Cellular and molecular effects of prolonged low-level sodium arsenite exposure on human hepatic HepaRG cells. Toxicological Sciences, 162(2), pp.676-687.
91. Dumont, P., Royer, V., Pascal, T., Dierick, J.-F., Chainiaux, F., Frippiat, C., Eliaers, F., Remacle, J., and Toussaint, O., 2001. Growth kinetics rather than stress cause accelerated telomere shortening in cultures of human diploid fibroblasts in oxidative stress-induced premature senescence. FEBS Lett. 503, 109-112.
92. Durante M., Loeffler J. S., 2010. Charged particles in radiation oncology. Nat. Rev. Clin. Oncol. 7, 37–43. 10.1038/nrclinonc.2009.183.
93. Schroeder, E.A. and Brunet, A., 2015. Lipid profiles and signals for long life. Trends in Endocrinology & Metabolism, 26(11), pp.589-592.

94. Escorcia, W., Ruter, D.L., Nhan, J. and Curran, S.P., 2018. Quantification of lipid abundance and evaluation of lipid distribution in Caenorhabditis elegans by nile red and oil red O staining. JoVE (Journal of Visualized Experiments), (133), p.e57352.
95. Feng, Q., Li, P., Leung, P.C. and Auersperg, N., 2004. Caspase-1ζ, a new splice variant of the caspase-1 gene. Genomics, 84(3), pp.587-591.
96. Feng, Y., De Franceschi, G., Kahraman, A., Soste, M., Melnik, A., Boersema, P.J., De Laureto, P.P., Nikolaev, Y., Oliveira, A.P. and Picotti, P., 2014. Global analysis of protein structural changes in complex proteomes. Nature biotechnology, 32(10), p.1036.
97. Ferbeyre, G., de Stanchina, E., Querido, E., Baptiste, N., Prives, C. and Lowe, S.W., 2000. PML is induced by oncogenic ras and promotes premature senescence. Genes & development, 14(16), pp.2015-2027.
98. Firsanov, D.V., Solovjeva, L.V. and Svetlova, M.P., 2011. H2AX phosphorylation at the sites of DNA double-strand breaks in cultivated mammalian cells and tissues. Clinical epigenetics, 2(2), pp.283-297.
99. Flor, A.C., Wolfgeher, D., Wu, D. and Kron, S.J., 2017. A signature of enhanced lipid metabolism, lipid peroxidation and aldehyde stress in therapy-induced senescence. Cell death discovery, 3(1), pp.1-12.
100. Forsburg, S.L., 2004. Eukaryotic MCM proteins: beyond replication initiation. Microbiology and Molecular Biology Reviews, 68(1), pp.109-131.
101. Freibaum, B.D., Chitta, R.K., High, A.A. and Taylor, J.P., 2010. Global analysis of TDP-43 interacting proteins reveals strong association with RNA splicing and translation machinery. Journal of proteome research, 9(2), pp.1104-1120.
102. Freund, A., Laberge, R.M., Demaria, M. and Campisi, J., 2012. Lamin B1 loss is a senescence-associated biomarker. Molecular biology of the cell, 23(11), pp.2066-2075.
103. Frias, C., Pampalona, J., Genesca, A. and Tusell, L., 2012. Telomere dysfunction and genome instability. Front Biosci, 17(11), pp.2181-2196.
104. Fridlyanskaya, I., Alekseenko, L. and Nikolsky, N., 2015. Senescence as a general cellular response to stress: a mini-review. Experimental gerontology, 72, pp.124-128.
105. Fujimoto, T., and R.G. Parton. 2011. Not just fat: the structure and function of the lipid droplet. Cold Spring Harb. Perspect. Biol. 3:a004838. http://dx.doi .org/10.1101/cshperspect.a004838
106. Fujimoto, T., Ohsaki, Y., Cheng, J., Suzuki, M. and Shinohara, Y., 2008. Lipid droplets: a classic organelle with new outfits. Histochem. Cell Biol. 130, 263-279.

107.Fulda, S., Gorman, A.M., Hori, O. and Samali, A., 2010. Cellular stress responses: cell survival and cell death. International journal of cell biology, 2010.

108.Gallouzi, I.E., Brennan, C.M., Stenberg, M.G., Swanson, M.S., Eversole, A., Maizels, N. and Steitz, J.A., 2000. HuR binding to cytoplasmic mRNA is perturbed by heat shock. Proceedings of the National Academy of Sciences, 97(7), pp.3073-3078.

109.Gao, T., Furnari, F. and Newton, A.C., 2005. PHLPP: a phosphatase that directly dephosphorylates Akt, promotes apoptosis, and suppresses tumor growth. Molecular cell, 18(1), pp.13-24.

110.Georgakilas, A.G., Martin, O.A. and Bonner, W.M., 2017. p21: a two-faced genome guardian. Trends in molecular medicine, 23(4), pp.310-319.

111.Gewirtz, D., 1999. A critical evaluation of the mechanisms of action proposed for the antitumor effects of the anthracycline antibiotics adriamycin and daunorubicin. Biochemical pharmacology, 57(7), pp.727-741.

112.Ghisolfi, L., Dutt, S., McConkey, M.E., Ebert, B.L. & Ander- son, P., 2012. Stress granules contribute to a-globin homeostasis in differentiating erythroid cells. Biochem. Bio- phys. Res. Commun. 420, 768–774.

113.Gingras, A.C., Raught, B. and Sonenberg, N., 1999. eIF4 initiation factors: effectors of mRNA recruitment to ribosomes and regulators of translation. Annual review of biochemistry, 68(1), pp.913-963.

114.Goodnow, R.A., 2017. Platform Technologies in Drug Discovery and Validation. Academic Press.

115.Goodpaster, B.H., Chomentowski, P., Ward, B.K., Rossi, A., Glynn, N.W., Delmonico, M.J., Kritchevsky, S.B., Pahor, M. and Newman, A.B., 2008. Effects of physical activity on strength and skeletal muscle fat infiltration in older adults: a randomized controlled trial. Journal of applied physiology, 105(5), pp.1498-1503.

116.Götte, B., Panas, M.D., Hellström, K., Liu, L., Samreen, B., Larsson, O., Ahola, T. and McInerney, G.M., 2019. Separate domains of G3BP promote efficient clustering of alphavirus replication complexes and recruitment of the translation initiation machinery. PLoS pathogens, 15(6), p.e1007842.

117.Gourlay, C.W. and Ayscough, K.R., 2005. The actin cytoskeleton: a key regulator of apoptosis and ageing?. Nature reviews Molecular cell biology, 6(7), pp.583-589.

118.Greenspan, P., Mayer, E. U., Fowler, S. D., 1985. Nile red: a selective fluorescent stain for intracellular lipid droplets. J Cell Biol. 100:965-973.

119.Gross, D.A., C. Zhan, and D.L. Silver. 2011. Direct binding of triglyceride to fat storage-inducing transmembrane proteins 1 and 2 is important for lipid droplet formation. Proc. Natl. Acad. Sci. USA. 108:19581–19586. http:// dx.doi.org/10.1073/pnas.1110817108

120.Gross, D.A., Zhan, C. and Silver, D.L., 2011. Direct binding of triglyceride to fat storage-inducing transmembrane proteins 1 and 2 is important for lipid droplet formation. Proceedings of the National Academy of Sciences, 108(49), pp.19581-19586.

121.Gross, D.A., E.L. Snapp, and D.L. Silver. 2010. Structural insights into triglyc- eride storage mediated by fat storage-inducing transmembrane (FIT) protein 2. PLoS ONE. 5:e10796. http://dx.doi.org/10.1371/journal.pone .0010796

122.Guil, S., Long, J.C. and Cáceres, J.F., 2006. hnRNP A1 relocalization to the stress granules reflects a role in the stress response. Molecular and cellular biology, 26(15), pp.5744-5758.

123.Gunasekaran, U. and Gannon, M., 2011. Type 2 diabetes and the aging pancreatic beta cell. Aging (Albany NY), 3(6), p.565.

124.Hall, B.M., Balan, V., Gleiberman, A.S., Strom, E., Krasnov, P., Virtuoso, L.P., Rydkina, E., Vujcic, S., Balan, K., Gitlin, I.I. and Leonova, K.I., 2017. p16 (Ink4a) and senescence-associated β-galactosidase can be induced in macrophages as part of a reversible response to physiological stimuli. Aging (Albany NY), 9(8), p.1867.

125.Haltiwanger, R.S., 2002. Regulation of signal transduction pathways in development by glycosylation. Current opinion in structural biology, 12(5), pp.593-598.

126.Harris, S.L. and Levine, A.J., 2005. The p53 pathway: positive and negative feedback loops. Oncogene, 24(17), pp.2899-2908.

127.Hastie, N.D., Dempster, M., Dunlop, M.G., Thompson, A.M., Green, D.K., Allshire, R.C., 1990. Telomere reduction in human colorectal carcinoma and with ageing. Nature 346, 866–868.

128.Hayflick, L. and Moorhead, P.S., 1961. The serial cultivation of human diploid cell strains. Experimental cell research, 25(3), pp.585-621.

129. Hayflick, L. The limited in vitro lifetime of human diploid cell strains. Exp. Cell Res. 37, 614–636 (1965).

130.Hayflick, L., Moorhead, P.S., 1961. The serial cultivation of human diploid cell strains. Exp. Cell Res. 25, 585–621.

131.He, J., Goodpaster, B.H. and Kelley, D.E., 2004. Effects of weight loss and physical activity on muscle lipid content and droplet size. Obesity research, 12(5), pp.761-769.

132.He, S. and Sharpless, N.E., 2017. Senescence in health and disease. Cell, 169(6), pp.1000-1011.

133.Henne, W.M., Reese, M.L. and Goodman, J.M., 2018. The assembly of lipid droplets and their roles in challenged cells. The EMBO journal, 37(12), p.e98947.

134.Herbig, U., Jobling, W.A., Chen, B.P., Chen, D.J. and Sedivy, J.M., 2004. Telomere shortening triggers senescence of human cells through a pathway involving ATM, p53, and p21CIP1, but not p16INK4a. Molecular cell, 14(4), pp.501-513.

135.Herranz, N. and Gil, J., 2018. Mechanisms and functions of cellular senescence. The Journal of clinical investigation, 128(4), pp.1238-1246.

136.Hofmann, S., Cherkasova, V., Bankhead, P., Bukau, B. and Stoecklin, G., 2012. Translation suppression promotes stress granule formation and cell survival in response to cold shock. Molecular biology of the cell, 23(19), pp.3786-3800.

137.Hua, Y. and Zhou, J., 2004. Survival motor neuron protein facilitates assembly of stress granules. FEBS letters, 572(1-3), pp.69-74.

138.Huang, Y., Yan, C.H. and Fu, S.B., 2005. The cloning and expression of apoptosis associated gene ANNEXIN A2 induced by p53 gene. Zhonghua yi xue yi chuan xue za zhi= Zhonghua yixue yichuanxue zazhi= Chinese journal of medical genetics, 22(6), pp.661-664.

139.Irvine, K., Stirling, R., Hume, D. and Kennedy, D., 2004. Rasputin, more promiscuous than ever: a review of G3BP. Int J Dev Biol, 48(10), pp.1065-1077.

140.Itahana, K., Campisi, J. and Dimri, G.P., 2004. Mechanisms of cellular senescence in human and mouse cells. Biogerontology, 5(1), pp.1-10.

141.Itahana, K., Dimri, G. and Campisi, J., 2001. Regulation of cellular senescence by p53. European Journal of Biochemistry, 268(10), pp.2784-2791.

142.Ivanov, A., Pawlikowski, J., Manoharan, I., van Tuyn, J., Nelson, D.M., Rai, T.S., Shah, P.P., Hewitt, G., Korolchuk, V.I., Passos, J.F. and Wu, H., 2013. Lysosome-mediated processing of chromatin in senescence. Journal of Cell Biology, 202(1), pp.129-143.

143.Jackson, J.G. and Pereira-Smith, O.M., 2006. Primary and compensatory roles for RB family members at cell cycle gene promoters that are deacetylated and downregulated in doxorubicin-induced senescence of breast cancer cells. Molecular and cellular biology, 26(7), pp.2501-2510.

144.Jain, S., Wheeler, J.R., Walters, R.W., Agrawal, A., Barsic, A. and Parker, R., 2016. ATPase-modulated stress granules contain a diverse proteome and substructure. Cell, 164(3), pp.487-498.

145.Jun, J.I. and Lau, L.F., 2017. CCN2 induces cellular senescence in fibroblasts. Journal of cell communication and signaling, 11(1), pp.15-23.

146.Kahlem, P., Dörken, B. and Schmitt, C.A., 2004. Cellular senescence in cancer treatment: friend or foe?. The Journal of clinical investigation, 113(2), pp.169-174.

147.Kahvejian, A., Svitkin, Y.V., Sukarieh, R., M'Boutchou, M.N. and Sonenberg, N., 2005. Mammalian poly (A)-binding protein is a eukaryotic translation initiation factor, which acts via multiple mechanisms. Genes & development, 19(1), pp.104-113.

148.Karpievitch, Y.V., Polpitiya, A.D., Anderson, G.A., Smith, R.D. and Dabney, A.R., 2010. Liquid chromatography mass spectrometry-based proteomics: biological and technological aspects. The annals of applied statistics, 4(4), p.1797.

149.Kaushik, S. and Cuervo, A.M., 2016. AMPK-dependent phosphorylation of lipid droplet protein PLIN2 triggers its degradation by CMA. Autophagy, 12(2), pp.432-438.

150.Kedersha, N. and Anderson, P., 2007. Mammalian stress granules and processing bodies. Methods in enzymology, 431, pp.61-81.

151.Kedersha, N., Chen, S., Gilks, N., Li, W., Miller, I.J., Stahl, J. and Anderson, P., 2002. Evidence that ternary complex (eIF2-GTP-tRNAi Met)–deficient preinitiation complexes are core constituents of mammalian stress granules. Molecular biology of the cell, 13(1), pp.195-210.

152.Kedersha, N., Chen, S., Gilks, N., Li, W., Miller, I.J., Stahl, J. and Anderson, P., 2002. Evidence that ternary complex (eIF2-GTP-tRNAi Met)–deficient preinitiation complexes are core constituents of mammalian stress granules. Molecular biology of the cell, 13(1), pp.195-210.

153.Kedersha, N., Cho, M.R., Li, W., Yacono, P.W., Chen, S., Gilks, N., Golan, D.E. and Anderson, P., 2000. Dynamic shuttling of TIA-1 accompanies the recruitment of mRNA to mammalian stress granules. The Journal of cell biology, 151(6), pp.1257-1268.

154.Kedersha, N., Ivanov, P. and Anderson, P., 2013. Stress granules and cell signaling: more than just a passing phase?. Trends in biochemical sciences, 38(10), pp.494-506.

155.Kedersha, N., Panas, M.D., Achorn, C.A., Lyons, S., Tisdale, S., Hickman, T., Thomas, M., Lieberman, J., McInerney, G.M., Ivanov, P. and Anderson, P., 2016. G3BP–Caprin1–USP10 complexes mediate stress granule condensation and associate with 40S subunits. Journal of Cell Biology, 212(7).

156.Kedersha, N., Stoecklin, G., Ayodele, M., Yacono, P., Lykke-Andersen, J., Fritzler, M.J., Scheuner, D., Kaufman, R.J., Golan, D.E. and Anderson, P., 2005. Stress granules and

processing bodies are dynamically linked sites of mRNP remodeling. The Journal of cell biology, 169(6), pp.871-884.

157.Kedersha, N., Tisdale, S., Hickman, T. and Anderson, P., 2008. Real- time and quantitative imaging of mammalian stress granules and processing bodies. Methods in enzymology, 448, pp.521-552.

158.Kedersha, N.A. and Anderson, P., 2002. Stress granules: sites of mRNA triage that regulate mRNA stability and translatability. Biochemical Society Transactions, 30(6), pp.963-969.

159.Kedersha, N.L., Gupta, M., Li, W., Miller, I. and Anderson, P., 1999. RNA-binding proteins TIA-1 and TIAR link the phosphorylation of eIF-2α to the assembly of mammalian stress granules. The Journal of cell biology, 147(7), pp.1431-1442.

160.Kim, Y.H. and Park, T.J., 2019. Cellular senescence in cancer. BMB reports, 52(1), p.42.

161.Kimmel, A.R., D.L. Brasaemle, M. McAndrews-Hill, C. Sztalryd, and C. Londos. 2010. Adoption of PERILIPIN as a unifying nomenclature for the mammalian PAT-family of intracellular lipid storage droplet proteins. J. Lipid Res. 51:468–471. http://dx.doi.org/10.1194/jlr.R000034

162.Kimura, K., Cuvier, O. and Hirano, T., 2001. Chromosome Condensation by a Human Condensin Complex inXenopus Egg Extracts. Journal of Biological Chemistry, 276(8), pp.5417-5420.

163.Kobayashi, T., Winslow, S., Sunesson, L., Hellman, U. and Larsson, C., 2012. PKCα binds G3BP2 and regulates stress granule formation following cellular stress. PloS one, 7(4), p.e35820.

164.Koopman, R., Schaart, G., and Hesselink, M. K. C. 2001. Optimisation of oil red O staining permits combination with immunofluorescence and automated quantification of lipids. Histochem Cell Biol. 116:63-68.

165.Kuerschner, L., Moessinger, C. and Thiele, C., 2008. Imaging of lipid biosynthesis: how a neutral lipid enters lipid droplets. Traffic, 9(3), pp.338-352.

166.Kuilman, T., Michaloglou, C., Vredeveld, L.C., Douma, S., van Doorn, R., Desmet, C.J., Aarden, L.A., Mooi, W.J. and Peeper, D.S., 2008. Oncogene-induced senescence relayed by an interleukin-dependent inflammatory network. Cell, 133(6), pp.1019-1031.

167.Kulju, K.S. and Lehman, J.M., 1995. Increased p53 protein associated with aging in human diploid fibroblasts. Experimental cell research, 217(2), pp.336-345.

168.Kuo, M.L., Sy, A.J., Xue, L., Chi, M., Lee, M.T.C., Yen, T., Chiang, M.I., Chang, L., Chu, P. and Yen, Y., 2012. RRM2B suppresses activation of the oxidative stress pathway and is up-regulated by p53 during senescence. Scientific reports, 2(1), pp.1-9.

169.Lambert, K.A.T.H.L.E.E.N. and Pirt, S.J., 1979. Growth of human diploid cells (strain MRC-5) in defined medium; replacement of serum by a fraction of serum ultrafiltrate. Journal of cell science, 35(1), pp.381-392.

170.Lavut, A. and Raveh, D., 2012. Sequestration of highly expressed mRNAs in cytoplasmic granules, P-bodies, and stress granules enhances cell viability. PLoS genetics, 8(2), p.e1002527.

171.Lee, B.Y., Han, J.A., Im, J.S., Morrone, A., Johung, K., Goodwin, E.C., Kleijer, W.J., DiMaio, D. and Hwang, E.S., 2006. Senescence- associated β- galactosidase is lysosomal β-galactosidase. Aging cell, 5(2), pp.187-195.

172.Lee, S. and Lee, J.S., 2019. Cellular senescence: A promising strategy for cancer therapy. BMB reports, 52(1), p.35.

173.Li, H., Collado, M., Villasante, A., Strati, K., Ortega, S., Cañamero, M., Blasco, M.A. and Serrano, M., 2009. The Ink4/Arf locus is a barrier for iPS cell reprogramming. Nature, 460(7259), pp.1136-1139.

174.Li, Y., Nichols, M.A., Shay, J.W. and Xiong, Y., 1994. Transcriptional repression of the D-type cyclin-dependent kinase inhibitor p16 by the retinoblastoma susceptibility gene product pRb. Cancer research, 54(23), pp.6078-6082.

175.Li, Y.R., King, O.D., Shorter, J. and Gitler, A.D., 2013. Stress granules as crucibles of ALS pathogenesis. Journal of cell biology, 201(3), pp.361-372.

176.Li, Y.R., King, O.D., Shorter, J. and Gitler, A.D., 2013. Stress granules as crucibles of ALS pathogenesis. Journal of cell biology, 201(3), pp.361-372.

177.Lian, X.J. and Gallouzi, I.E., 2009. Oxidative stress increases the number of stress granules in senescent cells and triggers a rapid decrease in p21waf1/cip1 translation. Journal of Biological Chemistry, 284(13), pp.8877-8887.

178.Lichtenthaler, H.K., 1998. The stress concept in plants: an introduction. Annals of the New York Academy of Sciences, 851, p.187.

179.Lin, P., Mobasher, M.E. and Alawi, F., 2014. Acute dyskerin depletion triggers cellular senescence and renders osteosarcoma cells resistant to genotoxic stress-induced apoptosis. Biochemical and biophysical research communications, 446(4), pp.1268-1275.

180.Lindsey, J., McGill, N.I., Lindsey, L.A., Green, D.K., Cooke, H.J., 1991. In vivo loss of telomeric repeats with age in humans. Mutat. Res. 256, 45–48.

181.Lingner, J., Cooper, J.P. and Cech, T., 1995. Telomerase and DNA end replication: no longer a lagging strand problem?. Science, 269(5230), pp.1533-1535.

182.Liu, B., Zhou, Z. and Lam, Y.W., 2011. Quantitative nucleolar proteomics reveals nuclear re-organization during stress-induced senescence in mouse fibroblast. BMC cell biology, 12(1), pp.1-13.

183.Lizardo, D.Y., Lin, Y.L., Gokcumen, O. and Atilla-Gokcumen, G.E., 2017. Regulation of lipids is central to replicative senescence. Molecular BioSystems, 13(3), pp.498-509.

184.Logar, D.B., Komadina, R., Preželj, J., Ostanek, B., Trošt, Z. and Marc, J., 2007. Expression of bone resorption genes in osteoarthritis and in osteoporosis. Journal of bone and mineral metabolism, 25(4), pp.219-225.

185.Londos, C., Brasaemle, D. L., Schultz, C. J., Segrest, J. P. and Kimmel, A. R., 1999. Perilipins, ADRP, and other proteins that associate with intracellular neutral lipid droplets in animal cells. Semin Cell Dev Biol. 10:51-58.

186.López-Otín, C., Blasco, M.A., Partridge, L., Serrano, M. and Kroemer, G., 2013. The hallmarks of aging. Cell, 153(6), pp.1194-1217.

187.Ludwig, C., Gillet, L., Rosenberger, G., Amon, S., Collins, B.C. and Aebersold, R., 2018. Data- independent acquisition- based SWATH- MS for quantitative proteomics: a tutorial. Molecular systems biology, 14(8), p.e8126.

188.Lukas, C., Falck, J., Bartkova, J., Bartek, J. and Lukas, J., 2003. Distinct spatiotemporal dynamics of mammalian checkpoint regulators induced by DNA damage. Nature cell biology, 5(3), pp.255-260.

189.Lumba, M.A., Willis, L.M., Santra, S., Rana, R., Schito, L., Rey, S., Wouters, B.G. and Nitz, M., 2017. A β-galactosidase probe for the detection of cellular senescence by mass cytometry. Organic & biomolecular chemistry, 15(30), pp.6388-6392.

190.Lyu, Y.L. and Liu, L.F., 2012. Doxorubicin cardiotoxicity revisited: ROS versus Top2. Recent Advances in Cancer Research and Therapy, pp.351-369.

191.Ma, B., He, L.F., Zhang, Y.L., Chen, M., Wang, L.L., Yang, H.W., Yan, T., Sun, M.X. and Zheng, C.Y., 2015. Characteristics and viral propagation properties of a new human diploid cell line, walvax-2, and its suitability as a candidate cell substrate for vaccine production. Human vaccines & immunotherapeutics, 11(4), pp.998-1009.

192.MacMillan-Crow, L.A. and Thompson, J.A., 1999. Tyrosine modifications and inactivation of active site manganese superoxide dismutase mutant (Y34F) by peroxynitrite. Archives of biochemistry and biophysics, 366(1), pp.82-88.

193.Mahboubi, H. and Stochaj, U., 2017. Cytoplasmic stress granules: Dynamic modulators of cell signaling and disease. Biochimica et Biophysica Acta (BBA)-Molecular Basis of Disease, 1863(4), pp.884-895.

194.Mailand, N., Falck, J., Lukas, C., Syljuåsen, R.G., Welcker, M., Bartek, J. and Lukas, J., 2000. Rapid destruction of human Cdc25A in response to DNA damage. Science, 288(5470), pp.1425-1429.

195.Mak, H.Y., 2012. Lipid droplets as fat storage organelles in Caenorhabditis elegans thematic review series: lipid droplet synthesis and metabolism: from yeast to man. Journal of lipid research, 53(1), pp.28-33.

196.Marcus, R.L., Addison, O., Kidde, J.P., Dibble, L.E. and Lastayo, P.C., 2010. Skeletal muscle fat infiltration: impact of age, inactivity, and exercise. The journal of nutrition, health & aging, 14(5), pp.362-366.

197.Marthandan, S., Priebe, S., Hemmerich, P., Klement, K. and Diekmann, S., 2014. Long-term quiescent fibroblast cells transit into senescence. PLoS One, 9(12).

198.Martin, S. and Parton, R.G., 2005, April. Caveolin, cholesterol, and lipid bodies. In Seminars in cell & developmental biology (Vol. 16, No. 2, pp. 163-174). Academic Press.

199.Martin, S. and Parton, R.G., 2006. Lipid droplets: a unified view of a dynamic organelle. Nature reviews Molecular cell biology, 7(5), pp.373-378.

200.Martinon, F., Burns, K. and Tschopp, J., 2002. The inflammasome: a molecular platform triggering activation of inflammatory caspases and processing of proIL-β. Molecular cell, 10(2), pp.417-426.

201.Matsuki, H., Takahashi, M., Higuchi, M., Makokha, G.N., Oie, M. and Fujii, M., 2013. Both G3BP1 and G3BP2 contribute to stress granule formation. Genes to Cells, 18(2), pp.135-146.

202.Matthews, C., Gorenne, I., Scott, S., Figg, N., Kirkpatrick, P., Ritchie, A., Goddard, M. and Bennett, M., 2006. Vascular smooth muscle cells undergo telomere-based senescence in human atherosclerosis: effects of telomerase and oxidative stress. Circulation research, 99(2), pp.156-164.

203.Mazroui, R., Huot, M.E., Tremblay, S., Filion, C., Labelle, Y. and Khandjian, E.W., 2002. Trapping of messenger RNA by Fragile X Mental Retardation protein into cytoplasmic granules induces translation repression. Human molecular genetics, 11(24), pp.3007-3017.

204.Mazroui, R., Sukarieh, R., Bordeleau, M.E., Kaufman, R.J., Northcote, P., Tanaka, J., Gallouzi, I. and Pelletier, J., 2006. Inhibition of ribosome recruitment induces stress granule formation

independently of eukaryotic initiation factor 2α phosphorylation. Molecular biology of the cell, 17(10), pp.4212-4219.

205.McDermott, M., Wakelam, M. J. O. and Morris, A. J., 2004. Phospholipase D. Biochem. Cell Biol. 82, 225-253.

206.McHugh, D. and Gil, J., 2018. Senescence and aging: Causes, consequences, and therapeutic avenues. Journal of Cell Biology, 217(1), pp.65-77.

207.McIlwain, D.R., Berger, T. and Mak, T.W., 2013. Caspase functions in cell death and disease. Cold Spring Harbor perspectives in biology, 5(4), p.a008656.

208.Meagher, M., Epling, L.B. and Enemark, E.J., 2019. DNA translocation mechanism of the MCM complex and implications for replication initiation. Nature communications, 10(1), pp.1-13.

209.Melk, A., Kittikowit, W., Sandhu, I., Halloran, K.M., Grimm, P., Schmidt, B.M. and Halloran, P.F., 2003. Cell senescence in rat kidneys in vivo increases with growth and age despite lack of telomere shortening. Kidney international, 63(6), pp.2134-2143.

210.Michaloglou, C., Vredeveld, L.C., Soengas, M.S., Denoyelle, C., Kuilman, T., Van Der Horst, C.M., Majoor, D.M., Shay, J.W., Mooi, W.J. and Peeper, D.S., 2005. BRAF E600-associated senescence-like cell cycle arrest of human naevi. Nature, 436(7051), pp.720-724.

211.Mijit, M., Caracciolo, V., Melillo, A., Amicarelli, F. and Giordano, A., 2020. Role of p53 in the Regulation of Cellular Senescence. Biomolecules, 10(3), p.420.

212.Millner, A., Lizardo, D.Y. and Atilla- Gokcumen, G.E., 2020. Untargeted Lipidomics Highlight the Depletion of Deoxyceramides during Therapy- Induced Senescence. Proteomics, 20(10), p.2000013.

213.Mishima, K., Handa, J.T., Aotaki-Keen, A., Lutty, G.A., Morse, L.S. and Hjelmeland, L.M., 1999. Senescence-associated beta-galactosidase histochemistry for the primate eye. Investigative ophthalmology & visual science, 40(7), pp.1590-1593.

214.Moding, E.J., Kastan, M.B. and Kirsch, D.G., 2013. Strategies for optimizing the response of cancer and normal tissues to radiation. Nature reviews Drug discovery, 12(7), pp.526-542.

215.Mollet, S., Cougot, N., Wilczynska, A., Dautry, F., Kress, M., Bertrand, E. and Weil, D., 2008. Translationally repressed mRNA transiently cycles through stress granules during stress. Molecular biology of the cell, 19(10), pp.4469-4479.

216.Morgunova, G.V., Kolesnikov, A.V., Klebanov, A.A. and Khokhlov, A.N., 2015. Senescence-associated β-galactosidase—A biomarker of aging, DNA damage, or cell proliferation restriction?. Moscow University biological sciences bulletin, 70(4), pp.165-167.

217.Moujaber, O., Mahboubi, H., Kodiha, M., Bouttier, M., Bednarz, K., Bakshi, R., White, J., Larose, L., Colmegna, I. and Stochaj, U., 2017. Dissecting the molecular mechanisms that impair stress granule formation in aging cells. Biochimica et Biophysica Acta (BBA)-Molecular Cell Research, 1864(3), pp.475-486.

218.Muñoz-Espín, D. and Serrano, M., 2014. Cellular senescence: from physiology to pathology. Nature reviews Molecular cell biology, 15(7), pp.482-496.

219.Munro, J., Steeghs, K., Morrison, V., Ireland, H. and Parkinson, E.K., 2001. Human fibroblast replicative senescence can occur in the absence of extensive cell division and short telomeres. Oncogene, 20(27), pp.3541-3552.

220.Murphy, D.J., 2001. The biogenesis and functions of lipid bodies in animals, plants and microorganisms. Progress in lipid research, 40(5), pp.325-438.

221.Nagano, T., Nakano, M., Nakashima, A., Onishi, K., Yamao, S., Enari, M., Kikkawa, U. and Kamada, S., 2016. Identification of cellular senescence-specific genes by comparative transcriptomics. Scientific reports, 6(1), pp.1-13.

222.Nakagawa, H. and Opitz, O.G., 2007. Inducing cellular senescence using defined genetic elements. In Biological Aging (pp. 167-178). Humana Press.

223.Nakano, M., Nakashima, A., Nagano, T., Ishikawa, S., Kikkawa, U. and Kamada, S., 2013. Branched-chain amino acids enhance premature senescence through mammalian target of rapamycin complex I-mediated upregulation of p21 protein. PloS one, 8(11).

224.Nanni, S., Melandri, G., Hanemaaijer, R., Cervi, V., Tomasi, L., Altimari, A., Van Lent, N., Tricoci, P., Bacchi, L. and Branzi, A., 2007. Matrix metalloproteinases in premature coronary atherosclerosis: influence of inhibitors, inflammation, and genetic polymorphisms. Translational Research, 149(3), pp.137-144.

225.Narita, M., Nuñez, S., Heard, E., Narita, M., Lin, A.W., Hearn, S.A., Spector, D.L., Hannon, G.J. and Lowe, S.W., 2003. Rb-mediated heterochromatin formation and silencing of E2F target genes during cellular senescence. Cell, 113(6), pp.703-716.

226.Nishio, K., Inoue, A., Qiao, S., Kondo, H. and Mimura, A., 2001. Senescence and cytoskeleton: overproduction of vimentin induces senescent-like morphology in human fibroblasts. Histochemistry and cell biology, 116(4), pp.321-327.

227.Noda, A., Hirai, Y., Hamasaki, K., Mitani, H., Nakamura, N. and Kodama, Y., 2012. Unrepairable DNA double-strand breaks that are generated by ionising radiation determine the fate of normal human cells. Journal of cell science, 125(22), pp.5280-5287.

228.Nonhoff, U., Ralser, M., Welzel, F., Piccini, I., Balzereit, D., Yaspo, M.L., Lehrach, H. and Krobitsch, S., 2007. Ataxin-2 interacts with the DEAD/H-box RNA helicase DDX6 and interferes with P-bodies and stress granules. Molecular biology of the cell, 18(4), pp.1385-1396.

229.North, B.J. and Sinclair, D.A., 2012. The intersection between aging and cardiovascular disease. Circulation research, 110(8), pp.1097-1108.

230.Oda, Y., Huang, K., Cross, F.R., Cowburn, D. and Chait, B.T., 1999. Accurate quantitation of protein expression and site-specific phosphorylation. Proceedings of the National Academy of Sciences, 96(12), pp.6591-6596.

231.Ohsaki, Y., Maeda, T. and Fujimoto, T. 2005. Fixation and permeabilization protocol is critical for the immunolabeling of lipid droplet proteins. Histochem Cell Biol. 124:445-452.

232.Olovnikov, A.M., 1973. A theory of marginotomy: the incomplete copying of template margin in enzymic synthesis of polynucleotides and biological significance of the phenomenon. Journal of theoretical biology, 41(1), pp.181-190.

233.Olzmann, J.A. and Carvalho, P., 2019. Dynamics and functions of lipid droplets. Nature reviews Molecular cell biology, 20(3), pp.137-155.

234.Omer, A., Patel, D., Lian, X.J., Sadek, J., Di Marco, S., Pause, A., Gorospe, M. and Gallouzi, I.E., 2018. Stress granules counteract senescence by sequestration of PAI- 1. EMBO reports, 19(5).

235.Palangi, F., Samuel, S.M., Thompson, I.R., Triggle, C.R. and Emara, M.M., 2017. Effects of oxidative and thermal stresses on stress granule formation in human induced pluripotent stem cells. Plos one, 12(7), p.e0182059.

236.Pan, C., Xue, B.H., Ellis, T.M., Peace, D.J., Diaz, M.O., 1997. Changes in telomerase ac- tivity and telomere length during human T lymphocyte senescence. Exp. Cell Res. 231, 346–353.

237.Paradis, V., Youssef, N., Dargère, D., Bâ, N., Bonvoust, F., Deschatrette, J. and Bedossa, P., 2001. Replicative senescence in normal liver, chronic hepatitis C, and hepatocellular carcinomas. Human pathology, 32(3), pp.327-332.

238.Pascal, T., Debacq-Chainiaux, F., Chrétien, A., Bastin, C., Dabée, A.F., Bertholet, V., Remacle, J. and Toussaint, O., 2005. Comparison of replicative senescence and stress-induced premature senescence combining differential display and low-density DNA arrays. FEBS letters, 579(17), pp.3651-3659.

239.Passos, J.F., Nelson, G., Wang, C., Richter, T., Simillion, C., Proctor, C.J., Miwa, S., Olijslagers, S., Hallinan, J., Wipat, A. and Saretzki, G., 2010. Feedback between p21 and reactive oxygen production is necessary for cell senescence. Molecular systems biology, 6(1).

240.Passos, J.F., Saretzki, G., Ahmed, S., Nelson, G., Richter, T., Peters, H., Wappler, I., Birket, M.J., Harold, G., Schaeuble, K. and Birch-Machin, M.A., 2007. Mitochondrial dysfunction accounts for the stochastic heterogeneity in telomere-dependent senescence. PLoS biology, 5(5).

241.Pirkkala, L., Nykänen, P. and Sistonen, L.E.A., 2001. Roles of the heat shock transcription factors in regulation of the heat shock response and beyond. The FASEB Journal, 15(7), pp.1118-1131.

242.Pitt, J.J., 2009. Principles and applications of liquid chromatography-mass spectrometry in clinical biochemistry. The Clinical Biochemist Reviews, 30(1), p.19.

243.Pol, A., Gross, S.P. and Parton, R.G., 2014. Biogenesis of the multifunctional lipid droplet: lipids, proteins, and sites. Journal of cell biology, 204(5), pp.635-646.

244.Protter, D.S. and Parker, R., 2016. Principles and properties of stress granules. Trends in cell biology, 26(9), pp.668-679.

245.Provost, E., Weier, C.A. and Leach, S.D., 2013. Multiple ribosomal proteins are expressed at high levels in developing zebrafish endoderm and are required for normal exocrine pancreas development. Zebrafish, 10(2), pp.161-169.

246.Raghuram, G.V. and Mishra, P.K., 2014. Stress induced premature senescence: a new culprit in ovarian tumorigenesis?. The Indian journal of medical research, 140(Suppl 1), p.S120.

247.Ramaswami, M., Taylor, J.P. and Parker, R., 2013. Altered ribostasis: RNA-protein granules in degenerative disorders. Cell, 154(4), pp.727-736.

248.Rayess, H., Wang, M.B. and Srivatsan, E.S., 2012. Cellular senescence and tumor suppressor gene p16. International journal of cancer, 130(8), pp.1715-1725.

249.Rohwedder, A., Zhang, Q., Rudge, S.A. and Wakelam, M.J., 2014. Lipid droplet formation in response to oleic acid in Huh-7 cells is mediated by the fatty acid receptor FFAR4. Journal of cell science, 127(14), pp.3104-3115.

250.Rokudai, S., Laptenko, O., Arnal, S.M., Taya, Y., Kitabayashi, I. and Prives, C., 2013. MOZ increases p53 acetylation and premature senescence through its complex formation with PML. Proceedings of the National Academy of Sciences, 110(10), pp.3895-3900.

251.Russo, A.J., Magro, P.G., Hu, Z., Li, W.W., Peters, R., Mandola, J., Banerjee, D. and Bertino, J.R., 2006. E2F-1 overexpression in U2OS cells increases cyclin B1 levels and cdc2 kinase activity and sensitizes cells to antimitotic agents. Cancer research, 66(14), pp.7253-7260.

252.Sabin, R.J. and Anderson, R.M., 2011. Cellular Senescence-its role in cancer and the response to ionizing radiation. Genome integrity, 2(1), p.7.

253.Saitou, M., Lizardo, D.Y., Taskent, R.O., Millner, A., Gokcumen, O. and Atilla-Gokcumen, G.E., 2018. An evolutionary transcriptomics approach links CD36 to membrane remodeling in replicative senescence. Molecular Omics, 14(4), pp.237-246.

254.Sato, S., Fukasawa, M., Yamakawa, Y., Natsume, T., Suzuki, T., Shoji, I., Aizaki, H., Miyamura, T. and Nishijima, M., 2006. Proteomic profiling of lipid droplet proteins in hepatoma cell lines expressing hepatitis C virus core protein. Journal of biochemistry, 139(5), pp.921-930.

255.Sen, M., Akeno, N., Reece, A., Miller, A.L., Simpson, D.S. and Wikenheiser-Brokamp, K.A., 2017. p16 controls epithelial cell growth and suppresses carcinogenesis through mechanisms that do not require RB1 function. Oncogenesis, 6(4), pp.e320-e320.

256.Shammas, M.A., 2011. Telomeres, lifestyle, cancer, and aging. Current opinion in clinical nutrition and metabolic care, 14(1), p.28.

257.Sharpless, N.E. and Sherr, C.J., 2015. Forging a signature of in vivo senescence. Nature Reviews Cancer, 15(7), pp.397-408.

258.Shaw, J., Costa-Pinheiro, P., Patterson, L., Drews, K., Spiegel, S. and Kester, M., 2018. Novel sphingolipid-based cancer therapeutics in the personalized medicine era. In Advances in cancer research (Vol. 140, pp. 327-366). Academic Press.

259.Shay, J.W., Pereira-Smith, O.M. and Wright, W.E., 1991. A role for both RB and p53 in the regulation of human cellular senescence. Experimental cell research, 196(1), pp.33-39.

260.Shen, C., Wang, Z., Shankar, G., Zhang, X. and Li, L., 2008. A hierarchical statistical model to assess the confidence of peptides and proteins inferred from tandem mass spectrometry. Bioinformatics, 24(2), pp.202-208.

261.Sherr, C.J. and Roberts, J.M., 1999. CDK inhibitors: positive and negative regulators of G1-phase progression. Genes & development, 13(12), pp.1501-1512.

262.Shi, X., Wang, J., Lei, Y., Cong, C., Tan, D. and Zhou, X., 2019. Research progress on the PI3K/AKT signaling pathway in gynecological cancer. Molecular medicine reports, 19(6), pp.4529-4535.

263.Shtutman, M., Chang, B.D., Schools, G.P. and Broude, E.V., 2017. Cellular model of p21-induced senescence. In Oncogene-Induced Senescence (pp. 31-39). Humana Press, New York, NY.

264.Skinner, J.R., Shew, T.M., Schwartz, D.M., Tzekov, A., Lepus, C.M., Abumrad, N.A. and Wolins, N.E., 2009. Diacylglycerol enrichment of endoplasmic reticulum or lipid droplets

recruits perilipin 3/TIP47 during lipid storage and mobilization. Journal of Biological Chemistry, 284(45), pp.30941-30948.

265.Smith, J.R. and Pereira-Smith, O.M., 1996. Replicative senescence: implications for in vivo aging and tumor suppression. Science, 273(5271), pp.63-67.

266.Smits, M., van Rijn, S., Hulleman, E., Biesmans, D., van Vuurden, D.G., Kool, M., Haberler, C., Aronica, E., Vandertop, W.P., Noske, D.P. and Würdinger, T., 2012. EZH2-regulated DAB2IP is a medulloblastoma tumor suppressor and a positive marker for survival. Clinical cancer research, 18(15), pp.4048-4058.

267.Solomon, S., Xu, Y., Wang, B., David, M.D., Schubert, P., Kennedy, D. and Schrader, J.W., 2007. Distinct Structural Features ofCaprin-1 Mediate Its Interaction with G3BP-1 and Its Induction of Phosphorylation of Eukaryotic Translation Initiation Factor 2α, Entry to Cytoplasmic Stress Granules, and Selective Interaction with a Subset of mRNAs. Molecular and cellular biology, 27(6), pp.2324-2342.

268.Spector, D.L., 2006. SnapShot: cellular bodies. Cell, 127(5), pp.1071-e1.

269.Spitaler, M. and Cantrell, D.A., 2004. Protein kinase C and beyond. Nature immunology, 5(8), pp.785-790.

270.Stanulis-Praeger, B., 1987. Cellular senescence revisited: a review. Mechanisms of ageing and development, 38(1), pp.1-48.

271.Stein, G.H., Drullinger, L.F., Soulard, A. and Dulić, V., 1999. Differential roles for cyclin-dependent kinase inhibitors p21 and p16 in the mechanisms of senescence and differentiation in human fibroblasts. Molecular and cellular biology, 19(3), pp.2109-2117.

272.Stöhr, N., Lederer, M., Reinke, C., Meyer, S., Hatzfeld, M., Singer, R.H. and Hüttelmaier, S., 2006. ZBP1 regulates mRNA stability during cellular stress. The Journal of cell biology, 175(4), pp.527-534.

273.Storck, E.M., Özbalci, C. and Eggert, U.S., 2018. Lipid cell biology: a focus on lipids in cell division. Annual Review of Biochemistry, 87, pp.839-869.

274.Sun, X., Li, B., Li, X., Wang, Y., Xu, Y., Jin, Y., Piao, F. and Sun, G., 2006. Effects of sodium arsenite on catalase activity, gene and protein expression in HaCaT cells. Toxicology in vitro, 20(7), pp.1139-1144.

275.Suzuki, K., Mori, I., Nakayama, Y., Miyakoda, M., Kodama, S. and Watanabe, M., 2001. Radiation-induced senescence-like growth arrest requires TP53 function but not telomere shortening. Radiation research, 155(1), pp.248-253.

276.Takubo, K., Nakamura, K.I., Izumiyama, N., Furugori, E., Sawabe, M., Arai, T., Esaki, Y., Mafune, K.I., Kammori, M., Fujiwara, M. and Kato, M., 2000. Telomere shortening with aging in human liver. The Journals of Gerontology Series A: Biological Sciences and Medical Sciences, 55(11), pp.B533-B536.

277.Tan, S.L.W., Chadha, S., Liu, Y., Gabasova, E., Perera, D., Ahmed, K., Constantinou, S., Renaudin, X., Lee, M., Aebersold, R. and Venkitaraman, A.R., 2017. A class of environmental and endogenous toxins induces BRCA2 haploinsufficiency and genome instability. Cell, 169(6), pp.1105-1118.

278.Tauchi-Sato, K., Ozeki, S., Houjou, T., Taguchi, R. and Fujimoto, T., 2002. The surface of lipid droplets is a phospholipid monolayer with a unique fatty acid composition. Journal of Biological Chemistry, 277(46), pp.44507-44512.

279.Tchkonia, T., Morbeck, D.E., Von Zglinicki, T., Van Deursen, J., Lustgarten, J., Scrable, H., Khosla, S., Jensen, M.D. and Kirkland, J.L., 2010. Fat tissue, aging, and cellular senescence. Aging cell, 9(5), pp.667-684.

280.Tchkonia, T., Zhu, Y., Van Deursen, J., Campisi, J. and Kirkland, J.L., 2013. Cellular senescence and the senescent secretory phenotype: therapeutic opportunities. The Journal of clinical investigation, 123(3), pp.966-972.

281.Tourrière, H., Chebli, K., Zekri, L., Courselaud, B., Blanchard, J.M., Bertrand, E. and Tazi, J., 2003. The RasGAP-associated endoribonuclease G3BP assembles stress granules. The Journal of cell biology, 160(6), pp.823-831.

282.Toussain, O., Dumont, P., Dierick, J.F., Pascal, T., Frippiat, C., Chainiaux, F., Sluse, F., Eliaers, F. and Remacle, J., 2000. Stress-induced premature senescence. Essence of life, evolution, stress, and aging. Annals of the New York Academy of Sciences, 908, pp.85-98.

283.Toussaint, O., Dumont, P., Remacle, J., Dierick, J.F., Pascal, T., Frippiat, C., Magalhaes, J.P., Zdanov, S. and Chainiaux, F., 2002. Stress-induced premature senescence or stress-induced senescence-like phenotype: one in vivo reality, two possible definitions?. The Scientific World JOURNAL, 2, pp.230-247.

284.Toussaint, O., Medrano, E.E. and von Zglinicki, T., 2000. Cellular and molecular mechanisms of stress-induced premature senescence (SIPS) of human diploid fibroblasts and melanocytes. Experimental gerontology, 35(8), pp.927-945.

285.Tsai, Y.S., Lai, C.L., Lai, C.H., Chang, K.H., Wu, K., Tseng, S.F., Fazli, L., Gleave, M., Xiao, G., Gandee, L. and Sharifi, N., 2014. The role of homeostatic regulation between tumor suppressor DAB2IP and oncogenic Skp2 in prostate cancer growth. Oncotarget, 5(15), p.6425.

286.Turner, G., Webb, T., Wake, S. and Robinson, H., 1996. Prevalence of fragile X syndrome. American journal of medical genetics, 64(1), pp.196-197.

287.Van Deursen, J.M., 2014. The role of senescent cells in ageing. Nature, 509(7501), pp.439-446.

288.Van Treeck, B., Protter, D.S., Matheny, T., Khong, A., Link, C.D. and Parker, R., 2018. RNA self-assembly contributes to stress granule formation and defining the stress granule transcriptome. Proceedings of the National Academy of Sciences, 115(11), pp.2734-2739.

289.Vasile, E., Tomita, Y., Brown, L.F., Kocher, O. and Dvorak, H.F., 2001. Differential expression of thymosin β- 10 by early passage and senescent vascular endothelium is modulated by VPF/VEGF: evidence for senescent endothelial cells in vivo at sites of atherosclerosis. The FASEB Journal, 15(2), pp.458-466.

290.Vasileiou, P.V., Evangelou, K., Vlasis, K., Fildisis, G., Panayiotidis, M.I., Chronopoulos, E., Passias, P.G., Kouloukoussa, M., Gorgoulis, V.G. and Havaki, S., 2019. Mitochondrial Homeostasis and Cellular Senescence. Cells, 8(7), p.686.

291.Ventura, A., Kirsch, D.G., McLaughlin, M.E., Tuveson, D.A., Grimm, J., Lintault, L., Newman, J., Reczek, E.E., Weissleder, R. and Jacks, T., 2007. Restoration of p53 function leads to tumour regression in vivo. Nature, 445(7128), pp.661-665.

292.Vogeser, M. and Kirchhoff, F., 2011. Progress in automation of LC-MS in laboratory medicine. Clinical biochemistry, 44(1), pp.4-13.

293.Vogeser, M. and Seger, C., 2008. A decade of HPLC–MS/MS in the routine clinical laboratory—Goals for further developments. Clinical biochemistry, 41(9), pp.649-662.

294.Walther, T.C. and Farese Jr, R.V., 2012. Lipid droplets and cellular lipid metabolism. Annual review of biochemistry, 81, pp.687-714.

295.Wang, C.Y. and Lin, C.F., 2014. Annexin A2: its molecular regulation and cellular expression in cancer development. Disease markers, 2014.

296.Wang, H., Becuwe, M., Housden, B.E., Chitraju, C., Porras, A.J., Graham, M.M., Liu, X.N., Thiam, A.R., Savage, D.B., Agarwal, A.K. and Garg, A., 2016. Seipin is required for converting nascent to mature lipid droplets. Elife, 5, p.e16582.

297.Wang, Y.C., Peterson, S.E. and Loring, J.F., 2014. Protein post-translational modifications and regulation of pluripotency in human stem cells. Cell research, 24(2), pp.143-160.

298.Weiss, A.K., Albertini, E., Holzknecht, M., Cappuccio, E., Dorigatti, I., Krahbichler, A., Damisch, E., Gstach, H. and Jansen-Dürr, P., 2020. Regulation of cellular senescence by

eukaryotic members of the FAH superfamily–A role in calcium homeostasis?. Mechanisms of ageing and development, 190, p.111284.

299. Wek, R.C., Jiang, H.Y. and Anthony, T.G., 2006. Coping with stress: eIF2 kinases and translational control.

300. Wheeler, J.R., Matheny, T., Jain, S., Abrisch, R. and Parker, R., 2016. Distinct stages in stress granule assembly and disassembly. Elife, 5, p.e18413.

301. Wheeler, J.R., Matheny, T., Jain, S., Abrisch, R. and Parker, R., 2016. Distinct stages in stress granule assembly and disassembly. Elife, 5, p.e18413.

302. White, J.P. and Lloyd, R.E., 2012. Regulation of stress granules in virus systems. Trends in microbiology, 20(4), pp.175-183.

303. Whittemore, K., Vera, E., Martínez-Nevado, E., Sanpera, C. and Blasco, M.A., 2019. Telomere shortening rate predicts species life span. Proceedings of the National Academy of Sciences, 116(30), pp.15122-15127.

304. Wiley, C.D., Velarde, M.C., Lecot, P., Liu, S., Sarnoski, E.A., Freund, A., Shirakawa, K., Lim, H.W., Davis, S.S., Ramanathan, A. and Gerencser, A.A., 2016. Mitochondrial dysfunction induces senescence with a distinct secretory phenotype. Cell metabolism, 23(2), pp.303-314.

305. Wilfling, F., Thiam, A.R., Olarte, M.J., Wang, J., Beck, R., Gould, T.J., Allgeyer, E.S., Pincet, F., Bewersdorf, J., Farese Jr, R.V. and Walther, T.C., 2014. Arf1/COPI machinery acts directly on lipid droplets and enables their connection to the ER for protein targeting. Elife, 3, p.e01607.

306. Williams, E.G., Wu, Y., Jha, P., Dubuis, S., Blattmann, P., Argmann, C.A., Houten, S.M., Amariuta, T., Wolski, W., Zamboni, N. and Aebersold, R., 2016. Systems proteomics of liver mitochondria function. Science, 352(6291).

307. Wischhusen, J., Melero, I. and Fridman, W.H., 2020. Growth/differentiation factor-15 (GDF-15): from biomarker to novel targetable immune checkpoint. Frontiers in Immunology, 11, p.951.

308. Xi, C.H.E.N., Zhang, W., Gao, Y.F., Su, X.Q. and Zhai, Z.H., 2002. Senescence-like changes induced by expression of p21 Waf1/Cip1 in NIH3T3 cell line. Cell research, 12(3), pp.229-233.

309. Xu, M., Palmer, A.K., Ding, H., Weivoda, M.M., Pirtskhalava, T., White, T.A., Sepe, A., Johnson, K.O., Stout, M.B., Giorgadze, N., Jensen, M.D., LeBrasseur, N.K., Tchkonia, T., Kirkland, J.L., 2015. Targeting senescent cells enhances adipogenesis and meta- bolic function in old age. eLife 4, e12997.

310.Xue, W., Zender, L., Miething, C., Dickins, R.A., Hernando, E., Krizhanovsky, V., Cordon-Cardo, C. and Lowe, S.W., 2007. Senescence and tumour clearance is triggered by p53 restoration in murine liver carcinomas. Nature, 445(7128), pp.656-660.

311.Yang, L., Ding, Y., Chen, Y., Zhang, S., Huo, C., Wang, Y., Yu, J., Zhang, P., Na, H., Zhang, H. and Ma, Y., 2012. The proteomics of lipid droplets: structure, dynamics, and functions of the organelle conserved from bacteria to humans. Journal of lipid research, 53(7), pp.1245-1253.

312.Ye, X., Luke, B., Andresson, T. and Blonder, J., 2009. 18O stable isotope labeling in MS-based proteomics. Briefings in Functional Genomics and Proteomics, 8(2), pp.136-144.

313.Yosef, R., Pilpel, N., Papismadov, N., Gal, H., Ovadya, Y., Vadai, E., Miller, S., Porat, Z., Ben- Dor, S. and Krizhanovsky, V., 2017. p21 maintains senescent cell viability under persistent DNA damage response by restraining JNK and caspase signaling. The EMBO journal, 36(15), pp.2280-2295.

314.Youn, J.Y., Dyakov, B.J., Zhang, J., Knight, J.D., Vernon, R.M., Forman-Kay, J.D. and Gingras, A.C., 2019. Properties of Stress Granule and P-Body Proteomes. Molecular Cell, 76(2), pp.286-294.

315.Zdanov, S., Remacle, J. and Toussaint, O., 2006. Establishment of H2O2- Induced Premature Senescence in Human Fibroblasts Concomitant with Increased Cellular Production of H2O2. Annals of the New York Academy of Sciences, 1067(1), pp.210-216.

316.Zhang, R., Chen, W. and Adams, P.D., 2007. Molecular dissection of formation of senescence-associated heterochromatin foci. Molecular and cellular biology, 27(6), pp.2343-2358.

317.Zhang, Y., Gao, Y., Zhang, G., Huang, S., Dong, Z., Kong, C., Su, D., Du, J., Zhu, S., Liang, Q. and Zhang, J., 2011. DNMT3a plays a role in switches between doxorubicin- induced senescence and apoptosis of colorectal cancer cells. International journal of cancer, 128(3), pp.551-561.

318.Zhao, W., Zhao, J., Hou, M., Wang, Y., Zhang, Y., Zhao, X., Zhang, C. and Guo, D., 2014. HuR and TIA1/TIAL1 are involved in regulation of alternative splicing of SIRT1 pre-mRNA. International journal of molecular sciences, 15(2), pp.2946-2958.

10 Appendices

Table 7.1: Enriched GO terms (BP) (Overrepresented)

ID	Description	p.adjusted	q.value	Count	Gene ID
GO:0090150	establishment of protein localization to membrane	1.95E-07	1.71E-07	20	RPL4/RPL32/RPL14/RPL13A/RPL34/RPL18/RPL7/RPL35A/ RPL18A/RPL29/STOM/RPL36/RFTN1/MICALL1/KRT18/ RPS29/RPS13/RPL27/RPL21/RPL15
GO:0006605	protein targeting	4.06E-05	3.56E-05	19	RPL4/RPL32/RPL14/RPL13A/RPL34/RPL18/RPL7/RPL35A/ RPL18A/RPL29/STOM/RPL36/MICALL1/RPS29/RPS13/ RPL27/ATP5IF1/RPL21/RPL15
GO:0070972	protein localization to endoplasmic reticulum	2.89E-10	2.54E-10	17	RPL4/RPL32/RPL14/RPL13A/RPL34/RPL18/RPL7/RPL35A/ RPL18A/RPL29/RPL36/RPS29/RPS13/RPL27/RPL21/RPL15/ KDELR1
GO:0019080	viral gene expression	6.55E-08	5.76E-08	17	RPL4/RPL32/RPL14/RPL13A/RPL34/RPL18/RPL7/RPL35A/ RPL18A/RPL29/RPL36/RPS29/RPS13/RPL27/RPL21/RPL15/ HMGA2
GO:0006401	RNA catabolic process	0.000531816	0.000467093	17	RPL4/RPL32/RPL14/RPL13A/RPL34/RPL18/RPL7/RPL35A/ RPL18A/RPL29/RPL36/PSMB8/RPS29/RPS13/RPL27/RPL21/ RPL15

GO:0044282	small molecule catabolic process	0.000541489	0.000475588	17	ALDH4A1/TIGAR/MCCC2/APOE/PNP/UPP1/NT5E/SLC9A1/RENBP/CDA/ABAT/GPT/GCAT/CD44/ARG2/MCAT/INPP1
GO:0006413	translational initiation	1.92E-07	1.69E-07	16	RPL4/RPL32/RPL14/RPL13A/RPL34/RPL18/RPL7/RPL35A/RPL18A/RPL29/RPL36/RPS29/RPS13/RPL27/RPL21/RPL15
GO:0032984	protein-containing complex disassembly	0.000347466	0.000305178	15	LIMA1/SPTBN2/GBA/CAV1/MRPL13/MRPL44/MRPS18A/MRPL17/MRPL28/MRPL9/MRPL57/MRPS24/VAMP8/MRPL34/MRPL20
GO:0043062	extracellular structure organization	0.020506553	0.01801086	14	ALB/LCP1/LAMB3/APOE/COL18A1/FN1/SERPINB5/ITGA2/VIPAS39/LAMC2/COL12A1/ITGB4/CD44/CTSL
GO:0043588	skin development	0.025603959	0.0224879	14	MYO5A/KRT17/KRT14/ITGA2/KRT8/KRT20/ITGB4/GBA/KRT18/CTSL/PSAP/KRT75/KRT81/KRT79
GO:1901136	carbohydrate derivative catabolic process	2.48E-05	2.18E-05	13	PNP/UPP1/NT5E/SLC9A1/RENBP/CDA/FUCA2/GBA/CD44/PSAP/FUCA1/GPC1/GM2A
GO:0045862	positive regulation of proteolysis	0.020506553	0.01801086	13	PHB/FBXO22/APOE/FN1/PML/DAB2IP/GBA/CAV1/FAS/CASP1/ARL6IP5/RPS27L/ATP5IF1

GO:0034330	cell junction organization	0.024793159	0.021775776	11	LAMB3/ARVCF/FN1/KRT14/ITGA2/FLNC/SLC9A1/LAMC2/ITGB4/CAV1/NRP1
GO:0097193	intrinsic apoptotic signalling pathway	0.025603959	0.0224879	11	HMOX1/PML/DAB2IP/SOD2/CD44/CAV1/ARL6IP5/GPX1/RRM2B/RPS27L/CDKN1A
GO:0006414	translational elongation	0.000267746	0.00023516	10	MRPL13/MRPL44/MRPS18A/MRPL17/MRPL28/MRPL9/MRPL57/MRPS24/MRPL34/MRPL20
GO:0140053	mitochondrial gene expression	0.000917931	0.000806216	10	MRPL13/MRPL44/MRPS18A/MRPL17/MRPL28/MRPL9/MRPL57/MRPS24/MRPL34/MRPL20
GO:0002181	cytoplasmic translation	0.000149441	0.000131253	9	RPL32/RPL13A/RPL18/RPL35A/RPL18A/RPL29/RPL36/RPS29/RPL15
GO:0048144	fibroblast proliferation	0.020506553	0.01801086	6	FN1/PML/DAB2IP/CCNB1/S100A6/CDKN1A
GO:0051651	maintenance of location in cell	0.024793159	0.021775776	6	ALB/APOE/PML/GAA/CAV1/KDELR1
GO:0046466	membrane lipid catabolic process	0.008251999	0.007247713	5	GBA/SMPD1/PSAP/FUCA1/GM2A

Table 7.2: Enriched GO terms (BP) (Underrepresented)

ID	Description	p.adjusted	q.value	Count	GeneID
GO:0071103	DNA conformation change	3.37E-05	3.01E-05	11	POLE3/RECQL4/H1-10/H1-2/H1-4/H1-5/NCAPH/H1-1/CTCF/H4C9/H1-0
GO:0006310	DNA recombination	7.61E-05	6.79E-05	10	DCAF1/RECQL4/H1-10/H1-2/H1-4/H1-5/H1-1/YY1/PAXIP1/H1-0
GO:0071824	protein-DNA complex subunit organization	9.36E-05	8.36E-05	10	POLE3/UBTF/H1-10/H1-2/H1-4/H1-5/H1-1/CTCF/H4C9/H1-0
GO:0033044	regulation of chromosome organization	0.000307582	0.000274597	10	BRD4/DNMT1/H1-10/H1-2/H1-4/H1-5/H1-1/CTCF/PAXIP1/H1-0
GO:0018205	peptidyl-lysine modification	0.001008695	0.000900522	10	PHF10/POLE3/BRD4/DNMT1/H1-2/H1-4/H1-5/HMG20B/CTCF/PAXIP1
GO:0051052	regulation of DNA metabolic process	0.001558187	0.001391087	10	DNMT1/H1-10/H1-2/H1-4/H1-5/H1-1/UBE2V1/PAXIP1/H1-0/UBE2V2
GO:0016570	histone modification	0.002399986	0.002142611	10	PHF10/POLE3/BRD4/DNMT1/DCAF1/H1-2/H1-4/H1-5/CTCF/PAXIP1
GO:0045814	negative regulation of gene expression, epigenetic	2.73E-06	2.44E-06	9	POLE3/DNMT1/H1-10/H1-2/H1-4/H1-5/H1-1/H4C9/H1-0

GO:0060968	regulation of gene silencing	4.65E-06	4.15E-06	9	DNMT1/RIPK1/H1-10/H1-2/H1-4/H1-5/H1-1/H4C9/H1-0
GO:0006333	chromatin assembly or disassembly	3.27E-05	2.92E-05	9	POLE3/H1-10/H1-2/H1-4/H1-5/H1-1/CTCF/H4C9/H1-0
GO:0010639	negative regulation of organelle organization	0.020014765	0.017868381	8	DNMT1/H1-10/H1-2/H1-4/H1-5/BNIP3/H1-1/H1-0
GO:0008213	protein alkylation	0.001269659	0.001133501	7	BRD4/DNMT1/H1-2/H1-4/H1-5/CTCF/PAXIP1
GO:0043414	macromolecule methylation	0.025093552	0.022402518	7	BRD4/DNMT1/H1-2/H1-4/H1-5/CTCF/PAXIP1
GO:0045815	positive regulation of gene expression, epigenetic	4.45E-05	3.97E-05	6	H1-10/H1-2/H1-4/H1-5/H1-1/H1-0
GO:0002573	myeloid leukocyte differentiation	0.02564396	0.0228939	6	CAMK4/ANXA2/DHRS2/RIPK1/RUNX1/PIR
GO:0070534	protein K63-linked ubiquitination	0.007702041	0.006876074	4	UBE2T/UBE2E3/UBE2V1/UBE2V2
GO:0007422	peripheral nervous system development	0.01532058	0.0136776	4	NAB2/RUNX1/DAG1/NDRG1

GO:0071679	commissural neuron axon guidance	0.04420753	0.039466712	2	NCAM1/DAG1
GO:0009143	nucleoside triphosphate catabolic process	0.049975433	0.044616064	2	DUT/ENPP1
GO:0010940	positive regulation of necrotic cell death	0.049975433	0.044616064	2	RIPK1/BNIP3

Table 7.6: Enriched GO terms (BP) (Overrepresented)

ID	Description	p.adjusted	qvalue	Count	Gene ID
GO:0044282	small molecule catabolic process	1.41E-11	1.19E-11	30	BCKDHB/ALDH2/GCDH/ETFDH/HK2/DLD/HMGCL/TIGAR/DBT/MCCC2/APOE/ETFA/MLYCD/HADHA/IL4I1/UPP1/IVD/GLB1/ACADVL/AKR1C3/ABAT/GCAT/CD44/TST/MCCC1/ACOX3/ECH1 /QPRT/LONP2/INPP1
GO:0043062	extracellular structure organization	2.17E-07	1.84E-07	24	AGRN/ALB/LAMB3/TNC/QSOX1/APOE/COL18A1/SERPINB5/MELTF/ITGA2B/DPP4/MMP1/LAMC2/ICAM1/CD44/AEBP1/CCN1/APP/VCAM1/SERPINF2/CTSS/SERPINE1/TIMP1/MMP2
GO:0052548	regulation of endopeptidase activity	7.01E-05	5.92E-05	20	AHSG/FAM162A/SERPINB5/ITIH2/HTRA2/CASP4/TRADD/CD44/FAS/CRYAB/CASP1/CCN1/APP/GPX1/CYFIP2/PLAUR/SERPINF2/SERPINE1/TIMP1/HERPUD1
GO:0006631	fatty acid metabolic process	2.91E-05	2.45E-05	19	GCDH/ETFDH/DLD/ACSF2/MYO5A/ETFA/ERLIN2/CES2/MLYCD/ HADHA/IVD/ACADVL/AKR1C3/PDK1/CAV1/ACOX3/ECH1/GPX1/ LONP2
GO:2001233	regulation of apoptotic signaling pathway	0.000276988	0.000233791	18	FAM162A/HTRA2/TRAF1/SOD2/ICAM1/TRADD/CD44/CAV1/FAS/BNIP3/GPX1/PLAUR/RRM2B/BCL2L1/ATP5IF1/PPIF/SERPINE1/HERPUD1
GO:0072593	reactive oxygen species metabolic process	1.49E-05	1.26E-05	17	HK2/TIGAR/HBA1/AKR1C3/SOD2/ICAM1/CAV1/ASS1/CRYAB/CCN1/BNIP3/RAC2/GPX1/ARF4/ATP5IF1/NDUFAF2/CDKN1A

GO:0071496	cellular response to external stimulus	6.68E-05	5.64E-05	17	ALB/TNC/WIPI2/UPP1/TRPM4/AKR1C3/MIOS/ICAM1/FAS/PIEZO1/CASP1/BNIP3/LAMP2/VCAM1/WIPI1/CDKN1A/CD68
GO:0045862	positive regulation of proteolysis	0.000302844	0.000255614	17	FAM162A/APOE/MELTF/RCN3/HTRA2/CASP4/C6/NOP53/TRADD/CAV1/FAS/CASP1/CCN1/APP/CYFIP2/ATP5IF1/HERPUD1
GO:0006520	cellular amino acid metabolic process	0.000339974	0.000286954	17	BCKDHB/GCDH/DLD/HMGCL/DBT/MCCC2/IL4I1/IVD/CRTAP/CKB/NFS1/ABAT/GCAT/TST/MCCC1/FARS2/ASS1
GO:0070482	response to oxygen levels	0.000487332	0.000411331	17	HK2/FAM162A/TIGAR/DPP4/ABAT/PDK1/NOP53/ICAM1/TMEM199/CAV1/FAS/CRYAB/BNIP3/AK4/VCAM1/MMP2/CDKN1A
GO:0016042	lipid catabolic process	0.000299593	0.000252871	16	GCDH/ETFDH/APOE/ETFA/PLBD2/MLYCD/HADHA/IVD/ACADVL/AKR1C3/NAGA/ASAH1/ACOX3/ECH1/FUCA1/LONP2
GO:0006790	sulfur compound metabolic process	0.000510617	0.000430985	16	B3GALT6/GCDH/DLD/HMGCL/ACSF2/MCCC2/MLYCD/GNS/GLB1/GSTK1/GALNS/NFS1/PDK1/TST/MCCC1/GPX1
GO:0097193	intrinsic apoptotic signaling pathway	0.000784204	0.000661905	14	HTRA2/CASP4/SOD2/PDK1/CD44/CAV1/BNIP3/GPX1/PLAUR/RRM2B/BCL2L1/PPIF/HERPUD1/CDKN1A
GO:0030258	lipid modification	0.000343839	0.000290216	13	GCDH/ETFDH/APOE/ETFA/MLYCD/HADHA/IVD/ACADVL/DGKA/ACOX3/ECH1/LONP2/INPP1
GO:1901136	carbohydrate derivative catabolic process	0.000299593	0.000252871	12	AGRN/SGSH/MLYCD/UPP1/GNS/GLB1/GALNS/NGLY1/CD44/NAGA/AMPD3/FUCA1

GO:0010821	regulation of mitochondrion organization	0.001174612	0.000991428	11	HK2/FAM162A/TIGAR/HTRA2/BNIP3/RAC2/GPX1/PLAUR/ BCL2L1/ATP5IF1/PPIF
GO:0002576	platelet degranulation	0.000299593	0.000252871	10	ALB/AHSG/QSOX1/ITGA2B/APP/LAMP2/SERPINF2/ CYB5R1/SERPINE1/TIMP1
GO:0008637	apoptotic mitochondrial changes	0.000299593	0.000252871	10	HK2/FAM162A/SOD2/IFIT2/BNIP3/GPX1/PLAUR/BCL2L1/ ATP5IF1/PPIF
GO:0006022	aminoglycan metabolic process	0.001182841	0.000998374	10	B3GALT6/AGRN/SGSH/ITIH2/GNS/GLB1/GALNS/CD44/ GALNT5/FUCA1
GO:1903008	organelle disassembly	0.001182841	0.000998374	8	WIPI2/HK2/TIGAR/HTRA2/PELO/BNIP3/ATP5IF1/WIPI1

Table 7.7: Enriched GO terms (BP) (Underrepresented)

ID	Description	p.adjust	qvalue	Count	geneID
GO:0006260	DNA replication	1.95E-35	1.74E-35	53	MSH6/RRM2/RFC1/POLE4/WDHD1/DUT/POLE3/NASP/POLE/POLA1/ EGFR/CHTF18/PCLAF/RNASEH2A/CHAF1A/LIG1/MCM6/POLD1/PCNA/ SMC3/RECQL4/MCM4/CACYBP/HELB/CDK1/MCM7/MCM5/MCM2/ POLD2/MCMBP/NFIB/RBBP7/MCM3/POLA2/RFC4/CHAF1B/RFC3/ RFC2/RFC5/GINS1/RRM1/GINS4/PRIM1/CDC45/PRIM2/CHEK1/ POLD3/RBBP4/FEN1/FAM111A/DSCC1/GINS3/DDX11
GO:0071103	DNA conformation change	3.76E-27	3.36E-27	49	NCAPD2/TOP2A/SMC4/POLE3/NASP/CHTF18/SMCHD1/CHAF1A/ MCM6/RECQL4/MCM4/HELB/CDK1/SMARCAD1/CENPH/H1-10/H1-2/ MCM7/MCM5/MCM2/NCAPG/RBBP7/MCM3/RFC4/CHAF1B/RFC3/ H1-5/SMC2/RFC2/CCNB1/RFC5/GINS1/NCAPH/H11/GINS4/CTCF/ HAT1/H4C9/CDC45/CENPQ/RBBP4/NUSAP1/ASF1B/ASF1A/HMGB1/ DSCC1/DDX11/HMGB2/HMGB3
GO:0007059	chromosome segregation	3.34E-24	2.99E-24	45	RCC2/NUMA1/NCAPD2/TOP2A/SMC4/MKI67/RACGAP1/RAD51C/SMC3/ NDE1/KIF2C/TACC3/SMARCAD1/KIFC1/TRIP13/RAD21/MCMBP/STAG1/ NCAPG/MAD2L1/SMC2/KIF22/NDC80/CCNB1/NUF2/PRC1/ZWINT/NCAPH/ CTCF/SPAG5/DLGAP5/PDS5B/AURKB/PMF1/CENPQ/KIF4A/SPC25/FEN1/ CDCA8/NUSAP1/SKA1/KNSTRN/FAM83D/DSCC1/DDX11
GO:0048285	organelle fission	7.67E-18	6.86E-18	45	NUMA1/NCAPD2/TOP2A/SMC4/ANLN/MKI67/RACGAP1/RAD51C/SMC3/ NDE1/KIF2C/TACC3/KIFC1/TRIP13/RAD21/STAG1/NCAPG/MAD2L1/UBE2S/ SMC2/KNTC1/KIF22/NDC80/CCNB1/NUF2/PRC1/ZWINT/NCAPH/KIF11/ RANBP1/HSPA2/SPAG5/DLGAP5/PDS5B/CHEK1/AURKB/AURKA/UBE2C/ KIF4A/CDCA8/NUSAP1/KNSTRN/DSCC1/PDGFRB/CKS2
GO:0045787	positive regulation of cell cycle	5.20E-09	4.65E-09	30	RCC2/NUMA1/EGFR/ASNS/RACGAP1/RAD51C/PCNA/CDK1/RAD21/MAD2L1/ NDC80/CCNB1/CCN2/RANBP1/PRKCA/HSPA2/SPAG5/DLGAP5/CDC45/CHEK1/

					AURKB/AURKA/UBE2C/FEN1/NUSAP1/FAM83D/PDGFRB/DDX11/CKS2/CKS1B
GO:0051052	regulation of DNA metabolic process	3.86E-08	3.45E-08	30	MSH6/EGFR/ARRB2/CHTF18/SMCHD1/PCNA/SMC3/CACYBP/HELB/CDK1/SMARCAD1/H1-10/H1-2/KPNA2/RFC4/RFC3/H1-5/MSH2/RFC2/RFC5/H1-1/CHEK1/AURKB/DEK/UBE2V1/HMGB1/DSCC1/PDGFRB/DDX11/UBE2V2
GO:0006310	DNA recombination	2.64E-11	2.36E-11	29	MSH6/TOP2A/SMCHD1/RAD51C/MCM6/RECQL4/MCM4/HELB/SMARCAD1/H1-10/H12/MCM7/MCM5/MCM2/TRIP13/RAD21/KPNA2/MCM3/H1-5/MSH2/MORF4L1/H1-1/GINS4/CDC45/CHEK1/FEN1/HMGB1/HMGB2/HMGB3
GO:0071824	protein-DNA complex subunit organization	2.60E-10	2.32E-10	28	SMARCC1/POLE3/NASP/CHAF1A/MCM6/UBTF/MCM4/CENPH/H1-10/H1-2/MCM7/MCM5/MCM2/RBBP7/MCM3/CHAF1B/H1-5/H1-1/CTCF/HAT1/H4C9/CDC45/CENPQ/RBBP4/ASF1B/ASF1A/HMGB1/HMGB2
GO:0044843	cell cycle G1/S phase transition	4.23E-09	3.78E-09	26	RRM2/POLE4/POLE3/NASP/POLE/POLA1/EGFR/IQGAP3/CDK6/MCM6/TYMS/PCNA/MCM4/CDK1/MCM7/MCM5/MCM2/MCM3/POLA2/CCNB1/PRIM1/CDC45/PRIM2/AURKA/DHFR/FAM83D
GO:0006302	double-strand break repair	6.81E-10	6.09E-10	25	POLA1/SMCHD1/KDM2A/RAD51C/MCM6/RECQL4/MCM4/HELB/SMARCAD1/MCM7/MCM5/MCM2/TRIP13/RAD21/MCM3/MSH2/MORF4L1/GINS4/H4C9/CDC45/CHEK1/FEN1/DEK/DDX11/UBE2V2
GO:0071897	DNA biosynthetic process	2.66E-11	2.38E-11	24	RFC1/POLE4/POLE3/POLE/POLA1/ARRB2/CHTF18/PCLAF/LIG1/POLD1/TYMS/PCNA/POLD2/POLA2/RFC4/RFC3/RFC2/RFC5/CCN2/TK1/AURKB/POLD3/DSCC1/PDGFRB
GO:0006333	chromatin assembly or disassembly	2.45E-10	2.19E-10	23	SMARCC1/POLE3/NASP/SMCHD1/CHAF1A/HIRIP3/BAZ1B/CENPH/H1-10/H1-2/MCM2/RBBP7/CHAF1B/H1-5/H1-1/CTCF/HAT1/H4C9/CENPQ/RBBP4/ASF1B/ASF1A/HMGB2
GO:1902850	microtubule cytoskeleton organization	2.13E-11	1.90E-11	21	NUMA1/PCNT/RACGAP1/SMC3/SUN2/NDE1/TACC3/KIFC1/STAG1/MAD2L1/NDC80/CCNB1/NUF2/PRC1/KIF11/STMN1/AURKB/AURKA/KIF4A/SPC25/NUSAP1

	involved in mitosis				
GO:0032200	telomere organization	1.50E-09	1.34E-09	21	RFC1/POLE4/POLE3/POLE/POLA1/RAD51C/POLD1/PCNA/RECQL4/POLD2/POLA2/RFC4/RFC3/RFC2/RFC5/PRIM1/H4C9/PRIM2/AURKB/POLD3/FEN1
GO:0007051	spindle organization	4.00E-09	3.57E-09	21	NUMA1/PCNT/RACGAP1/SMC3/SUN2/HAUS5/TACC3/KIFC1/STAG1/NDC80/CCNB1/NUF2/PRC1/KIF11/STMN1/SPAG5/AURKB/AURKA/KIF4A/SPC25/KNSTRN
GO:0006338	chromatin remodeling	3.98E-07	3.56E-07	18	SMARCC1/POLE3/NASP/SMCHD1/BAZ1B/SMARCAD1/CENPH/KDM4A/RBBP7/H4C9/CHEK1/CENPQ/CBX3/RBBP4/HMGB1/MYSM1/HMGB2/HMGB3
GO:0022616	DNA strand elongation	1.19E-19	1.07E-19	16	POLE/POLA1/RNASEH2A/LIG1/PCNA/MCM4/MCM7/POLD2/MCM3/RFC4/RFC3/GINS1/GINS4/POLD3/FEN1/GINS3
GO:0006301	postreplication repair	3.37E-10	3.01E-10	13	RFC1/PCLAF/POLD1/PCNA/POLD2/RFC4/RFC3/MSH2/RFC2/RFC5/POLD3/UBE2V1/UBE2V2
GO:0050000	chromosome localization	1.38E-07	1.24E-07	13	NUMA1/NDE1/KIF2C/KIFC1/KIF22/NDC80/CCNB1/NUF2/SPAG5/DLGAP5/CENPQ/CDCA8/FAM83D
GO:0042769	DNA damage response, detection of DNA damage	8.92E-07	7.97E-07	9	RFC1/POLD1/PCNA/POLD2/RFC4/RFC3/RFC2/RFC5/POLD3

Table 7.8: Enriched GO terms (BP) (Overrepresented)

ID	Description	p.adjusted	qvalue	Count	Gene ID
GO:0044282	small molecule catabolic process	5.60E-05	4.80E-05	19	ALDH2/HADHB/TIGAR/APOE/ACOT8/MLYCD/IL4I1/ACAA1/ UPP1/CBR3/SLC9A1/GLB1/ABAT/SDSL/CD44/MCCC1/BPGM/ ABCD1/INPP1
GO:0052548	regulation of endopeptidase activity	0.00029581	0.000253673	18	AHSG/C3/SERPINB5/PML/CST3/CRADD/HTRA2/CASP4/CTSD/ CD44/FAS/CRYAB/CYFIP2/SERPINF2/IFI16/RPS27L/SERPINE1/ TIMP1
GO:0009615	response to virus	0.002101476	0.001802129	14	DDX58/PARP9/PML/IFIT1/IFIT3/IFIT2/OASL/ISG15/OAS2/IFI16/ BCL2L1/OAS1/TRIM22/HMGA2
GO:0045862	positive regulation of proteolysis	0.007685262	0.006590526	13	PHB/APOE/C3/PML/CRADD/HTRA2/CASP4/CTSD/CAV1/FAS/ CYFIP2/IFI16/RPS27L
GO:0006732	coenzyme metabolic process	0.008961221	0.00768473	13	TIGAR/PARP9/ACOT8/MLYCD/NADSYN1/CBR3/FDXR/MCCC1/ COQ5/BPGM/ABCD1/COQ6/TP53I3
GO:0043900	regulation of multi-organism process	0.015646372	0.013417606	13	DDX58/PARP9/APOE/PML/STOM/IFIT1/OASL/CAV1/ISG15/IFI16/ OAS1/TIMP1/HMGA2
GO:1901136	carbohydrate derivative catabolic process	0.001185717	0.001016816	11	MLYCD/UPP1/CST3/SLC9A1/GLB1/GALNS/CD44/ABCD1/FUCA1/ FBXO2/GPC2
GO:0034976	response to endoplasmic	0.008961221	0.00768473	11	ERLIN2/ERLIN1/ATP6V0D1/PML/CASP4/CAV1/TPP1/BCL2L1/FBXO2/ DERL1/GOSR2

	reticulum stress				
GO:0097193	intrinsic apoptotic signaling pathway	0.009247479	0.007930211	11	PML/HTRA2/CASP4/SOD2/CD44/CAV1/RRM2B/IFI16/RPS27L/ BCL2L1/CDKN1A
GO:0072593	reactive oxygen species metabolic process	0.017602621	0.015095195	10	TIGAR/HBA1/SOD2/CAV1/CRYAB/ABCD1/ARF4/VDAC1/ACP5/ CDKN1A
GO:0042180	cellular ketone metabolic process	0.020181476	0.017306702	9	ERLIN2/ERLIN1/MLYCD/CBR3/FDXR/CAV1/COQ5/ABCD1/COQ6
GO:0034340	response to type I interferon	0.006077421	0.005211715	8	IFIT1/IFIT3/IFIT2/OASL/GBP2/ISG15/OAS2/OAS1
GO:0060333	interferon-gamma-mediated signaling pathway	0.016540064	0.014183996	8	PARP9/PML/OASL/CD44/GBP2/OAS2/OAS1/TRIM22
GO:0098754	detoxification	0.016540064	0.014183996	7	ALB/APOE/HBA1/ACAA1/GSTK1/CLIC2/SOD2
GO:0010212	response to ionizing radiation	0.017602621	0.015095195	7	TIGAR/PML/CRYAB/IFI16/BCL2L1/HMGA2/CDKN1A
GO:0007031	peroxisome organization	0.008961221	0.00768473	6	PEX11B/ACOT8/MLYCD/ACAA1/GSTK1/ABCD1

GO:0051651	maintenance of location in cell	0.010647196	0.009130544	6	ALB/APOE/PML/GAA/CAV1/GPAA1
GO:0043574	peroxisomal transport	0.018595582	0.015946712	5	ACOT8/MLYCD/ACAA1/GSTK1/ABCD1
GO:0042159	lipoprotein catabolic process	0.01490579	0.012782517	3	APOE/CTSD/LYPLAL1
GO:1902931	negative regulation of alcohol biosynthetic process	0.017602621	0.015095195	3	APOE/ERLIN2/ERLIN1

Table 7.9: Enriched GO terms (BP) (Underrepresented)

ID	Description	p.adjusted	qvalue	Count	Gene ID
GO:0006260	DNA replication	4.16E-24	3.57E-24	35	MSH6/RRM2/TIMELESS/RFC1/DUT/POLE3/NASP/POLA1/RNASEH2A/LIG1/MCM6/POLD1/PCNA/RECQL4/MCM4/CDK1/MCM7/MCM5/MCM2/POLD2/MCMBP/MCM3/POLA2/RFC4/RFC2/RFC5/RRM1/GINS4/PRIM1/KAT7/PRIM2/POLD3/FEN1/DSCC1/GINS3
GO:0071103	DNA conformation change	1.71E-21	1.47E-21	35	NCAPD2/TOP2A/SMC4/POLE3/NASP/SMCHD1/MCM6/RECQL4/MCM4/CDK1/CENPH/H1-10/H1-2/MCM7/MCM5/MCM2/NCAPG/MCM3/RFC4/H15/SMC2/RFC2/CCNB1/RFC5/NCAPH/H1-1/GINS4/CTCF/HAT1/H4C9/ASF1B/HMGB1/DSCC1/HMGB2/HMGB3
GO:0007059	chromosome segregation	3.19E-21	2.74E-21	34	NUMA1/NCAPD2/TOP2A/SMC4/MKI67/RACGAP1/KIF2C/TACC3/KIFC1/TRIP13/MCMBP/NCAPG/MAD2L1/SMC2/KIF22/NDC80/CCNB1/NUF2/PRC1/ZWINT/NCAPH/CDC20/CTCF/SPAG5/SKA3/DLGAP5/AURKB/KIF4A/SPC25/FEN1/KIF14/KNSTRN/FAM83D/DSCC1
GO:0048285	organelle fission	1.60E-14	1.37E-14	32	NUMA1/NCAPD2/TOP2A/SMC4/ANLN/MKI67/RACGAP1/KIF2C/TACC3/KIFC1/TRIP13/NCAPG/MAD2L1/UBE2S/SMC2/KIF22/NDC80/CCNB1/NUF2/PRC1/ZWINT/NCAPH/KIF11/CDC20/SPAG5/DLGAP5/AURKB/KIF4A/KIF14/KNSTRN/DSCC1/CKS2
GO:0006310	DNA recombination	3.53E-12	3.03E-12	24	MSH6/TFRC/TIMELESS/TOP2A/SMCHD1/MCM6/RECQL4/MCM4/H1-10/H1-2/MCM7/MCM5/MCM2/TRIP13/KPNA2/MCM3/H1-5/H1-1/GINS4/FEN1/YY1/HMGB1/HMGB2/HMGB3
GO:0033044	regulation of chromosome organization	4.47E-09	3.84E-09	22	NUMA1/TOP2A/DNMT1/MKI67/TACC3/SIRT1/H1-10/H1-2/MCM2/TRIP13/MAD2L1/H1-5/ATAD2/NDC80/CCNB1/H1-1/CDC20/CTCF/KAT7/DLGAP5/AURKB/FEN1
GO:0051052	regulation of DNA	1.88E-07	1.61E-07	22	MSH6/TFRC/TIMELESS/DNMT1/SMCHD1/PCNA/CDK1/SIRT1/H1-10/H1-2/KPNA2/RFC4/H1-5/RFC2/RFC5/H1-1/AURKB/DEK/UBE2V1/HMGB1/DSCC1/UBE2V2

	metabolic process				
GO:0071824	protein-DNA complex subunit organization	2.13E-09	1.83E-09	21	SMARCC1/POLE3/NASP/MCM6/UBTF/MCM4/CENPH/H1-10/H1-2/MCM7/MCM5/MCM2/MCM3/H1-5/H1-1/CTCF/HAT1/H4C9/ASF1B/HMGB1/HMGB2
GO:0044843	cell cycle G1/S phase transition	9.84E-09	8.44E-09	20	RRM2/POLE3/NASP/POLA1/MCM6/TYMS/PCNA/MCM4/CDK1/MCM7/MCM5/MCM2/MCM3/POLA2/CCNB1/PRIM1/PRIM2/DHFR/KIF14/FAM83D
GO:0007051	spindle organization	4.05E-10	3.47E-10	18	NUMA1/RACGAP1/SUN2/TACC3/KIFC1/NDC80/CCNB1/NUF2/PRC1/KIF11/STMN1/CDC20/SPAG5/AURKB/KIF4A/SPC25/HDAC3/KNSTRN
GO:0071897	DNA biosynthetic process	5.84E-10	5.01E-10	18	RFC1/POLE3/POLA1/LIG1/POLD1/TYMS/PCNA/SIRT1/POLD2/POLA2/RFC4/RFC2/RFC5/TK1/CHRAC1/AURKB/POLD3/DSCC1
GO:0032200	telomere organization	1.43E-09	1.22E-09	17	RFC1/POLE3/POLA1/POLD1/PCNA/RECQL4/POLD2/POLA2/RFC4/RFC2/RFC5/PRIM1/H4C9/PRIM2/AURKB/POLD3/FEN1
GO:0006302	double-strand break repair	1.76E-07	1.51E-07	17	TIMELESS/POLA1/SMCHD1/MCM6/RECQL4/MCM4/MCM7/MCM5/MCM2/TRIP13/MCM3/GINS4/H4C9/FEN1/DEK/YY1/UBE2V2
GO:1902850	microtubule cytoskeleton organization involved in mitosis	4.05E-10	3.47E-10	16	NUMA1/RACGAP1/SUN2/TACC3/KIFC1/MAD2L1/NDC80/CCNB1/NUF2/PRC1/KIF11/STMN1/CDC20/AURKB/KIF4A/SPC25
GO:0006333	chromatin assembly or disassembly	3.02E-07	2.59E-07	15	SMARCC1/POLE3/NASP/SMCHD1/CENPH/H1-10/H1-2/MCM2/H1-5/H1-1/CTCF/HAT1/H4C9/ASF1B/HMGB2
GO:0022616	DNA strand elongation	3.93E-17	3.37E-17	13	POLA1/RNASEH2A/LIG1/PCNA/MCM4/MCM7/POLD2/MCM3/RFC4/GINS4/POLD3/FEN1/GINS3

GO:0045814	negative regulation of gene expression, epigenetic	1.95E-07	1.67E-07	13	POLE3/DNMT1/SMCHD1/SIRT1/H1-10/H1-2/H1-5/ATAD2/H1-1/CHRAC1/HAT1/H4C9/HMGB1
GO:0050000	chromosome localization	7.74E-08	6.64E-08	11	NUMA1/KIF2C/KIFC1/KIF22/NDC80/CCNB1/NUF2/SPAG5/DLGAP5/KIF14/FAM83D
GO:0006301	postreplication repair	9.66E-09	8.29E-09	10	RFC1/POLD1/PCNA/POLD2/RFC4/RFC2/RFC5/POLD3/UBE2V1/UBE2V2
GO:0042769	DNA damage response, detection of DNA damage	2.98E-07	2.56E-07	8	RFC1/POLD1/PCNA/POLD2/RFC4/RFC2/RFC5/POLD3

Table 7.10: Enriched GO terms (BP) (Overrepresented)

ID	Description	p.adjusted	qvalue	Count	Gene ID
GO:0052548	regulation of endopeptidase activity	0.011744895	0.010164168	15	C3/SERPINB5/SERPINA1/PML/CASP4/CD44/FAS/CASP1/APP/GPX1/MTCH1/IFI16/SERPINE1/BST2/TIMP1
GO:0044282	small molecule catabolic process	0.013948858	0.012071503	14	RBKS/ACAD11/TIGAR/APOE/PNP/ACOT8/IL4I1/UPP1/KYNU/SLC9A1/ABAT/CD44/INPP5K/CARNMT1
GO:0043900	regulation of multi-organism process	0.020348535	0.017609857	13	DDX58/APOE/PML/STOM/IFIT1/STAT1/GRN/PDE3A/IFI16/INPP5K/OAS1/BST2/TIMP1
GO:0034341	response to interferon-gamma	0.011744895	0.010164168	12	PML/KYNU/STAT1/CD44/CASP1/OAS2/IRF9/OAS1/BST2/TRIM22/MT2A/VAMP3
GO:0045861	negative regulation of proteolysis	0.016636901	0.014397766	12	C3/SERPINB5/SERPINA1/PML/CD59/CD44/APP/GPX1/IFI16/SERPINE1/BST2/TIMP1
GO:0043062	extracellular structure organization	0.03049282	0.026388838	12	AGRN/LCP1/LAMB3/APOE/SERPINB5/LAMC2/ITGB2/CD44/APP/APOC3/SERPINE1/TIMP1
GO:0072593	reactive oxygen species metabolic process	0.013948858	0.012071503	11	TIGAR/HBA1/SOD2/ITGB2/PRCP/BRCA1/GPX1/ARF4/ATP5IF1/HBB/ CDKN1A
GO:0097193	intrinsic apoptotic signaling pathway	0.013948858	0.012071503	11	PML/CASP4/SOD2/CD44/EPHA2/BRCA1/GPX1/RRM2B/IFI16/BCL2L1/CDKN1A

GO:0008202	steroid metabolic process	0.020348535	0.017609857	11	SQLE/APOE/ACOT8/IGFBP7/FDXR/FDFT1/SMPD1/CES1/APP/MSMO1/CYB5R1
GO:0009615	response to virus	0.020348535	0.017609857	11	DDX58/PML/IFIT1/STAT1/OAS2/IFI16/BCL2L1/IRF9/OAS1/BST2/TRIM22
GO:0007568	aging	0.026359778	0.022812056	11	PML/KYNU/ABAT/SOD2/ITGB2/APP/NAMPT/SERPINE1/TIMP1/CDKN1A/CD68
GO:0019058	viral life cycle	0.026359778	0.022812056	11	APOE/PML/STOM/IFIT1/EPHA2/IFI16/CTSB/INPP5K/OAS1/BST2/VAMP8
GO:0006631	fatty acid metabolic process	0.033654666	0.029125136	11	ACAD11/C3/CES2/ACOT8/ABHD5/ALOX5/BRCA1/CES1/GPX1/ MSMO1/APOC3
GO:0098754	detoxification	0.013948858	0.012071503	8	APOE/HBA1/SLC30A1/CLIC2/SOD2/GPX1/HBB/MT2A
GO:0010212	response to ionizing radiation	0.013948858	0.012071503	8	TIGAR/PML/BRCA1/NAMPT/GPX1/IFI16/BCL2L1/CDKN1A
GO:1902652	secondary alcohol metabolic process	0.013948858	0.012071503	8	SQLE/APOE/FDXR/FDFT1/SMPD1/CES1/APP/MSMO1
GO:0072524	pyridine-containing compound metabolic process	0.020631842	0.017855034	8	RBKS/TIGAR/PNP/NADSYN1/KYNU/APP/NAMPT/TP53I3

GO:1901136	carbohydrate derivative catabolic process	0.022109993	0.019134243	8	AGRN/PNP/UPP1/SLC9A1/CD44/FUCA1/GPC1/FBXO2
GO:0006733	oxidoreduction coenzyme metabolic process	0.026359778	0.022812056	8	RBKS/TIGAR/NADSYN1/KYNU/FDXR/APP/NAMPT/TP53I3
GO:0002886	regulation of myeloid leukocyte mediated immunity	0.020348535	0.017609857	5	DDX58/C3/ITGB2/IL13RA2/VAMP8

Table 7.11: Enriched GO terms (BP) (Underrepresented)

ID	Description	p.adjusted	qvalue	Count	Gene ID
GO:0007059	chromosome segregation	1.38E-27	1.17E-27	39	RCC2/CDC27/NCAPD2/TOP2A/SMC4/MKI67/KIF23/NDE1/KIF2C/SKA2/TACC3/RIOK2/PLK1/KIFC1/TRIP13/MCMBP/NCAPG/MAD2L1/SMC2/CIAO2A/KIF22/NDC80/CCNB1/NUF2/PRC1/ZWINT/NCAPH/TLK2/CDC20/CTCF/UBE2I/SPAG5/DLGAP5/AURKB/KIF4A/SPC25/FEN1/NUSAP1/FAM83D
GO:0048285	organelle fission	3.93E-22	3.31E-22	39	CDC27/CUL7/NCAPD2/TOP2A/SMC4/ANLN/MKI67/KIF23/NDE1/KIF2C/TACC3/RIOK2/PLK1/KIFC1/TRIP13/NCAPG/MAD2L1/UBE2S/SMC2/KIF22/NDC80/CCNB1/NUF2/PRC1/ZWINT/NCAPH/KIF11/CDC20/SPAG5/DLGAP5/CHEK1/AURKB/AURKA/UBE2C/FIGNL1/KIF4A/NUSAP1/PDGFRB/CKS2
GO:0006260	DNA replication	1.06E-26	8.91E-27	36	RRM2/RFC1/POLE4/DUT/POLE3/NASP/POLA1/RNASEH2A/LIG1/MCM6/POLD1/PCNA/MCM4/CDK1/MCM7/MCM5/MCM2/POLD2/MCMBP/MCM3/POLA2/RFC4/RFC2/RFC5/GINS1/RRM1/DTL/GINS4/PRIM1/CDC45/PRIM2/CHEK1/POLD3/FEN1/GINS2/GINS3
GO:0071103	DNA conformation change	1.07E-22	9.01E-23	35	NCAPD2/TOP2A/SMC4/POLE3/NASP/MCM6/MCM4/CDK1/CENPH/H1-10/H1-2/MCM7/MCM5/MCM2/NCAPG/MCM3/RFC4/H1-5/SMC2/RFC2/CCNB1/RFC5/GINS1/NCAPH/H1-1/GINS4/HELLS/CTCF/HAT1/CDC45/GINS2/NUSAP1/HMGB1/HMGB2/HMGB3
GO:0033044	regulation of chromosome organization	4.45E-13	3.75E-13	26	CDC27/TOP2A/DNMT1/MKI67/TACC3/RIOK2/PLK1/H1-10/H1-2/MCM2/SRC/TRIP13/MAD2L1/H1-5/NDC80/CCNB1/ATF7IP/H1-1/TLK2/CDC20/CTCF/DLGAP5/CDC45/CHEK1/AURKB/FEN1
GO:0006310	DNA recombination	5.44E-12	4.59E-12	23	TOP2A/MCM6/MCM4/H1-10/H1-2/MCM7/MCM5/MCM2/TRIP13/KPNA2/MCM3/H1-5/H1-1/GINS4/RAD51AP1/CDC45/CHEK1/FIGNL1/FEN1/GINS2/HMGB1/HMGB2/HMGB3

GO:0044843	cell cycle G1/S phase transition	6.86E-12	5.78E-12	23	RRM2/POLE4/POLE3/NASP/POLA1/CDK6/MCM6/TYMS/PCNA/ MCM4/CDK1/MCM7/MCM5/MCM2/MCM3/POLA2/CCNB1/PRIM1/ CDC45/PRIM2/AURKA/DHFR/FAM83D
GO:0045787	positive regulation of cell cycle	9.58E-09	8.07E-09	22	RCC2/ASNS/PCNA/KIF23/CDK1/SRC/MAD2L1/NDC80/CCNB1/ DTL/SPAG5/DLGAP5/CDC45/CHEK1/AURKB/AURKA/UBE2C/ FEN1/NUSAP1/FAM83D/PDGFRB/CKS2
GO:0071824	protein-DNA complex subunit organization	4.39E-10	3.70E-10	21	POLE3/NASP/MCM6/UBTF/MCM4/CENPH/H1-10/H1-2/MCM7/ MCM5/MCM2/MCM3/H1-5/ATF7IP/H1-1/HELLS/CTCF/HAT1/ CDC45/HMGB1/HMGB2
GO:0051052	regulation of DNA metabolic process	2.33E-07	1.96E-07	21	DNMT1/PCNA/CDK1/H1-10/H1-2/SRC/KPNA2/RFC4/H1-5/RFC2/RFC5/ ATF7IP/H1-1/RAD51AP1/CHEK1/AURKB/FIGNL1/UBE2V1/HMGB1/ PDGFRB/UBE2V2
GO:0071897	DNA biosynthetic process	1.66E-11	1.40E-11	19	RFC1/POLE4/POLE3/POLA1/LIG1/POLD1/TYMS/PCNA/SRC/POLD2/ POLA2/RFC4/RFC2/RFC5/TK1/DTL/AURKB/POLD3/PDGFRB
GO:1902850	microtubule cytoskeleton organization involved in mitosis	8.16E-13	6.88E-13	18	KIF23/NDE1/TACC3/PLK1/KIFC1/MAD2L1/NDC80/CCNB1/NUF2/ PRC1/KIF11/STMN1/CDC20/AURKB/AURKA/KIF4A/SPC25/NUSAP1
GO:0032200	telomere organization	3.67E-10	3.10E-10	17	RFC1/POLE4/POLE3/POLA1/POLD1/PCNA/SRC/POLD2/POLA2/RFC4/RFC2/ RFC5/PRIM1/PRIM2/AURKB/POLD3/FEN1
GO:0007051	spindle organization	7.83E-10	6.60E-10	17	KIF23/TACC3/PLK1/KIFC1/NDC80/CCNB1/NUF2/PRC1/KIF11/STMN1/ CDC20/SPAG5/AURKB/AURKA/KIF4A/SPC25/HDAC3
GO:0000075	cell cycle checkpoint	2.02E-08	1.71E-08	17	TOP2A/PCNA/CDK1/PLK1/TRIP13/MAD2L1/NDC80/CCNB1/ZWINT/ CDC20/DTL/MAP3K20/ZWILCH/CDC45/CHEK1/AURKB/AURKA

GO:0006302	double-strand break repair	3.41E-07	2.87E-07	16	POLA1/MCM6/MCM4/MCM7/MCM5/MCM2/TRIP13/MCM3/GINS4/RAD51AP1/CDC45/CHEK1/FIGNL1/FEN1/GINS2/UBE2V2
GO:0022616	DNA strand elongation	1.08E-21	9.07E-22	15	POLA1/RNASEH2A/LIG1/PCNA/MCM4/MCM7/POLD2/MCM3/RFC4/GINS1/GINS4/POLD3/FEN1/GINS2/GINS3
GO:0000910	cytokinesis	1.05E-07	8.85E-08	14	CUL7/ANLN/CEP55/KIF23/PLK1/ANXA11/CHMP3/CKAP2/PRC1/STMN1/AURKB/AURKA/KIF4A/NUSAP1
GO:0006301	postreplication repair	1.66E-10	1.40E-10	11	RFC1/POLD1/PCNA/POLD2/RFC4/RFC2/RFC5/DTL/POLD3/UBE2V1/UBE2V2
GO:0042769	DNA damage response, detection of DNA damage	5.38E-09	4.54E-09	9	RFC1/POLD1/PCNA/POLD2/RFC4/RFC2/RFC5/DTL/POLD3

Table 7.12: Enriched GO terms (BP) (Overrepresented)

ID	Description	p.adjusted	qvalue	Count	Gene ID
GO:0052548	regulation of endopeptidase activity	0.001222127	0.00101488	11	PCSK1N/CD44/FAS/CRYAB/CASP1/GPX1/CYFIP2/ DHCR24/PLAUR/TFPI2/TIMP1
GO:0034341	response to interferon-gamma	0.000883011	0.000733271	10	KYNU/STAT1/CD44/SHFL/CASP1/OAS2/IFITM3/OAS1/ TRIM22/MT2A
GO:0043900	regulation of multi-organism process	0.005973412	0.004960449	9	APOE/STOM/IFIT1/STAT1/SHFL/IFITM3/OAS1/TIMP1/HMGA2
GO:0072593	reactive oxygen species metabolic process	0.002515044	0.002088546	8	BCR/HBA1/PTK2B/CRYAB/GPX1/SESN2/ATP5IF1/CDKN1A
GO:0016042	lipid catabolic process	0.005736917	0.004764059	8	ACAD11/APOE/ACAA1/ECH1/APOC3/SESN2/FUCA1/SMPDL3B
GO:0009615	response to virus	0.005736917	0.004764059	8	IFIT1/STAT1/SHFL/OAS2/IFITM3/OAS1/TRIM22/HMGA2
GO:0019058	viral life cycle	0.007001331	0.005814055	8	APOE/STOM/IFIT1/SHFL/CTSB/IFITM3/OAS1/HMGA2
GO:0045861	negative regulation of proteolysis	0.007364646	0.006115761	8	PCSK1N/CD44/CRYAB/GPX1/DHCR24/PLAUR/TFPI2/TIMP1
GO:0006631	fatty acid metabolic process	0.007998968	0.006642515	8	ACAD11/CES2/ACAA1/ECH1/GPX1/MSMO1/APOC3/SESN2
GO:0045862	positive regulation of proteolysis	0.007998968	0.006642515	8	APOE/PTK2B/FAS/CASP1/PSMD10/CYFIP2/ATP5IF1/BTRC

GO:0044282	small molecule catabolic process	0.015660434	0.013004761	8	ACAD11/APOE/ACAA1/KYNU/CD44/ECH1/QPRT/SESN2
GO:0098754	detoxification	0.001222127	0.00101488	7	APOE/HBA1/ACAA1/MGST3/GPX1/SESN2/MT2A
GO:0000302	response to reactive oxygen species	0.003543672	0.002942742	7	APOE/HBA1/STAT1/PTK2B/CRYAB/GPX1/SESN2
GO:0034340	response to type I interferon	0.002225806	0.001848357	6	IFIT1/STAT1/SHFL/OAS2/IFITM3/OAS1
GO:1902652	secondary alcohol metabolic process	0.015006171	0.012461447	5	APOE/FDFT1/MSMO1/DHCR24/ERG28
GO:0016125	sterol metabolic process	0.018908859	0.015702323	5	APOE/FDFT1/MSMO1/DHCR24/ERG28
GO:0051702	interaction with symbiont	0.016313924	0.013547433	4	APOE/STOM/GPX1/HMGA2
GO:0002021	response to dietary excess	0.007911096	0.006569544	3	GDF15/APOE/PCSK1N
GO:1901797	negative regulation of signal transduction by p53 class mediator	0.013438149	0.011159328	3	CD44/PSMD10/RRM2B
GO:0055090	acylglycerol homeostasis	0.016313924	0.013547433	3	APOE/APOC3/SESN2

Table 7.13: Enriched GO terms (BP) (Underrepresented)

ID	Description	p.adjusted	qvalue	Count	Gene ID
GO:0048285	organelle fission	8.51E-14	7.30E-14	26	NCAPD2/TOP2A/SMC4/ANLN/MKI67/TACC3/KIFC1/TRIP13/NCAPG/MAD2L1/SMC2/NDC80/CCNB1/NUF2/PRC1/ZWINT/NCAPH/KIF11/CDC20/HSPA2/SPAG5/AURKB/AURKA/CDCA8/NUSAP1/DSCC1
GO:0006260	DNA replication	1.21E-17	1.04E-17	25	RRM2/RFC1/DUT/POLE3/NASP/RNASEH2A/LIG1/MCM6/MCM4/CDK1/MCM7/MCM5/MCM2/POLD2/NFIB/MCM3/POLA2/RFC2/RRM1/PRIM1/PRIM2/POLD3/FEN1/DSCC1/GINS3
GO:0007059	chromosome segregation	2.46E-16	2.11E-16	25	NCAPD2/TOP2A/SMC4/MKI67/TACC3/KIFC1/TRIP13/NCAPG/MAD2L1/SMC2/NDC80/CCNB1/NUF2/PRC1/ZWINT/NCAPH/CDC20/SPAG5/AURKB/SPC25/FEN1/CDCA8/NUSAP1/FAM83D/DSCC1
GO:0071103	DNA conformation change	5.55E-16	4.76E-16	25	NCAPD2/TOP2A/SMC4/POLE3/NASP/MCM6/MCM4/CDK1/CENPH/H1-10/MCM7/MCM5/MCM2/NCAPG/MCM3/H1-5/SMC2/RFC2/CCNB1/NCAPH/BRD2/H1-1/NUSAP1/DSCC1/HMGB2
GO:0044843	cell cycle G1/S phase transition	8.05E-11	6.91E-11	19	RRM2/POLE3/NASP/CDK6/MCM6/TYMS/MCM4/CDK1/MCM7/MCM5/MCM2/MCM3/POLA2/CCNB1/PRIM1/PRIM2/AURKA/DHFR/FAM83D
GO:0033044	regulation of chromosome organization	7.05E-08	6.05E-08	17	TOP2A/DNMT1/MKI67/TACC3/H1-10/MCM2/SRC/TRIP13/MAD2L1/H1-5/NDC80/CCNB1/H1-1/CDC20/AURKB/FEN1/SNCA
GO:0010639	negative regulation of organelle organization	2.37E-06	2.04E-06	16	TOP2A/DNMT1/PICK1/H1-10/MCM2/SRC/TRIP13/MAD2L1/H1-5/NDC80/CCNB1/STMN1/H1-1/CDC20/AURKB/SNCA
GO:0060249	anatomical structure homeostasis	3.33E-05	2.86E-05	15	RFC1/POLE3/LTF/SRC/POLD2/POLA2/ITGB3/RFC2/CCN2/CA2/PRIM1/PRIM2/AURKB/POLD3/FEN1

GO:1902850	microtubule cytoskeleton organization involved in mitosis	2.47E-10	2.12E-10	14	TACC3/KIFC1/MAD2L1/NDC80/CCNB1/NUF2/PRC1/KIF11/ STMN1/CDC20/AURKB/AURKA/SPC25/NUSAP1
GO:0071897	DNA biosynthetic process	1.64E-08	1.41E-08	14	RFC1/POLE3/LIG1/TYMS/SRC/POLD2/POLA2/RFC2/CCN2/ TK1/CHRAC1/AURKB/POLD3/DSCC1
GO:0006310	DNA recombination	2.36E-06	2.03E-06	14	TOP2A/MCM6/MCM4/H1-10/MCM7/MCM5/MCM2/TRIP13/ KPNA2/MCM3/H1-5/H1-1/FEN1/HMGB2
GO:0071824	protein-DNA complex subunit organization	3.01E-06	2.58E-06	14	POLE3/NASP/MCM6/MCM4/CENPH/H1-10/MCM7/MCM5/MCM2/ MCM3/H1-5/BRD2/H1-1/HMGB2
GO:0045787	positive regulation of cell cycle	4.77E-05	4.09E-05	14	ASNS/CDK1/SRC/MAD2L1/NDC80/CCNB1/CCN2/HSPA2/SPAG5/ AURKB/AURKA/FEN1/NUSAP1/FAM83D
GO:0007051	spindle organization	1.13E-07	9.74E-08	13	TACC3/KIFC1/NDC80/CCNB1/NUF2/PRC1/KIF11/STMN1/CDC20/ SPAG5/AURKB/AURKA/SPC25
GO:0032200	telomere organization	4.76E-06	4.09E-06	11	RFC1/POLE3/SRC/POLD2/POLA2/RFC2/PRIM1/PRIM2/AURKB/ POLD3/FEN1
GO:0022616	DNA strand elongation	1.50E-11	1.29E-11	9	RNASEH2A/LIG1/MCM4/MCM7/POLD2/MCM3/POLD3/FEN1/GINS3
GO:0050000	chromosome localization	5.92E-05	5.08E-05	7	KIFC1/NDC80/CCNB1/NUF2/SPAG5/CDCA8/FAM83D
GO:0009262	deoxyribonucleotide metabolic process	6.96E-06	5.97E-06	6	RRM2/DUT/TYMS/SHMT1/RRM1/NUDT1

GO:0006301	postreplication repair	4.87E-05	4.18E-05	6	RFC1/POLD2/RFC2/POLD3/UBE2V1/UBE2V2
GO:0051383	kinetochore organization	1.35E-05	1.16E-05	5	SMC4/CENPH/SMC2/NDC80/NUF2